PB97-185912

NTIS
Information is our business.

SEISMIC RESPONSE OF COLUMN/CAP BEAM TEE CONNECTIONS WITH CAP BEAM PRESTRESSING

CALIFORNIA UNIV., SAN DIEGO, LA JOLLA

DEC 96

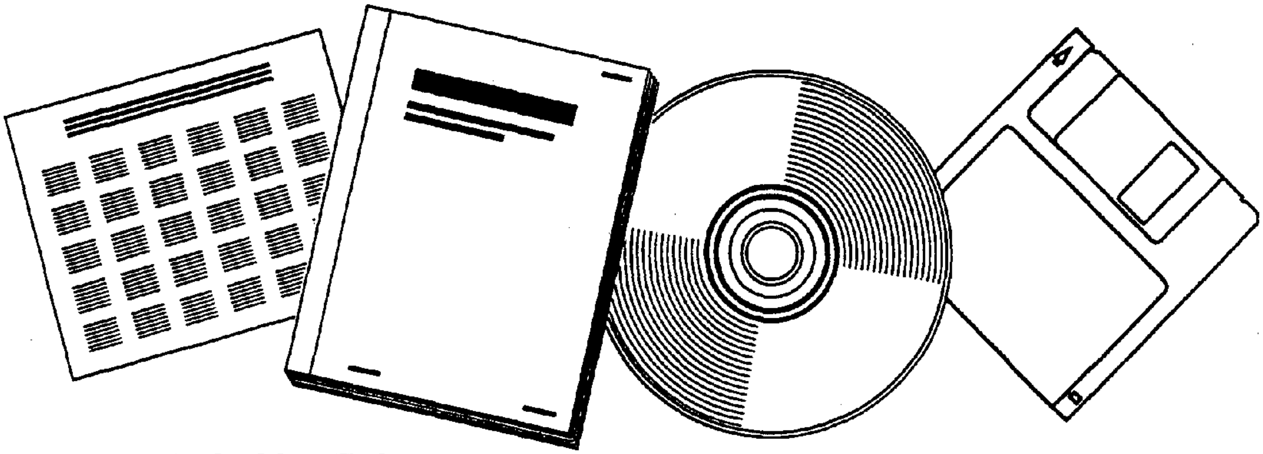

U.S. DEPARTMENT OF COMMERCE
National Technical Information Service

PB97-185912

STRUCTURAL SYSTEMS
RESEARCH PROJECT

Report No.
SSRP - 96/09

SEISMIC RESPONSE OF COLUMN/CAP BEAM TEE CONNECTIONS WITH CAP BEAM PRESTRESSING

by

Sri Sritharan
M.J. Nigel Priestley
Frieder Seible

Final Report on a Research Project funded by Caltrans
under Contract No. 59V374.

December 1996

Division of Structural Engineering
University of California, San Diego
La Jolla, California 92093-0085

REPRODUCED BY: NTIS
U.S. Department of Commerce
National Technical Information Service
Springfield, Virginia 22161

University of California, San Diego
Division of Structural Engineering
Structural Systems Research Project

Report No. SSRP-96/09

SEISMIC RESPONSE OF COLUMN/CAP BEAM TEE CONNECTIONS WITH CAP BEAM PRESTRESSING

by

Sri Sritharan
Graduate Research Assistant

M.J. Nigel Priestley
Frieder Seible
Professors of Structural Engineering

Final Report on a Research Project funded by Caltrans
under Contract No. 59V374.

Division of Structural Engineering
University of California, San Diego
La Jolla, California 92093-0085

December 1996

Technical Report Documentation Page

1. Report No. SSRP-96/09	2 PB97-185912	3. Recipient's Catalog No.
4. Title and Subtitle Seismic Response of Column/Cap Beam Tee Connections with Cap Beam Prestressing		5. Report Date December 1996
		6. Performing Organization Code
7. Author(s) S. Sritharan, M.J.N. Priestley and F. Seible		8. Performing Organization Report No.
9. Performing Organization Name and Address Division of Structural Engineering School of Engineering University of California, San Diego La Jolla, California 92093-0085		10. Work Unit No. (TRAIS)
		11. Contract or Grant No. RTA 59V374
12. Sponsoring Agency Name and Address California Department of Transportation Engineering Service Center 1801 30th Street Sacramento, California 95816		13. Type of Report and Period Covered Task 5 Final Report (1 of 2)
		14. Sponsoring Agency Code N/A

15. Supplementary Notes

16. Abstract

Concrete bridge joints in California were detailed with no shear reinforcement in the 1950s. The probable consequence of such poor detailing was demonstrated on an as-built bridge tee (interior) joint from the Santa Monica Viaduct in Los Angeles. When a redesign of this joint was considered with the conventional design methods based upon the maximum joint shear forces, it resulted in a considerable amount of joint reinforcement, causing congestion of steel within the joint. This has been identified as a major construction problem in concrete bridge construction.

Three redesigns of the prototype joint were sought with the objective of reducing the amount of reinforcing steel within the joint, thereby ensuring constructability. In all three designs, force transfer models were employed in determining the appropriate amount of joint reinforcement rather than using the joint shear forces as the design parameter. The first tee joint was designed with conventional reinforcement while the cap beams of the other two units were detailed with partial and full prestressing. Considering that the cap beam prestressing assists in transmitting the shear forces across the joint, the joint reinforcement in the latter units was further reduced when compared to the first unit. The suitability of the redesigned details was verified by subjecting half scale test models to simulated seismic loading. The response of all three redesigned units was satisfactory and complied to the current seismic design criteria. Some damage occurred to the joint of the reinforced concrete unit while the joint damage of the prestressed units was limited to only minor cracking. There was a clear indication that cap beam prestressing proportionally enhances the seismic performance of the joint.

When the cap beam was designed with full prestressing, it was also shown that precast construction can be adopted as an alternative to cast-in-place construction for building multi-column concrete bents. The details of the joint design, seismic performance of all three redesigned units and some design recommendations are presented in this report.

17. Key Words Bridge, Reinforced Concrete, Seismic Design, Joint, Tee Joint, Prestressing, Precast, Force-Transfer Mechanism, Strut-and-tie Model		18. Distribution Statement	
19. Security Classification (of this report) Unclassified	20. Security Classification (of this page) Unclassified	21. No. of Pages 296	22. Price

Form DOT F 1700.7 (8-72) Reproduction of completed page authorized

DISCLAIMER

The contents of this report reflect the views of the authors who are responsible for the facts and accuracy of the data presented herein. The contents do not necessarily reflect the official views or policies of the State of California or the Federal Highway Administration. This report does not constitute a standard, specification or regulation.

ABSTRACT

Concrete bridge joints in California were detailed with no shear reinforcement in the 1950s. The probable consequence of such poor detailing was demonstrated on an as-built bridge tee (interior) joint from the Santa Monica Viaduct in Los Angeles. When a redesign of this joint was considered with the conventional design methods based upon the maximum joint shear forces, it resulted in a considerable amount of joint reinforcement, causing congestion of steel within the joint. This has been identified as a major construction problem in concrete bridge construction.

Three redesigns of the prototype joint were sought with the objective of reducing the amount of reinforcing steel within the joint, thereby ensuring constructability. In all three designs, force transfer models were employed in determining the appropriate amount of joint reinforcement rather than using the joint shear forces as the design parameter. The first tee joint was designed with conventional reinforcement while the cap beams of the other two units were detailed with partial and full prestressing. Considering that the cap beam prestressing assists in transmitting the shear forces across the joint, the joint reinforcement in the latter units was further reduced when compared to the first unit. The suitability of the redesigned details was verified by subjecting half scale test models to simulated seismic loading. The response of all three redesigned units was satisfactory and complied to the current seismic design criteria. Some damage occurred to the joint of the reinforced concrete unit while the joint damage of the prestressed units was limited to only minor cracking. There was a clear indication that cap beam prestressing proportionally enhances the seismic performance of the joint.

When the cap beam was designed with full prestressing, it was also shown that precast construction can be adopted as an alternative to cast-in-place construction for building multi-column concrete bents. The details of the joint design, seismic performance of all three redesigned units and some design recommendations are presented in this report.

ACKNOWLEDGEMENTS

Large-scale tests on bridge tee joints presented in this report were performed at the Charles Lee Powell Laboratory of the University of California, San Diego. A number of technical personnel of UCSD assisted in the experimental investigation. Among them G. Smith, J. Ward and M. Baumann deserve special mention for their contribution in the construction and testing of the large-scale joints. Thanks are also due to L. Berman, D. Bowers, D. Castillo, R. Collins, M. Ellery, C. Lathem, C. McDaniel, R. Miner, L. Mitchell, P. Nelson, C. Stearns, and M. Veletzos for their assistance.

This study is made possible by funding from California Department of Transportation under contract No. 59V374.

LIST OF SYMBMOLS

A_g	Gross section area.
A_h	Cross sectional area of a hoop or spiral.
A_{ps}	Cross sectional area of post-tensioning bar.
A_{sc}	Area of longitudinal column reinforcement.
A_v	Area of shear reinforcement.
a	Effective depth of compression force.
a_b	Effective depth of the beam concrete compression force under positive moment.
a'_b	Effective depth of the beam concrete compression force under negative moment.
a_c	Effective depth of the column concrete compression force.
B	Bottom joint panel dimension.
b_w	Cap beam width.
b_j	Joint width.
C_B	Cap beam compression force under positive moment.
C'_B	Cap beam compression force under negative moment.
C_c	Column compression force.
C_c	Concrete compression force.
C_s	Steel compression force.
c	Neutral axis depth.
D	Diameter of column.
D	Diagonal joint panel dimension.
D_i	Diagonal compression strut.
D'	Diameter of column core measured to centerline of spirals or hoops.
d	Distance from tension reinforcement to the compression face (effective depth).
d	Joint panel width.
d_b	Diameter of reinforcement bar.
d_{bl}	Diameter of longitudinal reinforcement bar.
E_c	Youngs Modulus of concrete.
F	Actuator (or seismic) force.

F	Cap beam prestress force.
F_I	Actuator force required for ideal moment.
F_{max}	Maximum actuator force.
F_{min}	Minimum actuator force.
F_Y	Actuator force required for yield moment.
f	Flexibility coefficient.
f'_c	Unconfined concrete compression strength.
f'_{cc}	Compression strength of confined concrete.
f_h	Average joint axial stress in the horizontal direction.
f_l	maximum effective lateral stress.
f'_l	Effective lateral confining stress.
f_s	Steel stress.
f_v	Average joint axial stress in the vertical direction.
f_{yc}	Yield strength of longitudinal column reinforcement.
f_{yh}	Yield strength of transverse reinforcement.
G	Concrete shear modulus.
H	Height.
h	Joint panel height.
h_b	Cap beam depth.
h_c	Column depth.
I_{eff}	Cracked section (effective) second moment of area.
I_{gross}	Uncracked section second moment of area.
K_e	Confinement effectiveness coefficient.
L	Length of an idealized column or cap beam.
l	Instantaneous length.
l_a	Anchorage length.
l_c	Clear length.
l_{eff}	Effective length of a concrete member.
l_g	Gauge length of a curvature cell.
l'_g	Modified gauge length of a curvature cell to account for strain penetration.

l_p	Plastic hinge length.
l_{sp}	Equivalent strain penetration length.
l_w	Distance between linear potentiometers within a curvature cell.
M	Moment.
M_b	Cap beam positive moment.
M'_b	Cap beam negative moment.
M_c	Column moment.
M^o_c	Overstrength column capacity.
M_{cr}	Cracking moment.
M_p	Plastic moment.
M_I	Ideal moment.
M_Y	Yield moment.
M_U	Ultimate moment.
m	Model unit.
P	Axial force.
P_b	Cap beam axial force corresponding positive moment.
P'_b	Cap beam axial force corresponding negative moment.
P_c	Column axial force.
p	Prototype structure
p_c	Joint principal compression stress.
p_t	Joint principal tension stress.
SF	Scale factor
s	Spacing of transverse reinforcement.
T_a	Tension force in the bottom beam reinforcement.
T_b	Cap beam tension force under positive moment.
T'_b	Cap beam tension force under negative moment.
T_b	Tension force in beam shear reinforcement.
T_c	Column tension force.
T_s	Steel tension force.
u_i	Joint panel nodal displacements.

$v_{j,max}$	Maximum joint shear stress.
V	Shear force.
V_b	Cap beam shear corresponding to positive moment.
V'_b	Cap beam shear corresponding to negative moment.
V_c	Column shear force.
V_c	Concrete contribution to shear resistance.
V_d	Dead load shear force.
V_{jh}	Average horizontal joint shear force.
V_{jv}	Average vertical joint shear force.
V_p	Shear strength due to axial force.
V_r	Total shear resistance.
V_s	Shear resistance of steel reinforcement.
v_j	Joint shear stress.
v_{jh}	Horizontal joint shear stress.
v_{jv}	Vertical joint shear stress.
α	Inclination of diagonal compression strut.
β	Inclination of external joint strut.
γ	Joint shear strain.
Δ_c	Total fixed base column displacement.
Δ'_e	Elastic displacement component beyond yielding.
Δ_p	Plastic deformation.
Δ_s	Shear deformation.
Δ_{sy}	Shear deformation at ideal strength.
Δ_t	Total displacement.
Δ_x	Joint horizontal extension.
Δ_y	Yield displacement.
Δ_y	Joint vertical extension.
Δ'_y	Elastic displacement at first yield.
Δ_l	Displacement measured by a linear potentiometer within a curvature cell.

Δ_2	Displacement measured by a linear potentiometer within a curvature cell.
$\Delta\theta_x$	Joint rotation in x direction.
$\Delta\theta_y$	Joint rotation in y direction.
ε_c	Concrete strain.
ε_{cu}	Ultimate concrete compression strain.
ε_s	Steel strain.
ε_{su}	Steel strain at maximum tensile stress.
ε_{su}	Strain at the ultimate stress f_{su}.
ε_y	Yield strain of steel reinforcement.
θ	Angle of inclined flexure-shear cracking.
θ_p	Plastic hinge rotation.
λ_o	Overstrength factor.
μ_m	Member displacement ductility.
μ_s	System displacement ductility.
μ_Δ	System displacement ductility.
μ_ϕ	Curvature ductility of a concrete section.
ρ_l	Longitudinal steel ratio.
ρ_s	Volumetric ratio of joint horizontal reinforcement.
ρ_s	Volumetric ratio of confining steel.
ϕ_f	Flexural strength reduction factor.
ϕ_m	Curvature.
ϕ_p	Plastic curvature.
ϕ_S	Strength reduction factor for shear.
ϕ_Y	Yield curvature.
ϕ'_Y	First yield curvature.
ϕ_u	Ultimate curvature.
ξ	Equivalent viscous damping coefficient

TABLE OF CONTENTS

DISCLAIMER i

ABSTRACT ii

ACKNOWLEDGEMENTS iii

LIST OF SYMBOLS iv

TABLE OF CONTENTES ix

1 INTRODUCTION 1

1.1 Overview 1

1.2 Background 3

1.3 Research Significance 4

1.4 Units of Measurements 9

2 ANALYTICAL PROCEDURES 11

2.1 Moment-Curvature Analysis 11

2.2 Elastic Deformation 13

2.3 Plastic Hinge Length and Plastic Deformation 14

2.4 Shear Deformation 15

2.5 Member Ductility 15

2.6 Joint Deformation 16

2.7 Beam Flexibility 19

2.8 System Ductility 19

2.9 Predicted Response of Test Units 21

3 INTRODUCTION TO EXPERIMENTAL STUDY 23

3.1 As-Built Test Unit 23

3.1.1 Prototype Structure 23

3.1.2 Model Specimen SM3 28

3.1.3 Test Set Up Used for SM3 32

3.1.4 Instrumentation and Loading Sequence 32
3.1.5 Performance of SM3 34
3.2 Test Units IC Series 43
3.2.1 Prototype Structure 44
3.2.2 Modeling of Prototype 47
3.2.3 Test Set Up 48
3.2.4 Construction of Test Units 53
3.2.5 Instrumentation 53
3.2.6 Loading Sequence 58

4 INTERIOR JOINT WITH A REINFORCED CONCRETE CAP BEAM 61
4.1 Design Procedure 61
4.1.1 Column 61
4.1.2 Cap Beam 61
4.1.3 Interior Joint 63
4.2 Reinforcement Detailing 70
4.2.1 Column 70
4.2.2 Cap Beam 72
4.2.3 Interior Joint 72
4.3 Material Properties 75
4.4 Predicted Response 76
4.4.1 Cracking under Gravity Load 76
4.4.2 Cracking in the Column 76
4.4.3 Cracking in the Cap Beam 77
4.4.4 Cracking in the Joint Region 77
4.4.5 Force Displacement Response 77
4.5 Observation During the Test 78
4.5.1 Application of Dead Load 78
4.5.2 Force Control 78
4.5.3 Displacement Control 82

4.6 Experimental Results 91
4.6.1 Force-Displacement Hysteresis Curve 92
4.6.2 Moment-Curvature Response 92
4.6.3 Joint Deformation 99
4.6.4 Displacement Components 110
4.6.5 Strain Gauge Histories 113
4.6.6 Strain Profiles 121
4.7 Discussion 131

5 INTERIOR JOINT WITH A PARTIALLY PRESTRESSED CAP BEAM 143
5.1 Design Procedure 143
5.1.1 Column 143
5.1.2 Cap Beam 143
5.1.3 Interior Joint 143
5.2 Reinforcement Detailing 145
5.2.1 Column 146
5.2.2 Cap Beam 146
5.2.3 Interior Joint 148
5.3 Cap Beam Prestressing 148
5.4 Material Properties 152
5.5 Predicted Response 152
5.5.1 Gravity Load Response 153
5.5.2 Cracking in the Column 153
5.5.3 Cracking in the Cap Beam 153
5.5.4 Cracking in the Joint Region 153
5.5.5 Force-Displacement Response 154
5.6 Observation under Repeated Cyclic Loading 154
5.6.1 Application of Dead Load 154
5.6.2 Initial Damage 154
5.6.3 Force Control 155

5.6.4 Displacement Control 155
5.7 Experimental Results 162
5.7.1 Force-Displacement Hysteresis Curve 162
5.7.2 Moment-Curvature Response 167
5.7.3 Joint Deformation 169
5.7.4 Displacement Components 176
5.7.5 Strain Gauge Histories 180
5.7.6 Strain Profiles 188
5.8 Discussion 194

6 INTERIOR JOINT WITH A PRECAST FULLY PRESTRESSED CAP BEAM .. 197
6.1 Design Procedure 197
6.1.1 Column 197
6.1.2 Cap Beam 197
6.1.3 Interior Joint 198
6.2 Reinforcement Detailing 199
6.2.1 Column 203
6.2.2 Cap Beam 203
6.2.3 Interior Joint 203
6.3 Construction Procedure 204
6.3.1 Cap Beam Prestressing 204
6.4 Material Properties 211
6.5 Predicted Response 212
6.5.1 Gravity Load Response 212
6.5.2 Cracking in the Column 212
6.5.3 Cracking in the Cap Beam 212
6.5.4 Cracking in the Joint Region 212
6.5.5 Force-Displacement Response 213
6.6 Observation under Repeated Cyclic Loading 213
6.6.1 Application of Dead Load 213

6.6.2 Force Control 214

6.6.3 Displacement Control 217

6.7 Experimental Results 227

6.7.1 Force-Displacement Hysteresis Curve 228

6.7.2 Moment-Curvature Response 231

6.7.3 Joint Deformation 234

6.7.4 Displacement Components 243

6.7.5 Strain Gauge Histories 246

6.7.6 Strain Profiles 251

6.8 Discussion 262

7 DISCUSSION AND DESIGN RECOMMENDATIONS 265

7.1 Alternative Joint Design Approach 265

7.2 Discussion of Test Results 267

7.3 Design Recommendations 278

7.3.1 Reinforced Concrete Joints 278

7.3.2 Prestressed Concrete Joints 279

REFERENCES 279

APPENDIX A ANALYSIS OF JOINT CRACKING 285

APPENDIX B FORCE-DISPLACEMENT ENVELOPES 289

APPENDIX C ANALYSIS OF HYSTERESIS LOOPS 293

CHAPTER 1

INTRODUCTION

1.1 Overview

Capacity design philosophy [14] is now commonly adopted for seismic design of reinforced concrete structures in the United States. This design philosophy, which has been developed over the past two decades, ensures a desirable performance for a structure even under the maximum credible earthquake expected during its life time. Undesirable failure modes such as severe damage to joint regions and shear failure of structural members are precluded in the capacity design approach.

Elastic response is preferred to a ductile response for beam-column joints in concrete structures subjected to seismic loading because: (a) designing joints to respond in a highly ductile manner is practically impossible, and (b) allowing significant damage to the joint regions may lead to catastrophic failure of the entire structure. Elastic design approach for joints consistent with the above argument is adopted in the current design codes, in which the joint reinforcement content is determined for the maximum joint shear forces developed at the ultimate strength of the structure. Further, additional constraints to limit maximum joint shear stresses, to provide minimum confining steel and to assure minimum anchorage length for the longitudinal reinforcement in adjacent members are incorporated to obtain satisfactory performance of the joints, and hence a desirable response for the structure as a whole.

Design guidelines provided in the current codes were developed empirically, based largely on laboratory tests on beam/column joints from building frames. However, considerable discrepancies exist between design codes because joint behavior is treated differently in different codes. For example, the U.S. approach [3] emphasizes confinement by transverse reinforcement as the key element for satisfactory response whereas the New Zealand approach [27] requires shear transfer using truss mechanisms adapted from beam shear design. In both cases shear tends to be isolated as an independent force, rather than as a component of a complete, rational force transfer mechanism within the joint region.

A regulatory document governing bridge design in the United States is published by AASHTO [1]. Although the design specifications of this document are generally comparable to those of the ACI code, it provides little directions for the design of bridge cap beam/column connections. Comparing a bridge tee joint to an exterior building joint, the vertical reinforcement of the tee joint can be obtained using the ACI code. Since joint shear stresses are equal in the vertical and horizontal directions, a similar reinforcement quantity can be justified as horizontal joint shear reinforcement as well. If this approach based upon the maximum joint shear forces is considered, it generally results in a considerable amount of joint reinforcement, causing congestion of steel in the joint region [23]. In building frames, the amount of joint reinforcement is dictated by the overstrength capacity of the beams, which is generally smaller than that of a typical bridge column. Axial load and longitudinal steel content are high in bridge columns when compared to beams in building frames. Consequently, higher overstrength moments and higher joint shear stresses are developed in bridge structures. Further, because of reserve capacity of the longitudinal column reinforcement and due to the fact that a part of the moment capacity of the beam is provided by the slab whose reinforcement is anchored outside the joint, the design of building joints cause relatively less congestion in building joints [26].

Seismic design of concrete bridge joints were not properly understood in the pre-1960 era. Several arguments were taken for granted to simplify seismic design procedures without properly understanding (a) the magnitude of joint shear forces, and (b) the mechanisms necessary for force transfer from one structural member to another. The shear forces which are induced within a joint are typically 4-6 times higher than those developed in adjacent beam or column members. However, no joint reinforcement was provided to assist force transfer through the joint whereas the columns and cap beams were designed with shear reinforcement in accordance to the code provisions.

Probable consequence of such poor joint detailing was not appreciated until the 1989 Loma Prieta earthquake which caused significant damage to bridge structures in northern California. Failure to some bridges, including the double deck Cypress Viaduct, was partly attributed to the damage that occurred to the cap beam/column joints [6]. In several cases, distress to cap beam/column connections were also observed in the bay area. As a result, a vigorous research program was initiated in California, examining the competence of as-built joints and retrofit measures for poorly designed connections, as well as establishing efficient alternative details for designing new bridge joints [20]. The research presented in this report is the first phase of such an ongoing investigation conducted at the Charles Lee Powell Laboratory of the University of California, San Diego (UCSD), in which alternative reinforcement detailing is sought for interior cap beam/column connections, with the primary objective of reducing the congestion of steel within joints. The use of cap beam prestress to assist force transfer through the joint, and thereby reducing steel content within joints, was given particular emphasis in the investigation.

1.2 Background

Competence of an as-built tee joint with a circular column from pre-1960 design was examined in an earlier study at UCSD [12]. A three fourth scale model of the interior joint from Bent 793+57 of the Santa Monica Viaduct in Los Angeles, California, which was referred to as SM3, was used for this purpose. It was demonstrated that the performance of unreinforced tee joints is not dependable, and that joint shear failure is likely to occur prior to developing flexural capacity in the columns. A similar observation was also made in a study at the University of California, Berkeley, where seismic performance of an old bridge tee joint with a rectangular column was examined, followed by an investigation on possible retrofitting techniques of such poorly detailed concrete joints [11]. For developing alternative joint detailing in the current study, the previously tested joint of the Santa Monica Viaduct was redesigned so that the effectiveness of new joint details could be assessed with respect to the response of SM3.

In designing the joints with alternative reinforcement details, force transfer mechanisms based on simple strut-and-tie models were considered. A comprehensive discussion on detailing bridge joints based on force transfer mechanisms and thereby reducing reinforcement content within joints was presented by Priestley [17]. Of the proposed alternative design methods, the detailing procedure requiring the least amount of reinforcement, was chosen as the basis of the study presented in this report. In detailing each of the new joints, it was ensured that the column longitudinal reinforcement was anchored adequately into the joint so that the plastic flexural capacity of the column could be developed. The test program included three tee joints, the first unit with a fully reinforced concrete cap beam, the second unit with a partially prestressed cap beam, and the third unit with a precast fully prestressed cap beam. By varying prestress in the bent cap, the influence of cap beam prestressing on the joint performance was also studied.

1.3 Research Significance

In older concrete bridges, no reinforcement was provided to carry the joint shear forces. An example of this is shown in Figure 1.1 in which the reinforcement details of the as-built test model SM3 is given. Another design deficiency of this detailing is that the longitudinal column bars are prematurely terminated within the joint. As shear demand increases, joint cracking occurs when the joint principal tensile stress exceeds the cracking strength of concrete. If there is no reinforcement to carry the tensile forces induced within the joint and evenly distribute cracking, only a few large diagonal cracks develop in the joint region. Consequently, a rapid deterioration in the force resisting ability of the system ensues. If the longitudinal column bars are not extended as close to the top of the beam as possible, they will not be effectively anchored into the joint strut.

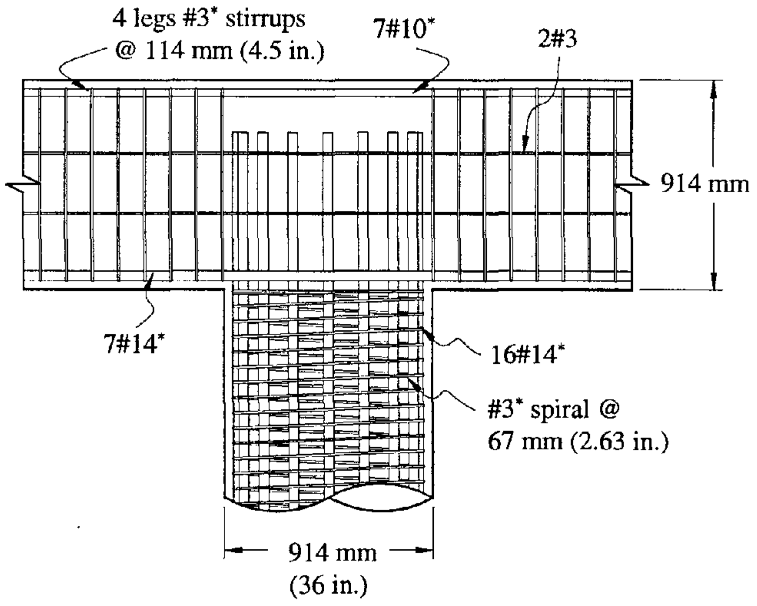

Note: *Grade 40 (276 Mpa) steel, d_b = 9.5 mm for #3, d_b = 32.2 mm for #10, and d_b = 43.0 mm for #14 rebar.

Figure 1.1 Reinforcement details of an as-built interior cap beam/column joint representing pre-1960 design.

As cracks widen and damage the joint, these bars, particularly the most extreme tension reinforcement, can easily pull out from the joint, not allowing the column overstrength capacity to be attained.

The test by MacRae *et al.* [12] on the as-built joint from the Santa Monica Viaduct demonstrated the shear failure of unreinforced joints. Cracking in the joint was first developed at a horizontal force corresponding to column theoretical ideal flexural strength. The horizontal load continued to increase up to displacement ductility 1.5. At this displacement, which recorded the maximum resistance, only 74 percent of the ideal flexural strength was developed. Progressive cracking of the joint gradually deteriorated force resisting ability of the system at larger ductilities and the test was terminated when the joint was severely damaged. More detail of the behavior of this test unit is discussed in Section 3.1.5.

Inadequate performance of unreinforced joints has not been frequently observed in past earthquakes. This is partly because poor detailing of other structural members, particularly the columns, did not allow member capacity to be developed and thus joints were not tested for the maximum demand expected under large earthquakes. Minor damage which occurred to the cap beam/column interior joint region may have gone unnoticed as these regions are generally hidden in box girder bridges. Cracking and some damage to outrigger knee joints were found to be common in the 1989 Loma Prieta earthquake. Joint damage observed in I-980 Bent #38 is shown in Figure 1.2 along with similar joint damage observed under laboratory condition [7].

Detailing bridge joints based on the maximum joint shear stresses results in robust joints. However, as indicated previously, the amount of reinforcement requires within the joint regions is unnecessarily conservative, causing construction problems. An example of this is shown in Figure 1.3 where the half scale cap beam/column tee joint considered in the current investigation (see Figure 4.4) was detailed for the maximum joint shear forces. The longitudinal column reinforcement of this unit is only 1.85 percent. If a larger reinforcement ratio is considered in the column, more joint reinforcement will be required than is shown in Figure 1.3. Therefore, alternative design methods for bridge joints are imperative. An elevated freeway structure may contain thousands of beam/column joints. Reducing congestion of steel within joints can considerably reduce construction time and cost in these structures.

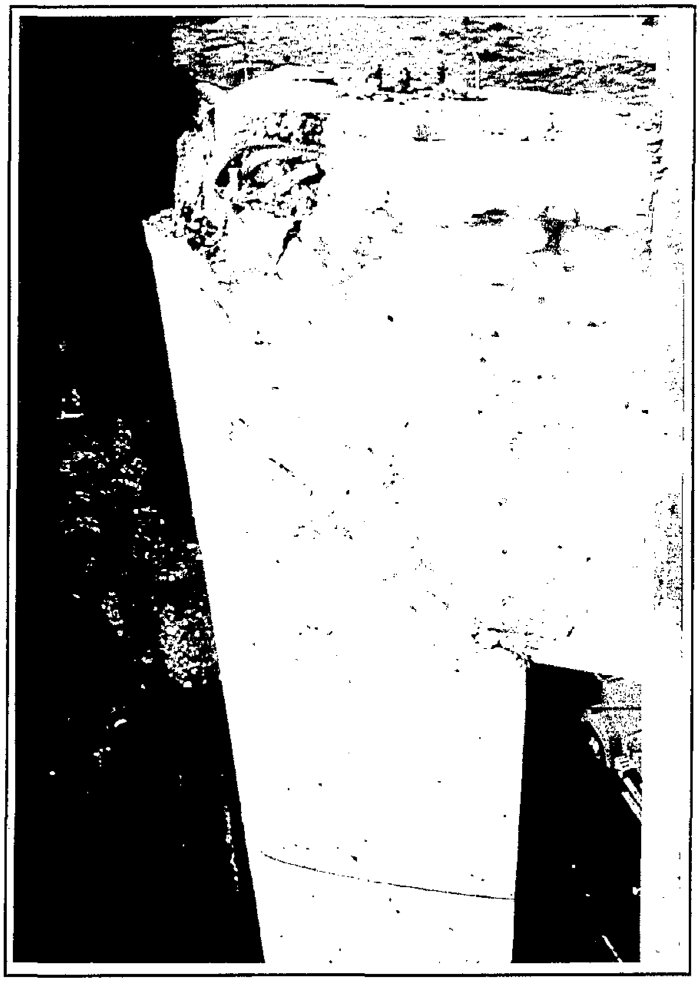

(a) Damage to outrigger knee joint of I-980 Bent #38 in the Loma Prieta earthquake.

(b) Damage to 1/3 scale model of I-980 Bent #38 knee joint in the laboratory test [7].

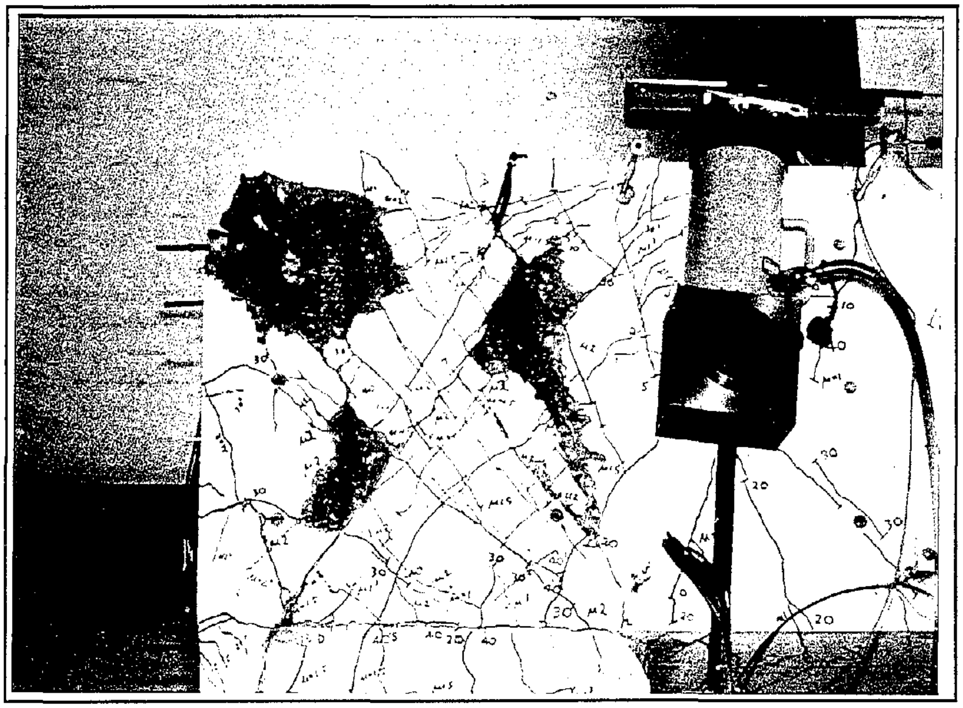

Figure 1.2 Comparison of joint damage observed in a prototype and laboratory model.

Reproduced from best available copy.

In the current investigation, three cap beam/column interior joints were designed with reduced joint reinforcement and yet ensuring dependable performance under seismic loading. From the response of large scale test units incorporating these details, it is shown that the proposed details are efficient alternatives to the current design practice.

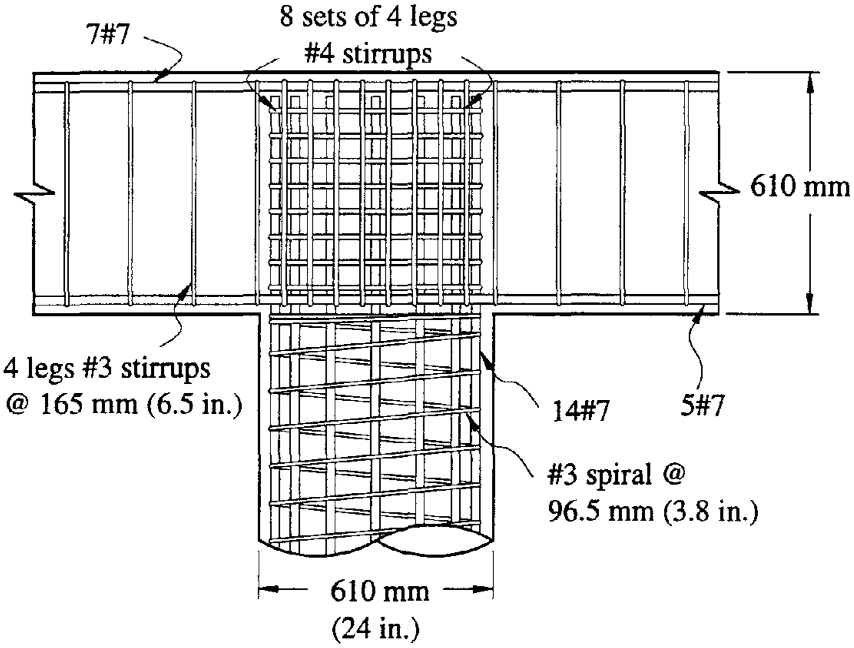

8 sets of 4 legs
#4 stirrups
7#7
610 mm
4 legs #3 stirrups
@ 165 mm (6.5 in.)
14#7
5#7
#3 spiral @
96.5 mm (3.8 in.)
610 mm
(24 in.)

Note: $d_b = 9.5$ mm for #3, $d_b = 12.7$ mm for #4, and $d_b = 22.2$ mm for #7.

Figure 1.3 Detailing of a tee joint based upon the maximum joint shear forces.

1.4 Units of Measurements

In accordance with the Caltrans policy, S.I. units are used in this report. Equivalent American units are also provided wherever possible for convenience.

CHAPTER 2

ANALYTICAL PROCEDURES

2.1 Moment-Curvature Analysis

Theoretical strengths and deformation capacities of structural members discussed in this report were assessed using a simple moment-curvature analysis as described in this section. Moment-curvature analyses were performed using the King's program [9] considering the Mander *et al.* model [13] to estimate the influence that steel confinement has on stress-strain behavior of concrete.

A typical moment-curvature response obtained for a reinforced concrete section from the King's program is shown in Figure 2.1. In this study, the yield moment, $\mathbf{M}_y$, was taken as the theoretical moment which induced experimentally measured yield strain in the most extreme tension reinforcement of the section. Corresponding curvature was ϕ'_y and this was referred to as the first yield curvature. Ideal moment capacity, $\mathbf{M}_I$, was defined as the moment which was required to develop concrete strain $\varepsilon_c = 0.005$ at the extreme compression fiber. This was consistent with procedures commonly adopted at the initiation of this study. Yield curvature, ϕ_y, which defines the curvature ductility was determined as follows:

$$\phi_y = \frac{\mathbf{M}_I}{\mathbf{M}_y}\phi'_y \qquad (2.1)$$

Curvature ductility capacity, μ_ϕ, of the concrete section is therefore:

$$\mu_\phi = \frac{\phi_u}{\phi_y} \qquad (2.2)$$

where ϕ_u is the ultimate curvature at which ultimate concrete compression strain, ε_{cu}, was achieved. Considering the influence of confinement of the transverse reinforcement, the ultimate compression strain was approximated as follows:

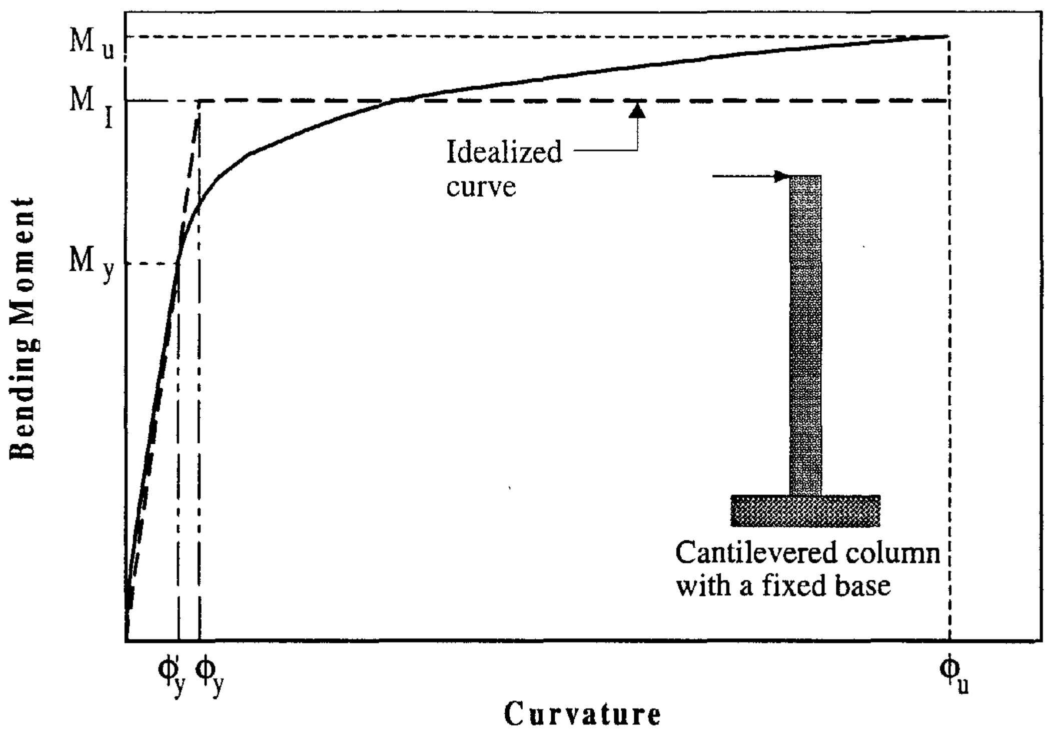

Figure 2.1 Moment-curvature response of a cantilevered column and theoretical idealization.

$$\varepsilon_{cu} = 0.004 + \frac{1.4\rho_s f_{yh} \varepsilon_{su}}{f'_{cc}} \tag{2.3}$$

where $\rho_s = 4A_h/D's$ is the volumetric ratio of confining steel for a circular section, A_h is the cross sectional area of hoop or spiral, D' is the diameter of core concrete measured to centerline of hoops, s is the spacing of the transverse reinforcement, f_{yh} is the yield strength of the transverse reinforcement, ε_{su} is the steel strain at the maximum tensile stress and f'_{cc} is the compressive strength of confined concrete, which was obtained from Eq. 2.4.

$$f'_{cc} = f'_c\left(2.254\sqrt{1+\frac{7.94f'_l}{f'_c}} - \frac{2f'_l}{f'_c} - 1.254\right) \tag{2.4}$$

In the above expression, f'_l and f'_c represent the effective lateral confining pressure and the unconfined concrete compressive strength respectively. For a circular section, f'_l was taken as:

$$f'_l = K_e f_l = 0.95 * \frac{2 f_{yh} A_h}{D' s} \tag{2.5}$$

where f_l is the maximum effective lateral confining pressure and K_e is the confinement effectiveness coefficient which is typically taken as 0.95 for circular sections [19].

2.2 Elastic Deformation

Based on the moment-curvature analysis obtained from the King's program, the yield displacement, Δy, of a cantilevered column was defined from yield curvature using simple bending theory as given below:

$$\Delta_y = \frac{1}{3} \phi_y l_{eff}^2 \tag{2.6}$$

where l_{eff} is the effective length of the concrete member and is defined as:

$$\left.\begin{aligned} l_{eff} &= l_c + 0.022 f_y d_{bl} \quad \text{(SI units)} \\ &= l_c + 0.15 f_y d_{bl} \quad \text{(psi units)} \end{aligned}\right\} \tag{2.7}$$

The length of the member from critical section to point of contraflexure is represented in the above equation by l_c and the second term accounts for strain penetration into the supporting element as described in the following section. It is believed that the member length is effectively increased due to strain penetration of longitudinal column reinforcement [18].

The yield displacement defined in Eq. 2.6 is the only elastic component for a column with an idealized elastic perfectly plastic moment-curvature response as shown in Figure 2.1. In reality, elastic displacement will continue to occur beyond yielding due to strain hardening of the reinforcement. If the elastic displacement at first yield is defined as:

$$\Delta'_y = \frac{1}{3}\phi'_y l_{eff}^2 \tag{2.8}$$

then the additional elastic displacement component beyond first yield can be obtained as follows:

$$\Delta'_e = \left(\frac{M}{M_y} - 1\right)\Delta'_y \quad \text{for } M > M_y \tag{2.9}$$

When the additional elastic component given in Eq. 2.9 is considered, the force-displacement characteristic of the column can be obtained with a better accuracy.

2.3 Plastic Hinge Length and Plastic Deformation

The plastic deformation, Δ_p, which occurs beyond first yield was obtained using the plastic curvature, ϕ_p, and a theoretical plastic hinge length, l_p, as described below:

$$\phi_p = \phi_m - \frac{M}{M_y}\phi'_y \tag{2.10}$$

$$\left.\begin{aligned} l_p &= 0.08l_c + 0.022f_y d_{bl} \geq 0.044f_y d_{bl} \quad \text{(SI units)} \\ &= 0.08l_c + 0.15f_y d_{bl} \geq 0.3f_y d_{bl} \quad \text{(psi units)} \end{aligned}\right\} \tag{2.11}$$

where ϕ_m is the curvature, f_y is the yield stress and d_{bl} is the diameter of longitudinal reinforcement, and l_c is the distance from the critical section to the point of contraflexure. A minimum plastic hinge length of $0.044f_y d_{bl}$ was emphasized in Eq. 2.11, as recommended by Priestley *et al.* [19], to allow strain penetration into the column as well as into the supporting member such as a joint or footing. The plastic displacement, Δ_p, was then calculated as follows:

$$\Delta_p = l_p \phi_p l_c \tag{2.12}$$

In the above expression the term l_c was used instead of $(l_c - 0.5l_p)$ as generally considered [15] for calculating displacement due to plastic rotation at the critical section. This modification was introduced to remain consistent with Eq. 2.11 which assumes some strain penetration of the longitudinal reinforcement into the supporting member, allowing plastic rotation to be centered close to the critical section.

2.4 Shear Deformation

Shear deformation of a concrete member subjected to severe cracking was approximated by reducing the shear stiffness in proportion to the flexural stiffness [18]:

$$\Delta_s = \frac{V l_c}{0.9 A_g G}\left[\frac{E_c I_{gross}}{E_c I_{eff}}\right] \tag{2.13}$$

where Δ_s is the shear deformation, **V** is the shear force, $\mathbf{0.9A_g}$ is the effective shear area for circular columns, **G** is the shear modulus which was taken as $\mathbf{0.4E_c}$, $\mathbf{E_c}$ is the elastic modulus of concrete, and $\mathbf{I_{gross}}$ and $\mathbf{I_{eff}}$ are respectively gross and effective second moment of area of the member. More accurate procedures are available where shear deformation is a significant component of the total displacement. For this study, where shear deformations were comparatively small, the approximate form of Eq. 2.13 was deemed to be adequately accurate.

2.5 Member Ductility

From the expressions given in Eqs. 2.6, 2.9, 2.12 and 2.13, the total column displacement, Δ_t, beyond yielding of the reinforcement was readily obtained from Eq. 2.14.

$$\Delta_t = \Delta_y + \Delta_e' + \Delta_p + \Delta_s \tag{2.14}$$

The displacement ductility of the member, μ_m, was then defined as

$$\mu_m = \frac{\Delta_t}{\Delta_y + \Delta_{sy}} = \frac{\Delta_t}{\Delta_c} \tag{2.15}$$

where Δ_{sy} and Δ_c are respectively the shear deformation and total fixed base column displacement corresponding to the theoretical ideal load. When flexibility of a connecting member such as a joint or beam is included in the above expression, it defines the system ductility and is discussed in the following sections.

2.6 Joint Deformation

The total deformation of a joint can be represented by five independent modes, namely pure shear, extension in x and y directions, and flexural deformation in x and y directions [21]. The deformation due to shear is expected to be the largest contributing mode for the experiments presented in this report. In Figure 2.2, the five independent joint modes are shown and the formula for calculating each deformation mode from the nodal displacements are given in Eq. 2.16.

$$\begin{Bmatrix} \gamma \\ \Delta\theta_x \\ \Delta\theta_y \\ \Delta_x \\ \Delta_y \end{Bmatrix} = \begin{bmatrix} \frac{1}{2h} & \frac{1}{2d} & \frac{1}{2h} & -\frac{1}{2d} & -\frac{1}{2h} & -\frac{1}{2d} & -\frac{1}{2h} & \frac{1}{2d} \\ -\frac{1}{h} & 0 & \frac{1}{h} & 0 & -\frac{1}{h} & 0 & \frac{1}{h} & 0 \\ 0 & \frac{1}{d} & 0 & -\frac{1}{d} & 0 & \frac{1}{d} & 0 & -\frac{1}{d} \\ -\frac{1}{2} & 0 & \frac{1}{2} & 0 & -\frac{1}{2} & 0 & \frac{1}{2} & 0 \\ 0 & \frac{1}{2} & 0 & -\frac{1}{2} & 0 & \frac{1}{2} & 0 & -\frac{1}{2} \end{bmatrix} \begin{Bmatrix} u_1 \\ u_2 \\ u_3 \\ u_4 \\ u_5 \\ u_6 \\ u_7 \\ u_8 \end{Bmatrix} \tag{2.16}$$

In order to obtain the nodal displacements of the joint, a joint panel instrumentation consisting of five linear potentiometers as shown in Figure 3.25 was typically employed. The nodal displacements of the joint was obtained from the panel deformation as follows:

For the joint panel configuration shown in Figure 2.3, let the initial lengths of the potentiometers be $\mathbf{B_0}$ (bottom), $\mathbf{T_0}$ (top), $\mathbf{N_0}$ (north), $\mathbf{S_0}$ (south) and $\mathbf{D_0}$ (diagonal). The instrumentation lengths in the deformed mode were then defined as in Eq. 2.17 – 2.21 using the measured changes in lengths.

$$\mathbf{B = B_0 + \Delta B = d + \Delta B} \tag{2.17}$$

$$\mathbf{T = T_0 + \Delta T = d + \Delta T} \tag{2.18}$$

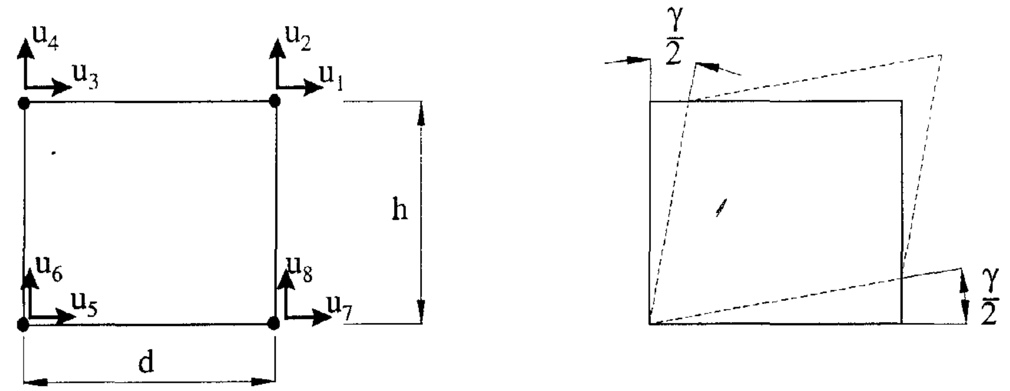
u_4
u_3
u_2
u_1
h
u_6
u_5
u_8
u_7
d
$\frac{\gamma}{2}$
$\frac{\gamma}{2}$

(a) Joint panel nodal displacements

(b) Mode 1 - pure shear

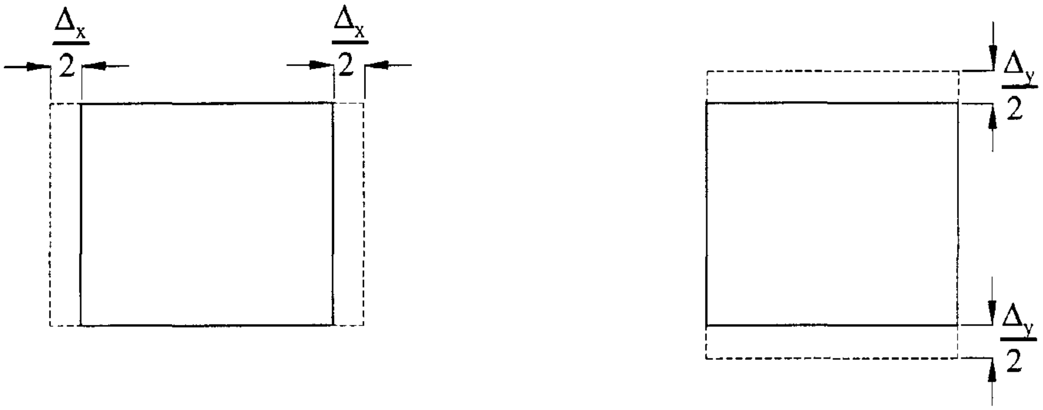
$\frac{\Delta_x}{2}$
$\frac{\Delta_x}{2}$
$\frac{\Delta_y}{2}$
$\frac{\Delta_y}{2}$

(c) Mode 2 - extension in x direction

(d) Mode 3 - extension in y direction

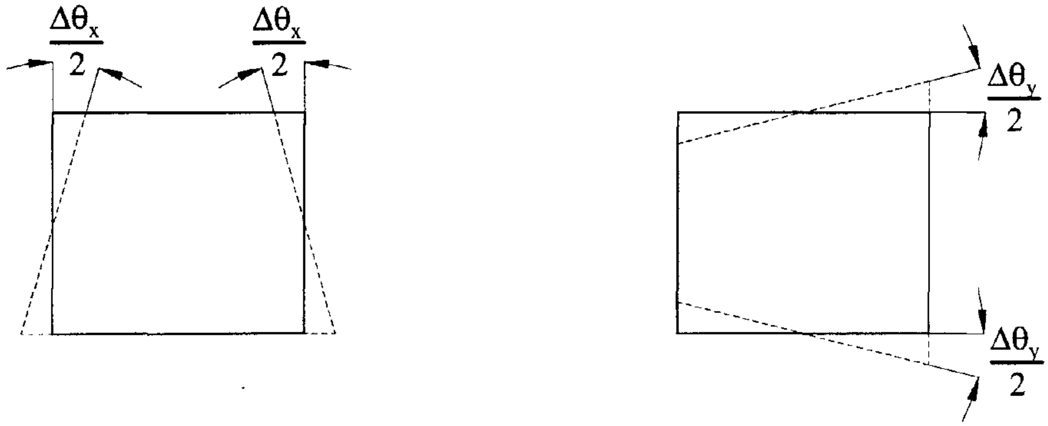
$\frac{\Delta\theta_x}{2}$
$\frac{\Delta\theta_x}{2}$
$\frac{\Delta\theta_y}{2}$
$\frac{\Delta\theta_y}{2}$

(e) Mode 4 - curvature about x axis

(f) Mode 5 - curvature about y axis

Figure 2.2 Decomposition of joint panel deformation into five independent modes.

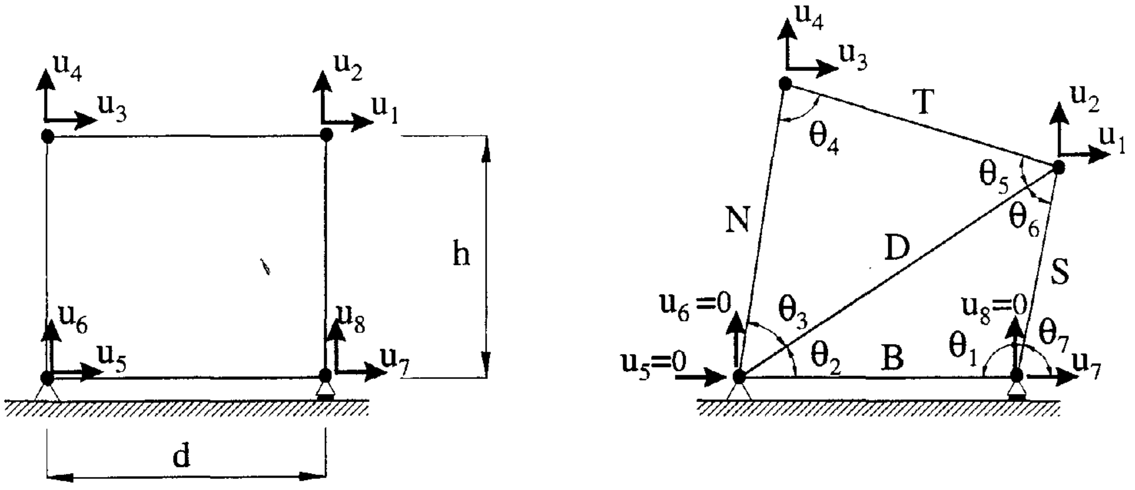
u4
u3
u2
u1
h
u6
u5
u8
u7
d
u4
u3
T
u2
u1
θ4
θ5
N
θ6
D
S
u6 =0
θ3
u8=0
θ7
u5=0
θ2
B
θ1
u7

(a) Original geometry

(b) Deformed geometry

Figure 2.3 Joint panel deformation.

$$\mathbf{N = N_0 + \Delta N = h + \Delta N} \tag{2.19}$$

$$\mathbf{S = S_0 + \Delta S = h + \Delta S} \tag{2.20}$$

$$\mathbf{D = D_0 + \Delta D = \sqrt{d^2 + h^2} + \Delta D} \tag{2.21}$$

By establishing the geometry of the joint from Eqs. 2.22 – 2.25 and assuming $\mathbf{u_8 = 0}$, the remaining nodal displacements were calculated using Eqs. 2.26 – 2.32 with respect to the reference node 3.

$$\boldsymbol{\theta_1 = \cos^{-1}\left(\frac{B^2 + S^2 - D^2}{2BS}\right)} \tag{2.22}$$

$$\boldsymbol{\theta_2 = \cos^{-1}\left(\frac{B^2 + D^2 - S^2}{2BD}\right)} \tag{2.23}$$

$$\boldsymbol{\theta_3 = \cos^{-1}\left(\frac{N^2 + D^2 - T^2}{2ND}\right)} \tag{2.24}$$

$$\theta_7 = \pi - \theta_1 \tag{2.25}$$

$$u_1 = S\cos\theta_7 \tag{2.26}$$

$$u_2 = S\sin\theta_7 - h \tag{2.27}$$

$$u_3 = N\cos(\theta_2 + \theta_3) \tag{2.28}$$

$$u_4 = N\sin(\theta_2 + \theta_3) \tag{2.29}$$

$$u_5 = 0 \tag{2.30}$$

$$u_6 = 0 \tag{2.31}$$

$$u_7 = B - d = \Delta B \tag{2.32}$$

The assumption $\mathbf{u_8 = 0}$ does not introduce any error in the joint deformation components when calculated from Eq. 2.16, but it implies that the rigid body rotation of the joint is zero. During the test, the rigid body rotation was separately monitored by placing two linear potentiometers beneath the joint as discussed in Section 3.2.5.

2.7 Beam Flexibility

In the above example, if the column is connected to a beam instead of a foundation, the flexibility of the beam, depending on how it is supported, will introduce additional rotation to the joint as shown in Figure 2.4. This will also increase the displacement at the top of the column.

2.8 System Ductility

For the tee joint tests reported in the following chapters, the column was connected to a flexible cap beam. The displacement at the top of the column was, therefore, influenced by the joint deformation and bending of the beam as shown in Figure 2.4. At yield, the displacement at the top of the column was:

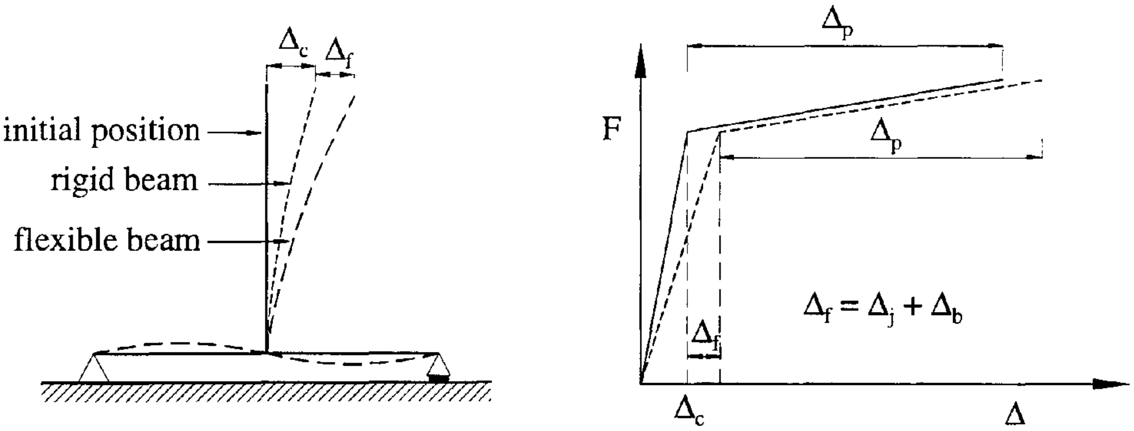
Δ_c
Δ_f
initial position
rigid beam
flexible beam
Δ_p
F
Δ_p
$\Delta_f = \Delta_j + \Delta_b$
Δ_f
Δ_c
Δ

(a) Displacement at yield

(b) Force-displacement response

Figure 2.4 Influence of cap beam flexibility on displacement ductility capacity.

$$\Delta_y = \Delta_c + \Delta_j + \Delta_b \tag{2.33}$$

where Δ_j is the displacement component due to joint deformation and Δ_b is the contribution from the flexibility of the cap beam. Hence, the total displacement at the top of the column was:

$$\Delta_t = \Delta_c + \Delta_j + \Delta_b + \Delta_p \tag{2.34}$$

The displacement capacity of the system was then defined as:

$$\mu_s = \frac{\Delta_t}{\Delta_y} = 1 + \frac{\Delta_p}{\Delta_c + \Delta_j + \Delta_b} = 1 + \frac{(\mu_m - 1)}{(1 + f)} \tag{2.35}$$

where μ_s is the system ductility and **f** is the flexibility coefficient. The displacement ductilities referred in this report are system ductilities unless otherwise mentioned. Because the flexibility of the system affects the yield displacement more than the total displacement, the ductility capacity of the system is always smaller than the member ductility capacity of the column.

2.9 Predicted Response of Test Units

The theoretical force-displacement response envelope of each test unit was obtained prior to the test using measured steel properties and estimated compressive strength of concrete. A simple model was considered by representing each structural member with a beam-column element. Elastic stiffness corresponding to the cracked section was used for members when the applied bending moment was greater than the theoretical flexural cracking moment of the section. Length of each flexural member was taken to the center of joint, ignoring any special modeling of the beam/column connection. Member end regions are sometimes represented by rigid elements to model the inflexible behavior of the joint [2]. However, due to strain penetration of the longitudinal steel, the actual joint behavior is likely to be between the model which considers rigid member ends and that completely ignores modeling of the joint as considered in this report. This aspect is further investigated in Section 4.6.4 where the response of the first unit is examined using experimental data.

The total horizontal displacement at the top of the column was estimated from four components. Two of these were the flexural elastic and plastic deformations of the column with a fixed base as discussed in Sections 2.2 and 2.3. The third component was the shear deformation associated with the column and the fourth component was due to joint rotation introduced by bending of the beam. Since the joint was not explicitly modeled, the joint deformation components were ignored. This is likely to introduce large error in the theoretical prediction when significant damage occurs to the cap beam/column connection. The axial deformation of the beam was expected to be small, and hence this component was also ignored.

CHAPTER 3

INTRODUCTION TO EXPERIMENTAL STUDY

Following the recommendations made in a study by the Seismic Safety Review Panel [16] on the expected performance of the Santa Monica Viaduct in Los Angeles, an interior cap beam/column joint, representative of as-built reinforcement detail, was tested at UCSD. A summary of this test, and modeling and testing procedure adopted for redesigned units incorporating joint reinforcement based on force transfer models are presented in this chapter.

3.1 As-Built Test Unit

The as-built test unit, SM3, was a ¾ scale model of the interior cap beam/column joint from Bent #793+57 of the Santa Monica Viaduct. This is a three column bent located south east of Griffith Avenue (Figure 3.1). Construction procedure of the as-built unit and its response under reverse cyclic loading are given in detail by MacRae *et al.* [12]. A brief summary of this report, giving relevant information to the current investigation, is presented below.

3.1.1 Prototype Structure

The reinforcement used in the prototype structure was Grade 40 steel. The column which is 1219 mm (48 in.) in diameter, contains 16#18 (d_b = 57 mm) bars, yielding 3.5 percent longitudinal steel (Figure 3.2). The volumetric ratio of spiral in the column is 0.5 percent. No joint shear reinforcement was provided in the cap beam/column connection (see Figure.3.2). The column reinforcement, which had embedment length of 16 bar diameters, was anchored into the joint with straight bar ends and terminated at 3/4 of the beam depth from the interface. The cap beam longitudinal reinforcement details are shown in Figure 3.3 while beam shear reinforcement, and the slab and web details are presented in Figure 3.4. As illustrated by Priestley *et al.* [19], several design deficiencies including no joint reinforcement and premature termination of column bar into the joint which are common in existing old bridge structures, are seen in the details of the prototype bent.

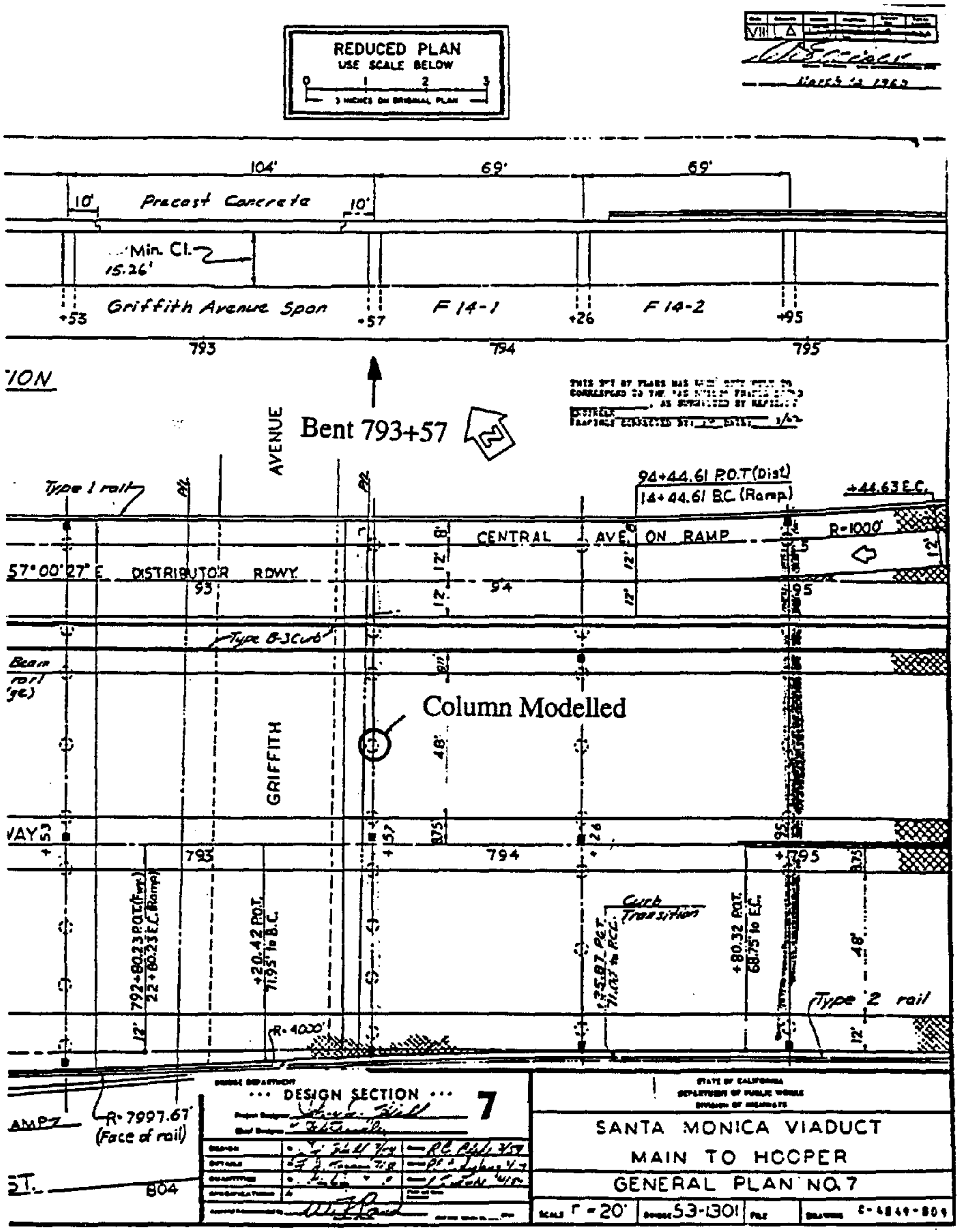

REDUCED PLAN
USE SCALE BELOW
104'
69'
69'
10'
Precast Concrete
10'
Min. Cl. 15.26'
Griffith Avenue Span
F 14-1
F 14-2
+53
+57
+26
+95
793
794
795
Bent 793+57
AVENUE
94+44.61 P.O.T.(Dist)
14+44.61 B.C.(Ramp)
+44.63 E.C.
Type 1 rail
CENTRAL AVE. ON RAMP
R=1000'
57°00'27" E
DISTRIBUTOR RDWY.
Type B-3 Curb
Column Modelled
GRIFFITH
Curb Transition
Type 2 rail
R=4000'
R=7997.67' (Face of rail)
DESIGN SECTION
7
SANTA MONICA VIADUCT
MAIN TO HOOPER
GENERAL PLAN NO. 7
1" = 20'
53-1301

Figure 3.1 Plan and elevation of prototype structure.

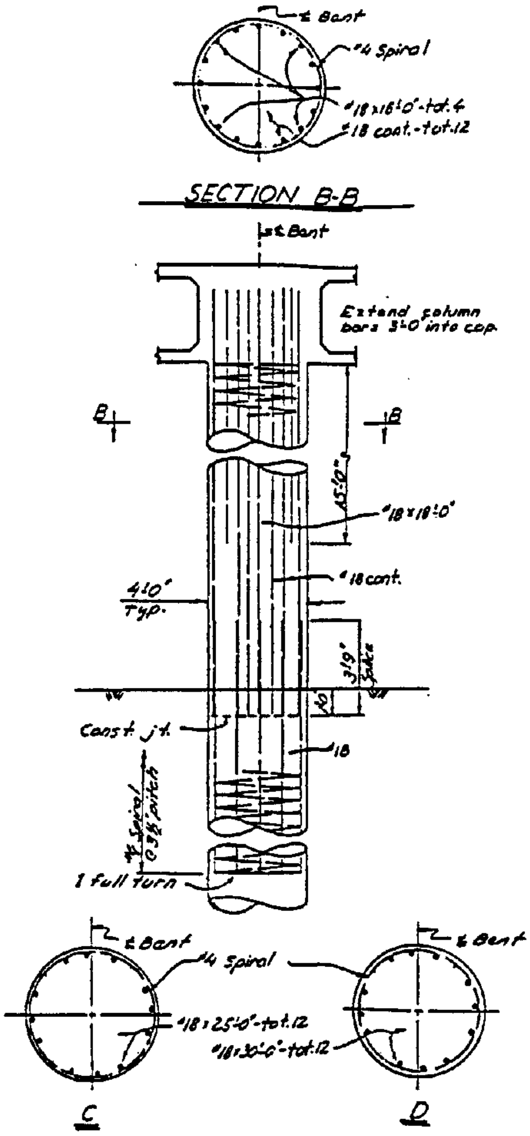
℄ Bent
#4 Spiral
#18 x 18'-0"-tot.4
#18 cont.-tot.12
SECTION B-B
℄ Bent
Extend column bars 3'-0" into cap.
B
B
15'-0"
#18 x 18'-0"
#18 cont.
4'-0" Typ.
3'-9" Jacket
10"
Const. jt.
#18
#4 Spiral @ 3½" pitch
1 full turn
℄ Bent
#4 Spiral
℄ Bent
#18 x 25'-0"-tot.12
#18 x 30'-0"-tot.12
C
D

Note: Splices in spiral reinforcement shall be made by welding or by a lap of 80 dia. for deformed bars, or 120 dia. for plain bars.

Figure 3.2 Prototype column details.

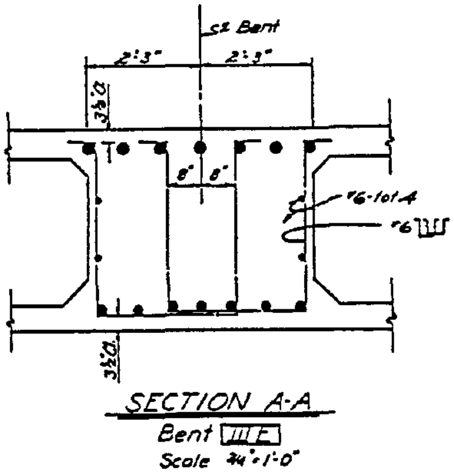
℄ Bent
2'-3"
2'-3"
3½ Cl.
8"
8"
#6-1of4
#6
3½ Cl.
SECTION A-A
Bent IIIF
Scale ¾"=1'-0"

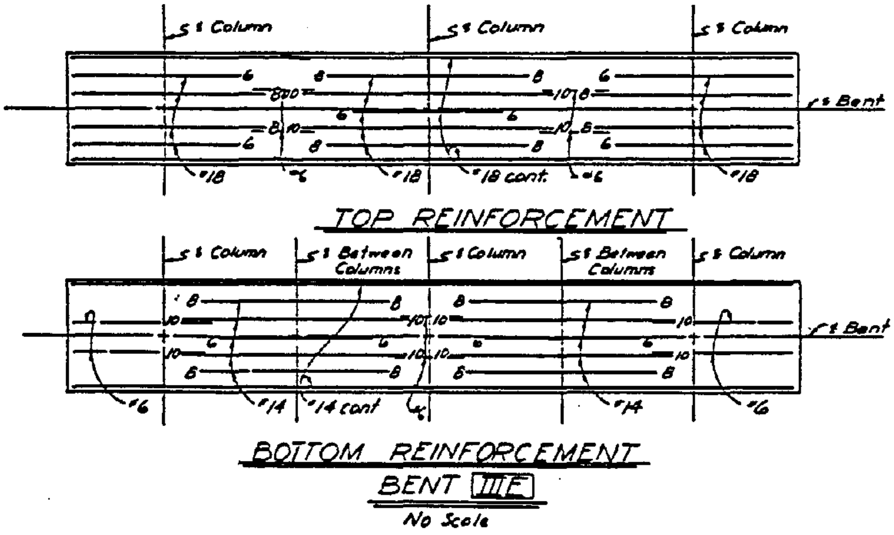
℄ Column
℄ Column
℄ Column
℄ Bent
#18
#6
#18
#18 cont.
#6
#18
TOP REINFORCEMENT
℄ Column
℄ Between Columns
℄ Column
℄ Between Columns
℄ Column
℄ Bent
#6
#14
#14 cont
#6
#14
#6
BOTTOM REINFORCEMENT
BENT IIIF
No Scale

Figure 3.3 Prototype cap beam main longitudinal steel.

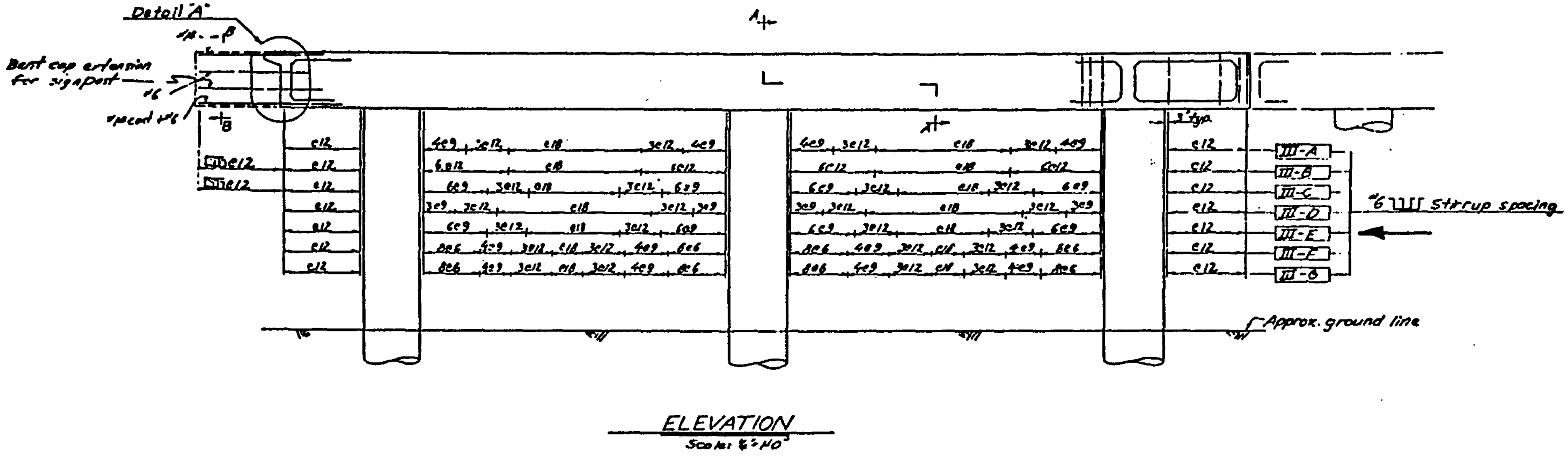
Detail "A"
Bent cap extension for signpost
Approx. ground line
#6 Stirrup spacing
III-A
III-B
III-C
III-D
III-E
III-F
III-G
ELEVATION
Scale: 1/8" = 1'-0"

(a) Shear stirrup spacing (Bent IIIE)

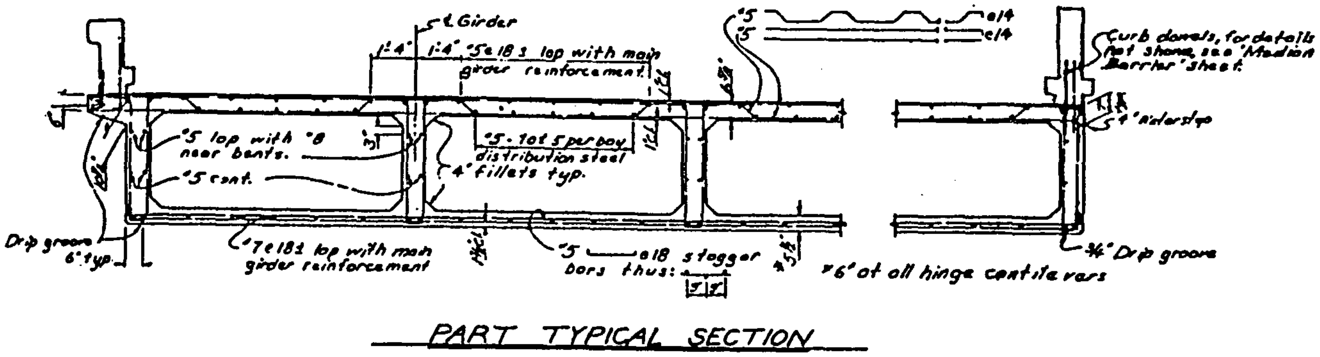
℄ Girder
1'-4" #5 e18 1/2 lap with main girder reinforcement
#5 lap with #8 near bents.
#5 cont.
#5 - 10 1/2 5 per bay distribution steel
4" fillets typ.
#7 e18 1/2 lap with main girder reinforcement
#5 e18 stagger bars thus:
#6 at all hinge cantilevers
Drip groove 6" typ.
3/4" Drip groove
Curb dowels, for details not shown, see "Median Barrier" sheet.
PART TYPICAL SECTION

(b) Slab and web steel details.

Figure 3.4 Prototype superstructure reinforcement details.

3.1.2 Model Specimen SM3

The as-built test unit SM3 was constructed in an inverted position and was tested under reverse cyclic loading. Reinforcement details of SM3, which had a combination of Grade 40 and Grade 60 steel, are shown in Figure 3.5-3.7. In order to match the column capacity of the prototype structure, the column of SM3 was provided with 16#14 (d_b = 57.2 mm) Grade 40 longitudinal reinforcement. They were anchored directly into the joint with a similar embedment length (i.e. 16 bar diameters). Transverse reinforcement content of 0.5 percent was duplicated in the column by providing #3 (d_b = 9.5 mm) spiral at 67 mm (2.625") spacing. Clear height of the column from the center of loading to the joint interface in SM3 was 2743 mm (108 in.), which corresponded to the distance between the joint interface and point of contraflexure in the prototype structure.

A sway mechanism with plastic hinges restricted to the top and bottom of columns is favored for the design of multi-column bents of bridge structures subjected to dynamic loading. Based on inadequate detailing provided for the cap beam, it was anticipated in the preliminary calculation [16] that plastic hinging would first develop in the bent cap as opposed to in the columns. The contribution of slab steel was ignored in this calculation as recommended in the ACI code [3]. However, in order to obtain realistic estimates of the yield capacity and ideal strength of the cap beam, the influence of longitudinal deck and soffit steel needs to be taken into account. MacRae *et al.* [12] reevaluated the capacity of the bent cap assuming the slab steel located within a distance of one half the beam depth plus six times the thickness of slab from the center of column effectively contributes to the moment resistance of the beam. This approach, which is consistent with the Caltrans practice [4], showed that yielding of the longitudinal beam reinforcement should not occur and that a column hinging mechanism would develop. Consequently, slab outstand from the cap beam of 762 mm (30 in) was included in the model (see Figure 3.6) to appropriately simulate the behavior as expected in the prototype structure. The beam length of 5283 mm (208 in) was chosen in order to accommodate reaction blocks and tie downs at the appropriate locations.

As seen in the prototype detail, no joint reinforcement was provided for SM3 and consequently a joint shear failure was expected. However, it was unclear if the strength degradation of the system associated with the joint failure would be gradual or rapid. It was also a concern if joint shear failure would trigger a punching shear failure of the column through the deck under gravity loads.

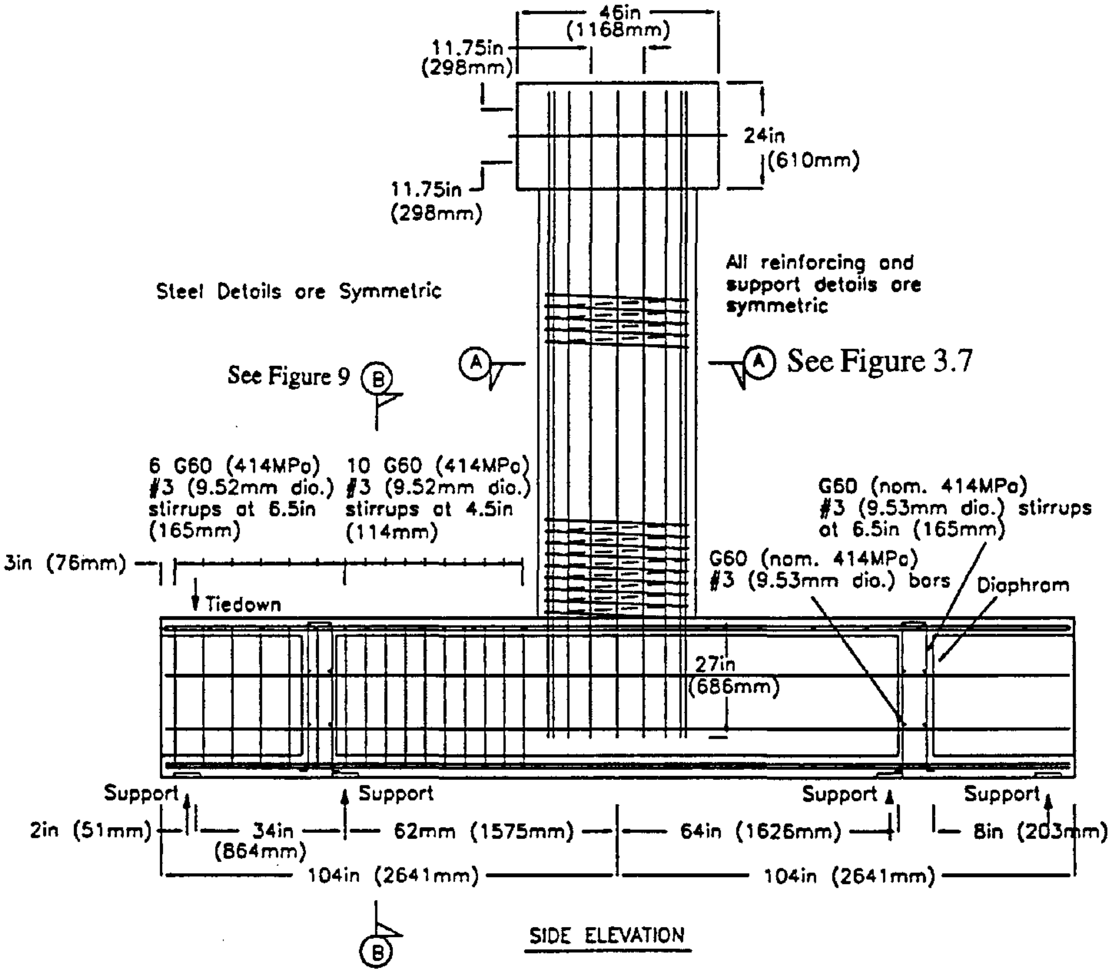
46in
(1168mm)
11.75in
(298mm)
11.75in
(298mm)
24in
(610mm)
Steel Details are Symmetric
All reinforcing and support details are symmetric
See Figure 9
B
A
A
See Figure 3.7
6 G60 (414MPa) #3 (9.52mm dia.) stirrups at 6.5in (165mm)
10 G60 (414MPa) #3 (9.52mm dia.) stirrups at 4.5in (114mm)
G60 (nom. 414MPa) #3 (9.53mm dia.) stirrups at 6.5in (165mm)
G60 (nom. 414MPa) #3 (9.53mm dia.) bars
Diaphram
3in (76mm)
Tiedown
27in
(686mm)
Support
Support
Support
Support
2in (51mm)
34in
(864mm)
62mm (1575mm)
64in (1626mm)
8in (203mm)
104in (2641mm)
104in (2641mm)
B
SIDE ELEVATION

Figure 3.5 Side elevation and reinforcement details of as-built unit SM3.

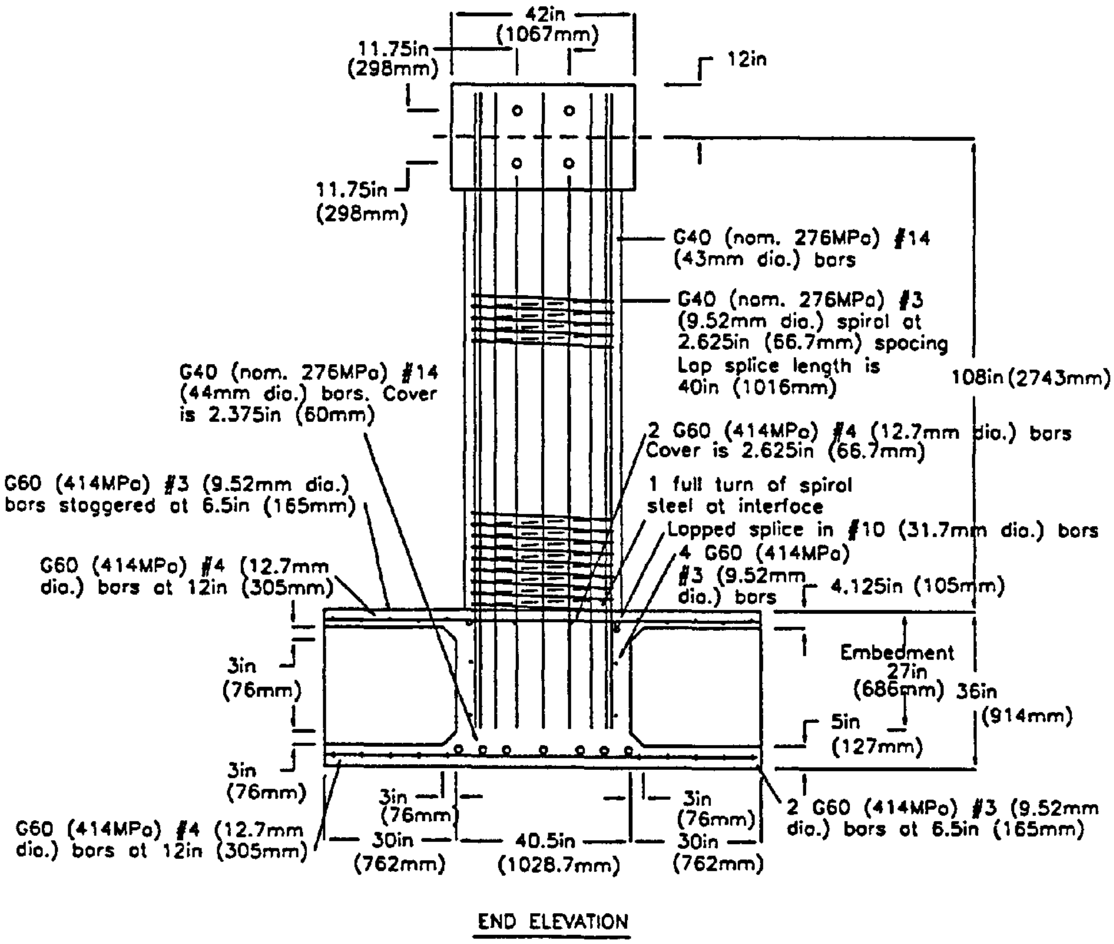
42in
(1067mm)
11.75in
(298mm)
12in
11.75in
(298mm)
G40 (nom. 276MPa) #14
(43mm dia.) bars
G40 (nom. 276MPa) #3
(9.52mm dia.) spiral at
2.625in (66.7mm) spacing
Lap splice length is
40in (1016mm)
108in (2743mm)
G40 (nom. 276MPa) #14
(44mm dia.) bars. Cover
is 2.375in (60mm)
2 G60 (414MPa) #4 (12.7mm dia.) bars
Cover is 2.625in (66.7mm)
G60 (414MPa) #3 (9.52mm dia.)
bars staggered at 6.5in (165mm)
1 full turn of spiral
steel at interface
Lapped splice in #10 (31.7mm dia.) bars
4 G60 (414MPa)
#3 (9.52mm
dia.) bars
4.125in (105mm)
G60 (414MPa) #4 (12.7mm
dia.) bars at 12in (305mm)
Embedment
27in
(686mm)
36in
(914mm)
3in
(76mm)
5in
(127mm)
3in
(76mm)
3in
(76mm)
3in
(76mm)
G60 (414MPa) #4 (12.7mm
dia.) bars at 12in (305mm)
2 G60 (414MPa) #3 (9.52mm
dia.) bars at 6.5in (165mm)
30in
(762mm)
40.5in
(1028.7mm)
30in
(762mm)
END ELEVATION

Figure 3.6 End elevation and reinforcement details of as-built unit SM3

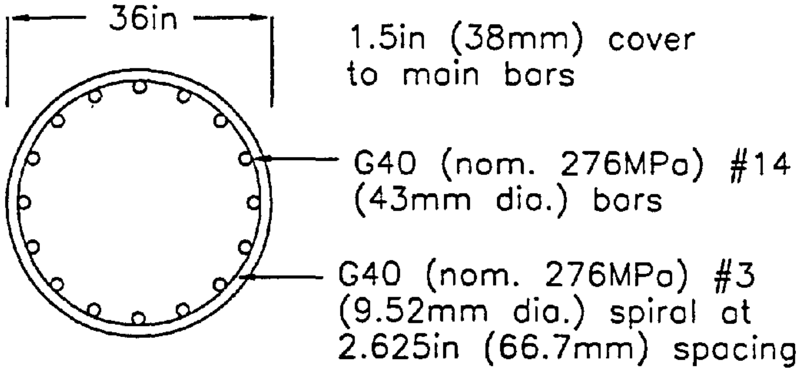
36in
1.5in (38mm) cover to main bars
G40 (nom. 276MPa) #14 (43mm dia.) bars
G40 (nom. 276MPa) #3 (9.52mm dia.) spiral at 2.625in (66.7mm) spacing

Section A–A From Figure 3.5

(a)

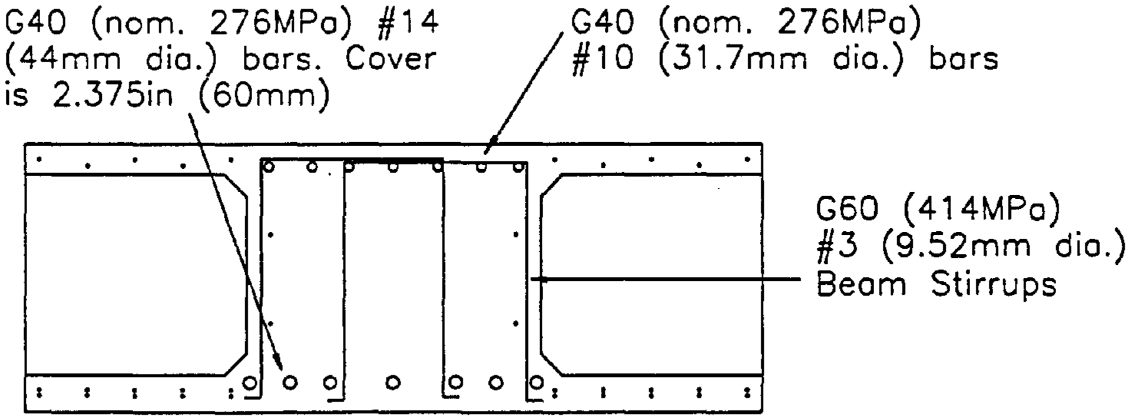
G40 (nom. 276MPa) #14 (44mm dia.) bars. Cover is 2.375in (60mm)
G40 (nom. 276MPa) #10 (31.7mm dia.) bars
G60 (414MPa) #3 (9.52mm dia.) Beam Stirrups

Beam Section B–B From Figure 3.5

(b)

Figure 3.7 Column and cap beam cross sections of as-built unit SM3.

3.1.3. Test Set up used for SM3

The test set up of SM3, as schematically shown in Figure 3.8, was selected so that the forces at the beam ends adjacent to the joint and at the critical section of the column could be modeled as correctly as possible, and hence realistic forces could be simulated in the joint region. The specimen was provided with two vertical reaction blocks at 1574 mm (62 in.) either side of the column centerline. Two tie downs were also placed further away at 2488 mm (98 in) to obtain appropriate cap beam positive moments at the column face. Estimated axial load on the column of SM3 at the maximum displacement was 1068 kN (240 kips). Although this load was critical for the investigation of possible punching type failure of the column through the beam and deck, a lower axial load of 579 kN (130 kips) was preferred to obtain a better distribution of forces at the member ends adjacent to the joint. Application of a lower axial load should not have altered the joint behavior significantly compared to what is expected in the prototype structure. Additional load cycles with higher axial loads were applied at the large ductilities to examine punching shear failure. The variation of axial force during the test is described in detail in the following section.

3.1.4 Instrumentation and Loading Sequence

The test unit was extensively instrumented with strain gauges and external devices (Figure 3.9) and the reduced data is presented in reference [12].

Figure 3.10 shows the complete lateral load sequence applied to unit SM3 and variation of the axial load introduced during the test. In accordance with standard practice, the first portion of the test was performed under force control and the remainder was under displacement control. Axial load in the column was kept at 579 kN (130 kips) for the most part of the test. Beyond yielding of the column bars, additional cycles with increased axial loads were considered. An axial load equal to 150 percent of the estimated gravity load was applied at the end of the test after the joint had suffered severe damage (see Figure 3.15).

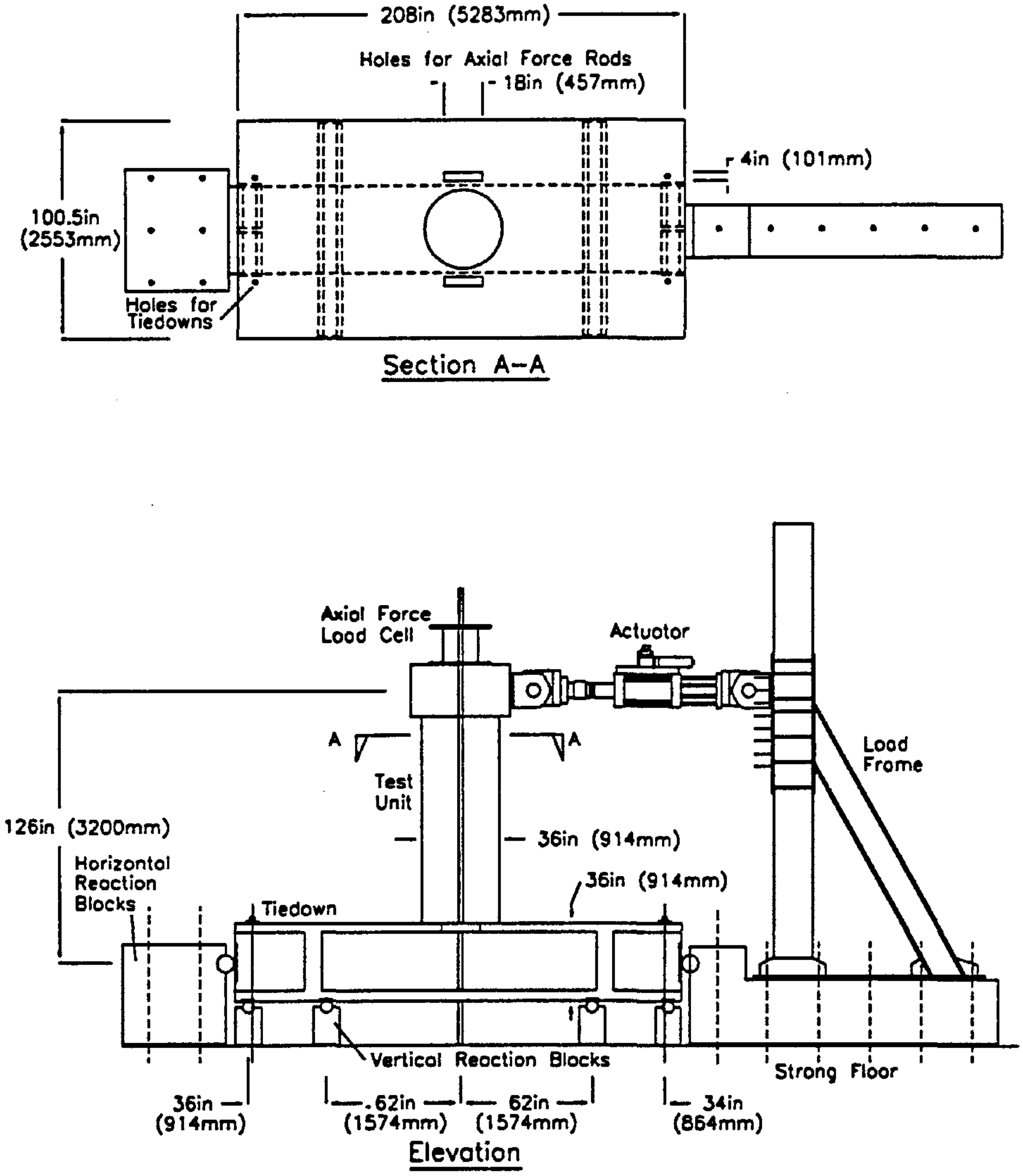
208in (5283mm)
Holes for Axial Force Rods
18in (457mm)
4in (101mm)
100.5in
(2553mm)
Holes for
Tiedowns
Section A-A
Axial Force
Load Cell
Actuator
A
A
Load
Frame
Test
Unit
126in (3200mm)
36in (914mm)
Horizontal
Reaction
Blocks
36in (914mm)
Tiedown
Vertical Reaction Blocks
Strong Floor
36in
(914mm)
62in
(1574mm)
62in
(1574mm)
34in
(864mm)
Elevation

Figure 3.8 Overall test set up of SM3 (also see Figure 3.9)

3.1.5 Performance of SM3

Joint shear cracking in the specimen was first observed at a horizontal load of 356 kN (80 kips), which is about 40 percent of the load corresponding to the ideal capacity of the column. Additional joint cracks were developed during the first cycle at 534 kN (120 kips). There was no significant changes observed in the next load step at 623 kN (140 kips), which induced the theoretical yield moment in the column. Further joint cracking and dilation in the joint region perpendicular to the loading direction was observed when the displacement was increased to that corresponding to system ductility of 1.0. Figure 3.11 shows the cracking on the east side of the joint after the first cycle at $\mu_\Delta = 1$. A significant number of joint shear cracks developed when the displacement was cycled at $\mu_\Delta = 1$ and at the end of third cycle the condition of the joint on the west side is shown in Figure 3.12. More joint cracking and the first encounter of concrete crushing in the joint region were observed at displacement ductility 1.5 (Figure 3.13). Crack pattern on the top of the soffit (as constructed) is shown in Figure 3.14 at $\mu_\Delta = 1.5$, which indicates that all of the slab steel effectively contributed to the moment resistance of the cap beam.

Large diagonal cracks developed in the joint at displacement ductility 2 and consequently a reduction in the load resisting ability of the system was first observed. From this point onwards, the damage was concentrated in the joint region and, as expected, the system deteriorated, but in a gradual fashion. At one point during the test, the actuator displaced the column at its full stroke. This took place because the displacement potentiometer, which was connected to the controller, was detached from the specimen and misguided the controller. The ductility corresponding to this displacement was estimated to be 14.9. However, it was noted [12] that there was no catastrophic failure occurred to the test unit (see Figure 3.15). At the end of the test, the concrete was removed in the joint region and it was found that the longitudinal column and beam bars were deformed as shown in Figure 3.16. The hysteretic force-displacement behavior of the system is depicted in Figure 3.17 and the gradual deterioration of the system can be clearly seen.

Despite increasing the axial load in the column during the test, no indication of a punching type failure was observed. Although the test was proved to be successful in terms of significantly reducing the cost required for retrofitting the Santa Monica Viaduct, it is clear from this test that damage to joints should be limited so that (a) the full capacity of the structure can be developed, (b) a dependable force-displacement

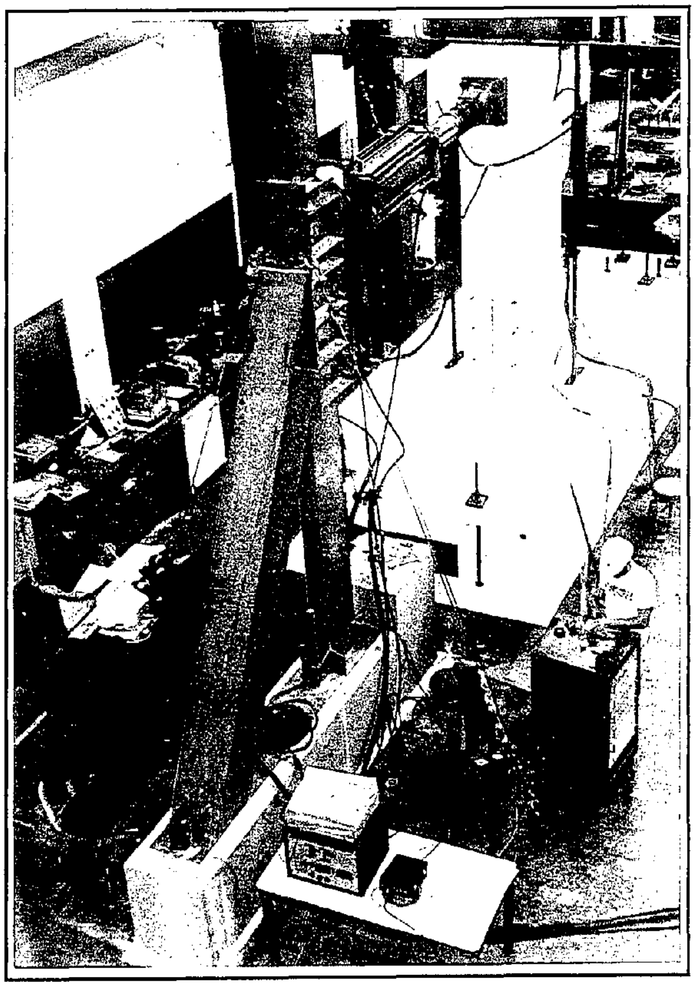

Figure 3.9 As-built unit SM3 prior to the test.

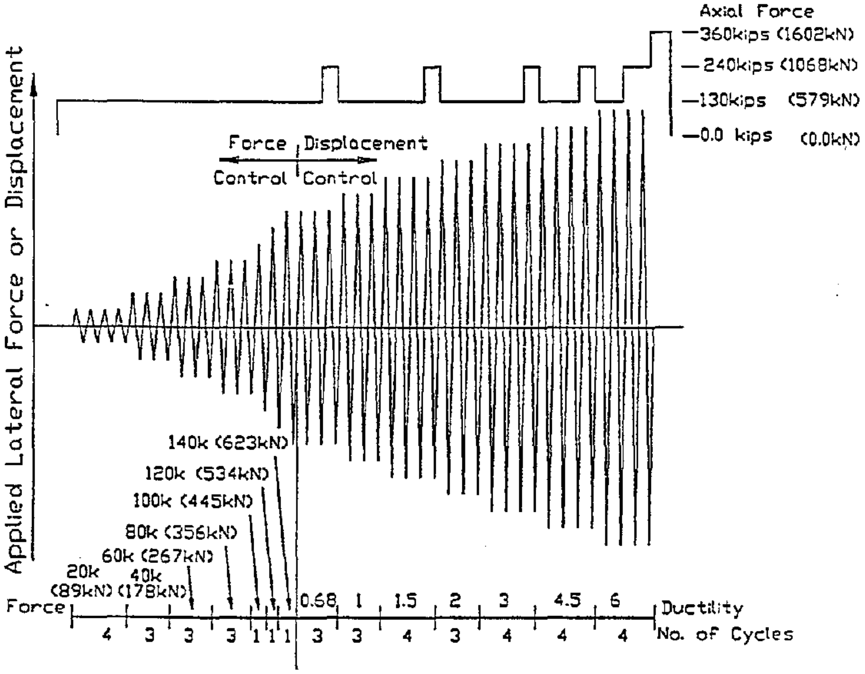

Figure 3.10 Applied lateral load sequence and axial load variation for SM3.

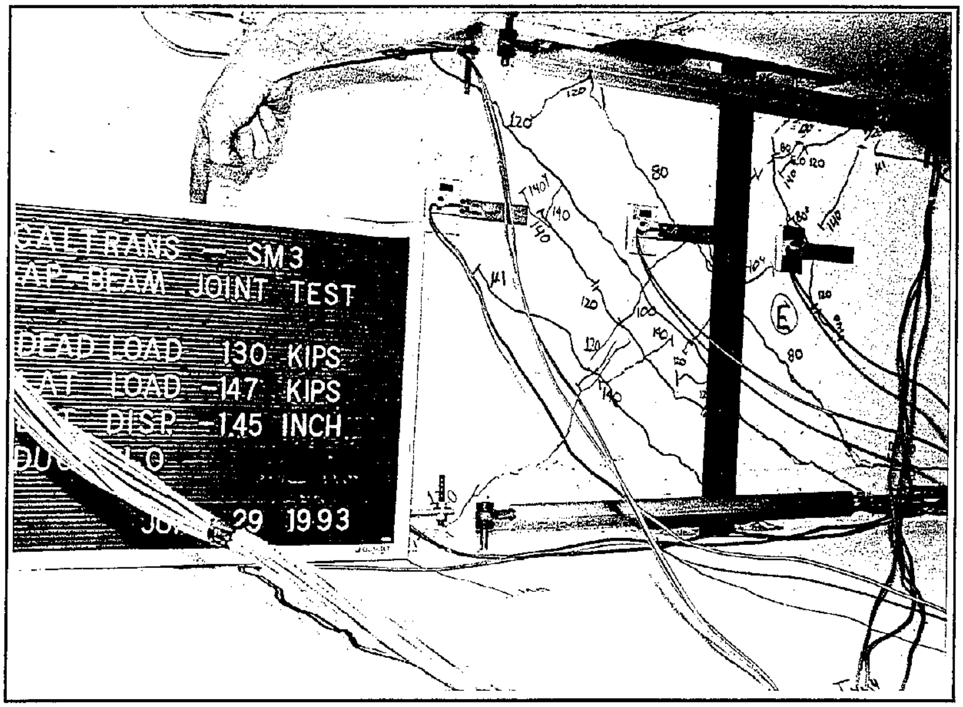
CALTRANS — SM3
AP-BEAM JOINT TEST
DEAD LOAD 130 KIPS
AT LOAD -147 KIPS
DISP -1.45 INCH
DU 1.0
29 1993
E

Figure 3.11 SM3 joint shear cracks on east side at $\mu_\Delta = -1$.

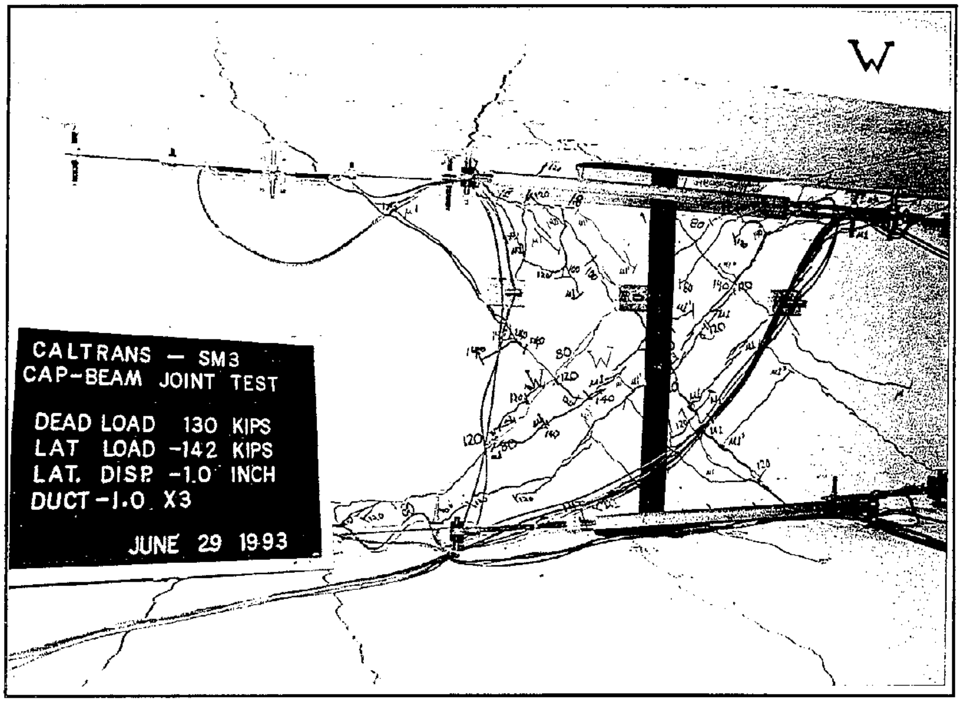
W
CALTRANS — SM3
CAP-BEAM JOINT TEST
DEAD LOAD 130 KIPS
LAT LOAD -142 KIPS
LAT. DISP. -1.0 INCH
DUCT -1.0 X3
JUNE 29 1993

Figure 3.12 SM3 joint shear cracks on west side at $\mu_\Delta = -1x3$.

Reproduced from best available copy.

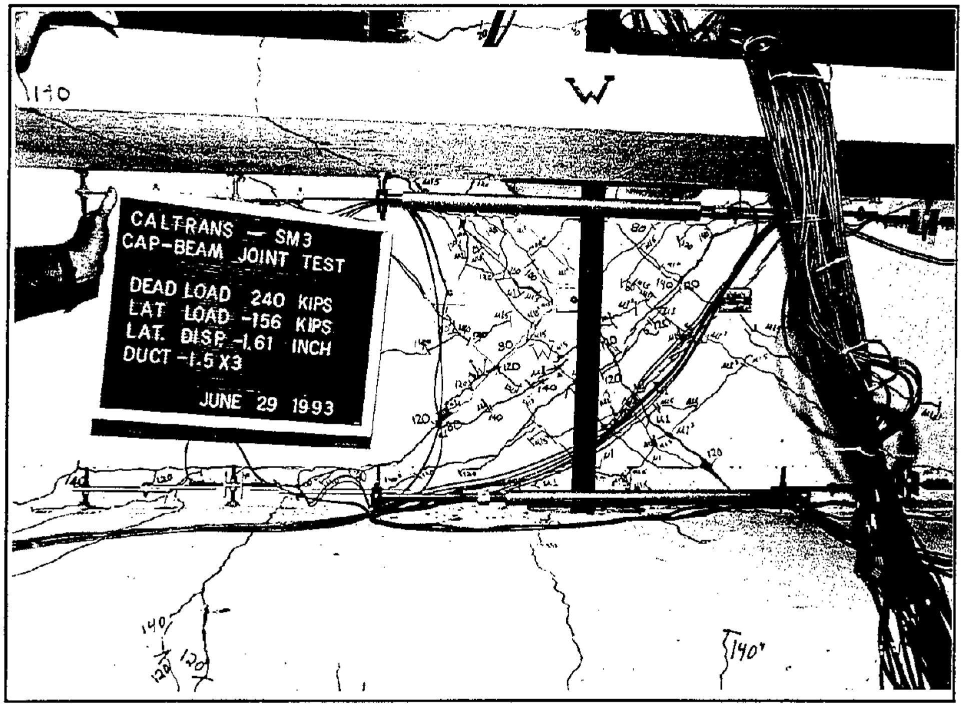
W
CALTRANS — SM3
CAP-BEAM JOINT TEST
DEAD LOAD 240 KIPS
LAT LOAD -156 KIPS
LAT. DISP -1.61 INCH
DUCT -1.5 X3
JUNE 29 1993
140
120

Figure 3.13 SM3 joint shear cracks on west side at $\mu_\Delta = -1.5x3$.

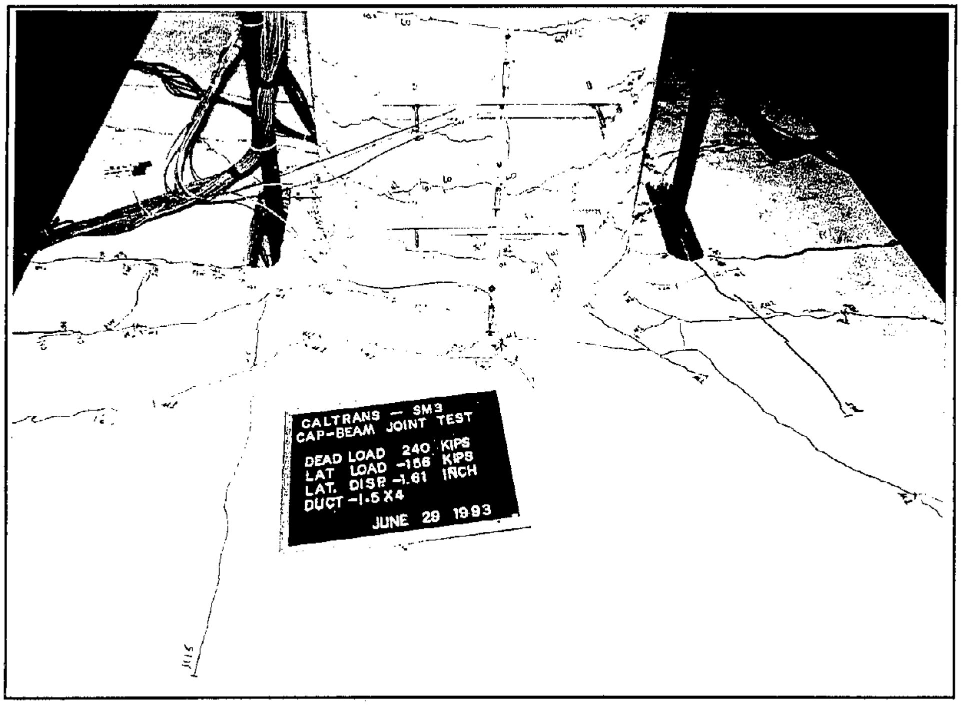
CALTRANS — SM3
CAP-BEAM JOINT TEST
DEAD LOAD 240 KIPS
LAT LOAD -156 KIPS
LAT. DISP -1.61 INCH
DUCT -1.5 X4
JUNE 29 1993

Figure 3.14 SM3 top slab cracks at $\mu_\Delta = -1x4$.

Reproduced from
best available copy.

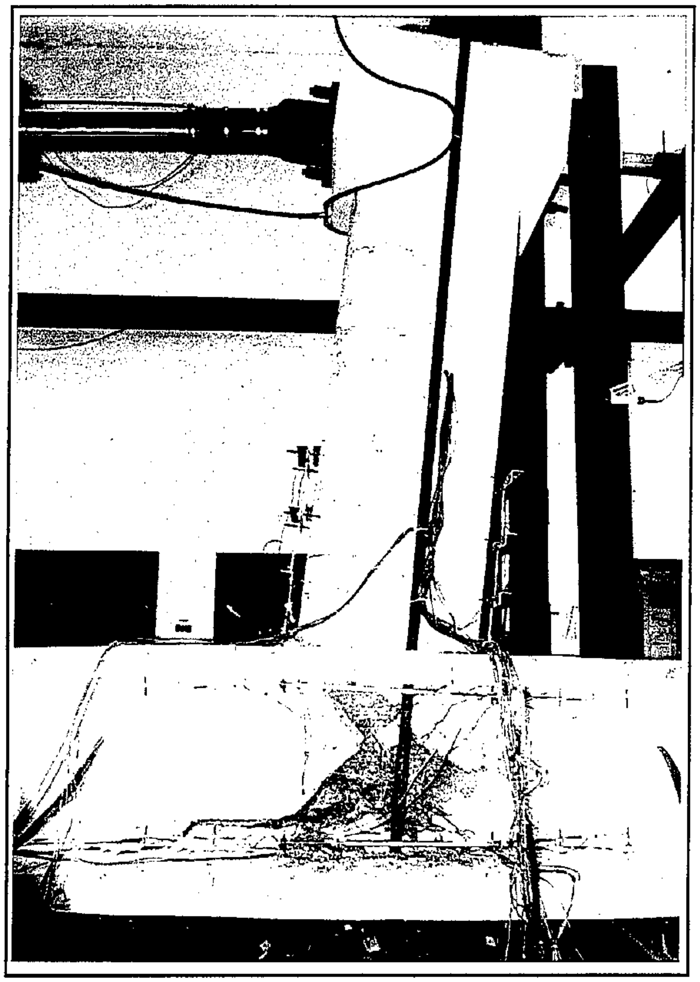

Figure 3.15 Overall deformation of SM3 at full stroke.

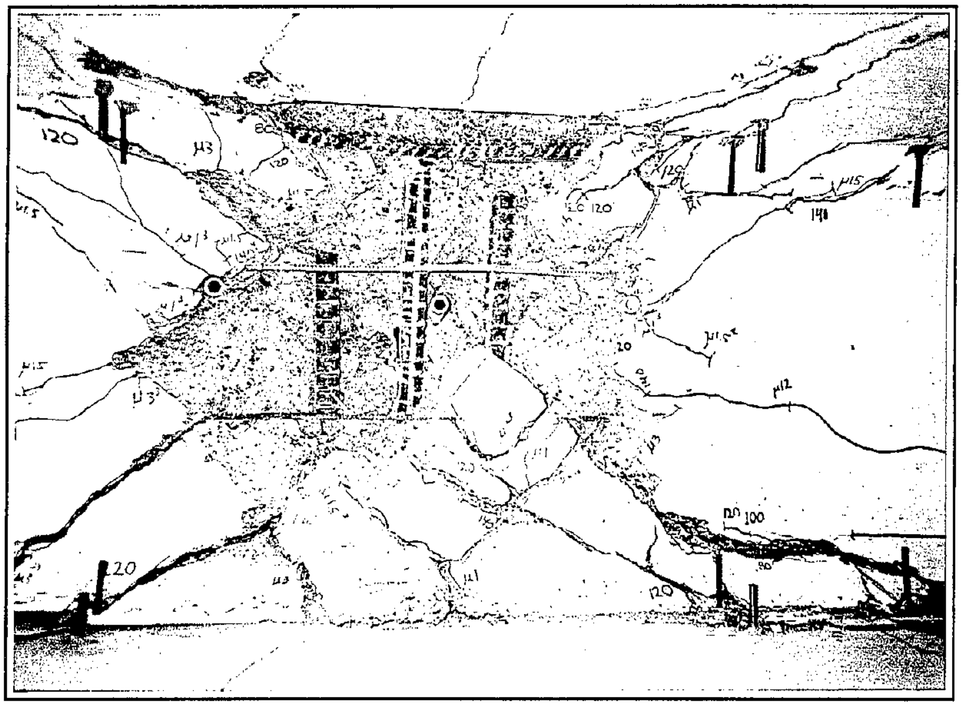
120
μ3
μ15
μ12
100
120

Figure 3.16 Deformed beam and column bars within the joint of SM3 at the end of test.

Reproduced from best available copy.

hysteretic behavior can be obtained, and (c) significant strength degradation of the system can be avoided. In the redesign of the tee joint, the damage was forced primarily to the plastic hinge region of the column and it is shown in Chapters 4, 5 and 6 that the full capacity of the column was developed with little or no strength degradation in each test unit with properly designed joint details. The energy absorption capacity of each redesigned unit was found to be much more dependable than that exhibited by as-built unit SM3.

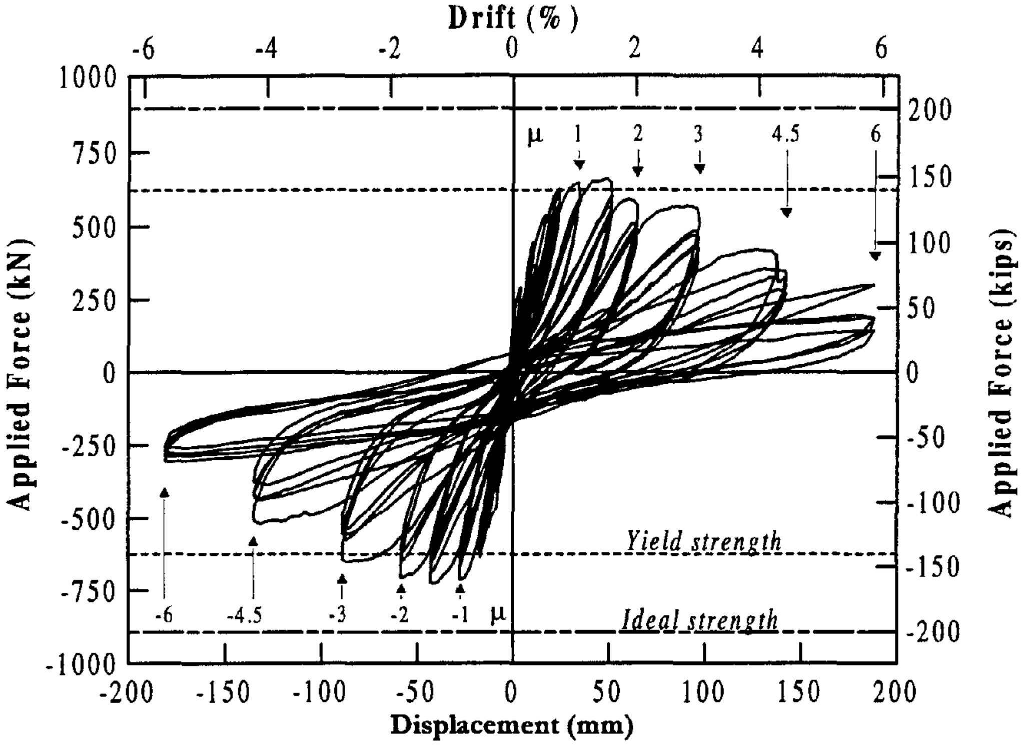

Figure 3.17 Hysteretic force-displacement response of as-built unit SM3

3.2 Test Units IC Series

Modeling technique, test set up, construction procedure, instrumentation and loading sequence applied to IC series specimens which incorporated the new detailing for the joints are given in this section. There were three specimens tested. The columns of all three units had almost similar ideal capacities, but the beams and joints contained different detailing. The first of this series was IC1 which was designed with a conventionally reinforced concrete bent cap. The joint of this unit was detailed with external joint reinforcement. The second unit, IC2, contained a partially prestressed cap beam and the third unit incorporated a precast fully prestressed beam. The joint reinforcement in the second and third units were reduced compared to that provided in the first unit as the cap beam prestressing was considered to transfer part of the shear through the joint. No external joint reinforcement was provided in the latter units. The design of the test units and their performance under repeated cyclic loading are discussed in Chapters 4, 5 and 6 respectively.

3.2.1 Prototype Structure

Since the behavior of an as-built joint had already been established for a typical interior joint from the Santa Monica Viaduct, the test units IC series were considered as redesigns of the interior beam/column joint from three column Bent #793+57 (Figure 3.1). The reinforcement details of the prototype structure are described concisely in Section 3.1.1. It was thought appropriate to maintain the ideal capacity of the column as was in the as-built structure, and redesign the cap beam and joint so that a dependable behavior could be obtained under seismic loading.

The bending moment distribution of the cap beam under gravity, seismic and combined gravity plus seismic loading is presented in Figure 3.18 based on the calculation performed for the prototype structure in reference [16]. Ideal moment capacities were assumed to have developed in the columns as expected in the structure when current reinforcement details for the cap beam and joints are incorporated. Also, for simplicity, it was assumed that the capacities of all three columns were identical and that the seismic moment at the interior column was resisted equally by the cap beam positive and negative moments. This implies ability for redistribution of beam moments across the joint. No overstrength factors were considered in Figure 3.18 when estimating the column capacities. Considering an overstrength factor of 1.3, the bending moment distribution was reevaluated and a portion of it relevant to the current investigation is shown in Figure 3.19.

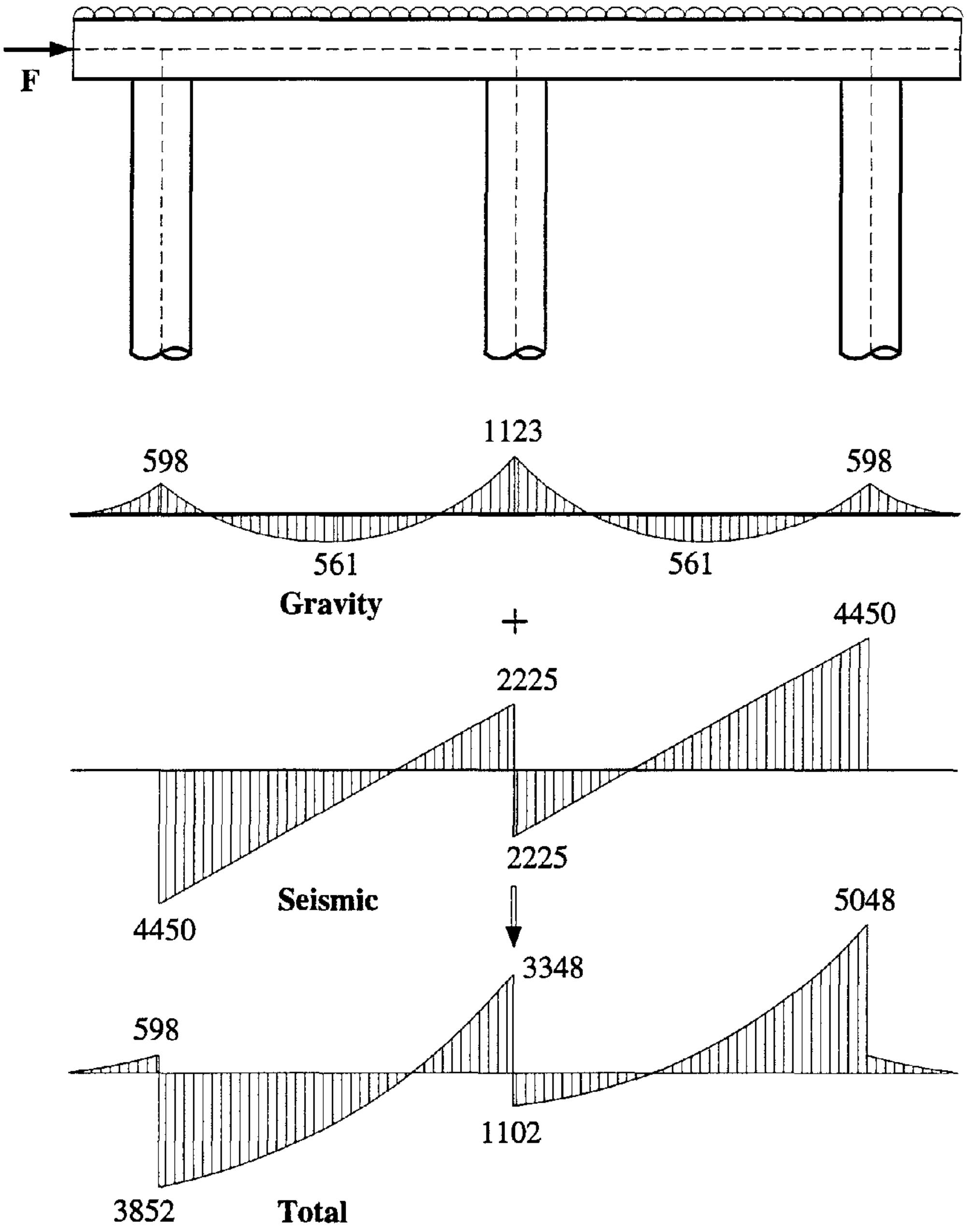
F
1123
598
598
561
561
Gravity
+
4450
2225
2225
Seismic
4450
5048
3348
598
1102
3852
Total

Note: Given bending moments are in kNm.
(1 kips-ft = 0.7376 kNm)

Figure 3.18 Bending moment distribution of the prototype bent cap based on the calculations given in reference [16].

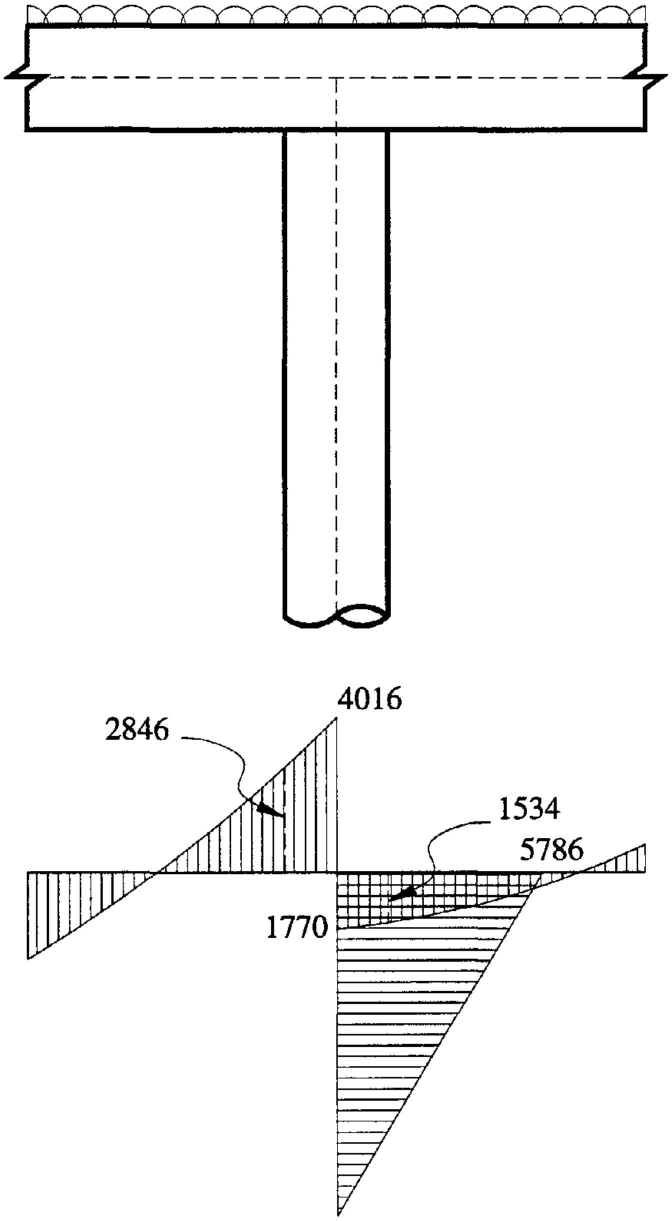
4016
2846
1534
5786
1770

Note: Given bending moments are in kNm.
(1 kips-ft = 0.7376 kNm)

Figure 3.19 Bending moment distribution in members framing into the tee joint at full scale.

3.2.2 Modeling of Prototype

It was decided that test units be built at half scale and tested inverted for convenience. In the testing procedure, it is necessary to apply forces that result in duplication of the stresses and strains in the model similar to those expected in the prototype structure [7]. A length scale factor **SF** = 0.5 results in the following relationship between the model and prototype:

$$\left.\begin{aligned}
\mathbf{Displacement_m} &= \mathbf{SF * Displacement_p} \\
&= \mathbf{0.5 * Displacement_p} \\
\mathbf{Area_m} &= \mathbf{SF^2 * Area_p = 0.25 * Area_p} \\
\mathbf{Force_m} &= \mathbf{SF^2 * Force_p = 0.25 * Force_p} \\
\mathbf{Bending\ Moment_m} &= \mathbf{SF^3 * Bending\ Moment_p} \\
&= \mathbf{0.125 * Bending\ Moment_p}
\end{aligned}\right\} \tag{3.1}$$

where **m** represents the model and **p** represents the prototype structure. Replacing **SF** = 0.75 in Eq. 3.1 provides modeling factors between the as-built unit SM3 and the prototype. Hence, the following relationships can be readily obtained between IC units and SM3:

$$\left.\begin{aligned}
&\mathbf{Displacement_{IC} = 0.667 * Displacement_{SM3}} \\
&\mathbf{Area_{IC} = 0.444 * Area_{SM3}} \\
&\mathbf{Force_{IC} = 0.444 * Force_{SM3}} \\
&\mathbf{Bending\ Moment_{IC} = 0.296 * Bending\ Moment_{SM3}}
\end{aligned}\right\} \tag{3.2}$$

The demand in a joint of a bridge structure is dictated by the capacity of the column framing into the joint provided that plastic hinging is developed, as preferred, in the column rather than in the cap beam. Therefore, if a desirable collapse mechanism for the prototype structure is developed, the demand in the joint would be higher than that was induced in the joint of the as-built unit SM3. Consequently, it follows that in order to test the redesigned joints to the maximum possible shear demand, the column capacity should be modeled appropriately. The ideal capacity of the column in the prototype structure was estimated to be 6033 kNm (4450 kips-ft) [16]. Hence, the equivalent column capacity in the model was 754 kNm (556 kips-ft). Since there are differences in the material properties of the prototype and model structures, the column reinforcement shown in Figure 4.4 was chosen for the test units. Longitudinal column steel consisted of 14#7 (d_b = 22.2 mm) bars with a steel ratio of 1.86 percent compared to 3.5 percent in the prototype structure. Transverse reinforcement was provided in the form of #3 (d_b = 9.5 mm) spiral @ 96.5 mm (3.8 in.) spacing, yielding a volumetric ratio of 0.52 percent. The ideal and ultimate capacities of this column section were found to be 694 kNm (512 kips-ft) and 769 kNm (567 kips-ft) respectively. As recommended in Section 3.2.3, an axial load of 400 kN (90 kips) was used in the analysis.

Given the uncertainties associated with material properties and strain hardening of steel, the overstrength capacity of the columns of the test units were taken as 30 percent higher than the predicted ultimate moment capacity for conservative reasons except for the third unit (see Section 6.1.2). This resulted in a maximum possible bending moment of 1000 kNm (737 kips-ft) in the column adjacent to the joint, and the beams were designed to resist this bending moment. The stresses and strains in the joints were estimated from equilibrium considerations of the member forces adjacent to the joint. Depending on the principal stress state, each joint was appropriately detailed with the objective of placing the minimum feasible amount of reinforcement within the joint.

Since the overstrength moment capacity is developed in the column adjacent to the joint, modeling of the deck or soffit was considered irrelevant as long as the beam was sufficiently detailed to resist the column moment. Avoiding deck and soffit slabs in the model was expected to ease complexity associated in identifying force transfer mechanisms of the joints.

As in SM3, the height of the column was selected such that the point of loading in the test units corresponded to the point of contraflexure in the prototype structure. The length of the cap beam was decided based on the testing arrangement as detailed in the following section.

3.2.3 Test Setup

To simplify the testing procedure, it was decided that the cap beam be simply supported at the ends. At the northern end of the beam the movements were restrained in the horizontal and vertical directions, and at the southern end it was constrained only in the vertical direction. To appropriately model the positive moment gradient, a support would have been required at 4572 mm (180 in.) from the center of the column. Also, two supports, as provided for the test of SM3, were necessary to obtain both positive and negative moment gradients similar to those expected in the prototype structure. Matching the moment gradients along the beam are not required to study the joint behavior as long as beam end forces adjacent to the joint are developed in the right proportion to resist the column moment. Hence, only one support at each side was justified. The supports for the cap beam of each test unit were located at 1219 mm (48 in.) from the center of column.

The test set up and overall dimensions of the test unit are shown in Figure 3.20, in which the specimen is inverted as in the test configuration. Axial load due to gravity on the column of a half scale model was 569 kN (128 kips) [16]. However, this value was not suitable to obtain the required cap beam moments at the joint interface. A lower value of 400 kN (90 kips) was chosen so that the ratios between the model and prototype cap beam bending moments at the column face as shown in Figure 3.21 were obtained at the ultimate strength of the structure. It was crucial to model the positive moment as accurately as possible because the external force transfer mechanism was to be developed on the tension side of the column (see Figure 4.3b). Thus, the positive moment was modeled with 100 percent accuracy and the corresponding negative moment was 129 percent of that calculated based on the prototype structure. A reduction in the column axial load may be slightly detrimental to the joint performance, giving conservative results.

Axial load distribution along the cap beam as modeled and as required based on the analysis of the prototype structure is shown in Figure 3.22. Again, it is emphasized that *it is not the distribution of forces along the cap beam, but the forces adjacent to the joint that are critical to the modeling procedure.* Axial compression in the cap beam acts to improve the joint performance with the opposite applying for the axial tension in the beam. Therefore, the implication is that the modeling of the cap beam axial load will underestimate the actual joint behavior in the push direction and overestimate it in the pull direction. Since the magnitude of the axial forces were small, there was no significant different in the joint performance was anticipated between the push and pull direction loading, as well as between the prototype structure and the test units. A considerable amount of axial load is applied when the cap beam is prestressed. The axial

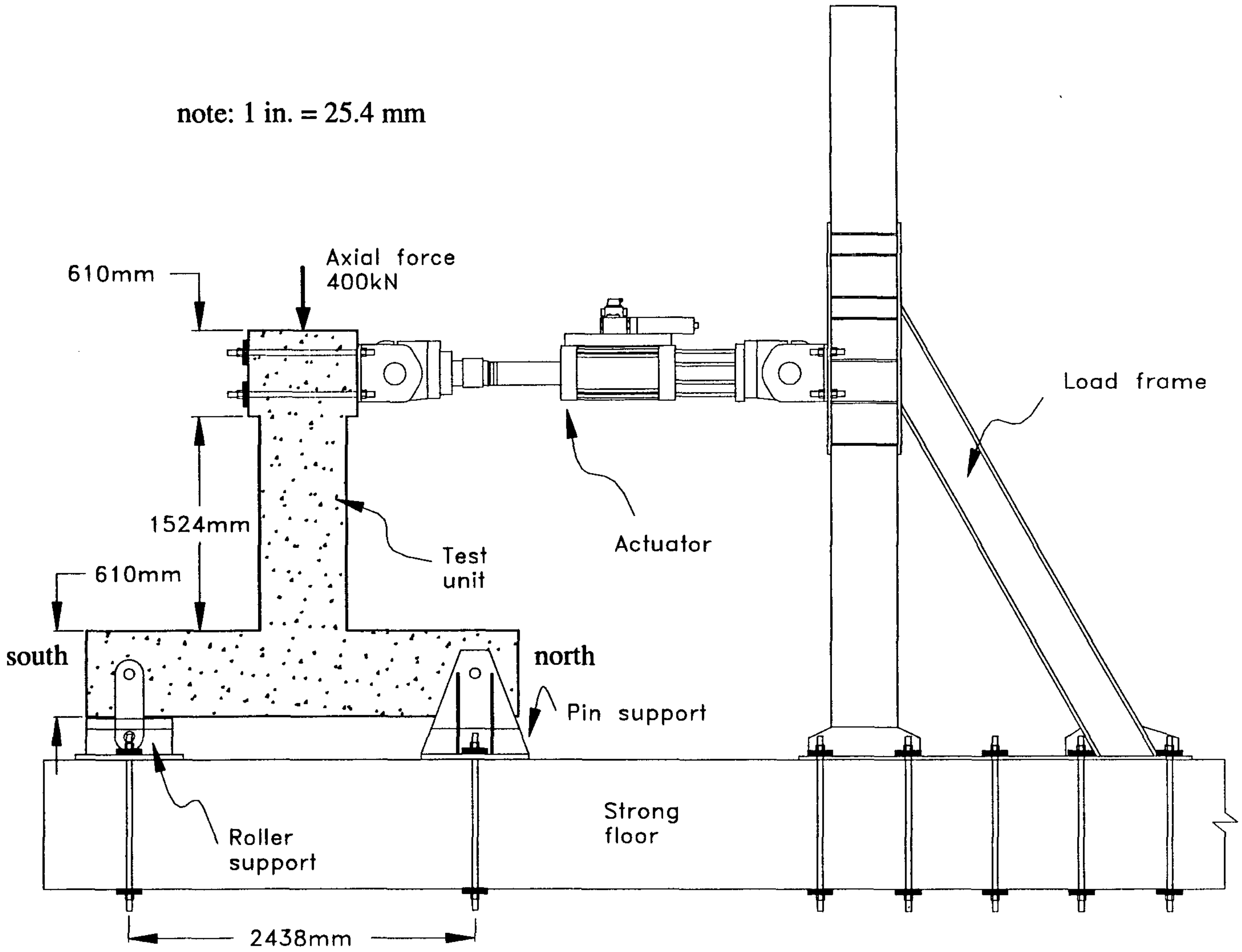
note: 1 in. = 25.4 mm

610mm
Axial force
400kN
1524mm
610mm
south
north
Test
unit
Actuator
Load frame
Pin support
Roller
support
Strong
floor
2438mm

Figure 3.20 Overall test set up of IC series interior joints.

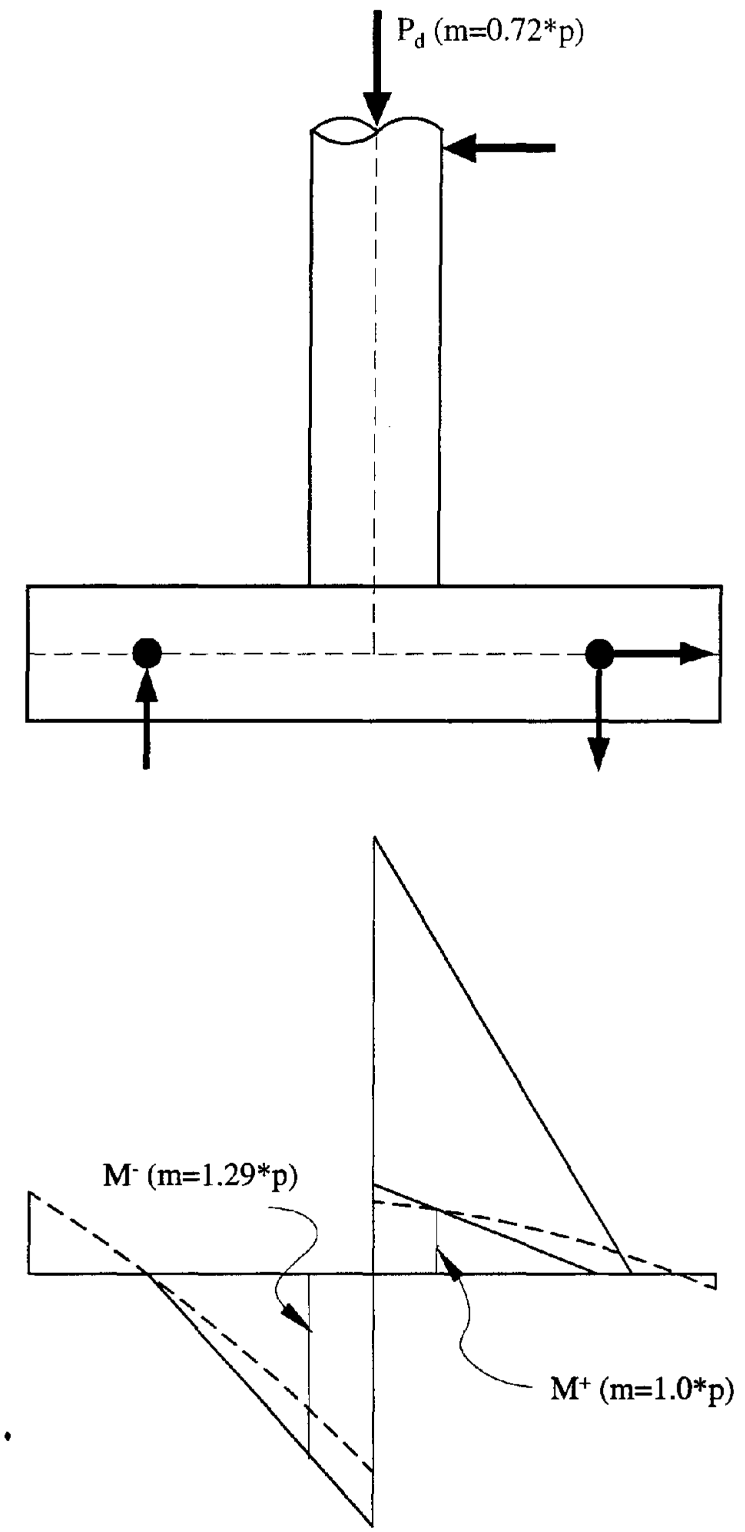
P_d (m=0.72*p)
M⁻ (m=1.29*p)
M⁺ (m=1.0*p)

Figure 3.21 Comparison of cap beam moments anticipated in the test models to those calculated on a half scale prototype structure in the interior joint region.

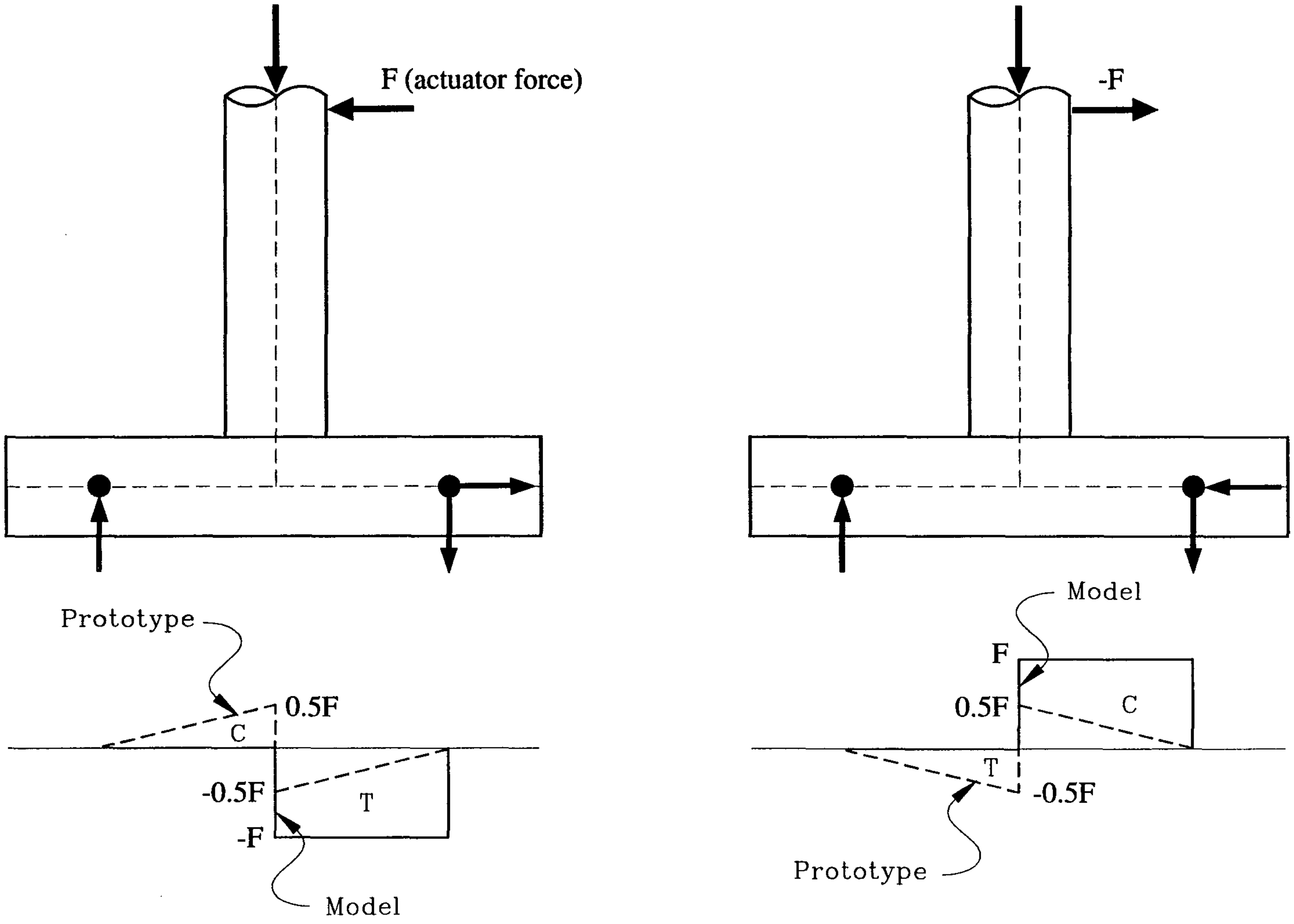

F (actuator force)
Prototype
0.5F
C
-0.5F
T
-F
Model
-F
Model
F
0.5F
C
T
-0.5F
Prototype

Figure 3.22 Distribution of cap beam axial force in the test unit and as expected in the prototype structure.

force distribution of the cap beam can then be obtained by adding the constant prestressing force to the force distribution shown in Figure 3.22.

3.2.4 Construction of Test Units

The first two test units were built simultaneously using monolithic construction. Each unit was cast in two concrete pours. The beams and joints were poured first and the columns were then cast with construction joints at the beam/column interface. Following the tests on the first two units, a third unit was designed with a fully prestressed cap beam. A precast construction was preferred for this unit since there was no continuous mild steel provided in the cap beam. The joint and column of this unit were built as a single module and the beam was constructed in two segments. The test unit was formed by connecting the two segments of the beam to either side of joint solely by prestressing. More details of the construction procedure adopted for this unit are presented in Section 6.3.

Standard concrete mix was used in all three units with a target compressive strength for concrete of 34.5 MPa (5 ksi) at the age of 28 days. High strength Grade 60 steel was used as reinforcement for the test units. Prestressing in the cap beams was applied using Dywidag bars, which were grouted a few days prior to the test. More details are given in the appropriate chapters.

3.2.5 Instrumentation

The test units were instrumented extensively with strain gauges, curvature devices, linear potentiometers, and a rotation device. Most of the strain gauges were mounted on the reinforcing steel in the joint region. Figures 3.23 and 3.24 define the strain gauge locations in the column, beam and joint reinforcement as provided for the first redesigned unit with a reinforced concrete bent cap (IC1). A similar distribution of gauges was considered for the two prestressed units. The procedure adopted for mounting the gauges may be found elsewhere [7]. As shown in Figure 3.25, the columns were provided with five sets and beam with eight sets (four on the west and four on the east side) of curvature devices (cells). Each curvature device consisted of two linear potentiometers. The

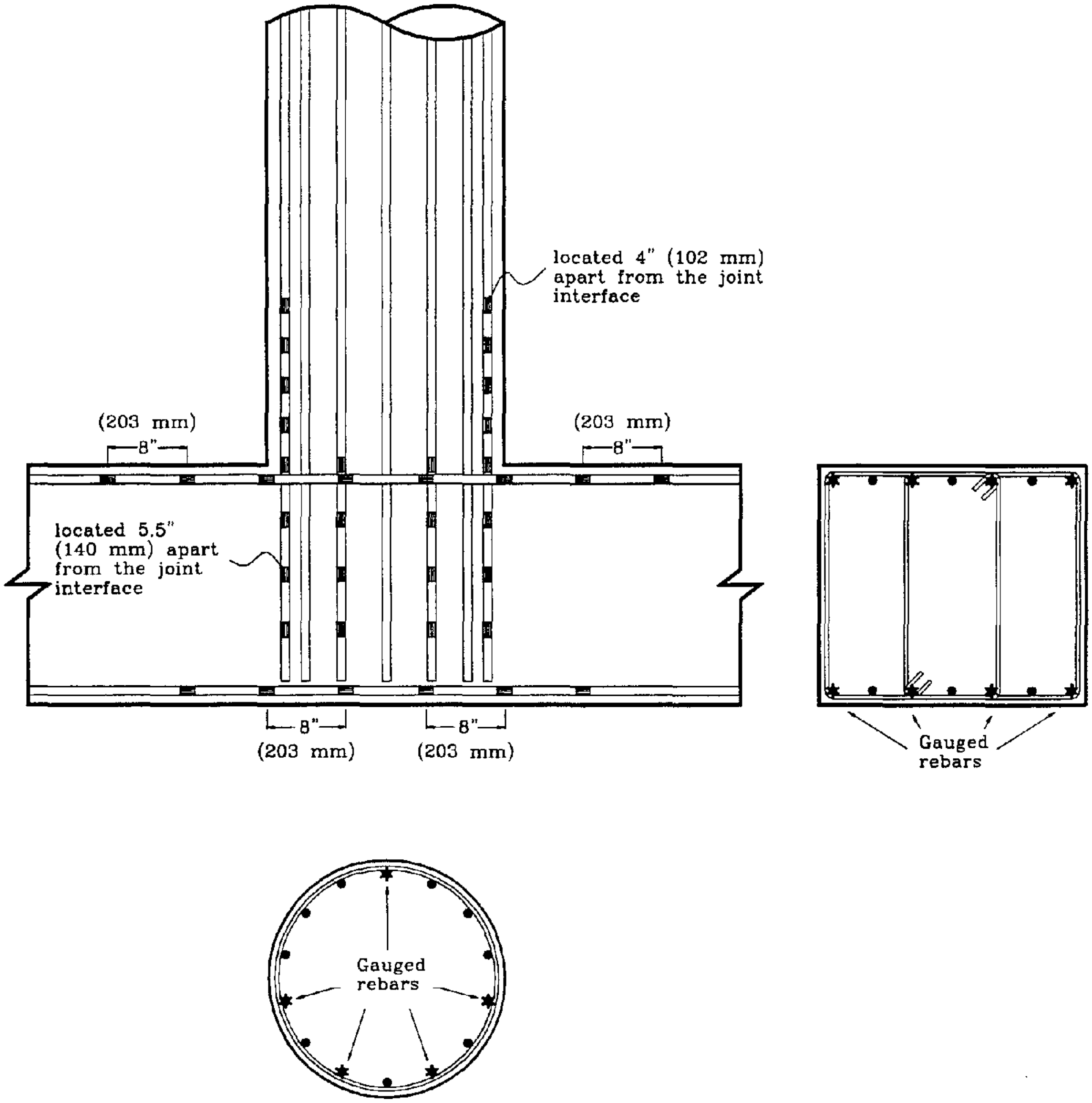
located 4" (102 mm) apart from the joint interface
(203 mm)
8"
(203 mm)
8"
located 5.5" (140 mm) apart from the joint interface
8"
(203 mm)
8"
(203 mm)
Gauged rebars
Gauged rebars

Figure 3.23 Location of strain gauges in the longitudinal column and beam reinforcement of test unit IC1.

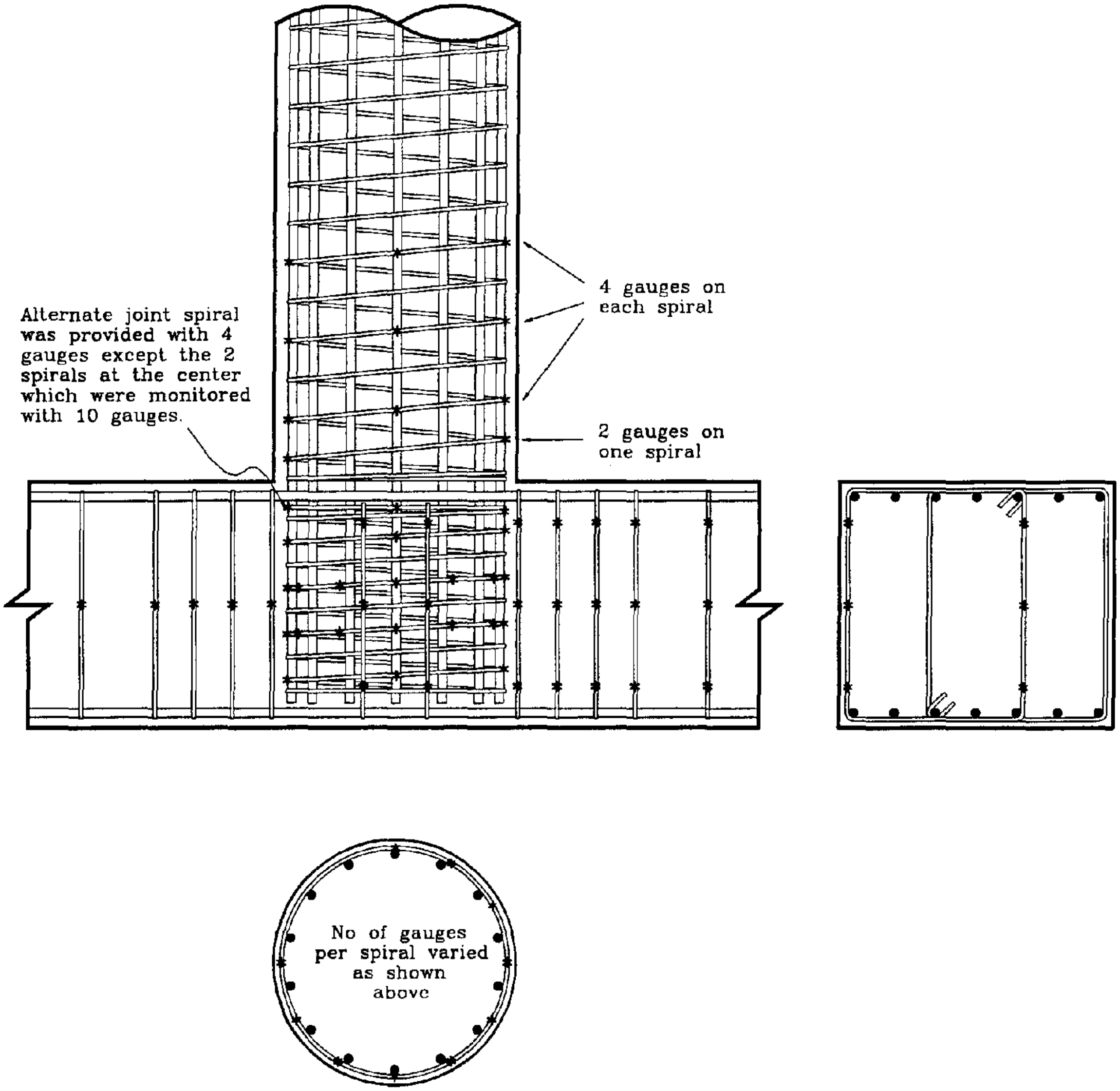
Alternate joint spiral was provided with 4 gauges except the 2 spirals at the center which were monitored with 10 gauges.
4 gauges on each spiral
2 gauges on one spiral
No of gauges per spiral varied as shown above

Figure 3.24 Location of strain gauges in the transverse reinforcement of test unit IC1.

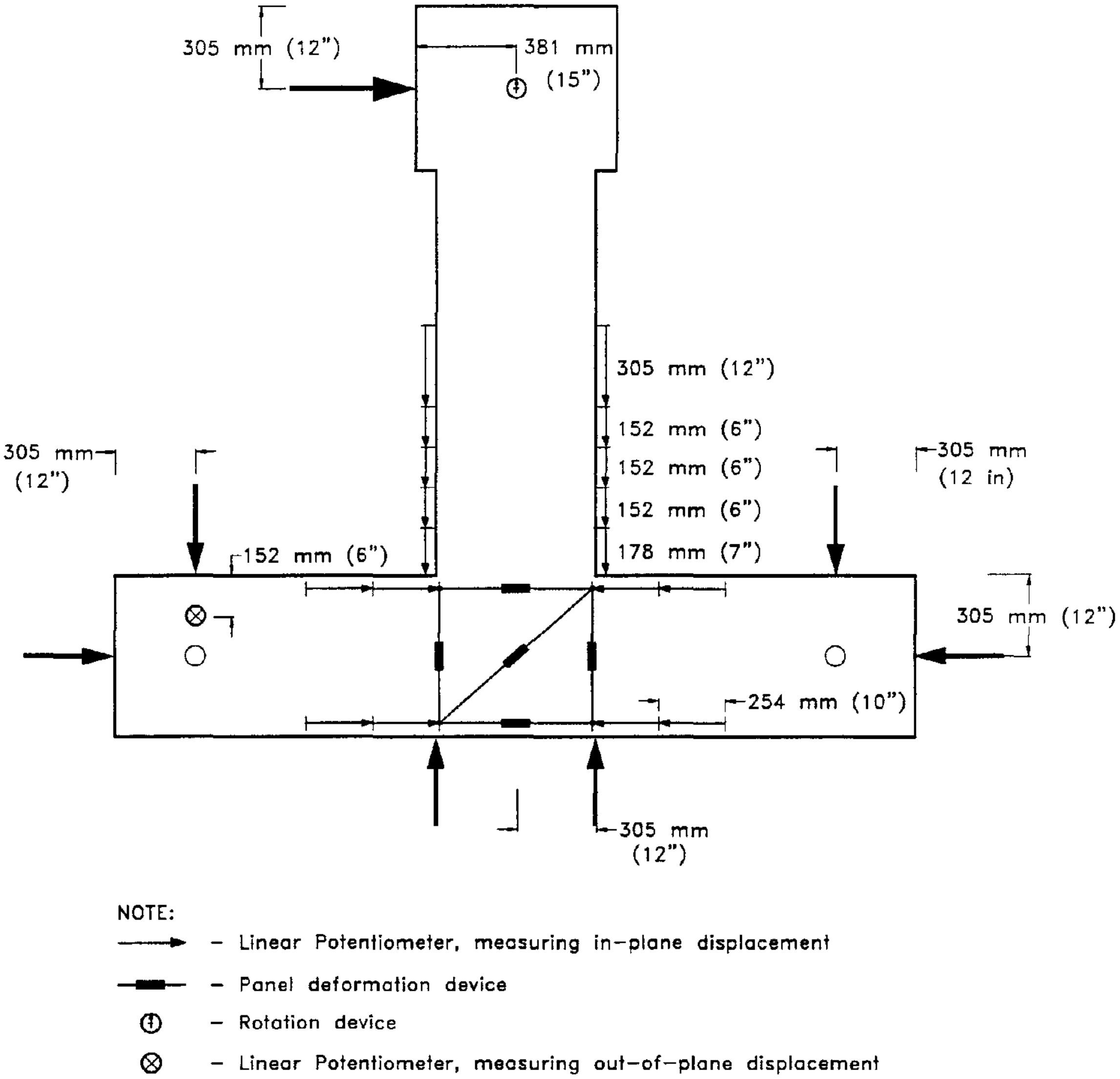

305 mm (12")
381 mm (15")
305 mm (12")
152 mm (6")
152 mm (6")
152 mm (6")
178 mm (7")
305 mm (12")
305 mm (12 in)
152 mm (6")
305 mm (12")
254 mm (10")
305 mm (12")
NOTE:
– Linear Potentiometer, measuring in-plane displacement
– Panel deformation device
– Rotation device
– Linear Potentiometer, measuring out-of-plane displacement

Figure 3.25 External instrumentation of redesigned cap beam/column interior joints.

curvature was obtained from the displacement measured in one potentiometer with respect to the other as detailed below:

$$\phi = \frac{\textbf{rotation}}{\textbf{gauge length}} = \frac{(\Delta_2 - \Delta_1)/l_w}{l_g} \tag{3.3}$$

where $(\Delta_2$-$\Delta_1)$ represents the relative extension within the curvature cell, l_w is the distance between the two linear potentiometers and l_g is the gauge length. When curvature is calculated in the column cell adjacent to the joint, a modified gauge length as given in Eq. 3.4 is considered:

$$l_g' = l_{sp} + l_g\left(1 - 1.67\frac{l_g}{l_c}\right) \tag{3.4}$$

where l_{sp} is the equivalent strain penetration length taken as $0.022f_yd_{bl}$ (in SI units). This modification is necessary to account for the base rotation resulting from strain penetration into the joint [18].

The joint deformation panel, which was formed from five linear potentiometers (Figure 3.25), was attached on the east and west side of the test units. By calculating the nodal displacements, the five independent joint deformations can be extracted as described in Section 2.5 from each set of joint panel instrumentation. The joint rotation introduced by bending of the beam was directly measured by placing two linear potentiometers beneath the joint at 610 mm (24 in.) distance apart. There were six linear devices placed with respect to fixed references in order to measure displacements at various locations on the specimen (see Figure 3.25). A rotation device was mounted at the center of the load stub to measure the rotation of the column from its original position under zero lateral load.

The cap beam of the second and third test units were designed with prestressing. In order to estimate the amount of prestressing applied to the beams, several demec points were glued to the top surface (as cast) and sides of the beam. Using a demountable mechanical strain gauge with a gauge length of 200 mm (7.87 in.), strains on the concrete surfaces were measured. Demec readings were taken at regular intervals starting from prior to prestressing the cap beam until the gravity load was applied. No readings were taken during the transverse lateral cyclic testing of the specimen. The prestressing bars were also mounted with strain gauges which were monitored during the entire test.

3.2.6 Loading Sequence

An identical loading sequence was planned for all three units. Gravity load was first applied as a concentrated force in the column and it was to be maintained during the lateral load test. Some variation in the axial load about the target load of 400 kN (90 kips) was, however, expected during the test. In Figure 3.26 the history of the axial load recorded for unit IC1 is shown and similar oscillations were also observed for the two prestressed units. In the calculations of all three units, the actual recorded axial load was considered wherever possible.

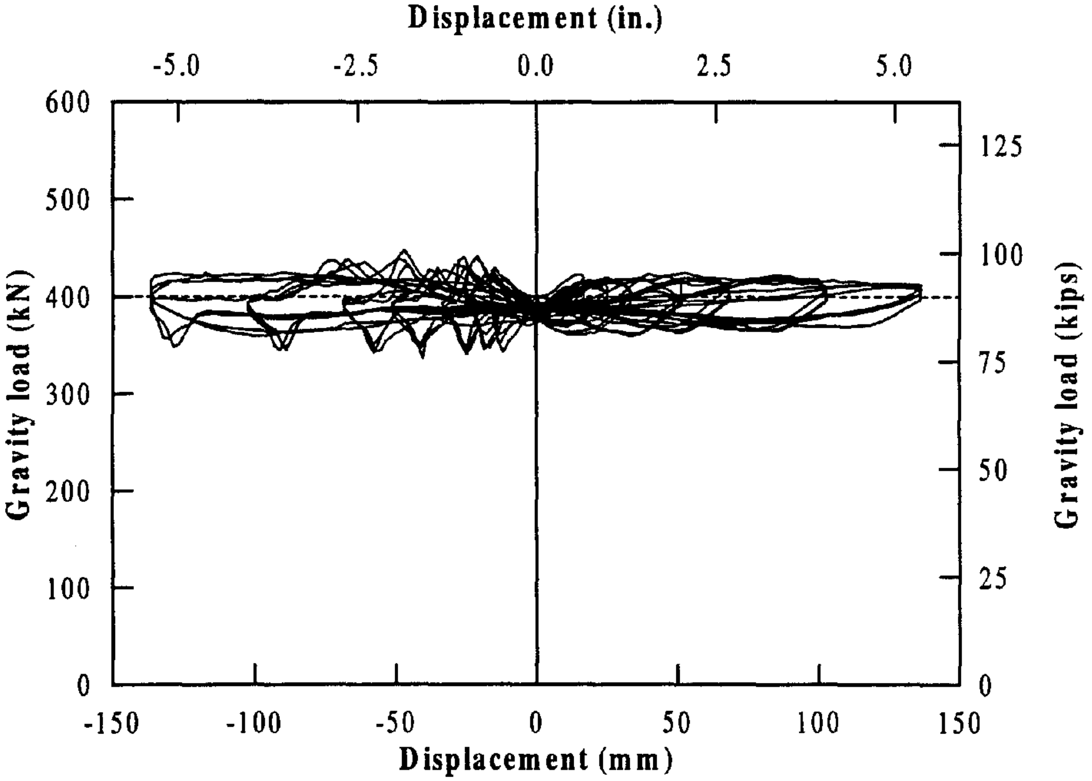

Figure 3.26 History of gravity load applied to test unit IC1.

The first part of the lateral load test was force controlled and the remainder, beyond yielding of the longitudinal column steel, was controlled by displacement. The horizontal force corresponding to the first yield was achieved in 4 steps with one cycle at each load step as shown in Figure 3.27. The displacement Δ'_y, measured at the first yield, was used for calculating the displacement corresponding to displacement ductility $\mu_\Delta = 1$ as shown below:

$$\Delta_y = \frac{M_I}{M_y}\Delta'_y \tag{3.5}$$

where M_y and M_I are theoretical yield moment and ideal moment capacity of the column respectively.

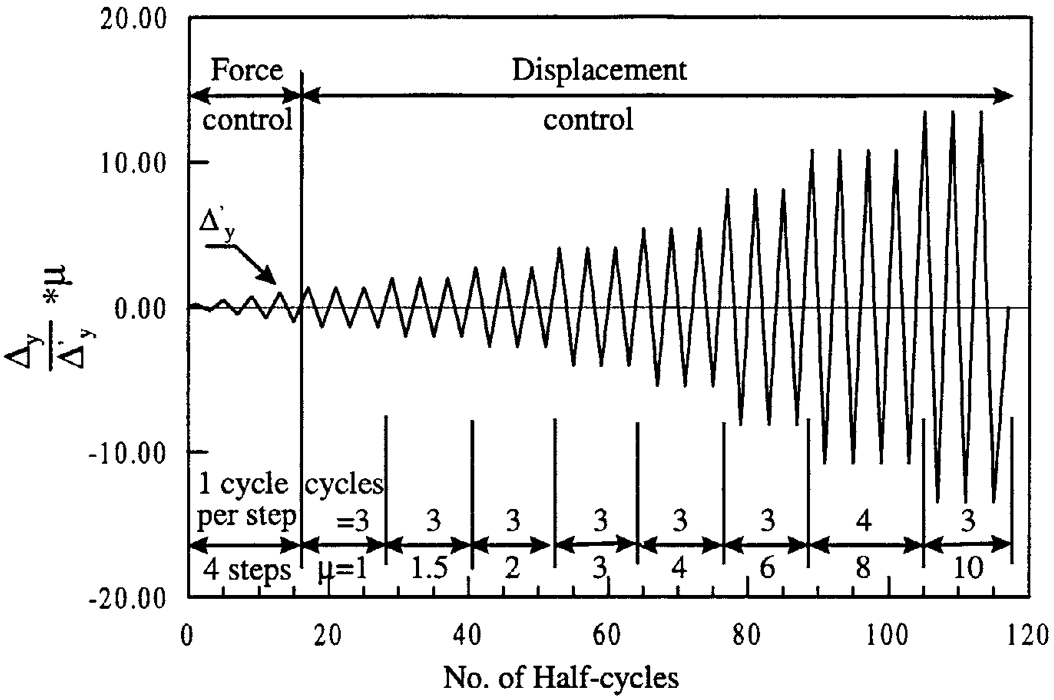

Figure 3.27 Lateral load sequence considered for redesigned test units with tee connections.

For the second part of the test, the displacement at the center of load stub, which was used to control the test, was increased in steps such that μ_Δ = 1, 1.5, 2, 3, 4, 6, 8 and 10 could be achieved. At each step, a minimum of three cycles were applied to observe the stability of the hysteresis loop (Figure 3.27). The test was terminated when a significant reduction in the force resisting ability of the system was observed.

CHAPTER 4

INTERIOR JOINT WITH A REINFORCED CONCRETE CAP BEAM

The reinforcement detailing of the first test unit IC1, which was designed with a fully reinforced concrete cap beam and external vertical joint reinforcement, is presented in this chapter. This is followed by a description of the performance of the test unit under repeated cyclic loading. Graphical representation of various data obtained during the test is also given in this chapter.

4.1 Design Procedure

4.1.1 Column

As specified in Section 3.2.2, the column reinforcement was chosen so that the prototype column capacity could be replicated. The shear resistance of the column was estimated using a three component UCSD model [19] which includes the contribution from the axial load, the concrete shear resisting mechanism, and the steel truss mechanism. It was ensured that no significant shear deformation would occur by limiting strains in the shear reinforcement to below yielding. More details relevant to the shear design may be found in Section 4.7.

4.1.2 Cap Beam

Assuming plastic hinging in the column and the maximum possible column moment being 1.3 times the predicted ultimate capacity (see Section 3.2.2), the beam positive and negative design moments and axial load distributions were estimated from equilibrium conditions (Figure 4.1). A comparison of the beam moments simulated in the test unit against those expected in an equivalent prototype structure was made in Section 3.2.3. In the prototype structure, the ratio between the negative and positive moment resistance of

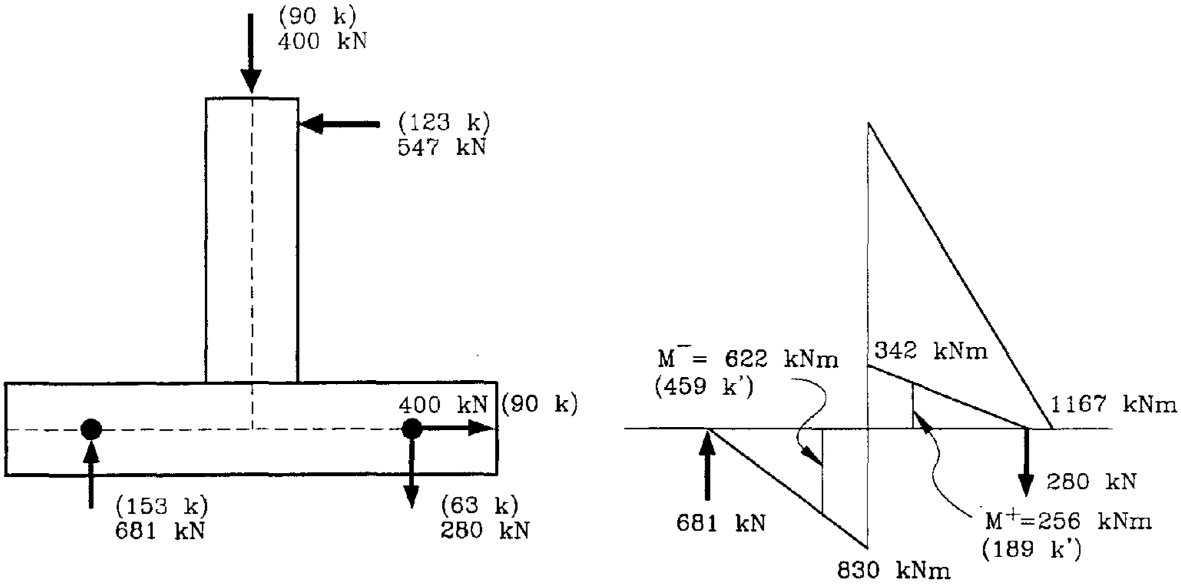
(90 k)
400 kN
(123 k)
547 kN
400 kN
(90 k)
(153 k)
681 kN
(63 k)
280 kN
M⁻= 622 kNm
(459 k')
342 kNm
1167 kNm
280 kN
681 kN
M⁺=256 kNm
(189 k')
830 kNm

(a) Tee joint test unit with external forces.

(b) Cap beam design moments under push direction loading. (1 kNm = 0.74 kips-ft)

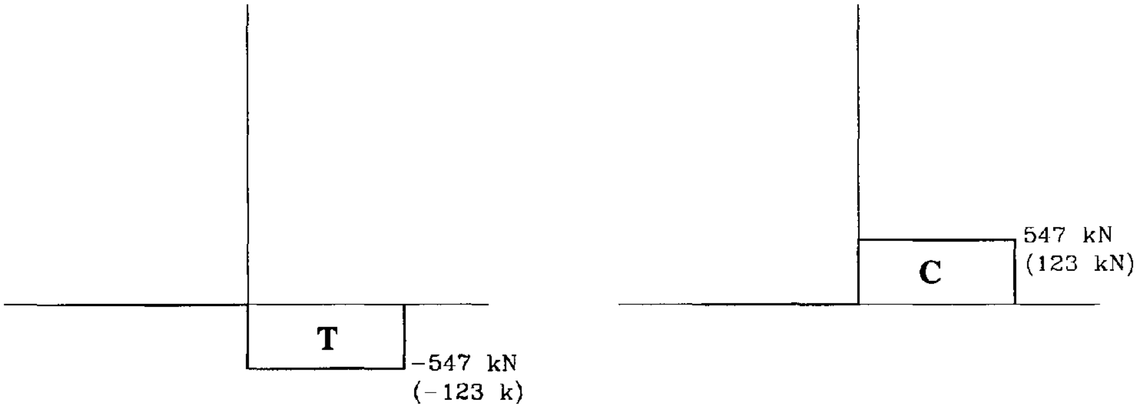
T
-547 kN
(-123 k)
C
547 kN
(123 kN)

(c) Cap beam axial load in the push direction.

(d) Cap beam axial load in the pull direction.

Figure 4.1 Design moments and distribution of axial load in the cap beam of test unit IC1.

the beam will be dictated by the cracked stiffness of the sections adjacent to the joint. However, as described in Section 3.2.1, it was assumed that column moment at the center of the joint would be resisted equally by the positive and negative beam moments. This was taken into account when determining the appropriate locations for the beam supports. For the test set up considered for IC series units (Figure 3.20), it was not possible to simulate moment redistribution in the cap beam unless the axial force in the column was varied systematically to maintain equilibrium. Since a constant axial force was preferred in the column, no moment redistribution was permitted in the beam of the test unit.

To protect the beam from any inelastic action, the cap beam was detailed such that yield moments at the critical sections adjacent to the joint should be greater than the beam design moments. This design criteria was considered to be fairly conservative. Therefore, flexural strength reduction factor $\phi_f = 1.0$ was used in the design. The reason for adopting a conservative approach in the beam detailing was that an external joint mechanism was designed to develop in the beam region adjacent to the joint as discussed in the following section. An alternative design procedure is recommended for capacity protected sections by Priestley *et al.* [19]. They propose that it is adequate to detail the cap beam by limiting (a) the concrete strain to 0.004 in the extreme compression fiber, and (b) the tensile strain to 0.015 in the longitudinal steel. The reason for restricting steel strain to 0.015 is that crack widths in the structural member can be kept to an acceptable serviceable limit. Considering that a flexural strength reduction factor $\phi_f = 1.0$ was used in the beam design of the test unit as opposed to $\phi_f = 0.9$ recommended in reference [19], the design approach of Priestley *et al.* suggests that the detailing of the beam of the test unit embodied additional strength of about 10-20 percent. Additional longitudinal reinforcement necessary for the joint mechanism was also provided consistent with the requirement given in the following section.

4.1.3 Interior Joint

In order to reduce congestion of reinforcing steel within the joint, a reduced amount of joint reinforcement was sought in the design of the interior cap beam/column connection. Unlike in the conventional approach (e.g. ACI 318-95 [3]), the maximum joint shear force was ***not*** regarded as a design parameter for establishing the joint reinforcement. Instead, it was detailed to ensure that the longitudinal column bars could be anchored adequately into the joint and that no significant damage would occur to the joint region, allowing overstrength moment capacity of the column to be developed at the critical section adjacent to the joint interface. Although anchorage of the column bars could be achieved partly by providing hooks or bends at the top of column bars, this was not favored as this detail causes excessive congestion of steel in the joint, and it would also be difficult to place the longitudinal deck steel at the top of the joint. Therefore, it was preferred that longitudinal column steel be anchored directly into the joint with straight bars and this was achieved by considering a force transfer mechanism as described below.

In designing bridge joints with force transfer mechanisms, the joint principal tensile stress, as calculated from Eq. 4.1, is used as an initial design parameter.

$$\mathbf{p_c, p_t = \frac{f_v + f_h}{2} \pm \sqrt{\left(\frac{f_v - f_h}{2}\right)^2 + v_j^2}} \qquad (4.1)$$

where $\mathbf{p_c}$ and $\mathbf{p_t}$ are the principal compression and tensile stresses respectively, $\mathbf{f_v}$ is the average axial stress in the vertical direction, $\mathbf{f_h}$ is the average axial stress in the horizontal direction and $\mathbf{v_j}$ is the joint shear stress averaged across the effective area of the joint. If the average joint shear force is used to calculate $\mathbf{v_j}$, the resulting stresses are referred to as the average principal stresses in this report. Similarly, the maximum principal stresses are obtained using the maximum joint shear force, which can be calculated considering the resultant tension and compression forces in members framing into the joint (see Appendix A). The average joint shear force can be obtained from the column overstrength moment as follows [19]:

$$\mathbf{V_{jh} \approx \frac{M_c^o}{h_b}} \qquad (4.2)$$

where $\mathbf{V_{jh}}$ is the average horizontal joint shear force, $\mathbf{M^o_c}$ is the column overstrength moment capacity, and $\mathbf{h_b}$ is the beam depth. Joint shear stresses in the vertical and horizontal directions are equal, and therefore the average joint shear stress can be calculated either from the horizontal or vertical joint shear force, which are related as shown in Eq. 4.3:

$$\mathbf{V_{jv} = \frac{V_{jh} h_b}{h_c}} \qquad (4.3)$$

where $\mathbf{V_{jv}}$ is the average joint vertical shear force, and $\mathbf{h_c}$ is the depth of column section. The difference between the average and maximum joint shear stresses is shown schematically in Figure 4.2 for a bridge tee joint considering the bending moment distribution along the cap beam.

In designing the joint of the test unit, the following design recommendations were considered based on the maximum principal tensile stress state of the joint [17]:

- If $\mathbf{p_t \leq 0.29\sqrt{f_c'}}\left(\mathbf{3.5\sqrt{f_c'}}\text{ in psi units}\right)$, joint shear cracking is not expected. Joint forces are transferred through the diagonal strut, and no dedicated joint steel is required. Only nominal joint reinforcement is provided.
- If $\mathbf{p_t > 0.42\sqrt{f_c'}}\left(\mathbf{5.0\sqrt{f_c'}}\text{ in psi units}\right)$, a complete force transfer mechanism is required for transmitting the joint shear forces. The detailing of the joint should be performed consistent with the force transfer models.
- For joint principal tensile stress between the above limits, a linear interpolation of the two reinforcement requirements can be considered.

In a recent publication [19], this design criteria have been revised, suggesting that the average principal tensile stress rather than its maximum value should be considered in the above recommendation. This modification was introduced appreciating that the damage within the joint should correlate to the average joint stresses. This revision would not have required any change to the joint design of this test unit. Nonetheless it can, in some cases, require a full force transfer model when the maximum principal stress is considered and suggest only a nominal joint steel when the average principal stress is used as the design parameter. This aspect is further discussed in Section 4.6.3. and in the following chapters based on the experimental results of other redesigned tee joints.

For the interior joint concerned in this section, the maximum principal tensile stress was estimated to be $\mathbf{0.84\sqrt{f_c'}}\left(\mathbf{10.1\sqrt{f_c'}}\text{ in psi units}\right)$ and consequently a full force transfer mechanism was originally justified. The average joint principal stress was later calculated to be $\mathbf{0.69\sqrt{f_c'}}\left(\mathbf{8.3\sqrt{f_c'}}\text{ in psi units}\right)$, requiring no change in the joint design approach. The detailing of the joint considering a complete joint force transfer mechanism was performed as illustrated in the following paragraphs.

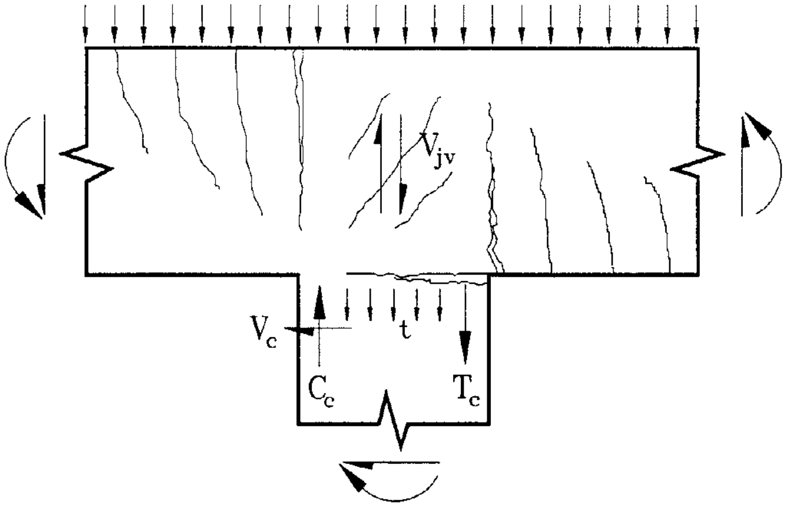
V_jv
V_c
t
C_c
T_c

(a) Bridge tee joint

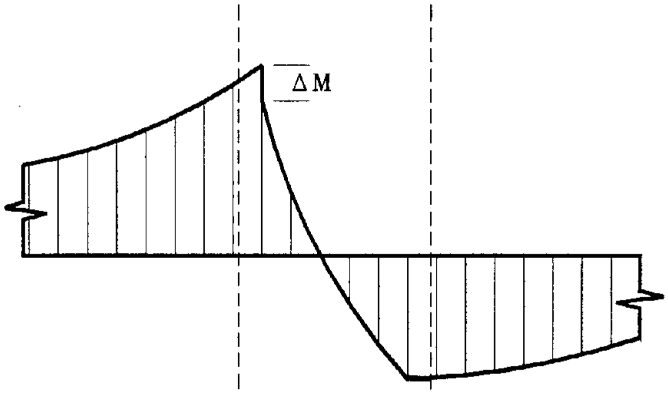

(b) Moments along cap beam

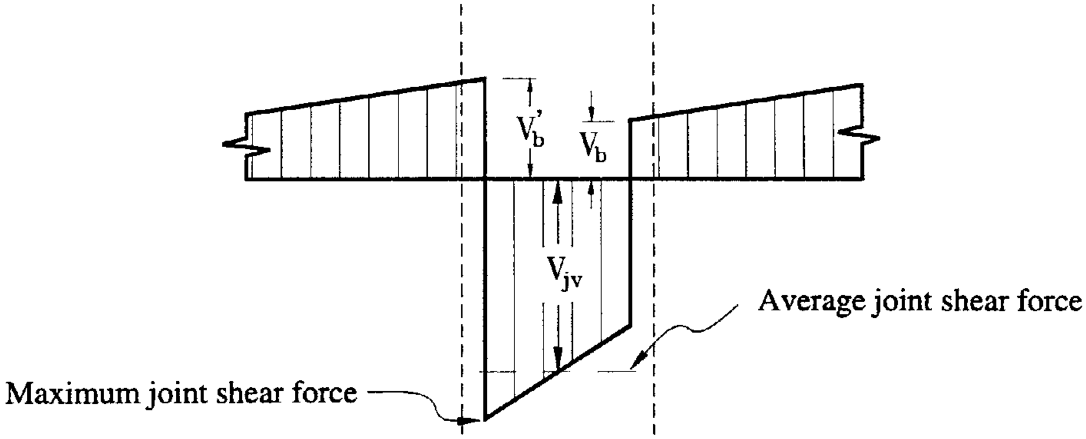
V_b'
V_b
V_jv
Average joint shear force
Maximum joint shear force

(c) Variation of vertical shear force

Figure 4.2 Comparison of average and maximum joint shear forces in a bridge tee joint [19].

Figure 4.3a shows the equilibrium condition of an interior cap beam/column joint and an idealized joint compression strut resulting from compression forces in members framing into the joint. The joint strut, in reality, will consist of a discrete number of distributed compression struts separated by diagonal cracks, and the boundaries of the struts will tend to be curved in the plane of loading. It was considered that column bars in compression, and tension bars carrying 50 percent of the total tension force, located obviously nearest to the neutral axis of the column section, can be anchored by bond into the diagonal compression strut. For the remaining 50 percent of the column tension force, which is likely to have anchorage problems due to large pull out forces in the reinforcement and small depth of the compression strut at the upper right hand corner, a force transfer mechanism illustrated in Figure 4.3b was envisaged [19,23]. The principal element of this mechanism is the development of compression strut D2. This external strut along with the internal joint strut D1 were assumed to provide a clamping effect to the extreme column tension reinforcement. Assuming that vertical components of struts D1 and D2 were equal and approximating the tension force of a circular section at its ultimate strength to:

$$T_c \approx 0.5\lambda_0 A_{sc} f_{yc} \tag{4.4}$$

where λ_0 is the overstrength factor of the column longitudinal steel, A_{sc} is the total area of the column bars and f_{yc} is the yield strength of longitudinal column reinforcement, the following reinforcement requirements were satisfied [19,23]:

- Area of external vertical stirrups required outside the joint was $0.16A_{sc}$. It was considered that this external joint reinforcement be placed over a distance equal to half the cap beam depth. The reinforcement provided to resist shear in the cap beam is not likely to be fully utilized under positive moment, and thus the reserve capacity of the cap beam shear reinforcement was supplemented towards the area of steel required outside the joint for force transfer.

- Although no vertical joint reinforcement was required by the mechanism, vertical reinforcement amounting to $0.08A_{sc}$ was placed within the joint to avoid severe joint cracking and to provide lateral resistance against buckling of the longitudinal top beam bars.

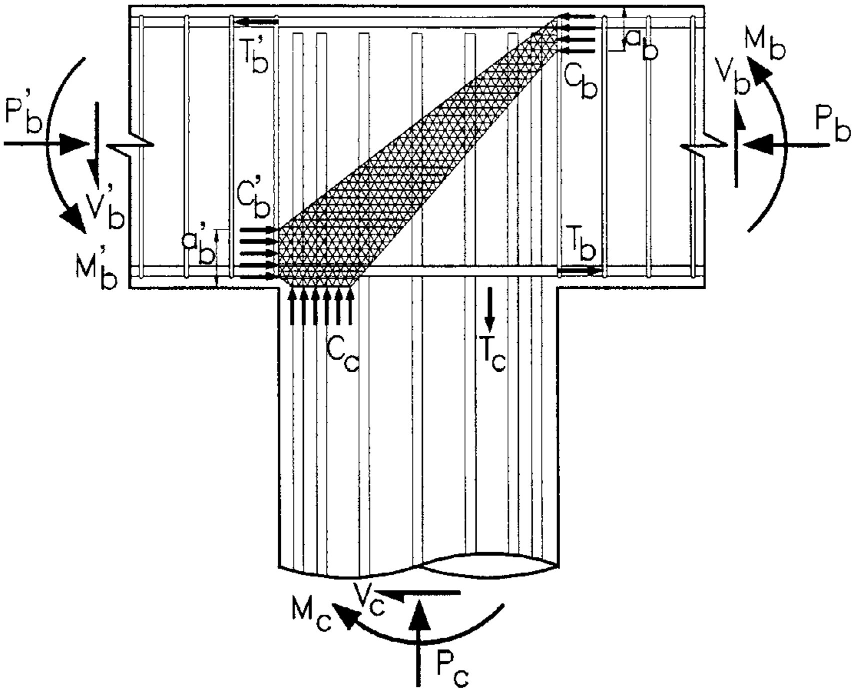

T'b
ab
Mb
Cb
Vb
P'b
Pb
C'b
V'b
a'b
Tb
M'b
Cc
Tc
Mc
Vc
Pc

(a) Member end forces and an idealized joint strut.

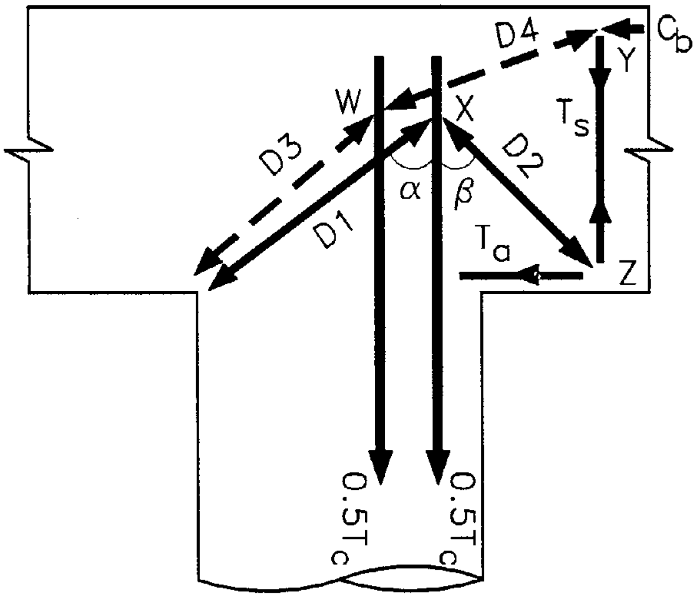

D4
Cb
Y
W
X
Ts
D3
D2
α
β
D1
Ta
Z
0.5Tc
0.5Tc

(b) Design force transfer mechanism.

Figure 4.3 Bridge column/cap beam tee connection.

- Volumetric ratio of the joint horizontal reinforcement, ρ_s, was obtained as follows:

$$\rho_s = \frac{0.3A_{sc}\lambda_o f_{yc}}{f_{yh} l_a^2} \tag{4.5}$$

where l_a is the anchorage length of the column bars in the joint, f_{yh} is the yield strength of spiral. This provision was to account for the unbalanced horizontal force induced at node X by struts D1 and D2 (Figure 4.3b).

- A minimum ρ_s value as given by Eq. 4.6 was ensured to provide some tensile resistance when cracking occurs in the joint region:

$$\rho_s = \begin{cases} \dfrac{0.29\sqrt{f_c'}}{f_{yh}} & \text{(SI units)} \\ \dfrac{3.5\sqrt{f_c'}}{f_{yh}} & \text{(psi units)} \end{cases} \tag{4.6}$$

where f_c' is the compressive strength of concrete. This minimum joint spiral requirement is about 50 percent of that recommended in the ACI code [3] for building joints when a compressive strength of 34.5 MPa (5 ksi) is considered.

- Additional bottom longitudinal beam reinforcement equivalent to $0.08A_{sc}$ was provided for the stability of strut D2 at node Z (Figure 4.3b).

- It was also considered that the column bars should be extended into the joint as close to the top of the beam as possible with a minimum embedment length, l_a, as given by the following equation:

$$l_a \geq \begin{cases} 0.30 d_{bl} f_{yc} \Big/ \sqrt{f_c'} & \text{(SI units)} \\ 0.025 d_{bl} f_{yc} \Big/ \sqrt{f_c'} & \text{(psi units)} \end{cases} \tag{4.7}$$

where d_{bl} is the diameter of longitudinal column reinforcement in mm. The anchorage length requirement given in Eq. 4.7, which assumes an average bond stress of $1.17\sqrt{f_c'}\left(14\sqrt{f_c'}\text{ in psi}\right)$ over the entire bar length embedded into the joint [19], provides a much reduced development length than that obtained from the ACI code [3] and Caltrans design specification [4].

Considering equilibrium at node Y (Figure 4.3b), it is obvious that the compression force C_b no longer acts horizontally at the cap beam/joint interface. Instead, the tension force T_s redirects C_b towards node W. The change of direction of the strut creates an additional clamping effect for the longitudinal column tension reinforcement, particularly for those located furthest from the extreme tension fiber of the column section. Experimental evidence of this phenomenon has been reported from tests on large-scale knee joints [8].

4.2 Reinforcement Detailing

The reinforcement detailing of the test unit is shown in Figure 4.4. Additional steel which was provided in the load stub and in 610 mm (24 in.) long support regions of the beam to avoid any undesirable failure due to stress concentration, are not shown. Horizontal ties and some short longitudinal bars were placed in the load stub while vertical stirrups required to carry the maximum reaction at the supporting points were provided at the ends of the beam to avoid shear failure.

Description of the reinforcement in each structural member is presented below while the construction of the test unit is shown in Figure 4.5.

4.2.1 Column

The reinforcement of the column was 14#7 ($d_b = 22.2$ mm) longitudinal bars and #3 ($d_b = 9.5$ mm) spiral at 96.5 mm (3.8 in.) pitch. This corresponded to longitudinal steel ratio of $\rho_l = 0.0186$ with volumetric transverse reinforcement ratio of $\rho_s = 0.0052$. Due to the difference in the grade of steel used in the Santa Monica Viaduct and in the test units, the longitudinal steel content provided in this column was about 53 percent of that in the prototype structure (Section 3.2.2), resulting in similar scaled flexural strengths.

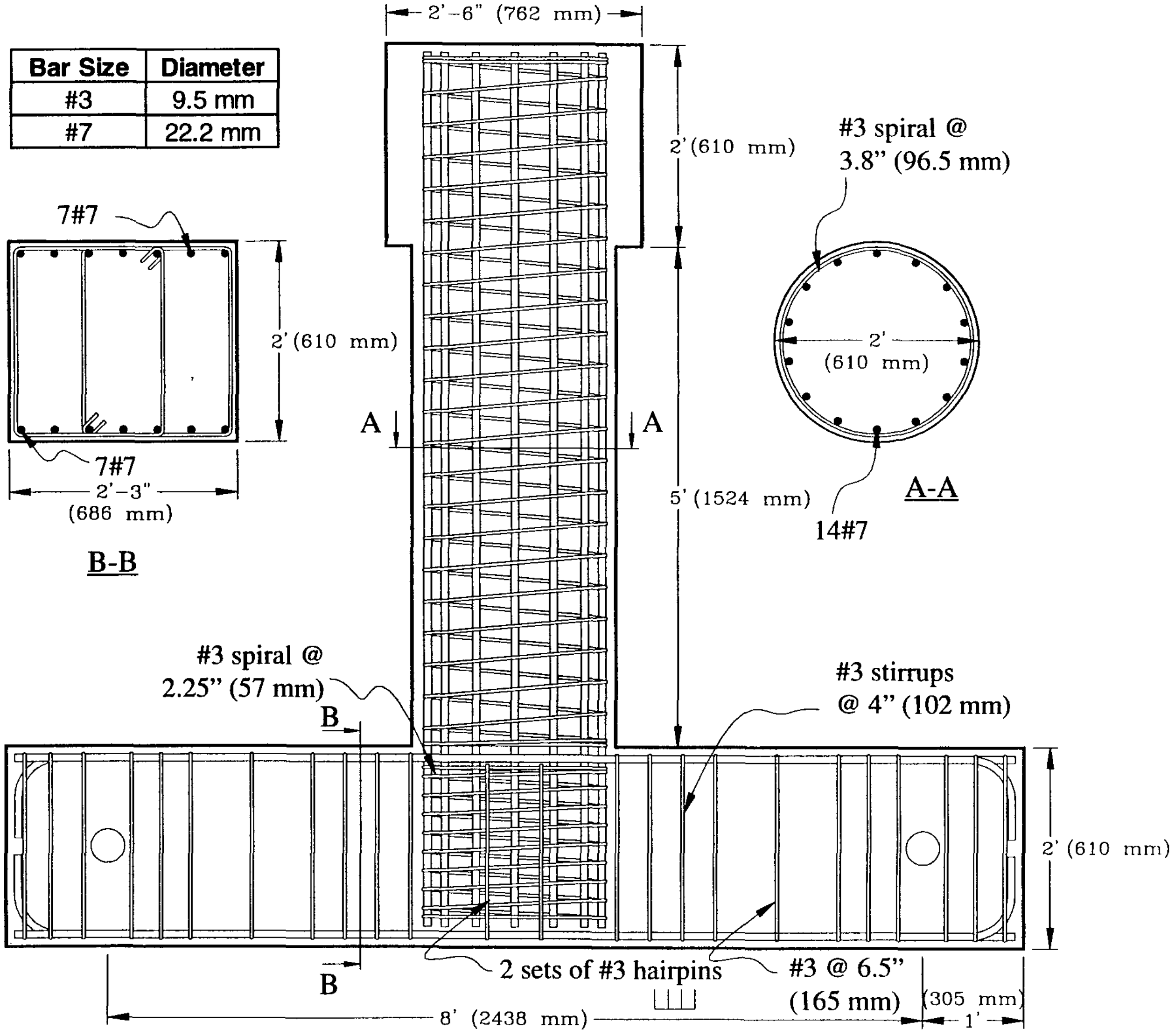
2'-6" (762 mm)
2'(610 mm)
5'(1524 mm)
#3 spiral @
3.8" (96.5 mm)
2'
(610 mm)
14#7
A-A
A
A
7#7
2'(610 mm)
7#7
2'-3"
(686 mm)
B-B
#3 spiral @
2.25" (57 mm)
B
B
#3 stirrups
@ 4" (102 mm)
2' (610 mm)
2 sets of #3 hairpins
#3 @ 6.5"
(165 mm)
(305 mm)
1'
8' (2438 mm)

Bar Size	Diameter
#3	9.5 mm
#7	22.2 mm

Figure 4.4 Key reinforcement details of the test unit with a reinforced concrete cap beam.

4.2.2 Cap Beam

The cap beam was reinforced with 7#7 (d_b = 22.2 mm) bars longitudinally at the top and bottom. There were only 5#7 tension bars required at the top (as constructed) to resist the positive moment and the remaining two bars were placed to support the joint force transfer mechanism as illustrated in Section 4.1.3. Shear design of the cap beam required only the nominal steel content, which was limited to $\mathbf{A_v/b_ws = 0.002}$. This was interpreted as 4 legs of #3 (d_b = 9.5 mm) stirrups at 203 mm (8.0 in), but a spacing of 165 mm (6.5 in.) was only feasible in the test unit. A reduced spacing of 102 mm (4 in.) was used for the stirrups in the beam region adjacent to the joint interface in order to satisfy the external vertical joint reinforcement requirement discussed in Section 4.1.3. This requirement resulted in 12.2 legs of #3 reinforcement be placed over 305 mm (12 in.) length along the beam from the joint interface and a total of 4 sets of 4 legs #3 stirrups were placed. No additional stirrups was considered necessary to satisfy the nominal shear reinforcement requirement in this portion of the beam. In Figure 4.6, the closely spaced beam transverse reinforcement adjacent to the column face can be identified.

4.2.3 Interior Joint

Volumetric ratio of horizontal reinforcement required in the joint, as obtained from Eq. 4.5, was 0.065. However, a larger reinforcement ratio of 0.087 was used, which was satisfied by a #3 (d_b = 9.5 mm) spiral @ 57 mm (2.25 in.) spacing. An increased amount of transverse joint reinforcement was provided because the design was originally performed for the prototype structure assuming a transverse rebar yield strength of 303 MPa (44 ksi) and the transverse reinforcement content was not later modified consistent with increased yield strength of 455 MPa (66 ksi). Also, a strength reduction factor of 0.85 was initially considered in the prototype design. Considering that no strength reduction factor is required in the joint design based on force transfer models, it is suggested that the above detailing resulted in 28 percent more steel in the test unit than is required by Eq. 4.5. According to the joint detail described in Section 4.1.3, nominal vertical reinforcement containing 8 legs #3 rebar was provided within the joint. Since this requirement was to control crack width in the joint region and to provide resistance against buckling of the longitudinal bottom (as cast) beam reinforcement, hairpin type stirrups, instead of closed ties, were used.

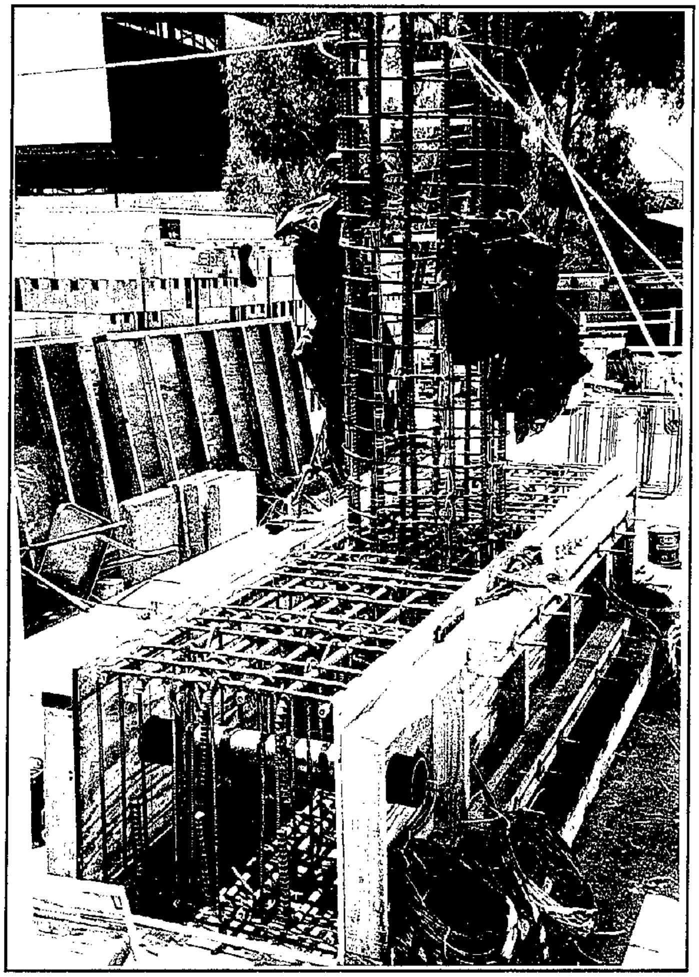

Figure 4.5 Construction of test unit IC1.

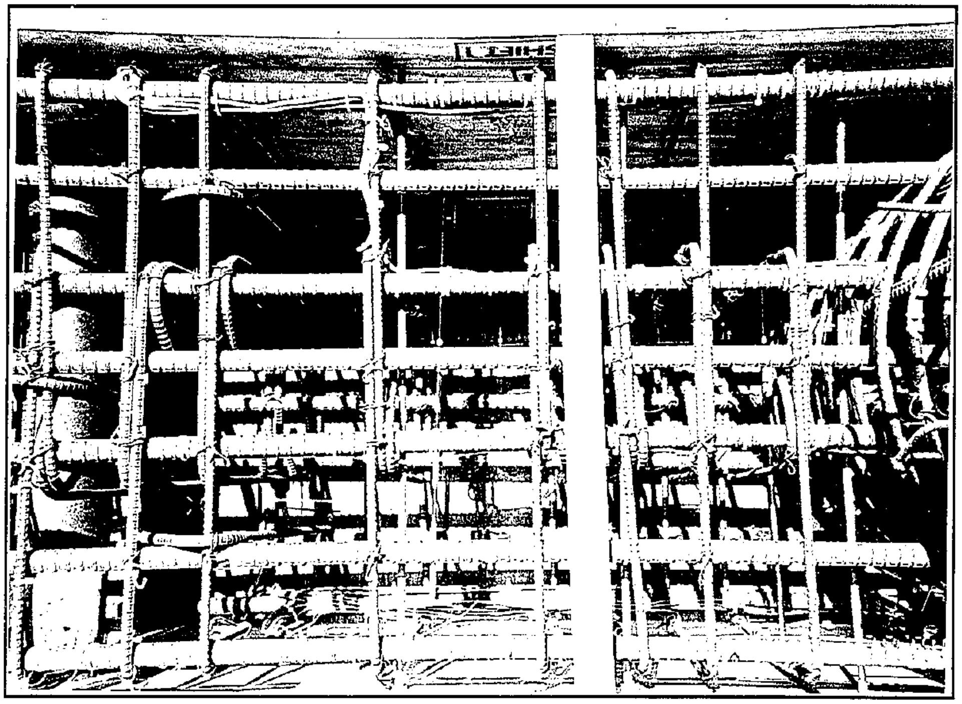

Figure 4.6 Transverse reinforcement detail in the cap beam adjacent to the joint.

Reproduced from best available copy.

The longitudinal column bars were extended into the joint as close to the top (i.e. bottom as constructed) of the beam as possible (Figure 4.4). Premature termination of column steel into the joint, as can be seen in the SM3 detailing (Figure 3.5), will not effectively anchor the column bars in the joint compression strut (Figure 4.3a) and should be avoided. The longitudinal column bars were extended into the joint up to 60 mm (2.375 in.) from the bottom (as cast) of the beam. This provided an embedment length of 550 mm (21.625 in.) which was almost the minimum required anchorage length for #7 (d_b = 22.2 mm) rebars according to Eq. 4.7.

4.3 Material Properties

Material properties of concrete and steel used in the test specimen were established from testing at UCSD's Charles Lee Powell Laboratory. The compression strength of concrete was measured at 7 days, 28 days and on the day of testing (D.O.T). Results are listed in Table 4.1. Each value in this table represents an average strength obtained from three unconfined concrete cylinders (152.4 mm diameter x 304.8 mm height), which were cast during the concrete pour. Tensile strength of concrete was not experimentally measured and this was taken as $\mathbf{0.62\sqrt{f_c'}}$ MPa $\left(\mathbf{7.5\sqrt{f_c'}} \text{ in psi units}\right)$ [14].

Table 4.1 Compressive strength of concrete used in test unit IC1.

Member	7 days		28 days		Day of Testing	
	MPa	ksi	MPa	ksi	MPa	ksi
Column	25.4	3.69	30.6	4.43	31.4	4.56
Cap beam and Joint	-	-	36.5	5.29	39.7	5.76

Uniaxial tensile testing was performed on three randomly selected coupons for each bar type and for each coupon a complete stress-strain relation was obtained until the peak stress was attained. The standard length of the sample was 914 mm (36 in.) except for the beam ties where 559 mm (22 in.) long specimens were used. The samples obtained from column and joint spirals did not have clearly defined yield points, which was expected since they were deformed prior to the testing in the process of making spirals.

Table 4.2 shows the average yield and ultimate strengths established for all the reinforcement.

Table 4.2 : Yield and ultimate strength of reinforcing steel of test unit IC1.

Description	Size	Yield Strength		Ultimate Strength	
	(diameter in mm)	MPa	ksi	MPa	ksi
Longitudinal column bar	#7 (22.2)	448	65.0	738	107.0
Column spiral	#3 (9.5)	431	62.5	669	97.0
Longitudinal beam bar	#7 (22.2)	433	62.8	726	105.3
Beam stirrups	#3 (9.5)	439	63.6	722	104.7
Joint spiral	#3 (9.5)	411	59.6	665	96.4

4.4 Predicted Response

Overall behavior of the test unit was predicted prior to the testing using the procedure outlined in Section 2.9. The expected response of unit IC1 is presented in the following sections.

4.4.1 Cracking under Gravity Load

Flexural cracking was expected in the cap beam when the gravity load of 400 kN (90 kips) was applied as a concentrated axial force in the column. No cracking was, however, expected within 813 mm (32 in.) from beam ends.

4.4.2 Cracking in the Column

Assuming that the concrete compressive strength of column on the day of testing would be 34.5 MPa (5 ksi) and that the tensile cracking strength would be 3.65 MPa (0.53 ksi), the flexural cracking capacity of the column was estimated to be 132 kNm (97 kips-ft). This corresponded to a horizontal actuator load of 72 kN (16.2 kips).

4.4.3 Cracking in the Cap Beam

Flexural cracking was expected in the bottom (as tested) of the beam under gravity load (Section 4.4.1). When the cap beam positive moment due to gravity and seismic exceeds the cracking moment, flexural cracks were expected to form on the top of the beam. A horizontal load required to cause flexural cracking at the top (as tested) of the cap beam was estimated to be 458 kN (103 kips), which was greater than the predicted theoretical ultimate horizontal force. Therefore, flexural cracking on the top of the beam was expected to develop only if the actual column capacity exceeds the theoretical ultimate moment by 8 percent.

4.4.4 Cracking in the Joint Region

Assuming that the first joint cracking should correspond to the horizontal load that induces maximum principal tensile stress of $0.29\sqrt{f'_c}$ MPa $\left(3.5\sqrt{f'_c} \text{ in psi units}\right)$, joint cracking was predicted at an actuator force of 222 kN (50 kips) in the push direction (see Appendix A for calculations). This horizontal load was about 60 percent of the ideal force estimated for the subassembly. The first joint cracking was expected in the push direction because the joint was subjected to axial tension in the horizontal direction. An axial compression is developed in the joint when the loading direction is reversed, and therefore cracking in the joint was expected at a higher lateral load in the pull direction.

4.4.5 Force-Displacement Response

The overall inelastic force-displacement envelope of the test unit was composed by calculating the response at several points in accordance with the procedure outlined in Chapter 2. These data points included events corresponding to flexural cracking in the beam under gravity, flexural cracking in the column, yielding of the column reinforcement and ultimate capacity of the column. Since the cap beam axial force varied in the push and pull direction of loading (Figure 4.1), for a given actuator force, the horizontal displacement in the two directions differed marginally. The predicted envelope of the force-displacement curve is shown in Figure 4.17a along with the experimentally measured force-displacement response (see Appendix B for numerical values, and predicted member and system ductility capacities).

4.5 Observation During the Test

The test unit was simply supported as discussed in Section 3.2.3 and subjected to a prescribed (Figure 3.27) transverse cyclic displacement pattern using a hydraulic actuator as shown in Figure 4.7 (also see Figure 3.20). The experimental observations made during the test are summarized in this section with the assistance of some photographic illustrations. In figures showing the photographs, ends of cracks were marked with a transverse bar and the corresponding load in kN or displacement ductility of the system. The damage of the test unit was observed at the peak displacements in the first and third loading cycles. The cracks, which were marked in the third cycle, were differentiated from those observed in the first loading cycle by adding a superscript "3" to the label indicating the system ductility (e.g. $\mu 1$ and $\mu 1^3$ represent cracks which developed at ductility one in the first and third loading cycles respectively). Also note that cracking corresponded to the push direction loading was marked in black while the pull direction cracks were identified in red. This procedure for marking cracks on the specimen was used consistently in all three redesigned units.

4.5.1 Application of Dead Load

Three flexural cracks formed in the cap beam when the axial load was applied in the column. Two of these cracks developed at the opposite column faces and the third crack formed in the center region of the joint. All three cracks were visible to half way up the beam depth. They were marked in green and can be seen in Figure 4.8. This behavior corresponded well with the predicted response in Section 4.4.1.

4.5.2 Force Control

Theoretical horizontal force required to induce yielding of the column reinforcement was applied in four steps. In each step, the force was cycled once. The observation made in each cycle is briefly described below:

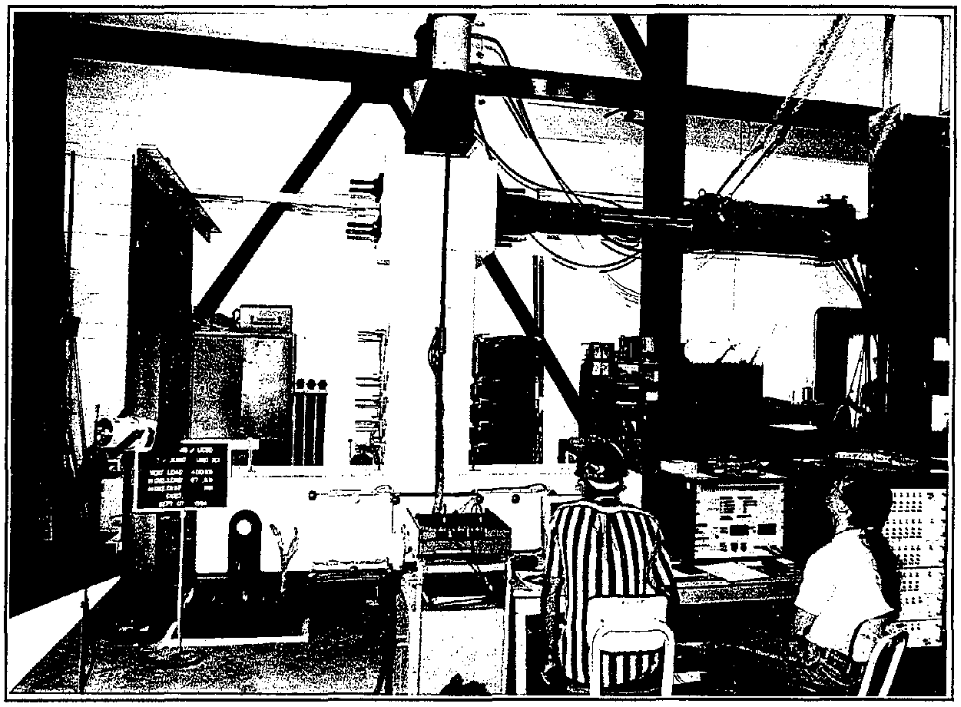

Figure 4.7 Overall test set up of interior test unit IC1.

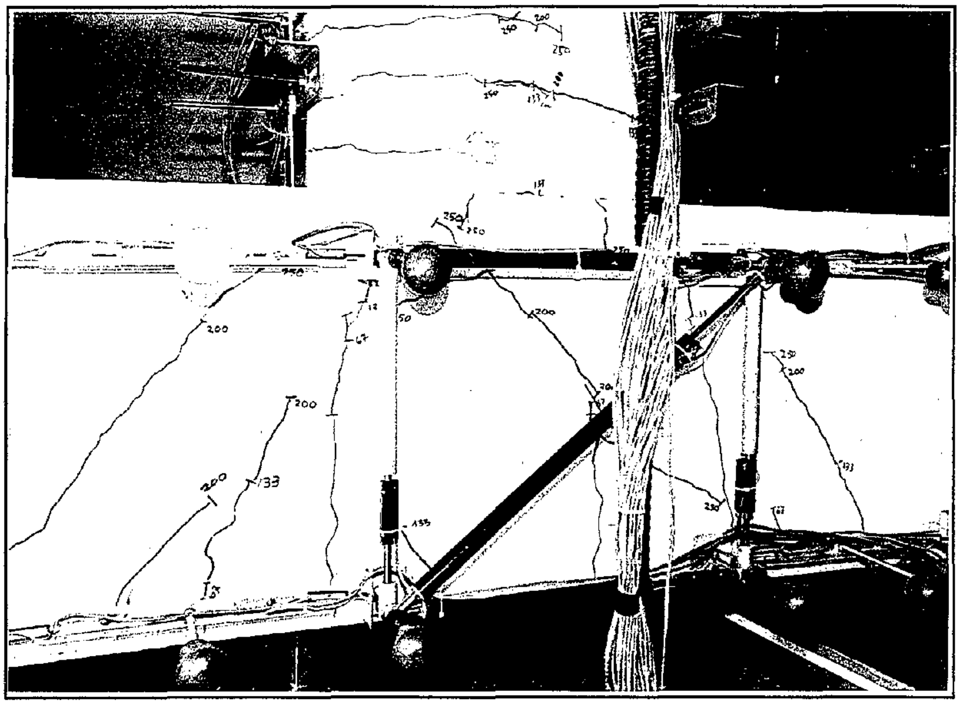
200
250
250
200
200
200
133
50
200
250
200
250

Figure 4.8 Cracking in the joint region at early stages of testing.

Reproduced from best available copy.

± 67 kN (15 kips)

No visible cracking developed in the joint or in the column of the test unit. Minor extension to the cap beam flexural cracks, which were formed under gravity load, was observed. In addition, new flexural cracks, one on either side of the joint, formed at the bottom (as tested) of the beam (Figure 4.8).

± 133 kN (30 kips)

There was still no joint diagonal cracking occurred. Flexural cracks developed on both sides of the column within 610 mm (24 in.) distance from the joint interface and equally spaced at an interval of about 152 – 178 mm (6 – 7 in.). Beam flexural cracks further extended some with inclination, indicating flexural-shear behavior (Figure 4.8).

± 200 kN (45 kips)

First joint cracking occurred at this horizontal force, which is 10 percent less than the predicted value in Section 4.4.4. In the push direction loading, inclined fine diagonal cracks, one on each side of the joint, were observed (Figure 4.8). No joint shear cracking was, however, visible under the pull direction. This was expected as the push direction loading applied a horizontal tension force in the joint while the pull direction loading induced an axial compression force. Significantly large inclined shear cracks were noticed in the cap beam. Some new flexural cracks and extension to old cracks were observed in the column.

± 250 kN (56 kips) - First Yield

Inclined shear cracks were first noted in the column as extensions to the flexural cracks which were formed in the previous load steps. Joint cracking observed under the horizontal load of +200 kN (45 kips) extended across the joint from corner to corner (Figure 4.8). First diagonal joint shear cracking was apparent in the pull direction loading which can be seen in Figure 4.9b. In both loading directions, vertical cracks developed in the joint, running from the column/joint interface for a depth of about 75 mm (3 in.) (see Figure 4.8).

4.5.3 Displacement Control

The displacement corresponding to ductility $\mu_\Delta = 1$ was estimated to be 17.1 mm (0.673 in.) using Eq. 3.5. The control of the system was now based on the horizontal displacement, which was increased to obtain appropriate ductilities. At each ductility level, a minimum of three cycles were applied. Observations made during this part of the test are described below:

3 cycles at $\mu_\Delta = \pm 1$ ($F_{max} = 284$ kN; $F_{min} = -292$ kN)

During the first displacement cycle, no significant damage was observed, except minor extension to old cracking and a diagonal crack across the joint in the pull direction loading. At this stage, it was noted that joint had cracked from corner to corner on both east and west sides in the two loading directions, and flexural cracks had developed to within 610 mm (24 in.) of point of contraflexure. At the peak displacements in the third cycle, the crack widths in the joint were found to be noticeably high. No new cracks or any significant extension to old cracks were noted in the specimen during subsequent cycling.

3 cycles at $\mu_\Delta = \pm 1.5$ ($F_{max} = 341$ kN; $F_{min} = -357$ kN)

In the first displacement cycle, cracking in the column was limited extension of the old flexural cracks with pronounced shear inclination (Figure 4.9a). Some extension to old cracks and development of new cracks were observed in the joint region (Figure 4.9b). The force resistance of the system dropped suddenly by about 20 kN (4.5 kips) soon after the peak displacement was first reached in the pull direction. No significant changes in the test unit were observed when additional cycles were imposed at this ductility.

3 cycles at $\mu_\Delta = \pm 2.0$ ($F_{max} = 360$ kN; $F_{min} = -376$ kN)

More new cracks and minor extension to old cracks were noticeable in the joint. A few vertical splitting cracks were first observed in the column as a sign of distress resulting from development of large bond stresses around the longitudinal column reinforcement or possibly due to radial dilation as a consequence of shear or confining actions of transverse rebar. When the column displacement was cycled, minor movement in the cover concrete along a crack in the center of the joint was seen. As can be seen in the hysteresis plot

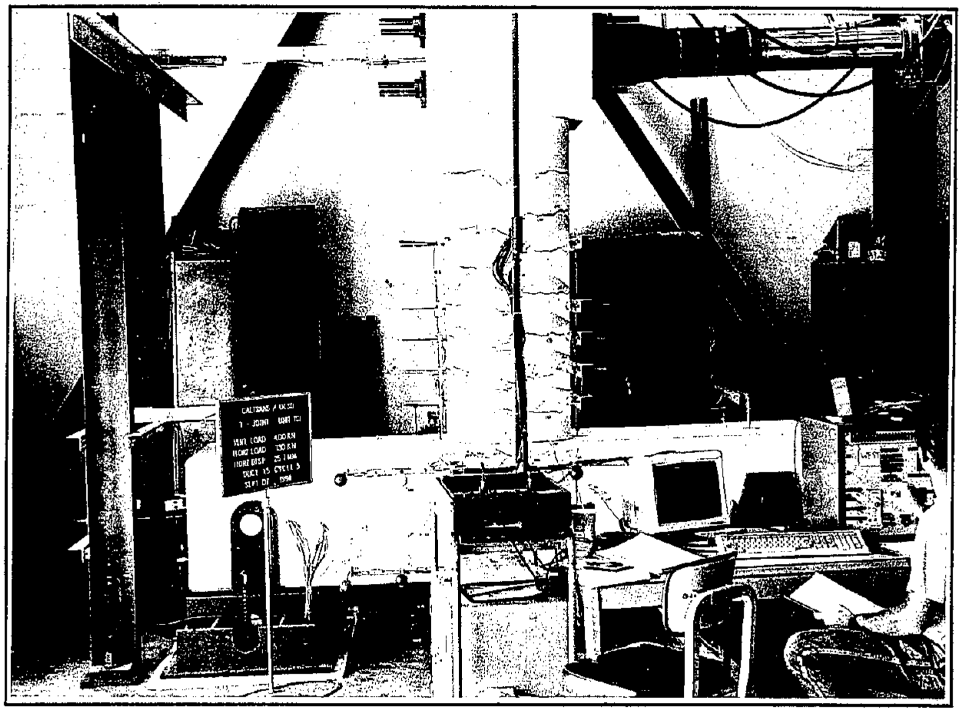
CALTRANS / UCSD
T - JOINT UNIT IC1
VERT LOAD 400 KN
HORZ LOAD 130 KN
HORZ DISP 25.7 MM
DUCT 1.5 CYCLE 3

(a) Cracking in the column

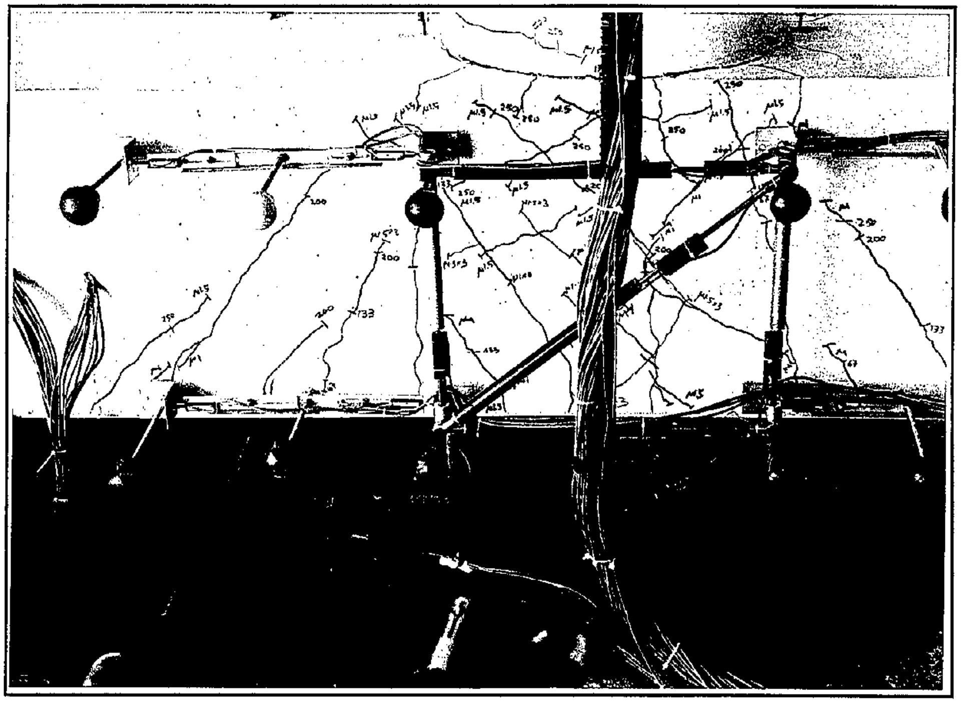

(b) Cracking in the joint and cap beam

Figure 4.9 Test unit IC1 at the end of 3rd cycle at $\mu_\Delta = 1.5$.

Reproduced from best available copy.

shown in Figure 4.17a, minor slipping in the system was encountered in the pull direction loading. It was suspected that this was caused due to the loose fit of the pin supporting the beam at the southern end (Figure 3.20). Driving a 0.635 mm (0.025 in.) thick aluminum plate between the steel tube and the pin did not appear to solve the problem.

3 cycles at $\mu_\Delta = \pm 3.0$ ($F_{max} = 381$ kN; $F_{min} = -402$ kN)

Crushing of cover concrete at the base of the column occurred when the displacement was first taken to the maximum in each direction. During the first cycle, crack width in the tension side of the column was found to be in excess of 1 mm (0.04 in.). Also the cracks, particularly in the center of joint opened up significantly, but the maximum crack width appeared to be smaller than that observed in the column. When the displacement was cycled, further damage was observed. At the peak displacements during the third cycle, first indication of concrete crushing in the joint, a considerable number of vertical splitting cracks in the column, and a shear crack in the beam at the north end of the support were seen. Crack widths at the base of the column and at 152 mm (6 in.) up the column from the joint interface reached about 3 mm (0.12in) and 2.5 mm (0.04 in.) respectively at the peak displacements. Corresponding crack width in the joint was about 1.5 mm (0.06 in.). At this stage, a uniformly distributed pattern of cracks had developed in the joint region (see Figure 4.10).

3 cycles at $\mu_\Delta = \pm 4.0$ ($F_{max} = 391$ kN; $F_{min} = -406$ kN)

During the first cycle at this ductility, a considerable number of new vertical splitting cracks in the column were seen. Extension of cracking was found to be common in the test unit. There was a flexural crack formed at the column/load stub interface. At the base of the column, the crack width was about 6 – 7 mm (0.24 – 0.28 in.). As the horizontal actuator load approached zero at the end of first cycle, the residual displacement of about -30 mm (-1.18 in.) was recorded, and all of the joint cracking appeared to be almost closed. The actuator load required to bring the column back to its original position was about 100 kN (22.5 kips). Spalling of cover concrete first occurred in the column during the third cyclic loading. The damage to the joint, as the number of cycles increased, was limited to minor extension of cracking. The condition of joint at the end of displacement cycle at this ductility appeared to be satisfactory (Figure 4.10).

3 cycles at $\mu_\Delta = \pm 6.0$ ($F_{max} = 410$ kN; $F_{min} = -434$ kN)

Cycle 1

Spalling of cover concrete extended to about 200 – 250 mm (7.9 – 9.8 in.) up the column from the interface. Minor spalling of concrete in the joint was seen during the first half cycle. As the column was displaced to its maximum negative value, a significantly large shear crack developed on the west side of the joint, which did not completely close during the load reversal (Figure 4.11). On the east side of the joint, it appeared that a large piece of cover concrete was about to spall off the joint.

Cycle 2

The main shear crack in the joint opened up significantly and a large amount of spalling of concrete in the joint was observed in the negative displacement half cycle.

Cycle 3

As shown in Figure 4.12, the large joint crack, which was formed during the first cycle, opened up significantly. Further spalling of joint cover concrete occurred and one of the two vertical ties provided in the joint was visible. During the second half of the displacement cycle, crushing of the concrete was seen in the cap beam. After spalling off more cover concrete in the column, the transverse reinforcement of the column close to the joint interface was visible. Deterioration of force resisting ability of the system during cycling appeared to be higher than that was observed in the previous ductilities.

4 cycles at $\mu_\Delta = \pm 8.0$ ($F_{max} = 318$ kN; $F_{min} = -357$ kN)

Cycle 1

Large joint shear deformation was seen, which was consistent with an observed drop in the horizontal force resistance of the system, implying joint rotation considerably influenced the displacement measured at the top of the column. In the reverse direction of loading, a large piece of concrete spalled off the joint on the east side (Figure 4.13). At this stage, it was unclear how deep the major joint crack had penetrated into the joint.

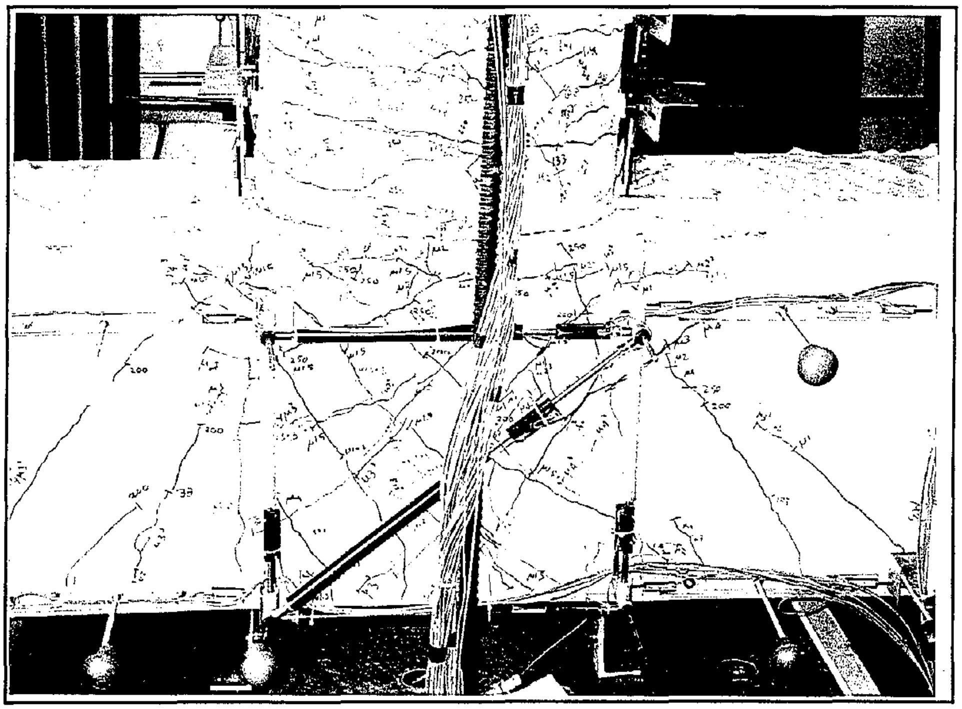

Figure 4.10 Condition of the joint at the end of $\mu_\Delta = 4x3$.

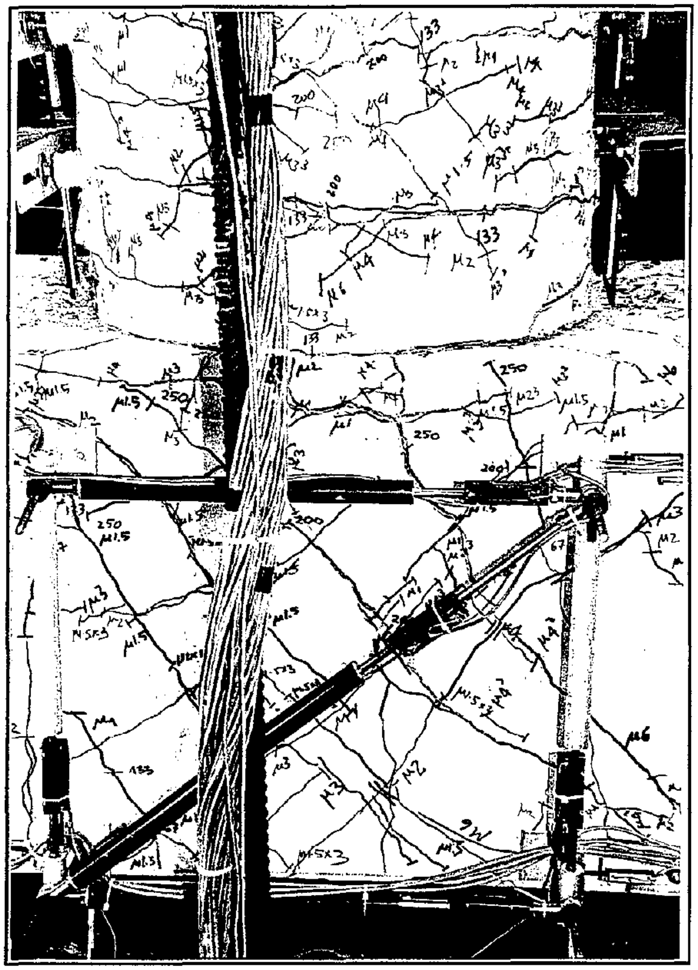

Figure 4.11 Development of major joint cracking during $\mu_\Delta = 6x1$.

Reproduced from best available copy.

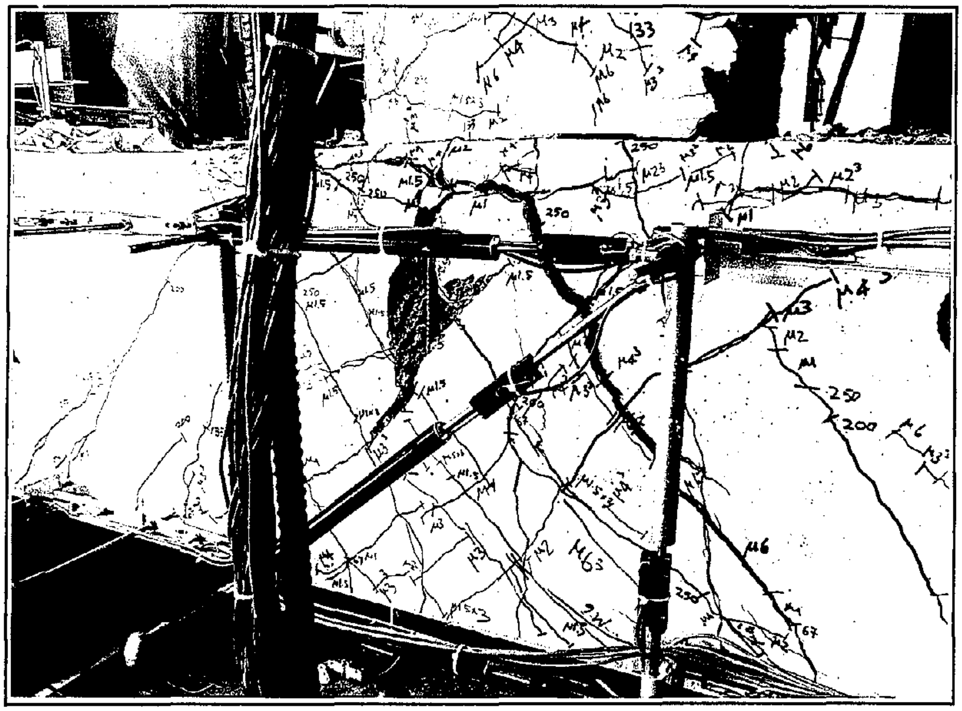

Figure 4.12 Damage on the east face of the joint at $\mu_\Delta = -6x3$. Note that the damage on the west face appeared less severe.

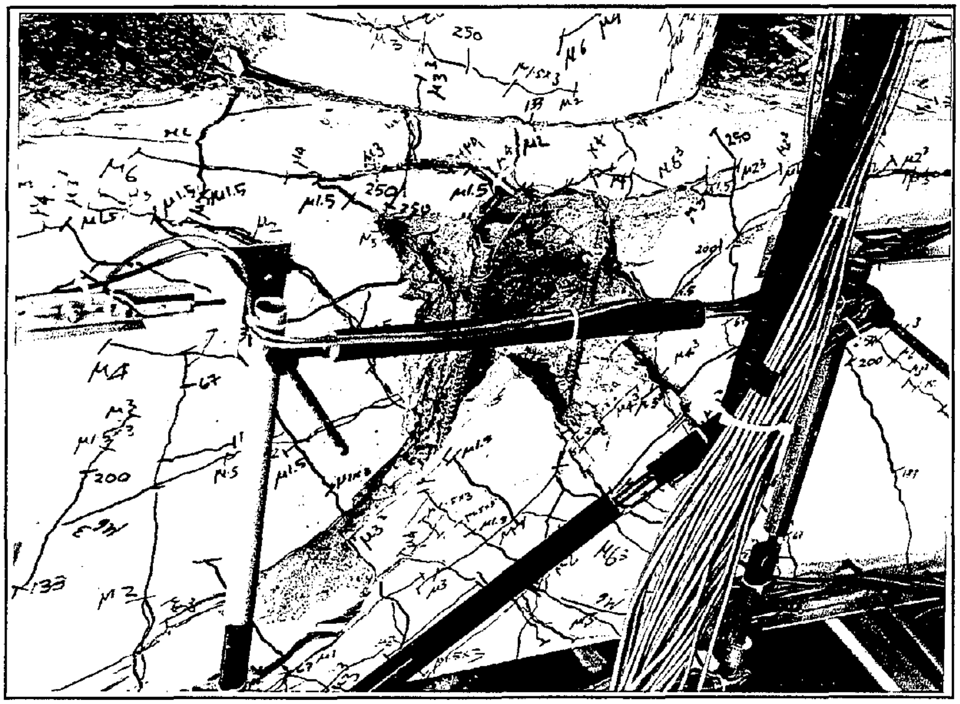

Figure 4.13 Condition of the joint at the end of first cycle at $\mu_\Delta = 8$.

Reproduced from
best available copy.

Some spalling of cover concrete also occurred at the top of the beam just outside the column.

Cycle 2

Loose concrete in the joint was removed before the second cycle and the condition of the test unit after imposing the peak displacement in the push direction is shown in Figures 4.14 and 4.15. Concrete spalling in the west side of the joint took place. A top longitudinal beam bar in the joint region was visible on the east side of the joint and can be seen in Figure 4.15.

Cycles 3 and 4

Further deterioration of the joint was seen. As shown in Figure 4.16, the longitudinal column bars on the south side appeared to have buckled between three spirals in the plastic hinge region. The second column spiral from the joint interface seemed to have almost reached the fracture point.

End of the Test

After removing all the external instrumentation, loose concrete in the joint was removed with a crowbar. The major shear cracks developed in the joint seemed to have penetrated right through the joint (see Figure 7.3). The vertical joint reinforcement provided in the form of hair pins did not provide necessary confinement to the joint core when the cover concrete was spalled off, as they were located outside the joint core.

4.6 Experimental Results

In this section, a summary of the reduced experimental data obtained during the test is presented in graphical form.

4.6.1 Force-Displacement Hysteresis Curve

The force-displacement curve obtained for the test unit and the corresponding hysteresis loop analysis are shown in Figure 4.17. A significant improvement in the energy dissipating ability of the system was achieved when compared to the performance of as-built unit SM3 (see Figure 3.17). The shape and stability of the loops are satisfactory up to a system ductility of 6 which corresponded to a drift of 4.8 percent. At ductility 8, significant strength degradation took place as the damage was mainly concentrated in the joint region (see Section 4.5.3). A good correlation between the predicted and measured force-displacement envelopes was obtained. Within the theoretical displacement capacity obtained from the Mander *et al.* confinement model [13], a satisfactory joint performance was obtained for the test unit. However, it is noted that this confinement model generally underestimates the displacement capacity as can be seen for prestressed units IC2 and IC3.

The area of the force-displacement loop and equivalent viscous damping are shown in Figures 4.17b and 4.17c at different ductilities for the first two loading cycles. The numerical values of the data points used in these figures are given in Appendix C. The area of the hysteretic loop increased almost linearly from ductility 2 to ductility 6. As joint damage increased, a reduction in the area of the hysteresis loop was obtained from $\mu = 6$ to 8. The equivalent viscous damping of the system corresponding to the second cycle increased from 3% at $\mu = 1$ to 22% at $\mu = 8$. A slightly larger damping values were obtained in the first cycle.

4.6.2 Moment-Curvature Response

There were five sets of curvature measurements taken in the column (Section 3.2.5 and Figure 3.25). In Figure 4.18 the moment-curvature relations established from the experimental data and theoretically predicted envelopes are shown for the two sets nearest to the joint interface. Theoretical bending moment within each column curvature cell was not constant and varied linearly. However, the maximum moments applied within the cells were considered as the appropriate bending moments corresponding to the measured curvature. This assumption was also applied to the cap beam.

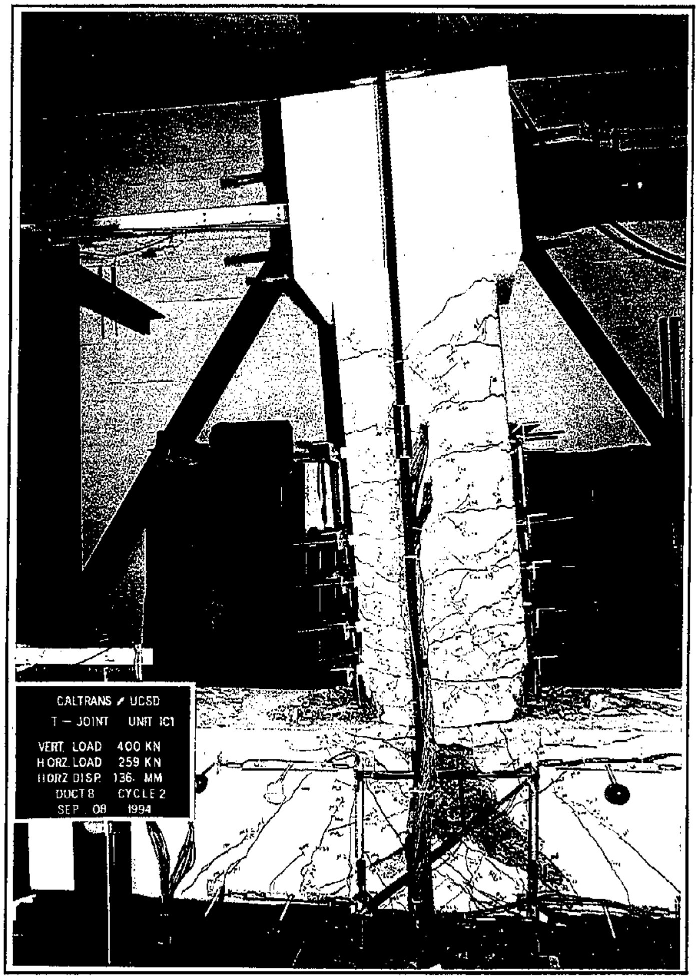
CALTRANS / UCSD
T – JOINT UNIT IC1
VERT. LOAD 400 KN
HORZ. LOAD 259 KN
HORZ. DISP. 136. MM
DUCT 8 CYCLE 2
SEP 08 1994

Figure 4.14 Test unit IC1 at the peak displacement at $\mu_\Delta = 8$.

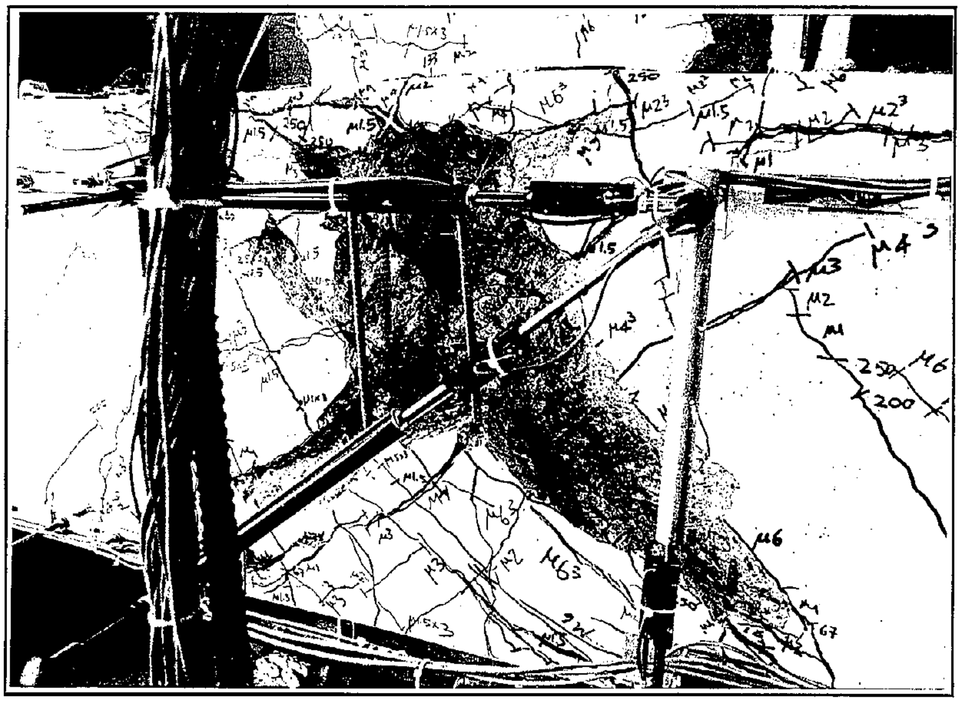
μ4
μ3
μ2
μ1
250
200
μ6
μ6

Figure 4.15 Condition of the joint on the east side at $\mu_\Delta = 8x2$.

Reproduced from best available copy.

Reproduced from
best available copy.

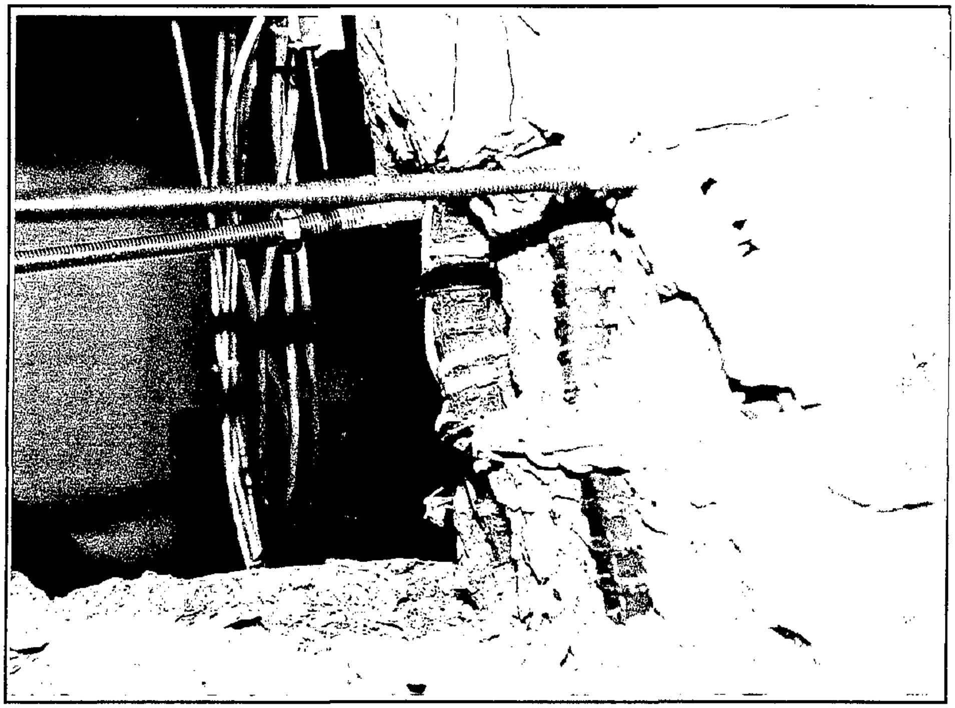

Figure 4.16 Buckling of longitudinal column bars in the hinge region at ductility 8.

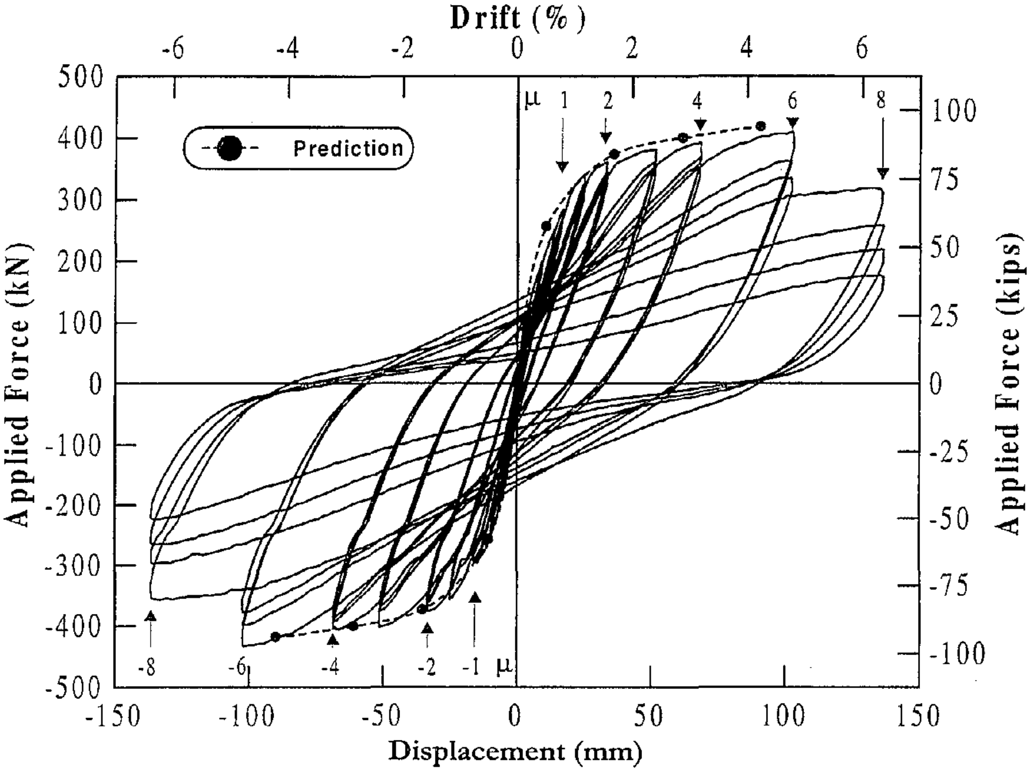

Figure 4.17a Force-displacement hysteresis plot for test unit IC1 accompanied by predicted envelope.

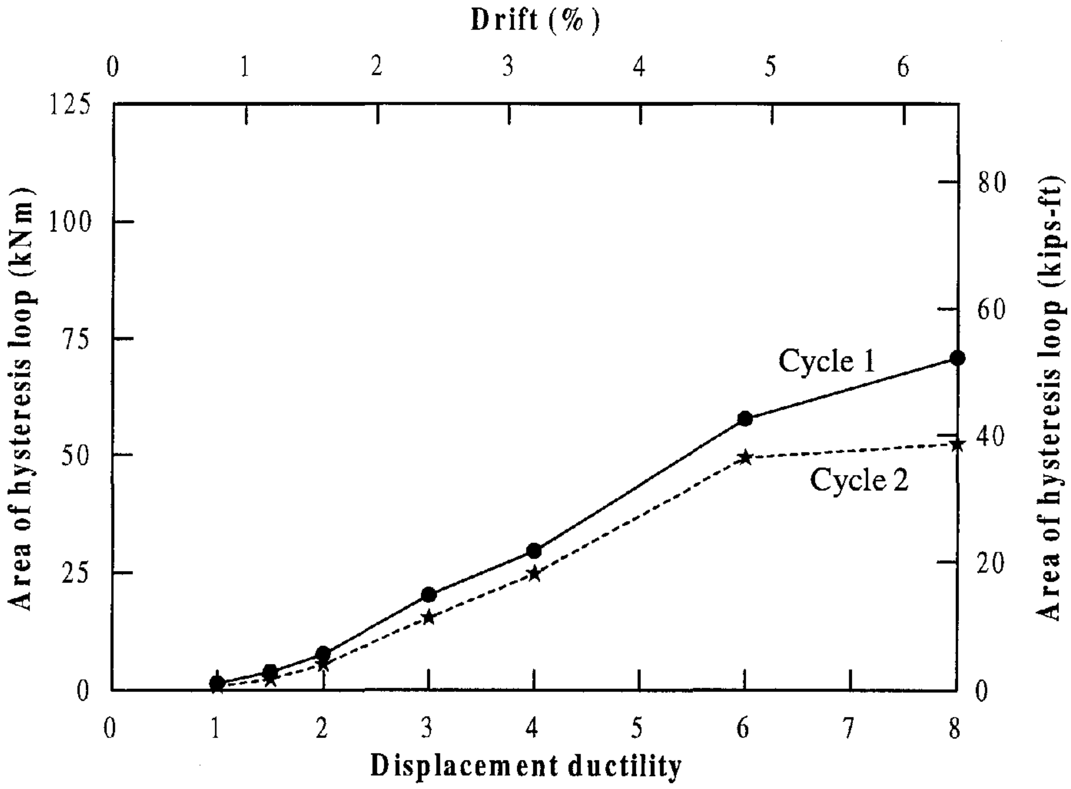

(b) Area of hysteresis loop

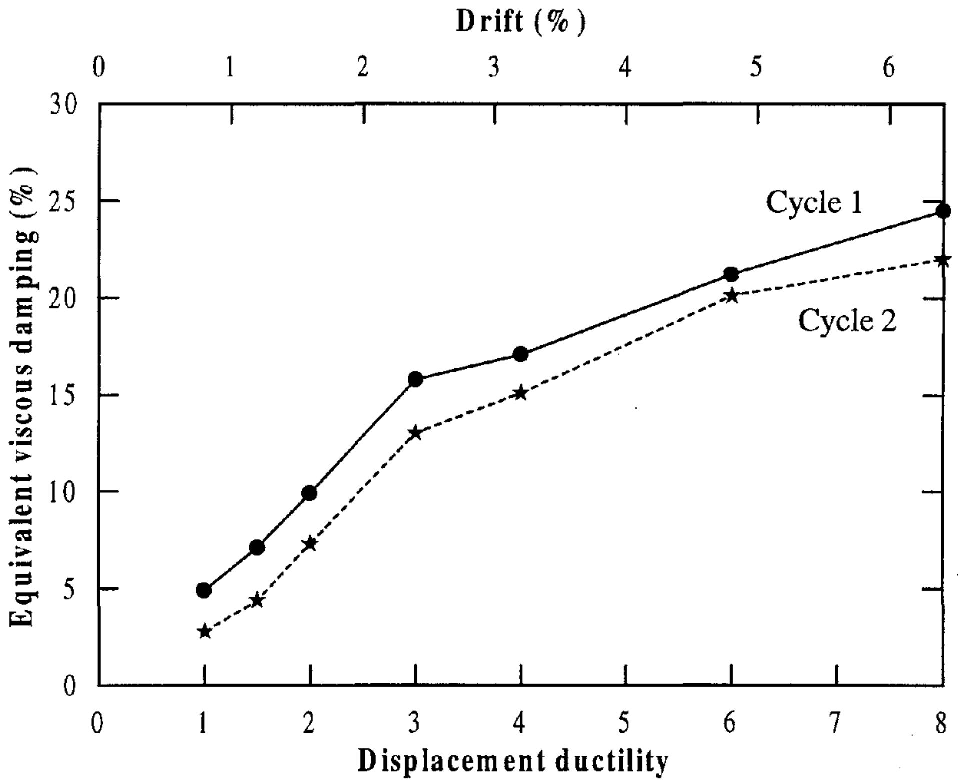

(c) Equivalent viscous damping

Figure 4.17 Force-displacement response and hysteresis loop analysis of unit IC1.

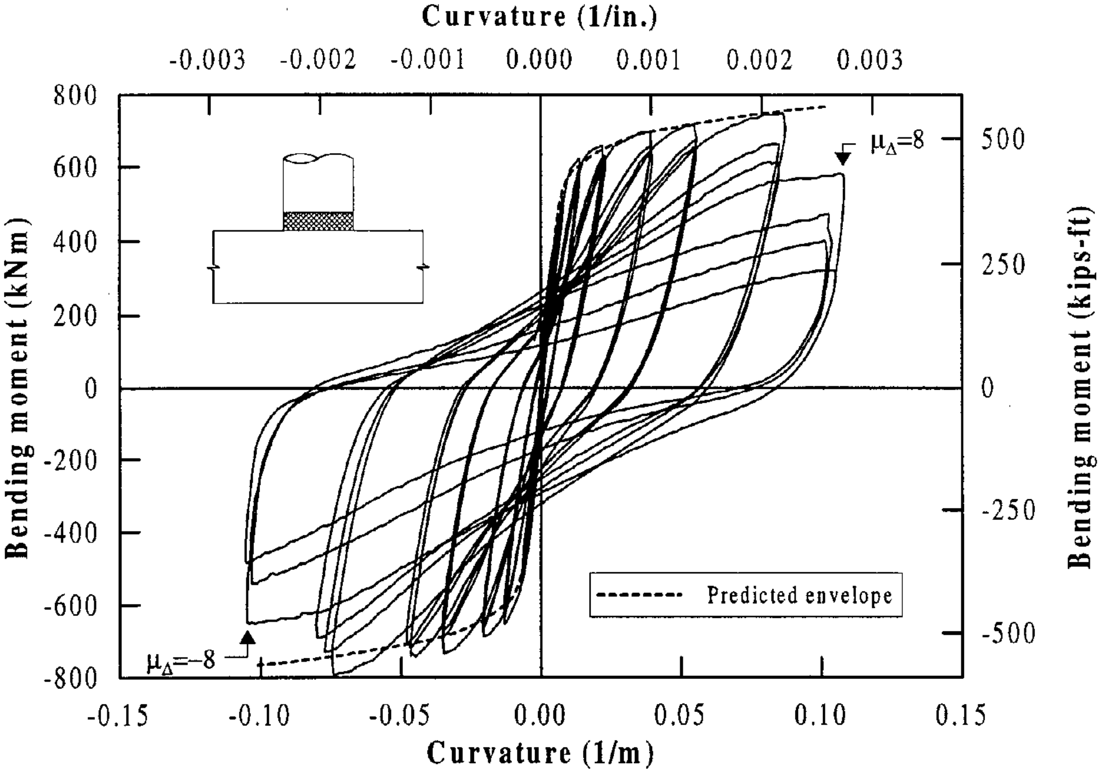

(a) adjacent to the joint interface

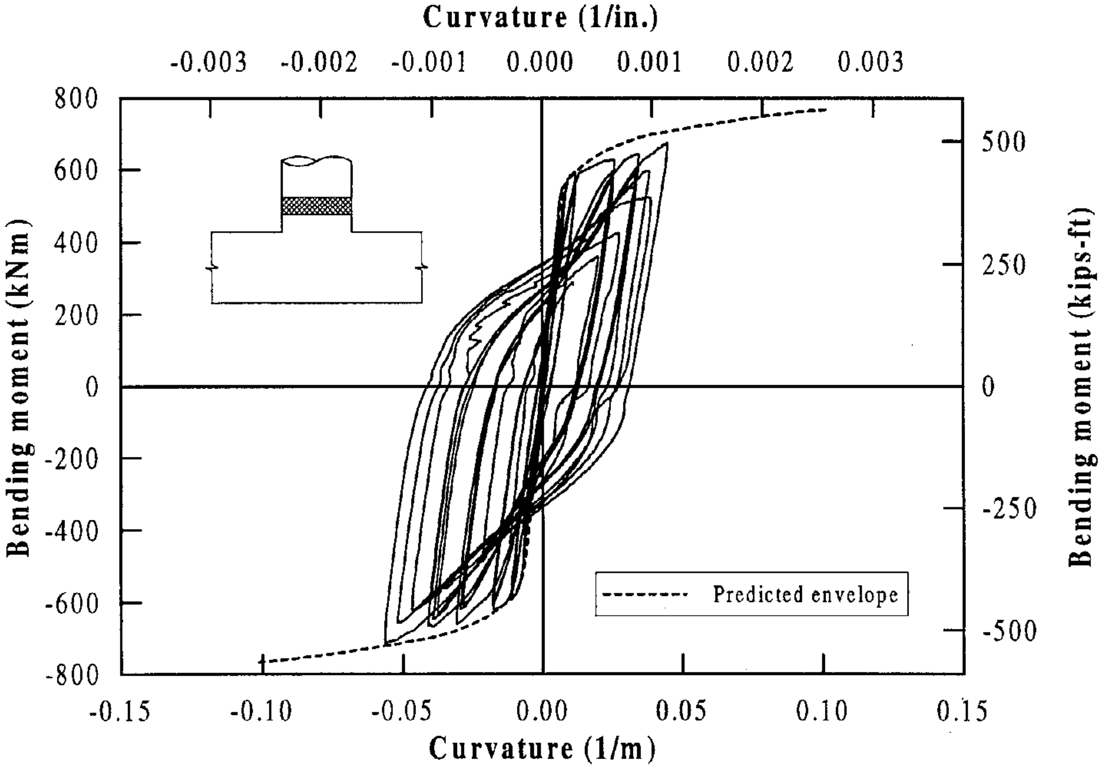

(b) 152 mm (6 in.) away from joint interface

Figure 4.18 Moment-curvature response in two column curvature cells nearest to the joint interface.

It is clear that most of the inelastic action in the column occurred close to the joint interface. Comparing the analytical and experimental moment curvature envelopes, it is seen that a good agreement was obtained for both curvature cells except at ductility 8 for the curvature cell located adjacent to the joint interface, where a much larger curvature was recorded for the applied bending moment. At this ductility, crushing of cover concrete was observed at the top (as cast) of the beam. This would have disturbed the curvature readings of this particular cell. A linear potentiometer in one of the top three curvature cells did not function properly during the test. The remaining two sets of curvature devices showed that inelastic action continuously decreased up the column and essentially a elastic response was obtained within the top cell. This observation can be verified in Figure 4.19 where column curvature profiles recorded during the first cycle at each load step are presented.

As anticipated, curvature measurements taken in the beam remained in the elastic range. A set of measurements obtained adjacent to the right and left sides of the joint are shown in Figure 4.20 along with the predicted envelopes. It is noted that the curvature scale used in this figure is 10 times smaller than that used for the columns in Figure 4.18. The cap beam axial load was zero for the left curvature cell and varied between -410 and +434 kN (i.e. between -92 kips and +98 kips) in the right curvature cell. However, the prediction of the envelope in the right curvature region was made using constant axial loads of -410 kN and +434 kN for the positive and negative moments respectively.

4.6.3 Joint Deformation

Two of the linear potentiometers attached on the east joint panel malfunctioned almost from the beginning of the test. Hence, the panel deformations obtained on the west side of the joint were used for deformation calculations. Joint stresses and strains, overall joint deformations, and independent deformation modes were obtained and they are represented in Figures 4.21 – 4.29.

In Figure 4.21 the variation of the maximum and average shear stresses calculated for the joint based on the experimental data are shown with respect to the column displacements. As was expected from the hysteretic response (Figure 4.17a), shear stresses increased until the column displacement corresponding to ductility 6 was reached. A significant drop in the maximum joint stress seen at ductility 8 is attributable to the significant joint

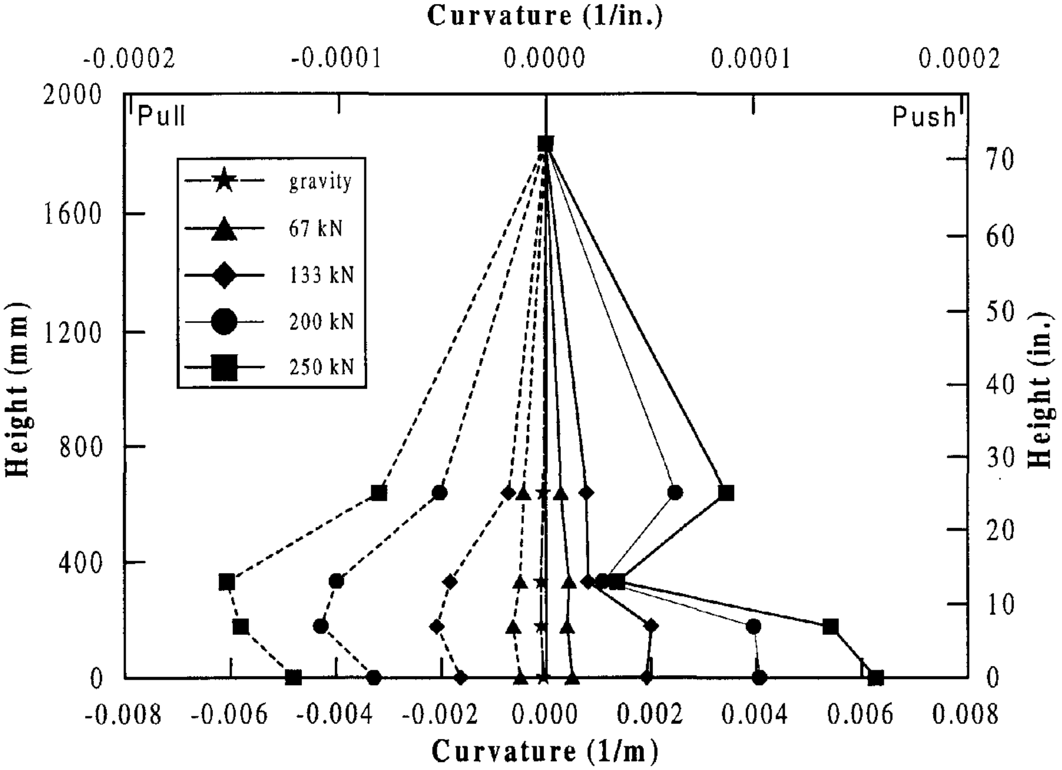

(a) Initial stages of testing

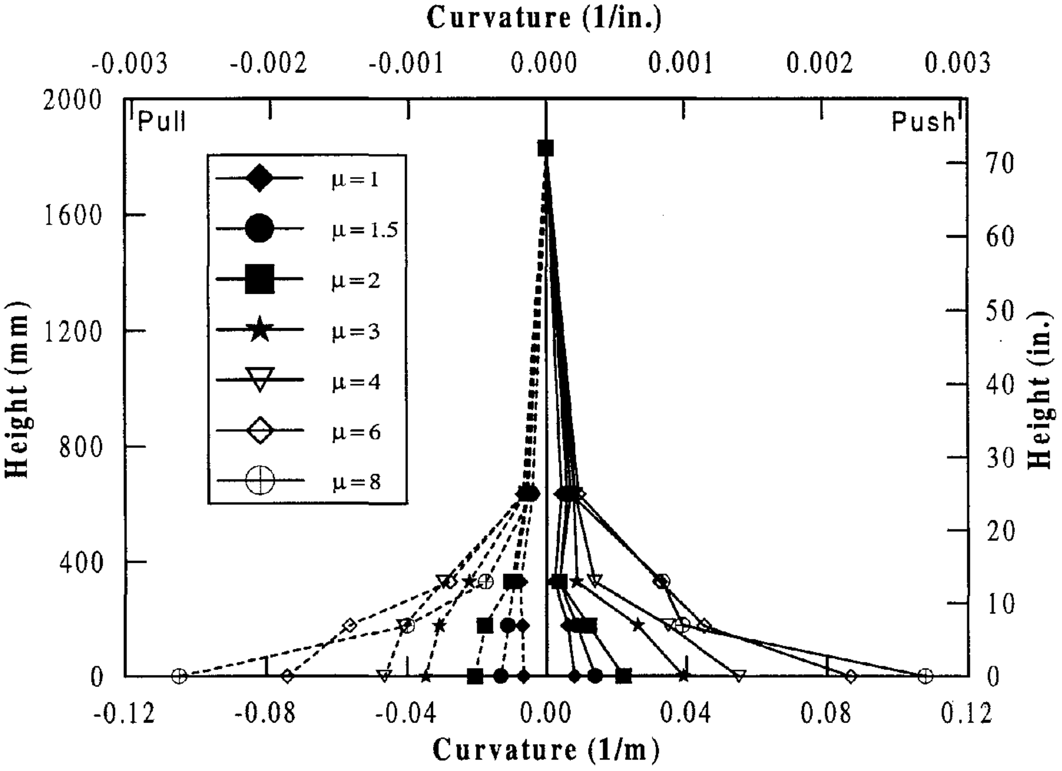

(b) Final stages of testing

Figure 4.19 Measured curvature profiles up the column.

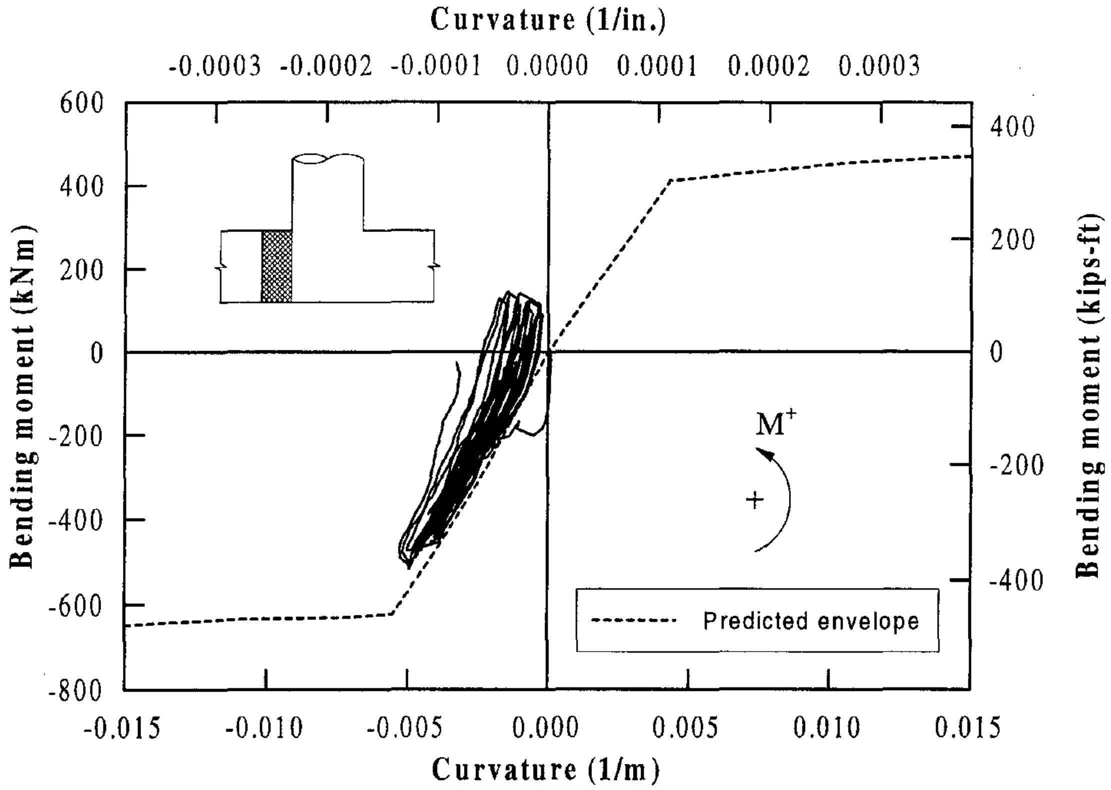

(a) left side of the joint

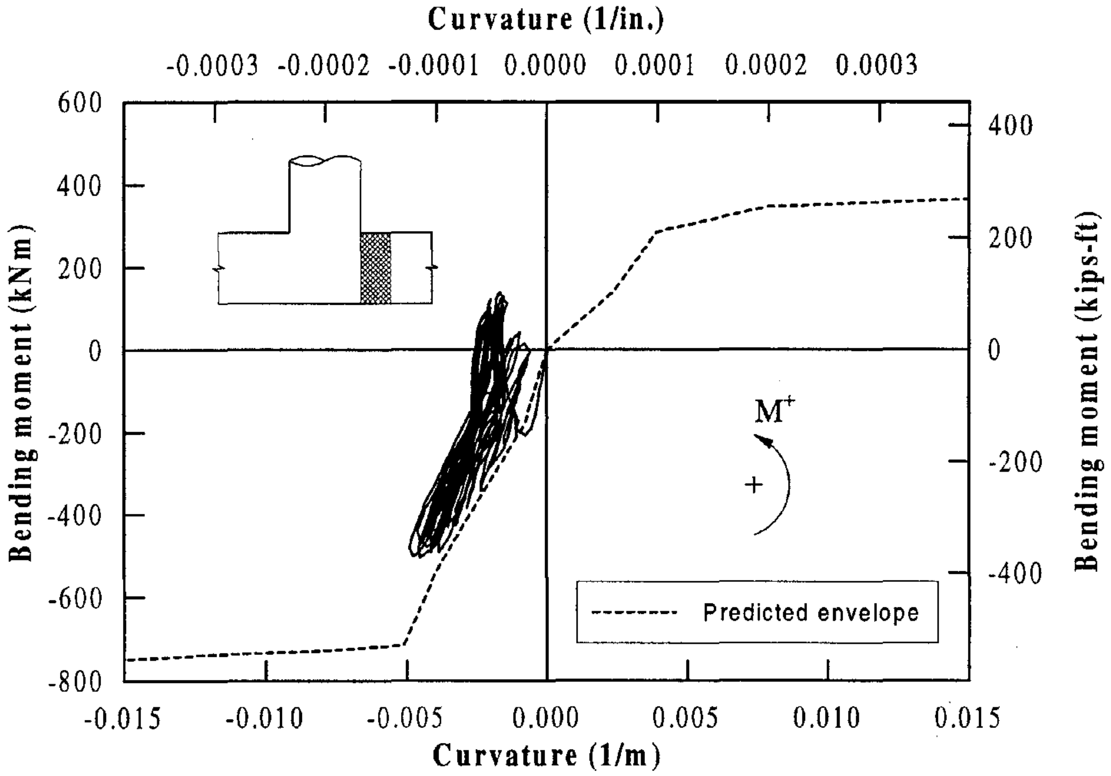

(b) right side of the joint

Figure 4.20 Moment-curvature response obtained in two beam curvature cells adjacent to the joint.

damage. The reduction in the joint stress was not significant when the average joint shear stress was considered. A similar observation can be made in Figure 4.22 where stress quantities as a function of experimentally calculated joint shear strains are shown. The joint deformation panel readings appeared to be reliable only up to the first push direction loading at displacement ductility 8 and the plot shown in Figure 4.22 are limited to ±0.01 strain. Higher shear strains, which were recorded during cycling at $\mu_\Delta = 8$, can be found in Figure 4.28. A crack formed adjacent to the right hand top curvature rod (see Figure 4.15) that was used to mount the joint panel devices. This may have disturbed the joint panel readings above $\mu_\Delta = 8x1$, and hence the data obtained beyond this point should be treated with caution.

The principal compression and principal tension stresses were calculated (Eq. 4.1) using the maximum and average joint shear stresses. The variations of these parameters with respect to the horizontal column displacements are shown in Figures 4.23 and 4.24 respectively. Again note in both figures the peak values at each ductility varied less significantly when the average joint stress was used in the calculation. This is true even at large ductilities where a considerable joint damage was encountered. The principal compression stress calculated from the maximum joint shear stress provided a peak value of $\mathbf{0.15f'_c}$ whereas the corresponding value calculated from the average shear stress reached a maximum of $\mathbf{0.1f'_c}$. The peak values of the principal tensile stress calculated from the maximum and average joint shear stresses were $\mathbf{0.83\sqrt{f'_c}}\left(\mathbf{10.0\sqrt{f'_c}}\text{ in psi units}\right)$ and $\mathbf{0.5\sqrt{f'_c}}\left(\mathbf{6\sqrt{f'_c}}\text{ in psi units}\right)$ respectively in SI units. Although the peak values of the principal tensile stress are slightly different from those estimated as a part of the design calculations (Section 4.1.3), both maximum and average principal tensile stresses suggest a full force transfer mechanism is necessary for the joint of IC1.

The angle of the principal plane as calculated using the average joint shear stress is shown in Figure 4.25 in terms of column displacement. For both push and pull direction loading, the principal stress plane was about 45° inclined to the horizontal axis. The cracking in the joint should be parallel to the principal stress plane and this trend was observed in the experiment as seen in Figure 4.11. When prestressing is applied in the cap beam, the principal stress plane rotates and cracking in the joint develop with a reduced inclination. This is further discussed in the subsequent chapters (Sections 5.7.3 and 6.7.3).

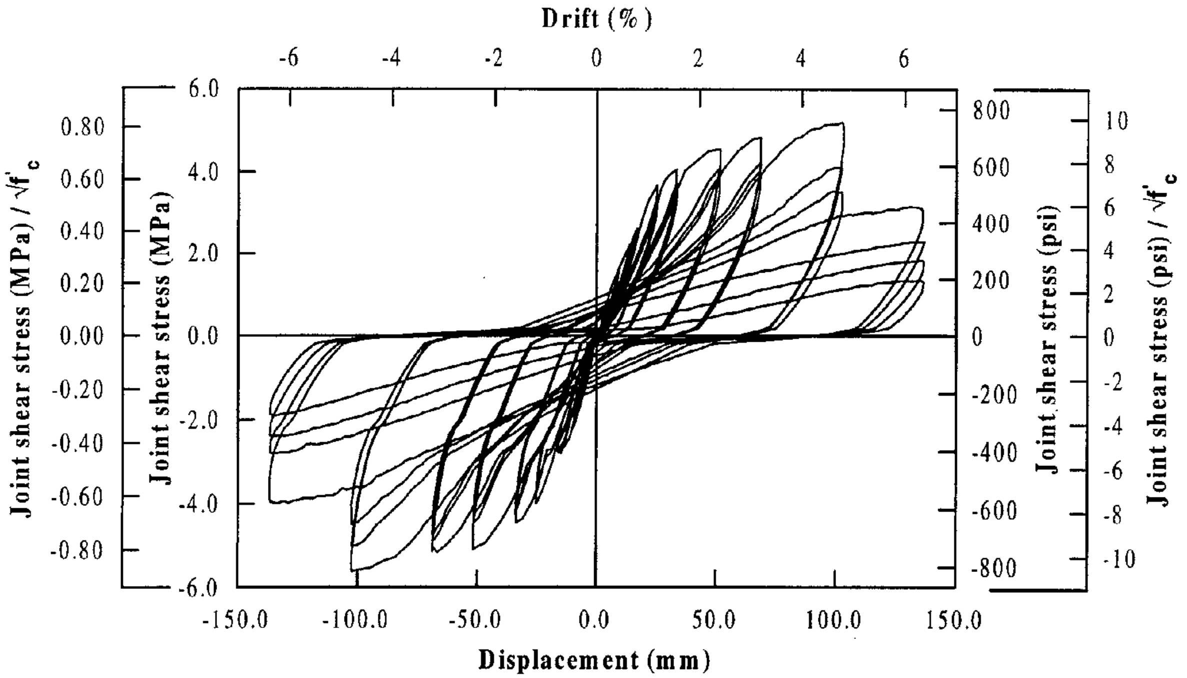

(a) Using maximum joint shear stress

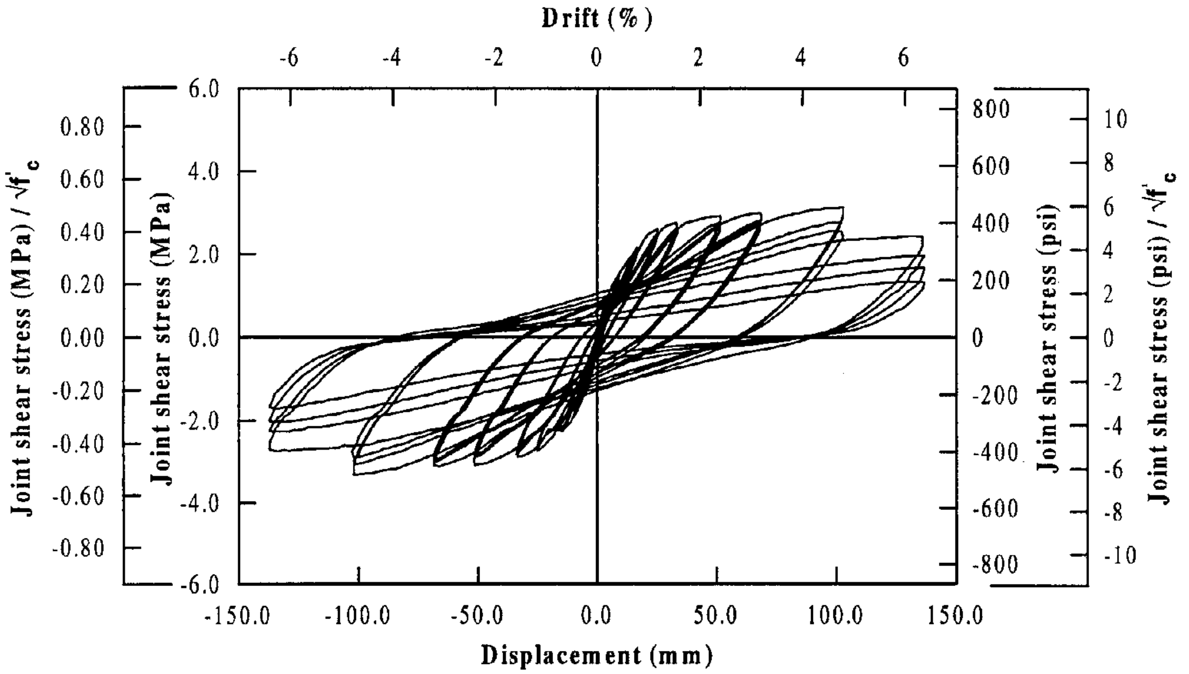

(b) Using average joint shear stress

Figure 4.21 Variation of joint shear stress as a function of column displacement.

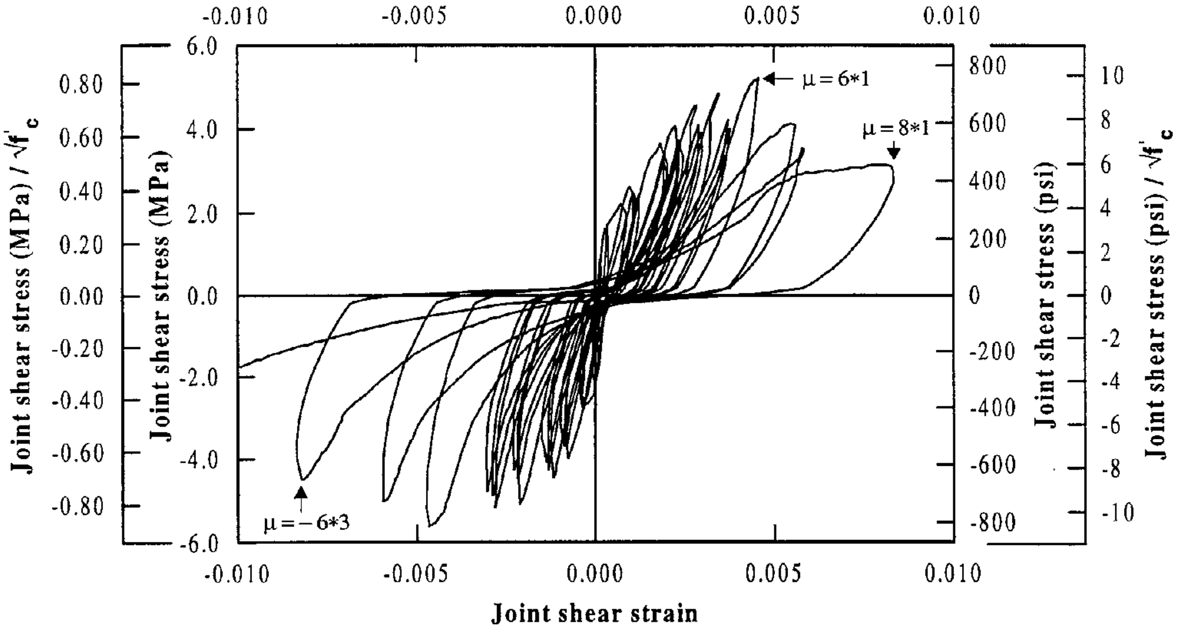

(a) Using maximum joint shear stress

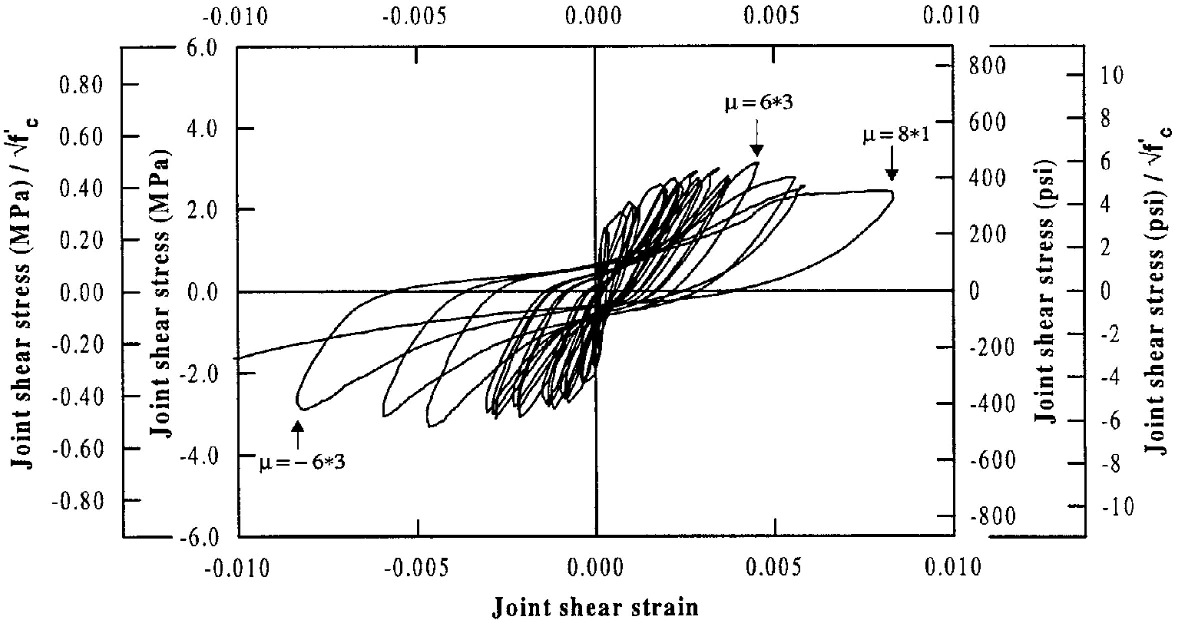

(b) Using average joint shear stress

Figure 4.22 Variation of joint shear stress as a function of joint shear strain.

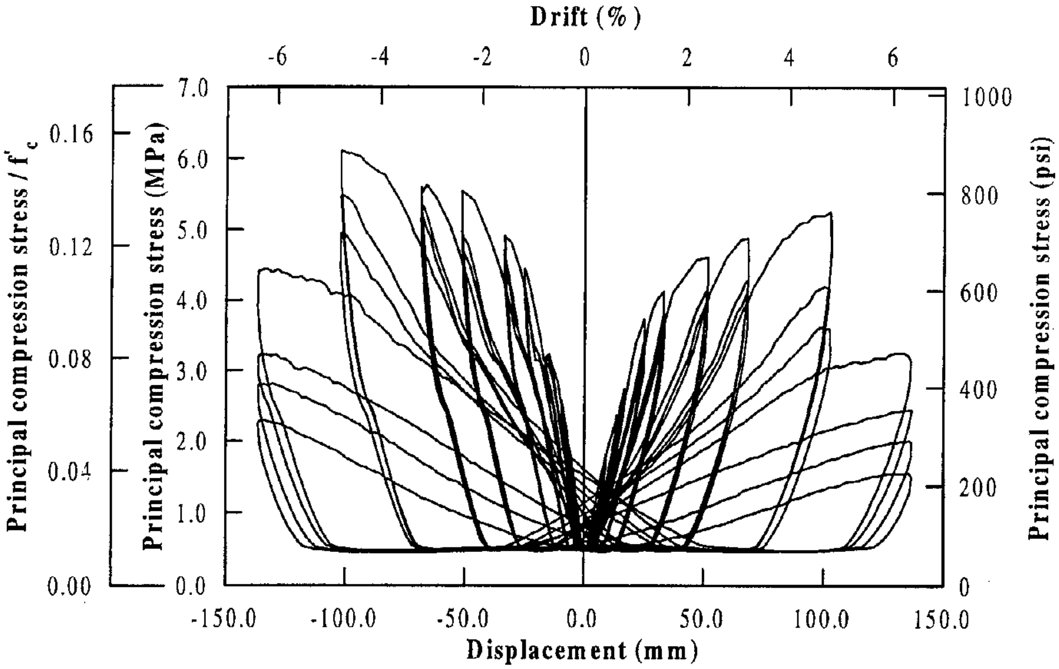

(a) Using maximum joint shear stress

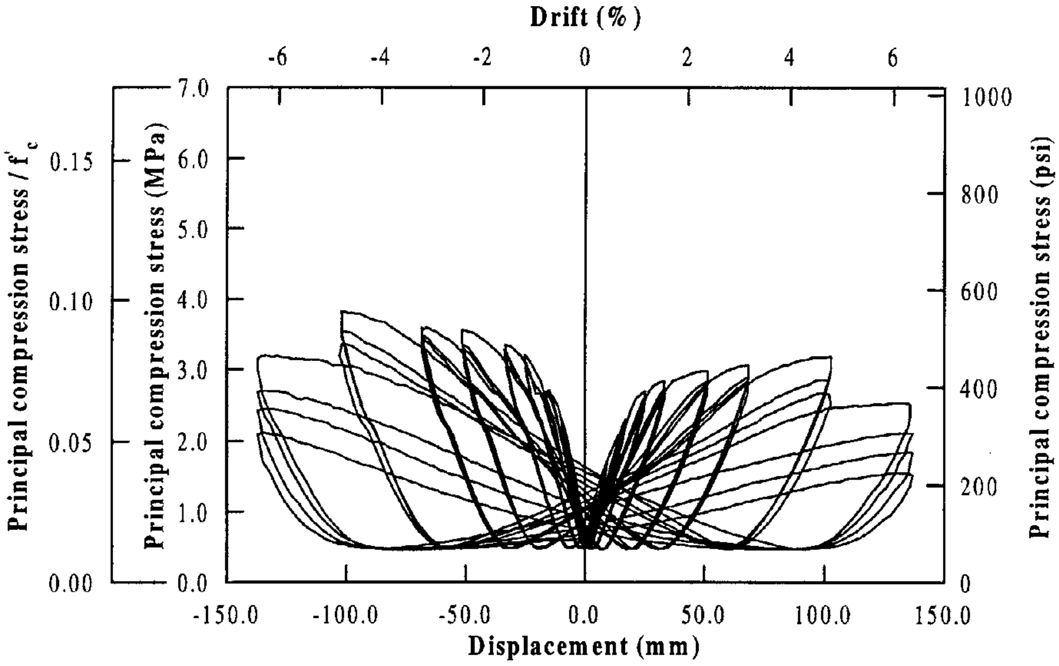

(b) Using average joint shear stress

Figure 4.23 Variation of joint principal compression stress as a function of column displacement.

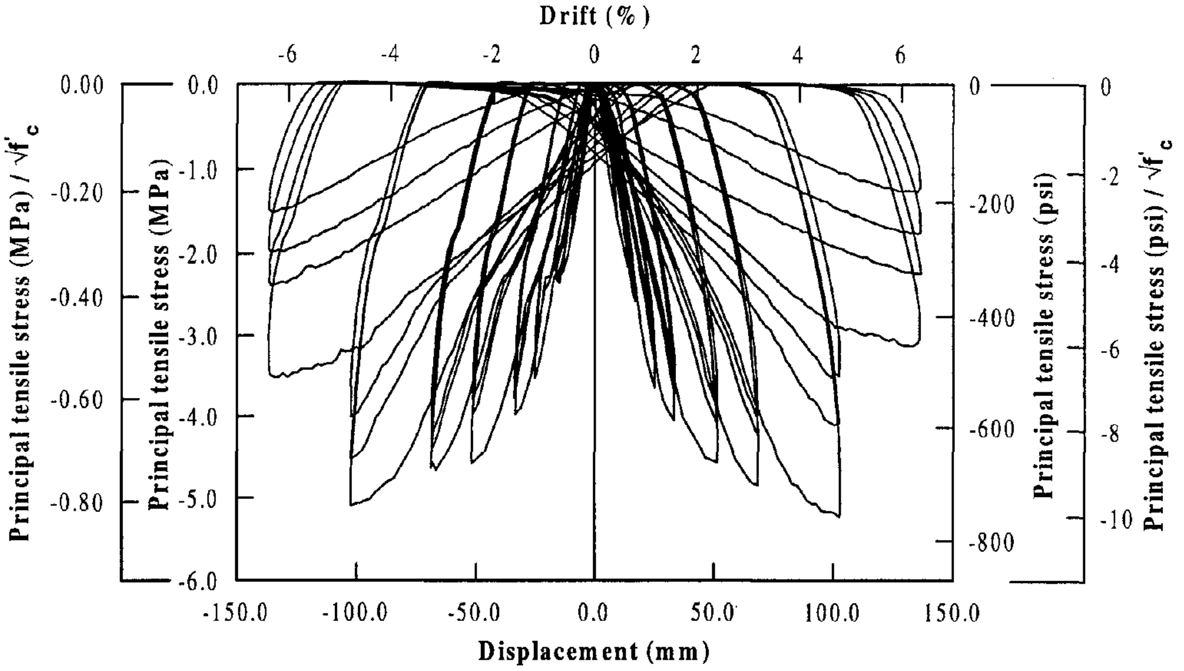

(a) Using maximum joint shear stress

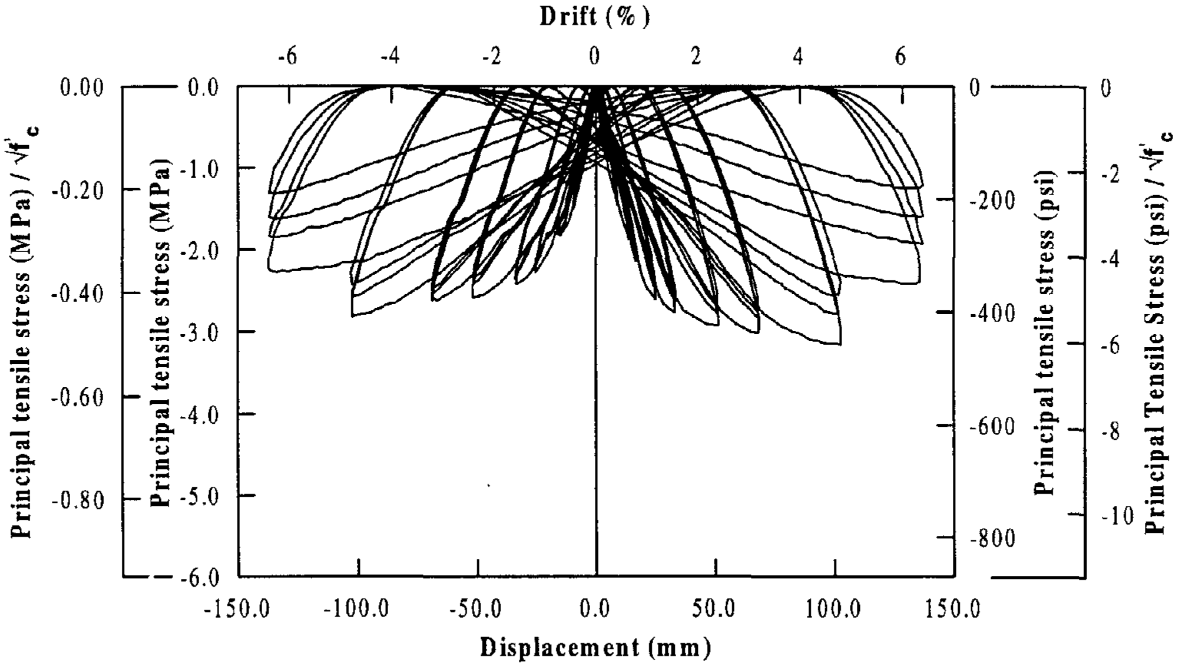

(b) Using average joint shear stress

Figure 4.24 Variation of joint principal tensile stress as a function of column displacement.

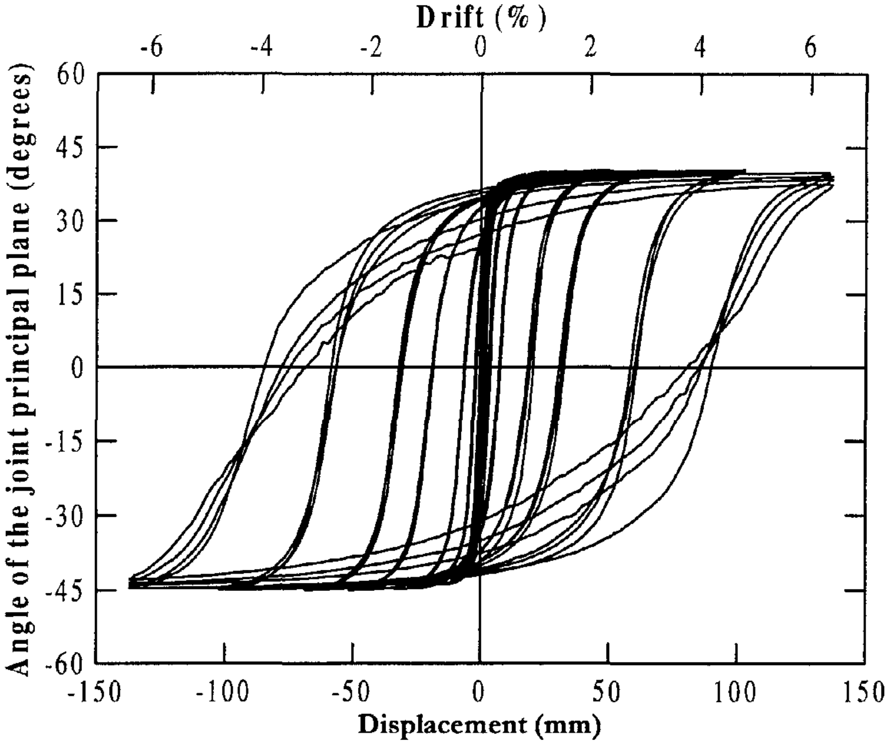

Figure 4.25 Angle of principal stress plane as obtained using the average joint shear stress.

The deformation that occurred to the joint can be depicted in several different ways. Two of these are shown in Figures 4.26 and 4.27 where the growth of joint panel area as a function of column displacement and displacements of three joint nodes with respect to the fourth node at displacement ductilities 1, 2, 4, 6 and 8 are shown. From both figures, it is obvious that joint area increased markedly at large ductilities, particularly after the major joint diagonal crack formed during the first cycle at $\mu_\Delta = 6$. The displacements of the joint nodes shown in Figure 4.27 indicate that joint shear strain and probably rigid body rotation of the joint increased marginally up to $\mu_\Delta = 6$ and significantly from $\mu_\Delta = 6$ to 8. This observation can be verified in Figures 4.28 and 4.29, which portray these parameters as a function of column displacement. A similar observation was made for the extension and flexural deformation of the joint in x and y directions, but they are not shown in this report.

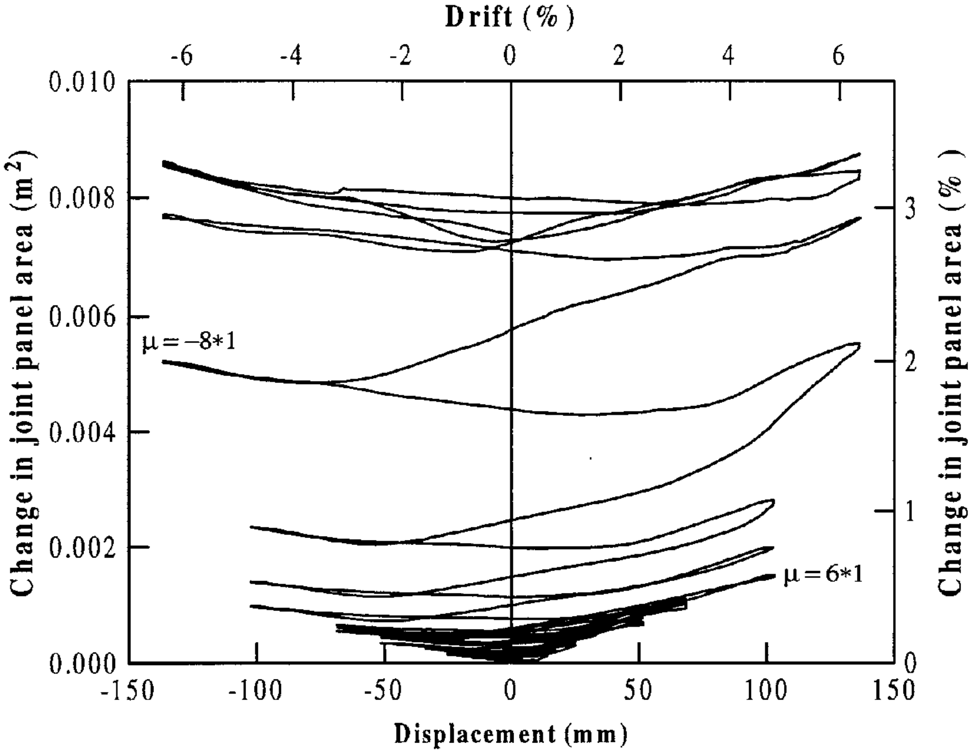

Figure 4.26 Growth of joint panel area as a function of column displacement.

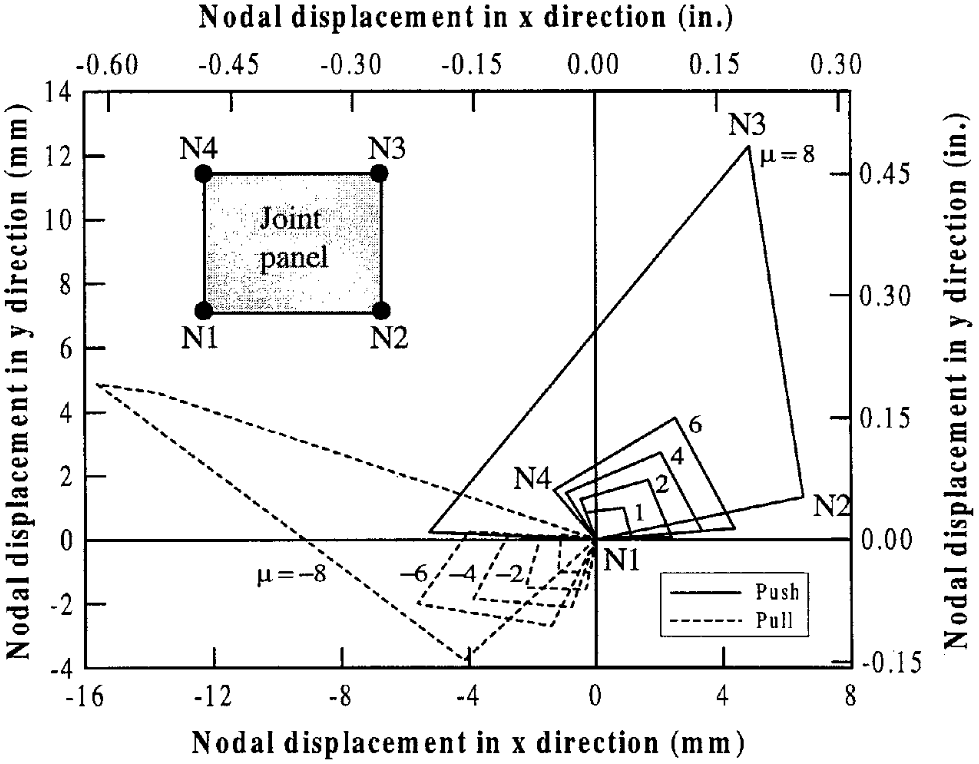

Figure 4.27 Representation of three joint nodal displacements with respect to the fourth node.

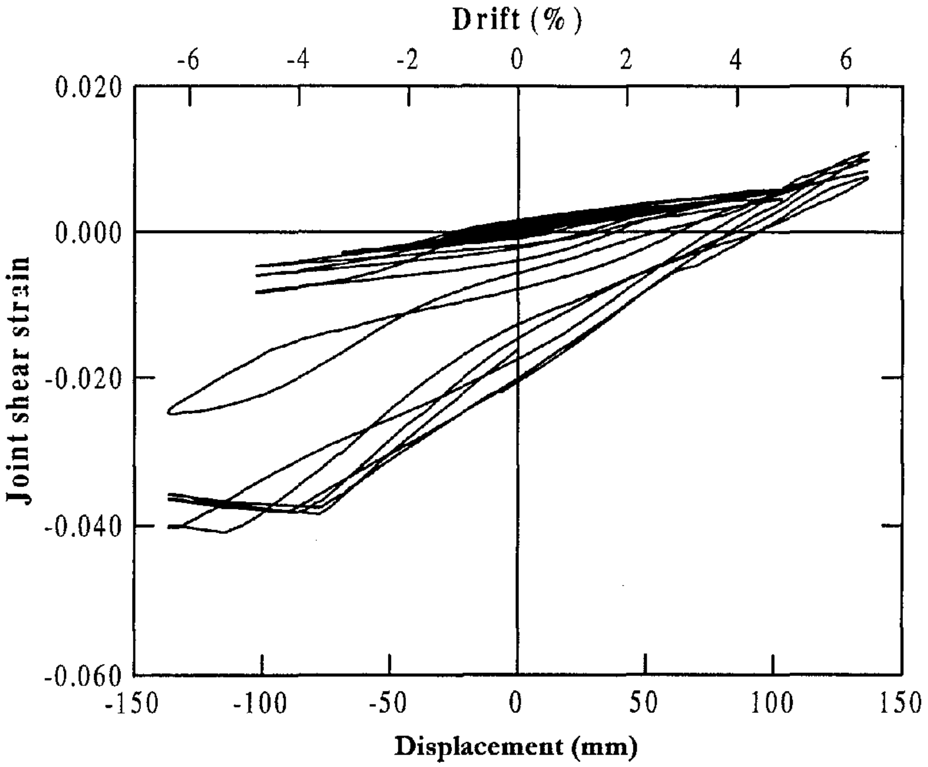

Figure 4.28 Joint shear strain as a function of horizontal column displacement.

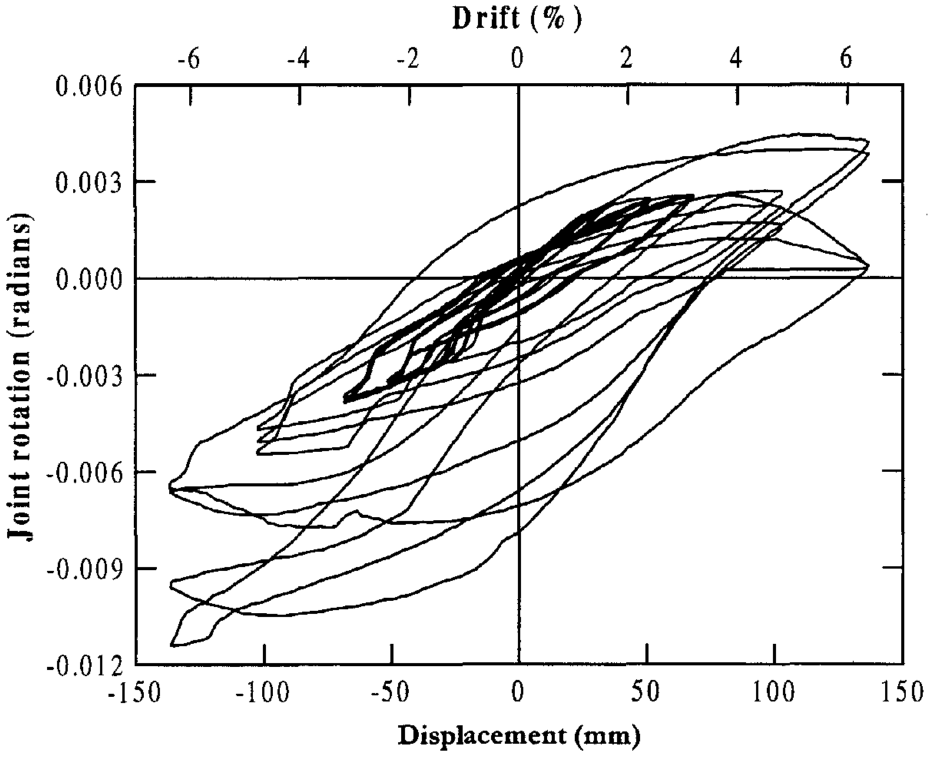

Figure 4.29 Rotation of the joint due to bending of the cap beam.

4.6.4 Displacement Components

As detailed in Section 2.8, theoretical prediction of the horizontal displacement at the top of column was comprised of four components, namely, elastic column flexure, plastic column flexure, column shear and joint rotation. From experimental measurements, estimates of column flexure (elastic plus plastic), joint rotation and joint shear were obtained. In Figure 4.30 - 4.33, experimental and theoretical displacement components are presented in various forms. The representation of experimental curves in these figures were formed by considering the readings which were obtained during the first cycle at ductilities 1, 2, 4, 6 and 8. Theoretically calculated displacements due to column shear was less than 1mm (0.04 in.), and this component was not considered in the figures.

The axial deformation of the cap beam was not directly measured during the test, but was estimated from the linear potentiometers placed at each end of the cap beam (Figure 3.25). This was found to vary from -0.6 mm (-0.024 in.) to -1.2 mm (-0.047 in.) in the push direction and from -0.4 mm (-0.016 in.) to -0.9 mm (-0.035 in.) in the pull direction as the displacement was increased from ductility 1 to ductility 8. The negative displacement estimated in the push direction contradicts the behavior expected from the variation of axial load induced in the cap beam. The axial load in the left portion of the beam was always zero while the right portion was subjected to an axial tension for the push direction loading and axial compression for the pull direction loading. It is believed that the axial deformation monitored during the test was dominated by shortening of the beam due to the curvature imposed on it rather than by the axial force. Since the magnitude of this component was expected to be very small, the contribution to the column displacement due to cap beam axial deformation was also ignored in this unit as well as in the two prestressed units.

Total displacements accumulated from column flexure and joint deformation as obtained from experimental observations and theoretical calculations are compared against the total measured displacement in Figures 4.30 and 4.31 respectively. A good agreement between the total measured and that obtained from individual components is generally seen in both figures. The accumulated displacements from the experimental calculations marginally overestimated the total measured displacement in the push loading direction while providing a better match in the pull direction except at $\mu_\Delta = 8$. As noted previously (see Figure 4.18a), the reading in the column curvature cell adjacent to the joint was disturbed as concrete crushing occurred on the top (as cast) of the beam. It is believed

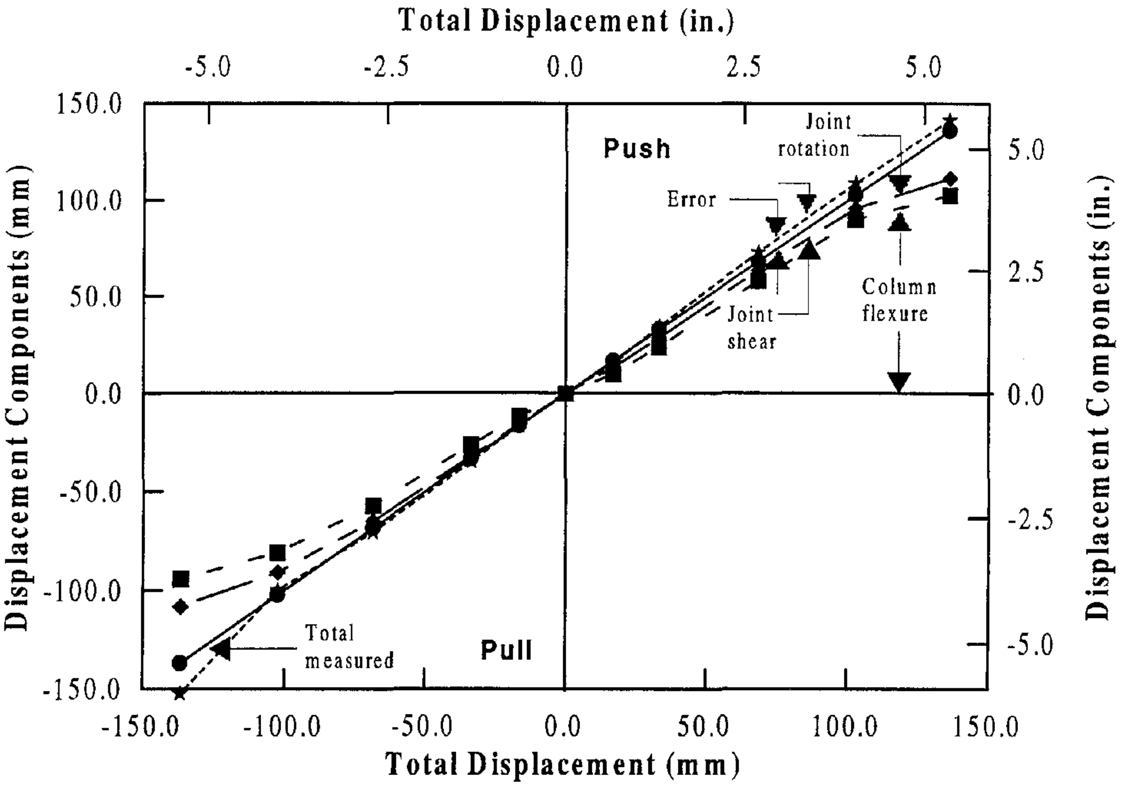

Figure 4.30 Comparison of the displacement accumulated from experimentally observed components to the total measured displacement.

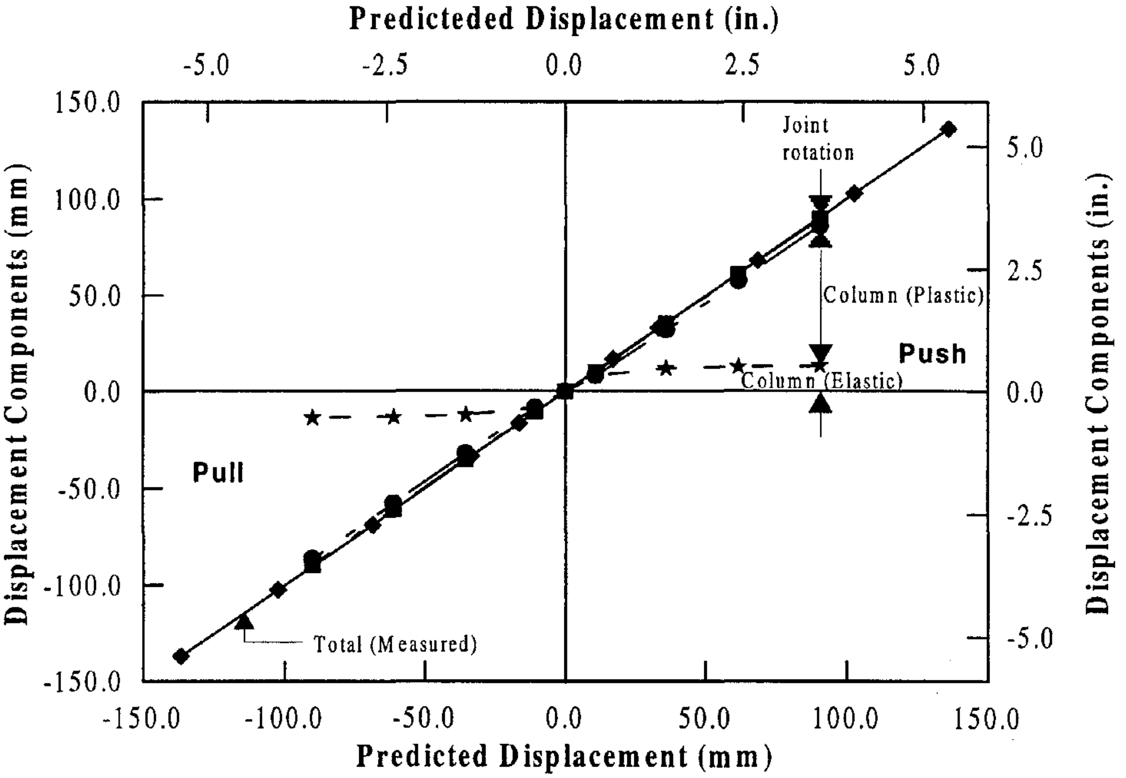

Figure 4.31 Comparison of the displacement accumulated from theoretically estimated components to the total measured displacement.

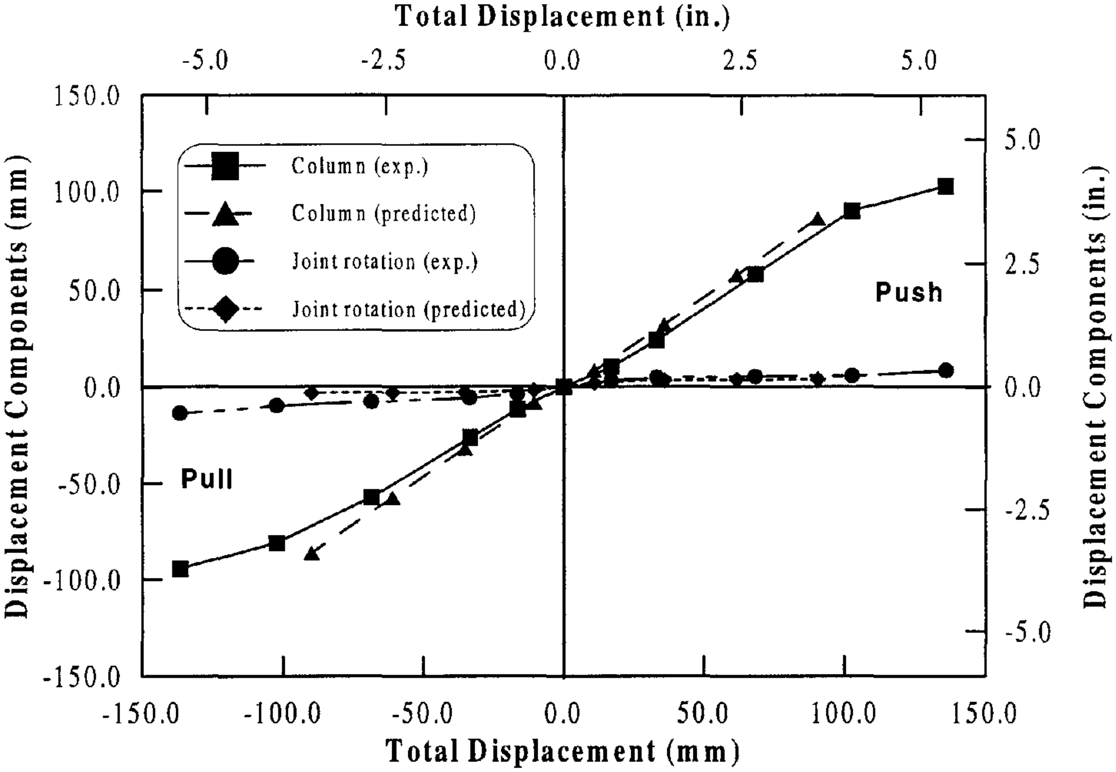

Figure 4.32 Comparison of experimentally obtained displacement components due to column flexure and joint rotation against the analytical values.

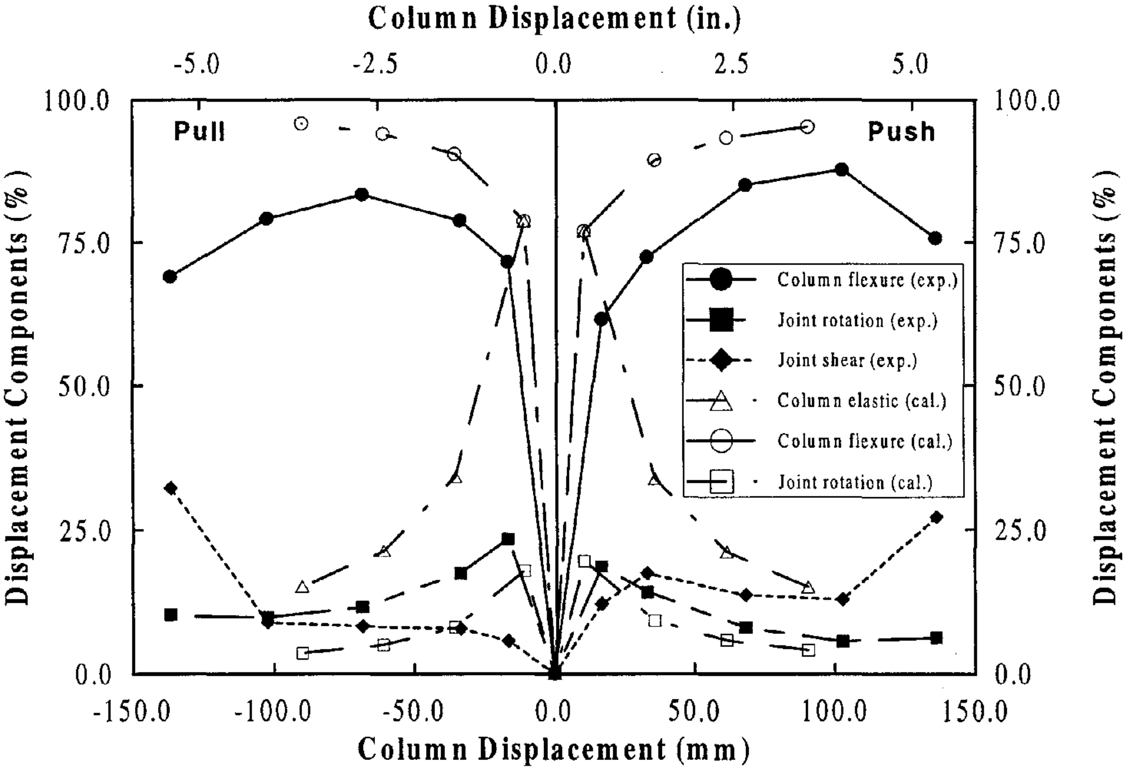

Figure 4.33 Representation of displacement components as percentage of the total horizontal displacement.

that this is largely responsible for the significant discrepancy between the measured and experimentally accumulated displacement at $\mu_\Delta = -8$. The displacement component due to joint shear and joint rotation could have also been slightly affected by the damage which occurred to the joint and bottom beam cover concrete respectively.

Theoretical and experimental values of displacement components due to column flexure and joint rotation are compared in Figure 4.32. A good agreement is seen between the theoretical and experimental values, although theoretical calculations slightly underestimated the component due to joint rotation and overestimated the flexural column displacement. Because the joint was not explicitly modeled in the theoretical calculation, and beam lengths were taken to the center of column, theoretical calculations should have overestimated the joint rotation. The differences between the theoretical and experimental values appear to be significant when the contribution of each component was obtained as a percentage of the total displacement (Figure 4.33). This is partly due to the fact that the theoretical calculations did not consider the joint shear contribution. The displacement due to joint shear contributed more in the push direction than in the pull direction loading. This is to be expected as the joint was subjected to axial tension in the push direction and axial compression in the pull direction as discussed in Section 3.2.3. As the damage was mainly concentrated in the joint region at $\mu_\Delta = 8$, joint shear significantly contributed to the total column displacement. This can be clearly seen in Figure 4.33.

4.6.5 Strain Gauge Histories

Of the many strain gauges mounted on the reinforcement of the test specimen, the variation of strain as a function of column displacement is shown only for a few selected gauges. Key values obtained on several other strain gauges are presented as strain profiles in the following section.

Strain gauge readings were expected to be small and corresponded to concrete strain at the beginning of the test. When the concrete cracked, the tension carrying capacity of the concrete dropped to almost zero and the reinforcement carried a large portion of the tensile force, therefore strain in the steel increased accordingly. At large deformations the force resisting ability of the system was reduced due to the joint damage and this should be reflected as a reduction in the strain gauge reading. Unfortunately, some of the strain gauges were damaged when the reinforcement was stressed beyond its yield strength and subjected to a reverse cyclic loading. The measurements taken in the gauges up to failure are reported herein.

Strain histories of three gauges mounted on the extreme longitudinal column tension reinforcement are presented in Figures 4.34 – 4.36. The strain history shown in Figure 4.34 is from a gauge within the joint, which was at 269 mm (10.6 in.) or 12.11 times the bar diameter from the bar end. At ductility 1.5, yield strength of the reinforcement was developed at this location. For reinforcement located at ½ and ¾ column diameters from the extreme compression fiber, yield strain was recorded at a distance equal to 5.83 times the bar diameter at ductility 4, but the gauges soon failed. The uniform bond stress required to develop yield strength of the column reinforcement within such a short bar length is $3\sqrt{f'_c}\left(36.7\sqrt{f'_c}\text{ in psi units}\right)$.

The strain history shown in Figure 4.35 corresponded to a gauge located at the joint interface. As anticipated, yield strain was reached at this location when the actuator load was increased to 250 kN (56.2 kips), which is the theoretically estimated force required to induce yield moment at the critical section of the column. The strain reading of another gauge placed at a similar location for the opposite direction loading was somewhat less than the yield strain at horizontal load of 250 kN (56.2 kips) and this can be seen in the strain profile plot shown in Figure 4.45. Gauges mounted on the column reinforcement away from the joint interface recorded strains well above the yield limit and an example of this is presented in Figure 4.36. This particular gauge was located at 305 mm (12 in.) from the joint interface and this region of the column was sparsely instrumented.

Several gauges were placed on the spiral reinforcement of the column and joint, and the readings obtained from four gauges are presented in Figures 4.37 – 4.40. The strain measurement of a gauge mounted on the east side of the first joint spiral from the bottom (as tested) of the beam is represented in Figure 4.37. The strain gauge reading suggests that yield strength was reached at ductility 2 at this particular location and significant amount of inelastic action took place at higher ductilities. Given that the loading direction was north-south, the high strain demand shown in Figure 4.37 was due to out-of-plane tension developed within the joint as a result of dilation of the core concrete. High strain demands were also observed in gauges placed on the west side of the joint spirals. Due to the confinement provided by the cap beam, a similar effect was not

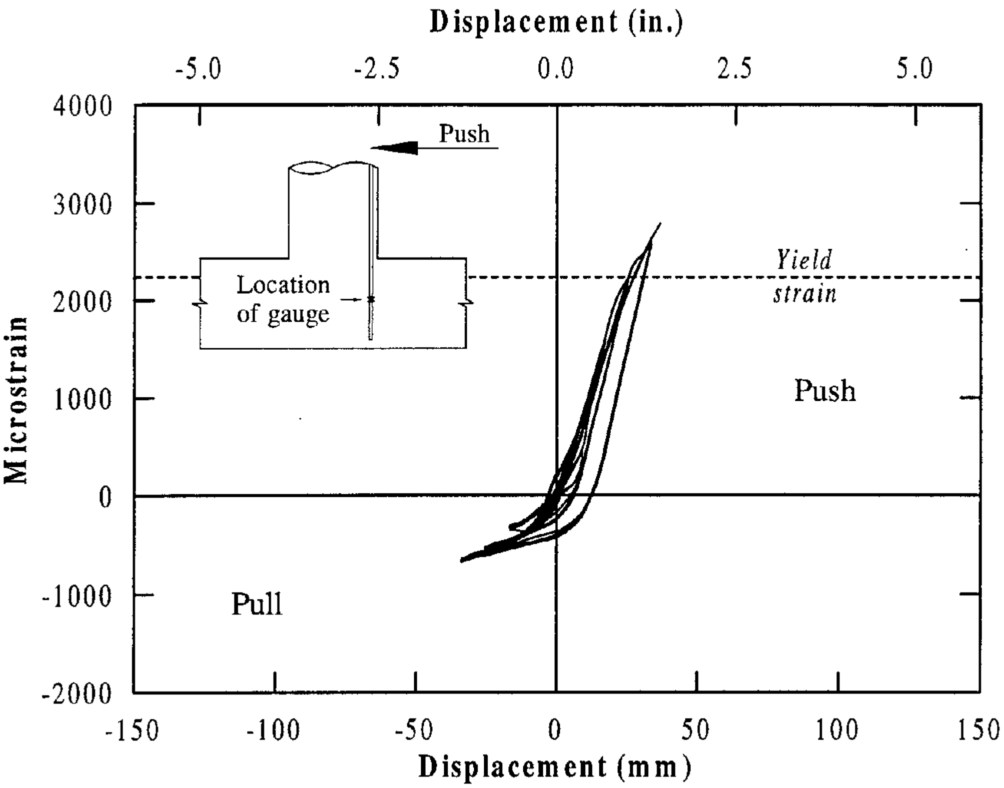

Figure 4.34 Strain gauge history of a gauge located within the joint on an extreme column tension reinforcement.

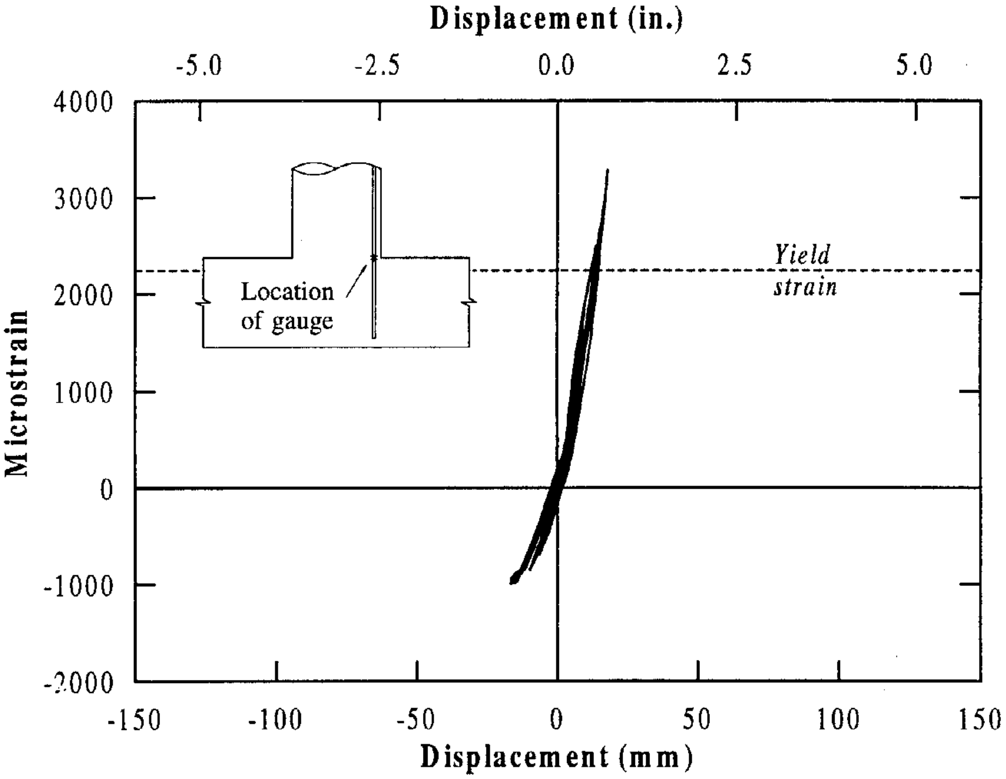

Figure 4.35 Strain history of a gauge located at the joint interface on an extreme column tension reinforcement.

expected on the gauges located on the north or south sides of the joint spirals, and this can be verified in the strain gauge profile plot presented in Figure 4.47.

Gauges placed on the north and south sides of the column spirals recorded the confinement effect whereas the shear demand was monitored on the east and west sides. In Figure 4.38 the strain reading of a gauge mounted on the north side of a column spiral at 194 mm (7.63 in.) from the joint interface is shown. It is apparent that the transverse reinforcement content provided in the prototype column was adequate to confine the concrete in the plastic hinge region. Comparable readings were obtained on several gauges located above and below this particular gauge as well as on the south side of the column.

Shear demand on the column transverse reinforcement is represented in Figure 4.39 by a strain gauge history obtained on the east side of the spiral at 441 mm (17.38 in.) from the

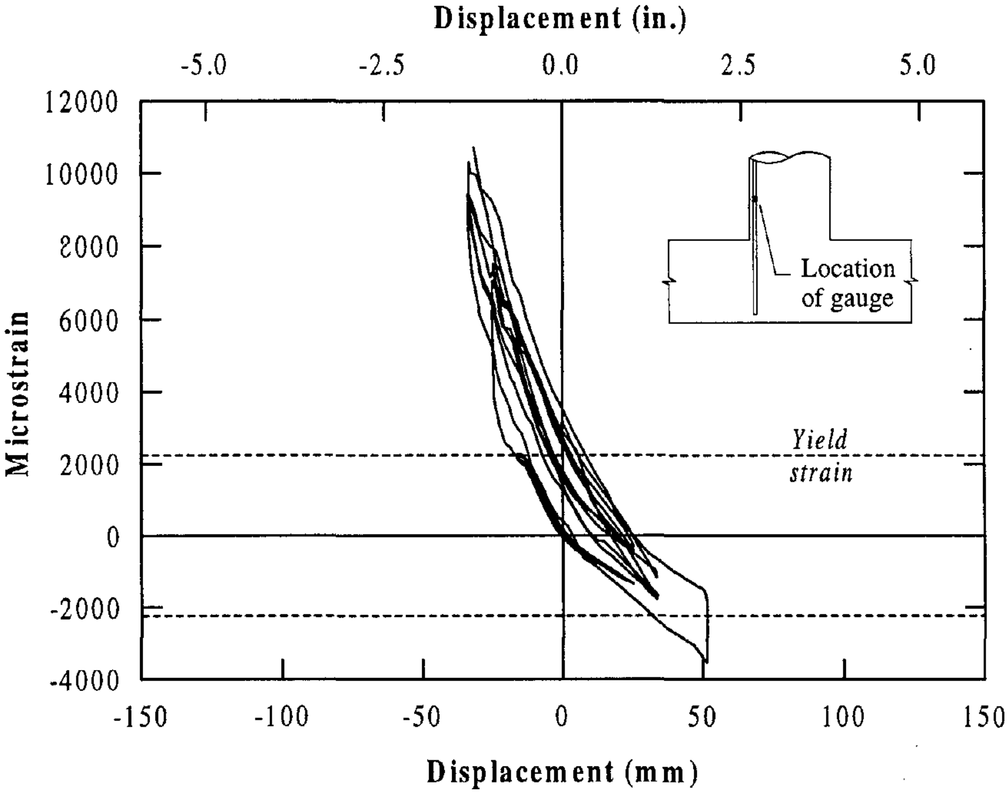

Figure 4.36 Strain history of a gauge mounted on an extreme longitudinal reinforcement away from the hinge region.

joint interface. The column shear force induced strains in excess of yield limit in this gauge and in the gauge located on the west side of the same spiral. The strain level at two spirals closer to the joint interface (i.e. 248 mm from the joint) was found to be less than or marginally reaching the yield strain on both sides, and an example of this is shown in Figure 4.40. There was no indication of column shear failure during the test up to ductility 6 and the shear force in the column dropped at ductility 8 due to joint damage. Shear cracks were much more pronounced and appeared to be leading to a shear failure of the column in the second unit, which duplicated the column detail of the first test unit, but consisted of a robust joint connecting the cap beam and column. This observation contradicts the design procedure outlined in Section 4.1.1, where it was ensured that shear strain in the spiral should be kept below the yield strain. An explanation to the difference between the expected and measured strain in the shear reinforcement is given in Section 4.7.

Three strain gauge histories from the longitudinal beam reinforcement are presented in Figures 4.41 – 4.43. The gauge shown in Figure 4.41 was mounted on a top (as constructed) beam reinforcement at the column face where tensile strains below yield in the push direction and small compression strains in the push direction were expected. Recorded strains in the push direction agree well with the expected behavior, but considerably high tensile strains instead of compression strains were recorded in the pull direction of loading. A similar response was observed in a number of gauges located at the column face. In the gauges placed at 203 mm (8 in.) away from the joint interface in the beam, compression strains were recorded under positive moments as were expected. This can be seen in the profile plots shown in Figures 4.52 and 4.53.

The strain history presented in Figure 4.42 corresponded to a gauge which was located within the joint on a top beam reinforcement at 203 mm (8 in) from the column face. Small strains were recorded in this gauge during the early stages of testing. At ductility 8, high compression strains were developed for both loading directions, presumably due to buckling of the reinforcement. In Figure 4.43, a strain history is shown for a bottom (as cast) longitudinal beam reinforcement at the column face. The response of this gauge also contradicts the behavior that was expected from simple beam theory. An analysis of this interior joint is currently underway [26], where an attempt is made to explain the

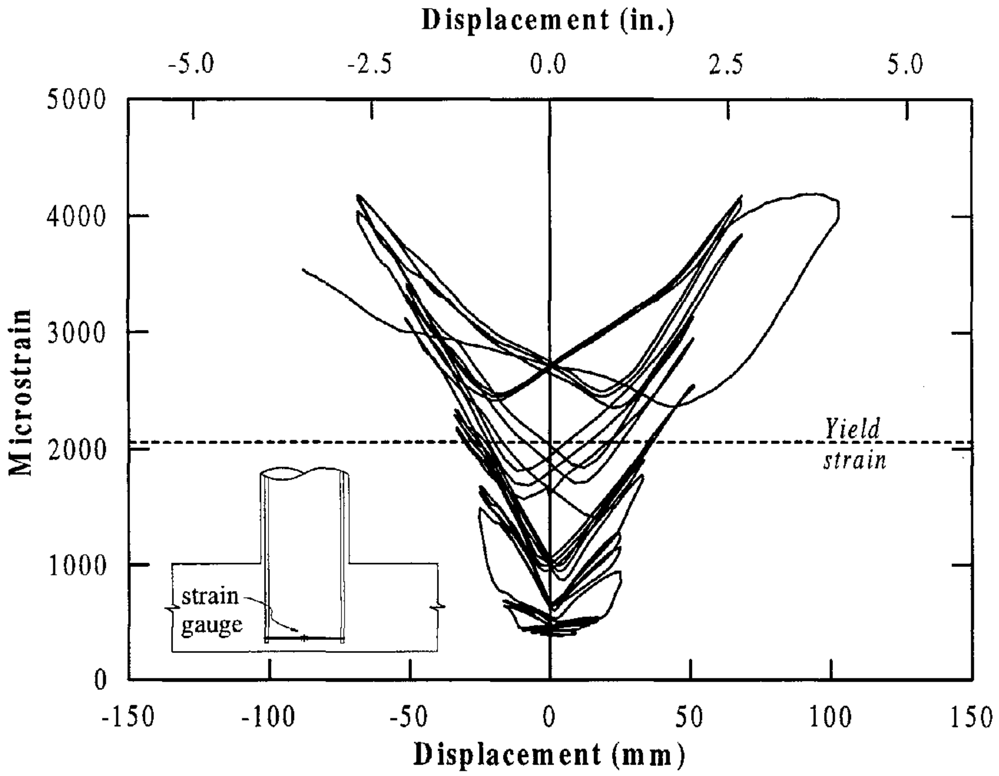

Figure 4.37 History of a joint spiral gauge measuring out-of-plane strain.

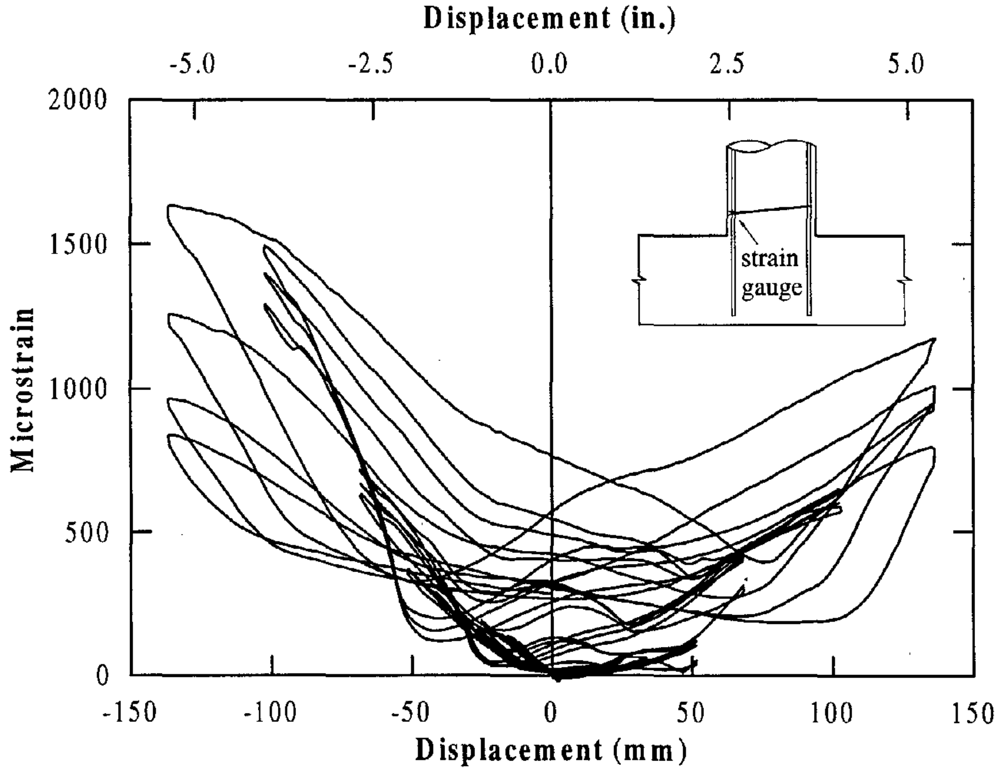

Figure 4.38 Column spiral gauge showing confinement strain in the hinge region.

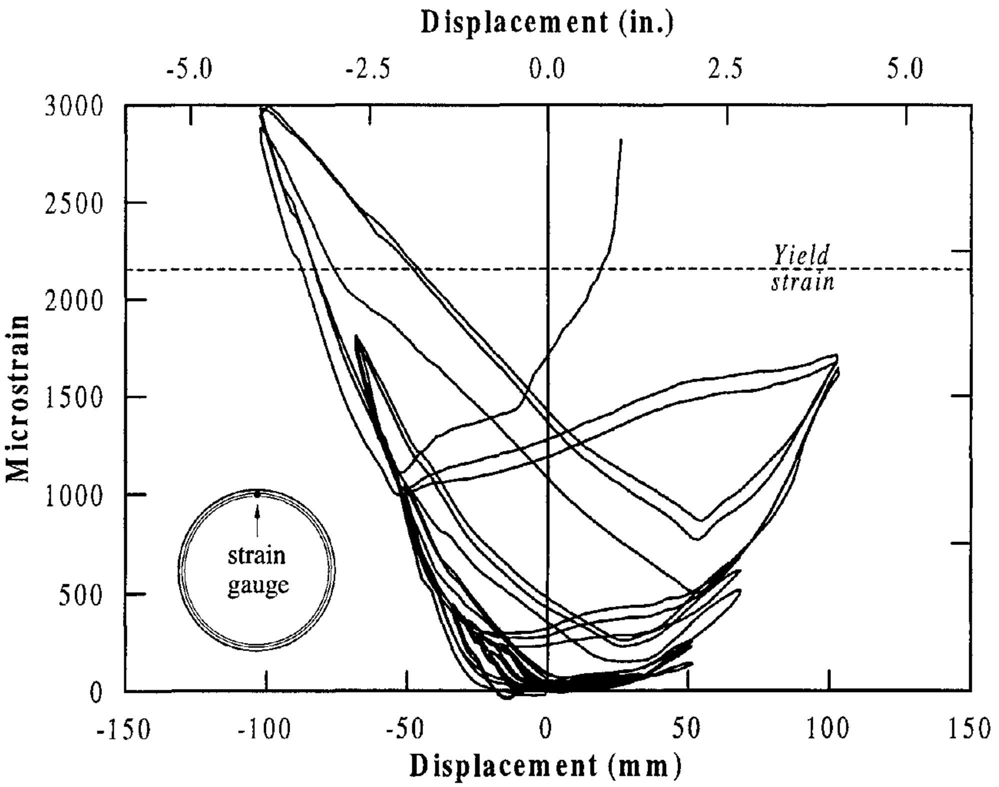

Figure 4.39 Strain history from a column shear reinforcement.

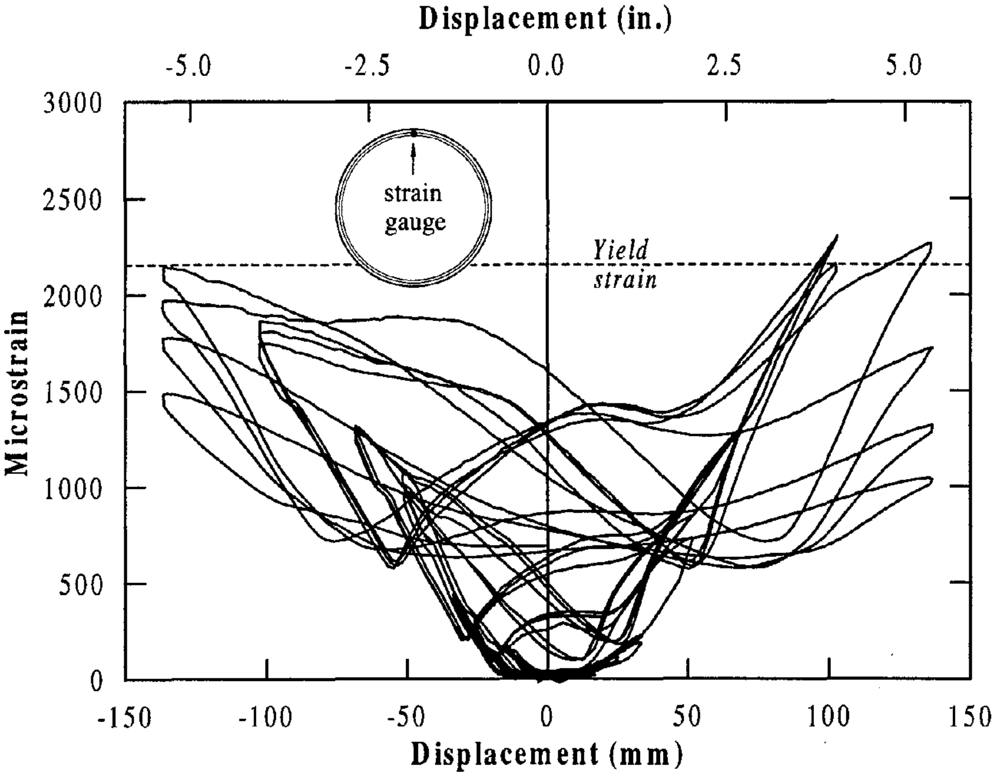

Figure 4.40 Strain history from a column shear reinforcement.

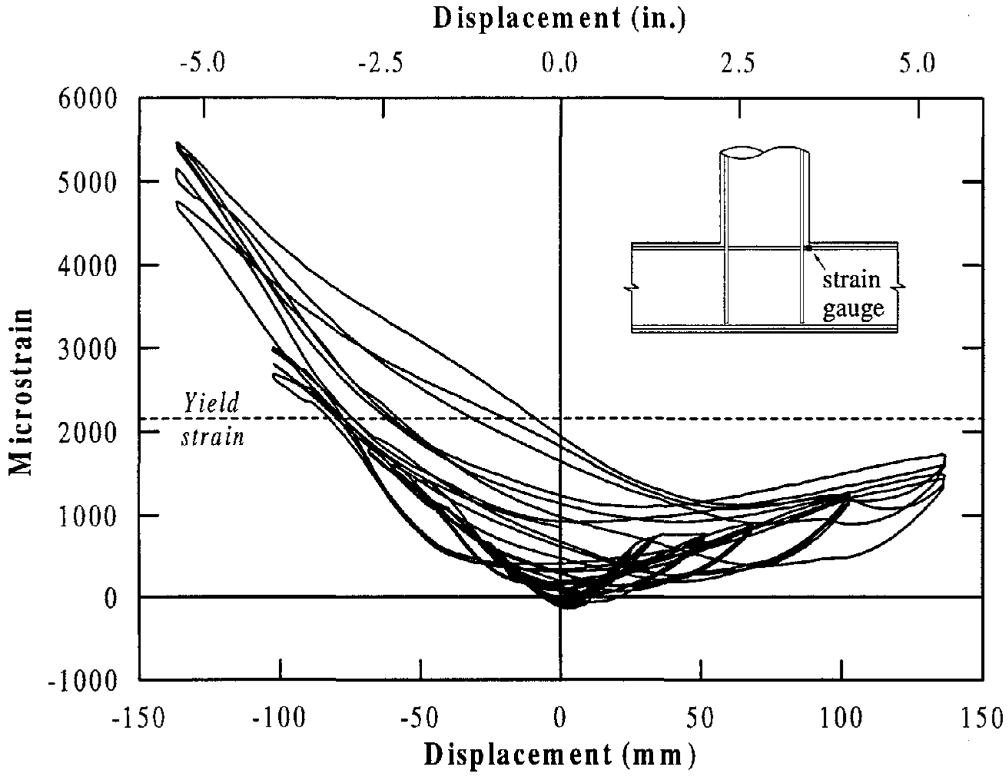

Figure 4.41 Strain history of a top beam reinforcement gauge located at the column face.

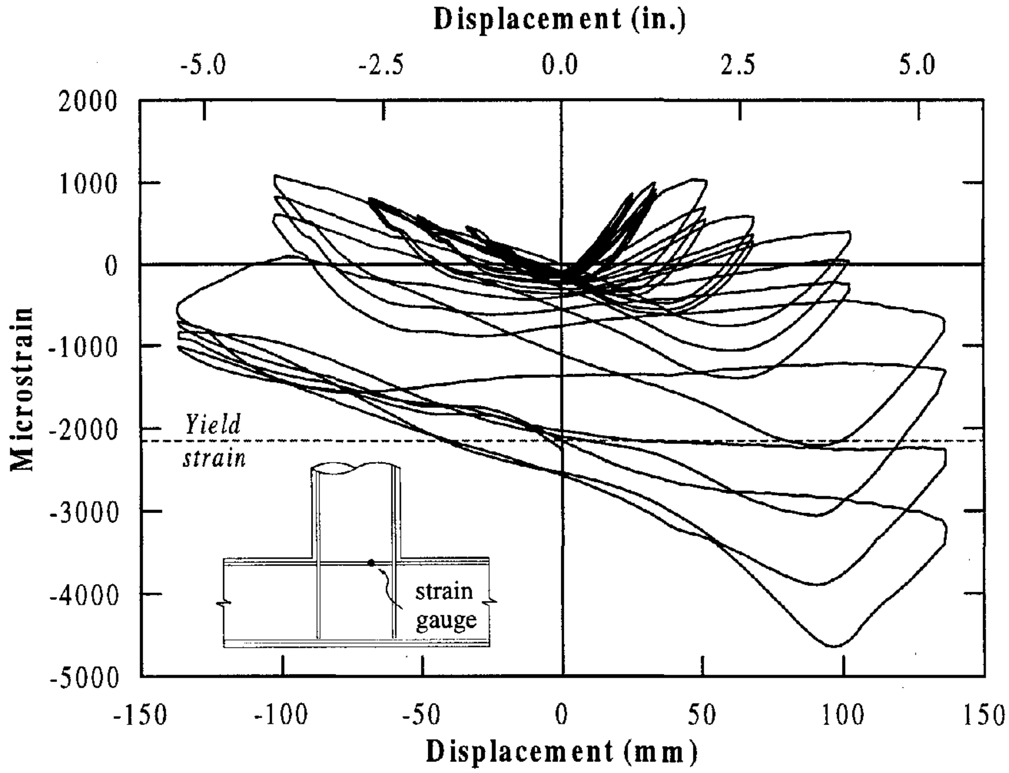

Figure 4.42 Strain history of a top beam reinforcement gauge located within the joint.

uncharacteristic strains developed in the longitudinal beam reinforcement in consideration to the joint force transfer mechanism.

Strain readings taken from the beam shear reinforcement are presented in detail in the profile plots. Strain history of one of the joint stirrup gauges is shown in Figure 4.44. This strain gauge, which was placed on an outer leg of the stirrup at mid height of the beam, reached yield strain at ductility 4 at which point the condition of the joint was considered satisfactory (Section 4.5.3). It appeared that significantly high strains were developed at this location at large ductilities.

4.6.6 Strain Profiles

Several strain profiles as obtained along or across the structural members are presented in this section. In each case, the strain values shown here are those recorded when the peak displacements were first achieved during the test (i.e. during the first loading cycle).

Strain profiles of two extreme longitudinal column bars are shown in Figures 4.45 and 4.46 in which significant strain penetration into the tee joint is seen from horizontal load of 200 kN (45 kips). A significant number of gauges mounted on the extreme tension reinforcement, particularly within the joint, failed for no obvious reason beyond displacement ductility 1.5. Of the two reinforcement, the nearest gauge to the bar end, where yield strain was developed, was at 269 mm (10.6 in.) and history of this gauge was shown previously in Figure 4.34. For column reinforcement located at ½ and ¾ column diameter from the extreme compression fiber, the yield strength was developed at 130 mm (5.1 in.) from the end of the bar.

Strain profiles obtained from column spirals are shown in Figures 4.47 and 4.48. The confinement effect of the transverse reinforcement is exhibited in Figure 4.47 from a series of gauges mounted on the south side of the column. Strain values up the height of the column appears to have remained within yield limit during the test. The strain demand imposed on the south side of the spirals located within the joint and in the plastic hinge region of the column is comparable although the spiral reinforcement in the joint was provided with smaller spacing. A similar observation was made for the gauges placed on the north side of the column.

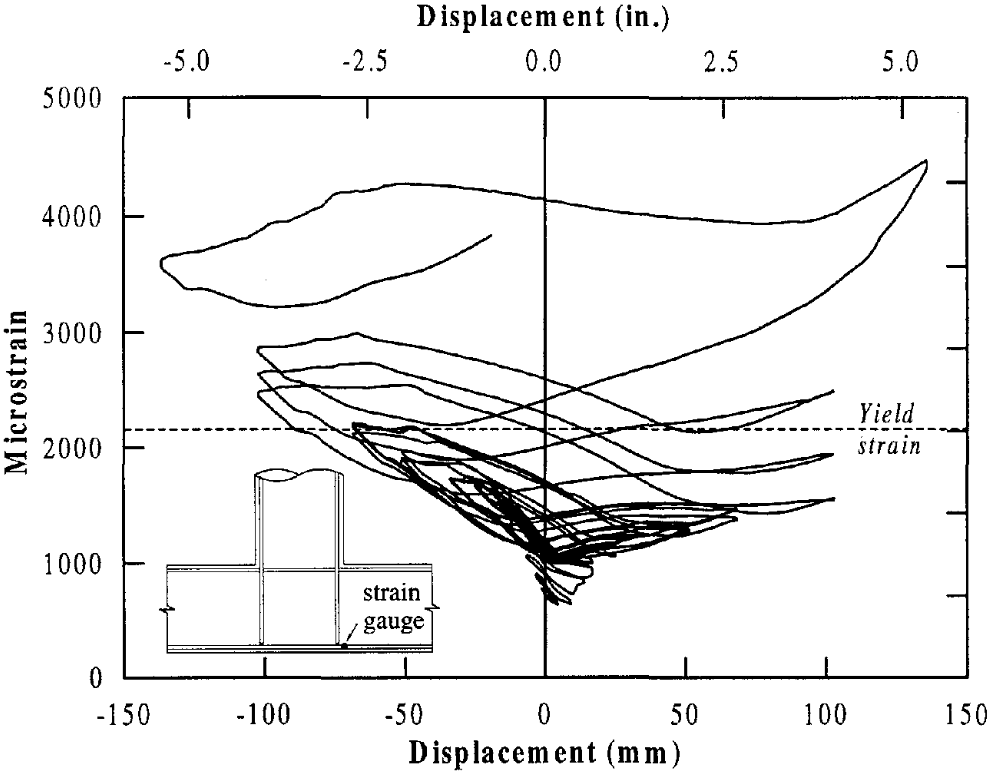

Figure 4.43 Strain history of a bottom beam reinforcement gauge located at the column face.

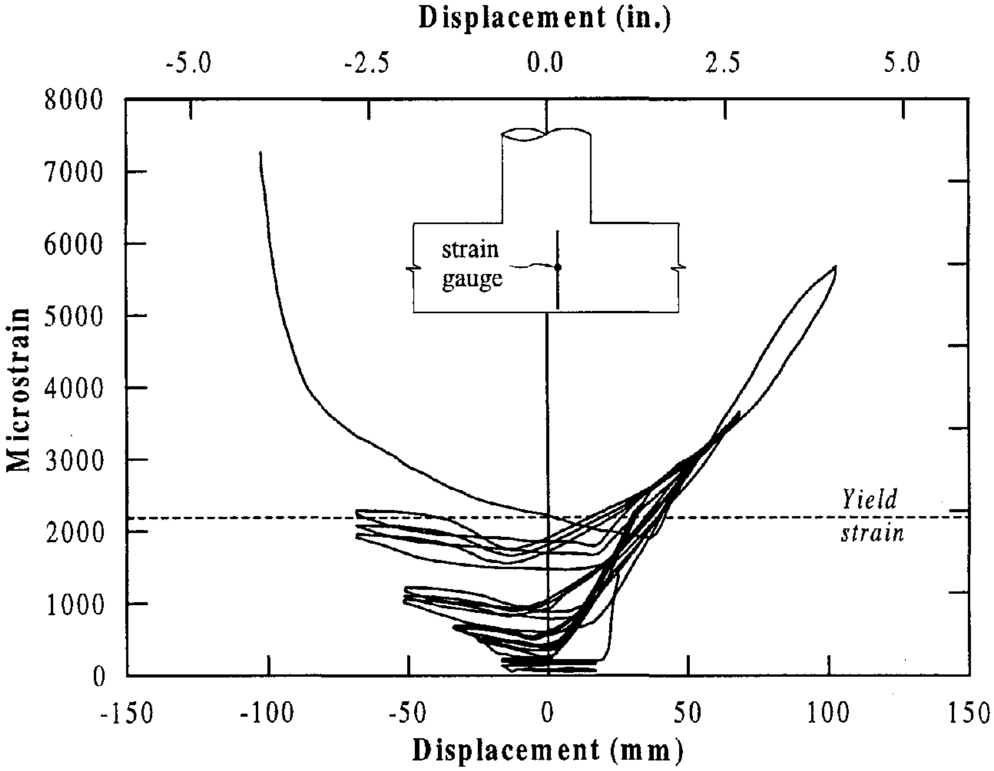

Figure 4.44 Strain history of a joint stirrup gauge at mid-height of the beam.

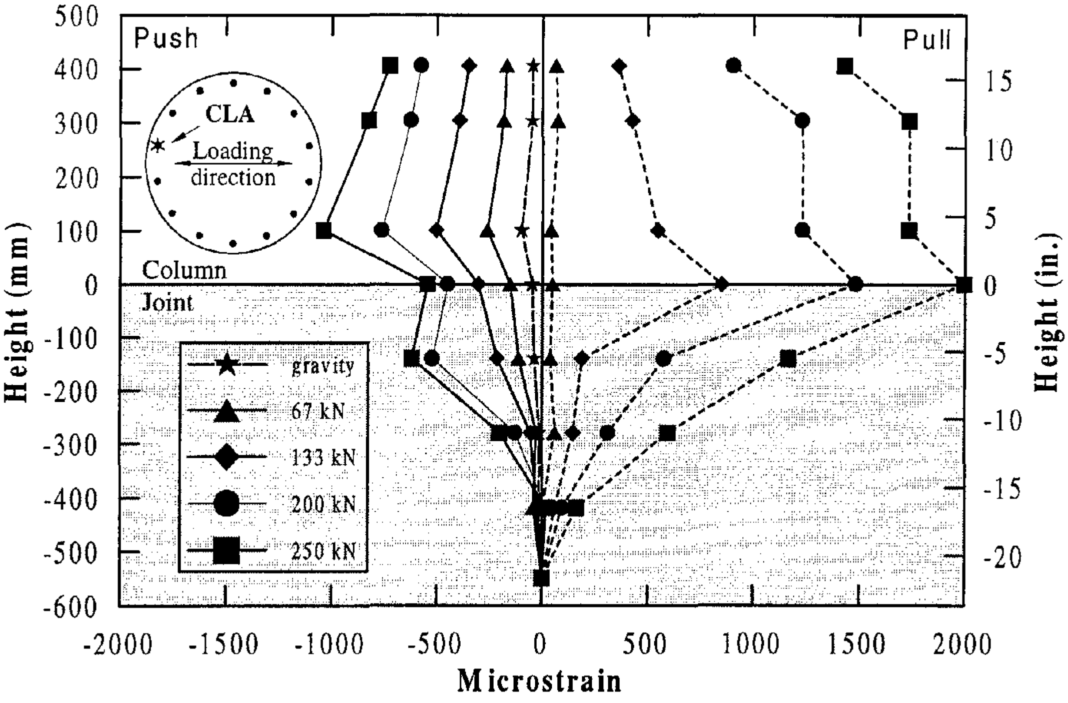

(a) Initial stages of testing

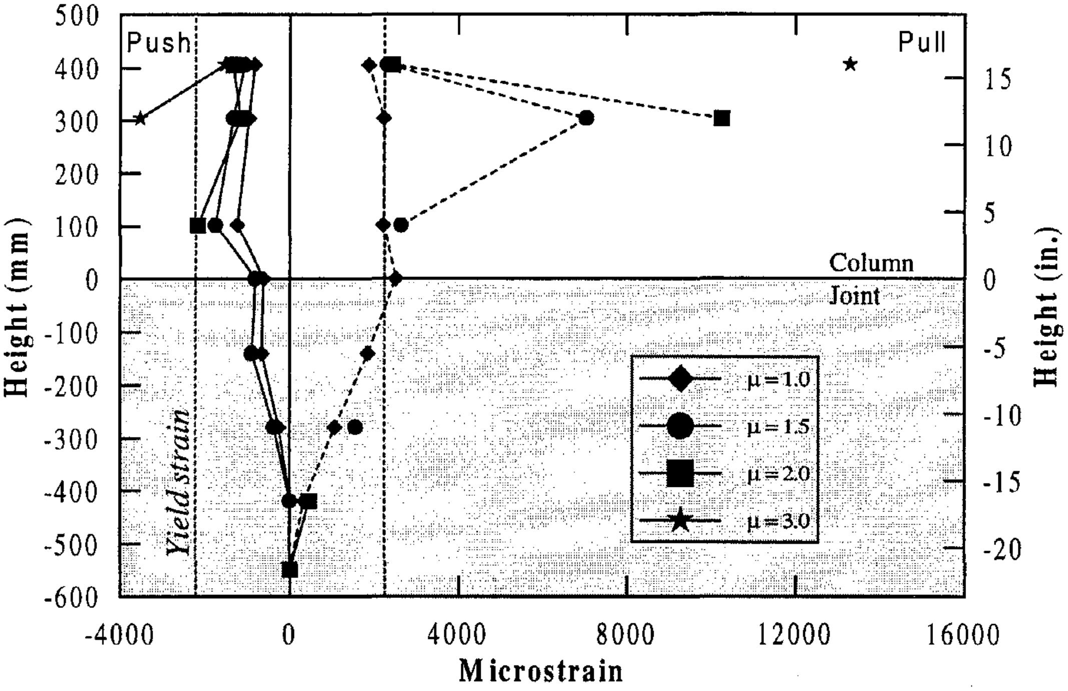

(b) At moderate ductilities

Figure 4.45 Strain profiles of a column longitudinal extreme tension reinforcement (CLA).

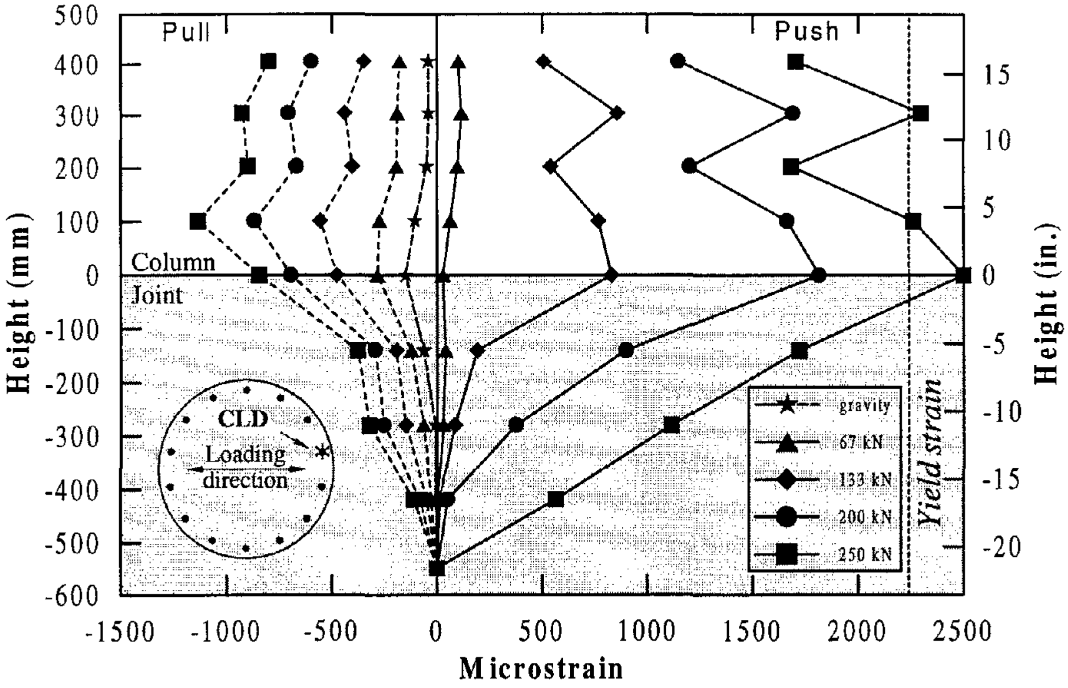

(a) Initial stages of testing

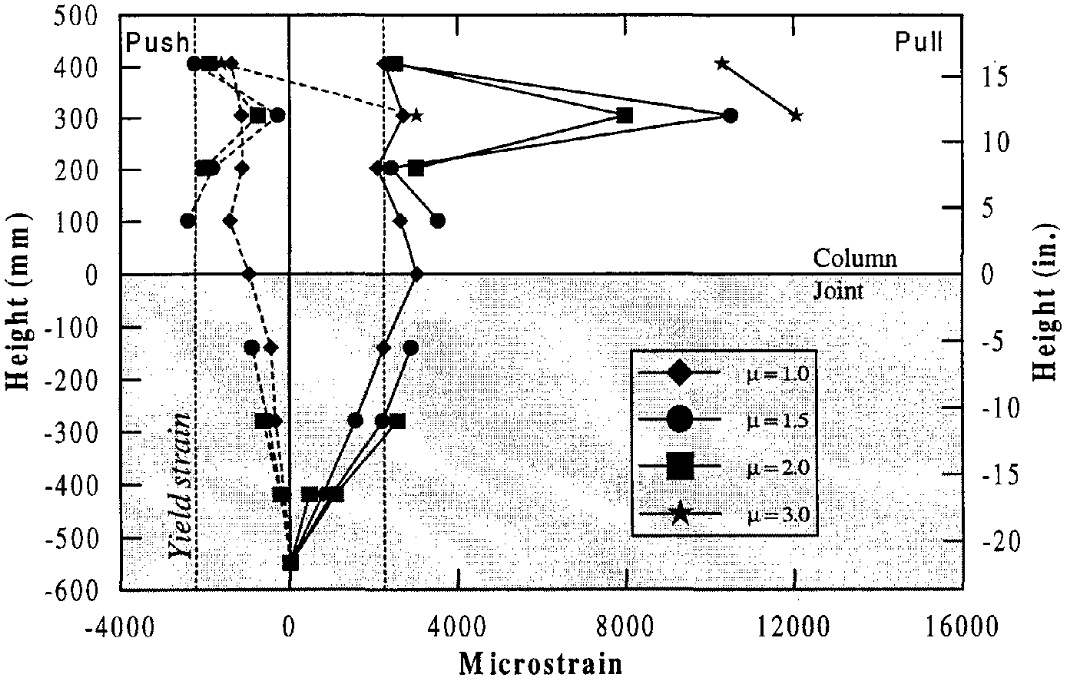

(b) At moderate ductilities

Figure 4.46 Strain profiles of a column longitudinal extreme tension reinforcement (CLD).

In Figure 4.48 strain profiles of the spiral gauges placed on the east side of the test unit is shown. These strains represent the shear contribution of the spirals in the column and out-of-plane transverse tension strain developed within the interior joint. Even though the column shear reinforcement was expected to remain elastic, strain gauge readings in excess of yield limit were recorded. An explanation for this disagreement between the expected and observed behavior is given in Section 4.7. The effect of out-of-plane transverse tension strain within the joint was dominant from the beginning when the gravity load was applied and the strain demand in the joint spirals increased with depth. Similar trends were also observed for the gauges on the west side of the specimen.

The second and third gauged joint spirals (see Figure 3.24) from the bottom (as cast) of the beam were provided with ten strain gauges to examine the variation of strain demand along the transverse reinforcement. Strain gauge profiles obtained from the third gauged spiral is shown in Figure 4.49 in which the effect of out-of-plane transverse strain is clearly seen. At small horizontal loads, no significant difference in the strain is seen (Figure 4.49a) between the gauges mounted in the loading plane and those in the out-of-plane to the loading direction. High strains were induced in the out-of-plane direction starting from a horizontal load of 250 kN (56.2 kips). The strain demand in the out-of-plane direction was noticeably higher than that in the in-plane direction at large displacement ductilities.

Four of the seven longitudinal bars placed at the top and bottom of the beam were strain gauged. Strain profiles of two bars each from the top and bottom reinforcement are shown in Figures 4.50 – 4.53. A regular strain pattern was observed for the bottom (as cast) reinforcement (Figures 4.50 and 4.51) while the strain profiles of the top beam bars appeared to be somewhat irregular. This trend was observed in the strain histories presented in Figures 4.41 and 4.42. When designing the cap beam it was ensured that the strain induced by positive and negative moments would be below yield at the ultimate limit state (see Section 4.1.2). In addition, the maximum column moment was considerably overestimated in the design, and hence the calculated beam design moments were highly conservative. Consequently, an elastic response of the beam should be expected. The moment-curvature response in the critical regions of the beam confirmed that the behavior was indeed elastic (Figure 4.20) and strain induced in the reinforcement should be well below the yield strain. On the contrary, the longitudinal beam reinforcement recorded strains in excess of yield in the beam segments as well as within

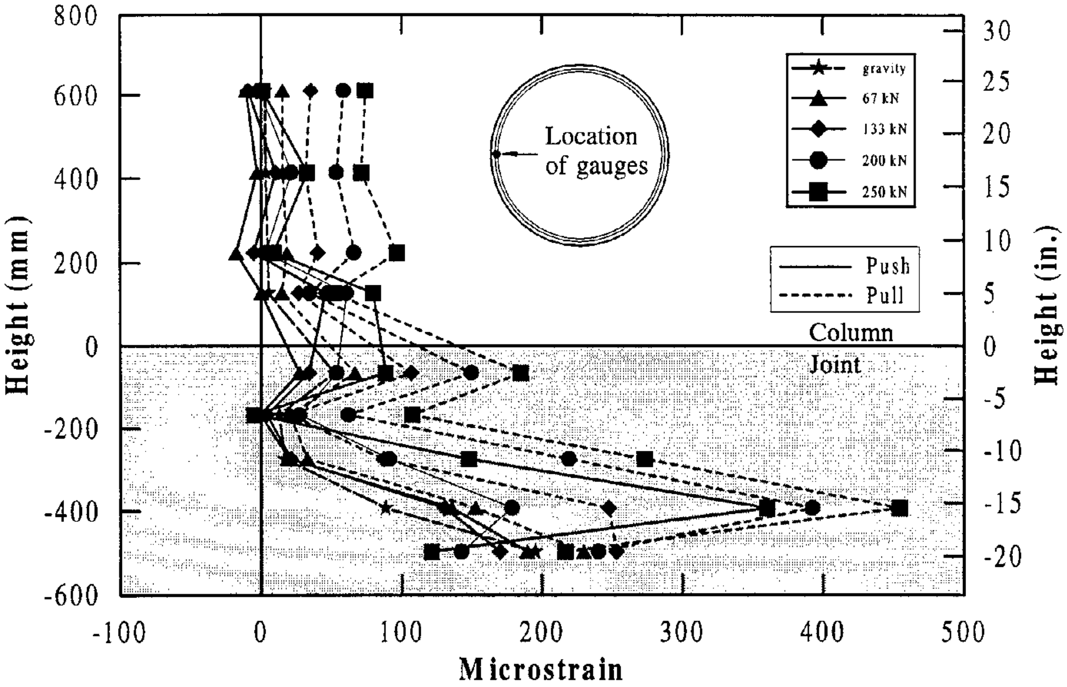

(a) Initial stages of testing

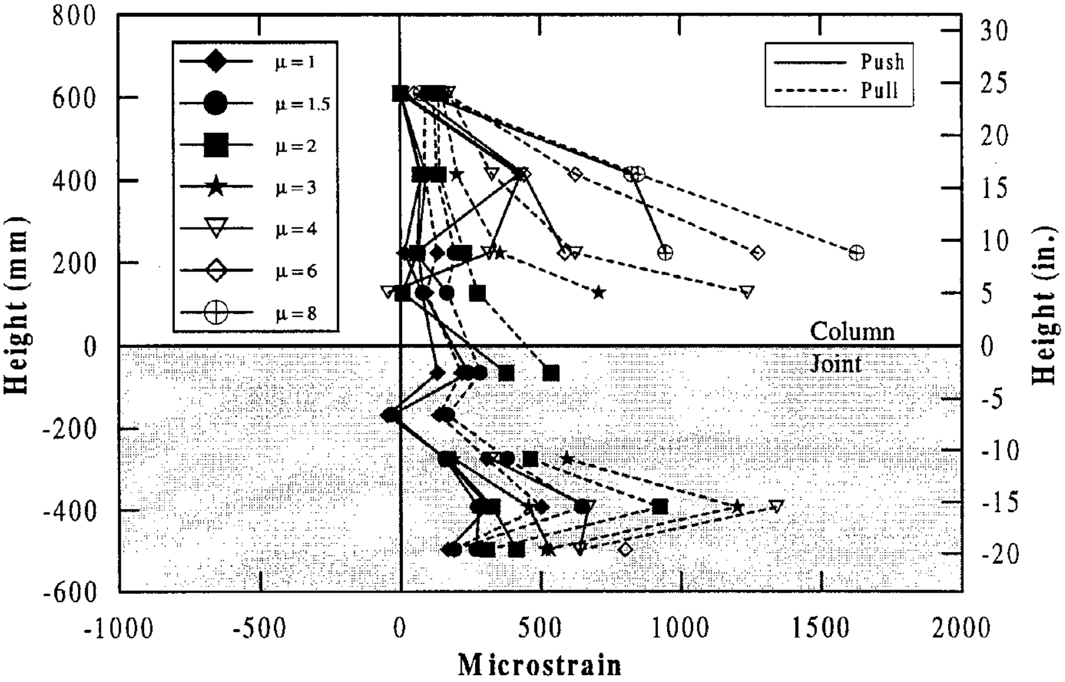

(b) Final stages of testing

Figure 4.47 Strain profiles of gauges mounted on the south side of column and joint spirals.

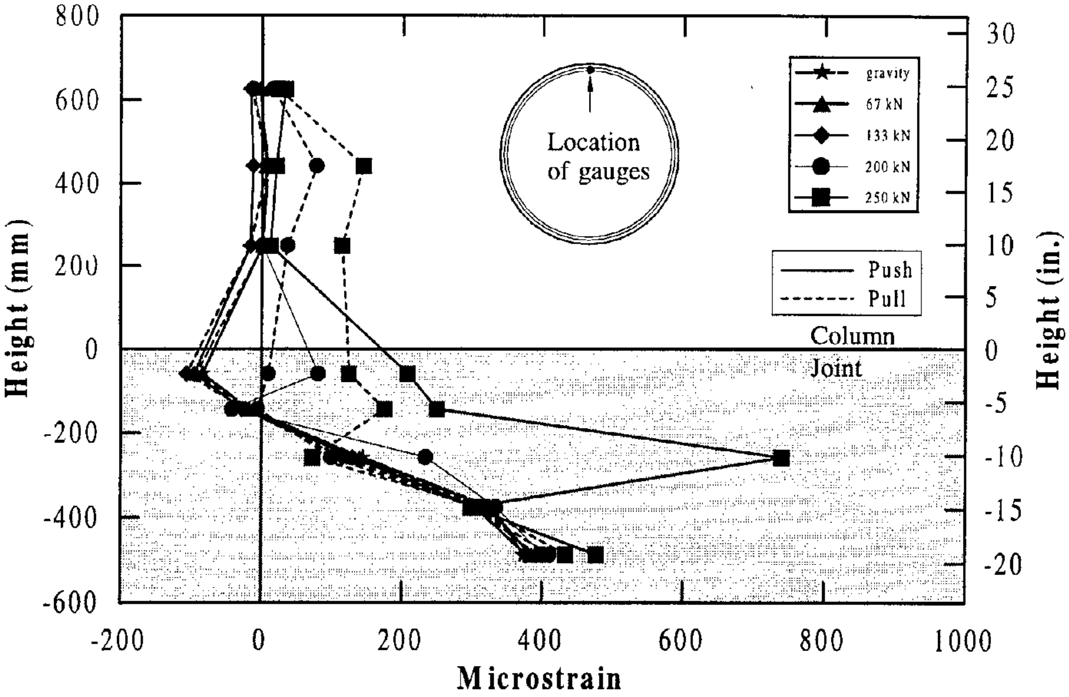

(a) Initial stages of testing

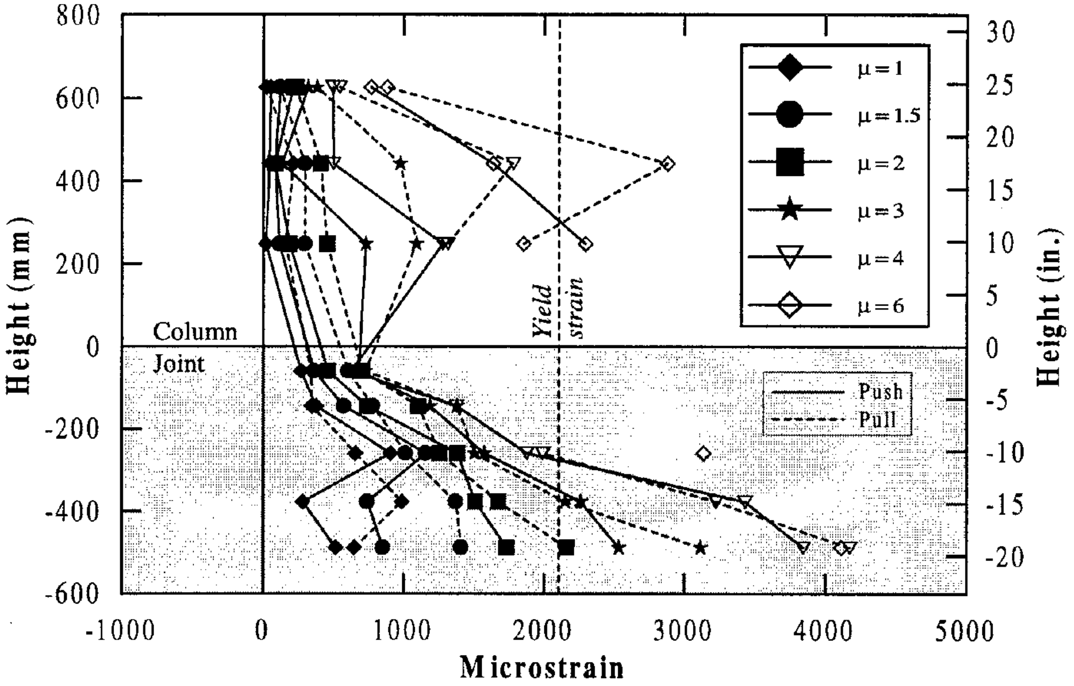

(b) Final stages of testing

Figure 4.48 Strain profiles of gauges mounted on the west side of column and joint spirals.

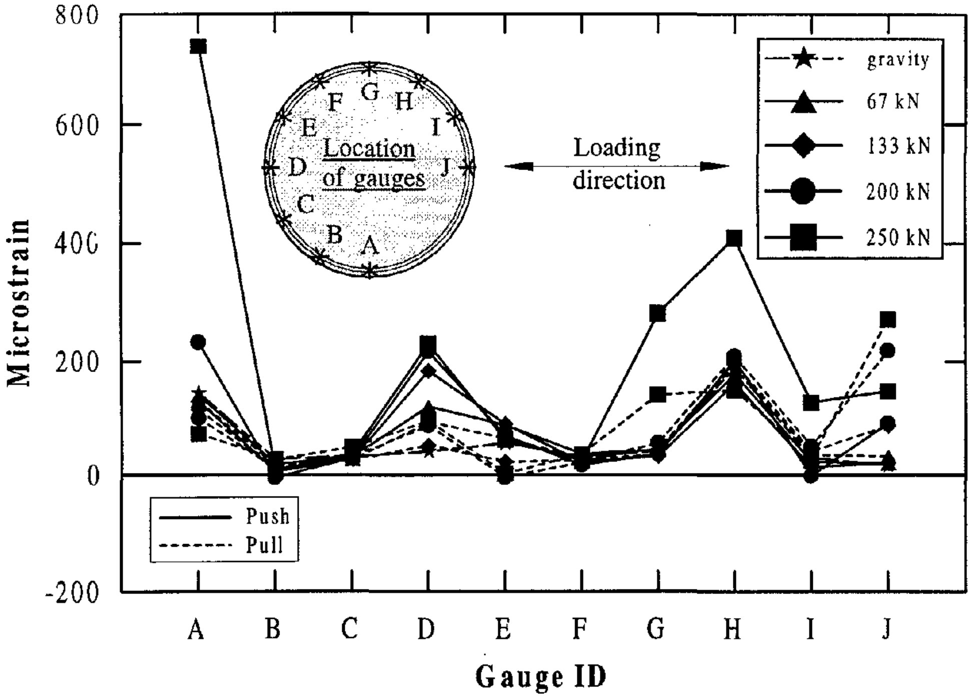

(a) Initial stages of testing

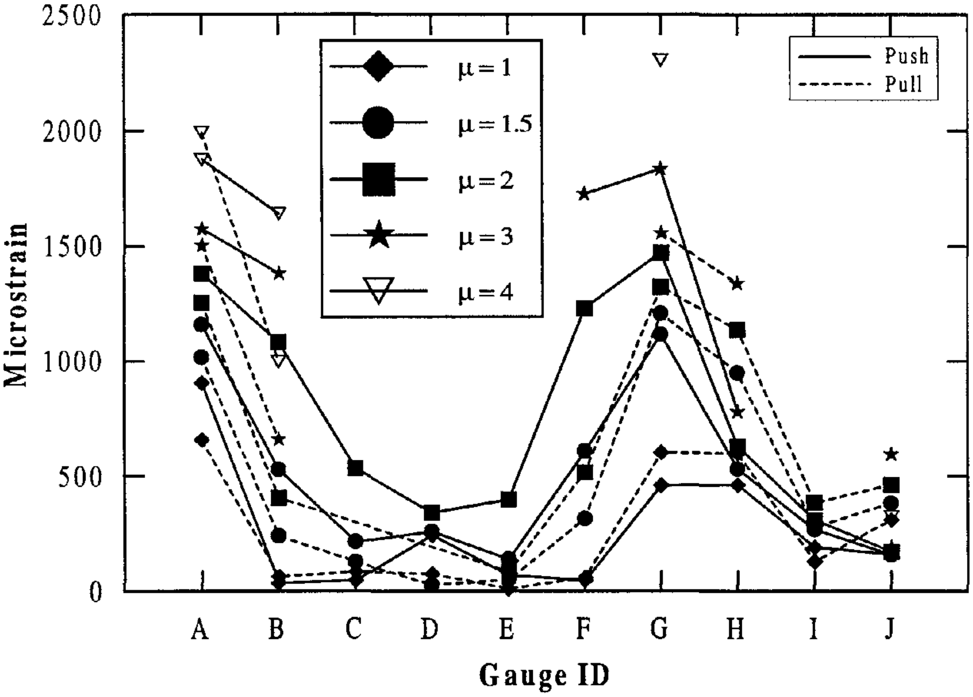

(b) At moderate ductilities

Figure 4.49 Strain profiles of gauges mounted on a joint spiral at mid-height of the beam.

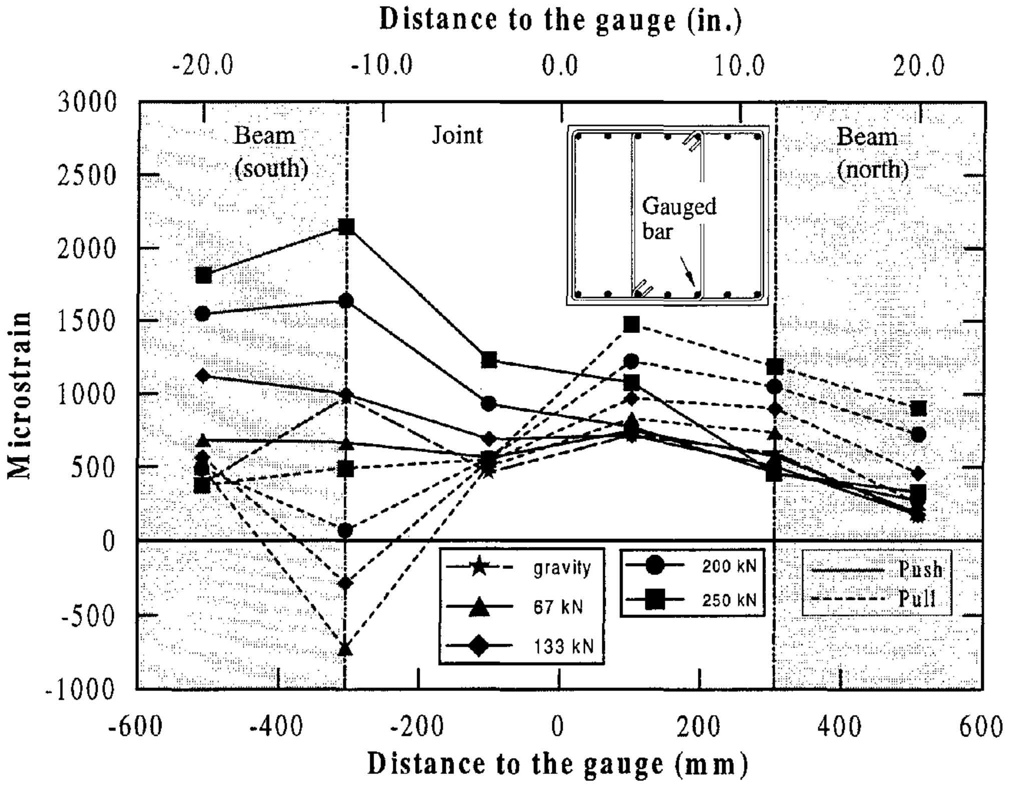

(a) Initial stages of testing

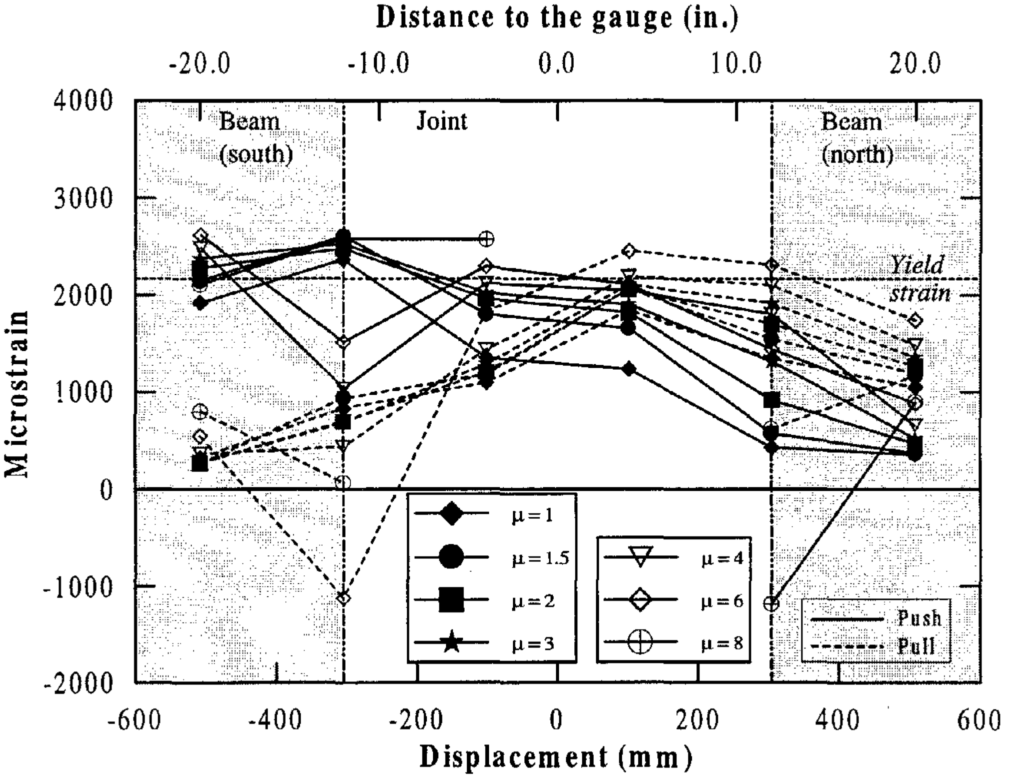

(b) Final stages of testing

Figure 4.50 Strain profiles along a bottom longitudinal beam reinforcement.

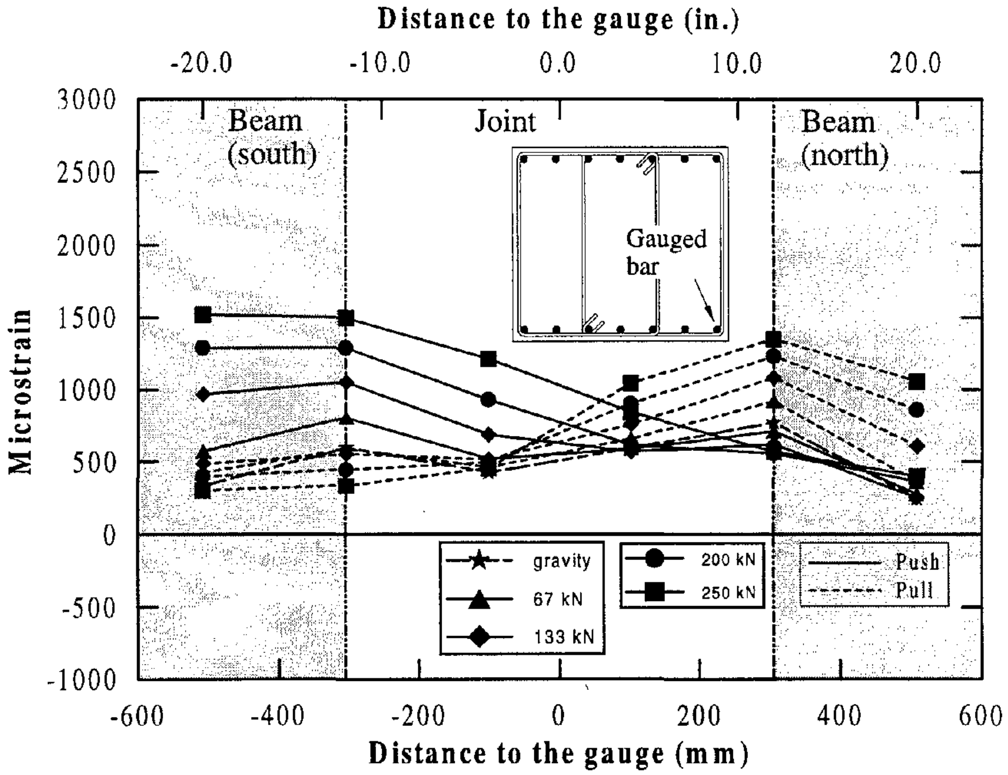

(a) Initial stages of testing

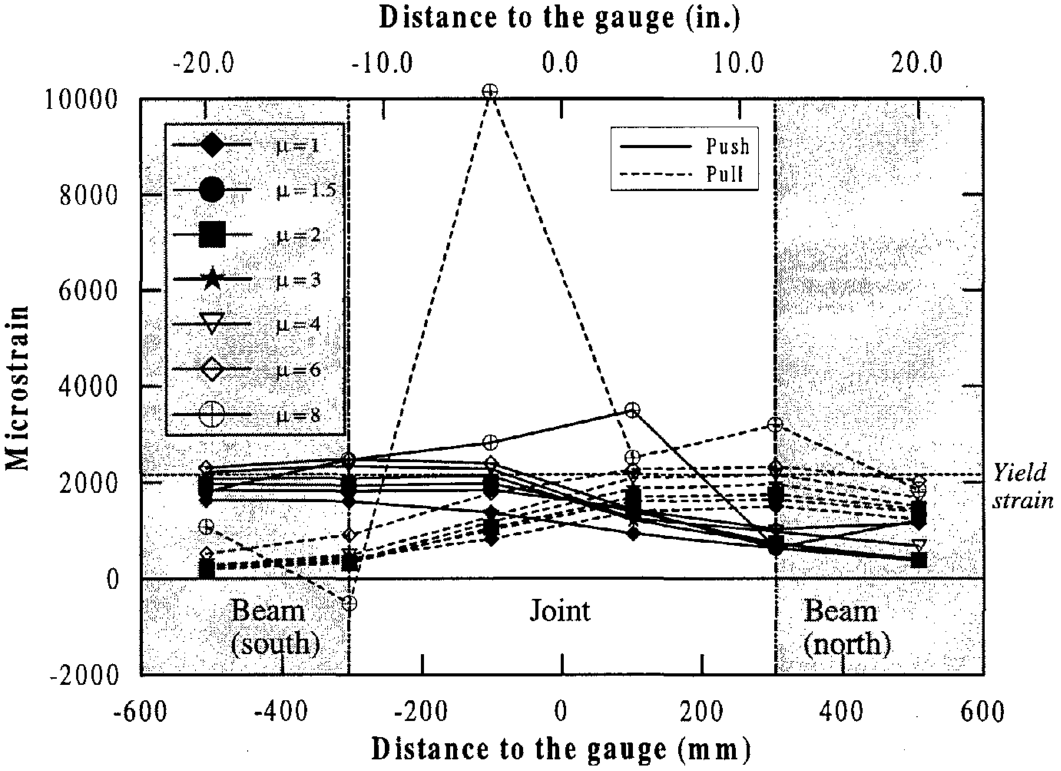

(b) Final stages of testing

Figure 4.51 Strain profiles of a bottom longitudinal beam reinforcement.

the joint. This is believed to have occurred as a result of joint force transfer mechanism and is further investigated in a companion report [26].

As can be seen in Figure 3.24, two legs of several cap beam stirrups were gauged at different depths of the beam. The strains obtained at the peak displacements during the first cycle at each loading step are shown in Figures 4.54 and 4.55 for the gauges mounted on the outer and inner legs of the stirrups at mid-height of the beam. Yielding of joint stirrups occurred at a displacement ductility of about 3. High strains were also recorded particularly in the outer legs of the stirrups placed outside the joint in the cap beam. Also shown in Figures 4.56 and 4.57 are the strain profiles recorded respectively at 5/6th of the beam depth (from the bottom as cast) in the outer legs and 1/6th of the beam depth in the inner legs of the stirrups. A significant inelastic strain was developed at the beam/joint interface in the inner leg for the push direction loading at ductility 6 (Figure 4.56). Since only a elastic recovery of the strain occurs during load reversal, a high strain was also recorded in the pull direction. The variation of strain in the stirrups as a function of beam depth can be identified by comparing all four figures. The strain gauge readings taken at different depths of the outer and inner legs of the stirrups were found to be comparable.

4.7 Discussion

A reinforced concrete cap beam/column tee joint was designed and tested under simulated seismic loading, and its performance is presented in this chapter. In detailing the joint region, an efficient force transfer mechanism was considered so that the amount of reinforcement required within the joint could be minimized. In the conventional design methods, the joint region is detailed for the maximum joint shear forces. This results in unnecessarily conservative detailing, causing congestion problems.

Within the expected displacement limits (i.e. column drifts of about 5%), the test unit performed satisfactorily. When the column displacement corresponding to 6.4% drift was imposed, a balanced failure of the column and joint occurred. Buckling of the longitudinal column reinforcement in the plastic hinge region and diagonal compression strut failure within the joint were encountered. In a real structure, some additional confinement to the joint would be given by the steel provided for the longitudinal response. Also, it is recommended that the joint vertical stirrups should be provided as closed ties instead of hairpins as were used in this test. Consequently, it can be stated that

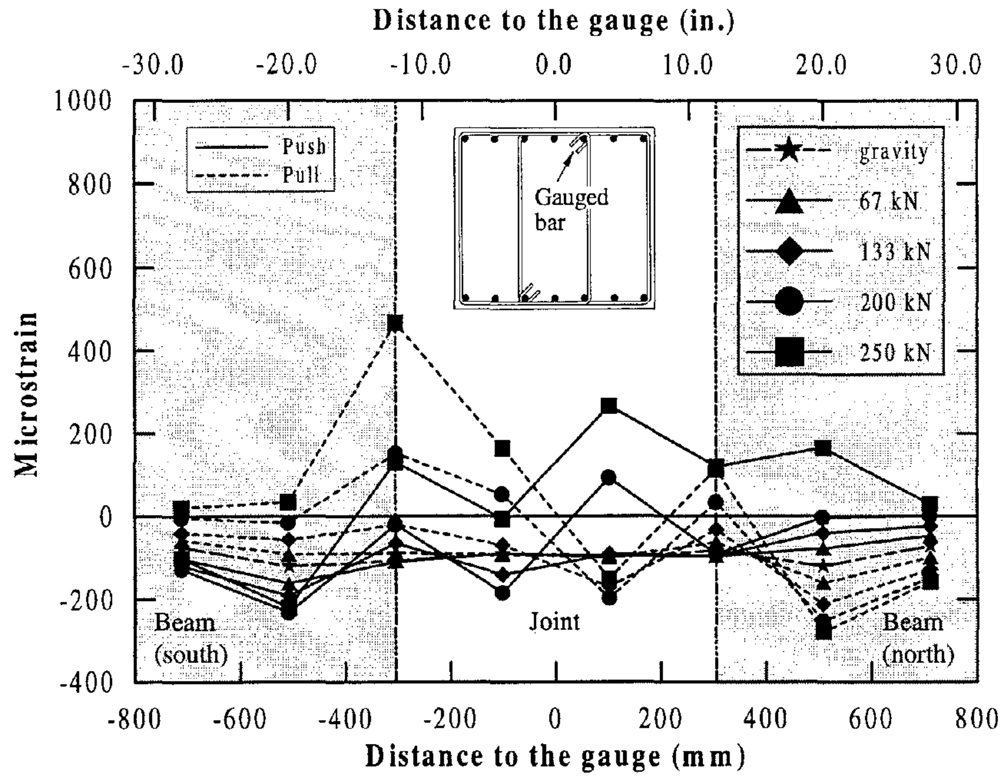

(a) Initial stages of testing

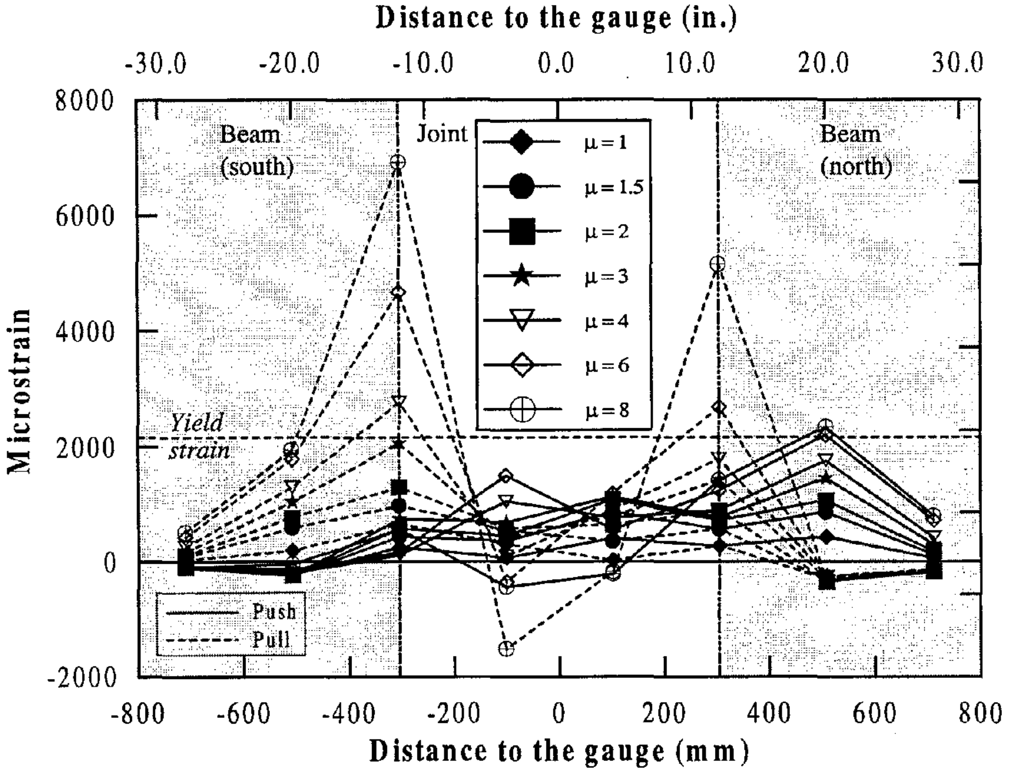

(b) Final stages of testing

Figure 4.52 Strain profiles along a top longitudinal beam reinforcement.

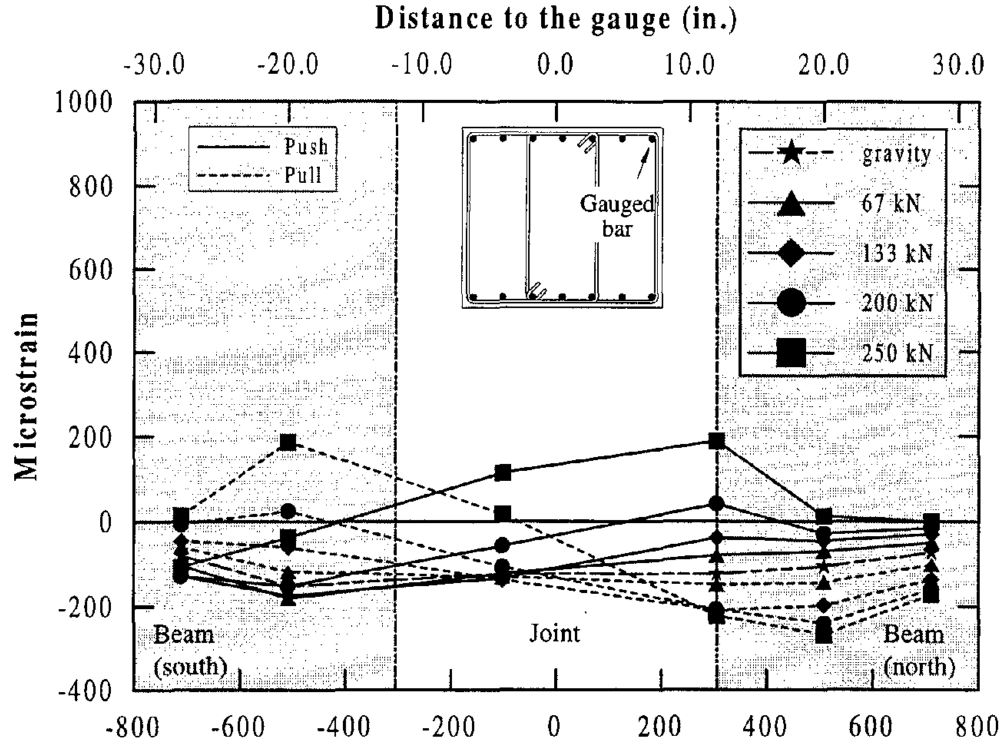

(a) Initial stages of testing

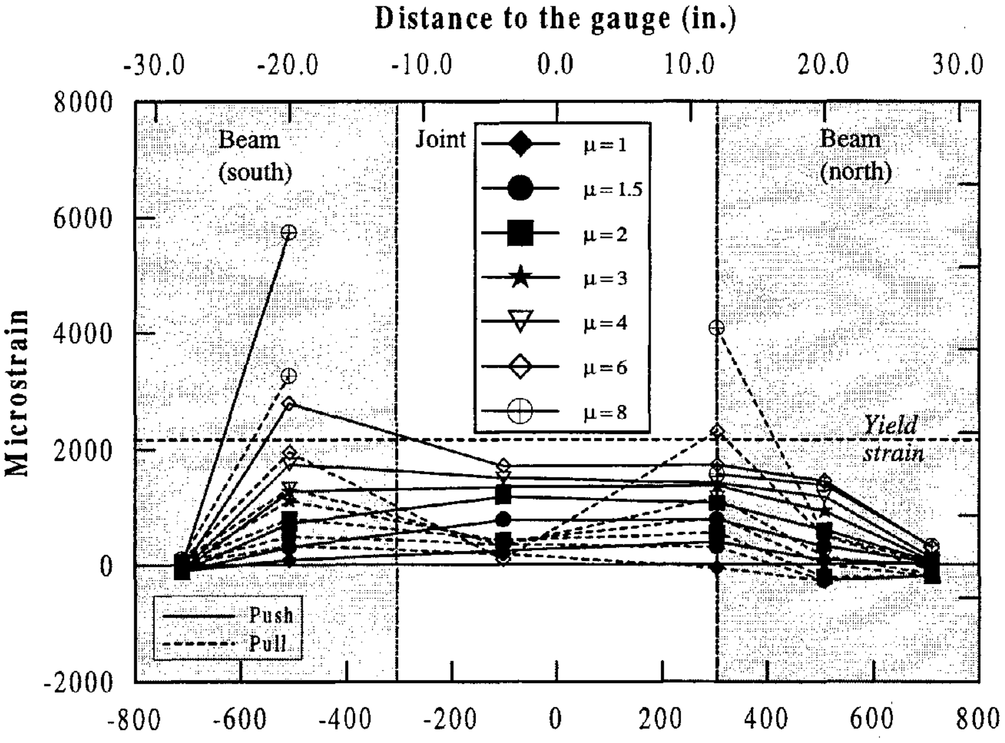

(b) Final stages of testing

Figure 4.53 Strain profiles along a top longitudinal beam reinforcement.

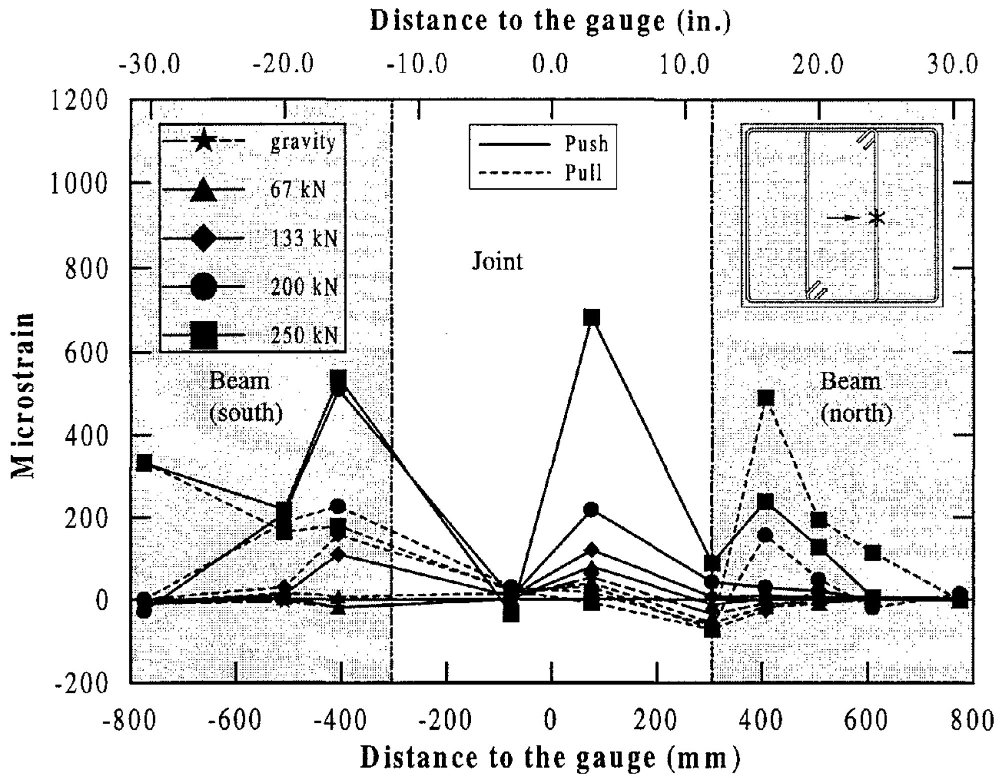

(a) Initial stages of testing

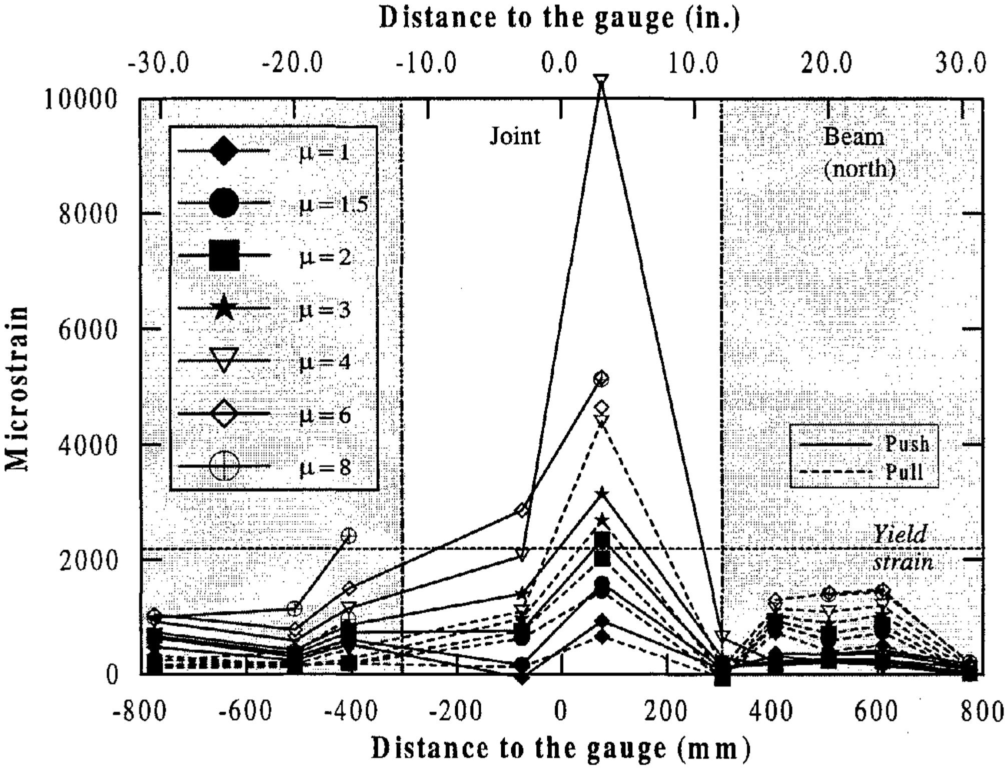

(b) Final stages of testing

Figure 4.54 Strain profiles of inner leg beam stirrups at mid-height.

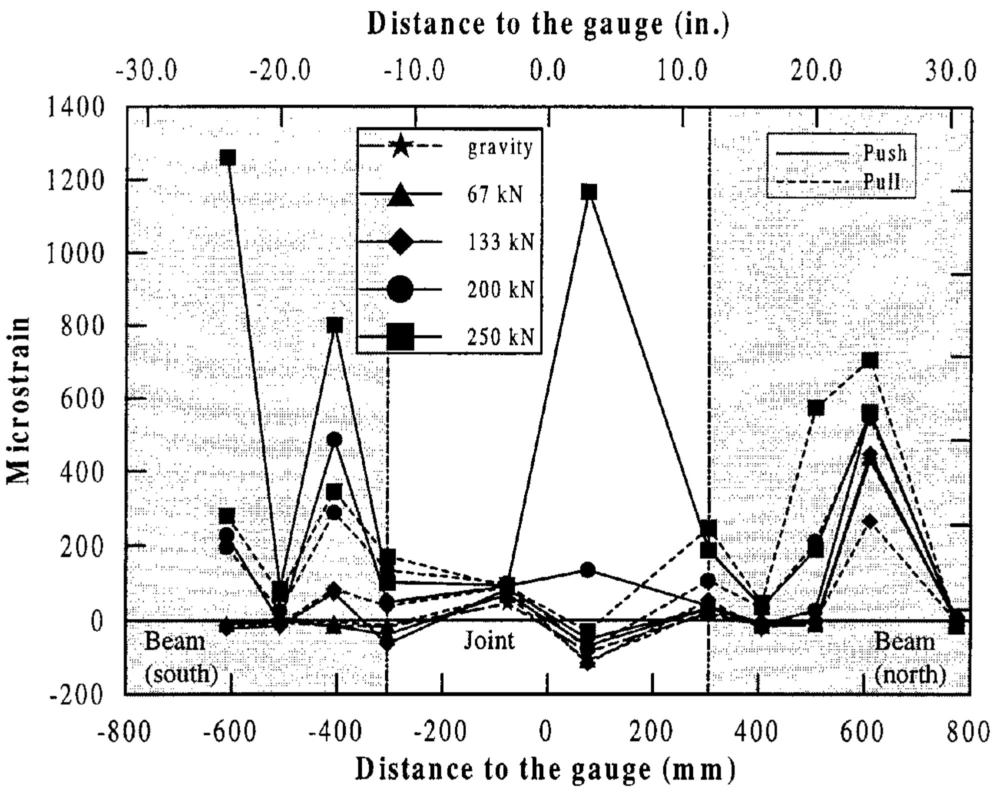

(a) Initial stages of testing

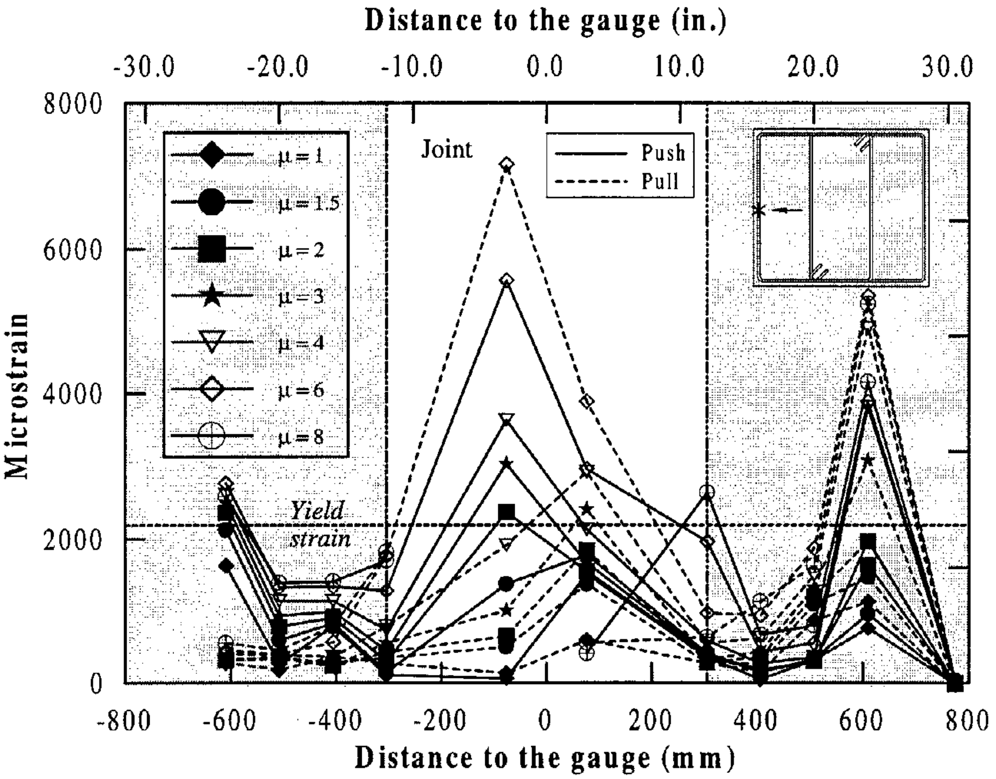

(b) Final stages of testing

Figure 4.55 Strain profiles of outer leg beam stirrups at mid-height.

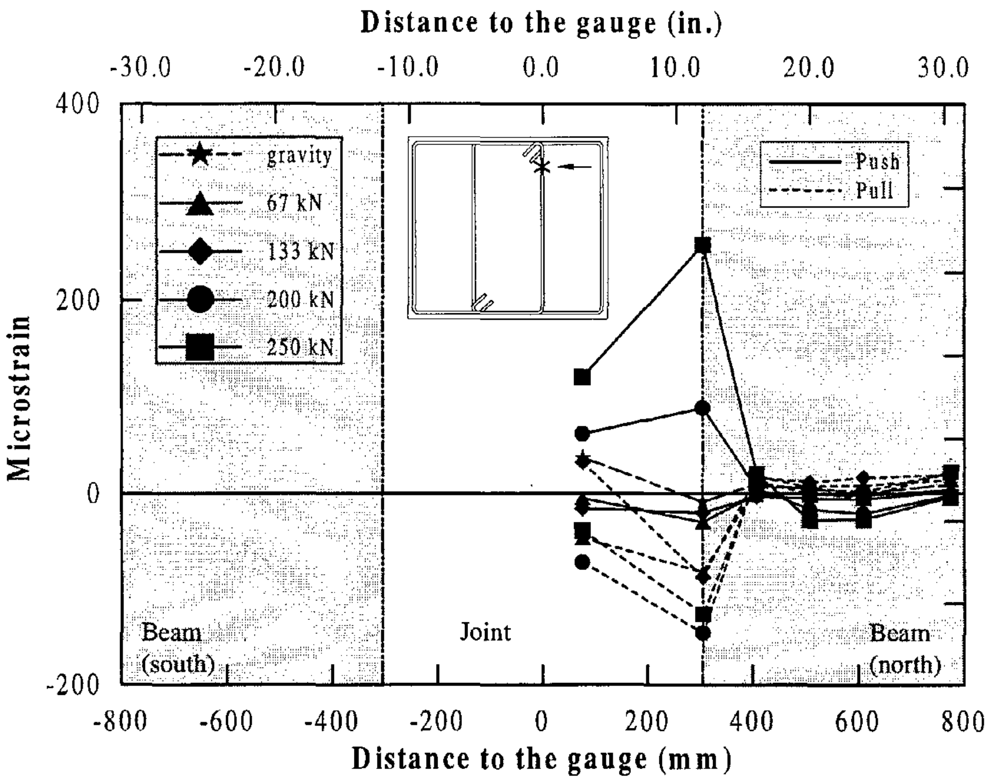

(a) Initial stages of testing

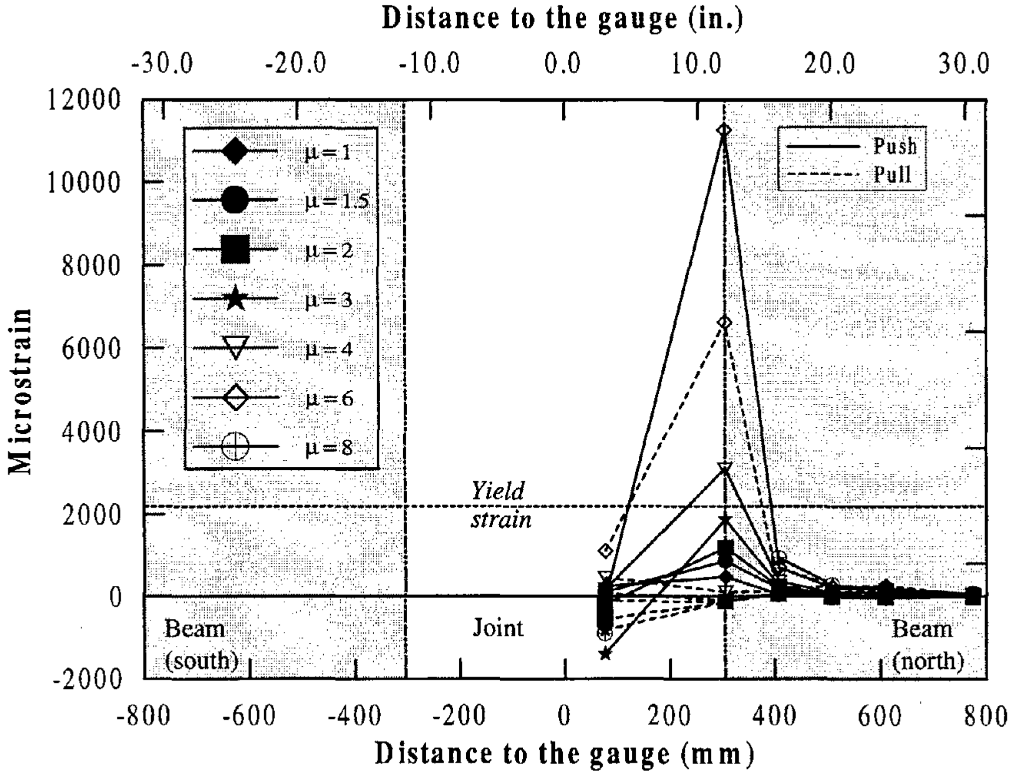

(b) Final stages of testing

Figure 4.56 Strain profiles of inner leg beam stirrups at 5/6th of beam depth.

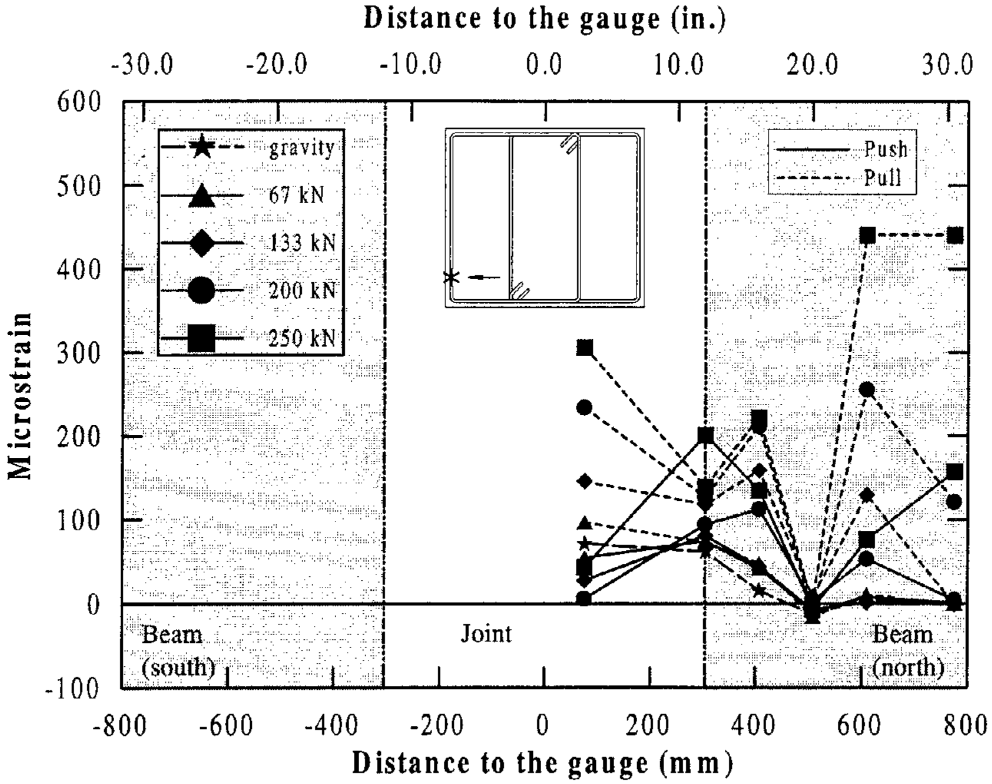

(a) Initial stages of testing

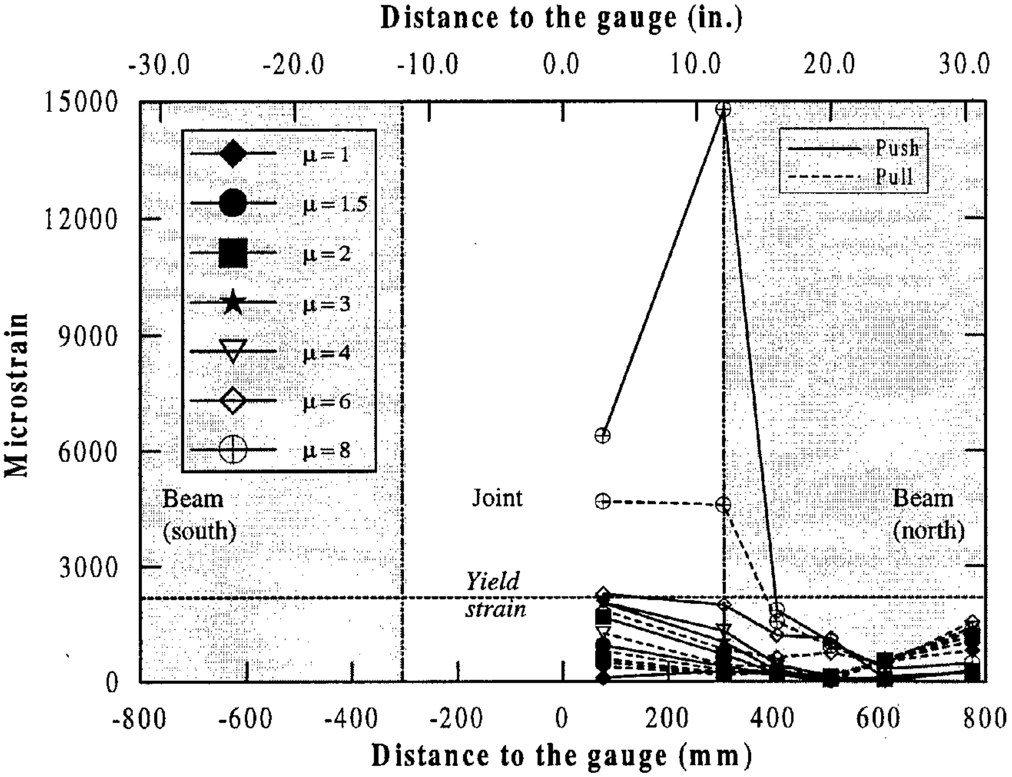

(b) Final stages of testing

Figure 4.57 Strain profiles of outer leg beam stirrups at 1/6th of beam depth.

a better joint performance and failure in the column can be expected for the force transfer mechanism considered for the joint design.

The overstrength capacity of the column was taken as 30 percent higher than the theoretical ultimate strength and this estimate was found to be excessively high, overestimating the cap beam design moments. The maximum column moment developed during the test was only 2.4 percent higher than the theoretical ultimate moment. The response of the column was dominated by flexural behavior with a plastic hinge forming adjacent to the joint interface. Shear cracks in the column did not appear to be significantly large, but strain gauge readings confirmed that yield strength was developed in the column shear reinforcement at some locations. In the design calculations, it was ensured that the column spirals were adequate to protect the column from any significant shear deformation and yielding of the spiral was *not* anticipated. This discrepancy is believed to have caused by the procedure which was used to estimate the shear resistance of the transverse reinforcement. As noted previously, a three component model was considered for the shear design as follows [19]:

$$\mathbf{V_r = V_c + V_s + V_p} \tag{4.8}$$

where $\mathbf{V_r}$ is the total shear resistance, $\mathbf{V_c}$ is the concrete component, $\mathbf{V_s}$ is the resistance from the spiral reinforcement, and $\mathbf{V_p}$ is the contribution from the axial force. Using the measured concrete and steel properties, the minimum contributions from $\mathbf{V_c}$ and $\mathbf{V_p}$ were estimated to be 67 kN (15 kisp) and 53 kN (12 kips) respectively. The applied maximum shear in the column was 436 kN (98 kips), requiring shear resistance of 316 kN (71 kips) from the spiral. The contribution shear resistance by spirals of a circular column was obtained as follows:

$$\mathbf{V_s = \frac{\pi}{2} \frac{A_h f_{yh} D'}{s} \cot\theta} \tag{4.9}$$

where $\mathbf{A_h}$ is the cross sectional area of the spiral, $\mathbf{f_{yh}}$ is the yield strength of spiral, $\mathbf{D'}$ is core diameter, $\mathbf{s}$ is the spacing of the shear reinforcement and θ is the angle of the critical inclined flexure-shear cracking. In the design calculations, $\mathbf{D'}$ = 568 mm (22.4 in) and $\theta = 30^\circ$ were considered. In a recent publication [10], it has been suggested that the term $\mathbf{D'}$

should be replaced with **(D'-c)** in Eq. 4.9 considering that only the portion of transverse reinforcement in the tension zone contributes for shear resistance. Based on the estimated $\mathbf{V_s}$ component listed in Table 4.3, both approaches suggest that the shear reinforcement provided in the column was adequate if $\theta = 30^\circ$ is considered. When $\theta = 45^\circ$ is assumed as used in the design codes, it is found that both methods suggest that the shear reinforcement in the column was insufficient although the second method indicates more severe shear damage in the column than the first method.

Table 4.4: Shear resistance contribution of column spiral (i.e. $\mathbf{V_s}$) considering different parameters. (Note: $\mathbf{V_{s,exp}}$ = 316 kN)

	using **D'** in Eq. 4.9	using **(D'-c)** in Eq. 4.9	using Eq. 4.10
$\theta = 30^\circ$	489 kN (110 kips)	365 kN (82 kips)	391 kN (88 kips)
$\theta = 35^\circ$	405 kN (91 kips)	298 kN (67 kips)	325 kN (73kips)
$\theta = 45^\circ$	285 kN (64 kips)	209 kN (47 kips)	227 kN (51 kips)

From experimental observation of this column and of the columns in other two prestressed units (IC2 and IC3), it was concluded that inclined shear cracking did not form at 30°. A more appropriate value for θ would be 35° for all three columns discussed in this report. Secondly, in Eq. 4.9, the shear resistance of each spiral is represented by an average value of $\frac{\pi}{2}\mathbf{A_h f_{yh}}$, which assumes the component resisting shear along the spiral varies from **0** to $\mathbf{A_h f_{yh}}$ within each quadrant. If **(D'-c)** term is considered in Eq. 4.9 instead of **D'**, then the average force per spiral should be modified accordingly. This results in Eq. 4.10 if it is assumed that the neutral axis depth of a circular section at ultimate is approximately at **D'/4** from the extreme compression fiber. Note that it is more appropriate to consider **(D-c-cover)** instead of **(D'-c)** in Eq. 10, but this modification is not expected to give any significant change in the $\mathbf{V_s}$ component for this particular case.

$$\mathbf{V_s = \frac{1.685 A_h f_{yh}\left(D' - c\right)}{s}\cot\theta} \tag{4.10}$$

Representation of $\mathbf{V_s}$ component as a function of neutral axis depth is presented in reference 10. When Eq. 4.10 is considered with $\theta = 35^\circ$, the predicted $\mathbf{V_s}$ component is 325 kN (73 Kips), suggesting that yielding of the shear was possible in the column of test unit IC1. When $\theta = 35^\circ$ is considered in Eq. 4.9 and $\theta = 30^\circ$ or 45° is used in Eq. 4.10, the resulting $\mathbf{V_s}$ component does not seem to explain the observed behavior.

In estimating the shear resistance of the transverse reinforcement in Eq. 4.10, two compensating approximations were made. The shear resistance of the concrete was taken as the minimum possible theoretical value [19] and it was assumed that all of the spirals within $\mathbf{(D'-c)cot\theta}$ were mobilized by the inclined shear cracks. When high shear strains were induced in the column transverse reinforcement, the column was subjected to large inelastic displacements, and subsequently the extreme longitudinal tension reinforcement in the column would have developed significantly large inelastic strains. This resulted in wider flexural cracks on the tension side of the column. Therefore, most of the cracking in the column at large ductilities appeared to be more like flexure-shear rather than pure shear (Figure 4.14), indicating that not all of the spirals within $\mathbf{(D'-c)cot\theta}$ could have been mobilized. If the column shear demand had continuously increased, steep inclined shear cracks would have developed with possibly $\theta = 30^\circ$ in order to mobilize all of the spirals within $\mathbf{(D'-c)cot\theta}$ to provide the necessary shear resistance. If the shear resistance provided by the spirals is insufficient, shear failure ensues by developing potential failure planes along the steep inclined cracks. This phenomena has been observed in typical tests on shear columns [28]. Based on this, it is concluded that the column of IC1 was far from failing in shear. The shear reinforcement provided in the column was perhaps close to the optimum amount required to ensure a flexural response. When the column is designed with the recent design recommendation [19], which considers $\theta = 35^\circ$, and strength reduction factor of 0.85 for all three components, a more conservative detailing is expected for shear resistance.

As stated in Section 4.1.2, the cap beam of the test unit was designed conservatively such that the strains in the longitudinal steel would remain within the yield limit. The bending moments induced at the critical sections of the beam during the test were less than the design moments. However, a number of gauges mounted on the longitudinal beam reinforcement indicated that yield strength was developed in several of these bars in the critical regions of the beam and within the joint at as low as ductility 4. The strains monitored in the longitudinal beam bars generally appeared to be high even at lower ductility levels. Further, the top longitudinal reinforcement recorded high strains with opposite sign at the column face. The damage to the beam was insignificant until the displacement ductility 8 was achieved, and therefore localized damage can not be attributed to these uncharacteristic behavior. It is believed that the joint force transfer mechanism was responsible for developing unexpected strains in the beam reinforcement and is currently being further investigated [26].

The first shear cracking within the joint was predicted at a horizontal force of 222 kN (50 kips) assuming that the cracking of the joint corresponds to that induces the maximum joint principal tensile stress of $\mathbf{0.29\sqrt{f'_c}}$ in S.I. units $\left(\mathbf{3.5\sqrt{f'_c}} \text{ in psi units}\right)$, and the first joint shear cracks developed at F = 200 kN (45 kips) during the test. The major shear diagonal crack, which led to a joint shear failure at the ultimate displacement, formed when the average joint principal tensile stress reached its peak value of $\mathbf{0.5\sqrt{f'_c}}$ $\left(\mathbf{6\sqrt{f'_c}} \text{ in psi units}\right)$. Further, in the design procedure, no comparison was made between the demand and capacity of the joint strut nor any limiting criteria was imposed in order to avoid crushing of concrete in the joint region. Despite the average joint principal compression stress reaching only a peak value of $\mathbf{0.1f'_c}$, a failure in the joint strut occurred as a result of concrete crushing. It is suggested that it is important to establish a simple rational procedure for ensuring that the demand in the joint strut does not exceed its capacity so that joint strut failure can be avoided. This aspect is investigated in a companion report dedicated for the analysis of the joint response [26].

A simple modeling of the test unit using beam-column elements to represent structural members captured the overall force-displacement behavior with sufficient accuracy. Cracked section properties of individual members and inelastic response of the column were estimated from a moment-curvature analysis. When the displacement components due to column flexure and joint rotation were compared with the theoretical estimates, the column flexure component was found to be slightly overestimated while the column displacement due to joint rotation was marginally underestimated. Experimentally measured displacement component due to joint shear appears to be significant and should be included in the displacement calculations.

CHAPTER 5

INTERIOR JOINT WITH A PARTIALLY PRESTRESSED CAP BEAM

The second test unit, IC2, was designed with a partially prestressed cap beam. Design details and seismic performance of this unit are reported in this chapter.

5.1 Design Procedure

5.1.1 Column

Since identical column capacities were considered in all three test units, the column reinforcement details of IC1 were replicated.

5.1.2 Cap Beam

The design moments of the cap beam were taken as those estimated for IC1 (Figure 4.1). In detailing the beam, it was considered that about 50 percent of the negative moment be transferred to prestressing and the remainder be designed with conventional reinforcement, resulting in a partially prestressed bent cap. As for unit IC1, no yielding was permitted in the longitudinal beam reinforcement.

5.1.3 Interior Joint

The maximum principal tensile and compression stresses of the joint at the ultimate limit state were estimated to be $\mathbf{0.52\sqrt{f_c'}}\left(\mathbf{6.3\sqrt{f_c'}}\text{ in psi}\right)$ and $\mathbf{0.23f_c'}$ respectively. According to the design criteria based upon the maximum joint principal tensile stress as described in Section 4.1.3, a full force transfer mechanism was required for transmitting the forces through the joint. Recognizing that the cap beam prestressing can contribute towards any horizontal unbalanced force within the joint, Eq. 4.5 for calculating the joint horizontal reinforcement was modified as follows [17]:

$$\rho_s = \frac{3.3}{D' f_{yh} l_a} \left[\frac{0.09 A_{sc} \lambda_o f_{yc} D'}{l_a} - F \right] \tag{5.1}$$

where $\mathbf{D'}$ is the diameter of the column core measured to centerline of the spirals and **F** is the cap beam prestressing. When equation 5.1 was considered for IC2, it resulted in a negative value, suggesting that only a nominal horizontal joint reinforcement consistent with Eq. 4.6 was necessary. Note that for this particular joint design, Eq. 5.1 gives $\rho_s = 0$ when **F** = 307 kN (69 kips) is used, which is less than 20 percent of the prestressing applied in the cap beam of the test unit (Section 5.2.2).

In addition, a nominal vertical joint reinforcement within the joint and appropriate amount of external stirrups in the cap beam were required as a part of the full force transfer mechanism (Section 4.1.3). Hairpin type vertical joint steel, as for IC1, was provided, but no additional stirrups outside the joint in the cap beam were considered necessary for the following reasons. When the cap beam is prestressed, the neutral axis depths in the beam sections adjacent to the joint increase when compared to an equivalent reinforced concrete unit (Figure 4.3a). Consequently, a broader joint diagonal strut develops in prestressed bridge joints as shown in Figure 5.1. This increases the embedment length of the column reinforcement into the diagonal strut. Since the cap beam prestressing is governed by the negative moment, the strut depth at the location of the most extreme column tension reinforcement is likely to be high. Considering that the longitudinal column reinforcement would be taken to the bottom (as cast) of the cap as much as possible (see Section 4.2.3) and equating the depth of joint strut at the most extreme tension bar to the neutral axis depth of the beam section adjacent to it, it was found that the column bars could be directly anchored into the joint diagonal strut by bond transfer alone if a uniform bond stress of $\mathbf{2.24\sqrt{f_c'}}\left(\mathbf{27\sqrt{f_c'}} \text{ in psi}\right)$ could be developed. Although an average bond stress of $\mathbf{1.17\sqrt{f_c'}}\left(\mathbf{14\sqrt{f_c'}} \text{ in psi}\right)$ was used in Eq. 4.7, higher bond stresses over twice as much as that used in Eq. 4.7 have been reported from experimental study on bridge joints [8,12]. Further, a better condition for bond transfer between the longitudinal column reinforcement and surrounding concrete is more likely in a prestressed joint due to the transverse pressure than it would be in an equivalent reinforced concrete joint [5]. Therefore, with the expectation of a good joint performance, it was concluded that all of the longitudinal column reinforcement could be directly anchored into the main diagonal strut by bond transfer and that no external joint mechanism requiring additional vertical stirrups in the cap beam would be required.

The prestressing alone was expected to provide the necessary shear resistance in the cap beam, so none of the nominal shear reinforcement provided in the beam would be utilized for resisting shear in the cap beam. Hence, if external joint struts need to be developed for a satisfactory performance of the joint, it can still be possible to a certain extend provided the beam longitudinal reinforcement has some reserve capacity. This was taken into consideration when detailing the bent cap (Section 5.2.2).

5.2 Reinforcement Detailing

Key reinforcement details of test unit IC2 are shown in Figure 5.2 and photos of the test unit taken after placing all the reinforcement are shown in Figures 5.3 and 5.4. A brief

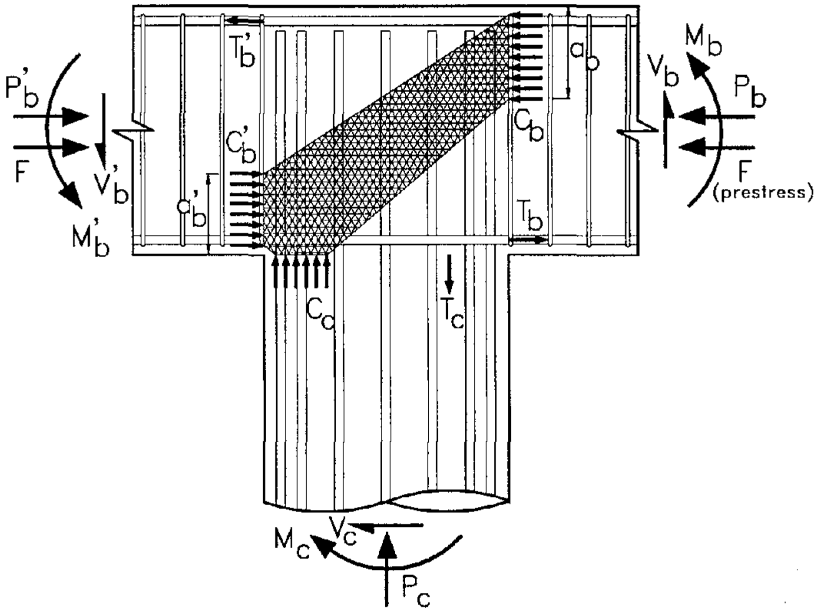

Figure 5.1 Forces acting on a bridge tee joint with a prestressed cap beam and an idealized joint strut.

summary of the column, beam and joint reinforcement is presented in the following sections.

5.2.1 Column

The longitudinal column reinforcement consisted of 14#7 (d_b = 22.2 mm) bars, providing a steel ratio of 1.86. The transverse reinforcement was #3 (d_b = 9.5 mm) spirals at 96.5 mm (3.8 in.) spacing, which yielded a volumetric ratio of 0.52 percent.

5.2.2 Cap Beam

The cap beam negative moment resistance was provided by 4#6 (d_b = 19.1 mm) tension reinforcing bars and a prestressing force of 1668 kN (375 kips). The cap beam prestressing was applied using four 32 mm (1.25 in.) diameter Dywidag bars, which were located at 60 percent of the dimensions of each quadrant (Figure 5.2), with each bar carrying 417 kN (94 kips). Since the bending moments induced by gravity were small and it was convenient to apply prestressing using Dywidag bars under laboratory conditions, prestressing in the bent cap was applied with zero eccentricity.

Prestressing moment alone was adequate to resist the positive bending moment in the beam. However, 4#6 bars were also placed as tension reinforcement in the top section (as constructed) of the beam. This was to satisfy the reinforcement requirement for developing the external joint mechanism as discussed in Section 5.1.3, although #4 (d_b = 19.1 mm) reinforcement could have been used instead of #6. Nominal shear reinforcement was required in the beam as for IC1, and this was represented by 4 legs of #3 (d_b = 9.5 mm) stirrups at 165 mm (6.5 in.) spacing.

In the beam end regions, additional vertical stirrups and #3 spirals (diameter = 179 mm and pitch = 51 mm), co-centered with each Dywidag bar, (Figure 5.3) were provided to resist bursting shear resulting from the anchorage of prestressing bars.

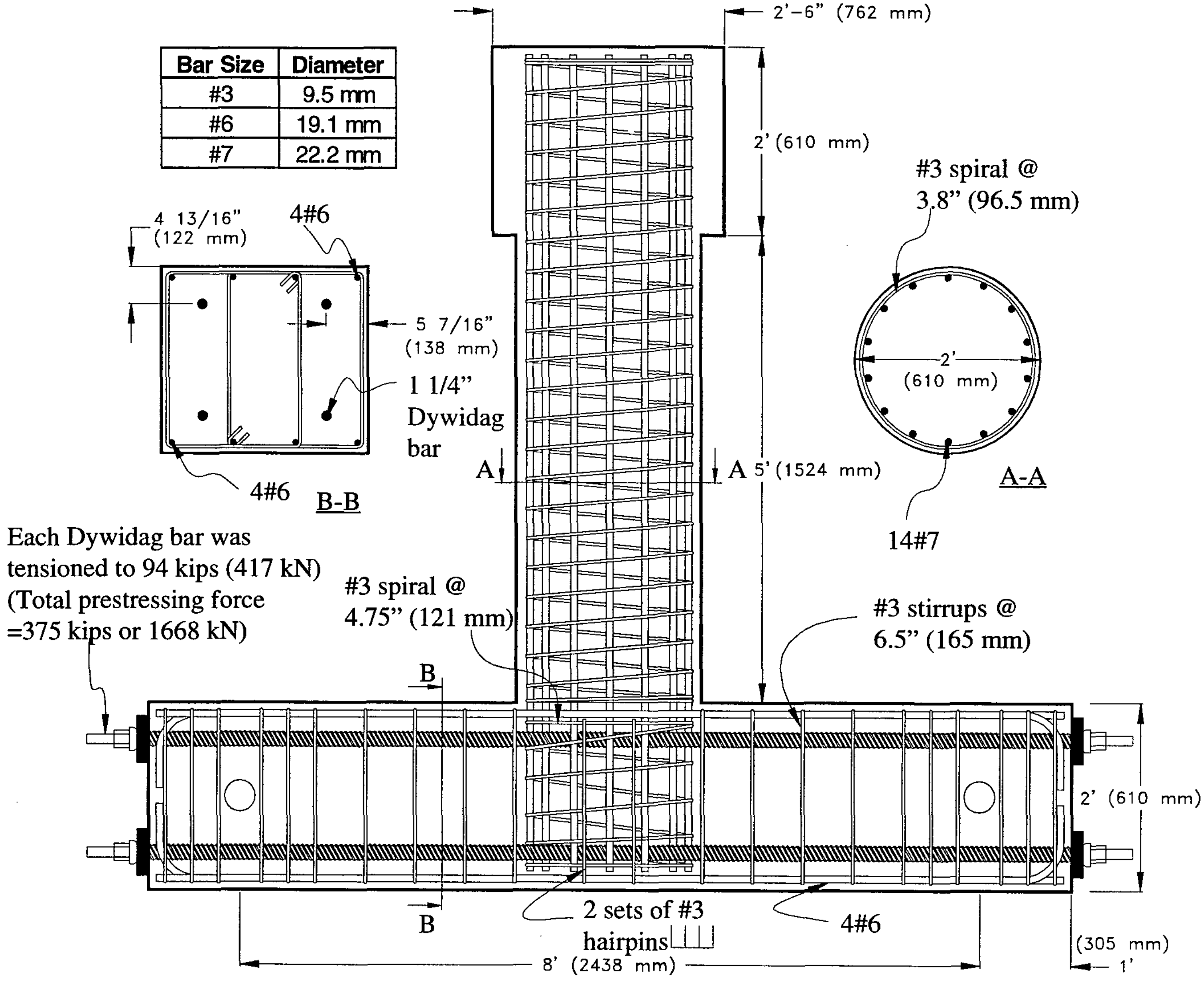
2'-6" (762 mm)
2' (610 mm)
#3 spiral @
3.8" (96.5 mm)
2'
(610 mm)
A-A
14#7
4 13/16"
(122 mm)
4#6
5 7/16"
(138 mm)
1 1/4"
Dywidag
bar
4#6
B-B
A
A
5' (1524 mm)
Each Dywidag bar was
tensioned to 94 kips (417 kN)
(Total prestressing force
=375 kips or 1668 kN)
#3 spiral @
4.75" (121 mm)
#3 stirrups @
6.5" (165 mm)
B
B
2' (610 mm)
2 sets of #3
hairpins
4#6
(305 mm)
1'
8' (2438 mm)

Bar Size	Diameter
#3	9.5 mm
#6	19.1 mm
#7	22.2 mm

Figure 5.2 Reinforcement details of the test unit with a partially prestressed bent cap.

5.2.3 Interior Joint

Consistent with Eq. 4.6, a nominal joint horizontal reinforcement consisting of #3 spiral at 121 mm (4.75 in.) was provided. The minimal vertical joint reinforcement was, also provided as for IC1 in the form of hairpins. This was satisfied by 2 sets of 4 legs #3 rebar within the joint. No additional external vertical stirrups were provided adjacent to the joint in the cap beam (Section 5.1.3). As discussed in Section 4.2.3 for the joint of IC1, the longitudinal column bars were taken to the bottom (as cast) of the cap as far as possible to avoid bond slipping of the reinforcement.

5.3 Cap Beam Prestressing

Most of the instrumentation necessary for the test was completed prior to the post-tensioning of the cap beam. This included mounting three strain gauges on each of the four prestressing bars. An initial set of readings on these instrumentation and demec points was taken just before the Dywidag bars were tensioned.

The target prestressing in the beam on the day of testing was 1668 kN (375 kips). Considering 15 percent for lock-out loss and 5 percent for loss due to time dependent effects of concrete and prestressing steel, it was decided that each Dywidag bar be tensioned to 500 kN (112.5 kips). In order to minimize bending of the beam during prestressing, the tension force required in the Dywidag bars was applied in two steps. In each step, 50 percent of the required force was applied first in the bars located in the opposite corners and then in the remaining two bars.

Immediately after prestressing, the average strain gauge reading of the prestressing bars indicated that the beam was subjected to a total prestressing force of 1786 kN (401.6 kips). The expected strain in the beam corresponding to the applied prestress was 140 μ strain. The average measured strain on the concrete surface was 160 μ strain and that obtained from the gauges mounted on the longitudinal beam reinforcement was 170 μ strain. These values are comparable to the expected strain which was calculated by estimating the elastic modulus based on the compressive strength of concrete.

After four hours from the end of prestressing, the prestress ducts were grouted using hydrostone mix. The standard grout mix was not preferred because of lack of spacing

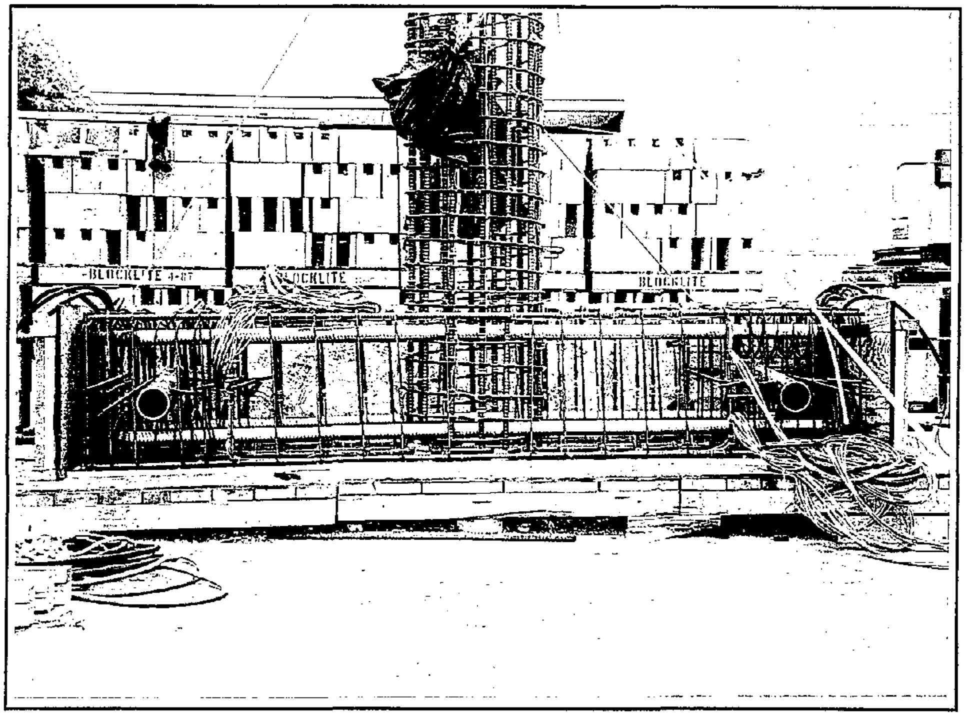

Figure 5.3 Construction of test unit IC2.

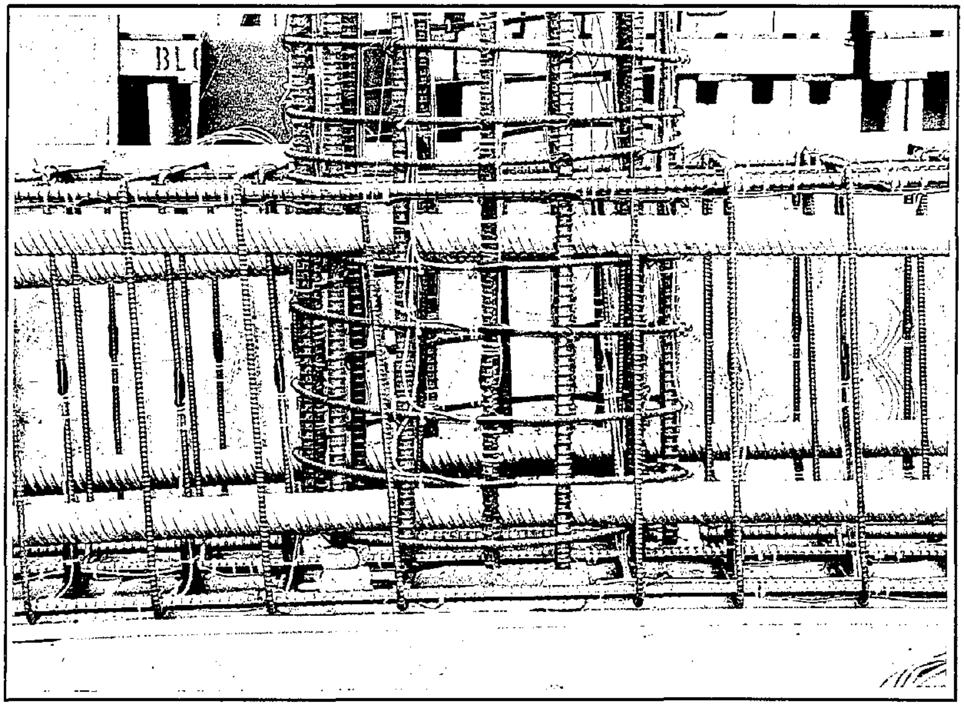

Figure 5.4 Joint reinforcement of test unit IC2 with a partially prestressed cap beam.

Reproduced from
best available copy.

between sheathing and strain gauged Dywidag bars. Using hyrostone mix as grouting material was not expected to have any significant influence on the response of the cap beam.

Readings on the specimen were continuously taken at regular intervals for the next five days until the unit was tested under lateral cyclic loading. In this short time interval, no significant changes were observed in the average strain obtained from both the demec readings on the concrete surface and the strain gauge recordings in the longitudinal beam reinforcement. The influence of ambient condition as well as the noise in the strain gauge readings appeared to be higher than that introduced by the time dependent effects of concrete and prestressing steel. This is not completely surprising because the beam was prestressed at the age of 77 days. Several of the strain gauges mounted on the Dywidag bars recorded strain drop, in the worst case up to 1800 μ strain, a few hours prior to applying the gravity load as a part of the cyclic testing procedure. Considering that the change in strain was not similar between gauges from the same prestressing bar and that there was no corresponding variation in strain observed in the longitudinal beam reinforcement nor in the demec readings, it was concluded that this strain drop was probably due to a disturbance that occurred to the signal conditioning cabinet. Of the total twelve gauges mounted on the prestressing bars, three of them did not register any significant strain drop, but the average strain variation in these three gauges between prestressing and day of testing was about 100 μ strain. This appeared excessive given that no appreciable change in the strain was monitored on the concrete surface nor in the longitudinal beam reinforcement.

Considering the complexity of the problem, it was concluded that a best estimate of the prestressing in the beam on the day of testing was 1737 kN (390 kips), 4 percent more than it was intended. This corresponded to a change of only 20 μ strain in each Dywidag bar due to time dependent effects, which was estimated based on selected gauge readings of the longitudinal beam reinforcement. Based on the strain gauge readings obtained prior to experiencing the significant strain drop, it was found that the prestressing in one of the four bars reduced more than that was seen in the other three bars. This was also accounted for when establishing the appropriate cap beam prestressing on the day of testing. An error of up to ±5 percent can be easily associated with the estimated prestressing force, but this is not considered to have any significant effect on the test results.

5.4 Material Properties

The material properties of concrete and steel were obtained as illustrated in Section 4.3. Listed in Tables 5.1 and 5.2 are respectively the compression strength of concrete at different ages and steel properties of the reinforcement. Each data point in the tables was established from testing on a minimum of three samples.

Table 5.1 Compressive strength of concrete used in test unit IC2.

Member	7 days		28 days		Day of Testing*	
	MPa	ksi	MPa	ksi	MPa	ksi
Column	25.4	3.69	30.6	4.43	34.6	5.02
Cap beam and Joint	-	-	36.5	5.29	40.5	5.87

*average of 6 samples, three of which were tested six days prior to D.O.T. on the day of prestressing.

Table 5.2 : Yield and ultimate strength of reinforcing steel of test unit IC2.

Description	Size	Yield Strength		Ultimate Strength	
	(diameter in mm)	MPa	ksi	MPa	ksi
Longitudinal column bar	#7 (22.2)	448	65.0	738	107.0
Column spiral	#3 (9.5)	431	62.5	669	97.0
Longitudinal beam bar	#6 (19.1)				
Beam stirrups	#3 (9.5)	439	63.6	722	104.7
Joint Spiral	#3 (9.5)	434	63.0	674	97.8
Prestressing Bar†	1-1/8 (31.8)	988	143.3	1131	164.0

†tested by the manufacturer

5.5 Predicted Response

The behavior of the test unit predicted prior to the test is presented in this section. The procedure adopted was similar to that used for IC1 (Section 4.4) but using a target cap beam prestressing of 1668 kN (375 kips).

5.5.1 Gravity Load Response

Compressive stress induced in the cap beam due to prestressing was 3.7 MPa (0.54 ksi). The estimated flexural cracking strength of the concrete was 3.9 MPa (0.57 ksi) and therefore no cracking in the cap beam was expected until a stress level in excess of 7.6 MPa (1.11 ksi) was induced in the beam. The application of gravity load corresponded to 3.9 MPa (0.57 ksi) in the extreme tension fiber of the beam, and consequently no cracking was expected under gravity load.

5.5.2 Cracking in the Column

As for test unit IC1, the flexural cracking at the critical section of the column was expected to form at a horizontal load of 72 kN (16.2 kips), based on nominal material strengths.

5.5.3 Cracking in the Cap Beam

Bending moment required to induce the flexural cracking stress, which was estimated in Section 5.5.1, was 357 kNm (263 kips-ft). Since the cap beam positive moment due to seismic and gravity loads was not expected to exceed 256 kNm (189 kips-ft), no flexural cracks would develop on the top (as constructed) of the beam. Negative bending moment was expected to reach the cracking moment at a horizontal load of 217 kN (49 kips).

5.5.4 Cracking in the Joint Region

Since the maximum joint principal tensile stress was expected to exceed $0.29\sqrt{f_c'}\left(3.5\sqrt{f_c'}\text{ in psi}\right)$, cracking in the joint region was anticipated. Although the joint cracking load was not calculated prior to the test, the horizontal load required for joint cracking was later estimated using Eq. 4.1 and the measured concrete strength on the day of testing. It was found that the first joint cracking was predicted to correspond to a horizontal load of 356 kN (80 kips) in the push loading direction (see Appendix A for calculations).

5.5.5 Force-Displacement Response

Overall force-displacement behavior obtained for the test unit from a push-over type analysis is included with the experimental response in Figure 5.10a (see Table B3 in Appendix B for numerical values). As was for the reinforced concrete joint, changes in structural behavior due to cracking in the column, yielding of longitudinal column steel, cracking in the beam, and development of maximum concrete strain in the column were taken into account in the analysis (Section 2.9).

A fixed base analysis of the column yielded a member displacement capacity $\mu_m = 6.81$. Using the procedure outlined in Section 2.8, the flexibility of the cap beam and joint at yield was estimated to give flexibility coefficient $f = 0.213$, hence resulting in predicted system ductility capacity of 5.79 for IC2.

5.6 Observation under Repeated Cyclic Loading

The experimental observation made during the test under lateral cyclic loading is given in this section.

5.6.1 Application of Dead Load

As anticipated from theoretical calculations (Section 5.5.1), no cracking developed in the specimen when the gravity load was applied.

5.6.2 Initial Damage

Due to an initial signal imbalance in the control system, when the hydraulics was turned on, the actuator applied an impulsive force to the specimen in the pull direction. Unfortunately there was no automatic triggering set for taking scans of gauge readings during this mishap, but a scan was manually obtained soon after the impulsive load was applied. It was found that the column was subjected to a horizontal load of 388 kN (87 kips) and the corresponding displacement at the center of load stub was 46.1 mm (1.81 in.), which was estimated to be approximately equal to a system ductility of 3.

The damage which occurred to the test unit due to the impulsive load was: development of flexure-shear cracks all the way up the column, minor crushing of concrete on the compression (north) side of the column close to the joint interface, some vertical splitting cracks on the tension (south) side in the plastic hinge region of the column, and diagonal shear cracking on both sides of the joint. All the cracks were marked in blue and labeled "μ3" on the specimen. Some of the initial damage can be seen in Figures 5.5 and 5.6.

The test unit was then unloaded and the horizontal displacement of the column was brought back to zero. This required an actuator force of 158 kN (36 kips) in the push direction. It was decided that the first three elastic cyclic loading steps were no longer necessary and that the testing be proceeded with the originally planned loading sequence (Figure 3.25) starting with a horizontal load of 250 kN (56 kips).

5.6.3 Force Control

The actuator force was taken to the level corresponding to the theoretical yield in the push direction in a single step. In the reverse direction, a similar load was expected to induce displacement beyond the elastic limit due to the initial damage, and hence a reduced force was applied. This horizontal force was determined such that the resulting displacement would be similar to that observed for the push direction loading.

± 250 kN (56 kips) - First Yield

In the push direction, flexural and inclined shear cracks developed almost all the way up the column. Diagonal joint shear cracking was seen on the east side of the joint (Figure 5.6), which was not expected at this horizontal load (Section 5.5.4). No flexural cracks were seen in the cap beam. All the tension cracks, which were developed during the impulsive force prior to the test, were completely closed. No new damage was seen in the test unit under pull direction loading.

5.6.4 Displacement Control

The estimated displacement corresponding to $\mu_\Delta = 1$ was 15.0 mm (0.590 in.) from Eq. 3.3. From this point onwards, a minimum of three cycles were applied at each ductility and the observed behavior is described below.

3 cycles at $\mu_\Delta = \pm 1$ ($F_{max} = 302$ kN; $F_{min} = -140$ kN)

In the push direction loading, the damage to the column and joint was limited to minor extension of the old cracks. No joint cracking had yet occurred on the west side. For both loading directions, flexural cracks formed at the column face in the cap beam under negative moment. The peak horizontal loads applied during this cycle were +302 kN (+68 kips) and -140 kN (-32 kips), and the theoretically estimated actuator force corresponding to that causing flexural cracking moment was 217 kN (49 kips) (Section 5.5.3). The condition of the test unit at the end of third cycle in the push direction loading is shown in Figure 5.6.

3 cycles at $\mu_\Delta = \pm 1.5$ ($F_{max} = 347$ kN; $F_{min} = -230$ kN)

Joint cracking occurred on the west side when the column was first displaced in the push direction loading. The horizontal load in this half cycle reached a maximum value of 347 kN (78 kips), which was 98 percent of the expected horizontal joint cracking load (Section 5.5.4 and Appendix A). Vertical splitting cracks were seen on the tension side of the column and on the joint close to the column/joint interface (see Figure 5.7). A minor extension of the cap beam flexural crack developed during the load reversal to the maximum negative displacement. No significant changes were observed in the test unit during cycling of the column displacement.

3 cycles at $\mu_\Delta = \pm 2.0$ ($F_{max} = 374$ kN; $F_{min} = -299$ kN)

In the first cycle, more vertical splitting cracks were seen on the tension side of the column for both loading directions. Extension of joint shear cracks was observed in the push direction while no additional joint damage was encountered in the pull direction. During cycling, minor extension of flexural cracks developed on the column with the maximum crack width reaching about 3 mm (0.118 in.) at the critical section. Cracking also developed on the top (as test) of the cap beam radiating from the tension side of the column for both loading directions, as a result of strain penetration of the longitudinal column reinforcement into the joint. Minor crushing of cover concrete occurred on the north side of the column which suffered a similar damage during the impulsive load.

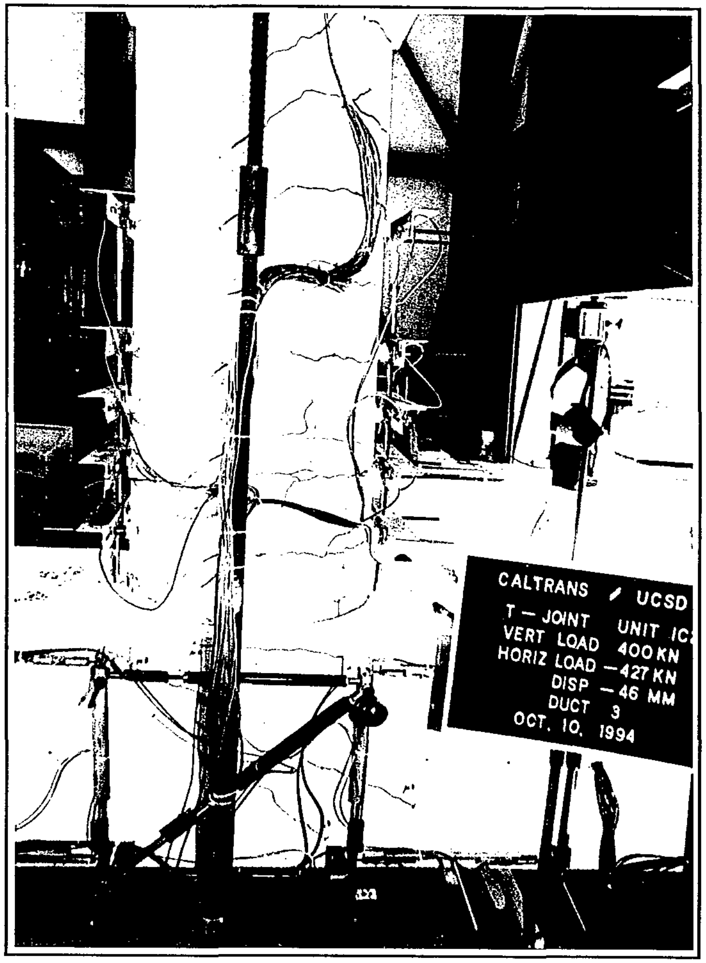
CALTRANS / UCSD
T – JOINT UNIT IC
VERT LOAD 400 KN
HORIZ LOAD –427 KN
DISP –46 MM
DUCT 3
OCT. 10, 1994

Figure 5.5 Initial damage that occurred to test unit IC2 due to an impulsive force in the pull direction.

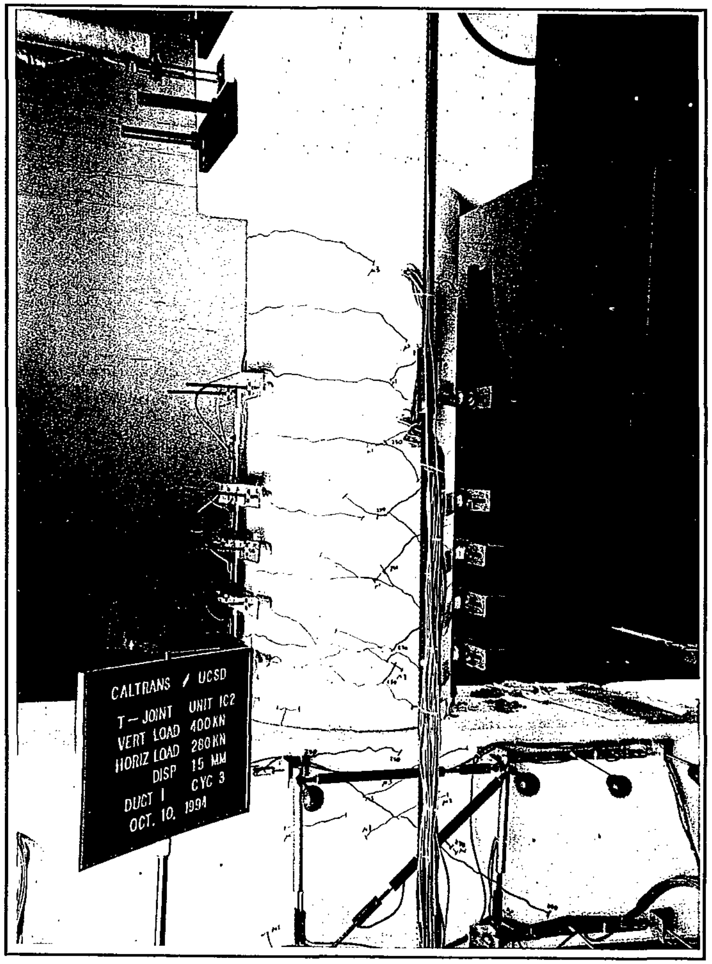
CALTRANS / UCSD
T – JOINT UNIT IC2
VERT LOAD 400 KN
HORIZ LOAD 280 KN
DISP 15 MM
DUCT 1 CYC 3
OCT. 10, 1994

Figure 5.6 Damage to test unit IC2 at the end of third cycle at ductility 1.

Reproduced from best available copy.

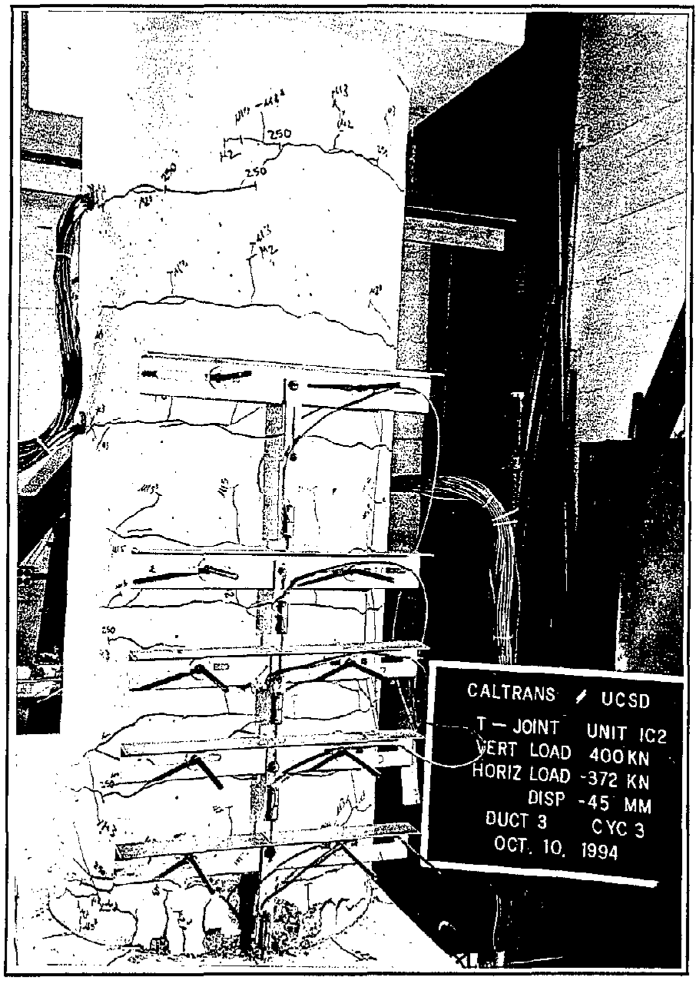
CALTRANS / UCSD
T – JOINT UNIT IC2
VERT LOAD 400 KN
HORIZ LOAD -372 KN
DISP -45 MM
DUCT 3 CYC 3
OCT. 10, 1994

(a) column damage on the north side

(b) Joint damage on the east face

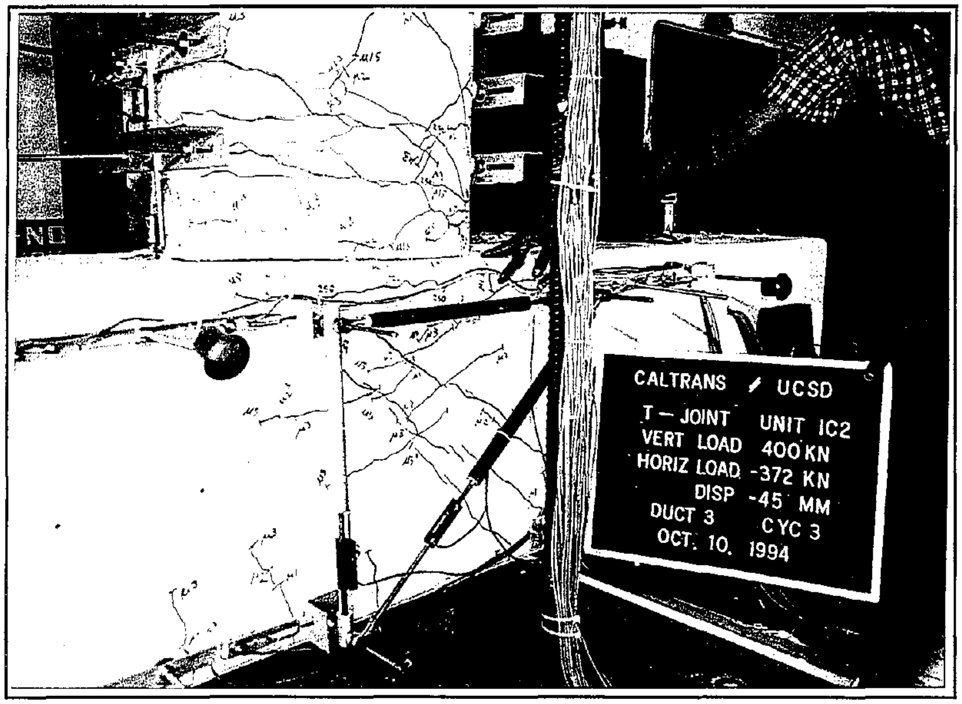
CALTRANS / UCSD
T – JOINT UNIT IC2
VERT LOAD 400 KN
HORIZ LOAD -372 KN
DISP -45 MM
DUCT 3 CYC 3
OCT. 10, 1994

Figure 5.7 Condition of test unit IC2 at the end of testing at $\mu_\Delta = 3$.

Reproduced from
best available copy.

3 cycles at $\mu_\Delta = \pm 3.0$ ($F_{max} = 405$ kN; $F_{min} = -371$ kN)

A new diagonal crack and extension of old cracks were noted on both sides of the joint during the first cycle in the push and pull direction loading. Crushing of cover concrete was first observed on the south side of the column close to the joint interface while more crushing occurred on the north side. More new cracks in the joint and extension of old cracks in the specimen occurred during the subsequent load cycles. In Figure 5.7, the damage to the north side of the column and east face of the joint are shown at the end of third cycle at ductility 3. It is clear that there was no significant joint deformation occurred at this stage.

3 cycles at $\mu_\Delta = \pm 4.0$ ($F_{max} = 415$ kN; $F_{min} = -389$ kN)

No significant damage occurred. More fine cracks developed in the joint with extension of most of the old cracks in the test unit. The width of the flexural crack at the base of the column was approximately 4 mm (0.158 in.). On either side, cover concrete spalled off the column for about 178 mm (7 in.) from the joint interface.

3 cycles at $\mu_\Delta = \pm 6.0$ ($F_{max} = 431$ kN; $F_{min} = -416$ kN)

New diagonal cracks and extension of old cracks were seen in the tee joint. New inclined large shear cracks were also developed in the column. Crack width at the base of the column was in excess of 5 mm (0.20 in.). During cycling of the column displacement, the cover concrete flaked off on the top of the cap beam in the vicinity of the column. At the end of cyclic loading at this ductility, the damage in the joint region appeared to be insignificant and can be seen in Figure 5.8.

4 cycles at $\mu_\Delta = \pm 8.0$ ($F_{max} = 418$ kN; $F_{min} = -421$ kN)

Shear cracks in the column opened up significantly and it appeared that shear failure was likely to occur in the column. These pronounced shear cracks can be identified in Figure 5.9, which shows the test unit at the peak displacement at ductility 8. A new joint crack developed in the pull direction loading, which was visible on both sides of the joint. The width of this new crack was about 0.5 mm (0.02 in.) and appeared to be larger than any of the previous joint cracks. During the third cycle, buckling of the longitudinal column reinforcement between three spirals occurred in the hinge region for both loading directions. In the subsequent cycle, two of the column tension bars fractured when the column was subjected to the pull direction loading and the test was, therefore, terminated by bringing the column to its original position.

End of the Test

All the loose concrete was removed at the end of the test and most of the damage that occurred to the test unit can be seen in Figure 7.3b. The inelastic displacement capacity of the column was completely developed with only minor damage to the cap beam and tee joint of the test unit.

5.7 Experimental Results

Based on the experimental data obtained during the test, the key results are presented in a reduced form in this section.

5.7.1 Force-Displacement Hysteresis Curve

In Figure 5.10, the force-displacement behavior of the test unit and the corresponding hysteresis loop analysis are shown. The energy absorption of the system as represented by the hysteretic loops increased when compared to the reinforced concrete unit IC1. The response of the test unit did not appear to have been significantly affected by the initial damage. Noticeable strength degradation first occurred in the system at ductility 8 due to buckling of the longitudinal column reinforcement. Some of these reinforcing bars fractured due to low cycle fatigue in the fourth loading cycle at this ductility in the pull direction loading and this was associated with a significant drop in the lateral force resistance of the test unit (Figure 5.10a).

Good agreement between the predicted and observed force displacement envelopes is seen in Figure 5.10a although the theoretical calculations underestimated the maximum displacement by 33 percent. The confinement model, which was used in the moment curvature analysis of the column, provides a conservative estimate for the maximum concrete compressive strain ε_{cu}, and hence a reduced (i.e. "safe") maximum displacement results from the analytical prediction. The discrepancy seen between the predicted and

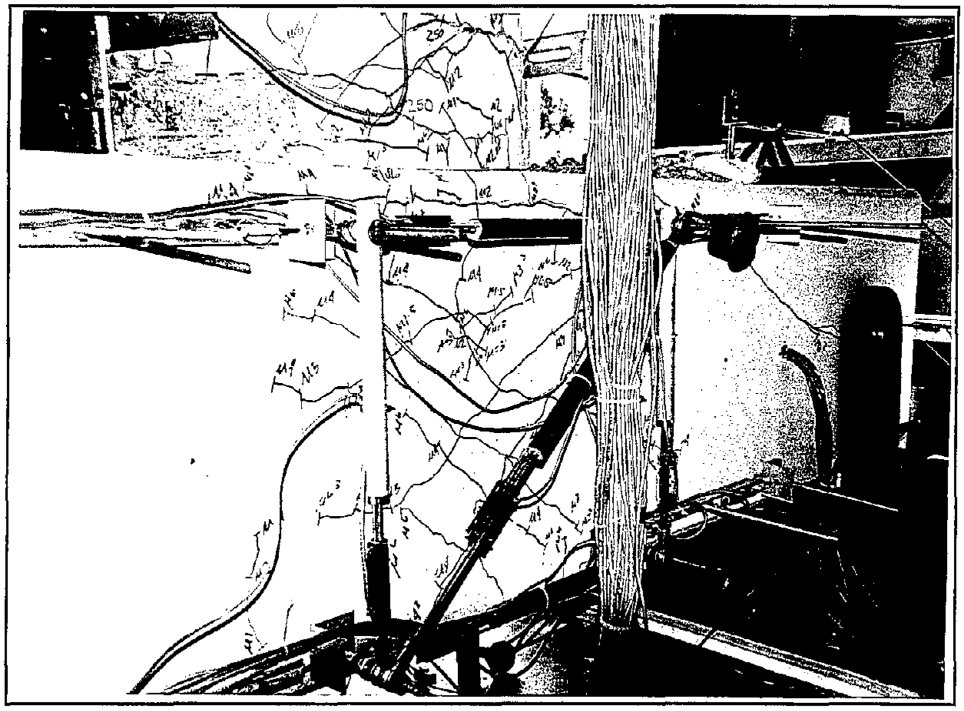

Figure 5.8 Damage to joint region of IC2 at the end of third cycle at $\mu_\Delta = 6$.

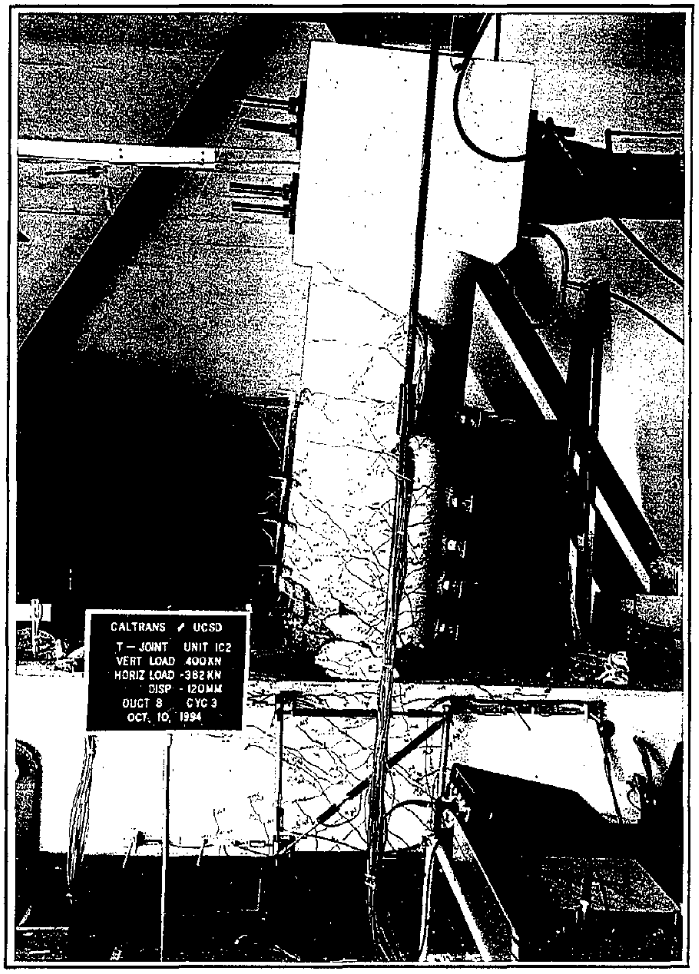
CALTRANS / UCSD
T – JOINT UNIT IC2
VERT LOAD 400KN
HORIZ LOAD -382KN
DISP -120MM
DUCT 8 CYC 3
OCT. 10, 1994

Figure 5.9 Test unit displaced at its maximum displacement at $\mu_\Delta = 8$.

Reproduced from best available copy.

observed envelopes in the pull direction loading up to displacement ductility 3 was due to the initial damage which occurred to the test unit. Yielding of the column reinforcement occurred during the impact load and this reduced the secant stiffness of the system, requiring a smaller actuator force to reach the target column displacement.

The area of the force-displacement loop and equivalent viscous damping are shown in Figures 5.10b and 5.10c at different ductilities for the first two loading cycles. The numerical values of the data points used in these figures are given in Appendix C. The area of the hysteretic loop increased linearly from ductility 4 to ductility 8. The equivalent viscous damping of the system corresponding to the second cycle increased from 5% at $\mu = 1$ to 24% at $\mu = 8$. A slightly larger damping values were obtained in the first cycle.

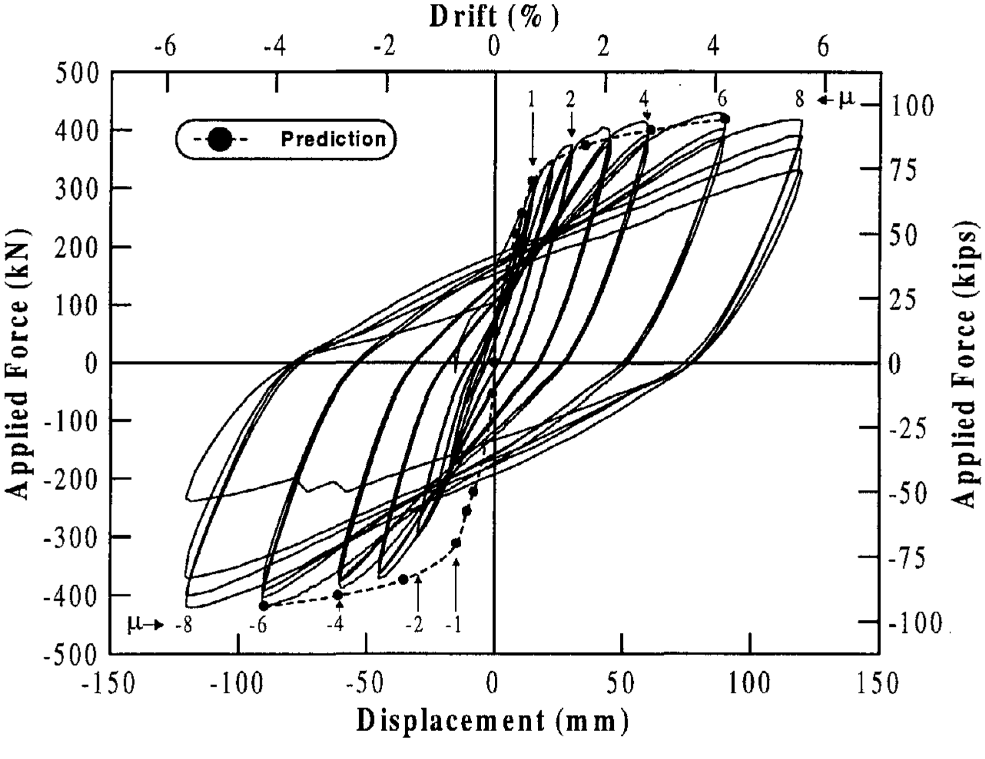

Figure 5.10a Force-displacement response of the partially prestressed test unit and predicted response envelope.

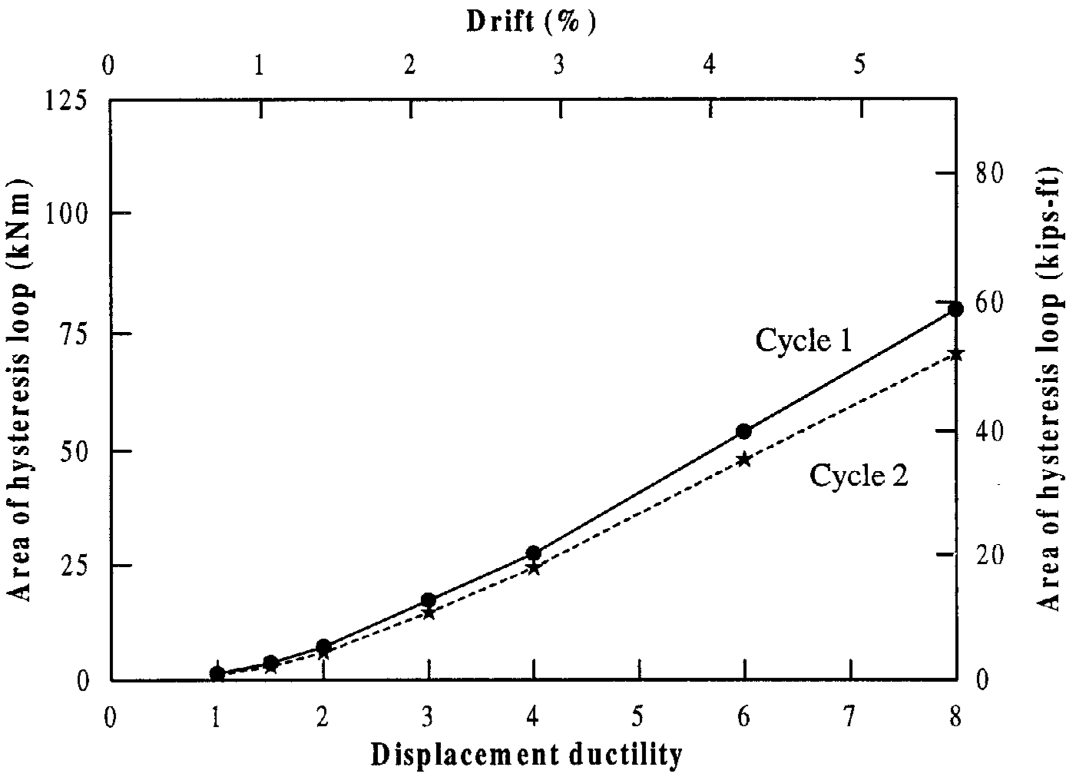

(b) Area of hysteresis loop

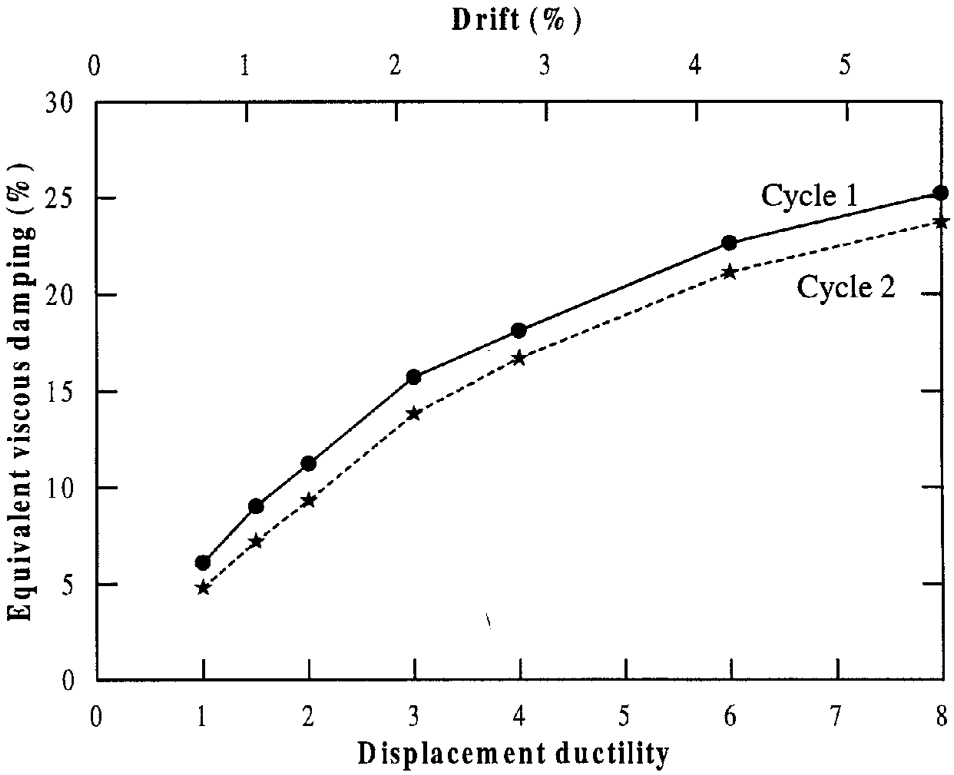

(c) Equivalent viscous damping

Figure 5.10 Force-displacement response and hysteresis loop analysis of unit IC1.

5.7.2 Moment-Curvature Response

Moment-curvature response of two column curvature cells located close to the joint interface are shown in Figure 5.11, accompanied by the theoretical response envelope calculated for the column section. The curvature measurements in both cells were obtained until the maximum column displacement was reached during the third cycle in the push direction at ductility 8. Significant inelastic deformations occurred within both curvature cells with the recorded peak curvature almost reaching the maximum theoretical value in the cell adjacent to the joint interface (Figure 5.11a). Given that the measured curvature was averaged over the gauge length, which included the strain penetration term in the cell adjacent to the joint as illustrated in Section 3.2.5, it can be stated that the curvature at the critical column section would have been higher than the theoretical ultimate curvature. The concrete confinement model should be corrected such that an accurate prediction of the maximum curvature response and hence a better estimate of the column displacement capacity can be obtained. The predicted moment-curvature envelope matches the recorded data satisfactorily in both cases.

The curvature measurements obtained in the remaining three cells showed that column curvature reduced up the column and essentially an elastic response was monitored in the top curvature cell. This observation can be verified in Figure 5.12 where the curvature profiles of the column are shown at different displacement ductilities.

The moment-curvature response obtained in the cap beam confirmed that the response of the beam was elastic during the cyclic testing of the specimen. In Figure 5.13, the curvature readings obtained in two beam curvature cells adjacent to the column face are shown as a function of the maximum bending moment induced within each cell. In the prediction of response envelopes, which satisfactorily captured the measured curvature, the cap beam prestressing was represented by a constant axial load. If the prestressing bars are appropriately modeled considering the actual stress-strain behavior of high yield reinforcement, a much larger ultimate moment and ductility capacity would have been obtained for the beam section with a similar initial stiffness. Since the beam was designed to respond elastically, the prediction shown in Figure 5.13 was considered to be adequate.

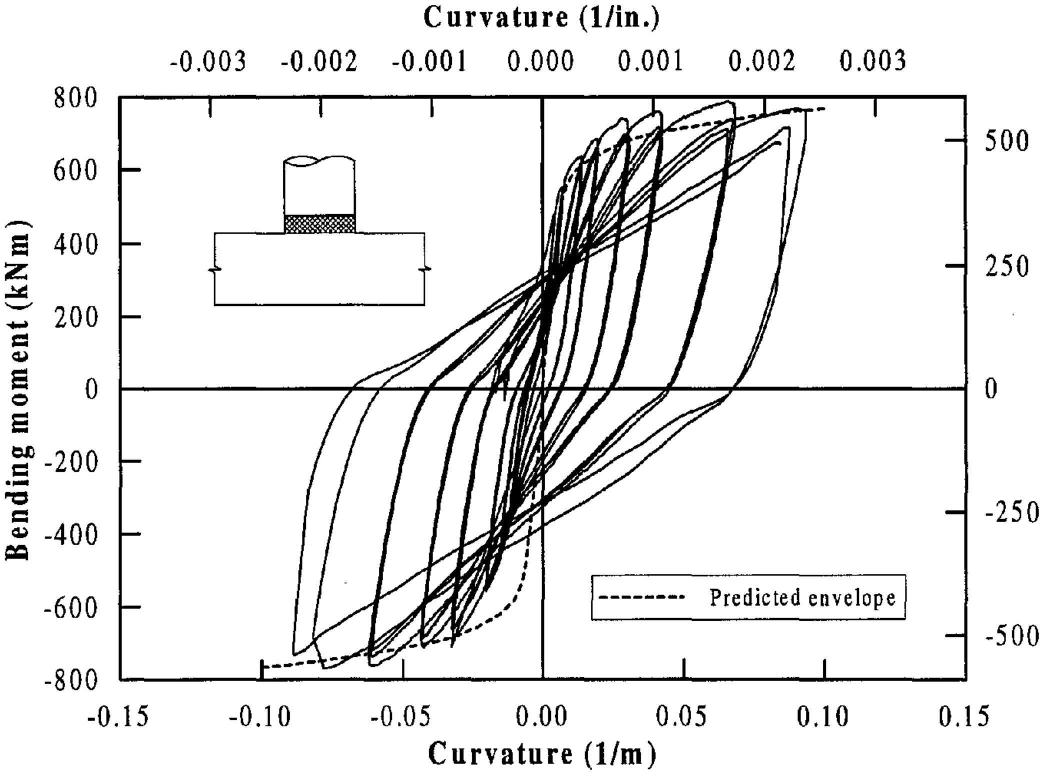

(a) adjacent to the joint interface

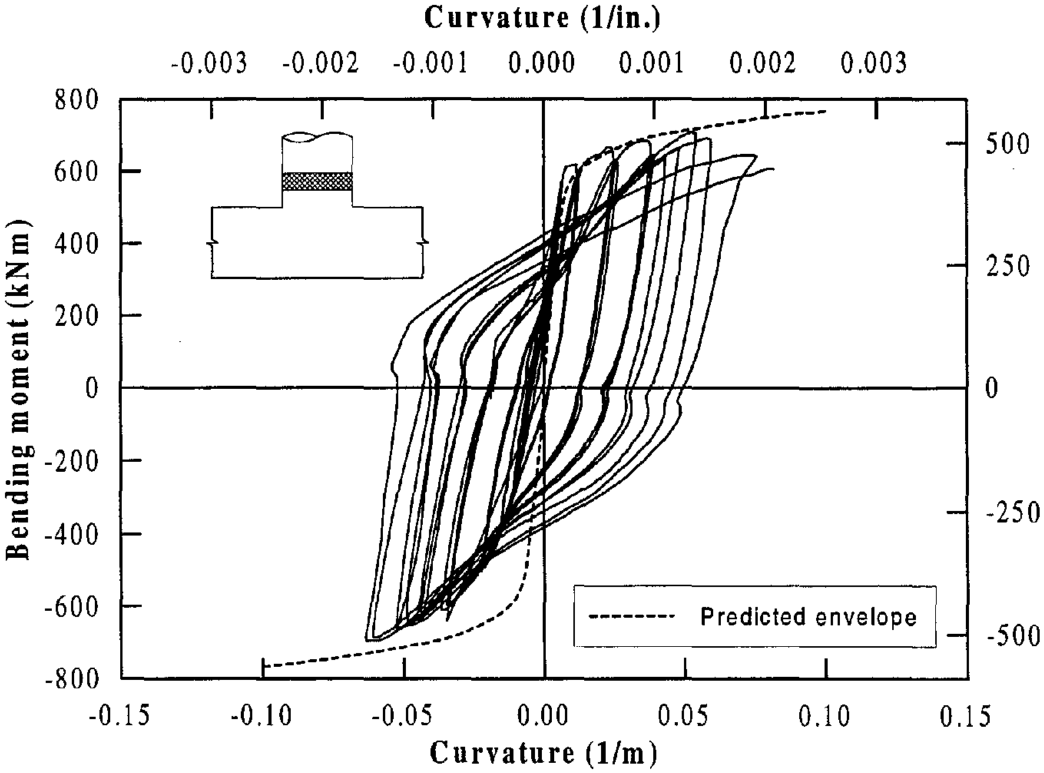

(b) 152 mm (6 in.) away from joint interface

Figure 5.11 Moment-curvature response of two column curvature cells close to the joint interface.

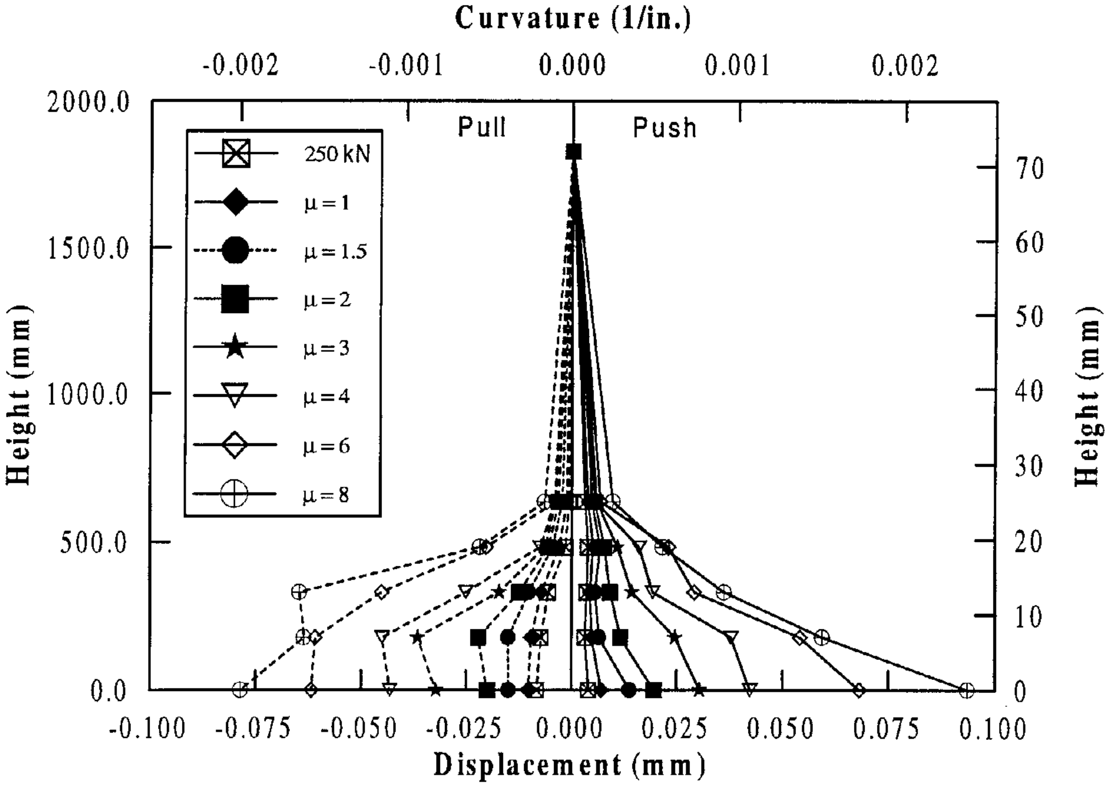

Figure 5.12 Measured curvature profiles up the column.

5.7.3 Joint Deformation

In contrast to the response of the reinforced concrete unit, joint IC2 with a partially prestressed cap beam performed well with significantly less joint deformation although the shear demand in the two joints was almost identical. The joint reinforcement provided in IC2 was less than that considered for IC1 based on a force transfer model, suggesting that the joint performance was clearly enhanced by the cap beam prestressing in the latter unit. Because of reduced joint deformation, the joint panel readings of IC2 were so low as to be affected by the noise in the system and only a limited information is presented herein. The panel readings of the west side were used for all the joint deformation calculations, as some of the potentiometer readings on the east side panel were unreliable.

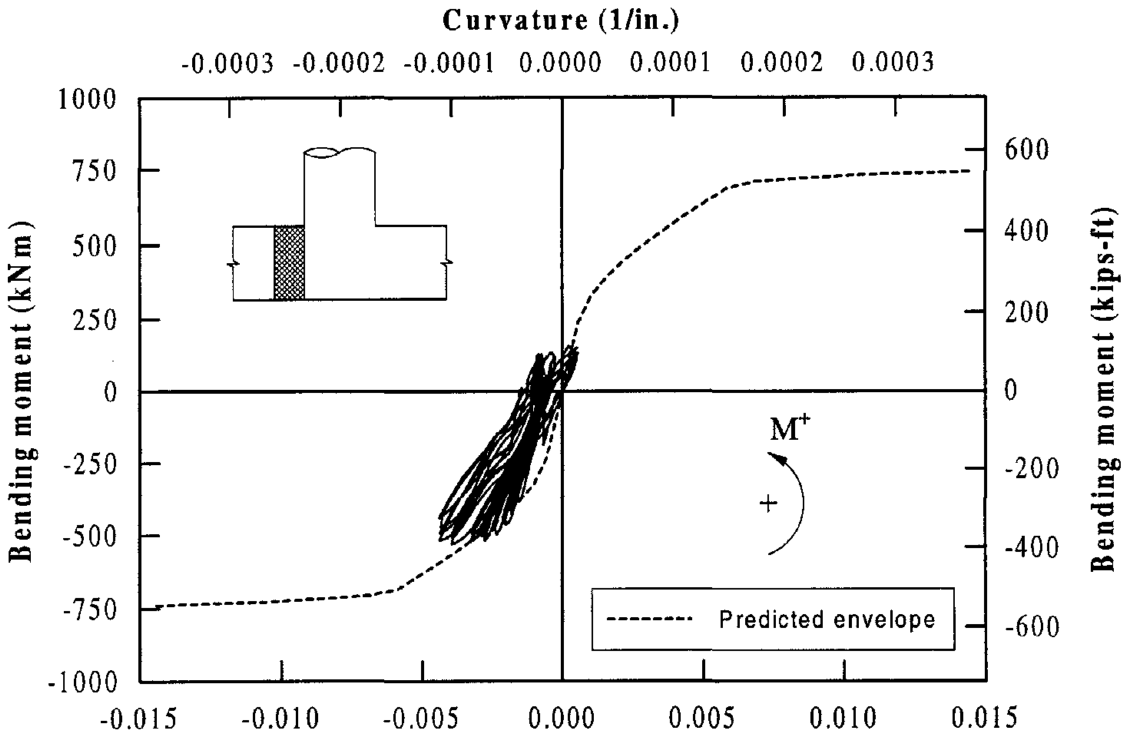

(a) left side of the joint

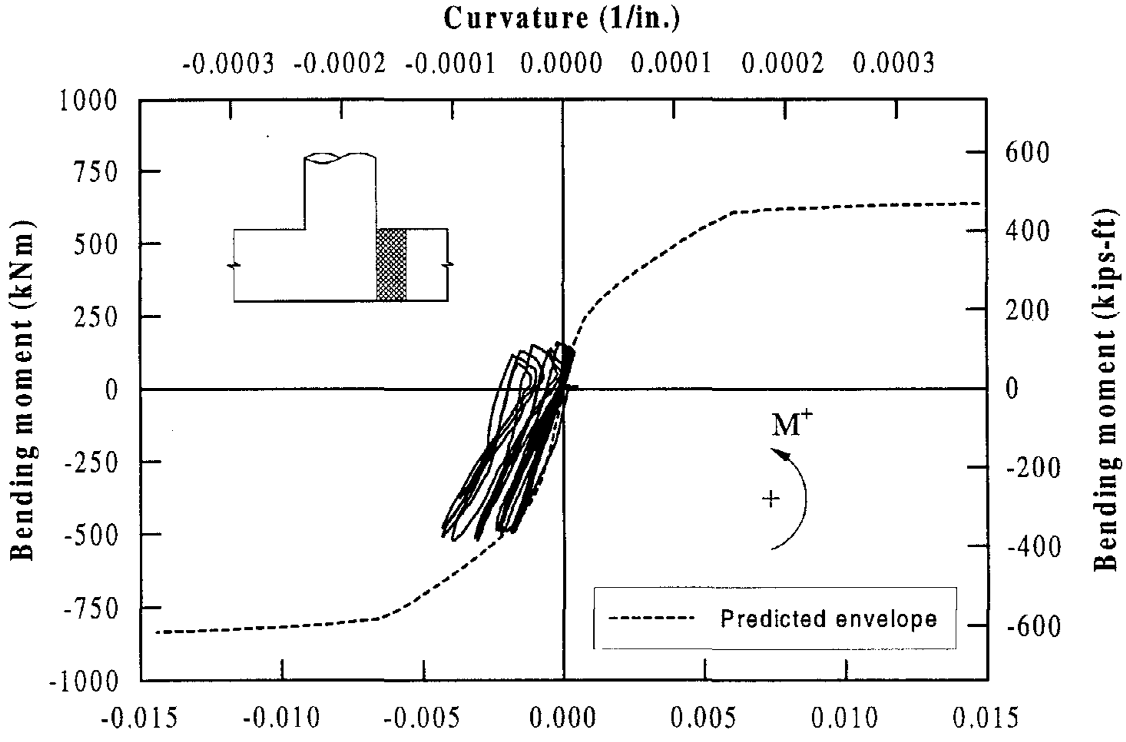

(b) right side of the joint

Figure 5.13 Moment-curvature response obtained in two beam curvature cells adjacent to the joint.

In Figure 5.14, the maximum and average joint shear stresses are plotted as a function of horizontal column displacement. The average joint shear stress corresponding to the peak displacement at each ductility appears to be constant, whereas an appreciable variation is seen in the maximum joint shear stress. Similarities between joint shear stresses of IC1 and IC2 can be seen by comparing Figure 4.21 to Figure 5.14. This is because a column hinging mechanism was developed in both units that had identical column reinforcement. The principal stresses of IC2 were, however, significantly different from those obtained for IC1 due to the axial compression introduced by the cap beam prestressing.

In Figures 5.15 and 5.16 the principal compression and tensile stresses for the joint of the partially prestressed unit are shown using both the maximum and average joint shear stresses. The peak values of the principal compression stresses were $\mathbf{0.20f'_c}$ and $\mathbf{0.16f'_c}$ when the maximum and average joint shear stresses were considered respectively. In Figure 5.16, the peak value of the principal tensile stress reached a maximum of $\mathbf{0.55\sqrt{f'_c}}\left(\mathbf{6.6\sqrt{f'_c}}\text{ in psi units}\right)$ when the maximum joint shear stress was considered and $\mathbf{0.24\sqrt{f'_c}}\left(\mathbf{2.9\sqrt{f'_c}}\text{ in psi units}\right)$ for the average joint shear stress. The peak of the maximum principal tensile stress, which is slightly higher than that estimated in the design calculation (Section 5.1.3), suggests that the joint should have been detailed with a full force transfer mechanism. The peak of the average joint principal tensile stress is more in line with the consideration that a nominal joint reinforcement would be adequate for a satisfactory joint performance, as was, in fact, obtained.

When comparing the principal stress plots to those of the other two joints, it can been seen that the principal tensile stress of the partially prestressed joint is smaller than that developed in the reinforced concrete joint. Similarly, the joint principal compression stress is less in the partially prestressed joint than in the equivalent fully prestressed joint (Chapter 6). Considering that the joint principal tensile stress determines the appropriate joint reinforcement based on force transfer models and that crushing of concrete in the joint strut is dictated by the principal compression stress, it is clear that a joint designed with a partially prestressed cap beam provides reduced joint reinforcement while maintaining the compression stress in the joint region well below the crushing strength of concrete. In the design of IC2, it was demonstrated that a partially prestressed joint whose joint principal compression was about 50 percent of the limiting value recommended in reference [19], can be designed with nominal joint reinforcement.

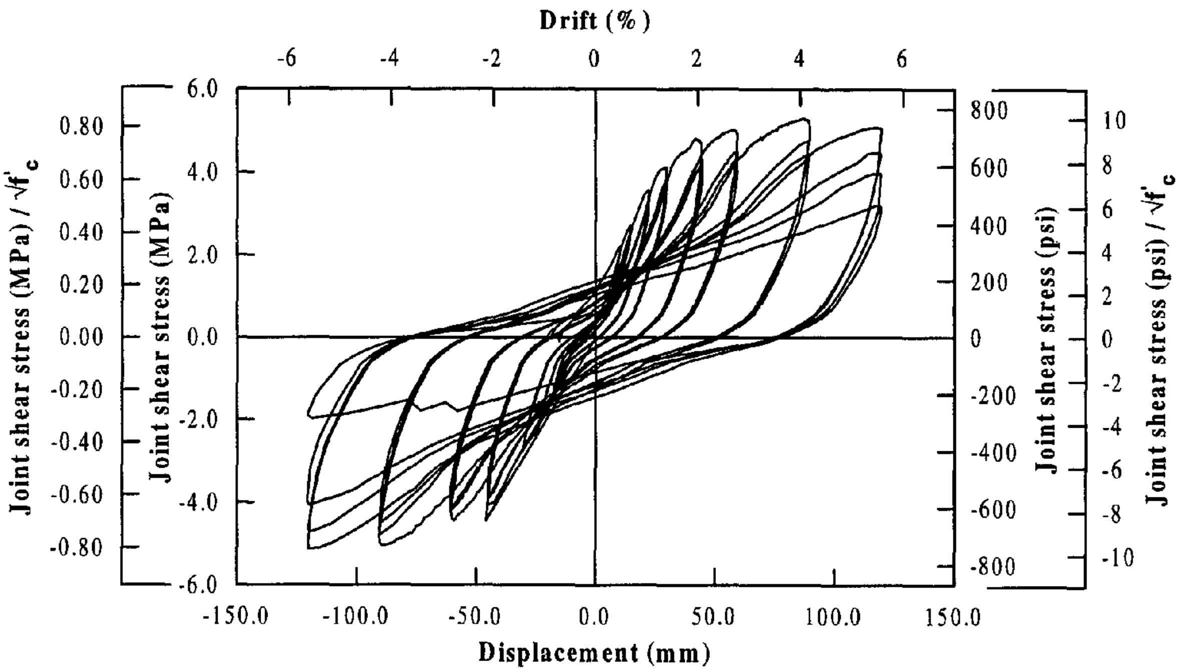

(a) Using maximum joint shear stress

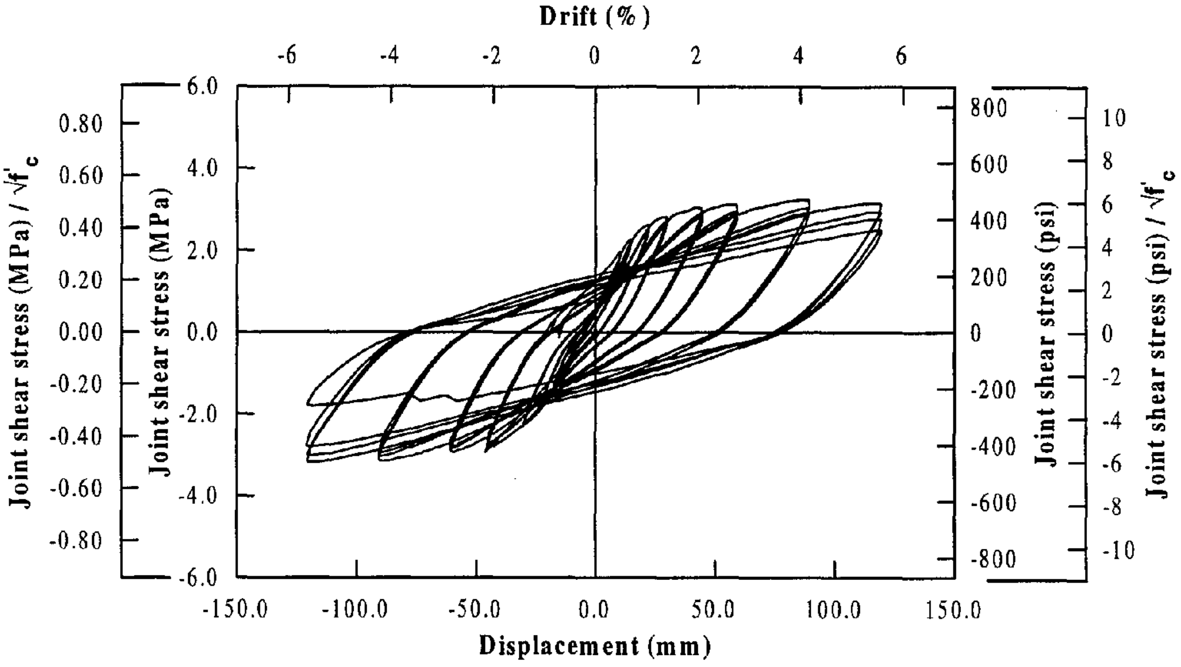

(b) Using average joint shear stress

Figure 5.14 Variation of joint shear stress as a function of column displacement.

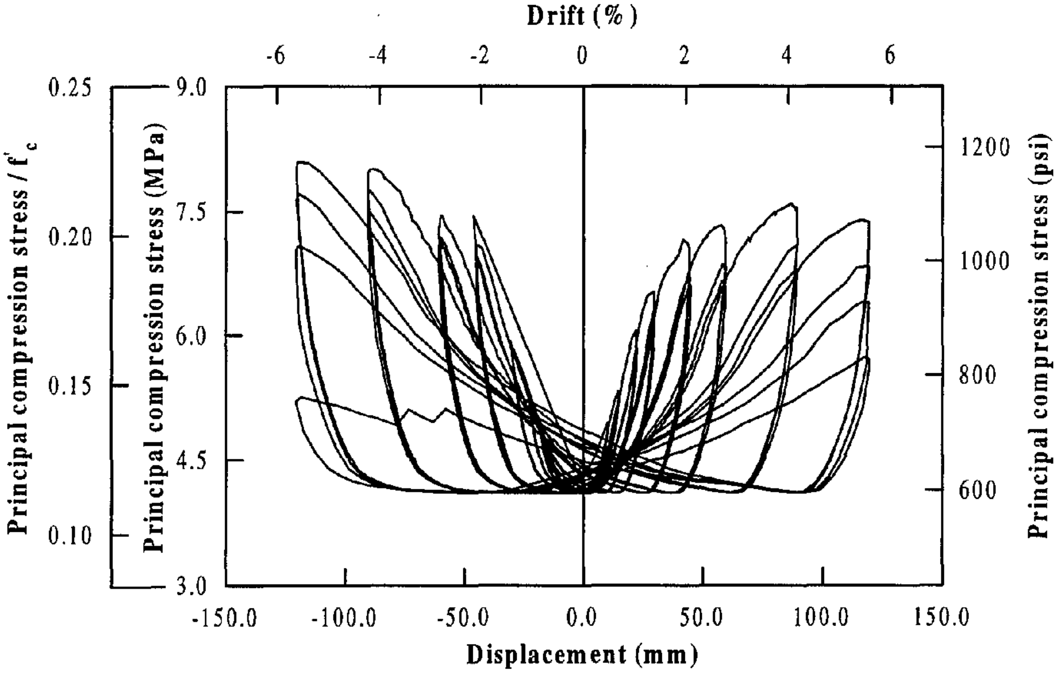

(a) Using maximum joint shear stress

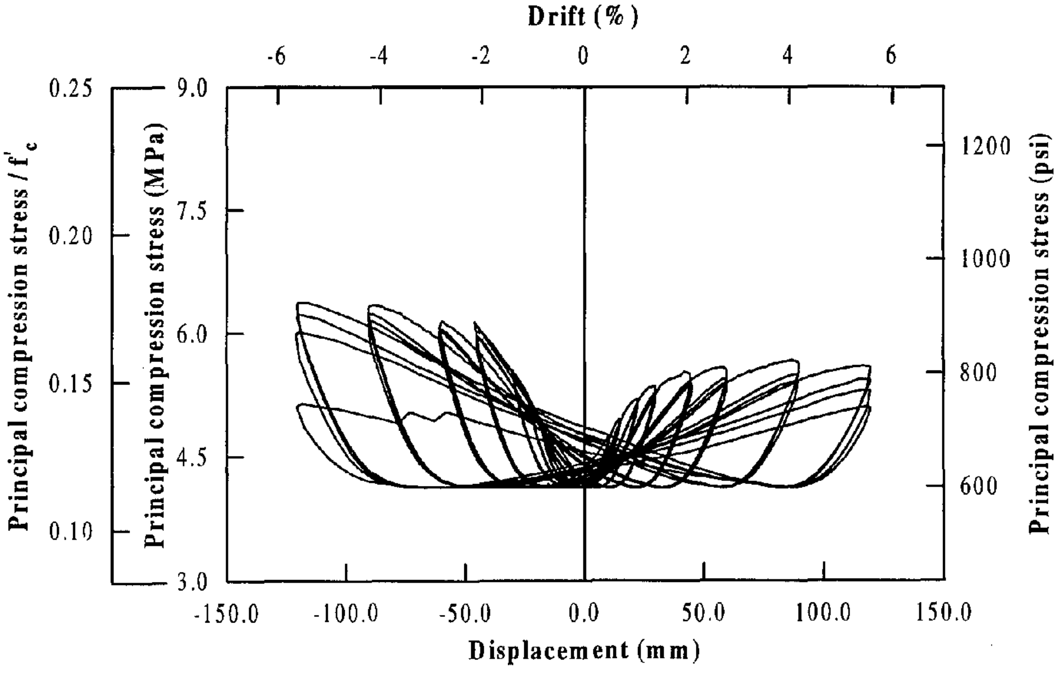

(b) Using average joint shear stress

Figure 5.15 Variation of joint principal compression stress as a function of column displacement.

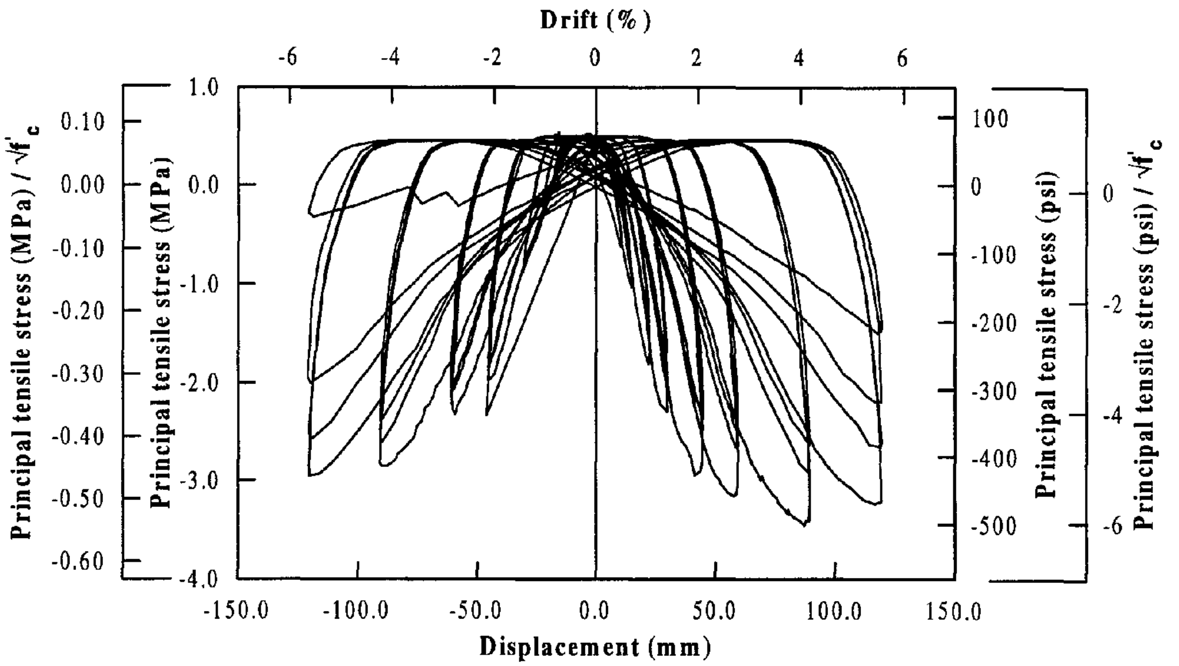

(a) Using maximum joint shear stress

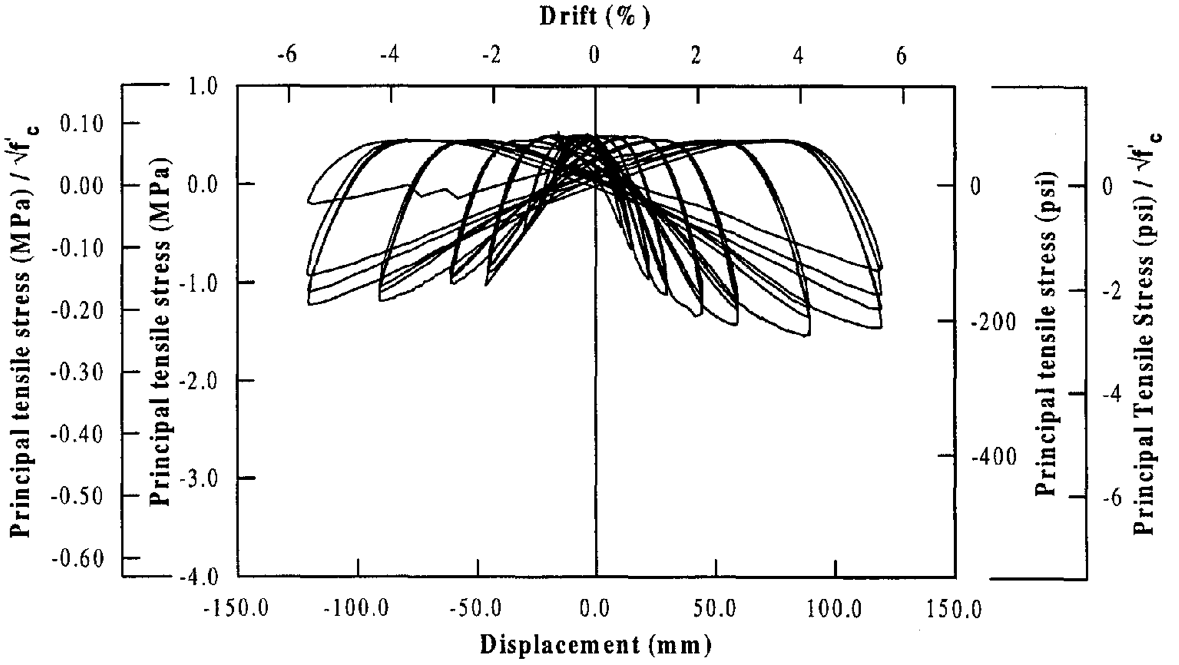

(b) Using average joint shear stress

Figure 5.16 Variation of joint principal tensile stress as a function of column displacement.

Further, an advantage of designing joints with a partially prestressed cap beams is that the joint principal stresses can be adjusted to satisfy design criteria by varying the amount of cap beam prestressing.

The angle of the principal stress plane as calculated from the average joint shear stresses is shown in Figure 5.17 as a function of column displacement. The angle corresponding to the peak displacement at large ductilities was about 30°. For the reinforced concrete joint, this was estimated to be 45° and the reduction of 15° was caused by the cap beam prestressing. Cracking in the joint region of IC2 occurred with an inclination between 30° - 40° (Figure 7.3b) whose median corresponded well with the peak angle of principal plane that was calculated using the maximum joint shear stress.

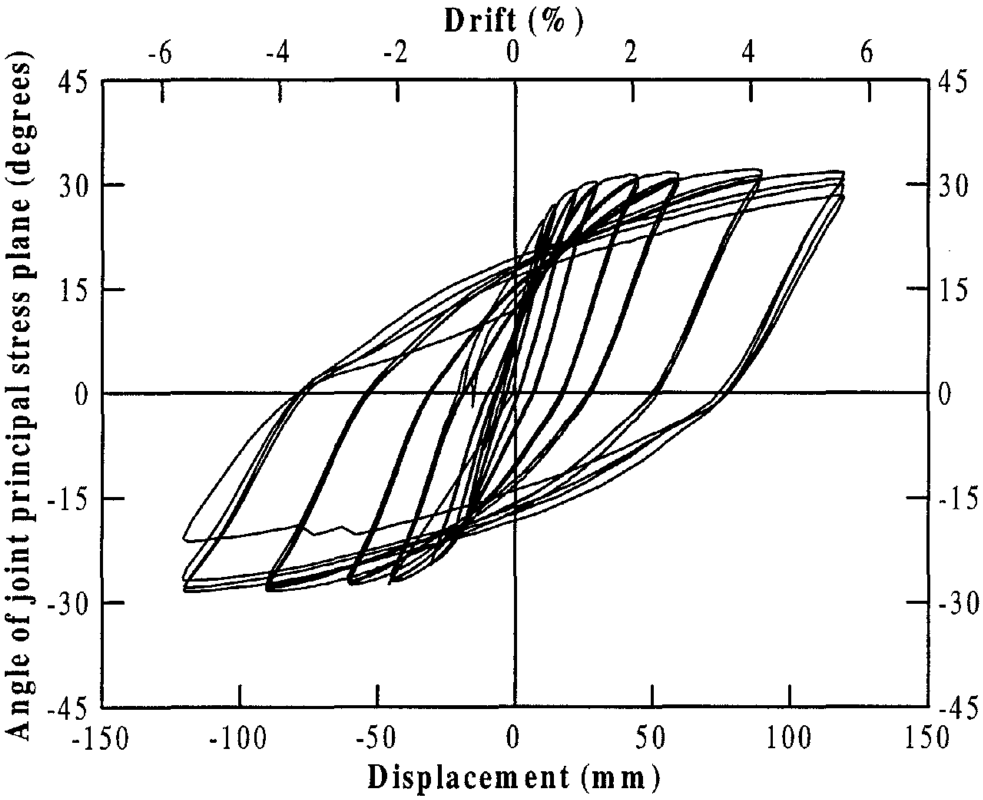

Figure 5.17 Angle of the joint principal stress plane as calculated using the average joint shear stress.

In Figure 5.18, growth of the joint panel area is represented as a function of column displacement, which confirms that the joint deformation of IC2 was negligibly small in comparison to that observed for the joint of IC1 (compare with Figure 4.26). Variation of shear strain calculated for the joint of IC2 seemed to have been affected by the initial damage that occurred to the joint and is not presented in this report. The experimentally observed rigid body rotation of the joint introduced by bending of the cap beam is shown in Figure 5.19. The maximum rotation of 0.003 radians was obtained at ductility 8, which contributed to about 5 percent of the total horizontal displacement (see also Figure 5.23).

5.7.4 Displacement Components

Components of the total horizontal displacement at the top of the column are depicted in various forms in Figures 5.20 – 5.23 as presented for IC1 in Figures 4.30 – 4.33. As mentioned in the previous section, a good estimate of the joint shear strain was not obtained. Therefore, the horizontal displacement due to joint shear was not considered in Figure 5.20, which shows the components of the column displacements as calculated from the experimental readings. Also shown in this figure is a comparison between the total measured displacement and that accumulated from column flexure and joint rotation. It is believed that the omission of displacement contribution due to joint shear is largely responsible for the error shown in Figure 5.20, which increases with displacement.

A good agreement between the accumulated displacement from theoretical estimates of column flexure and joint rotation and the total measured column displacement was obtained (Figure 5.21), but the maximum theoretical displacement underestimated the experimental value by 33 percent. In Figure 5.22, theoretical components due to column flexure and joint rotation are compared to those obtained from the experimental readings. A good agreement is again seen, although the predicted displacement component due to joint rotation was marginally underestimated and that due to column flexure was slightly overestimated. A similar observation was made for the reinforced concrete unit. The percentage contribution of the displacement components are shown in Figure 5.23 starting from the displacement corresponding to the first yield. Because of initial damage, the contribution due to column flexure was higher in the pull direction at low ductility when compared to the values in the push direction loading. As a result, almost

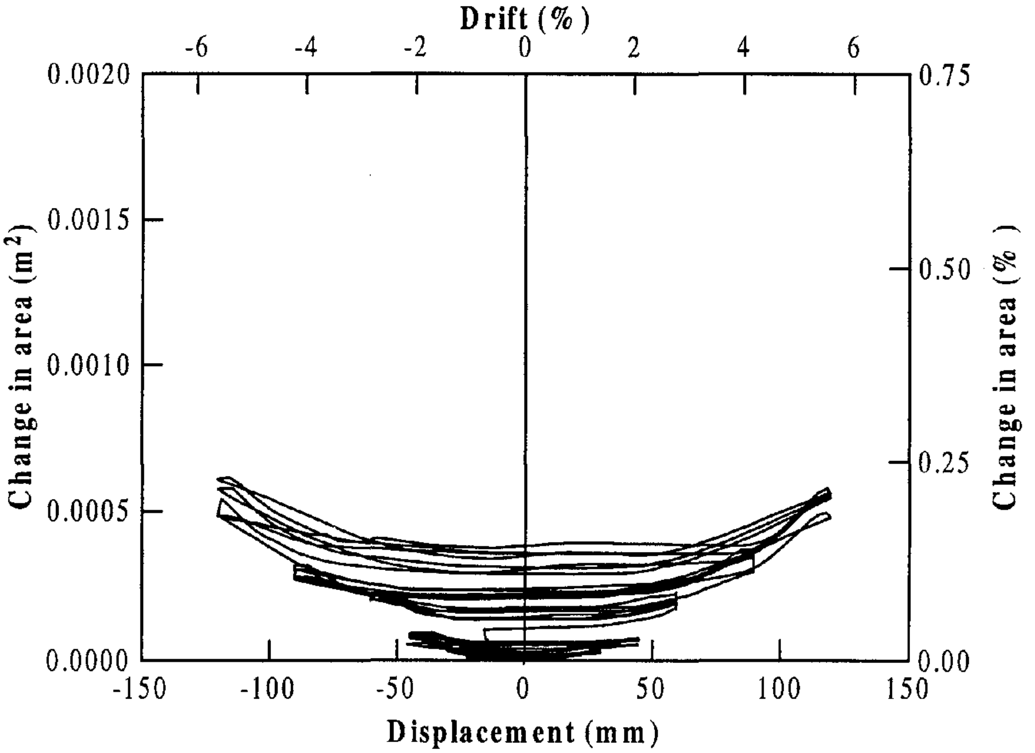

Figure 5.18 Growth of joint panel area as a function of column displacement.

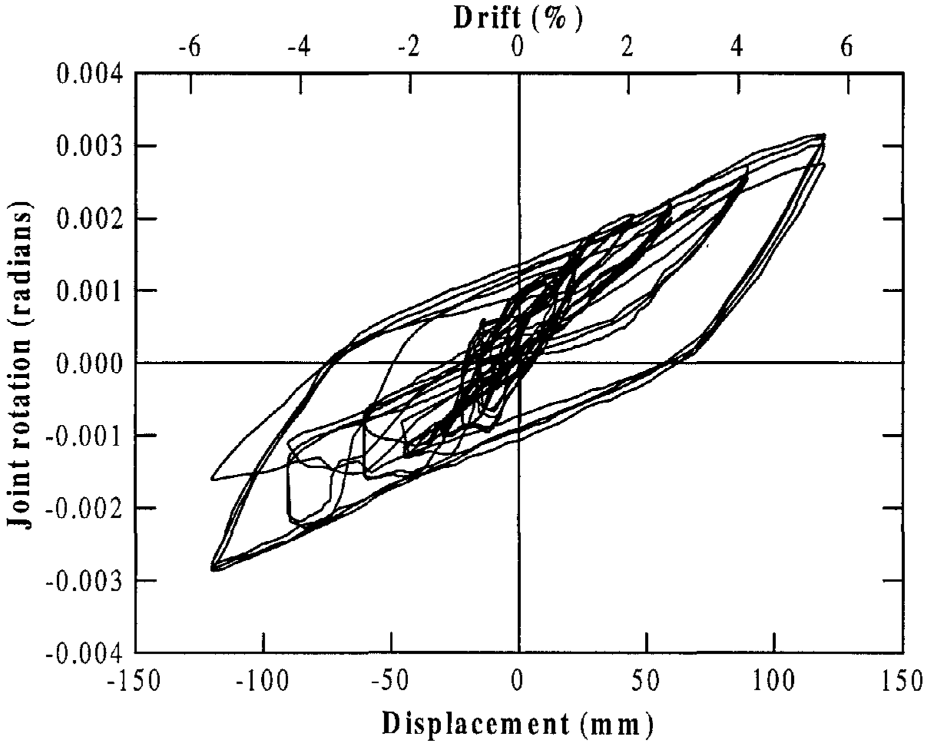

Figure 5.19 Joint rotation as introduced by bending of the cap beam.

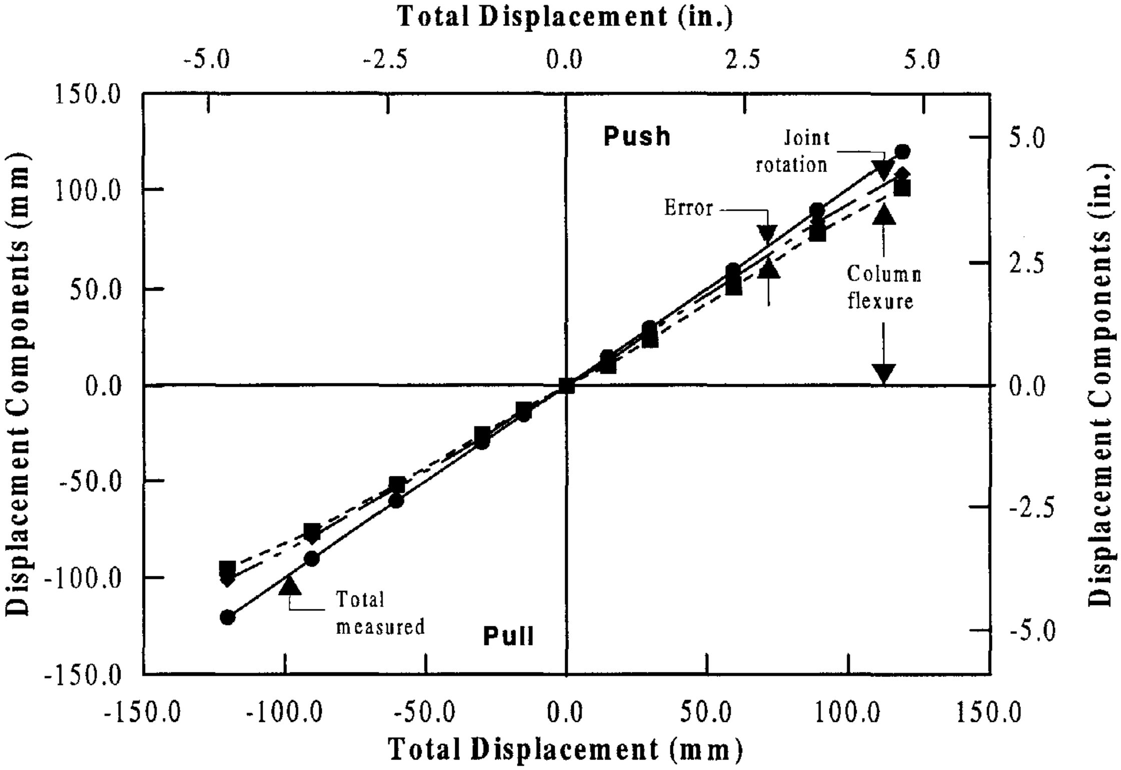

Figure 5.20 Comparison of the displacement accumulated from experimentally observed components to the total measured displacement.

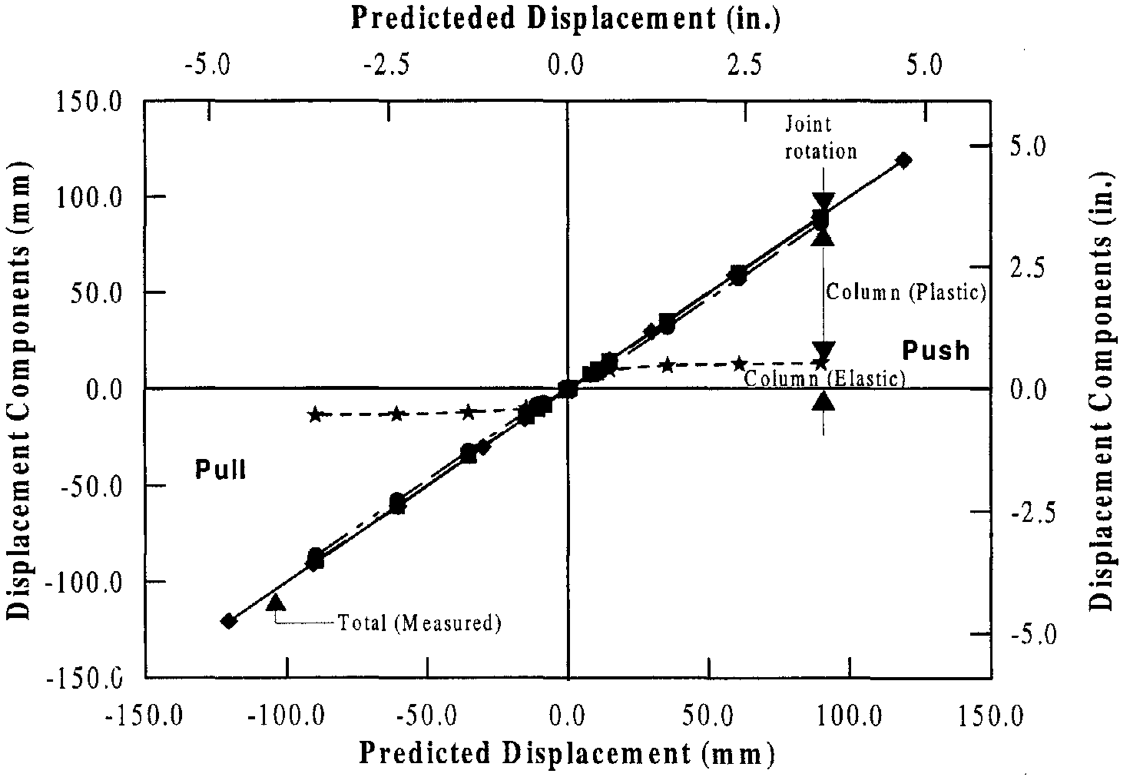

Figure 5.21 Comparison of the displacement accumulated from theoretically estimated components to the total measured displacement.

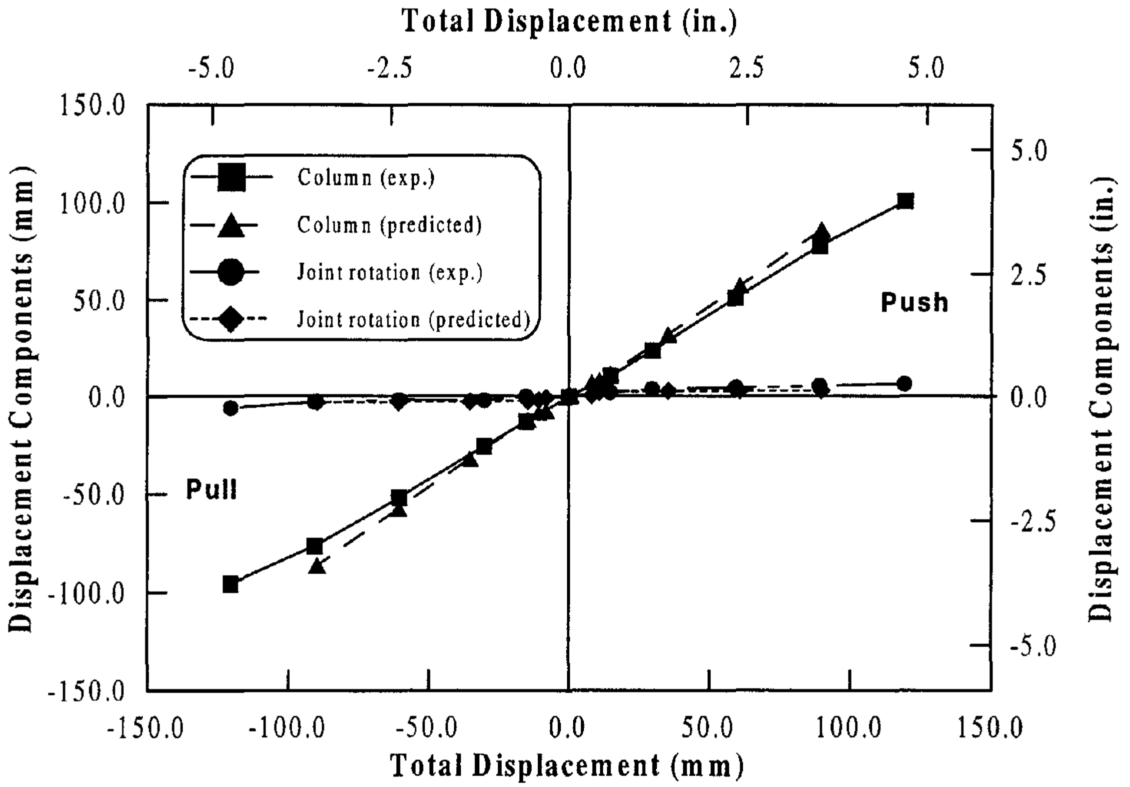

Figure 5.22 Comparison of experimentally obtained displacement components due to column flexure and joint rotation against the analytical values.

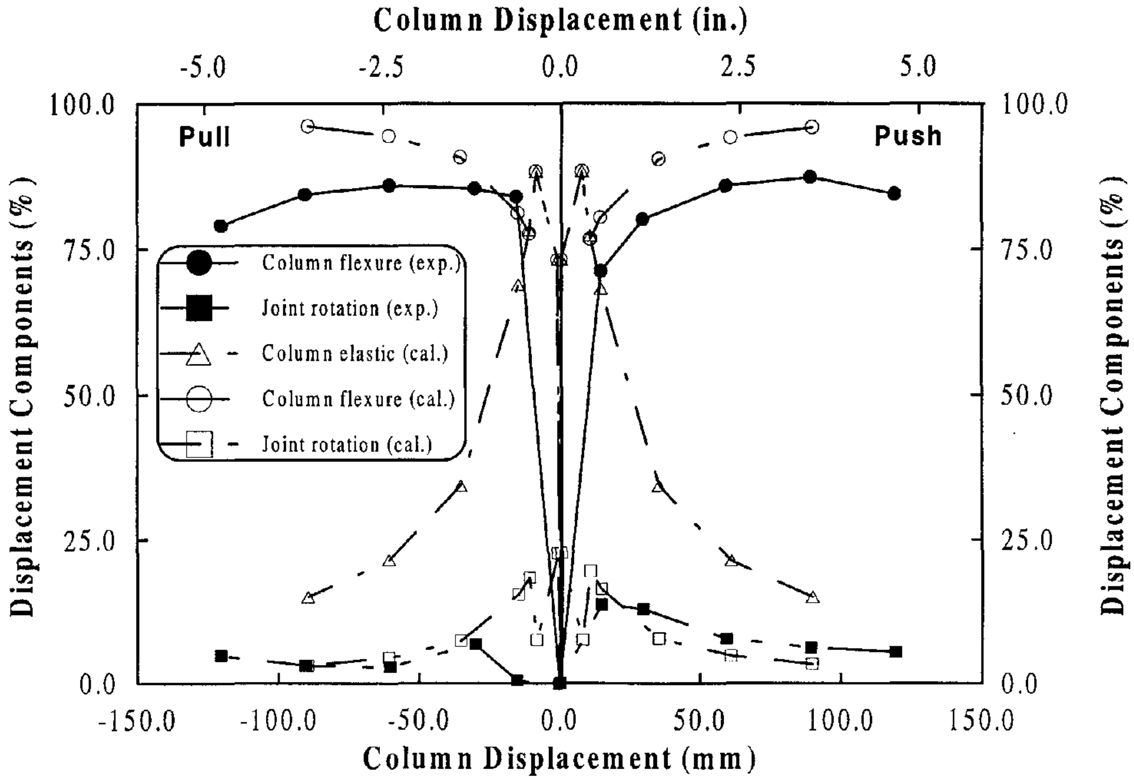

Figure 5.23 Representation of displacement components as percentage of the total horizontal displacement.

zero percent contribution due to joint rotation was obtained experimentally at ductility 1 in the pull direction.

5.7.5 Strain Gauge Histories

The only serious damage which occurred to the test unit due to the unexpected actuator force on the specimen prior to testing was to the internal instrumentation. Most of the strain gauges mounted on the longitudinal column reinforcement and some of the spiral gauges, particularly those located within the joint, failed during the cause of this incident. Consequently, only limited strain profile plots were obtained (see Section 5.7.6). Several strain histories are presented here as representative readings in the various regions of the test unit.

Two strain gauge histories from the longitudinal column reinforcement are presented in Figures 5.24 and 5.25. The first gauge was placed on an extreme tension reinforcement at the joint interface while the location of the second gauge was on an inner bar within the joint at 269 mm (10.6 in.) from the bar end. During the initial pull direction loading, both gauges were subjected to strains beyond yielding with the first gauge under compression and the second gauge under tension. The strain gauge history shown in Figure 5.25 for the gauge within the joint confirms that a significant strain penetration occurred into the joint.

In Figures 5.26 – 5.29, strain gauge histories of four spiral gauges are exhibited as a function of column displacement. The first two gauges were located in the first joint spiral from the bottom (as constructed): one on the south side perpendicular to the loading direction (Figure 5.26) and the other on the east side measuring the out-of-plane transverse strain (Figure 5.27). Because of the confinement provided by the cap beam and prestressing, the strain in the gauge on the south side was considerably less than that on the east side, where it appears that yielding of the reinforcement would have developed at ductility 8. A similar observation between in-plane and out-of-plane strains was made for the reinforced concrete joint IC1. When compared to IC2, much higher out-of-plane transverse strains were recorded in IC1 (see Figure 4.48).

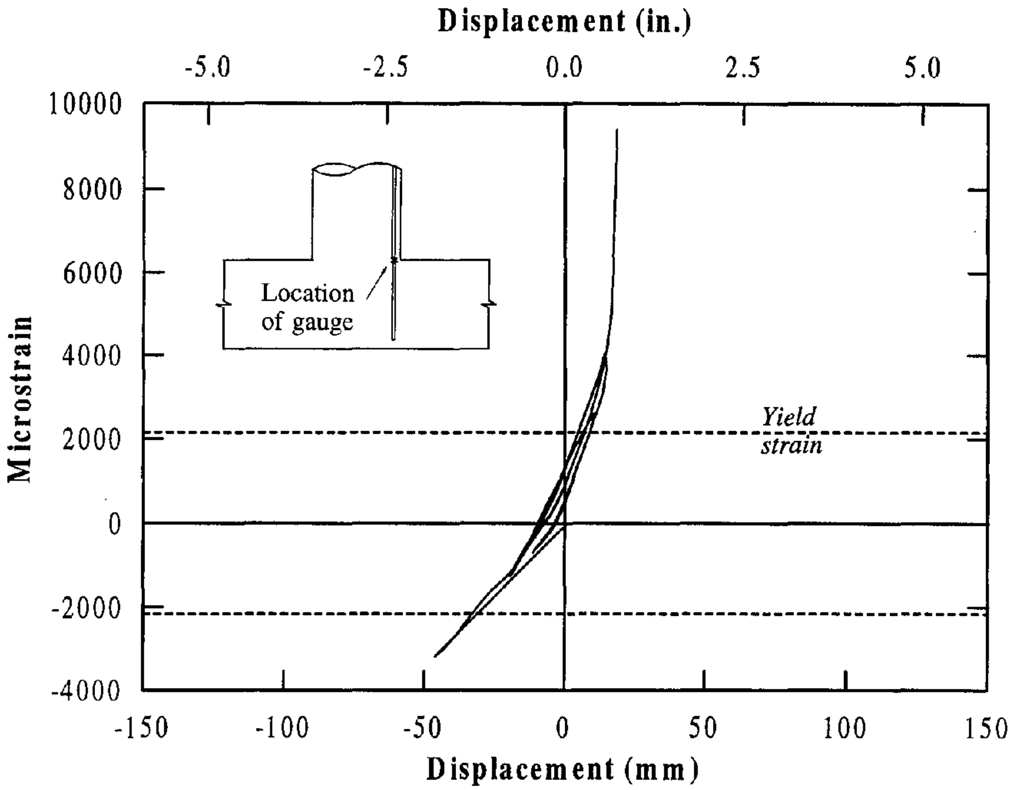

Figure 5.24 Strain history of a gauge located at the joint interface on an extreme column tension reinforcement.

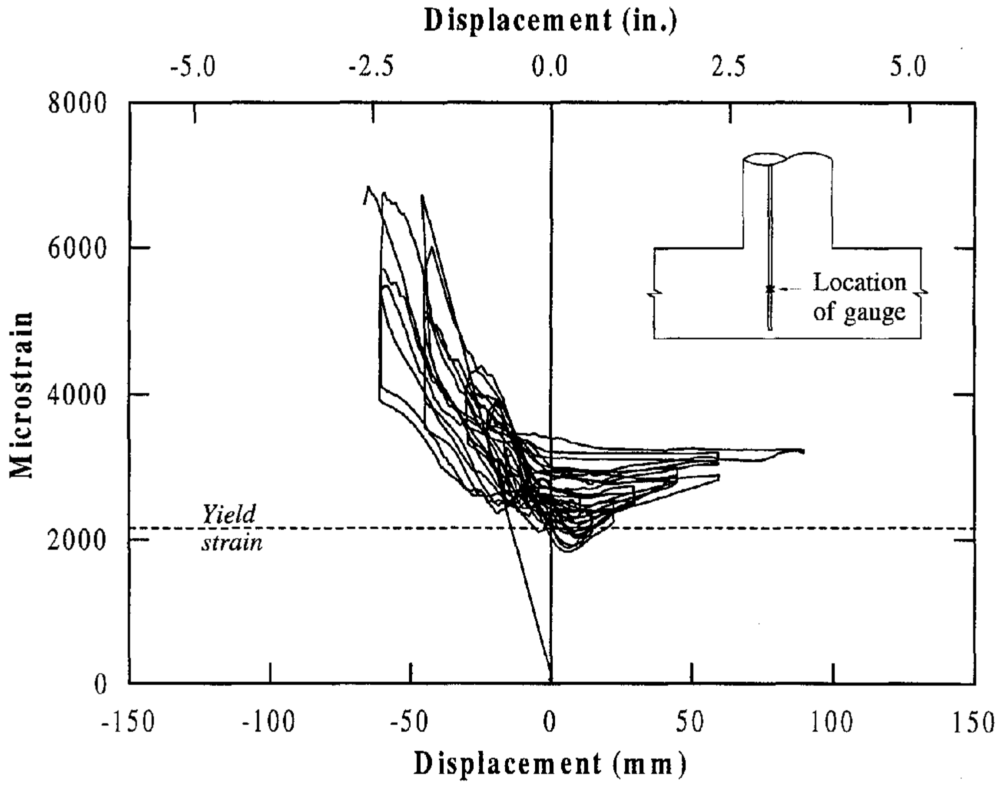

Figure 5.25 Strain history of a gauge located within the joint on a longitudinal column reinforcement.

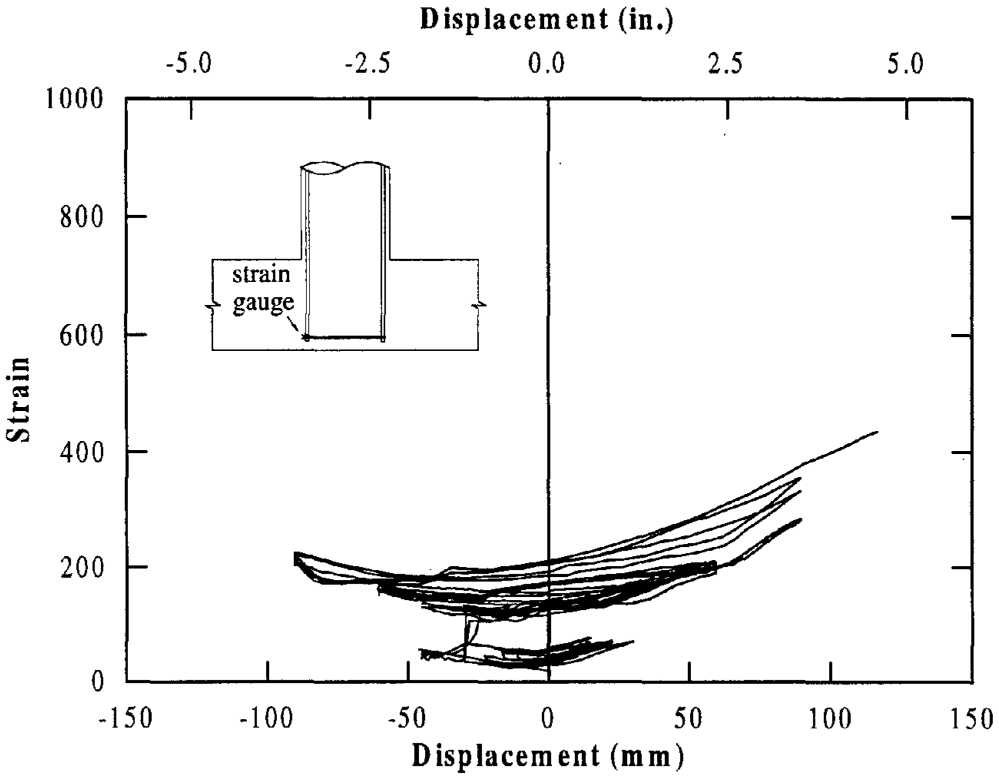

Figure 5.26 History of a joint spiral gauge measuring in-plane strain.

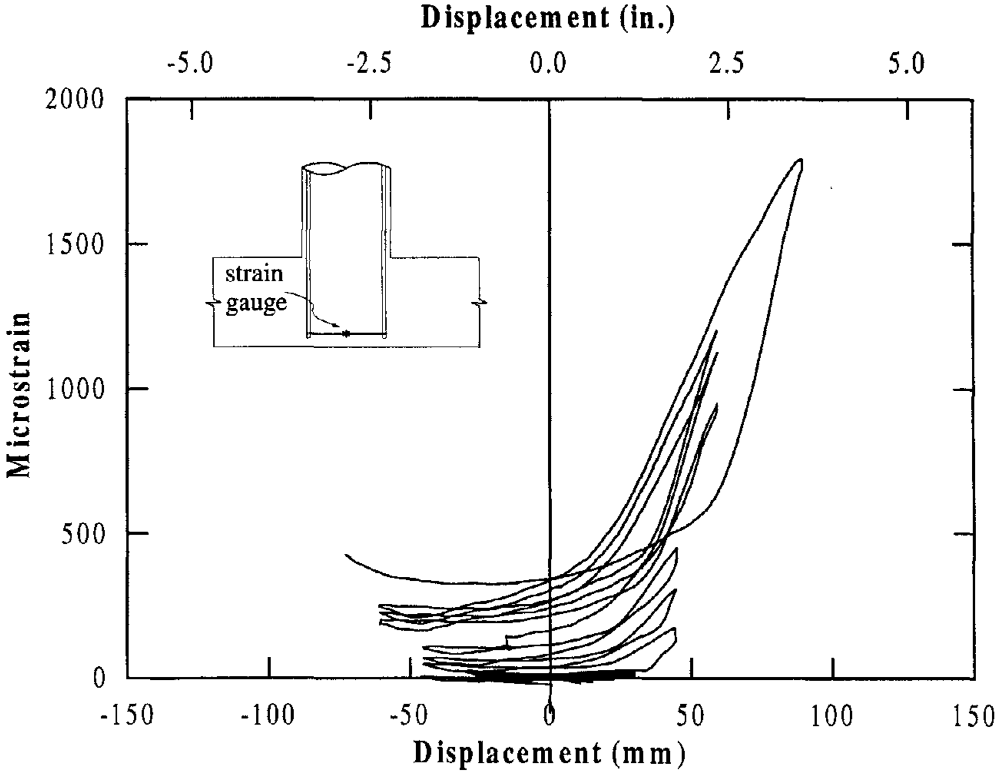

Figure 5.27 History of a joint spiral gauge measuring out-of-plane strain.

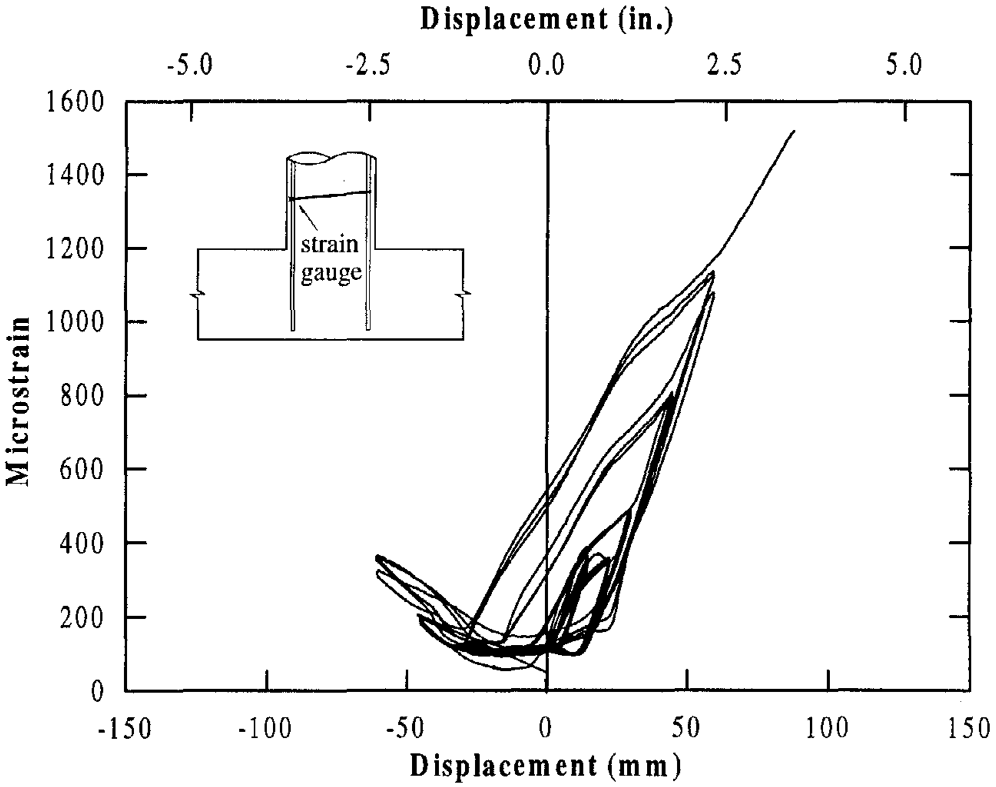

Figure 5.28 History of a column spiral gauge measuring confinement strain.

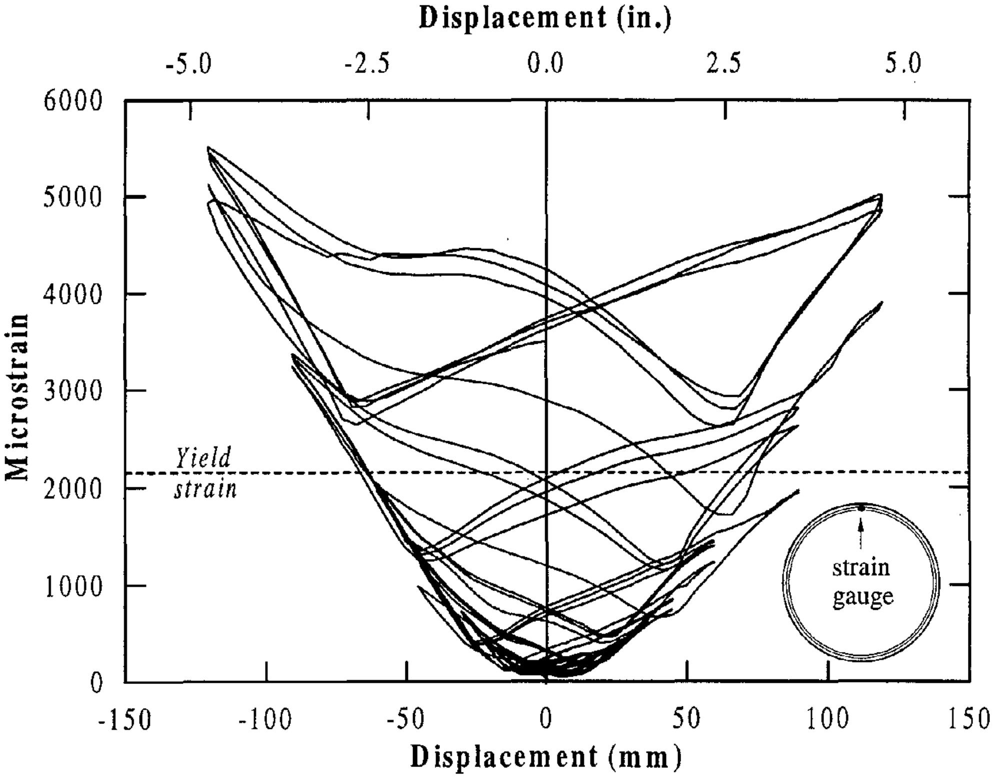

Figure 5.29 History of a column spiral gauge measuring shear strain.

The two spiral gauges shown in Figures 5.28 and 5.29 were located in the column with the first one showing the confinement effect and the other representing strain in the column transverse reinforcement due to shear. The strain gauge reading shown for the confinement was located at 419 mm (6.5 in.) from the joint interface and significantly larger strains would have developed in the spirals closer to the critical section of the column. As observed for IC1, strains well in excess of yield limit were developed in the shear reinforcement. Several other gauges also recorded similar strain histories.

In Figures 5.30 – 5.32, three strain gauge readings from the longitudinal beam reinforcement are presented. The first gauge (Figure 5.30) was on a bottom (as cast) beam reinforcement at the column face. The tension strain developed in this gauge under push direction loading corresponded to the maximum negative moment induced in the cap beam. The peak strain developed in the reinforcement was 65 percent of the yield

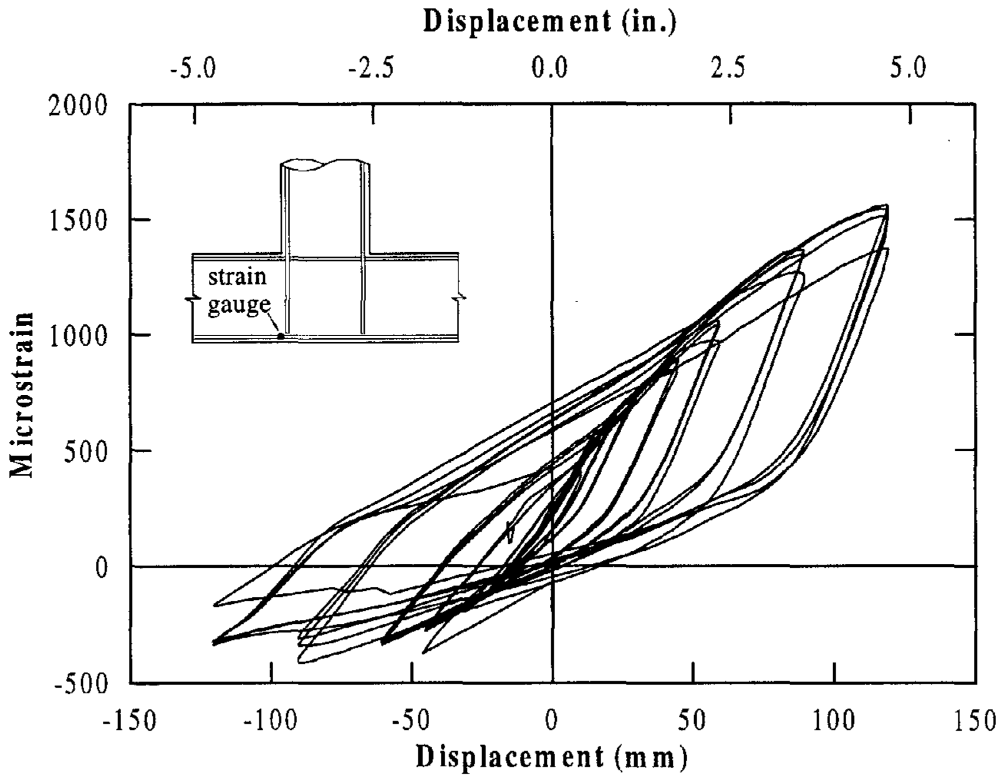

Figure 5.30 Strain history of a bottom reinforcement gauge located at the column face.

strain. The other two strain histories shown in Figures 5.31 and 5.32 corresponded to gauges on a top (as cast) beam reinforcement located 203 mm (8 in.) apart, one at the beam/joint interface and the other within the joint. Considering that the variation of stress in the reinforcement should be similar to that shown for the strain readings because the recorded strains in the reinforcement were almost within the yield limit, the following observations are made. When the pull direction load was applied to the column, it developed the maximum positive moment on the left side of the column face where the gauge shown in Figure 5.31 was located. In the design procedure (Section 5.2.2), there was no top reinforcement required in the cap beam and the prestressing alone was found to be adequate for resisting the positive moment. However, there were 4#6 bars, although 4#4 bars were adequate, provided in order to support the joint force transfer mechanism if required. It is surprising that yield strength was developed in the top beam reinforcement at ductility 8. Comparing Figure 5.31 to Figure 5.32, it is seen that almost an opposite behavior was obtained for the gauge located within the joint. When tensile yield strength was developed at the column face, the gauge within the joint recorded 50 percent of yield under compression. A bond stress required for the corresponding stress change in the bar within 203 mm (8 in.) would be $2.7\sqrt{f_c'}\left(32\sqrt{f_c'}\text{ in psi units}\right)$. During cycling of loading at ductility 8, the bar stress at the interface continued to reduce while at the gauge location within the joint yield strength was almost developed under compression. A similar behavior showing compression strain within a short distance into the joint and gradual increase in the strain during cyclic loading at ductility 8 was also observed in the other top beam reinforcement. An example may be seen in Figure 5.37, where a strain profile plot of one of these reinforcement is presented. However, the magnitudes of peak strains of this reinforcement and other top beam bars were smaller than that is seen in Figure 5.32.

As can be seen in the profile plots (Figure 5.38 and 5.39), the strains monitored in the beam stirrup reinforcement were small except in the joint region. Two strain histories are presented for joint stirrup gauges, which were located in the outer legs at mid height of the beam, in Figures 5.33 and 5.34. Yield strain was developed in both gauges, suggesting that the provided nominal joint reinforcement was adequate for the joint response. Because of their location at equal distance from the column center line, an opposite behavior reflecting the loading direction should be expected in the strain histories and this can be seen in the figures.

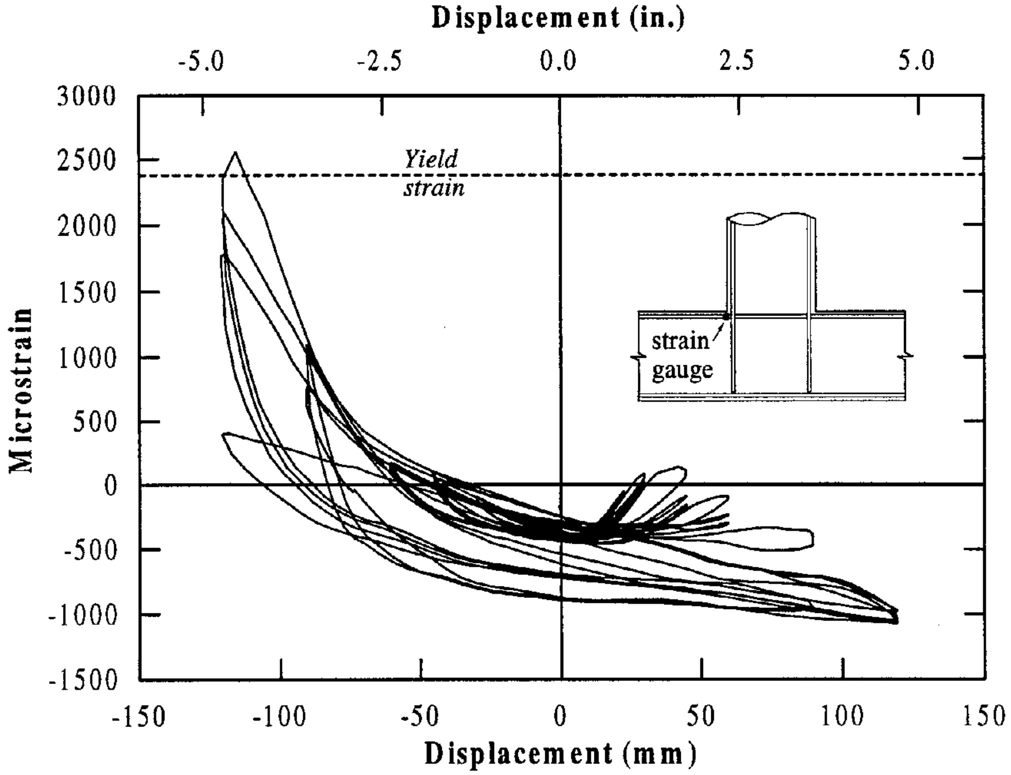

Figure 5.31 Strain history of a top beam reinforcement gauge located at the column face.

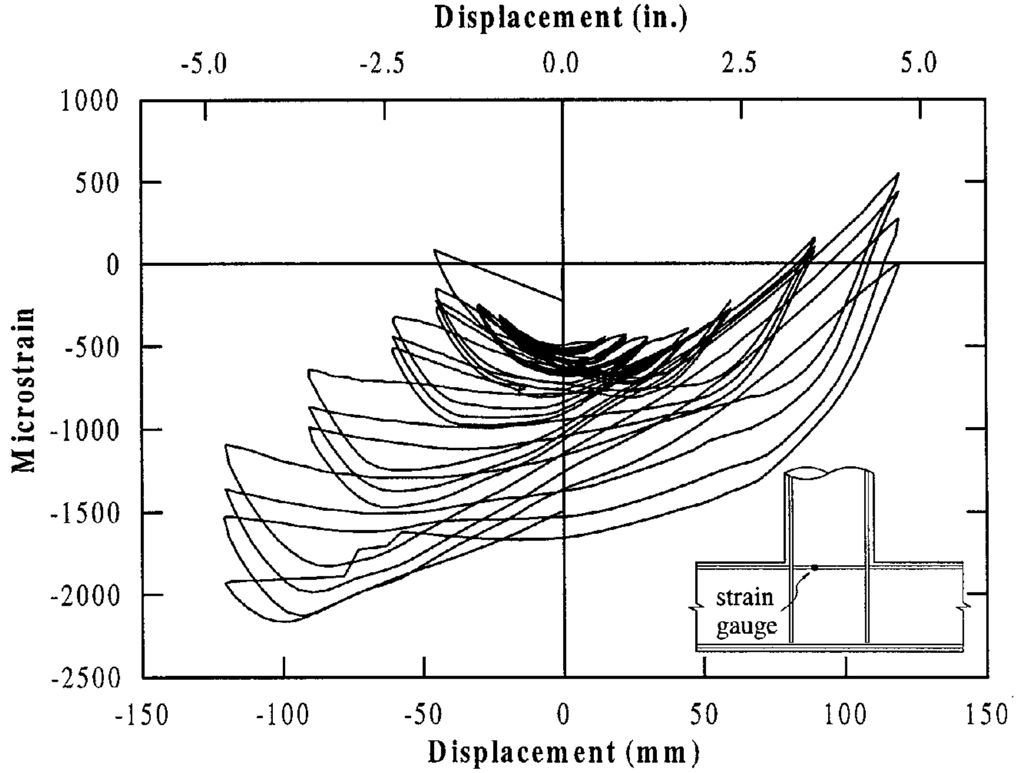

Figure 5.32 Strain history of a top beam reinforcement gauge located within the joint.

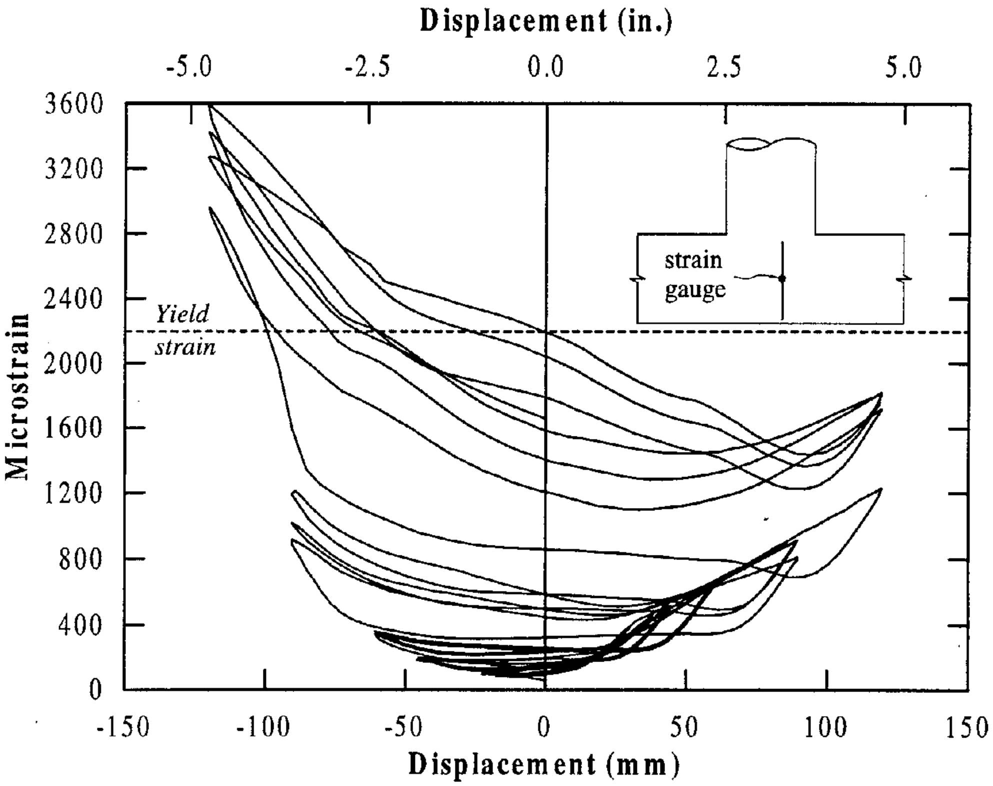

Figure 5.33 Strain history of a joint stirrup gauge at mid-height of the beam.

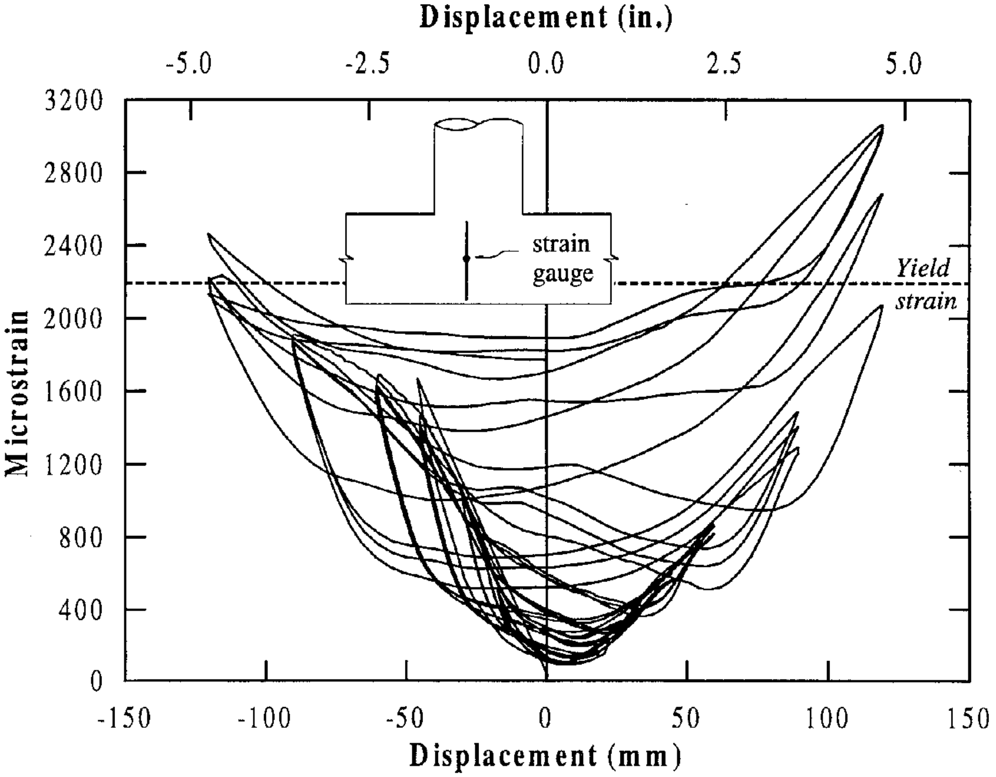

Figure 5.34 Strain history of a joint stirrup gauge at mid-height of the beam.

5.7.6 Strain Profiles

Good strain profile plots could not be obtained for the longitudinal and transverse column reinforcement as several strain gauges were damaged prior to the testing. Strain profiles were, however, established for the beam reinforcement and are presented below.

In Figures 5.35 – 5.37, strain profiles obtained along a bottom (as cast) and two top longitudinal beam reinforcement are shown. The maximum tensile strain developed in the bottom reinforcement under negative moments reached 63 percent of yield strain at the column face, which is similar to that was shown for another bottom beam reinforcement in Figure 5.30. These reinforcement were designed to yield at the peak horizontal load on the column. The conservative estimate of the column overstrength moment factor is largely responsible for obtaining considerably lower peak strain in the reinforcement than that was anticipated according to the design calculation. The maximum tensile strain measured in the top reinforcement at the column face was about 1000 μ strain in the push direction loading. For the pull direction, a gauge in one bar recorded strains beyond yield (also see Figure 5.31) while strains in the other bar were restricted to 700 μ strain. The remaining two top reinforcement were also gauged and the strains recorded in these bars were found to be closer to the latter. In the strain history plots presented in Figure 5.31 and 5.32, it was shown that when tensile strain developed at the column face due to positive moment, compression strain was recorded within the joint at 203 mm (8 in.) from the beam/joint interface. This was not expected to occur due to strain penetration into the joint. The profile plots shown in Figures 5.36 and 5.37 show a similar behavior for push and pull direction loading, and this is further investigated in reference [26].

The strain profiles obtained at mid-height of the inner and outer legs of beam stirrups are shown in Figure 5.38 and 5.39 respectively. Significantly high strains developed in stirrups within the joint with a few gauges recorded strains beyond yield, suggesting that the amount of vertical reinforcement provided within the joint was sufficient. As anticipated, the strains in the stirrups of the cap beam were negligibly small.

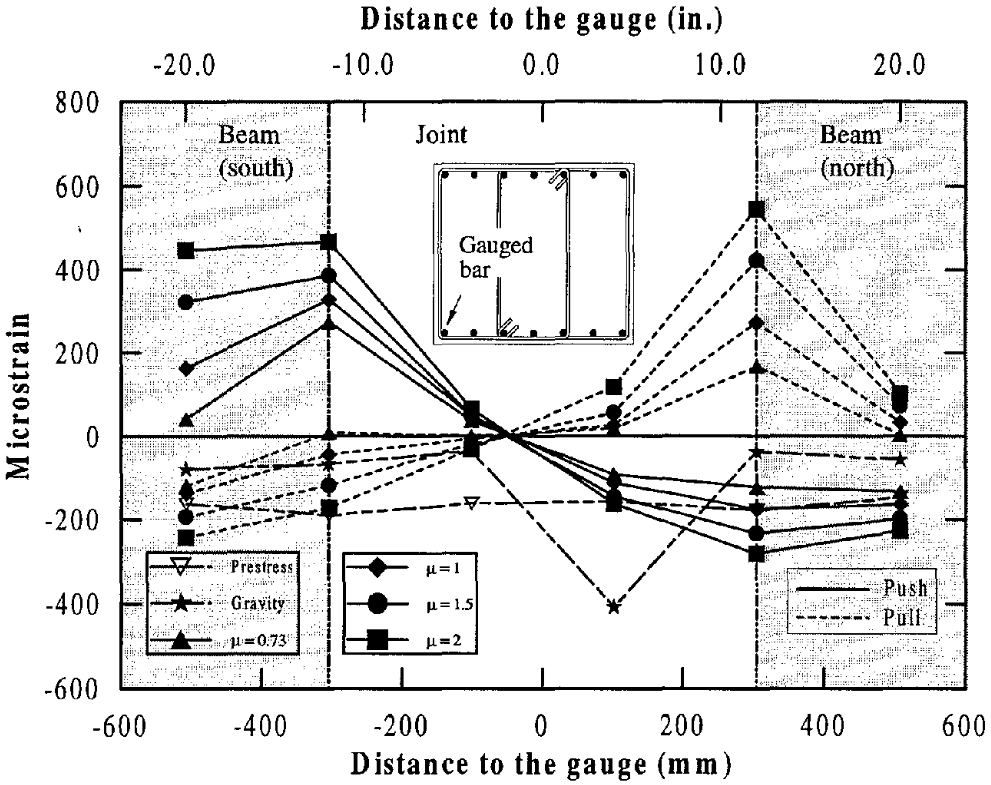

(a) Initial stages of testing

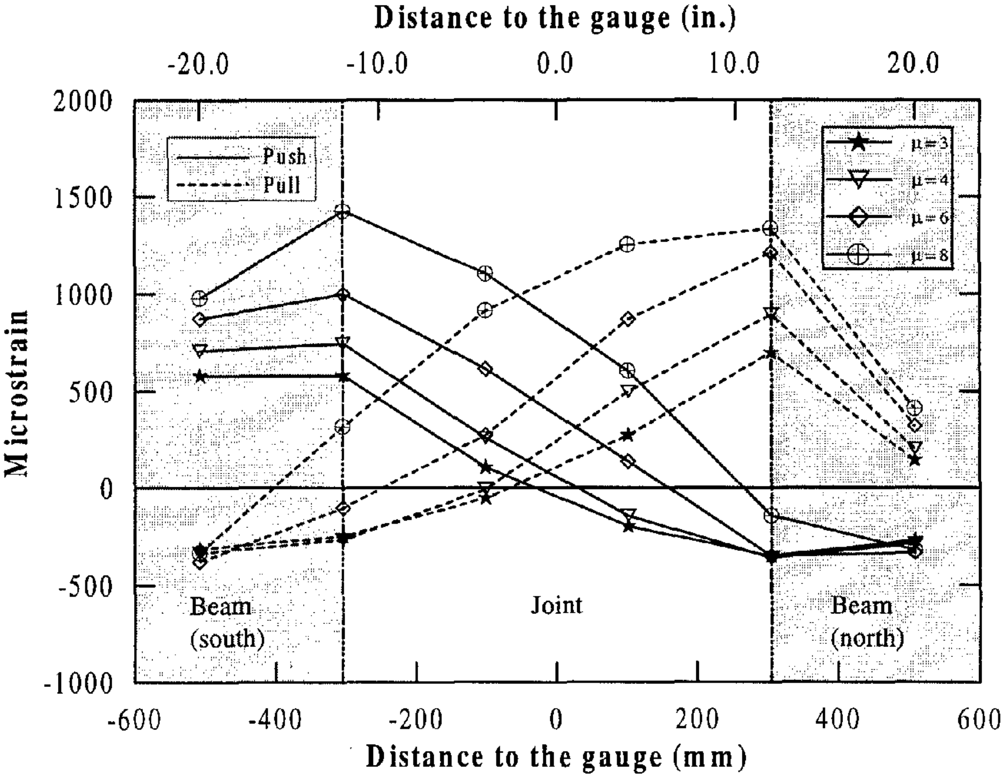

(b) Final stages of testing

Figure 5.35 Strain profiles along a bottom longitudinal beam reinforcement.

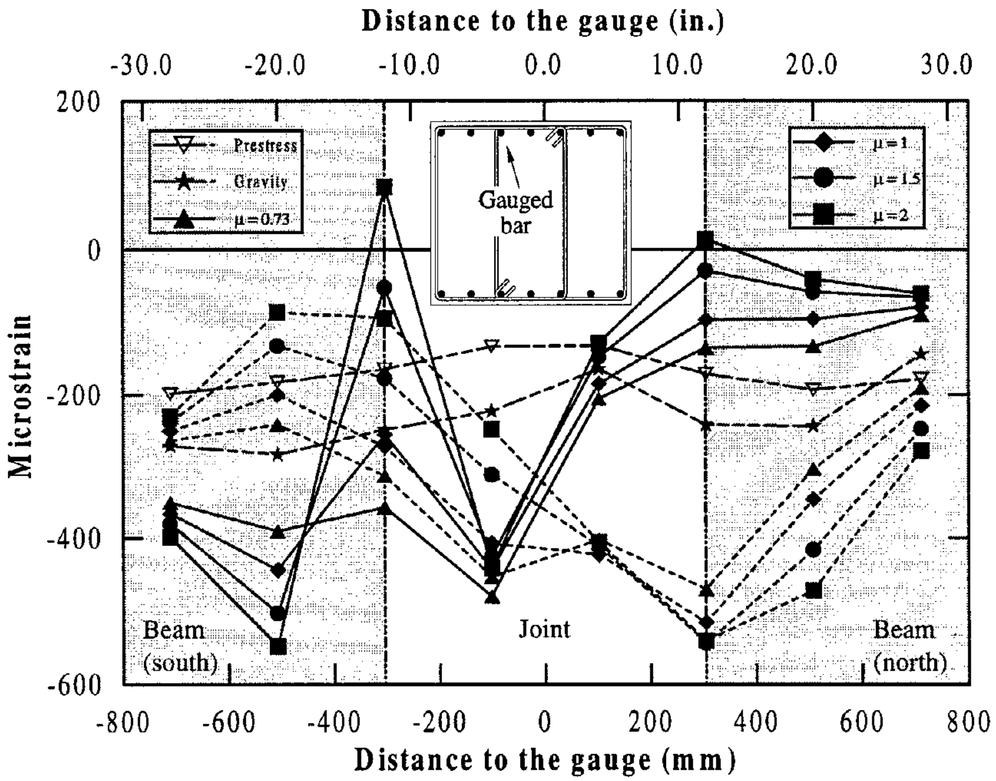

(a) Initial stages of testing

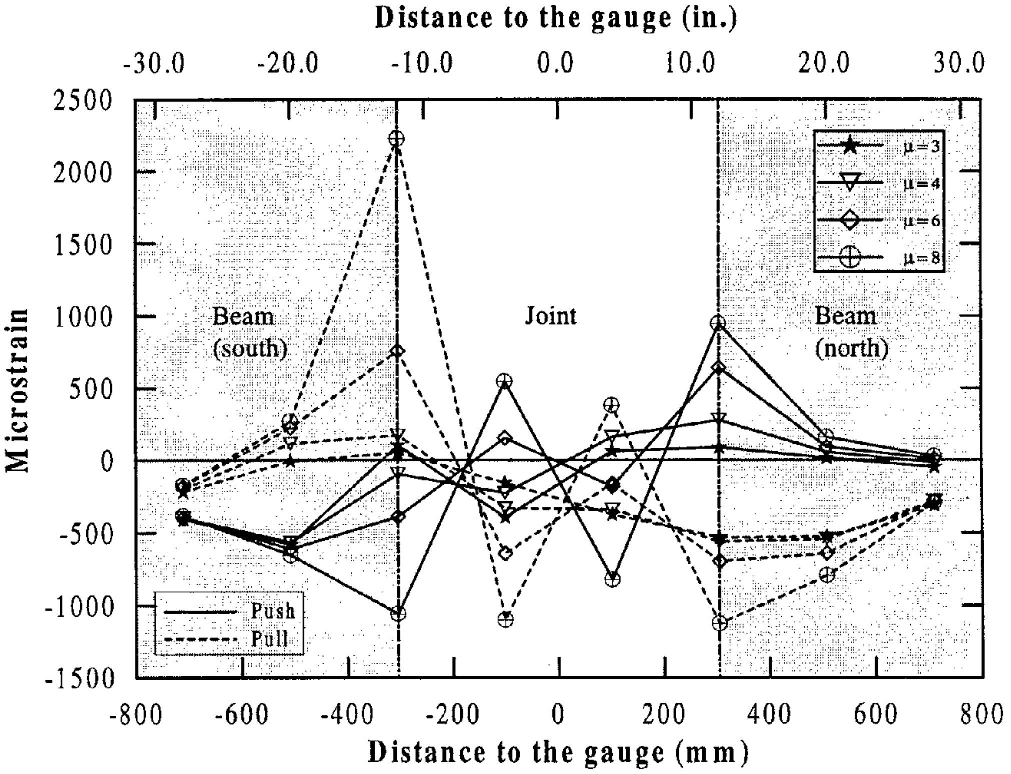

(b) Final stages of testing

Figure 5.36 Strain profiles along a top longitudinal beam reinforcement.

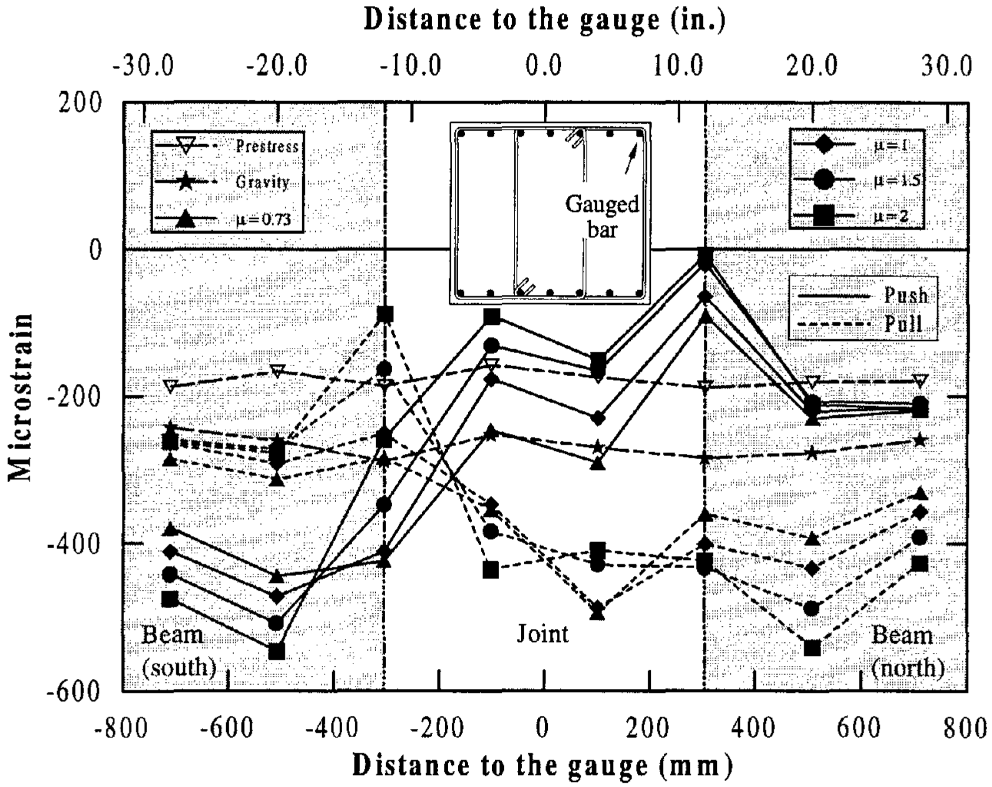

(a) Initial stages of testing

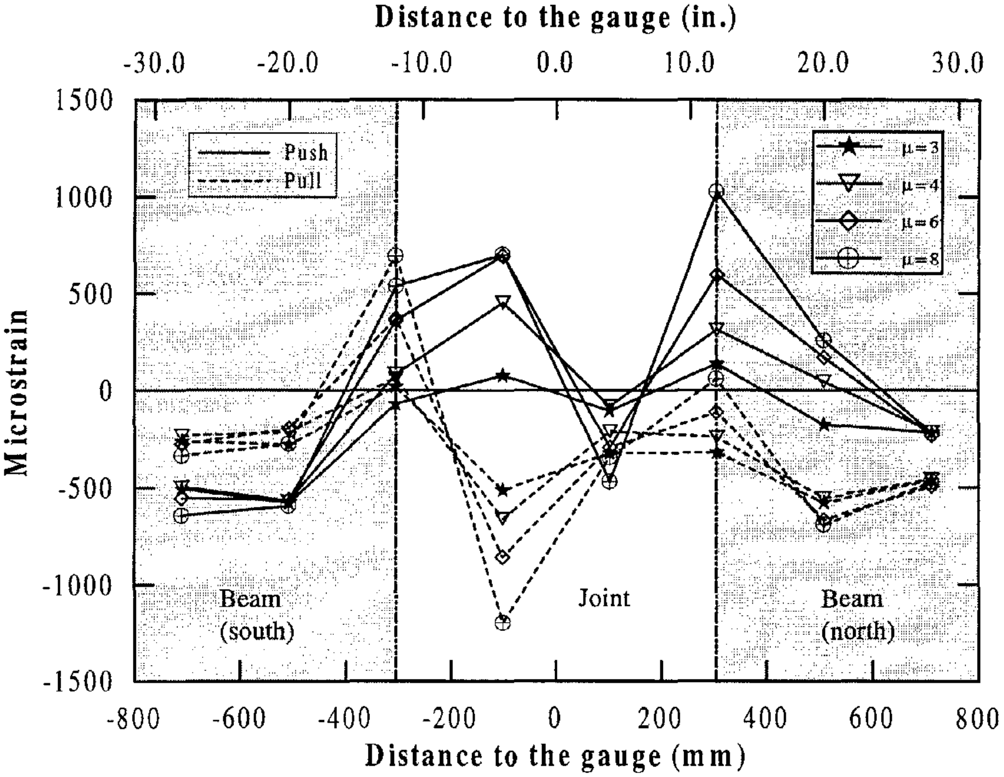

(b) Final stages of testing

Figure 5.37 Strain profiles along a top longitudinal beam reinforcement.

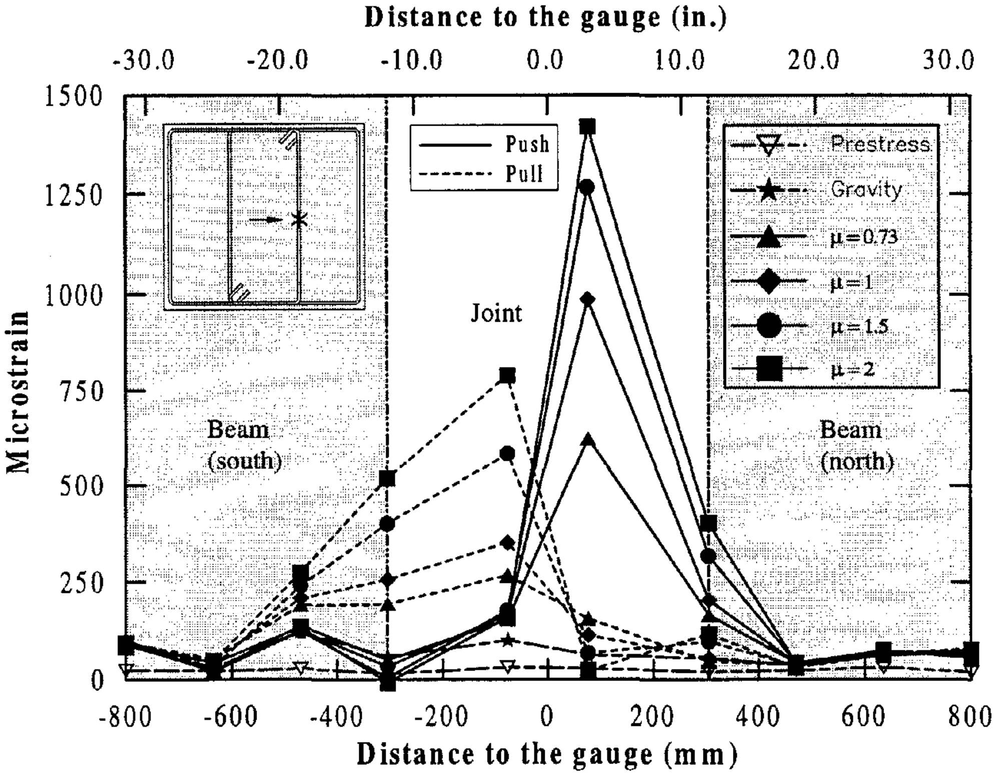

(a) Initial stages of testing

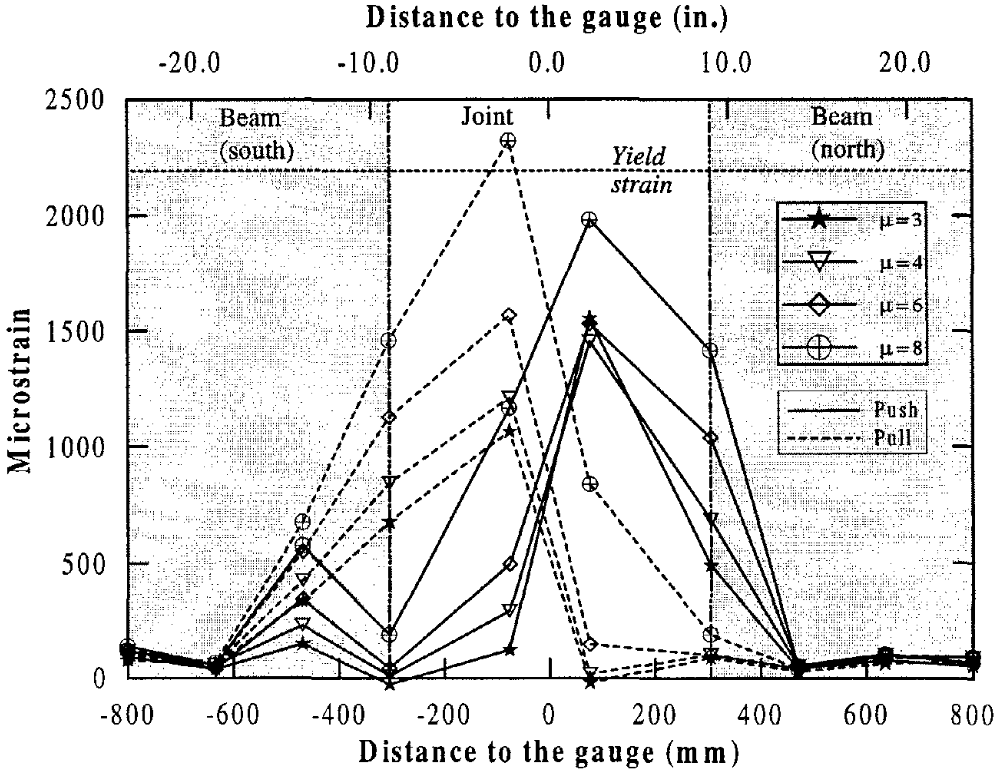

(b) Final stages of testing

Figure 5.38 Strain profiles of inner leg beam stirrups at mid-height.

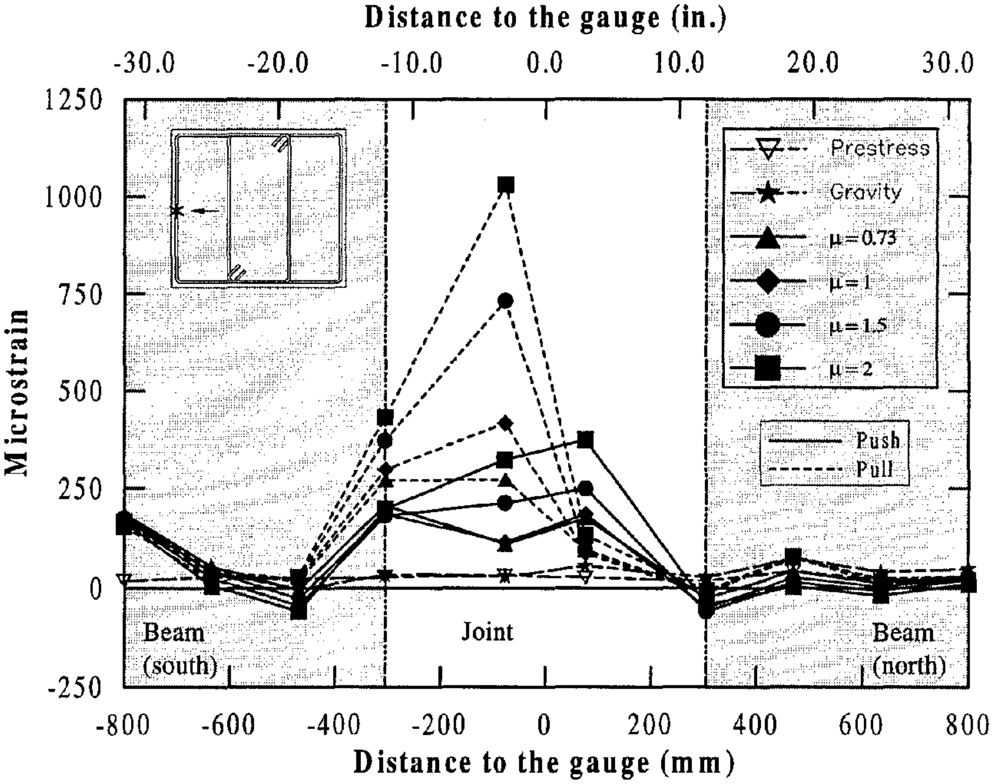

(a) Initial stages of testing

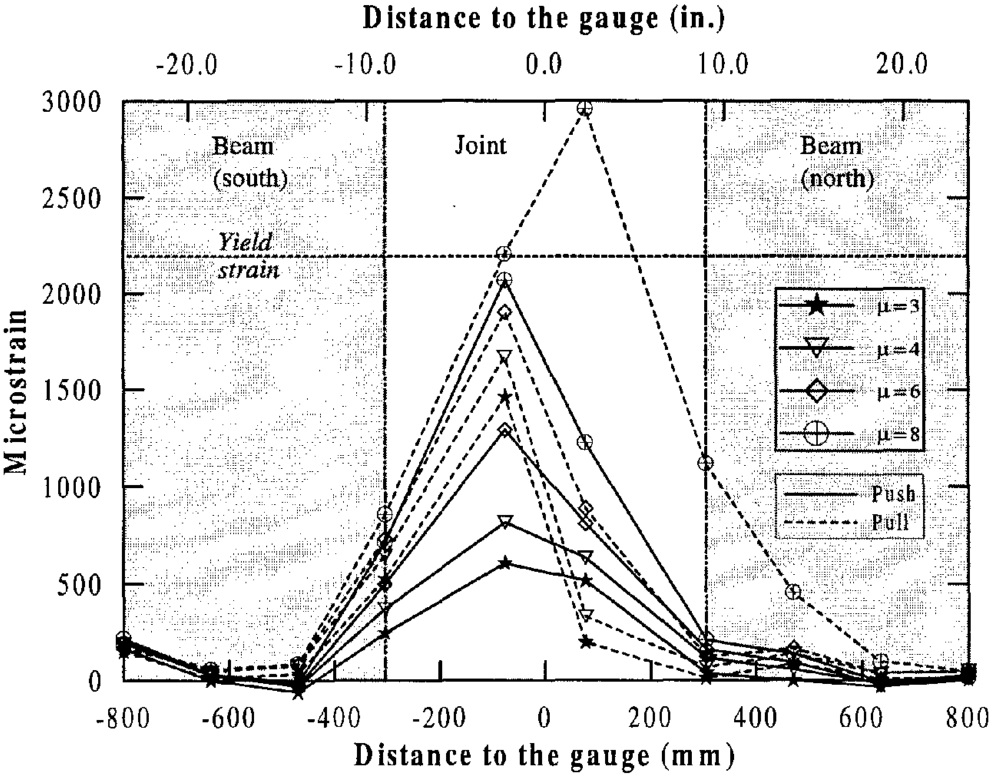

(b) Final stages of testing

Figure 5.39 Strain profiles of outer leg beam stirrups at mid-height.

5.8 Discussion

The seismic performance of a bridge tee joint designed with a partially prestressed cap beam is presented in this chapter. In detailing the joint region, a force transfer model was initially considered. Identifying that the longitudinal column reinforcement can be anchored directly into the joint strut, which was broadened by the cap beam prestressing, the joint reinforcement was reduced to the nominal requirements. In the design procedure, the cap beam was limited to respond elastically while the plastic hinging was forced in the column adjacent to the joint interface.

Prior to performing the cyclic test on the specimen, the test unit was unintentionally subjected to a horizontal load in the pull direction. There was some minor damage occurred to the test unit which did not significantly alter the overall behavior of IC2 under simulated seismic loading. However, the incident resulted in loss of several strain gauges.

A good hysteretic force-displacement response was obtained for the test unit with failure occurring in the plastic hinge region of the column as intended. At the peak displacement, the column drift corresponded to 5.6 percent, which was 33 percent higher than that predicted from theoretical calculations.

The overstrength moment capacity of the column was taken as 30 percent higher than the theoretical ultimate moment capacity. The maximum moment induced in the column during the test was only 1.8 percent higher when compared to the theoretical ultimate moment capacity. Inclined shear cracks developed in the column as extension to flexural cracks opened up significantly when the column was subjected to the maximum displacement. It appeared at the late stages of testing that shear failure in the column might be possible. The strain gauge reading from the column spirals supported this observation, by registering significantly high inelastic strains. Based on the argument presented in Section 4.7 for unit IC1 whose column detail was identical to that of IC2, it is concluded that the column was not insufficiently reinforced against shear failure.

There was almost no damage occurred to the cap beam, suggesting that it was very conservatively designed and that the longitudinal reinforcement content and/or the amount of cap beam prestressing applied to the beam could have been reduced. The unnecessarily high overstrength factor assumed for the moment capacity of the column was largely responsible for detailing the beam conservatively. Yielding in the beam reinforcement was, however, observed in some of the reinforcing bars at the column face probably due to some local effect and within the joint presumably as a part of joint mechanism. This is further investigated in a companion report [26].

A good seismic performance was obtained for the cap beam/column interior joint with the damage in the joint region limited to only minor cracking. The strain gauge measurements indicated that both horizontal and vertical joint reinforcement reached yield strength. When comparing the response of this joint to the equivalent reinforced concrete joint, it is obvious that the cap beam prestressing vastly improved the joint performance in unit IC2. A drawback of cap beam prestressing is that it elevates the principal compression stress within the joint, which can eventually cause crushing of concrete in the main diagonal strut, and hence a brittle failure of the joint. The advantage of partially prestressed cap beam is that the principal compression and tensile stresses can be manipulated by adjusting the prestressing so that such a failure can be avoided. When a large longitudinal reinforcement content is considered in the column, a fully prestressed detail is unlikely for the cap beam because the amount of prestressing required is typically high enough to cause failure of the joint strut. In such circumstances, a partially prestressed design of the bent cap will result in a good and simple joint detail as illustrated in this chapter.

CHAPTER 6

INTERIOR JOINT WITH A PRECAST FULLY PRESTRESSED CAP BEAM

The last test unit, IC3, of this series was designed with a fully prestressed cap beam. Since no continuous mild steel was required within the cap, the possibility of precast construction of concrete multi-column bents was also investigated. The design and construction of the test unit, as well as its behavior under simulated seismic loading are presented in this chapter.

6.1 Design Procedure

6.1.1 Column

In order to compare the results of this unit to those of the two previous units, identical flexural capacity of the column was retained. Hence, the longitudinal reinforcement detail of unit IC1 was duplicated in the column of IC3. Considering that pronounced shear cracking was observed in the two previous units and that additional confinement in the plastic hinge region of the column would delay buckling of the longitudinal column reinforcement further than that observed previously in IC1 and IC2, the volumetric ratio of the transverse reinforcement was increased from 0.0052 in IC1 (and IC2) to 0.0079 in IC3. This was expected to increase the ductility capacity of the column with no significant enhancement to its flexural moment capacity.

6.1.2 Cap Beam

Tensile tests performed on three coupons of longitudinal column steel resulted in average yield strength of 461 MPa (67 ksi) (see Table 6.2). The ideal and ultimate moment capacities estimated for the column using the measured yield strength were 697 kNm (514 kips-ft) and 814 kNm (600 kips-ft) respectively. The overstrength moment capacity of the column had been taken as 30 percent more than the nominal ultimate capacity for the two previous test units (IC1 and IC2). Considering that this approach significantly overestimated the actual capacities observed in the experiments, the overstrength column capacity of IC3 was taken as only 15 percent higher than the estimated ultimate moment capacity. Consequently, from equilibrium conditions, the required positive and negative cap beam moment resistance were estimated to be 220 kNm (162 kips-ft) and 602 kNm (444 kips-ft) respectively.

In designing the cap beam prestressing, a simple plastic analysis of the section (see Figure 6.1) was considered at the ultimate limit state with a strength reduction factor $\phi_f = 0.9$. For the cap beam width $b_w = 648$ mm (27 in.) and $f'_c = 34.5$ MPa (5 ksi), Eq. 6.1 resulted in cap beam prestressing of 2936 kN (660 kips), which was expected to induce an average stress of 7 MPa (i.e. $0.2f'_c$) in the beam. Limiting prestressing stress in the beam to about $0.2f'_c$ was considered necessary in order to keep concrete stresses within permissible values under serviceability conditions.

6.1.3 Interior Joint

The maximum principal tensile stress of the joint at the ultimate limit state was estimated, using Eq. 4.1, to be $0.43\sqrt{f'_c}\left(5.1\sqrt{f'_c}\text{ in psi}\right)$, which suggested that at least a part of the joint force should be transferred by a special mechanism. However, as for the interior joint of IC2 (section 5.1.3), only nominal joint shear reinforcement was provided. The maximum principal compression stress was expected to be $0.29f'_c$. This appeared excessive when compared to design criteria of building joints [25], where joints shear stresses are limited to $0.25f'_c$ providing, for this particular case, a maximum allowable joint principal compression stress of $0.27f'_c$. If the joints are adequately confined, the joint diagonal struts can be subjected to larger stresses. Therefore, no design modification was considered when the above limitation was marginally exceeded. The average joint principal tensile and compression stresses were later estimated to be $0.19\sqrt{f'_c}\left(2.3\sqrt{f'_c}\text{ in psi}\right)$ and $0.25f'_c$ respectively.

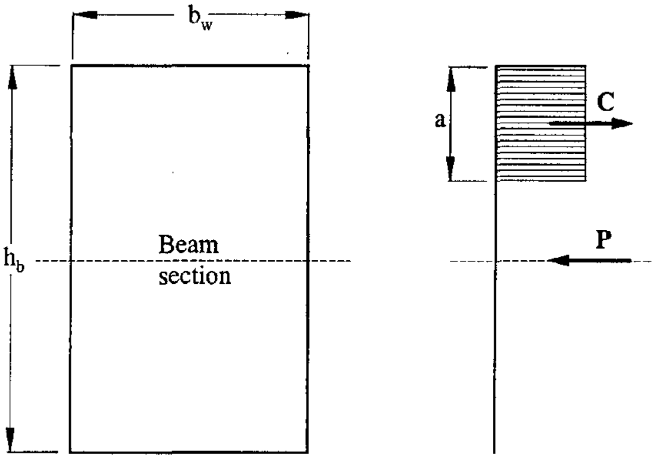

For equilibrium,

$$\left.\begin{aligned} &\mathbf{P = C = 0.85f_c' * b_w * a,}\ \text{and} \\ &\mathbf{P*\left(\frac{h_b - a}{2}\right) \geq \frac{M_{max}}{\phi_f}} \end{aligned}\right\} \qquad (6.1)$$

by substituting appropriate values in Eq. 6.1, it requires that

$$\mathbf{P \geq 2865\ kN\ (644\ kips)}$$

hence use

$$\mathbf{P = 2936\ kN\ (660\ kips)}$$

Figure 6.1 Plastic section analysis of the cap beam at the ultimate limit state.

Following the damage that occurred to the joint region of the first unit, which was designed with a fully reinforced concrete cap beam, the use of closed form vertical joint stirrups was preferred rather than that of hairpin ties. This was expected to give a better confinement to the joint core.

6.2 Reinforcement Detailing

Key reinforcement details of test unit IC3 are shown in Figure 6.2 while photographs of construction of the test unit are shown in Figures 6.3 and 6.4. A description of the reinforcement in the region of interest is given in the following sections.

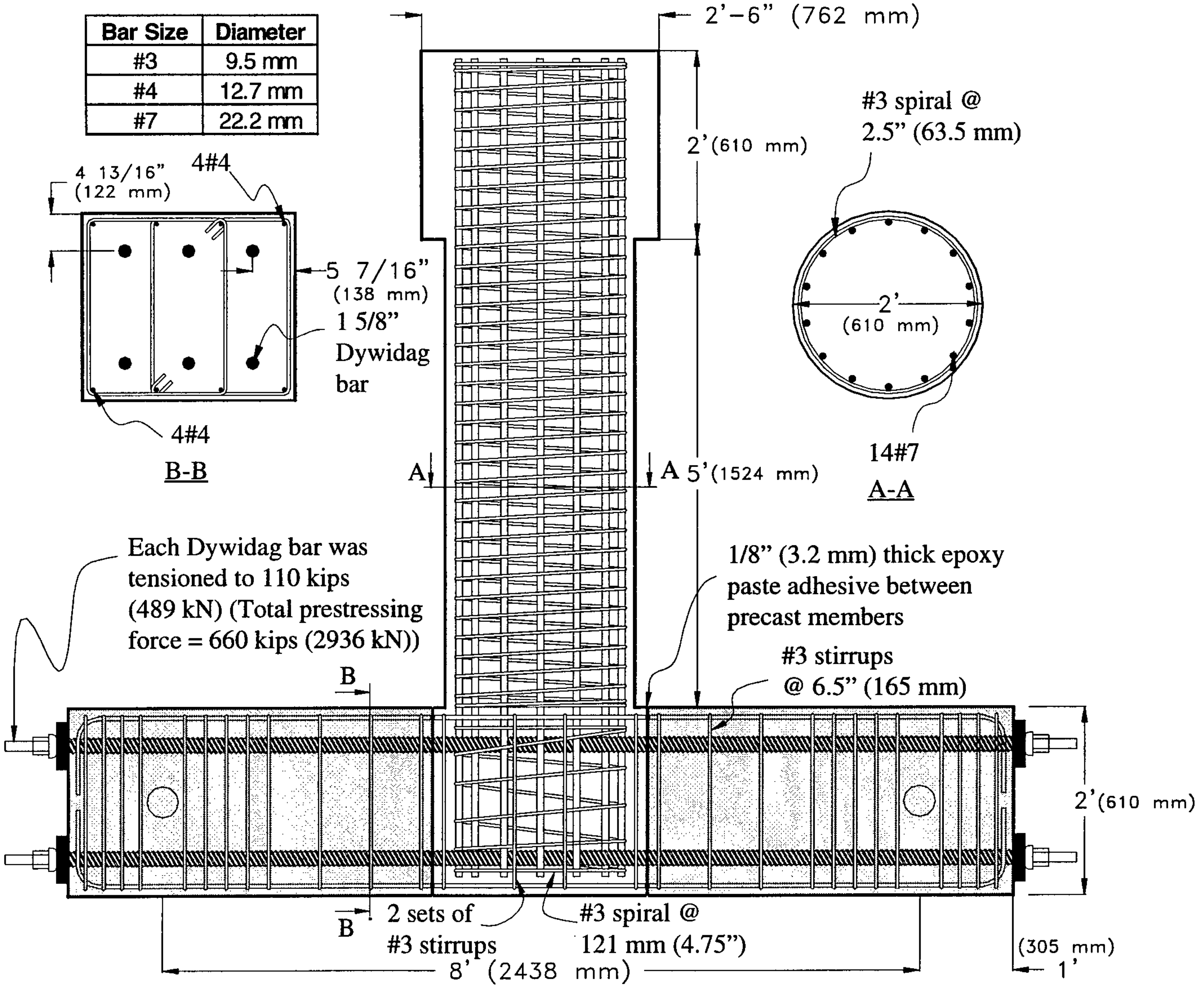

Bar Size	Diameter
#3	9.5 mm
#4	12.7 mm
#7	22.2 mm

2'-6" (762 mm)
2'(610 mm)
#3 spiral @
2.5" (63.5 mm)
2'
(610 mm)
14#7
A-A
A
A
5'(1524 mm)
4 13/16"
(122 mm)
4#4
5 7/16"
(138 mm)
1 5/8"
Dywidag
bar
4#4
B-B
Each Dywidag bar was
tensioned to 110 kips
(489 kN) (Total prestressing
force = 660 kips (2936 kN))
1/8" (3.2 mm) thick epoxy
paste adhesive between
precast members
#3 stirrups
@ 6.5" (165 mm)
B
B
2 sets of
#3 stirrups
#3 spiral @
121 mm (4.75")
8' (2438 mm)
2'(610 mm)
(305 mm)
1'

Figure 6.2 Key reinforcement details of the precast fully prestressed test unit IC3.

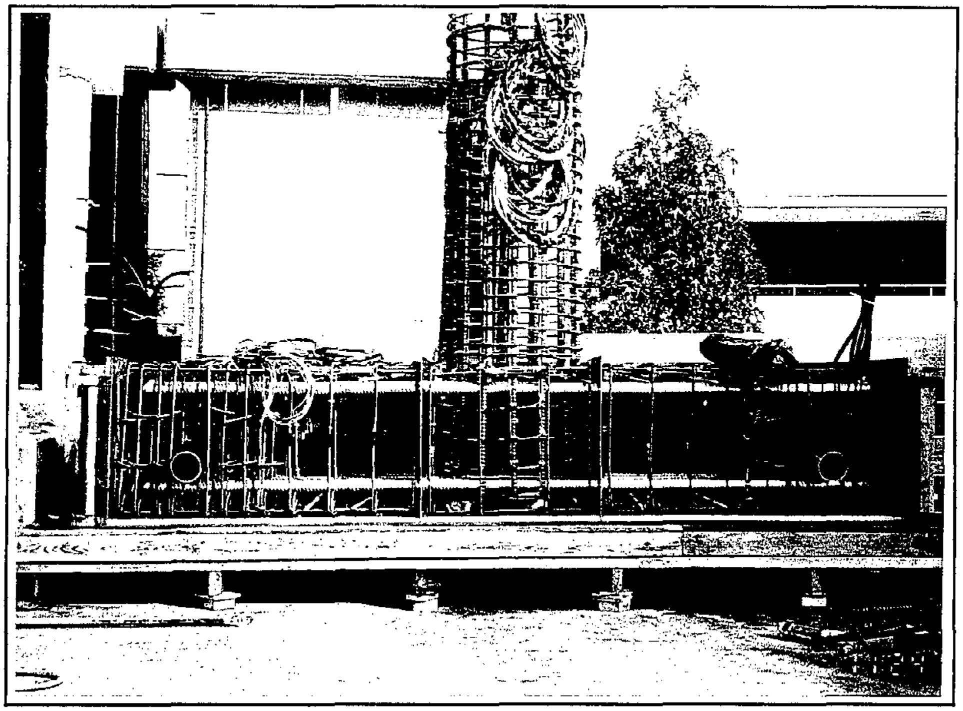

Figure 6.3 Construction of test unit IC3.

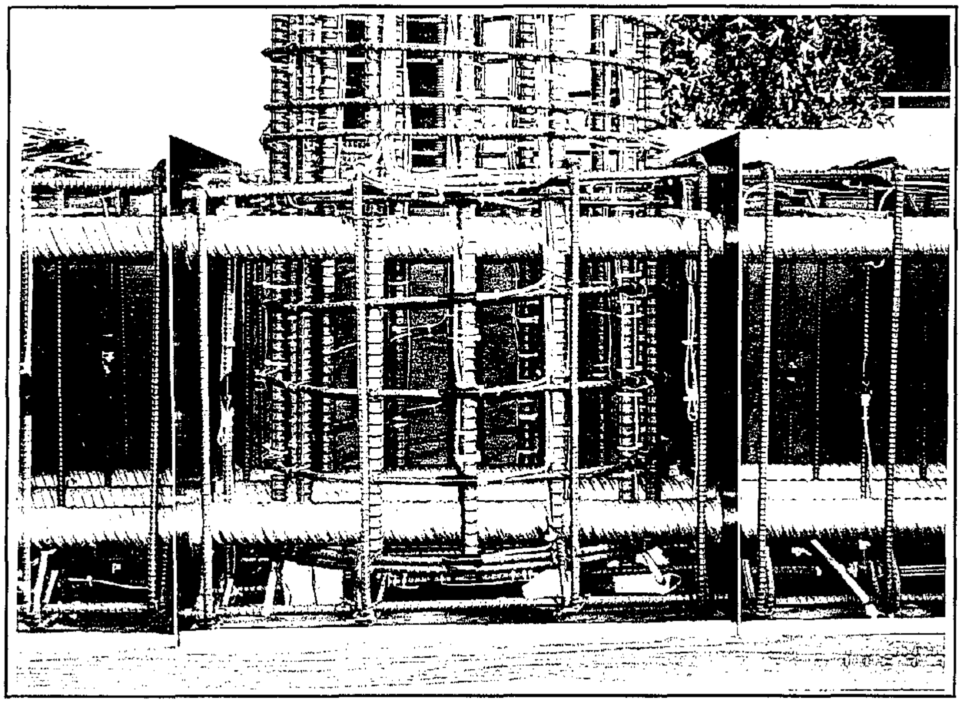

Figure 6.4 Joint reinforcement of test unit IC3 with a fully prestressed cap beam.

Reproduced from
best available copy.

6.2.1 Column

Column longitudinal reinforcement content of 1.86 percent was represented by 14#7 (d_b = 22.2 mm) bars. The spacing of #3 spiral was reduced from 96.5 mm (3.8 in.) in the first two units to 63.5 mm (2.5 in) in IC3, corresponding to a volumetric ratio of 0.79 percent.

6.2.2 Cap Beam

The required cap beam prestressing was applied using six 35 mm (1.375 in.) diameter Dywidag bars with each bar carrying 489 kN (110 kips). As can be seen in Figure 6.2, the prestressing bars were located as for IC2 with two additional bars passing through the center of column. Again, the cap beam prestressing was applied using straight bars with zero eccentricity. There was no continuous longitudinal mild steel reinforcement placed in the bent cap. However, in each precast segment of the cap, #4 (d_b = 12.7 mm) rebars were provided in the top and bottom corners primarily to support the vertical beam ties during construction. The use of longitudinal mild steel also facilitated strain measurements along the beam.

Nominal shear reinforcement, as for IC1 and IC2, was provided in the form of 4 legs #3 (d_b = 9.5 mm) stirrups at 165 mm (6.5 in) spacing. A friction mechanism was relied upon for shear transfer between precast members. By assuming a friction coefficient of 0.6 [3], it was concluded that the cap beam prestressing was adequate to transfer shear between precast beam segments and the joint. In the beam end regions, additional vertical stirrups and #3 spirals (diameter = 152 mm and pitch = 51 mm) outside each Dywidag bars were provided to resist bursting shear resulting from the anchorage of prestressing bars (see Figure 6.3).

6.2.3 Interior Joint

Joint detailing of the test unit was identical to that of the second test unit (see Section 5.2.3) except that the joint vertical stirrups were provided as closed ties.

6.3 Construction Procedure

As there was no continuous mild steel provided in the cap beam, feasibility of precast construction of concrete multi-column bents was also investigated as a part of this test. The interior joint of the test unit was built with the column as a single unit while the cap beam was constructed in two separate segments (see Figures 6.2 – 6.5). The precast elements were constructed in the laboratory using the procedure outlined below in order to ensure that the prestressing ducts in all three elements are perfectly aligned. The cap beam including the joint was cast in a single pour, with two 3.2 mm (0.125 in.) thick lightly greased steel plates separating the joint from the beam (see Figures 6.3 and 6.4). The cap beam segments and joint were pulled apart at the end of curing period (i.e. after 7 days) and the column was then built with a construction joint at the column/joint interface to form a single precast module consisting of the column and joint.

After the form work of the column was removed the test specimen was assembled by connecting the cap beam segments to either side of the tee joint (Figure 6.5). Because the steel plates separating the cap beam from the joint were greased prior to casting the beam, each concrete surface which was cast against the steel plates was very smooth and shiny. The surfaces forming the beam/joint interface were thus roughened using a wire brush to remove laitance. After placing a thin layer of epoxy paste between precast elements (Figure 6.6), the prestressing bars were hand tightened until the epoxy squeezed out of all four sides (Figure 6.7). The targeted thickness of the epoxy between the elements was 3.2 mm (0.125 in.), the same thickness as the steel plates used in the construction of the beam. The purpose of placing epoxy paste between precast elements was primarily to improve grouting procedure. Nevertheless, the presence of epoxy was expected to contribute to shear transfer across the interface.

6.3.1 Cap Beam Prestressing

The cap beam of the test unit was prestressed at the age of 48 days. All the strain gauges and external devices of the test specimen were connected to the data acquisition system, and an initial reading was obtained prior to prestressing the beam. An initial set of readings was also taken for the demec points. There were two strain gauges mounted on each of the six prestressing bars. Unfortunately, eight out of twelve strain gauges of the

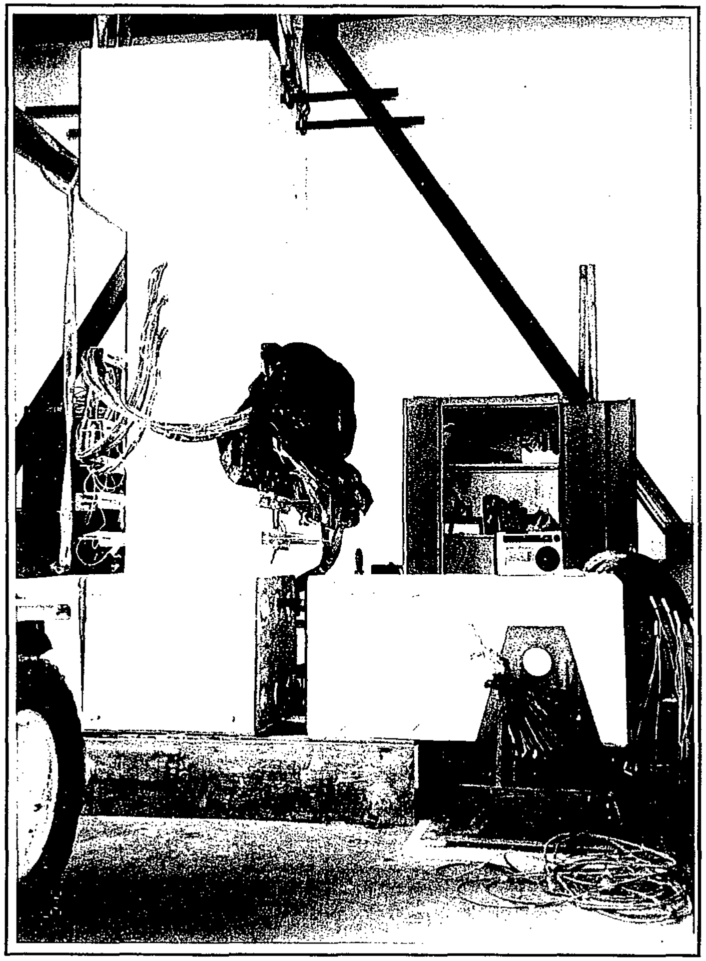

Figure 6.5 Forming test unit IC3 using precast modules.

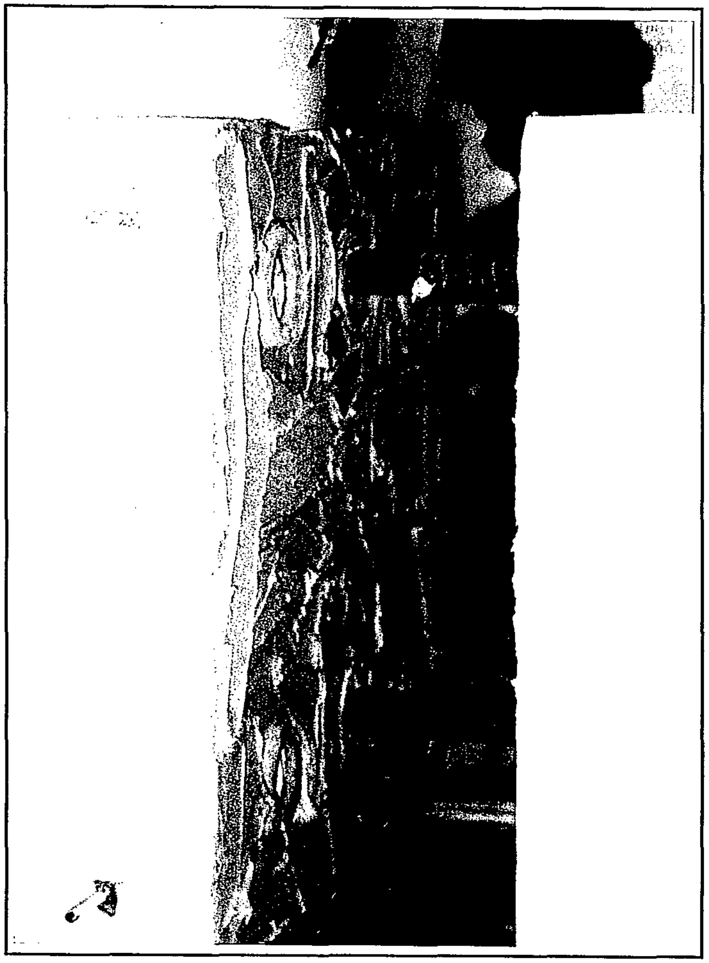

Figure 6.6 Placing epoxy paste between precast elements.

Reproduced from
best available copy.

Reproduced from best available copy.

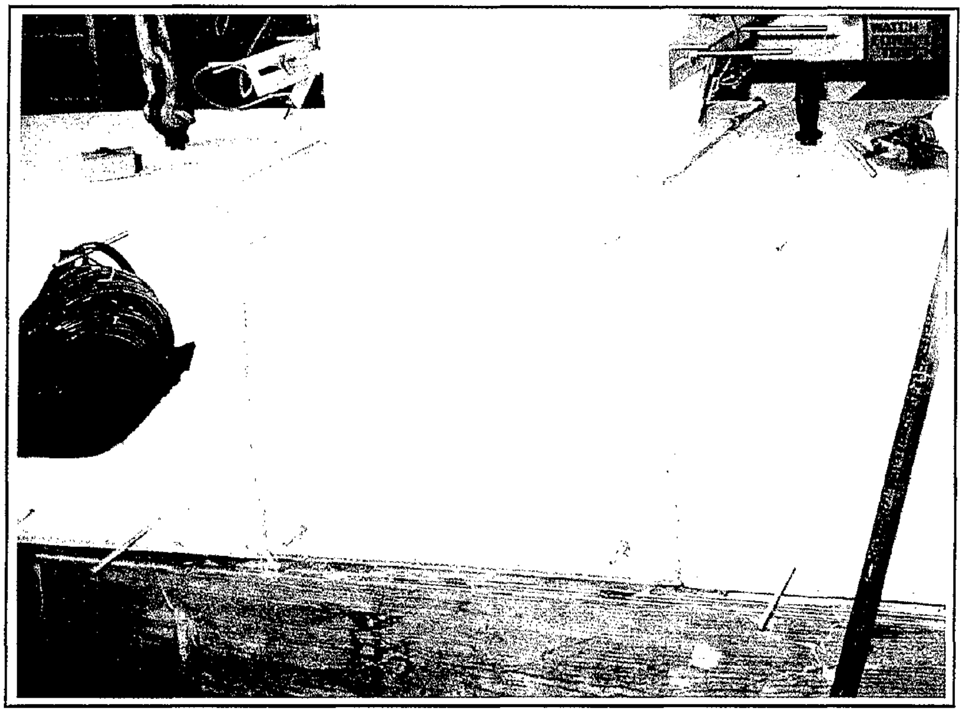

Figure 6.7 Joint region of IC3 after the test unit was assembled from precast modules.

prestressing bars failed during construction and an additional gauge failed during prestressing, leaving only three surviving gauges on three different bars. The reason for failure of an alarming number of gauges was due to lack of clear spacing between the prestressing ducts and Dywidag bars.

To achieve the target prestressing of 2936 kN (660 kips) on the day of testing, it was considered that 3523 kN (792 kips) force should be applied to the beam in total, allowing for an estimated 15 percent loss due to lock-out of the prestressing bars and an additional 5 percent loss due to time dependent effects of concrete and pretensioned steel as for IC2. The prestressing of the beam was performed in two steps and in each step about 50 percent of the total required tension was applied. In order to minimize bending of the cap beam during prestressing, the Dywidag bars located in the opposite corners were first tensioned and followed by the bars located in the center of the section (Figure 6.2).

The prestressing bars were stressed using a hydraulic system which was regulated by a pressure gauge which was attached to the hydraulic pump. Several scans of the gauges

6.4 Material Properties

The material properties of concrete and steel were obtained as illustrated in Section 4.3. Listed in Tables 6.1 and 6.2 are respectively the compressive strengths of concrete at different ages and the properties of the steel reinforcement. Each representative value given in the tables was established by testing three randomly selected samples.

The epoxy paste used between precast members was Sikadur 31 - High Mod Gel. It is a two component solvent-free, moisture-insensitive, high modulus, high strength epoxy paste adhesive. The expected properties of this material at the age of 14 days were compressive strength of 82.7 MPa (12 ksi), tensile strength of 24.8 MPa (3.6 ksi), and shear strength of 23.4 MPa (3.4 ksi).

Table 6.1 Compressive strength of concrete used in test unit IC3.

Member	7 days		28 days		Day of Testing	
	MPa	ksi	MPa	ksi	MPa	ksi
Column	26.2	3.80	33.9	4.62	33.2	4.82
Cap beam and Joint	26.2	3.80	32.3	4.68	36.1	5.23

Table 6.2 : Yield and ultimate strength of reinforcing steel of test unit IC3

Description	Size	Yield Strength		Ultimate Strength	
	(diameter in mm)	MPa	ksi	MPa	ksi
Longitudinal column bar	#7 (22.2)	461	66.9	744	107.9
Column spiral	#3 (9.5)	434	63.0	681	98.8
Longitudinal beam bar	#4 (12.7)	426	61.8	694	100.7
Beam stirrups	#3 (9.5)	452	65.5	670	97.2
Joint Spiral	#3 (9.5)	440	63.8	685	99.3
Prestressing Bar[†]	1-3/8 (34.9)	889	129	1034	150

[†] standard values, not established from testing

6.5 Predicted Response

The behavior of the test unit predicted prior to the test is presented in this section. The procedure adopted was similar to that used for IC1 (Section 4.4), but with an expected cap beam prestressing of 2936 kN (660 kips).

6.5.1 Gravity Load Response

The estimated flexural cracking stress of the concrete was 3.66 MPa (0.53 ksi). Considering that the prestressing induced compressive stress of 7.04 MPa (1.02 ksi), no cracking in the cap beam was expected until a flexural stress level in excess of 10.7 MPa (1.55 ksi) was developed. The application of the gravity load corresponded to 3.79 MPa (0.55 ksi) of stress in the extreme tension fiber and, consequently, no cracking was expected under this load.

6.5.2 Cracking in the Column

As for the two previous test units, the flexural cracking at the critical section of the column was expected to form at a horizontal load of 72 kN (16.2 kips).

6.5.3 Cracking in the Cap Beam

Based on the cracking strength estimated in Section 6.5.1, the flexural cracking moment of the beam was estimated to be 515 kNm (380 kips-ft). Since the cap beam positive moment due to gravity and seismic loads was not expected to exceed 210 kNm (155 kips-ft), no cracking was predicted on the top (as constructed) of the beam. Negative bending moment was expected to develop the cracking strength at a horizontal load of 415 kN (93 kips) and flexural cracks were expected to form at this stage.

6.5.4 Cracking in the Joint Region

Since the maximum joint principal tensile stress was expected to be greater than

$0.29\sqrt{f_c'}\left(3.5\sqrt{f_c'} \text{ in psi}\right)$, cracking in the joint region was anticipated. Although the joint cracking load was not calculated prior to the test, the horizontal force required for joint cracking was later estimated using Eq. 4.1. The measured concrete strength on the day of testing was considered in this calculation, which is given in Appendix A. It was concluded that the joint cracking should first occur under push direction loading at a horizontal force of 400 kN (90 kips).

6.5.5 Force-Displacement Response

Overall force-displacement behavior obtained for the test unit from a push-over type analysis is included with the experimental response in Figure 6.15 (see Table B5 in Appendix B for numerical values). Changes in structural behavior were taken into account during the analysis just as done for the two previous units. These changes included cracking in the column, yielding of longitudinal column steel, cracking in the beam, and the development of maximum concrete strain in the column.

The predicted displacement components and total displacement of the test unit are listed in Table B5 in Appendix B. A fixed base analysis of the column yielded a member displacement capacity $\mu_m = 8.50$. The flexibility of the cap beam and joint at yield was estimated to give $f = 0.092$, resulting in predicted system ductility capacity of 7.87 for IC3.

6.6 Observation under Repeated Cyclic Loading

Experimental observations made during the test under the prescribed loading (Section 3.2.6) are given in this section.

6.6.1 Application of Dead Load

As anticipated from theoretical calculations (Section 6.5.1), no cracking developed in the specimen when the gravity load was applied.

6.6.2 Force Control

The actuator force was incremented to the level corresponding to the theoretical yield strength was applied in four steps. In each step, only one loading cycle was applied and the observation made in each cycle is summarized below:

± 67 kN (15 kips)

Flexural cracks formed up to the column/load stub interface for the push direction loading while there were only three flexural column cracks visible for the pull direction loading. The unsymmetric column flexural cracks may be seen in Figure 6.8. It was suspected that there was an impact load applied to the specimen when the actuator was connected, and this was responsible for developing uneven cracking on the north and south sides of the column. The recorded actuator force prior to the testing confirmed that the column was subjected to horizontal loads up to 85 kN (19 kips). No sign of distress was observed on the beam nor in the joint.

± 133 kN (30 kips)

Extension of old cracks and formation of a few new cracks were found on both sides of the column although overall flexural cracking on either side still remained uneven (Figure 6.8). No cracking in the joint region or in the cap beam was visible.

± 200 kN (45 kips)

Damage on the column was restricted to minor extension of old cracks on the north side for the push direction loading while new cracks formed on the south side. Cracking on the column appeared to be comparable on both sides. No damage to the joint or cap beam was observed.

± 250 kN (56 kips) - First Yield

Minor extension to old cracks of the column was commonplace. For the push direction loading, a new flexural crack and a vertical splitting crack close to the critical section were developed on the north side of the column. The joint and the cap beam were yet to develop any cracking.

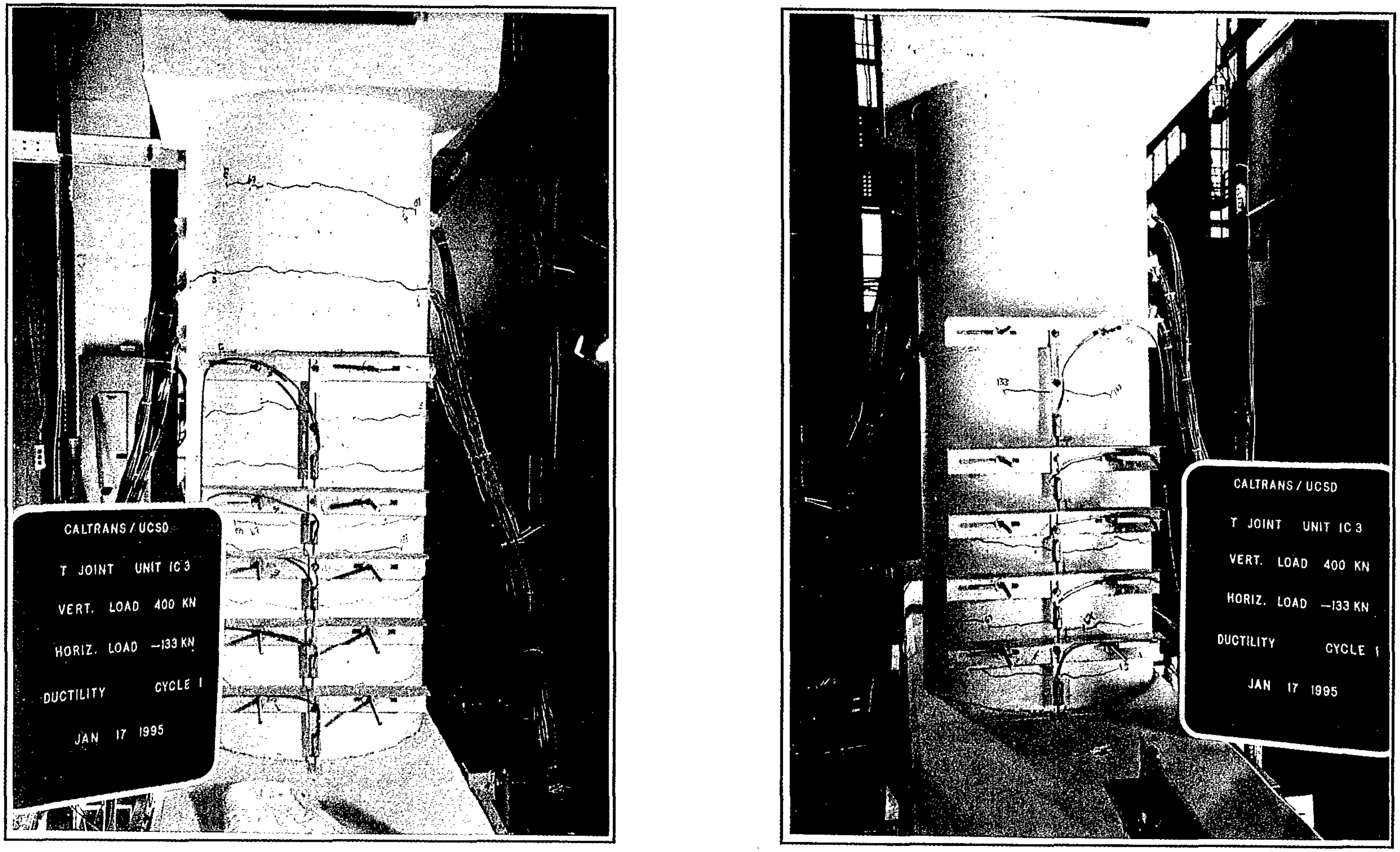
CALTRANS / UCSD
T JOINT UNIT IC 3
VERT. LOAD 400 KN
HORIZ. LOAD −133 KN
DUCTILITY CYCLE 1
JAN 17 1995
CALTRANS / UCSD
T JOINT UNIT IC 3
VERT. LOAD 400 KN
HORIZ. LOAD −133 KN
DUCTILITY CYCLE 1
JAN 17 1995

(a) North side

(b) South side

Figure 6.8 Cracking in the column of IC3 after load cycle F = ±133 kN (30 kips) was completed.

Reproduced from best available copy.

6.6.3 Displacement Control

The estimated displacement corresponding to $\mu_\Delta = 1$ was 15.0 mm (0.590 in.) from Eq. 3.3, similar to that used for the second unit IC2. From this point onwards, a minimum of three cycles were introduced at each ductility and the observed behavior is described below:

3 cycles at $\mu_\Delta = \pm 1$ ($F_{max} = 333$ kN; $F_{min} = -313$ kN)

A few inclined shear cracks developed as extension to old flexural and widespread vertical splitting cracks were observed on the tension sides developed in the column (Figures 6.9a and b). No damage was occurred to the beam or joint.

3 cycles at $\mu_\Delta = \pm 1.5$ ($F_{max} = 385$ kN; $F_{min} = -373$ kN)

First joint cracking was seen on the east face when the column was pushed to the peak displacement during the first cycle (Figure 6.9c). The peak actuator force recorded in this half cycle was 96 percent of the predicted horizontal load at first joint cracking (Section 6.5.4 and Appendix A). Shear cracks were not seen in the joint corresponding to pull direction loading at this ductility. Minor extension of the old cracks and new shear cracks were observed on the column. A significant number of vertical splitting cracks 2/3 way up the column from the interface were also seen (Figures 6.9a and b). The opening of the crack at the base of the column was about 2 – 3 mm (0.08 – 0.12 in.). No flexural crack was observed on the beam, but a horizontal crack between the top and bottom layers of prestressing bars was seen at each end face of the cap beam.

3 cycles at $\mu_\Delta = \pm 2.0$ ($F_{max} = 410$ kN; $F_{min} = -395$ kN)

The only significant observation was that the of crushing of the concrete was imminent at the base of the column. The west face of the joint cracked under push direction loading at a maximum actuator force of 409 kN (92 kips), which was 102 percent of the predicted joint cracking load. The joint damage at this stage appeared similar on both east and west sides. Joint cracking was, however, not yet developed for the pull direction loading.

3 cycles at $\mu_\Delta = \pm3.0$ ($F_{max} = 431$ kN; $F_{min} = -418$ kN)

During the first cycle, crushing of concrete was seen on both sides of the column in the plastic hinge region. Also found in this loading cycle was first joint cracking in the pull direction loading (Figure 6.10). As the displacement cycles were increased, crushed cover concrete spalled off the column. Extension of old flexural cracks, and more new shear and vertical splitting cracks were noted on the column. The crack width at the base of the column was about 3 – 4 mm (0.12 – 0.16 in.). Cracks also formed on the top (as tested) of the beam adjacent to the column and flaked off some surface concrete. This was believed to have been caused by significant strain penetration of the column reinforcement into the joint. Flexural cracks were not yet observed in the beam.

3 cycles at $\mu_\Delta = \pm4.0$ ($F_{max} = 426$ kN; $F_{min} = -432$ kN)

The condition of the test unit after 3 cycles at $\mu_\Delta = \pm4$ is shown in Figure 6.10 and a close up view of the column/joint interface is given in Figure 6.11. For both push and pull direction loading in the first cycle, flexural cracks were developed at the bottom (as cast) of the beam/joint interface. The average maximum horizontal load applied in this cycle was 428 kN (96 kips), which was 97 percent of the predicted beam cracking load. The cracks *did not* appear to have coincided with the epoxy seam provided between the precast elements. Minor extension and a new crack was noted in the joint region. Cracks opened up significantly in the column with crack width reaching up to 3 – 5 mm (0.012 – 0.20 in.) at the base. The damage, which is visible on the top (as cast) of the cap beam surrounding the column in Figure 6.11, was due to strain penetration of the longitudinal column bars into the joint.

3 cycles at $\mu_\Delta = 6.0$ ($F_{max} = 453$ kN; $F_{min} = -462$ kN)

Extension of old cracks and some new minor cracks were seen on the joint (Figure 6.12). Beam flexural cracks developed further. More cover concrete flaked off on the top of the cap beam adjacent to the column and the beam stirrups were visible. The column suffered further damage in a similar fashion to what was noted in the previous ductility. Spalling of cover concrete extended up to about 152 mm (6 in.) from the critical section. The crack width at the base of the column was about 4 – 5 mm (0.16 – 0.20 in.). The spreading of cracks into the load stub was also observed, but it was nothing of any significance.

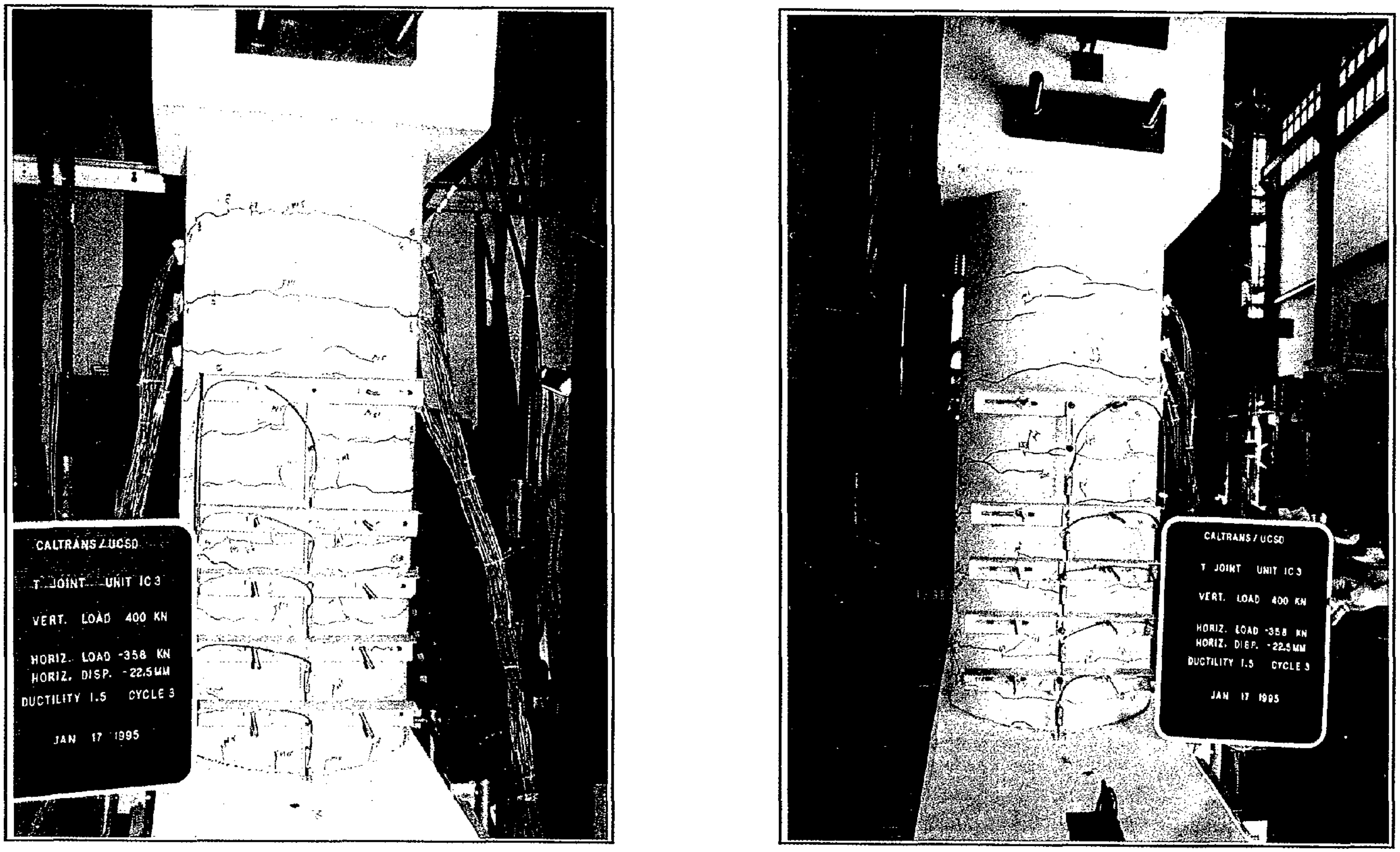
CALTRANS / UCSD
T JOINT UNIT IC3
VERT. LOAD 400 KN
HORIZ. LOAD -358 KN
HORIZ. DISP. -22.5MM
DUCTILITY 1.5 CYCLE 3
JAN 17 1995

(a) Damage on the north side of coumn

(b) Damage on the south side of column

Figure 6.9

Reproduced from best available copy.

Reproduced from best available copy.

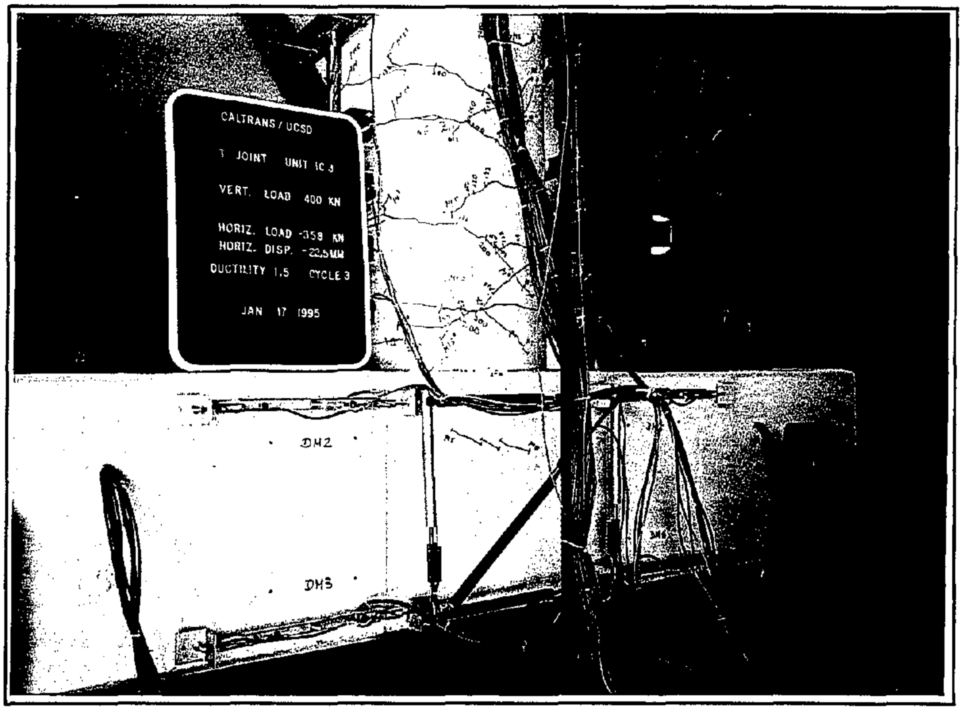

(c) Cracking on the east face of the joint region

Figure 6.9 Test unit IC3 at the end of third cycle at $\mu_\Delta = 1.5$.

4 cycles at $\mu_\Delta = \pm 8.0$ *(*$F_{max} = 441$ *kN;* $F_{min} = -462$ *kN)*

Four displacement cycles were imposed at this ductility since the two previous test units were subjected to a similar loading pattern. New shear cracks and extension of old cracks were marked on the joint, but the joint cracks appeared to be less severe on the west side (Figure 6.12). Flexural beam cracks were developed on the bottom of the joint at about 152 – 203 mm (6 – 8 in.) from the epoxy seam. However, the precast beam segments were yet to form any flexural cracks outside the epoxy seam. Further spalling of cover concrete on the top of the beam and in the plastic hinge region of the column occurred. The reduced spacing used for the transverse reinforcement of the column appeared to provide a much better confinement in the hinge region when compared to the observations made in the response of IC1 and IC2. No sign of buckling of the longitudinal column reinforcement was seen at this stage. More shear and vertical cracking was observed in the column, but were not marked except for the first cycle. The

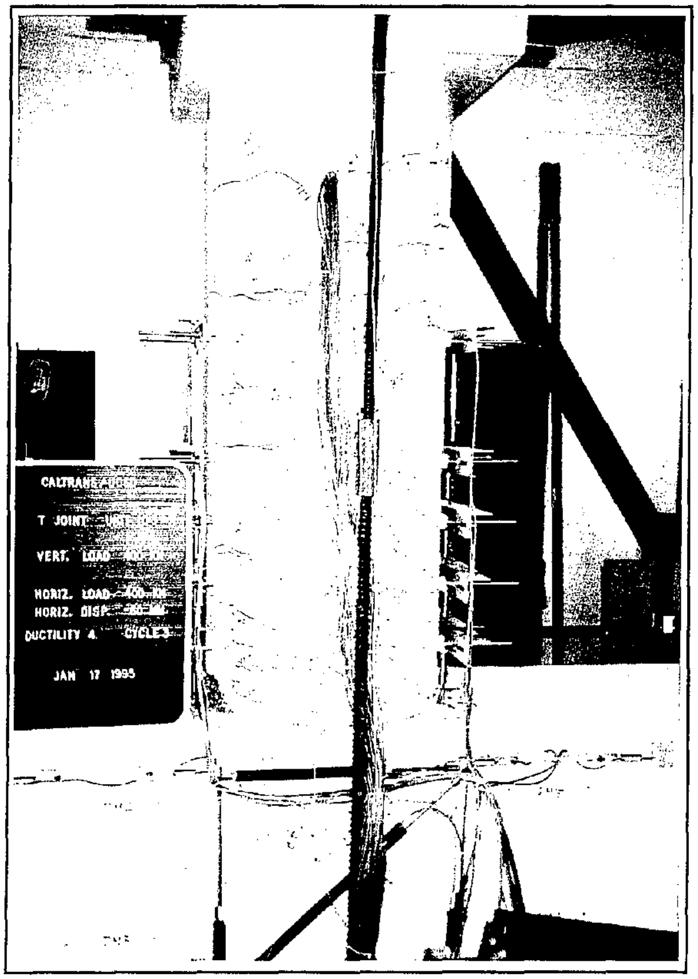
CALTRANS
T JOINT
VERT. LOAD
HORIZ. LOAD
HORIZ. DISP.
DUCTILITY 4. CYCLE 3
JAN 17 1995

Figure 6.10 Test unit IC3 at the end of $\mu_\Delta = -4x3$.

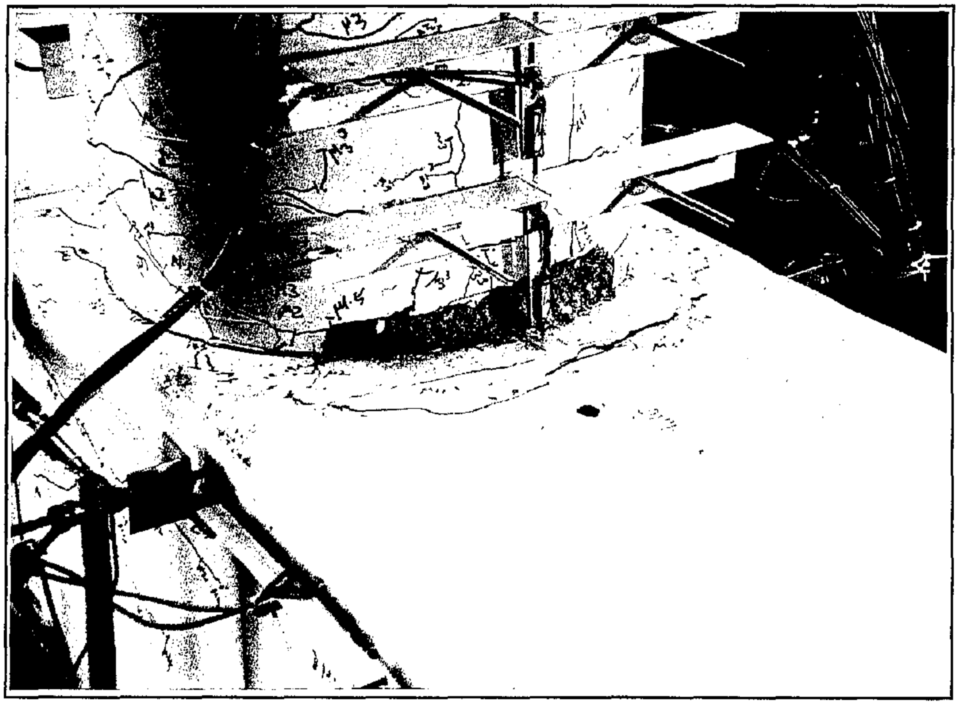

Figure 6.11 Damage to surface concrete on the top of beam at the end of $\mu_\Delta = -4x3$.

Reproduced from best available copy.

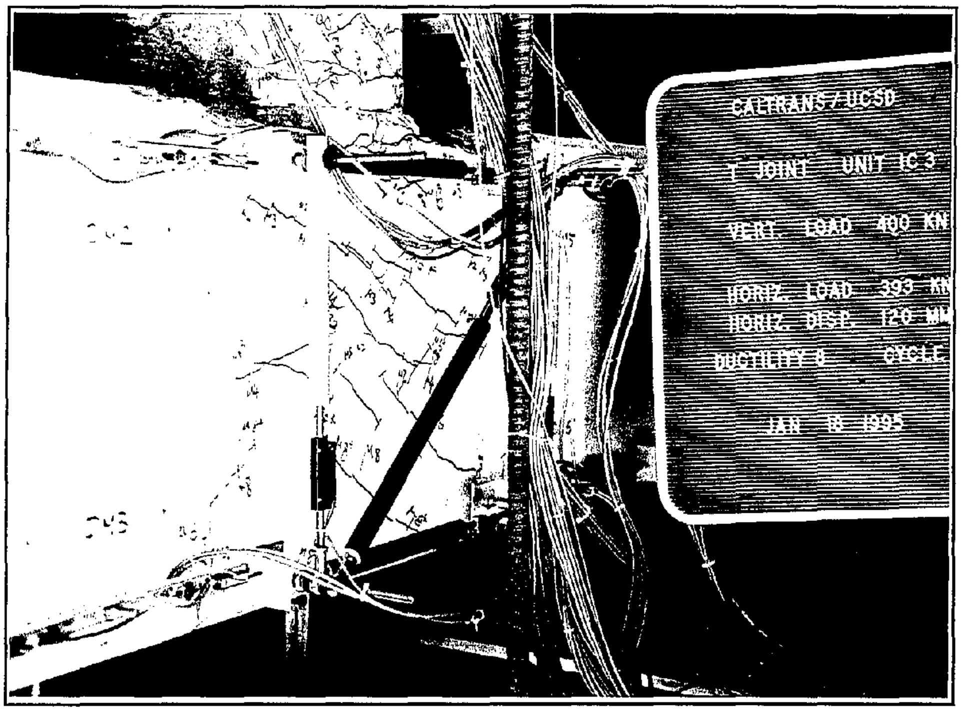
CALTRANS / UCSD
T JOINT UNIT IC3
VERT. LOAD 400 KN
HORIZ. LOAD 393 KN
HORIZ. DISP. 120 MM
DUCTILITY 8 CYCLE
JAN 18 1995

(a) East face

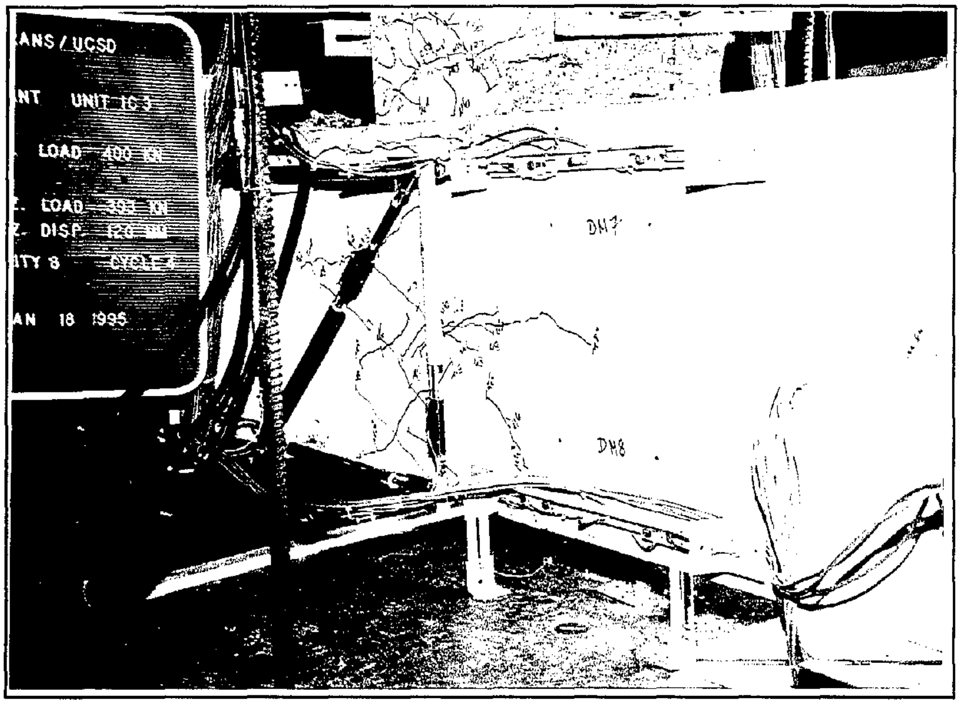
ANS / UCSD
NT UNIT IC 3
LOAD 400 KN
. LOAD 393 KN
. DISP 120 MM
ITY 8 CYCLE 4
AN 18 1995
DM7
DM8

(b) West face

Figure 6.12 Joint cracking in unit IC3 at the end of testing at $\mu_\Delta = 8$.

Reproduced from best available copy.

crack width at the base of the column was about 5 mm (0.20 in.), and that at 51 mm (2 in.) below the critical section in the joint was about 4 mm (0.16 in.). This crack formed during the test from ductility 4 to 6 due to strain penetration of the longitudinal column reinforcement.

3 cycles at $\mu_\Delta = \pm 10.0$ ($F_{max} = 409$ kN; $F_{min} = -443$ kN)

Figure 6.13 depicts the test unit at the end of the first cycle at ductility 10. During this first loading cycle, spalling of the cover concrete extended up the column for about 305 mm (12 in.) from the base. The extreme longitudinal column bars were appeared to have buckled in the hinge region for both loading directions. Joint cracks extended into the beam horizontally across the epoxy seam (Figure 6.14). Further minor cracking was also observed in the joint region. In the subsequent cycle, at least two column bars suffered significant buckling in the push direction and they fractured when they were subjected to tension during the reverse loading (Figure 6.14). A column spiral in the hinge region was also broken in the compression side from the pull direction loading. A third longitudinal column bar fractured on the south side during the third cycle. Significant buckling of the bars were seen on the north side, but none of none of the reinforcing bars was fractured. Damage to the test unit was clearly confined to the plastic hinge region of the column and the top of the beam as a result of strain penetration (Figure 6.14). The test unit all-in-all performed like a monolithic structure.

End of the Test

All the loose concrete was removed and it was clear that the damage was concentrated in the plastic hinge region of the column. No significant damage occurred in the cap beam or the joint (Figure 7.3c). The cracks in the joint region almost closed when the horizontal load was brought back to zero.

6.7 Experimental Results

From the extensive measurements taken during the test, the key results are presented in a reduced form in the following sections.

6.7.1 Force-Displacement Hysteresis Curve

In Figure 6.15, the force-displacement response of the specimen as recorded during the test is shown along with the predicted response envelope established in Section 6.5.5. Energy absorption capacity of the system, as indicated by the shape and stability of the hysteresis loops, was excellent. There was no significant strength degradation observed before system displacement ductility 10, which corresponded to a drift of about 7.0 percent. The first encounter of strength degradation, which occurred at ductility 10, was due to buckling of the longitudinal column compression bars in the plastic hinge region. The bars buckled during the first cycle for both push and pull direction loading, and this was followed by fracturing of three column bars and a spiral in the subsequent cycles (see Section 6.6.3 for further detail). The reduction in the force resistance of the system due to fracture of the reinforcement can be clearly seen in Figure 6.15.

In Figure 6.16, an analysis of the hysteresis loops obtained for the test unit is presented. The area of the force-displacement loop and equivalent viscous damping are shown in this figure at different ductilities for the first two loading cycles. The numerical values of the data points used in Figure 6.16 are given in Appendix C. The area of the hysteretic loop increased almost linearly from ductility 2. At displacement ductility 10, a sudden drop in the area of the loop occurred in the second cyclic loading as a result of the damage that occurred to the column in the hinge region. The equivalent viscous damping of the system increased from 5% at $\mu = 1$ to 30% at $\mu = 10$. At a given displacement, it was found that the energy absorption of the system and equivalent damping were higher for IC3 than those obtained for the two previous units (see Figure 7.2).

The comparison between the predicted and observed envelopes of the force-displacement response was satisfactory. Unlike for the two previous units, the estimated envelope slightly underestimated the force resistance at a given displacement. The test unit was subjected to a maximum displacement of 150 mm (5.91 in.), which was 31 percent higher than the predicted maximum displacement. A similar observation was made for the response of the second unit IC2. The predicted and observed displacement capacity of unit IC3 were 8.7 and 10 respectively.

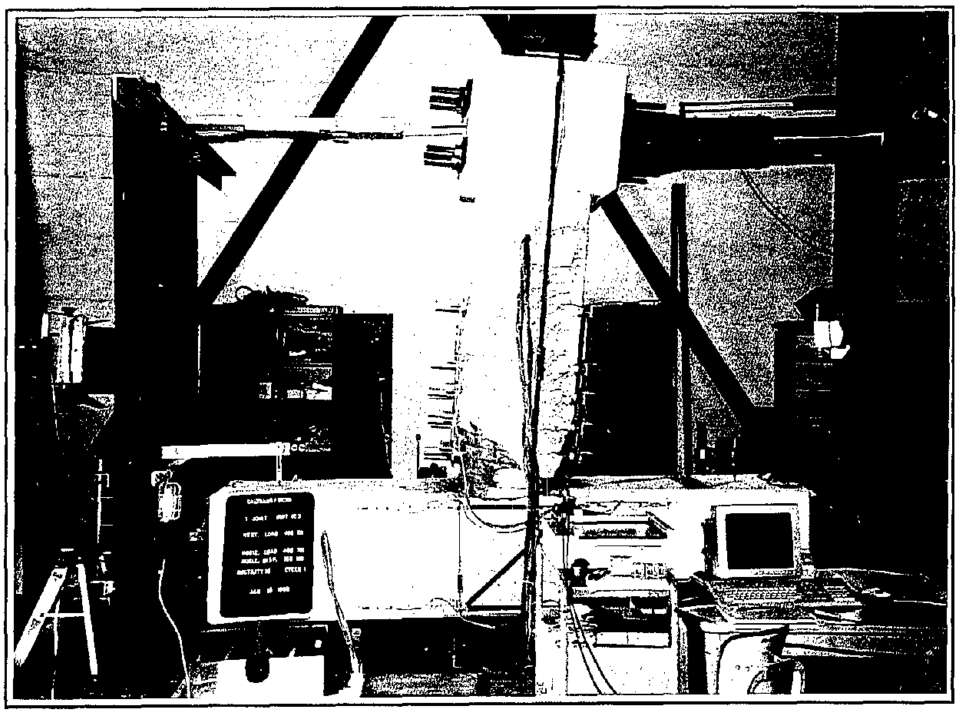

Figure 6.13 Test unit IC3 displaced at the maximum displacement at $\mu_\Delta = 10\text{x}1$.

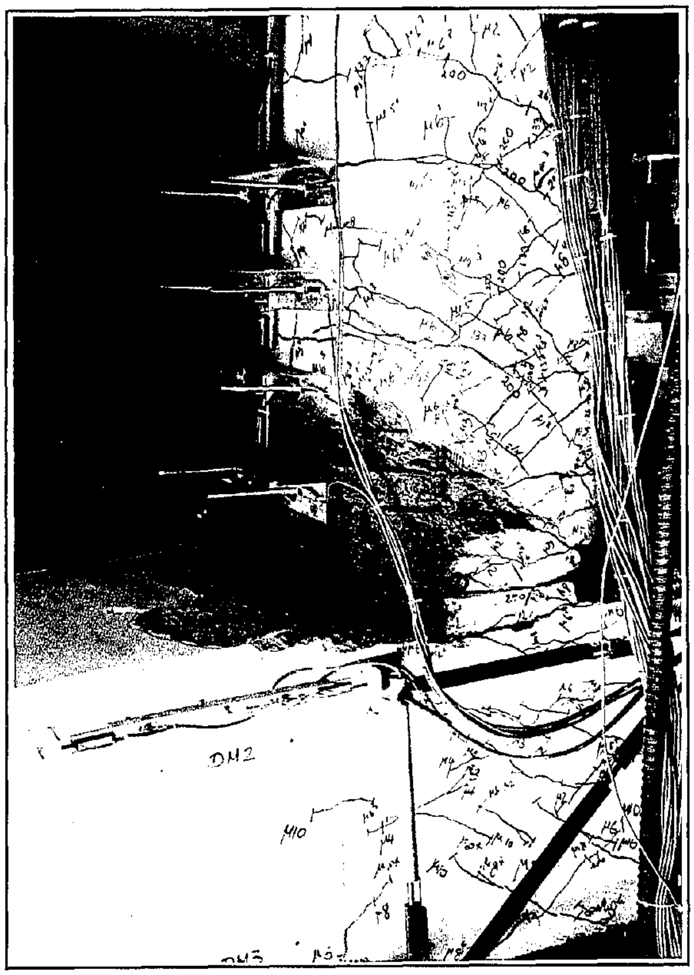

Figure 6.14 Damage to unit IC3 in the plastic hinge region of the column at the end of testing.

Reproduced from best available copy.

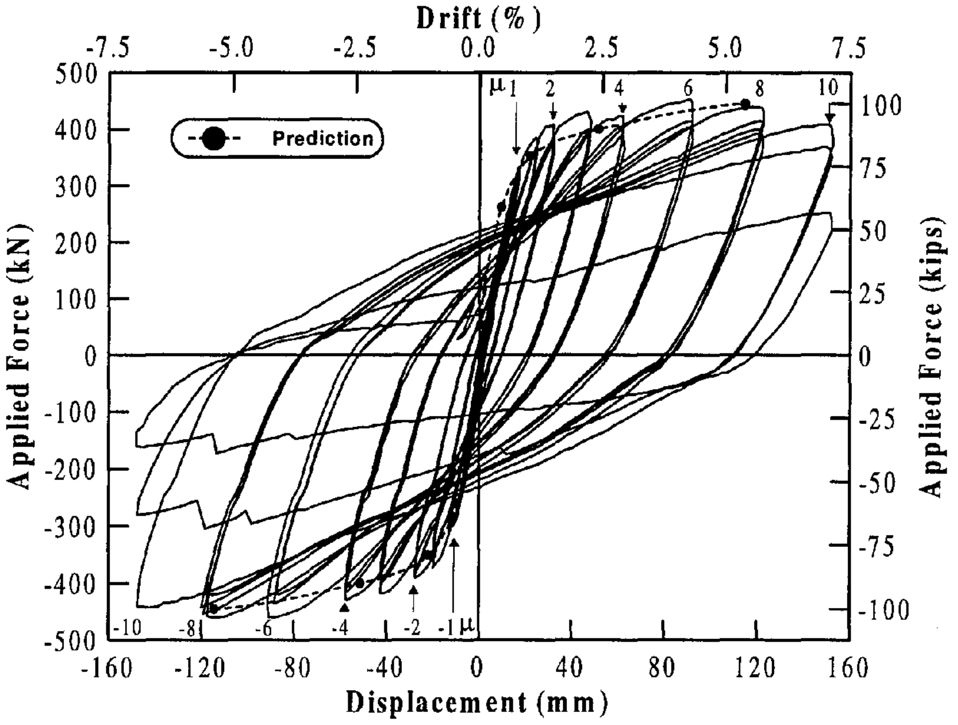

Figure 6.15 Force-displacement response of test unit IC3 with the predicted envelope.

6.7.2 Moment-Curvature Response

Of the five sets of column curvature devices, the two sets obtained closest to the joint interface are shown in Figure 6.17 accompanied by the predicted moment-curvature envelope of the column section. As noted in Section 4.6.2, for the experimental response, the maximum bending moment developed within each curvature cell was considered in Figure 6.17. It is clear that a significant inelastic response was recorded in the column region adjacent to the joint interface. The response of the first curvature device (Figure 6.16a) was recorded only up to the third cycle at ductility 6 as spalling of the top beam cover concrete disturbed the readings at larger displacements. Unsymmetric moment curvature seen for this curvature cell at ductility 6 suggests that the curvature readings might have been disturbed starting at a lower ductility level. Measured curvature up to ductility 1 was smaller in the curvature cell closest to the joint interface than that obtained in the second cell. This can be clearly seen in Figure 6.17, where curvature profiles up the column are plotted. Theoretical prediction of the envelope appeared to match the measured moment-curvature response satisfactorily.

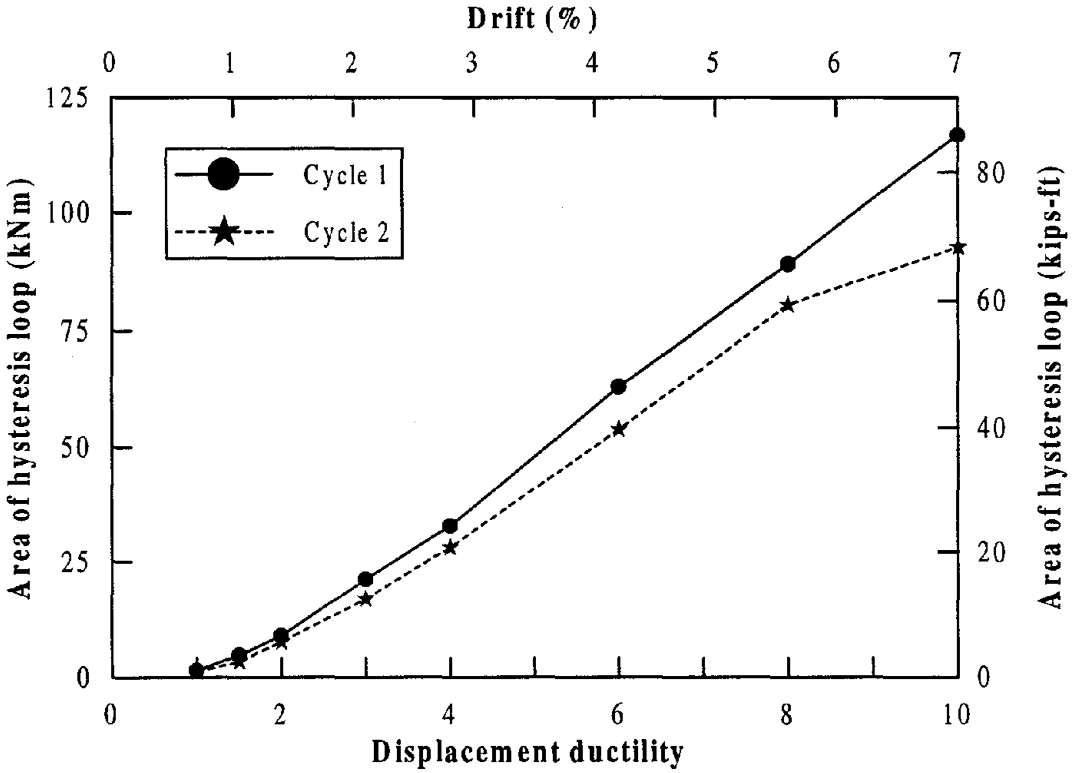

(a) Area of hysteresis loops

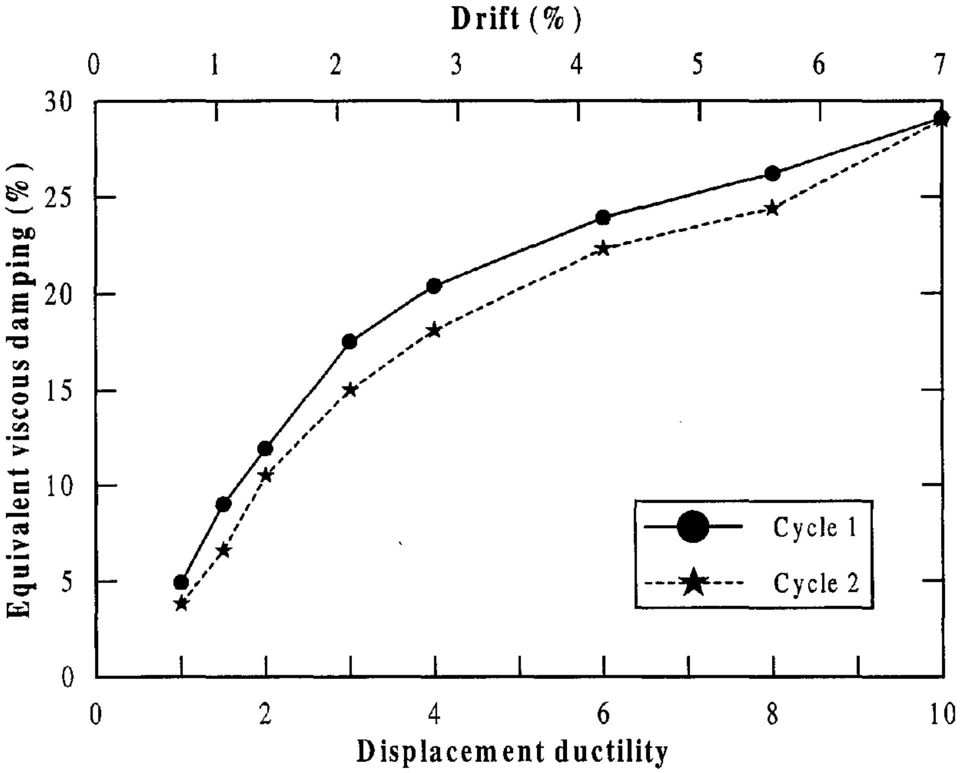

(b) Equivalent viscous damping

Figure 6.16 Analysis of the force-displacement hysteretic loops of test unit IC3.

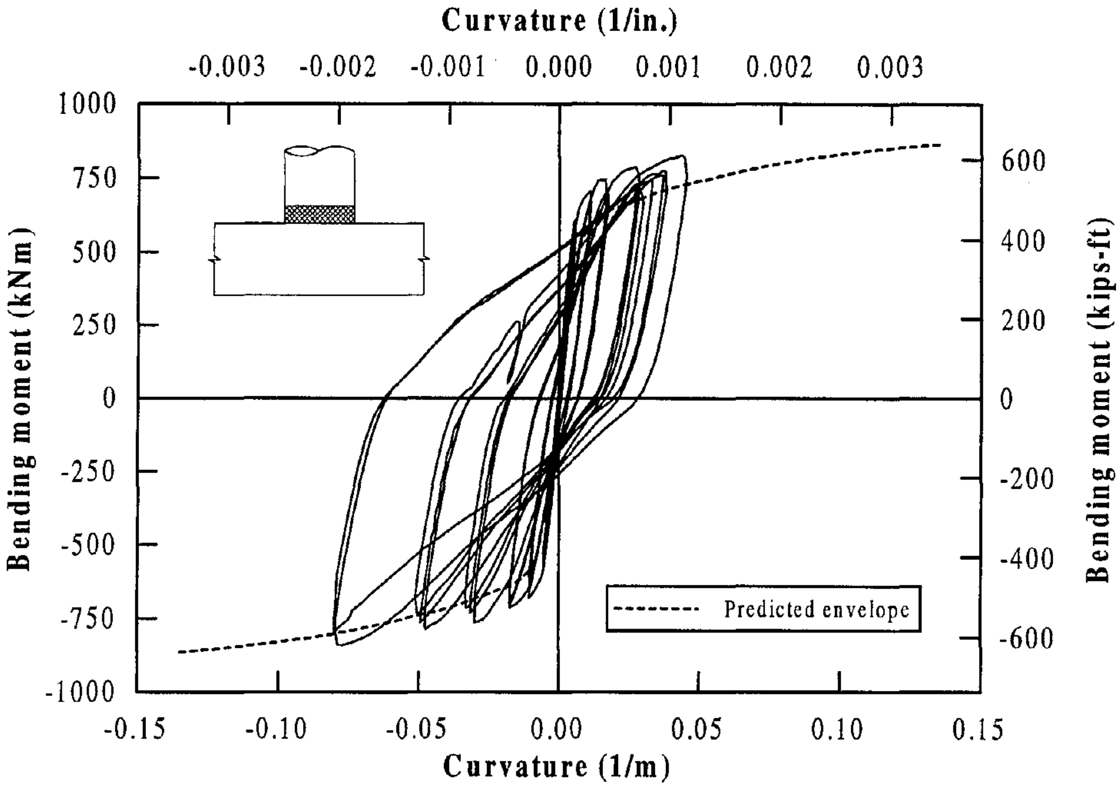

(a) adjacent to the joint interface

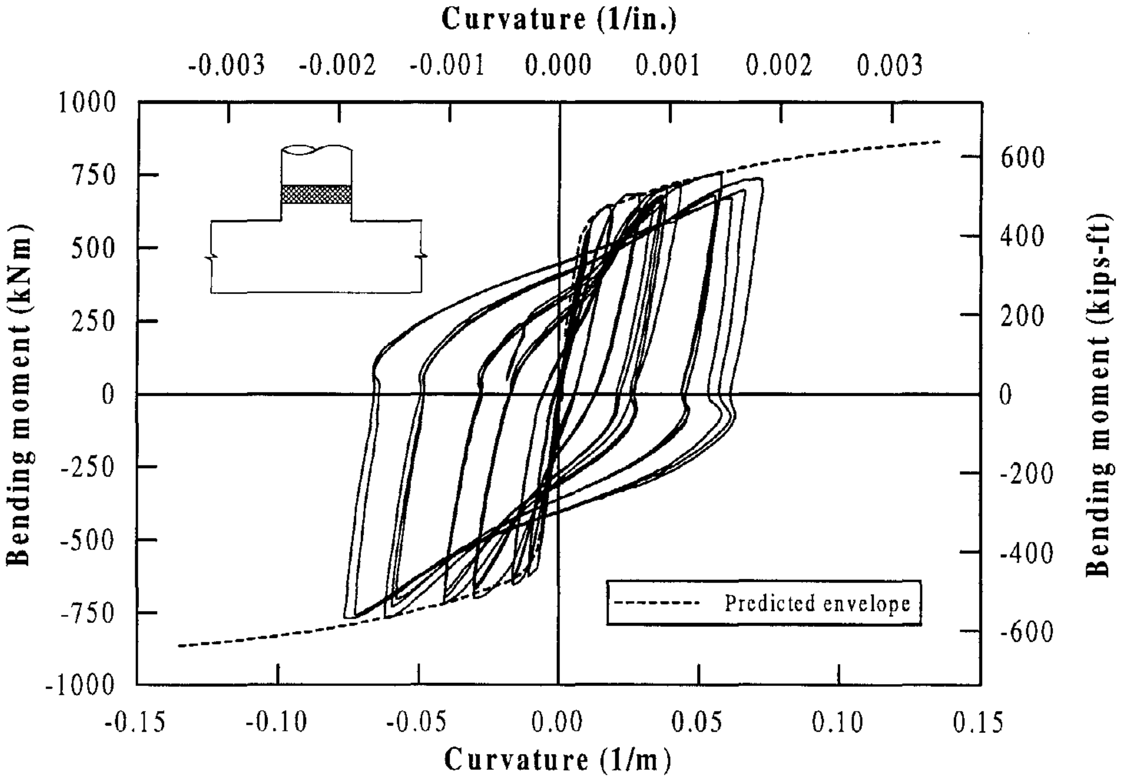

(b) 152 mm (6 in.) away from joint interface

Figure 6.17 Moment-curvature response in two column curvature cells nearest to the joint interface.

From the remaining sets of curvature measurements, it was noted that inelastic action reduced up the column height (Figure 6.18) and only an elastic response was obtained in the curvature device located furthest from the critical section. A similar observation was made in the response of IC1 and IC2.

The moment-curvature response obtained in the cap beam was essentially elastic. In Figure 6.19 the readings obtained in two curvature cells adjacent to the joint interface are plotted against predicted envelopes. The cap beam prestressing was represented as a constant axial load in determining the theoretical envelopes as for IC2. In both cases, a satisfactory agreement between the predicted and measured response envelopes was obtained.

6.7.3 Joint Deformation

The shear demand imposed upon the joint of IC3 was similar to that developed in the redesigned test units with reinforced concrete (IC1) and partially prestressed (IC2) cap beams. However, there was no significant joint deformation associated with the inelastic response of the test unit, resulting in small joint strains. As for the two previous units, the west side joint deformation panel was considered in establishing the measured joint response.

The maximum and average joint shear stresses as a function of horizontal column displacement are shown in Figure 6.20. Variation of stress with increasing ductility is noticeable when the maximum stress is considered, but the average stress appears to be almost constant at 3.3 MPa (480 psi) from ductility 2.0. The first significant reduction in the joint stress was at ductility 10 due to the damage which occurred to the column.

As for unit IC2, the cap beam prestressing significantly influenced the principal stresses in the joint region. In Figures 6.21 and 6.22 the principal compression and principal tensile stresses as calculated for the joint are presented as a function of the column displacement. In both cases, assuming a constant cap beam prestressing (i.e. 3002 kN), the principal stresses were obtained using the maximum and average joints shear stresses. The peak values of the principal compression stresses were $\mathbf{0.30f'_c}$ and $\mathbf{0.24f'_c}$ when the maximum and average joint stresses were considered respectively. In the design criteria

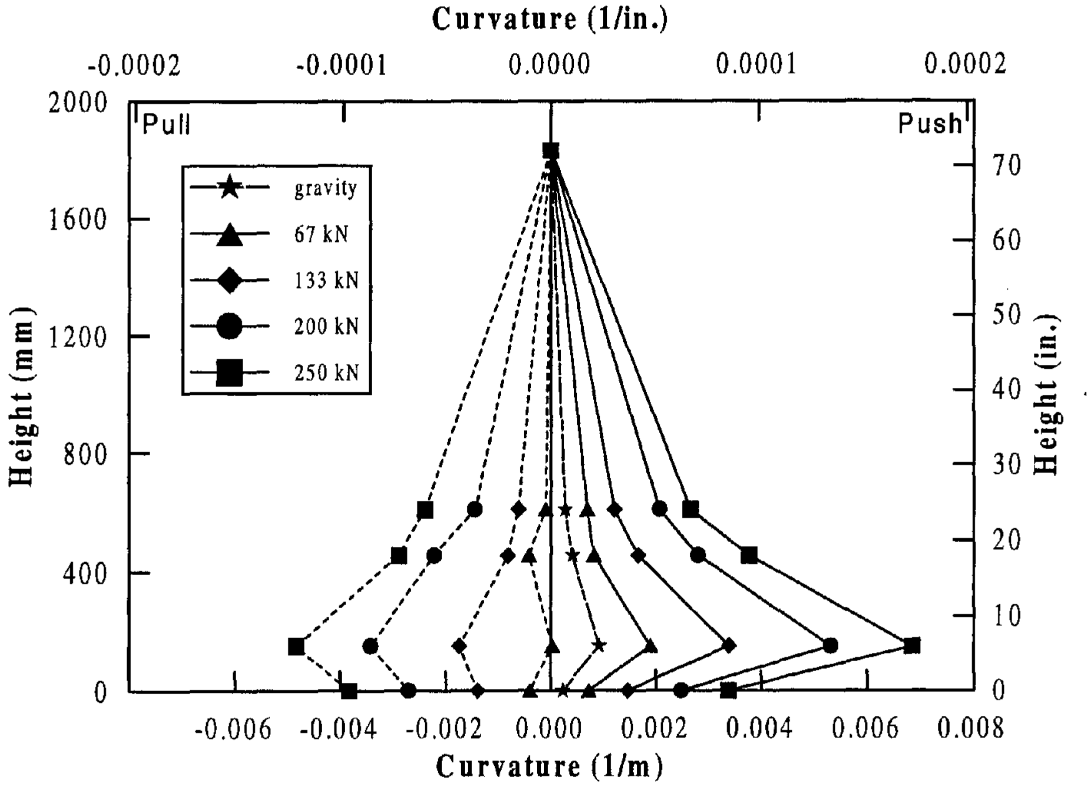

(a) Initial stages of testing

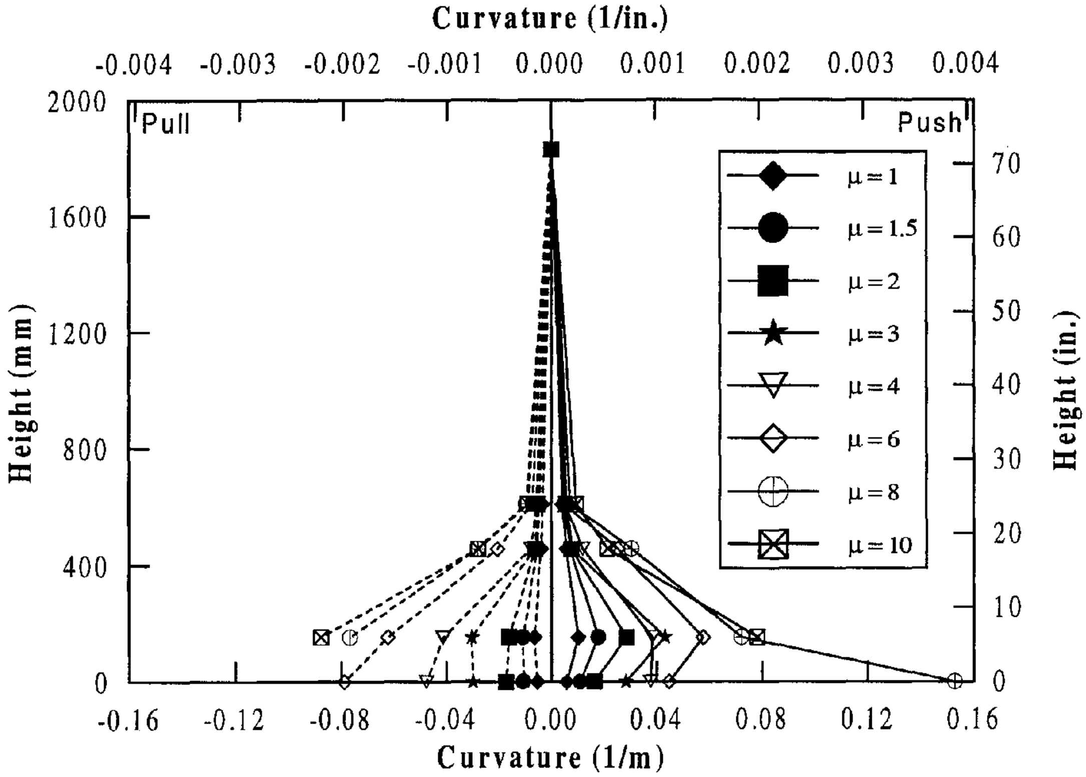

(b) Final stages of testing

Figure 6.18 Measured curvature profiles up the column.

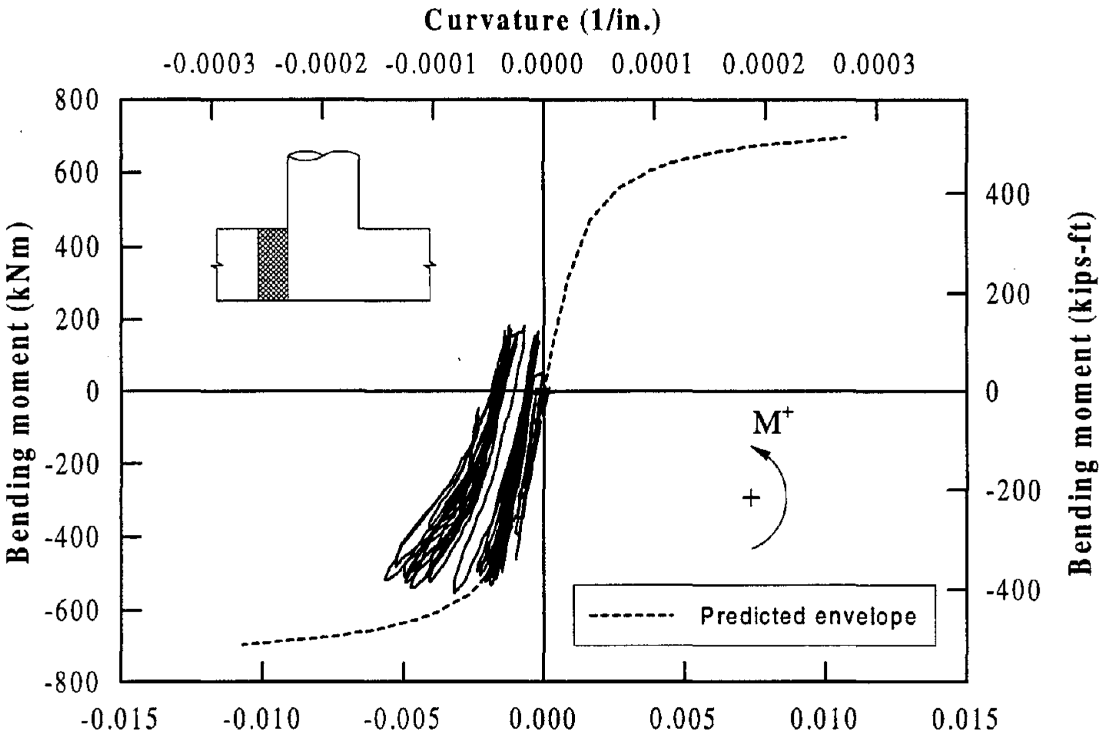

(a) left side of the joint

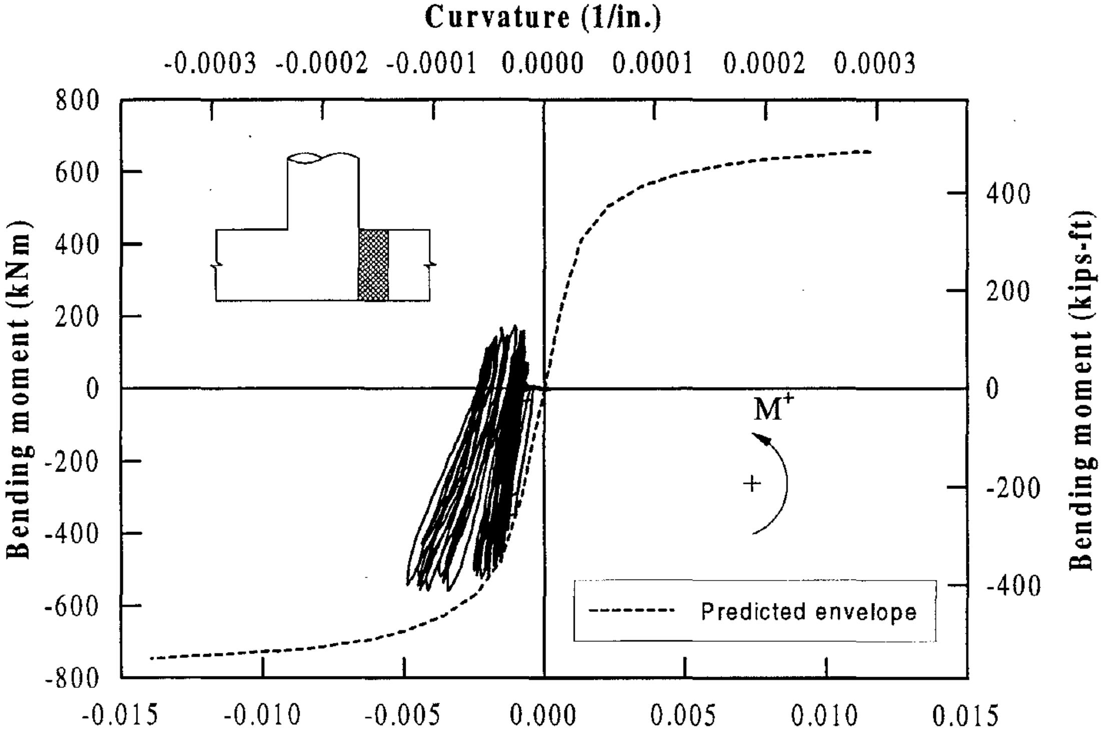

(b) right side of the joint

Figure 6.19 Moment-curvature response obtained in two beam curvature cells adjacent to the joint.

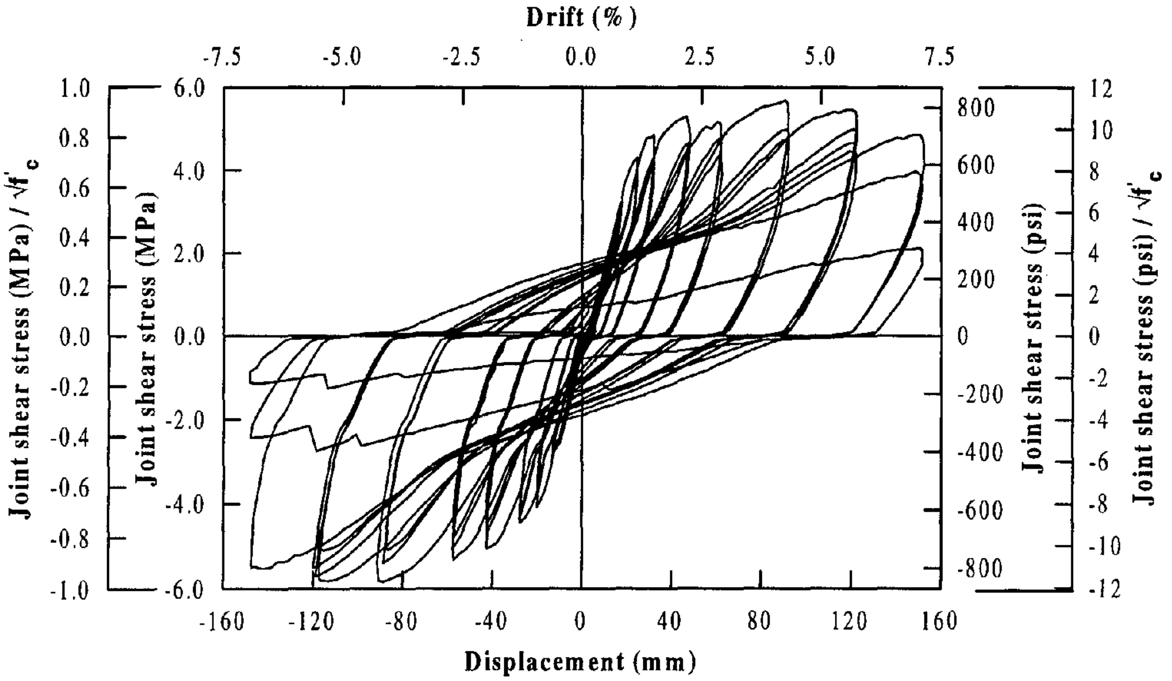

(a) Using maximum joint shear stress

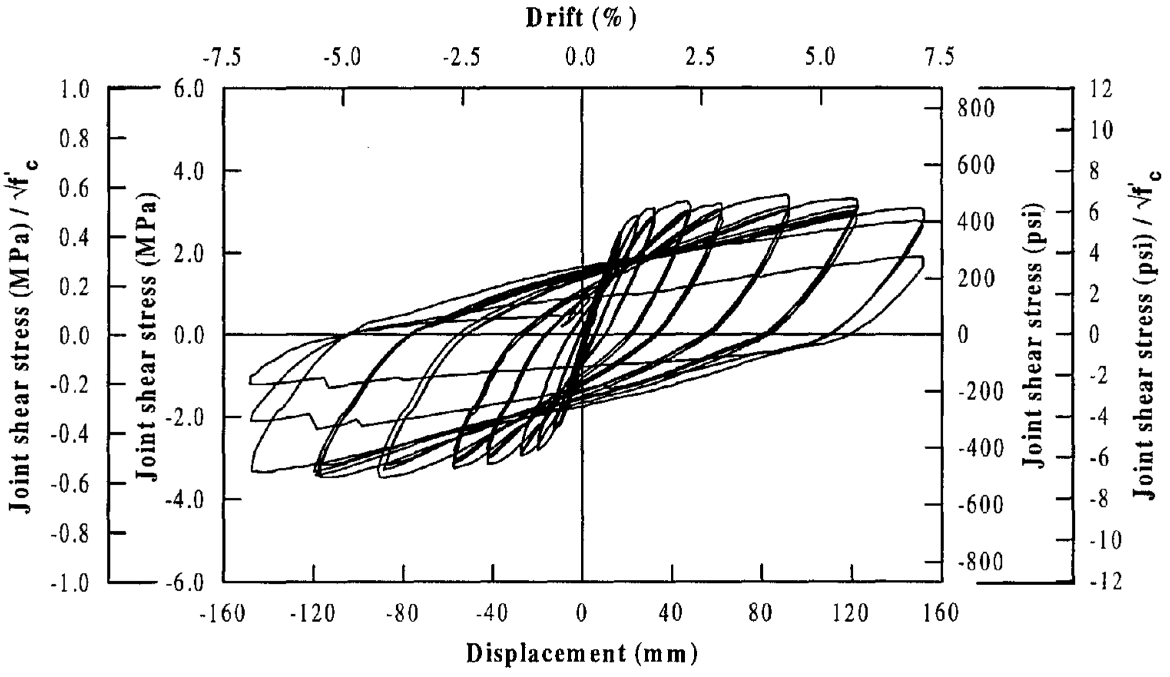

(b) Using average joint shear stress

Figure 6.20 Variation of joint shear stress as a function of column displacement.

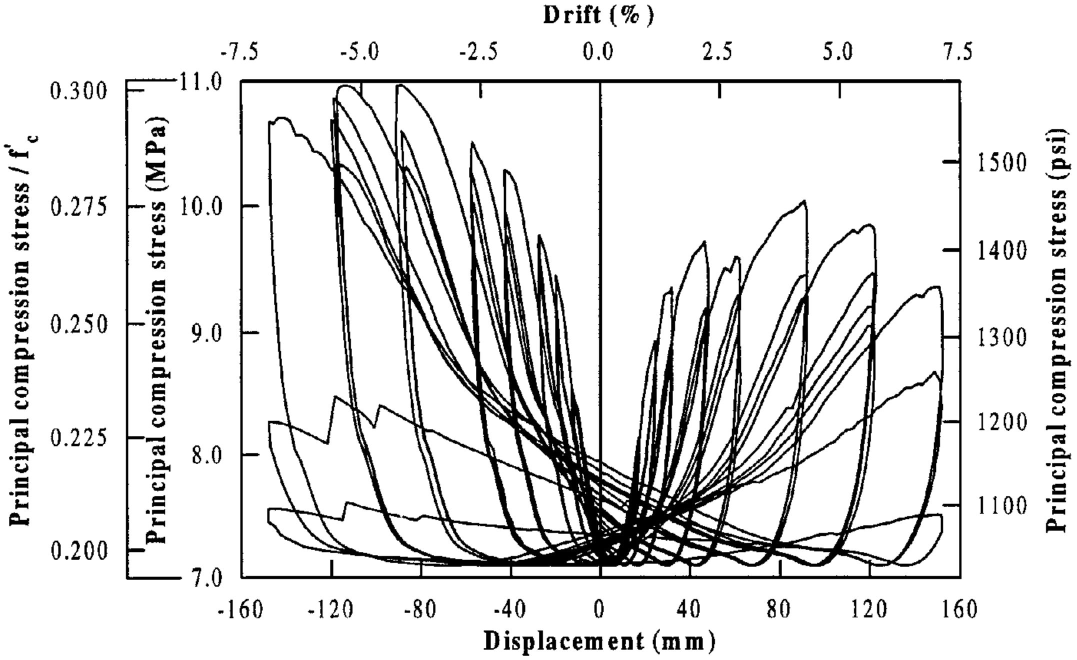

(a) Using maximum joint shear stress

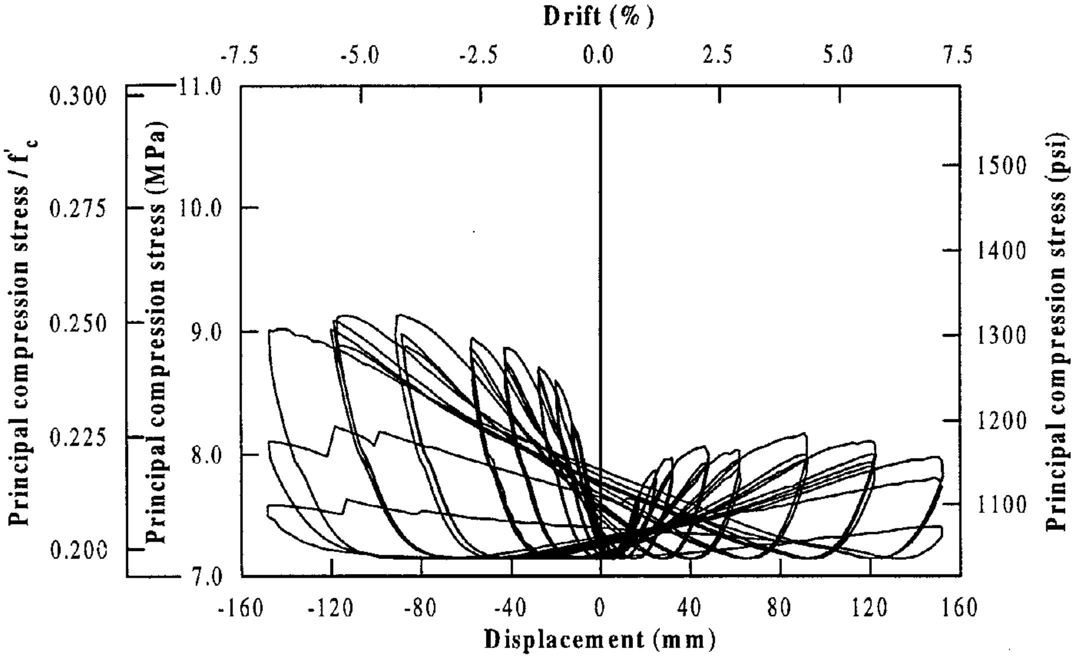

(b) Using average joint shear stress

Figure 6.21 Variation of joint principal compression stress as a function of column displacement.

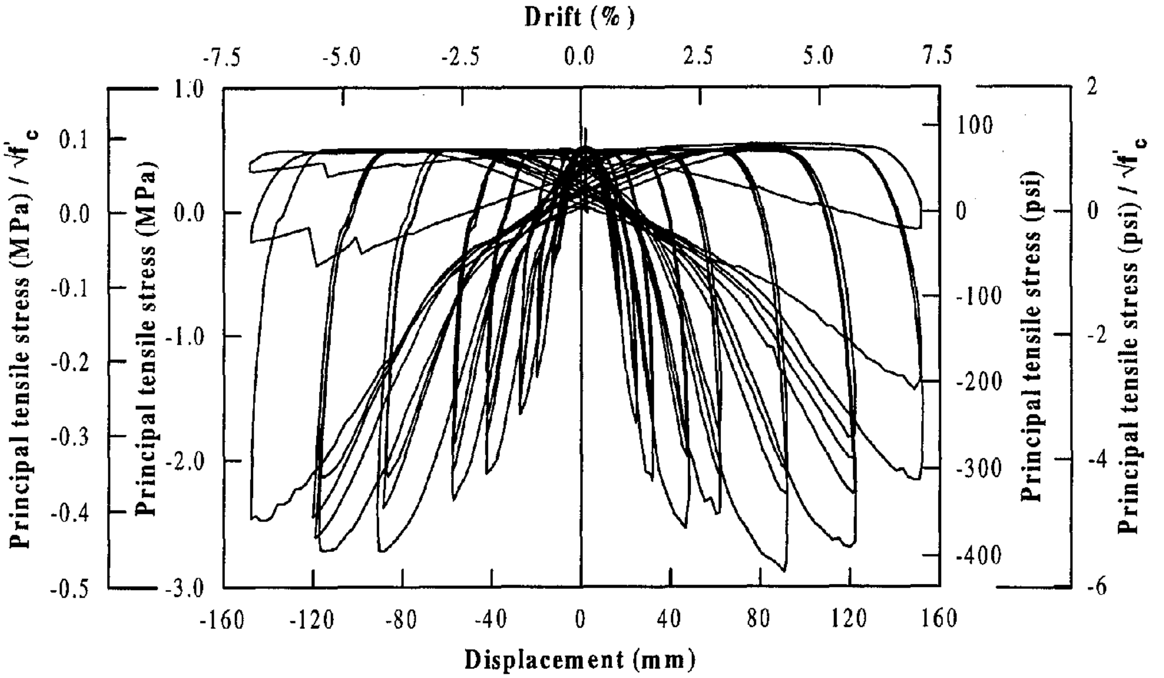

(a) Using maximum joint shear stress

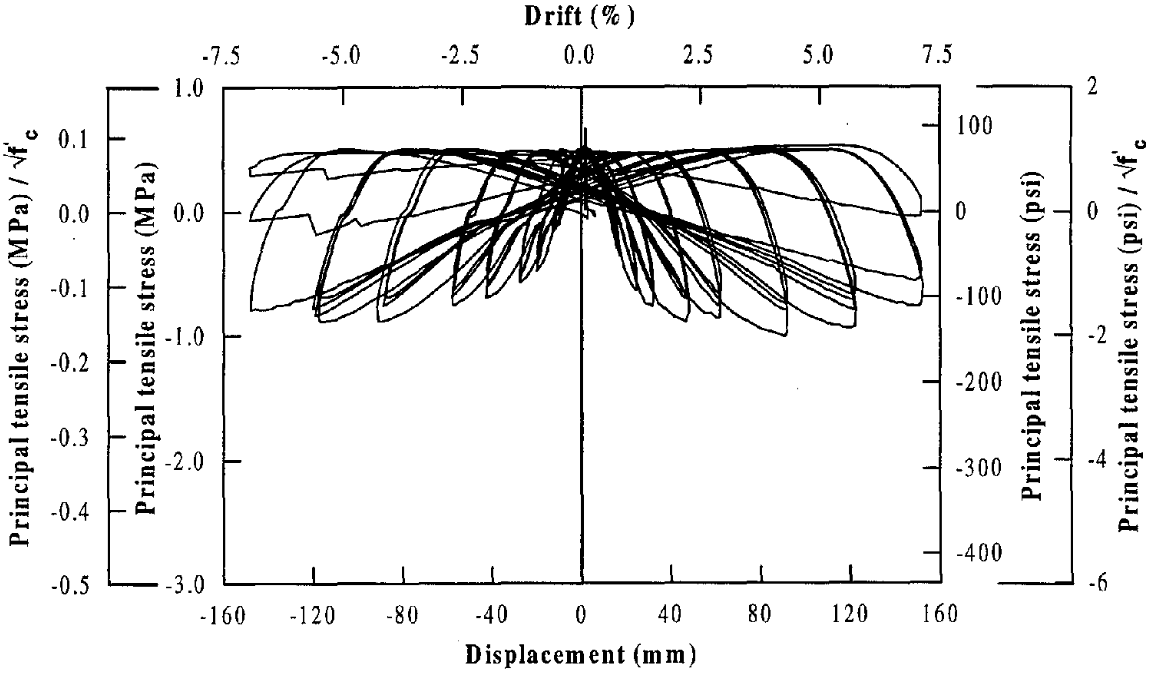

(b) Using average joint shear stress

Figure 6.22 Variation of joint principal tensile stress as a function of column displacement.

of building frames, the joint shear stresses are typically limited to $\mathbf{0.25f'_c}$ in order to avoid crushing of concrete in the joint diagonal strut [15]. If this is considered as the upper bound for joint shear stress in conjunction with applied vertical joint stress and measured compressive strength, it results in a limiting principal compression stress of $\mathbf{0.26f'_c}$ for this particular joint. This limiting stress is comparable to the average joint principal compression stress induced in the joint during the cyclic test, but smaller than the maximum joint principal compression stress. A similar comparison was made in the design calculation using the expected material strength (Section 6.1.3).

The principal tensile stress reached the peak values of $\mathbf{0.48\sqrt{f'_c}}\left(\mathbf{5.8\sqrt{f'_c}}\text{ in psi units}\right)$ and $\mathbf{0.17\sqrt{f'_c}}\left(\mathbf{2.0\sqrt{f'_c}}\text{ in psi units}\right)$ respectively when the maximum and average joint shear stresses were considered. Based on these values, which are higher than those estimated in the design calculations (Section 6.1.3), it appears that the joint should have been provided with a full force transfer mechanism if it was designed for the maximum principal tensile stress. However, the average joint principal tensile stress indicates that only a nominal joint reinforcement within the joint would be adequate. In the design of the test unit, it was argued that the joint diagonal strut could transfer the entire shear force and subsequently only a minimal amount of reinforcement was provided within the joint.

The angle of the joint principal plane as calculated using the average joint shear stress is shown in Figure 6.23. Unlike the reinforced concrete joint (Figure 4.25), where the principal stress plane changed swiftly between push and pull direction loadings, a gradual change in the angle is noted with the maximum value of about 24°. Cracking in the joint was much flatter (Figure 6.12) than that observed for IC1, with an average inclination of about 30°. This corresponded well with the principal stress angle that was calculated from the maximum joint shear stress. A similar comment was also made for the joint cracking observed on unit IC2 (Section 5.7.3).

Growth of joint panel area and joint shear strain as a fuction of column displacement are shown in Figures 6.24 and 6.25 respectively. Both parameters confirm that the joint damage associated with this particular test unit was much less than that was seen for the first test unit. The area of growth and joint strain recorded for the first unit was 20-30 times higher than those shown in Figures 6.24 – 6.25.

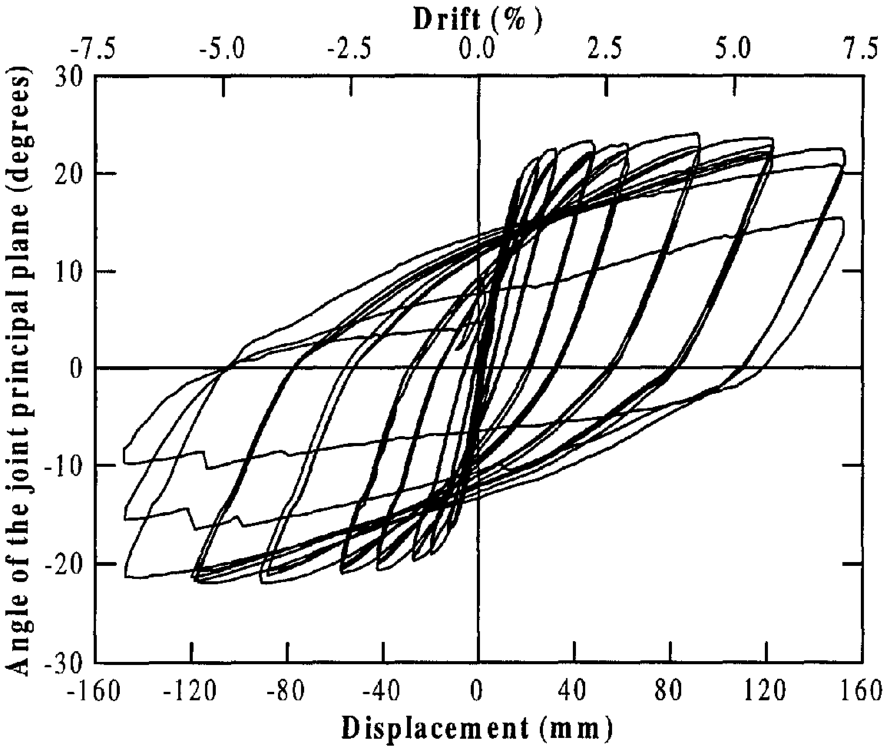

Figure 6.23 Angle of principal stress plane as obtained from the average joint shear stress.

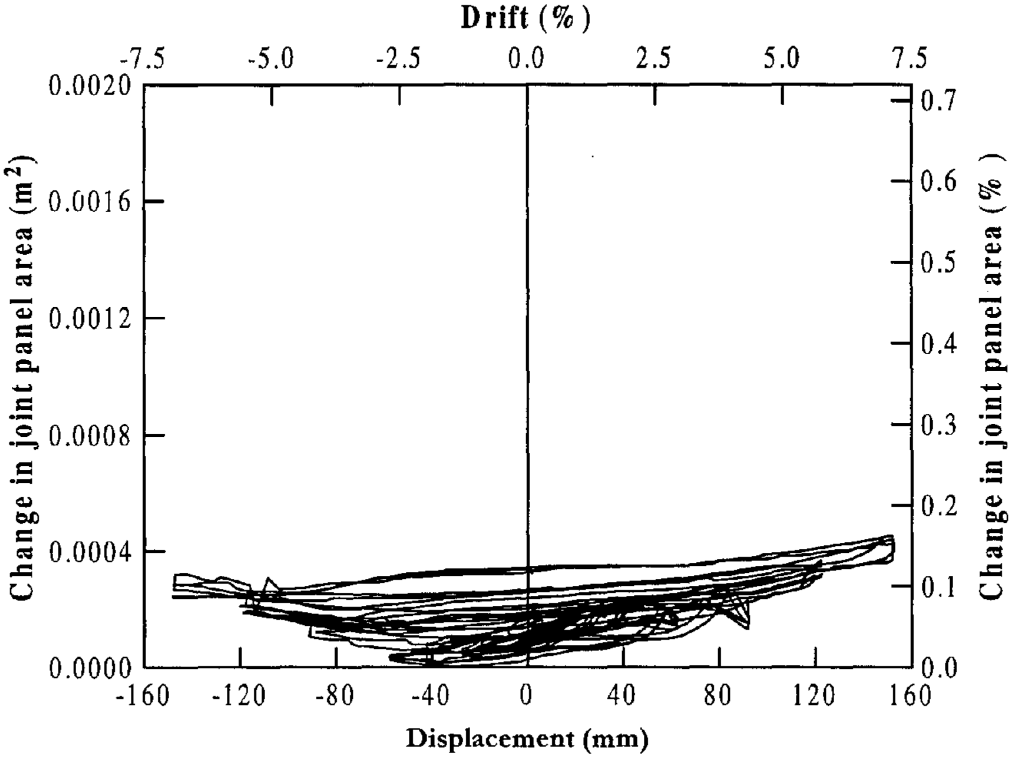

Figure 6.24 Growth of joint panel area as a function of column displacement.

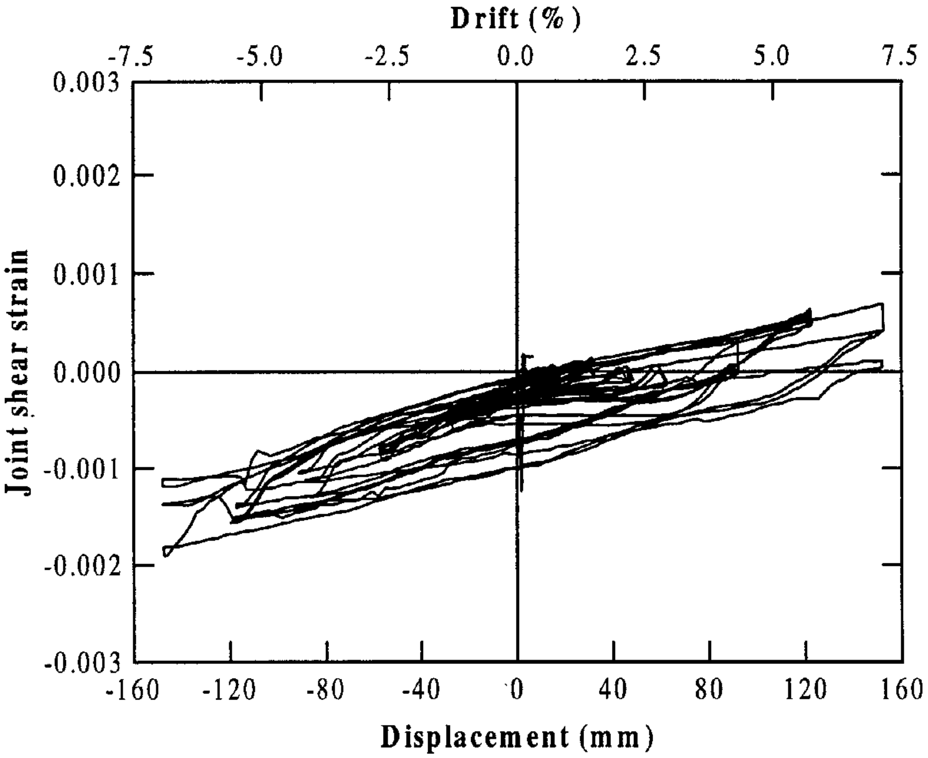

Figure 6.25 Joint shear strain as a function of horizontal column displacement.

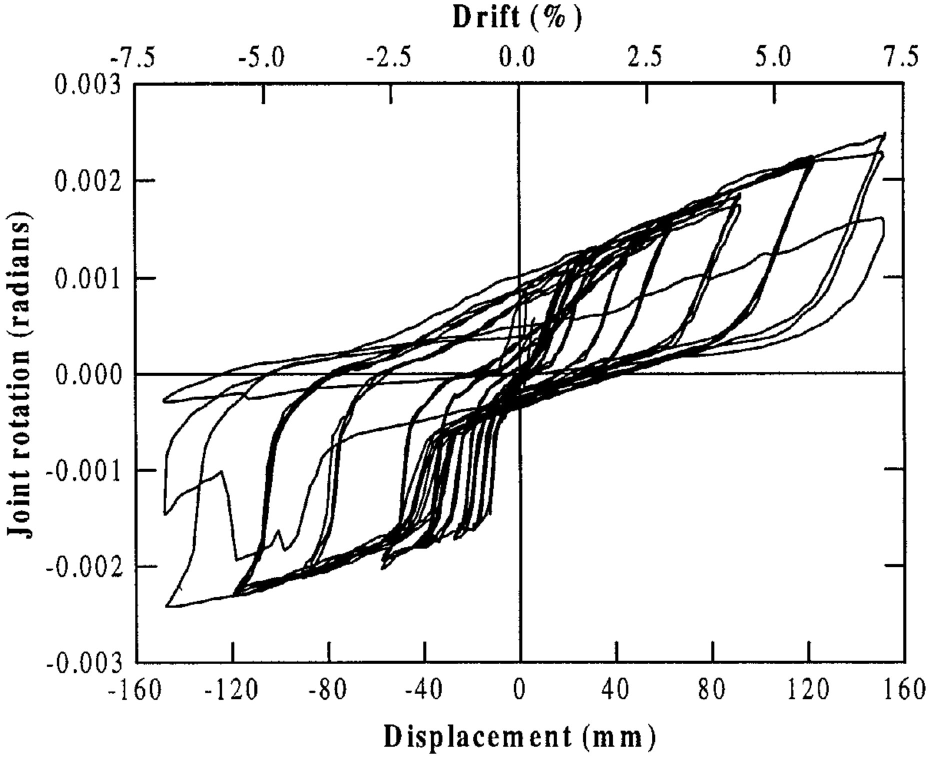

Figure 6.26 Rotation of the joint due to bending of the cap beam.

In Figure 6.25, the measured rigid body rotation of the joint due to bending of the cap beam is shown. The maximum joint rotation obtained for IC3 was slightly smaller than that observed for the equivalent partially prestressed joint. The displacement contribution due to joint rotation was 3.5 percent of the total displacement at ductility 10.

6.7.4 Displacement Components

As for the two previous tests, various components of the column horizontal displacement were examined and the numerical values are given in Appendix B. In Figures 6.27 and 6.28, total displacements accumulated from column flexure and joint rotation as obtained from experimental observations and theoretical calculations are compared against the total measured displacements at selected ductilities. In the experimental calculations, the component due to joint shear is not shown. As can be seen in Figure 6.25, the maximum shear strain, which was recorded at the peak displacement, yielded a horizontal column displacement of only 2.2 mm (0.087 in.). This was about 40 percent of that contributed by joint rotation due to bending of the cap beam. A good agreement between the total measured and that accumulated from column flexure and joint rotation is seen for both analytical and experimental values.

Theoretical and experimental displacement components due to column flexure and joint rotation are compared against each other in Figure 6.29. Again a good agreement is seen for both components although the peak displacement was underestimated in the theoretical prediction. Further, as for IC1 and IC2, analytical prediction slightly underestimated the joint rotation component while marginally overestimating the column flexure component. In Figure 6.30, displacement components as percentage of the total displacement are given, which show the percentage contribution due to joint rotation was higher at lower ductilities than at higher ductilities. At smaller ductilities ($\mu_\Delta < 6$), the experimentally obtained displacement contribution due to column flexure was smaller in the pull direction than in the push direction loading. The contribution in the push direction loading appears comparable to the observations made in the two previous units, suggesting that there may be an error involved in the experimental displacement components due to column flexure in the pull direction loading at low ductilities.

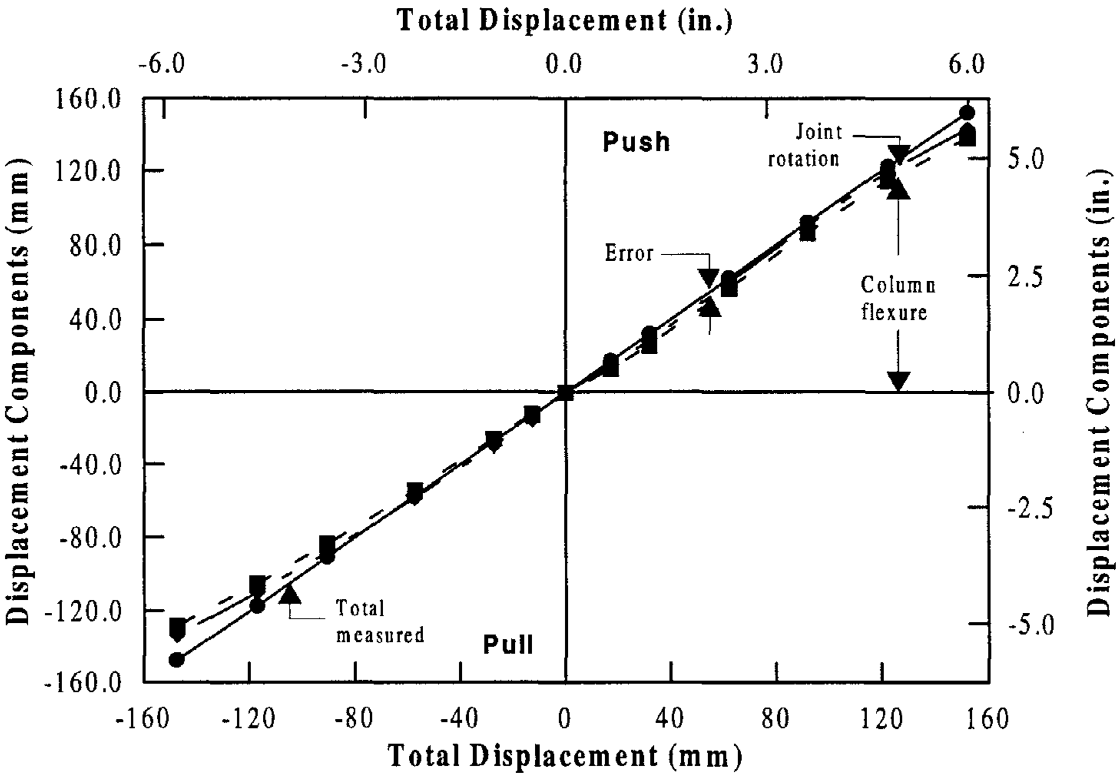

Figure 6.27 Comparison of the displacement accumulated from experimentally observed components to the total measured displacement.

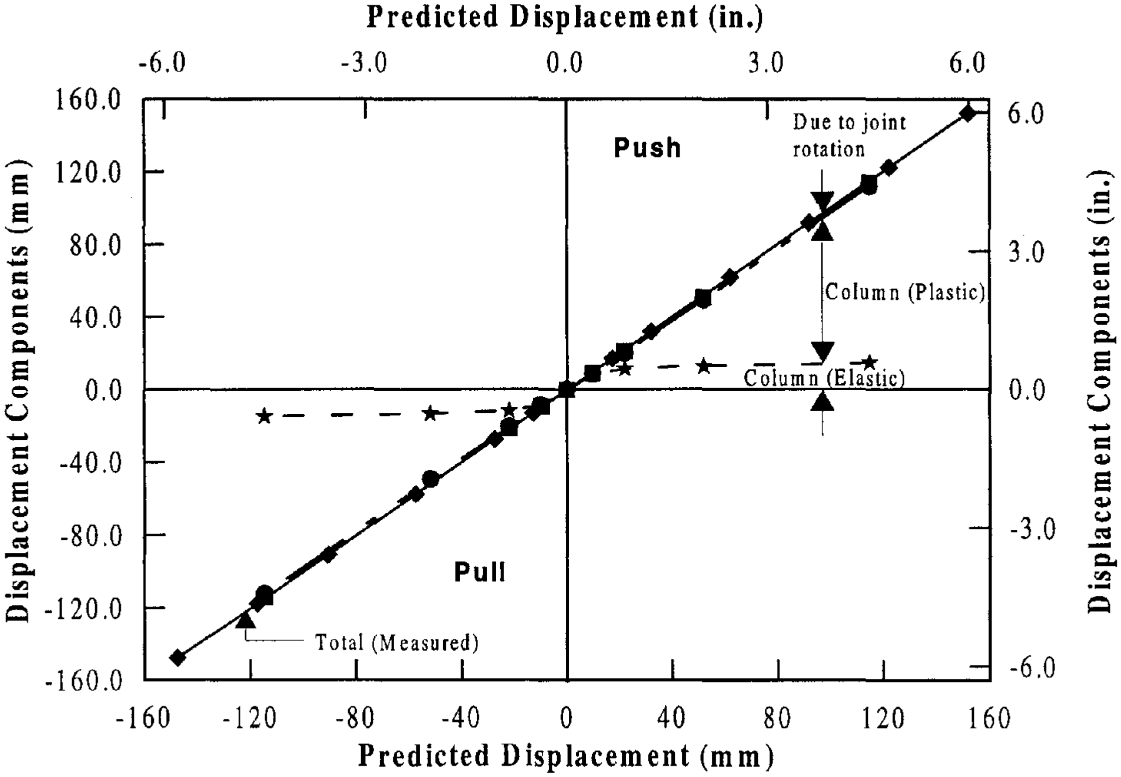

Figure 6.28 Comparison of the displacement accumulated from theoretically estimated components to the total measured displacement.

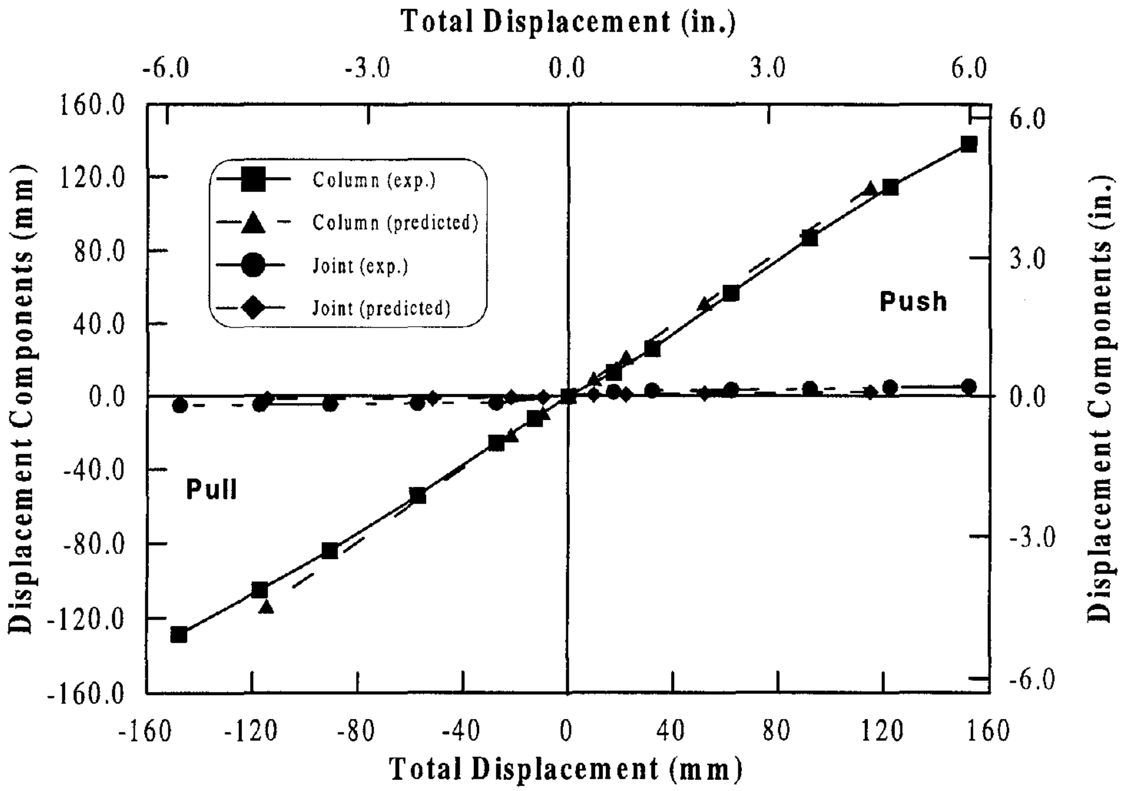

Figure 6.29 Comparison of experimentally obtained displacement components due to column flexure and joint rotation against the analytical values.

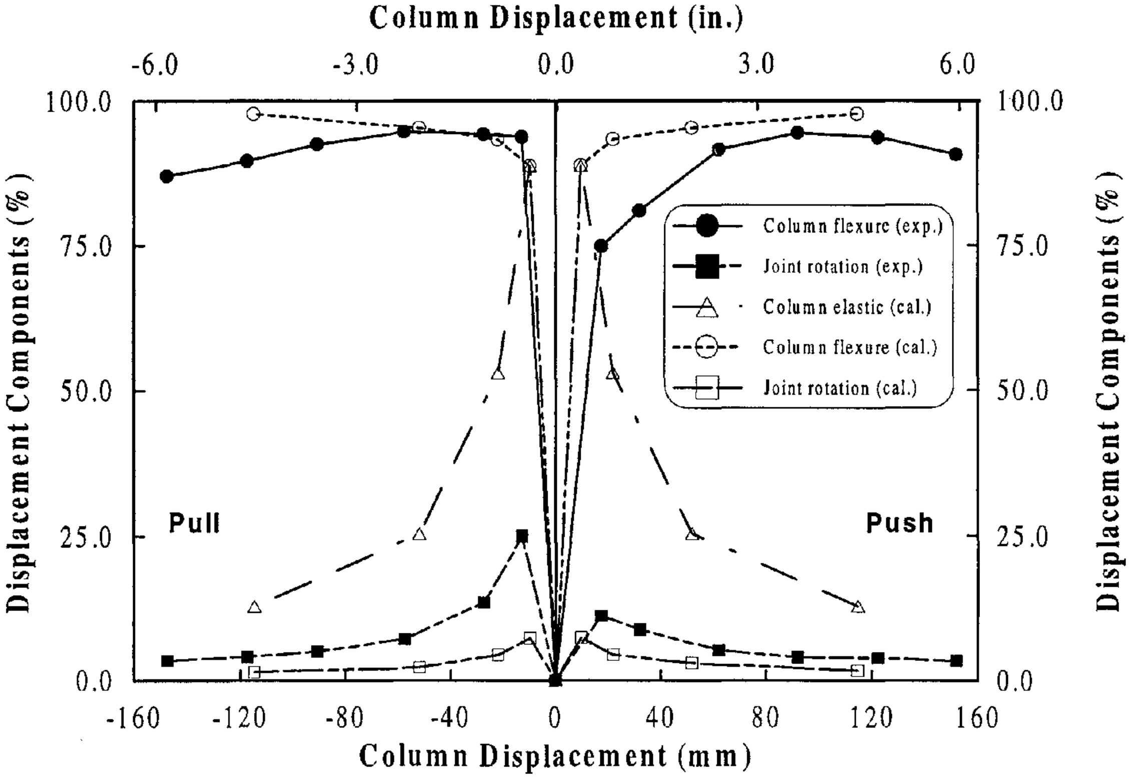

Figure 6.30 Representation of displacement components as percentage of the total horizontal displacement.

6.7.5 Strain Gauge Histories

The recorded histories of selected strain gauges are presented in this section as a function of the horizontal column displacement while key values of several other gauges are given as profile plots in the following section.

In Figure 6.31 the strain recorded on an extreme longitudinal column reinforcement at the joint interface is shown. Yielding of the bar did not occur when the horizontal load was taken to 250 kN (56 kips). Instead, the yield strain was recorded during loading between 250 kN and that corresponded to $\mu_\Delta = 1$. For the opposite direction loading, the yield strain was obtained in the critical column section when the target displacement approached to that corresponding to $\mu_\Delta = 1$.

Strain gauge histories of two column spiral gauges are presented in Figures 6.32 and 6.33. The strain data given in Figure 6.32 shows the confinement effect in the column plastic hinge region whereas the shear resistance provided by the column spiral is represented in

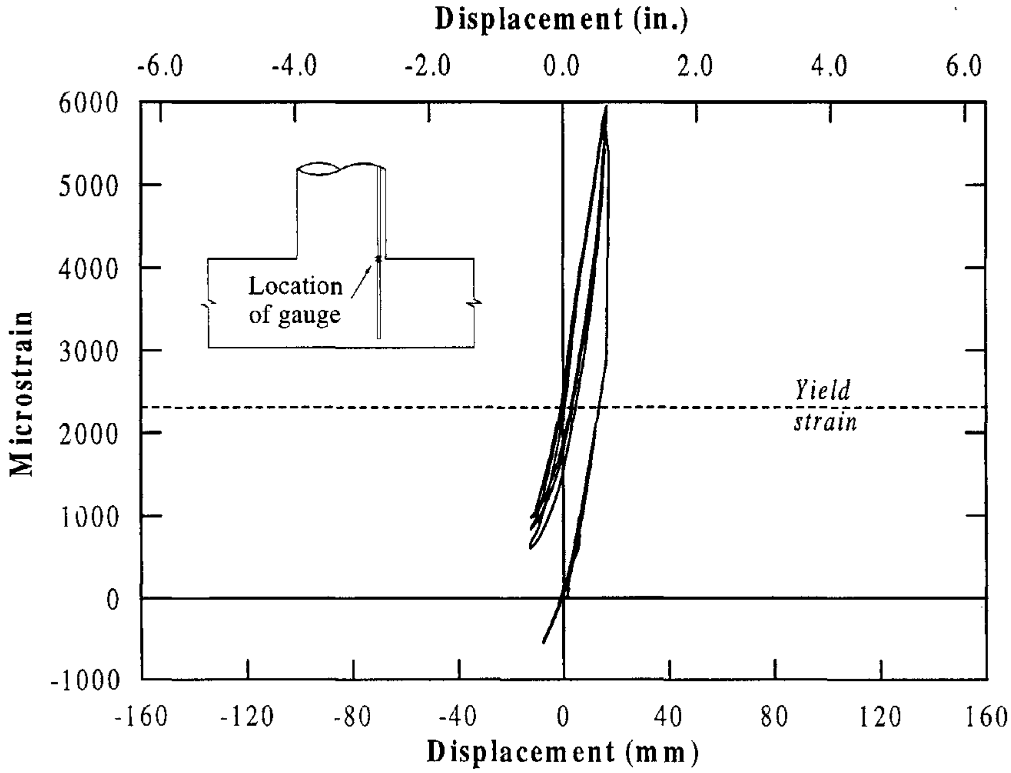

Figure 6.31 Strain gauge history of a gauge located at the joint interface on an extreme column tension reinforcement.

Figure 6.33. The gauge measuring the confinement was located on the south side of the column about 203 mm (8 in.) from the joint interface. Yielding of the spiral appeared to have occurred at ductility 6 at this location. There was another gauge placed closer to the joint interface and yield strain in this gauge was registered as the displacement was taken to that corresponding to $\mu_\Delta = 6$, but this gauge also failed soon after recording the yield strain. As for the two previous units, significant inelastic action was recorded in the column spiral gauge measuring shear strain despite increasing the shear reinforcement in this column when compared to the spiral contents of IC1 and IC2. Several other gauges measuring shear resistance of spiral contribution also exhibited significant inelastic behavior and this can be seen in the profile plot shown in Figure 6.40. This is further discussed in Section 6.8 in relation to the shear demand in the column. No significantly large strains were obtained in the gauges placed on the spirals within the joint and this may also be seen in the profile plots.

The strains monitored on the longitudinal beam steel were generally low. Some of the gauges within the joint, particularly those placed close to the center of joint, recorded strains above 0.0015. An example of this is shown in Figure 6.34. Given the location of this gauge, it is difficult to explain why higher tensile strains were recorded in the pull direction loading. This behavior was not identified in the previous units.

Of several gauges placed on the stirrups of the cap beam, strain records are shown for three gauges in Figures 6.35 – 6.37. The gauge shown in Figure 6.35 was mounted on an inner leg of the stirrup which was placed within the joint adjacent to the epoxy seam on the right side to the center of column. Large strains developed in the push direction loading are believed to have been induced by the compression struts anchored at the bottom left corner of the joint. The maximum strain measured on an outer leg of the same stirrup was found to be less than half of that is shown in Figure 6.35. Strains in the stirrups were relatively high in the center region of the joint. Two examples are shown in Figures 6.36 and 6.37. Both gauges, which were placed on the outer legs of the joint stirrups appeared to be similar although one recorded larger maximum strain than the other. The strain gauges placed in the inner legs of the same stirrups failed while approaching yield strain between ductility 6 and 8, indicating the nominal steel placed within the joint was adequate to provide the necessary confinement.

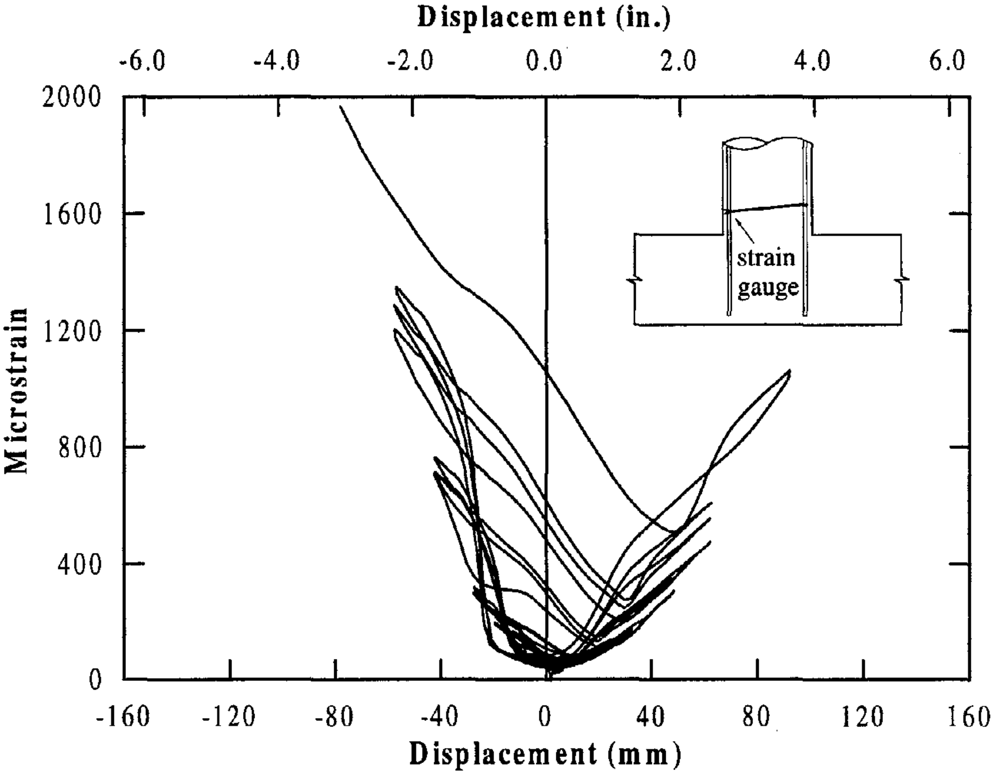

Figure 6.32 Column spiral gauge showing confinement strain in the hinge region.

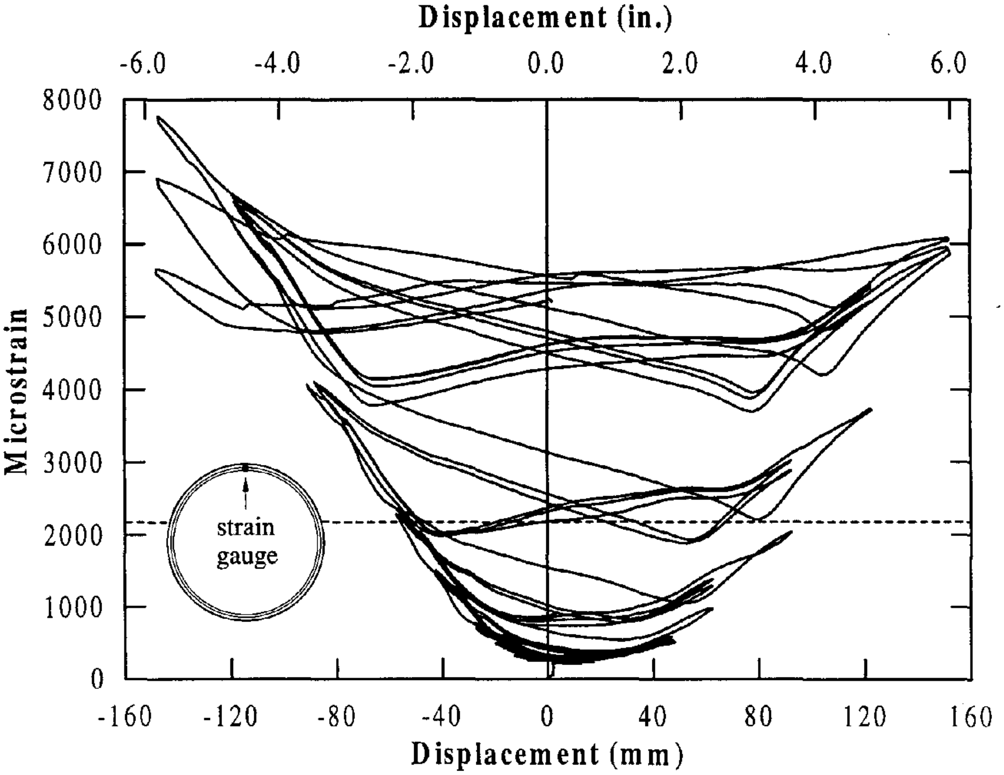

Figure 6.33 Strain history from a column shear reinforcement.

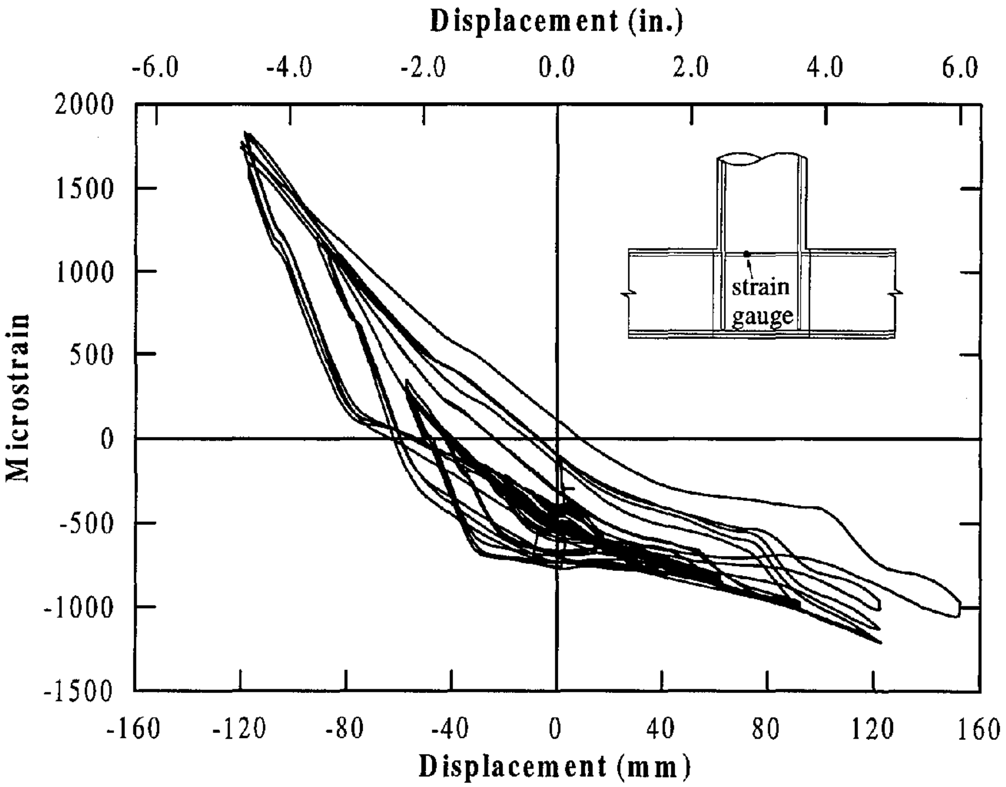

Figure 6.34 Strain history of a top beam reinforcement gauge located within the joint.

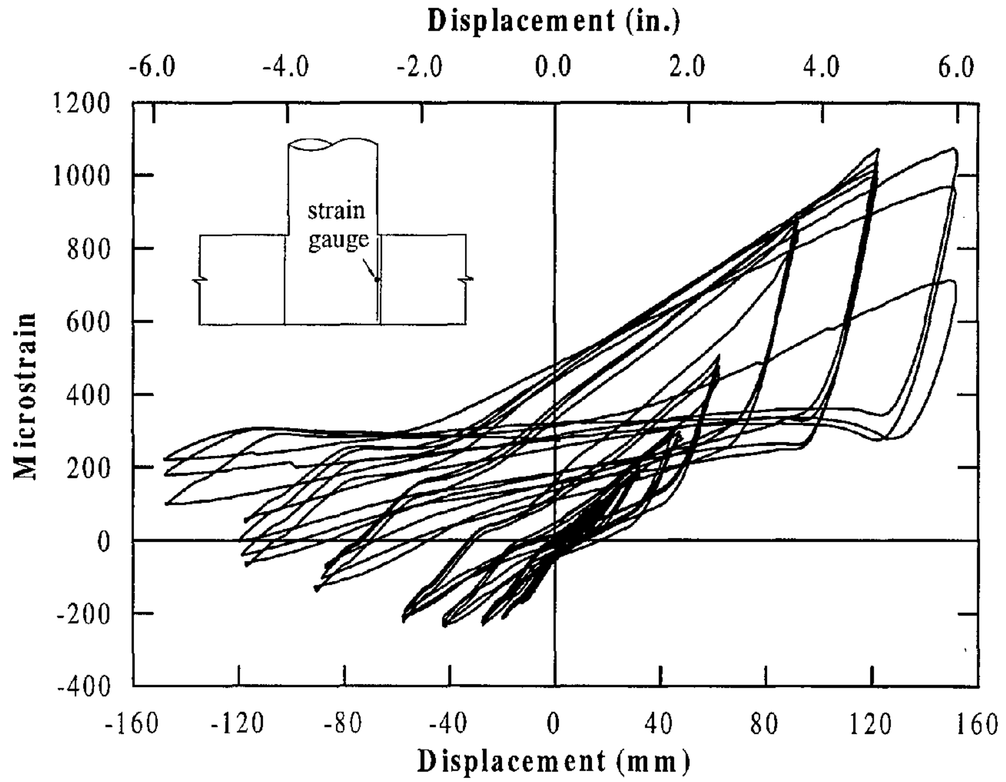

Figure 6.35 Strain history from an inner leg of a joint stirrup adjacent to the epoxy interface.

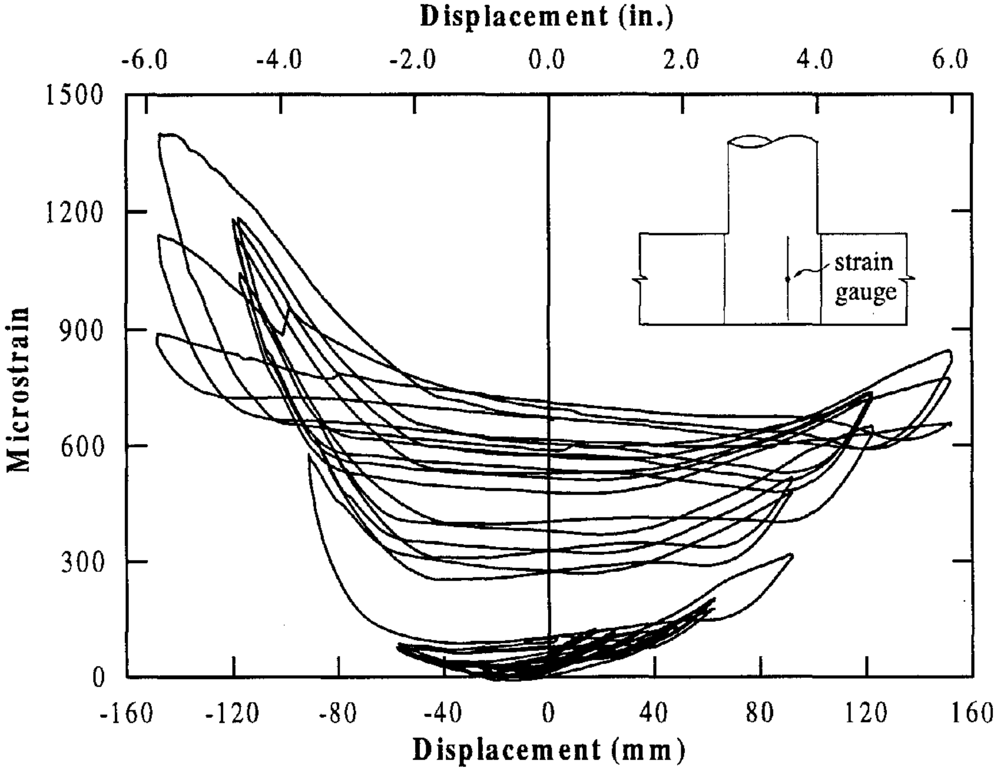

Figure 6.36 Strain history from an outer leg of a joint stirrup at mid height.

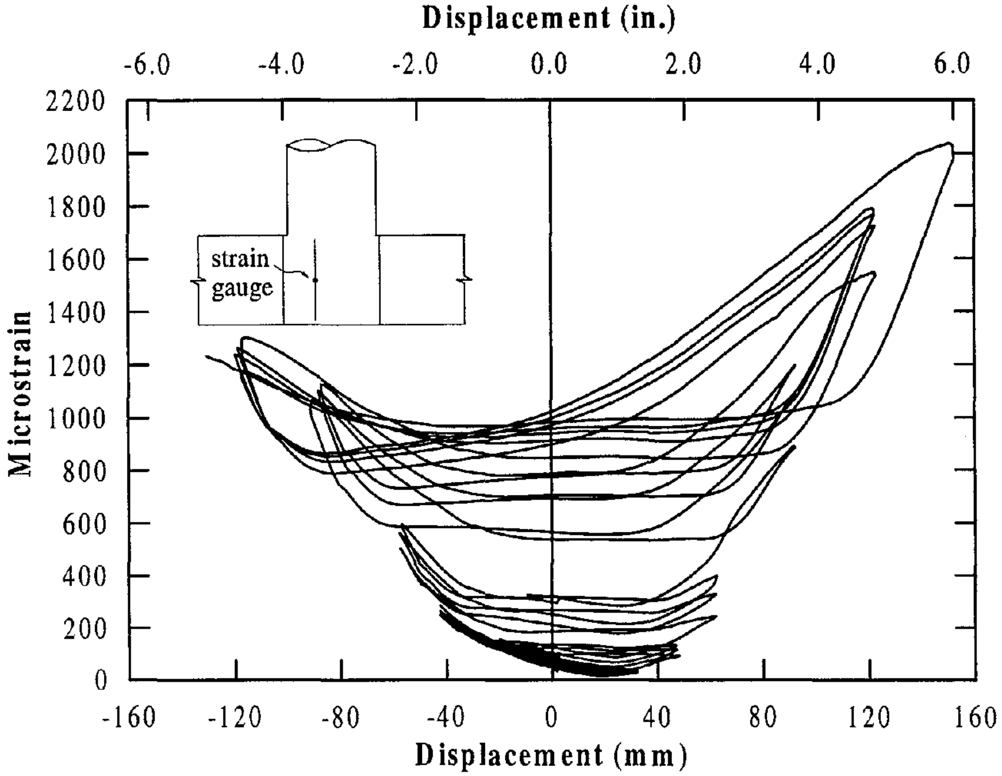

Figure 6.37 Strain history from an outer leg of a joint stirrup at mid height.

6.7.6 Strain Profiles

Strain profiles obtained in the column, beam and joint are presented in this section. The reported strains, as before, are the peak values recorded during the first cycle at each ductility. Note that there was only one cycle imposed during the first part of the test under force control and that the peak strains measured in each load step are also included in the profile plots.

In Figure 6.38 strain profiles of an extreme column longitudinal reinforcement are presented. As for the first unit, most of the strain gauges failed between displacement ductility 1.5 and 2.0. Significant strain penetration into the joint is seen from a horizontal load as low as 133 kN (30 kips). Strain in the longitudinal bar within the joint reduced relatively quickly with depth when compared to the equivalent reinforced concrete unit (Figures 4.45 and 4.46). This is possible because a broader joint strut was developed in IC3 (compare Figure 4.3a to Figure 5.1). As a result, it appeared that the yield strength of the column bars of the prestressed joint developed further away from the bar end than that was observed for the reinforced concrete unit IC1. The shortest bar length at which yield strength was recorded in unit IC1 was 130 mm (5.1 in.) compared to 269 mm (10.6 in.) in IC3. In reality, the column bars in the prestressed joints require the same, if not less, development length as that for the reinforced concrete counterpart. Because anchorage length of the column bars into the joint strut is effectively increased in the prestressed joint (see Figure 5.1), it is possible that a larger diameter bar can be anchored in the prestressed joint than in an equivalent reinforced concrete joint.

A series of gauges were mounted on the spirals of the column and joint to capture the confinement effect and shear demand on the transverse reinforcement. Figures 6.39 and 6.40 depict the strain profiles from the south and east side of the column respectively. In Figure 6.39, it is seen that strains due to confinement effect, which was recorded in the loading plane, gradually increased in the column spirals from the beginning of the test while the strain gauge readings below the interface within the joint remained to insignificant values for the entire test as the cap beam and prestressing provided the required confinement. A similar observation was also made for the gauges on the north side of the spirals. In the equivalent reinforced concrete joint, higher strains were recorded in the joint spirals than in the column transverse reinforcement at early stages of testing (Figure 4.47) despite the volumetric ratio of the spirals within the joint was 70 percent higher than that of the column. At large ductilities, comparable strains were recorded in the joint and in the plastic hinge region of the column in IC1. The volumetric ratio of the column spirals was increased by 52 percent in IC3 when compared to IC1, but strains monitored at large displacements appeared to be similar for both units. This statement is valid even at ductility 4 at which point no influence of buckling of longitudinal reinforcement on the strains monitored in the transverse steel was possible. For a given horizontal displacement at the top of column, a larger plastic rotation would have developed in the hinge region of the column in IC3 because of reduced flexibility of the cap beam and joint resulting from the prestressing. A larger plastic rotation in the column requires higher demand upon the transverse reinforcement confining the concrete in the hinge region. Consequently, energy absorption capacity was increased in IC3 at a given drift ratio (see Figure 7.2).

The spiral gauges from the east side of the test unit (Figure 6.40) represent the contribution of transverse reinforcement to the column shear resisting mechanism and transverse tension developed within the joint. Although shear cracks in the column of this unit appeared to be well controlled when compared to the two previous units, yield strength of the shear reinforcement was developed in the column, which was also observed on the opposite side. Shear demand in the column of IC3 was increased only by 5.5 percent while the spiral content was increased by 52 percent compared to the columns of IC1 and IC2. A further discussion on the capacity versus demand of the column shear reinforcement is given Section 6.8. Within the joint, the transverse strain remained insignificantly small during the test. The prestressing of the cap beam induced compression strain in the joint spirals, which was not recovered until the displacement ductility 3 was imposed. A comparable plot corresponding to the first unit was shown in Figure 4.48 where tensile strain as high as 0.004 was recorded as an effect of transverse dilation of the joint concrete. The gauges placed on the west side of IC3 joint spirals exhibited slightly larger strains within the joint. The first and second gauged joint spirals from the bottom of the joint (as tested) recorded strains for the most part of the test. It was found that strains in these gauges increased to about 0.0005 at ductility 8 and twice that at ductility 10.

The strain profile along the second gauged joint spiral from the end of the column bars is shown in Figure 6.41, in which the demand on the joint spirals as described above can be clearly seen. The loading direction was J-D and no significant changes in the strains of gauges at D and J are seen. Starting from compressive strains, strain values of gauges located at A and G gradually increased to tensile strains.

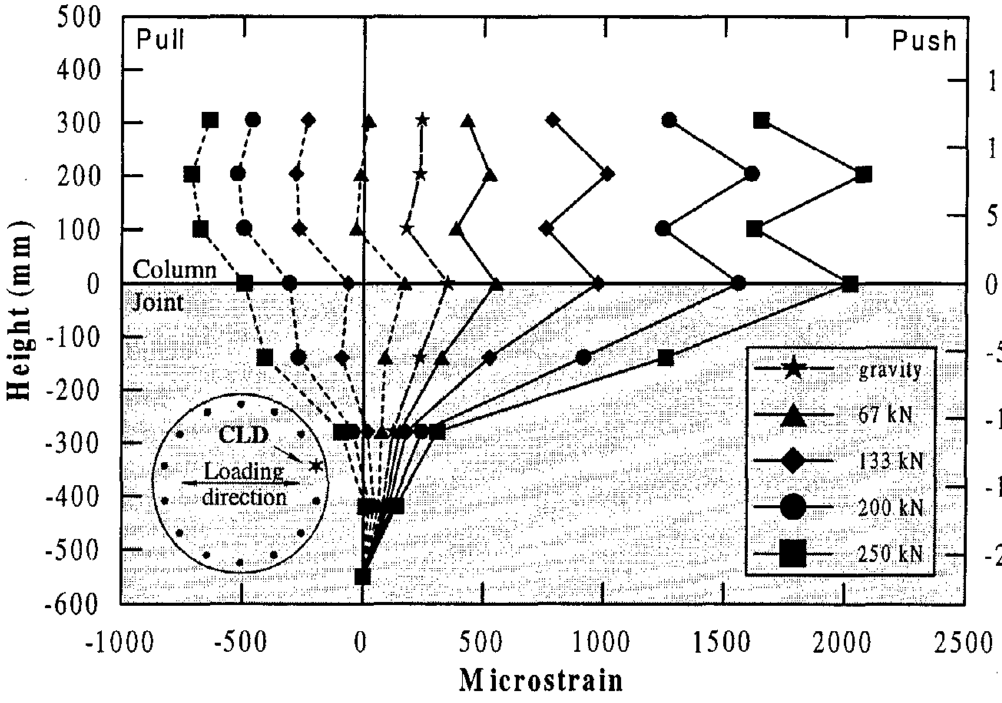

(a) Initial stages of testing

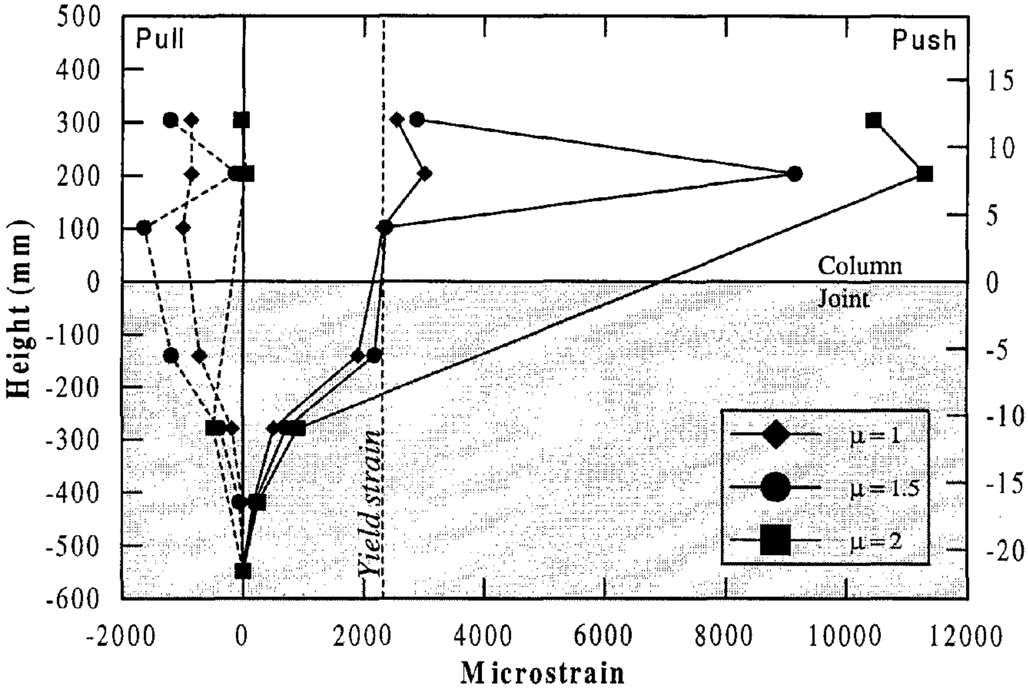

(b) At moderate ductilities

Figure 6.38 Strain profiles of a column longitudinal extreme tension reinforcement (CLD).

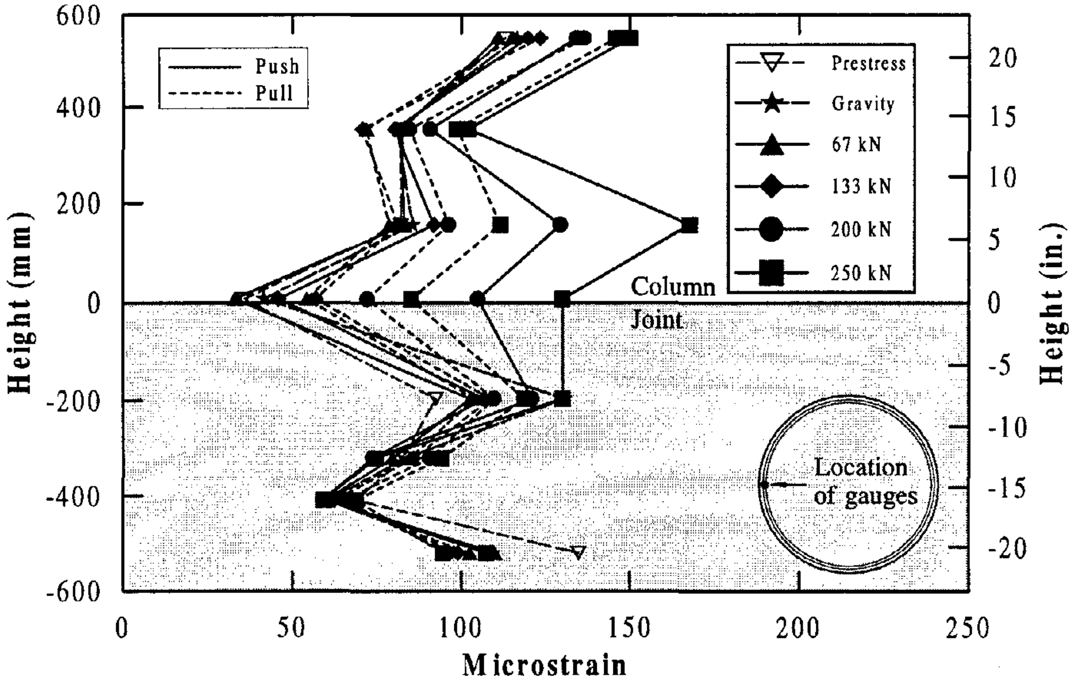

(a) Initial stages of testing

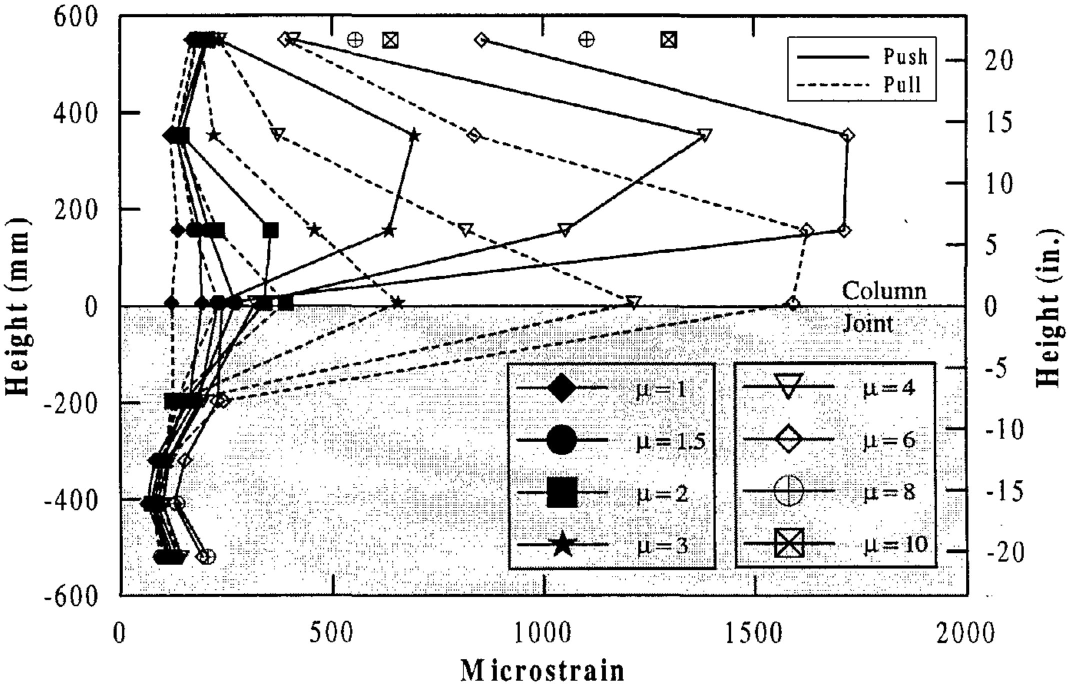

(b) Final stages of testing

Figure 6.39 Strain profiles of gauges mounted on the south side of column and joint spirals.

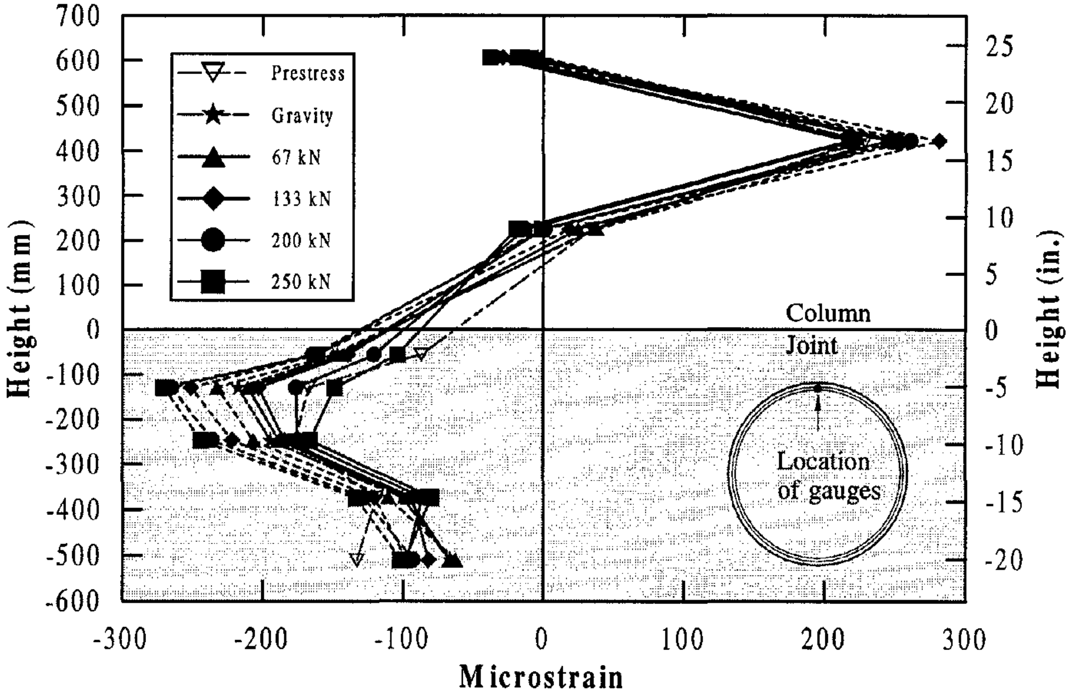

(a) Initial stages of testing

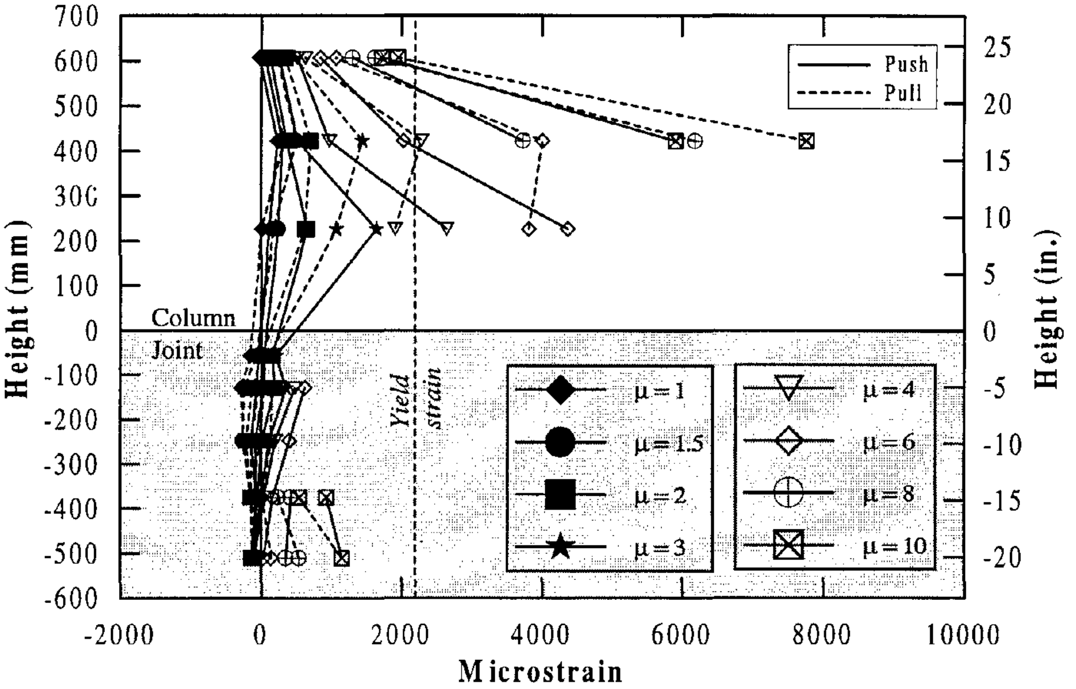

(b) Final stages of testing

Figure 6.40 Strain profiles of gauges mounted on the west side of column and joint spirals.

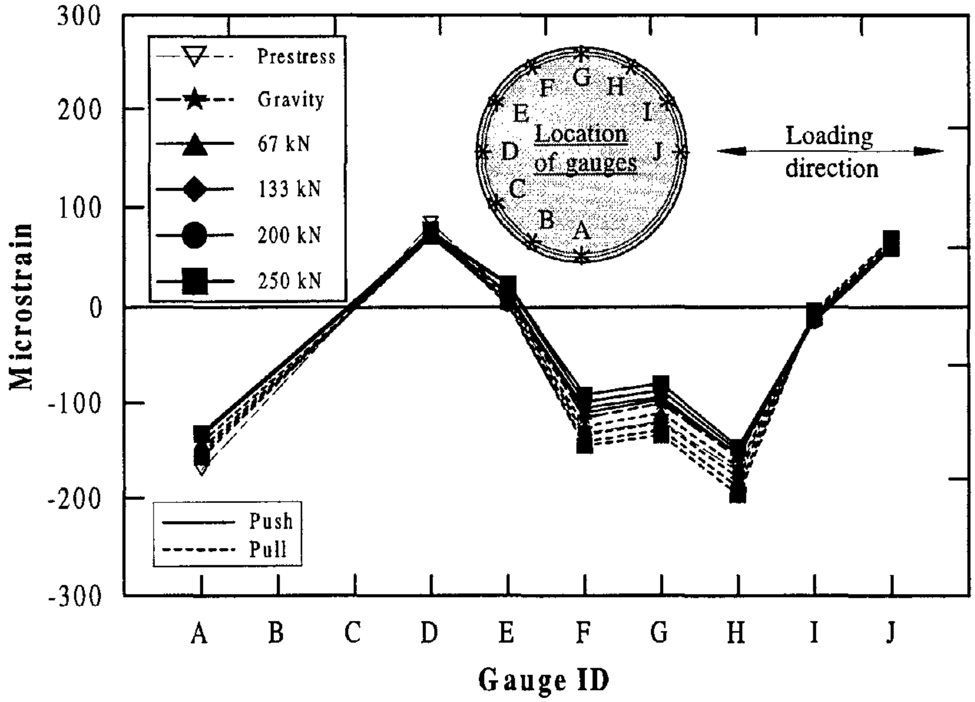

(a) Initial stages of testing

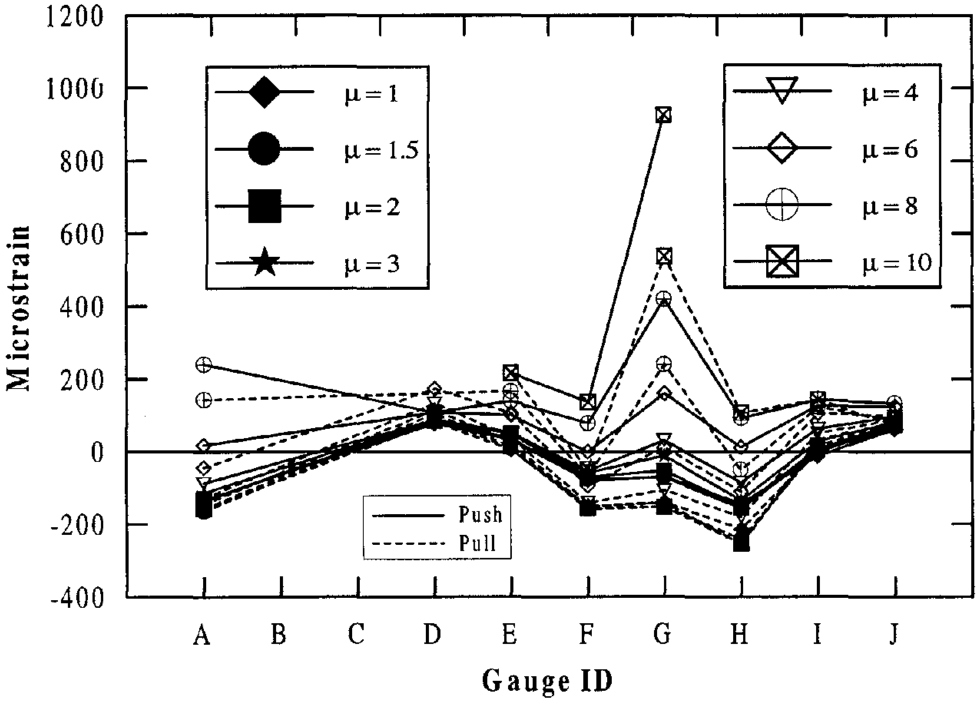

(b) At moderate ductilities

Figure 6.41 Strain profiles of gauges mounted on the second joint spiral from the bottom of the beam.

The strain profiles along a bottom (as tested) and top longitudinal beam reinforcement are shown in Figures 6.42 and 6.43 respectively. At each epoxy interface connecting the precast elements, the mild steel reinforcement was discontinued and thus the strain at the interface was considered to be zero, but in reality the corresponding concrete strain would have varied approximately linearly between the gauges located on either side of the epoxy seam. In both figures, it is noted that the cap beam compressive strain induced by the prestressing was reduced eventually by the negative cap beam moment, which was induced as a result of seismic lateral force in the column. The combination of gravity and the maximum negative moment in the bent cap was not, however, adequate to induce tension in the beam, indicating that the cap beam prestressing could have been reduced. This is consistent with the test observation that there was no flexural cracks formed away from the epoxy interface in the beam. In order to reduce conservatism in the design of this test unit, a reduced overstrength moment factor was used when establishing the maximum possible capacity of the column (Section 6.1.2). Perhaps, by further reducing the column overstrength factor, a reduced amount of cap beam prestressing could be obtained. The strains monitored in the longitudinal top beam reinforcement within the joint exceeded 0.001 in Figure 6.43. A gauge placed at the same section but closer to the center of the joint almost reached twice this strain and the history of this gauge was presented previously in Figure 6.34.

In Figures 6.44 and 6.45, the strain profiles of several gauges at mid height of inner and outer legs of beam stirrup reinforcement are presented. The strains in the cap beam stirrups were negligibly small, but higher values were recorded in the stirrups located either side of the epoxy paste (see Figure 6.2) and also in the joint stirrups placed within the column cage. At ductility 10, strain on an outer leg of a joint stirrup reached 0.002. The strain gauge placed on the inner leg of a joint stirrup failed between ductility 6 and 8 as it appeared to be approaching to the yield strain. When these strains monitored within the joint are compared to the strains of the joint spiral reinforcement, it is clear that the vertical joint stirrups were largely responsible for the joint mechanism and the contribution of the spirals was insignificant.

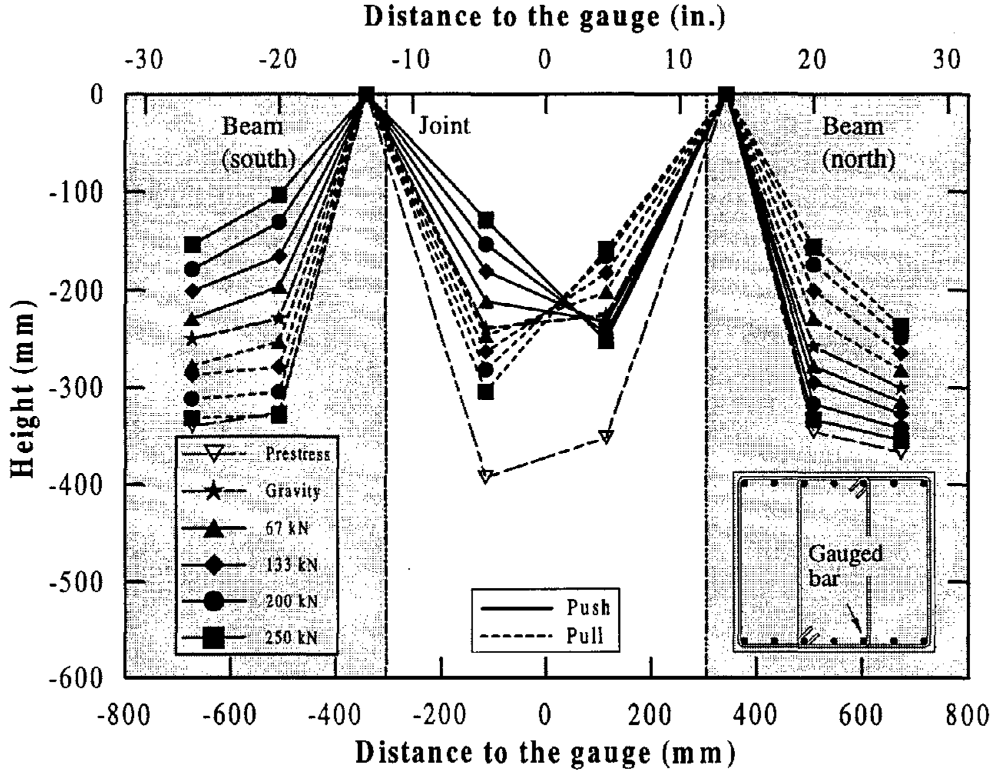

(a) Initial stages of testing

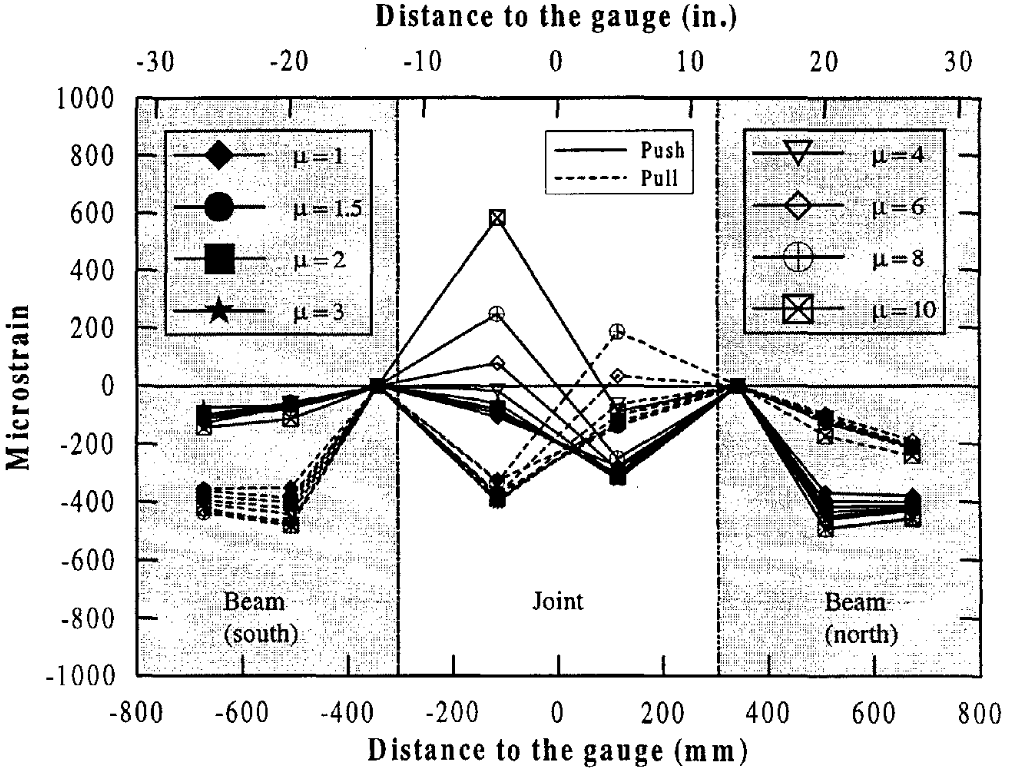

(b) Final stages of testing

Figure 6.42 Strain profiles along a bottom longitudinal beam reinforcement.

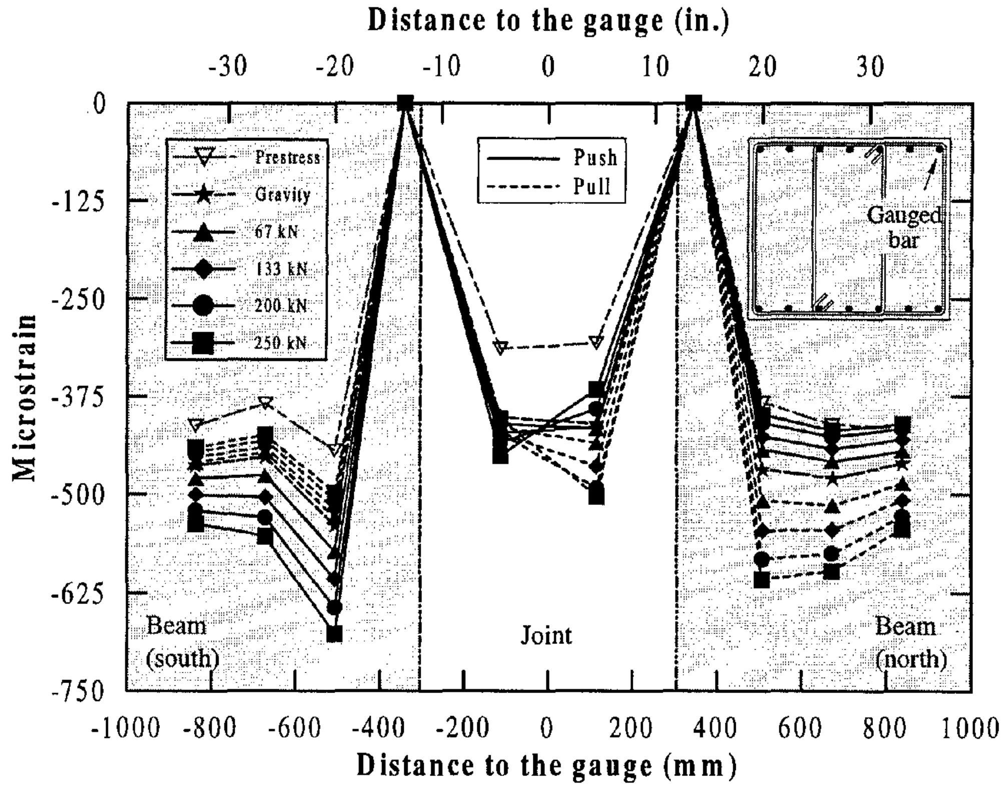

(a) Initial stages of testing

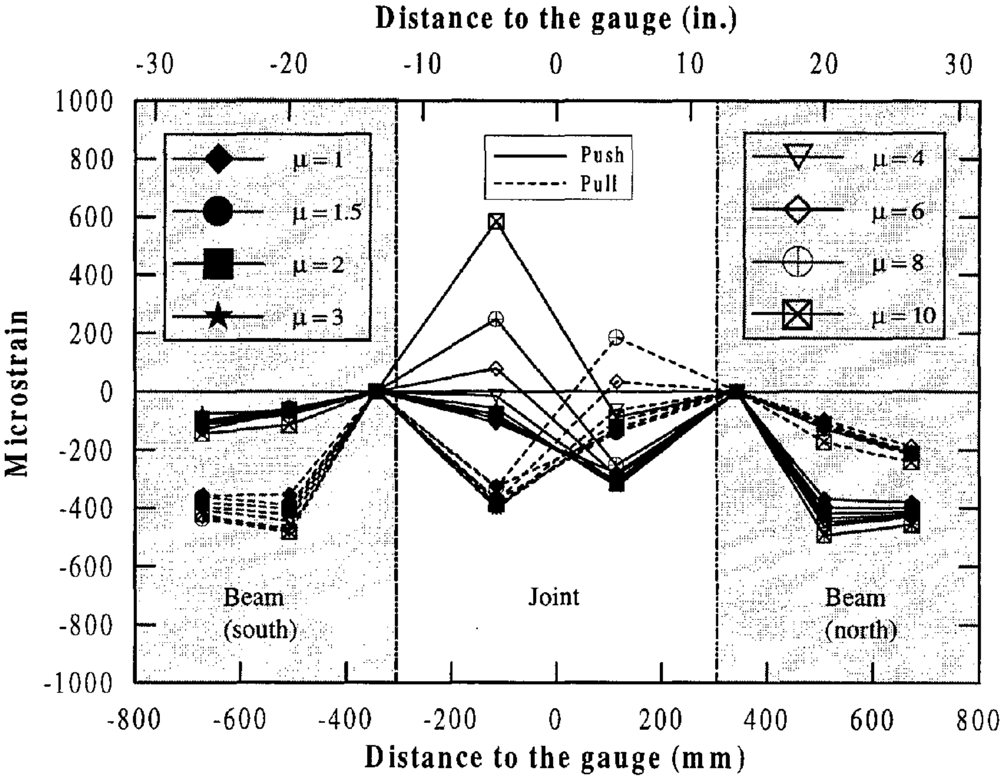

(b) Final stages of testing

Figure 6.43 Strain profiles along a top longitudinal beam reinforcement.

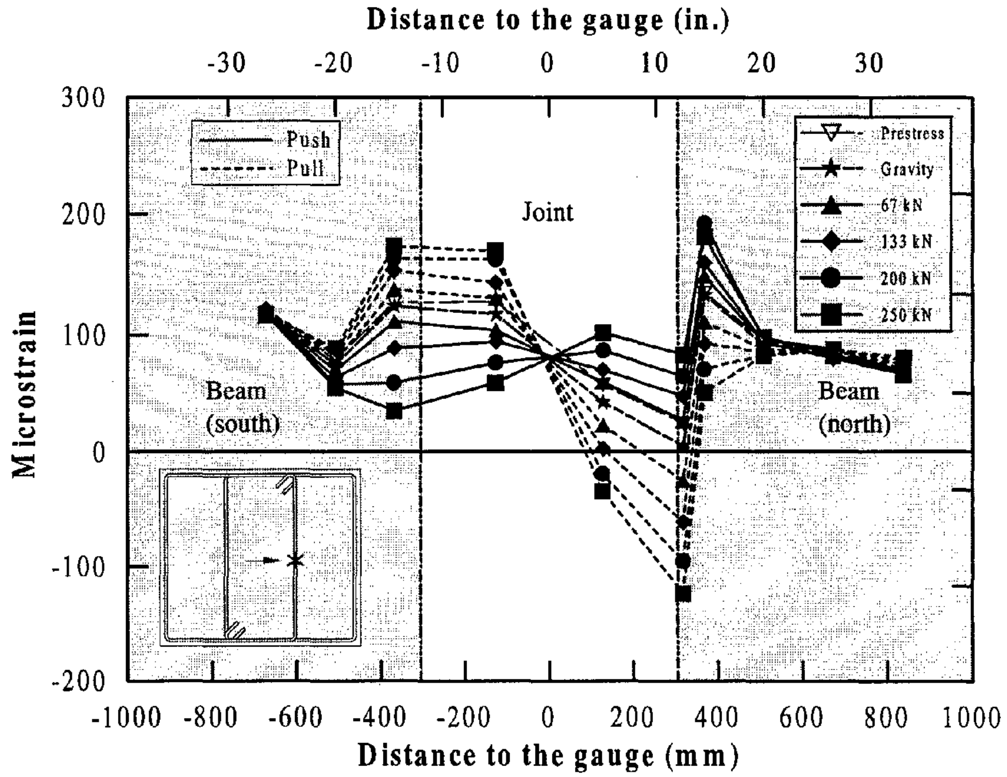

(a) Initial stages of testing

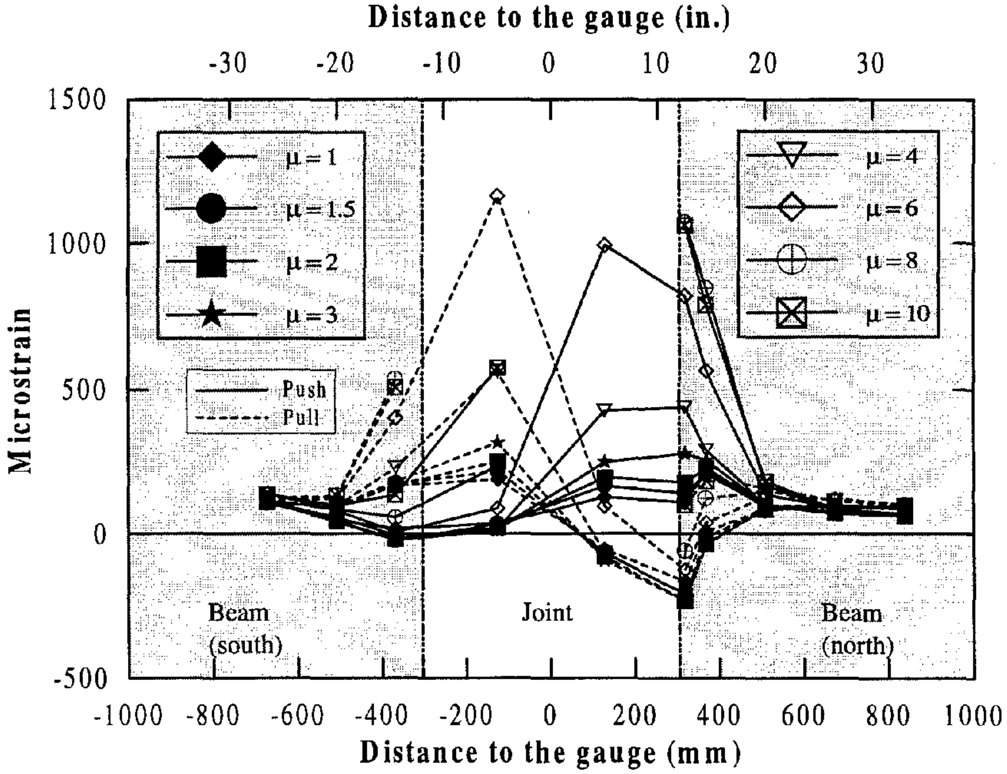

(b) Final stages of testing

Figure 6.44 Strain profiles of inner leg beam stirrups at mid-height.

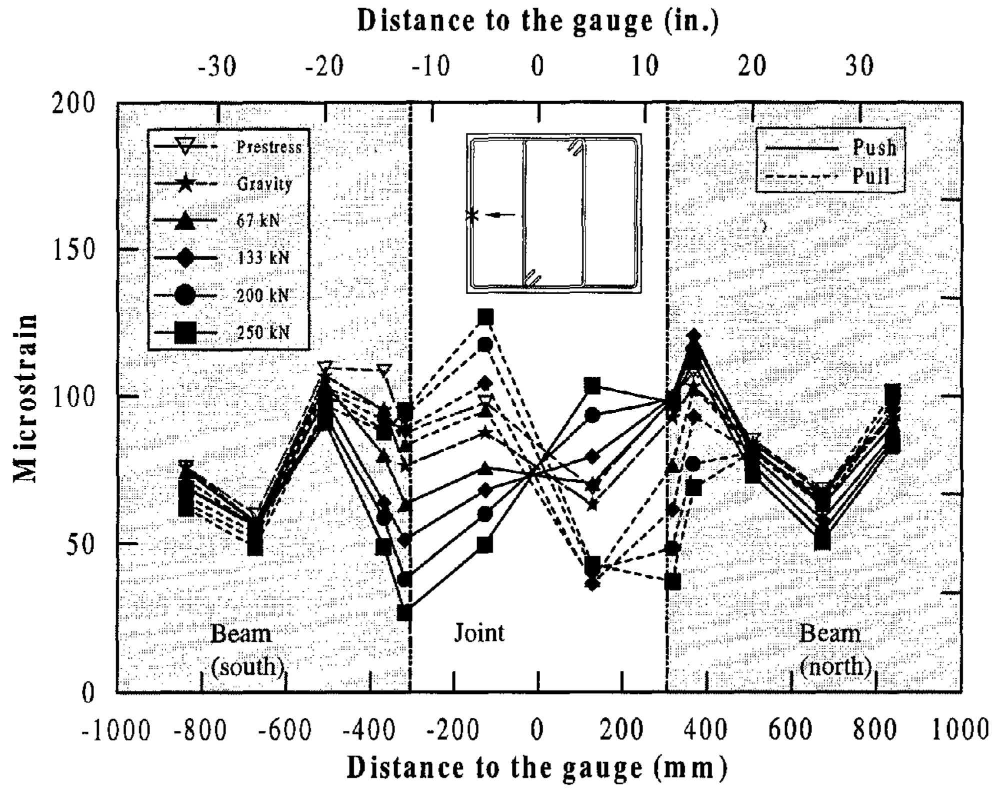

(a) Initial stages of testing

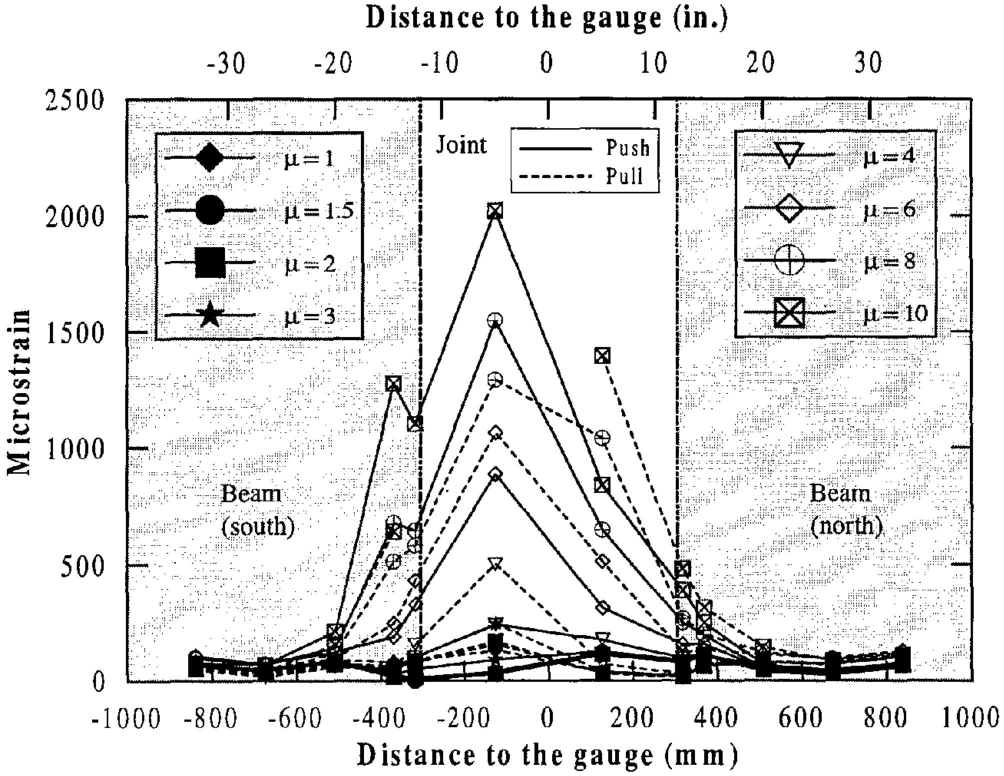

(b) Final stages of testing

Figure 6.45 Strain profiles of outer leg beam stirrups at mid-height.

6.8 Discussion

A precast fully prestressed tee connection was designed and tested under simulated seismic loading. The design detail and its seismic performance are described in this chapter. Although a force transfer mechanism similar to that was presented in Chapter 4 for the reinforced concrete joint was considered for designing the of IC3 joint, a reduced amount of joint steel was provided as for the partially prestressed joint (Chapter 5). This was possible because the cap beam prestressing broadened the joint diagonal strut such that all the longitudinal column reinforcement could be anchored directly into the joint by bond, suggesting no special mechanism for anchorage of the column bars. The average beam stress induced by prestressing was about $0.2f'_c$, which was considered to be an appropriate limit for satisfying serviceability design criteria.

An excellent hysteresis response was obtained for the test unit under simulated seismic loading with failure occurring in the plastic hinge region of the column at the ultimate limit state. At the peak displacement, the column drift corresponded to 7 percent, which was 31 percent higher than that estimated from theoretical calculations.

The overstrength capacity of the column was taken as 15 percent higher than the estimated ultimate moment capacity in the design calculations. It was found that the maximum horizontal load applied to the test unit was only 3.4 percent higher than that corresponding to the expected ultimate moment capacity.

Although the response of the column was predominately influenced by flexural behavior, significantly high inelastic strains were recorded in the shear reinforcement of the column. During the test, inclined shear cracks in the column did not appear to be as pronounced as those were seen for the columns of IC1 and IC2. This was thought to be consistent with the fact that transverse reinforcement content in the column of IC3 was increased by 52 percent while no significant change in the shear demand was imposed when compared to the columns of test units IC2 and IC3. Consequently, based on the calculations presented in Section 4.7, the shear demand was not expected induce yielding of the column spirals in IC3. The possible reason for recording strains beyond yield limit in the column spirals could be a localized effect, resulting from shear cracks crossing the gauged reinforcement.

The design of the cap beam was performed using a simple plastic analysis of the section using a strength reduction factor of 0.9. Almost no damage was occurred to the cap beam of the test unit, indicating that the column moment capacity was overestimated. In the design of IC1 and IC2, the overstrength flexural capacity of the column was taken as 30% higher than the theoretical ultimate moment capacity. In the design of IC3, only 15% ratio was considered between the overstrength and theoretical ultimate capacities. Considering the damage that occurred to the cap beam of IC3, it is suggested that it is sufficiently conservative to design the beam assuming that the overstrength column moment is only 5-10% higher than the theoretical ultimate capacity, provided the actual material properties of the reinforcement are taken into account, as for the design of test units presented in this report.

The seismic performance of the precast joint was excellent and outperformed the equivalent reinforced concrete joint. Because of the presence of prestressing in the joint, the damage was limited to only minor cracking and no significant shear deformation occurred to the joint. The theoretical force required to cause first joint cracking agreed well with the observation. The overall behavior of the precast joint was consistent with the capacity design philosophy and was similar to that would be expected on a fully prestressed monolithic joint.

CHAPTER 7

DISCUSSION AND DESIGN RECOMENDATIONS

7.1 Alternative Joint Design Approach

Following the poor seismic performance of an as-built tee joint from the Santa Monica Viaduct, redesigns of the prototype joint were sought. Attributing the inadequate performance of the as-built joint to the absence of joint shear reinforcement, the current design philosophy based upon the maximum joint shear forces was first considered to establish the required amount of joint reinforcement. The joint detailing resulting from this design approach was excessive and indicated potential congestion problems. This observation is consistent with the construction difficulties identified in practical situations.

Recognizing that the detailing of joints based on shear force results in unnecessarily conservative amounts of reinforcement because shear, which is a component of a complete rational force transfer mechanism, is treated as an independent force, alternative design methods based on force transfer models were considered to minimize the reinforcement within the joint. In detailing the joints using force transfer models, it was emphasized that the overstrength moment capacity of the column could be developed by ensuring adequate anchorage of the longitudinal reinforcement into the joint and that no significant damage would occur in the joint region. Consistent with this design approach, Caltrans has adopted an alternative detailing for the cap beam/column regions [29]. When the design of joint was performed consistent with force transfer models, a significant reduction in the joint reinforcement resulted when compared to the amount that was required by the conventional methods based on the maximum shear forces. A further reduction in the joint reinforcement was possible when the cap beam was designed with prestressing. The cap beam prestressing broadened the joint diagonal strut, creating a better bond condition for the longitudinal column bars. Also, the damage to the joint was reduced because of the precompression introduced in the joint due to prestressing.

In detailing the joints, it was preferred that the longitudinal column bars be anchored into the joint with straight bar ends. Providing bends or hooks at the end of the column bars is likely to enhance the anchorage of the reinforcement, but this detail can also create congestion within the joint. Another design deficiency inherent in the as-built joint from the Santa Monica Viaduct was the premature termination of column bars into the joint (Figure 3.2). A similar detail can also be identified in recently completed concrete bridges in California. Considering the possible consequence of such detailing [25], it was emphasized in the design of the redesigned joints that the column bars should be extended into the joint as close to the top beam reinforcement as possible.

7.2 Discussion of Test Results

Three redesigns of the as-built tee connection consistent with the new design philosophy were experimentally investigated. The cap beams of these units were designed varying amounts of prestressing. Consistent with the amount of beam prestressing, the joint region was detailed accordingly. The competence of the joint details was verified by subjecting half scale model units to simulated seismic loading. All three test units performed satisfactorily within the expected maximum displacement capacity of the system. The force-displacement envelopes of the measured response, which are compared against the response envelope of the as-built joint in Figure 7.1, show that redesigned units produced a significantly improved seismic performance when compared to the as-built joint. In Figure 7.1, the actuator force applied to the as-built unit was scaled to obtain the equivalent force required for a half scale model. Identical initial stiffness was obtained for all four units with the maximum displacement ductilities of 6, 8, 8 and 10 for SM3, IC1, IC2 and IC3 respectively. Joint shear deformation of the prestressed units, IC2 and IC3, was considerably smaller than that observed for the two reinforced concrete joints, IC1 and SM3, and this resulted in smaller maximum displacement for IC2 than for IC1 despite using identical reinforcement detailing in the two columns.

Comparison of the hysteresis loops and equivalent viscous damping as shown in Figure 7.2 confirms that the energy absorption increased as the amount of cap beam prestressing, presumably as a result of reduced joint deformation and increased inelastic rotation of the column. In Figure 7.2, the force-displacement response corresponding to relatively stable second loading cycle was considered.

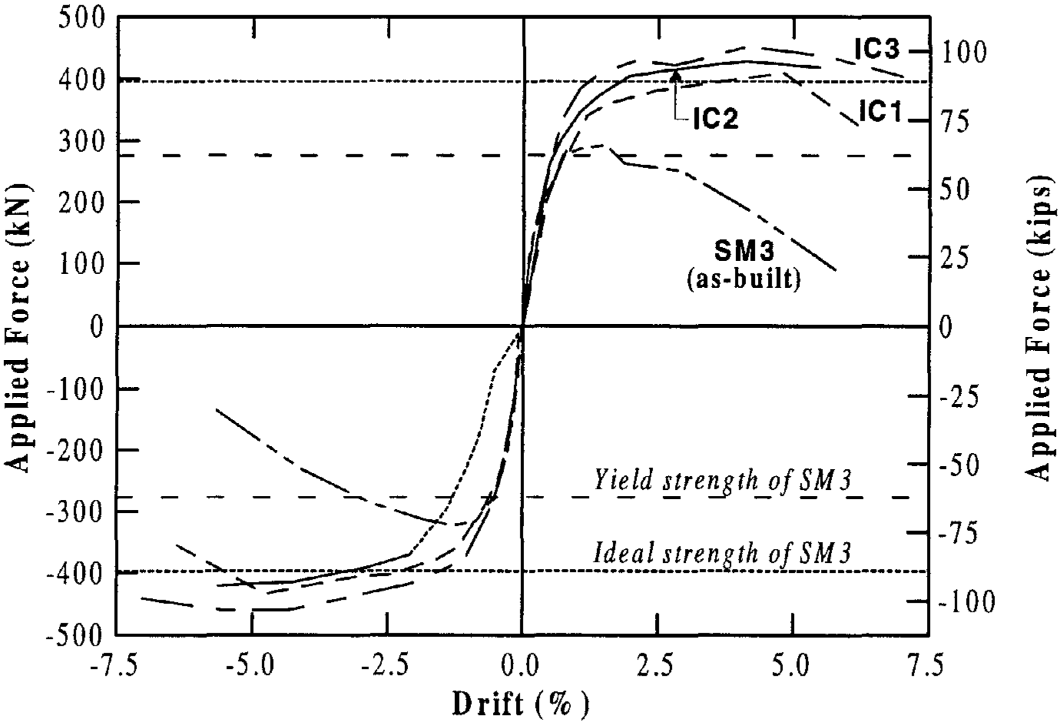

Figure 7.1 Comparison of the measured response envelopes of redesigned joints against that of the as built joint.

The strength deterioration seen for IC2 and IC3 at the maximum ductility was primarily due to the damage which occurred to the columns in the hinge region. This can be identified in Figure 7.3 where the damage occurred to each of the redesigned test units is shown. The strength degradation associated with IC1 at large ductilities was due to

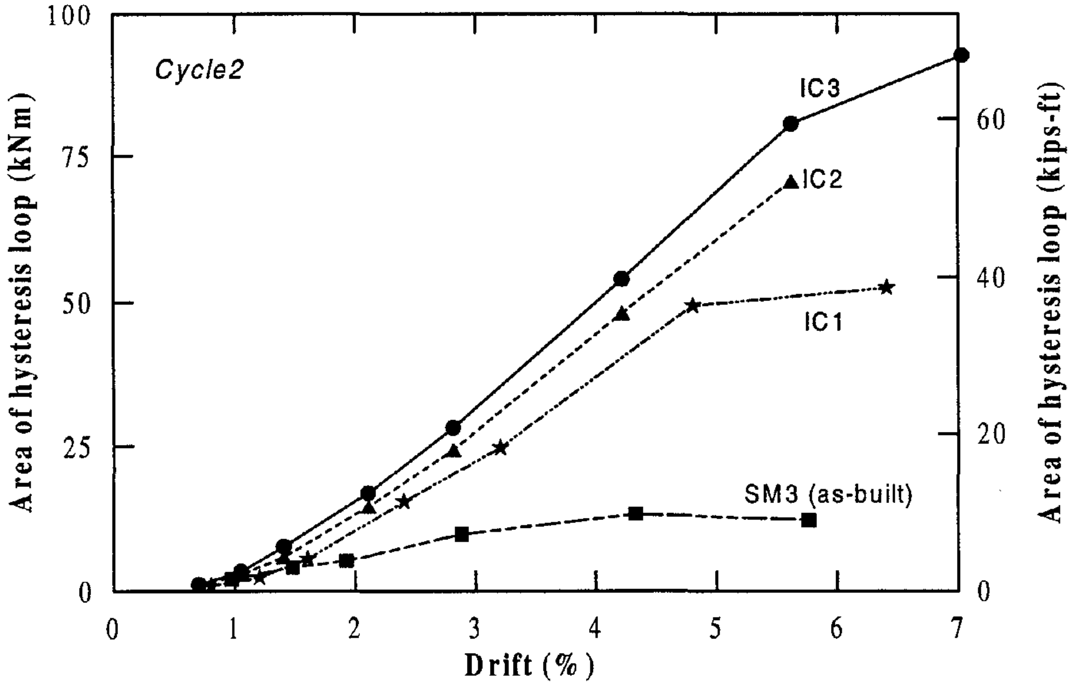

(a) Area of hysteresis loop

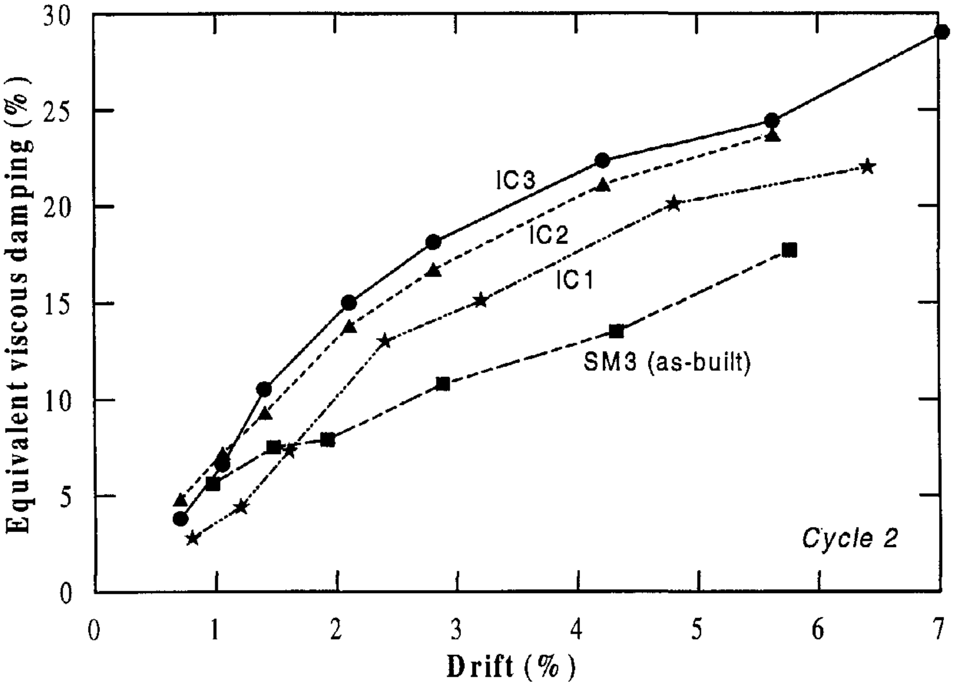

(b) Equivalent viscous damping

Figure 7.2 Comparison of energy dissipation capacity of the redesigned and as-built units.

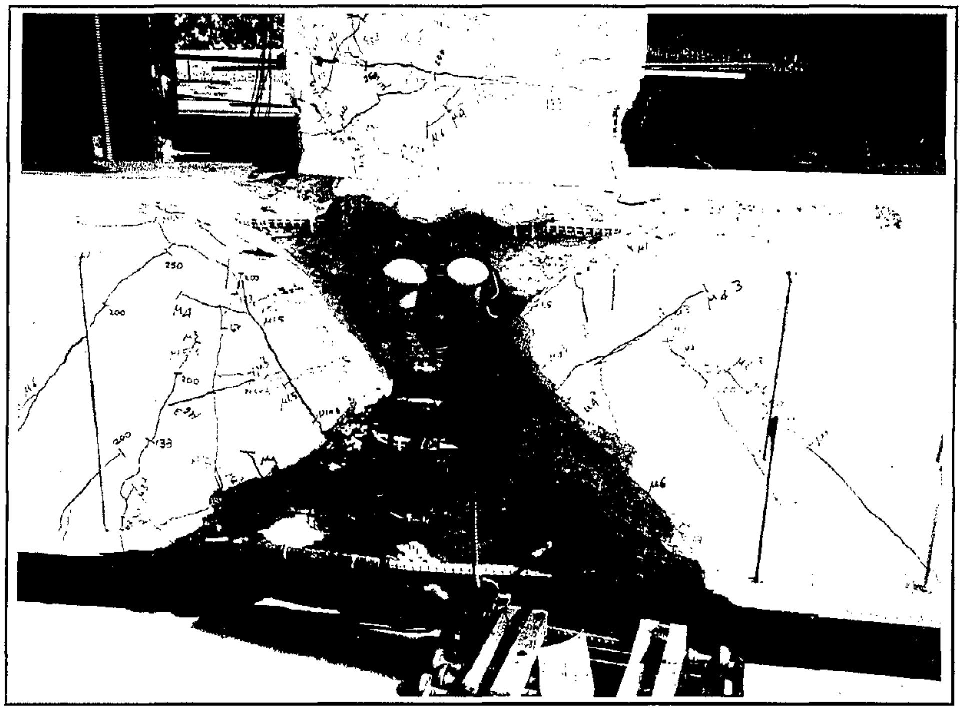

(a) IC1 - reinforced concrete joint

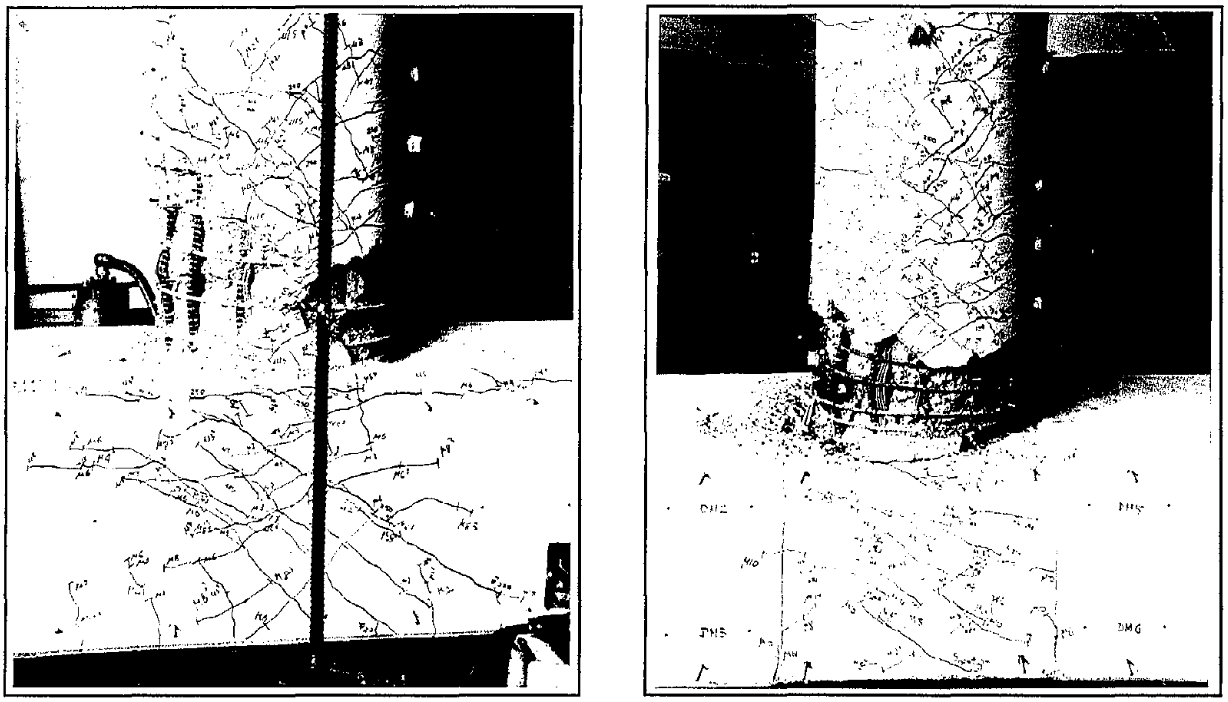

(b) IC2 - partially prestressed joint

(c) IC3 - precast fully prestressed joint

Figure 7.3 Condition of the redesigned units in the joint region after removing loose concrete.

Reproduced from
best available copy.

damage occurring to both the column and joint (Figure 7.3). The response of SM3, which never attained its theoretical flexural strength, was mainly influenced by the joint damage initiating at a low ductility level of 2.0. The negative stiffness seen in the force-displacement envelope, which was introduced mainly by the joint damage, was also similar for IC1 and SM3 for both loading directions.

The reinforcement provided in the joint region of the reinforced concrete unit, IC1, was slightly higher than that required by the force transfer model while the joint reinforcement in the prestressed units, IC2 and IC3, was reduced compared to that suggested by the mechanism in recognition that longitudinal column bars could be directly anchored into the joint strut. Although it was argued that the joint performance could be enhanced for the reinforced concrete unit by providing closed ties within the joint and accommodating the required joint reinforcement for the response in the longitudinal direction, it is concluded that prestressed joints undoubtedly outperformed the equivalent reinforced concrete joint. The amount of prestressing applied in the partially prestressed unit, IC2, was about 55 percent of that required in fully prestressed unit IC3. The precompression introduced in the joint of the partially prestressed unit was more than adequate to vastly improve the seismic performance of the joint when compared to that obtained for the equivalent reinforced concrete joint. The difference in the joint damage of the two prestressed joints was insignificant. Cracking initiated at a slightly reduced horizontal force in the partially prestressed joint and subsequently more cracking was seen at the ultimate limit state when compared to the fully prestressed joint.

The possibility of precast construction of bridge joints was investigated in the fully prestressed unit using the cap beam prestressing as a means of connecting the precast segments of the beam to cast-in-place or precast joint. Since bridge structures are designed to develop plastic hinges at column ends, it was demonstrated successfully that precast construction is a viable option for building multi-column concrete bents at no compromise to its hysteretic performance. Several other aspects of precast construction of multi-column bridge bents are currently investigated at UCSD [24].

The joint principal stresses were used in deciding the appropriate force transfer mechanism required for the joint and to ensure crushing of concrete would not occur in the joint main diagonal strut. In Figures 7.4 and 7.5, the envelopes of the principal tensile and compression stresses of the joints as calculated from the experimental measurements are compared for all three redesigned joints. In both figures, maximum and average principal stresses obtained using the maximum and average joint shear stresses are shown. The reinforced concrete joint experienced the largest principal tensile stress while the maximum principal compression stress was developed in the fully prestressed unit. In the partially prestressed joint, a reduced amount of prestressing was applied when compared to the fully prestressed joint. As a consequence, the principal stresses of this joint were bounded by those of the reinforced and fully prestressed joints, suggesting that the joint principal stresses can be manipulated in partially prestressed design by suitably changing the cap beam prestressing.

In designing the tee joints using force transfer mechanism, it was the maximum principal tensile stress which was used as the design parameter. Considering that the average joint principal tensile stress represents the damage potential more appropriately than the maximum stress, it has been suggested in a recent publication [19] that the design criteria of bridge joints should be based on the average stress. In Figure 7.4, it is shown that the design criteria described in Section 4.1.3 using limiting values of $\mathbf{0.29\sqrt{f_c'}}\left(\mathbf{3.5\sqrt{f_c'}}\text{ in psi units}\right)$ and $\mathbf{0.42\sqrt{f_c'}}\left(\mathbf{5.0\sqrt{f_c'}}\text{ in psi units}\right)$ better match the average principal tensile stress because the prestressed joints were designed with nominal joint reinforcement whereas the reinforced concrete joint was designed with a complete joint force transfer mechanism.

It is, however, recommended that when the joint design results in nominal reinforcement, it should be ensured that the depth of joint strut at the location of the most extreme tension bar is adequate to anchor the longitudinal column reinforcement by bond between steel and concrete. In this calculation, the depth of joint strut can be approximated to the

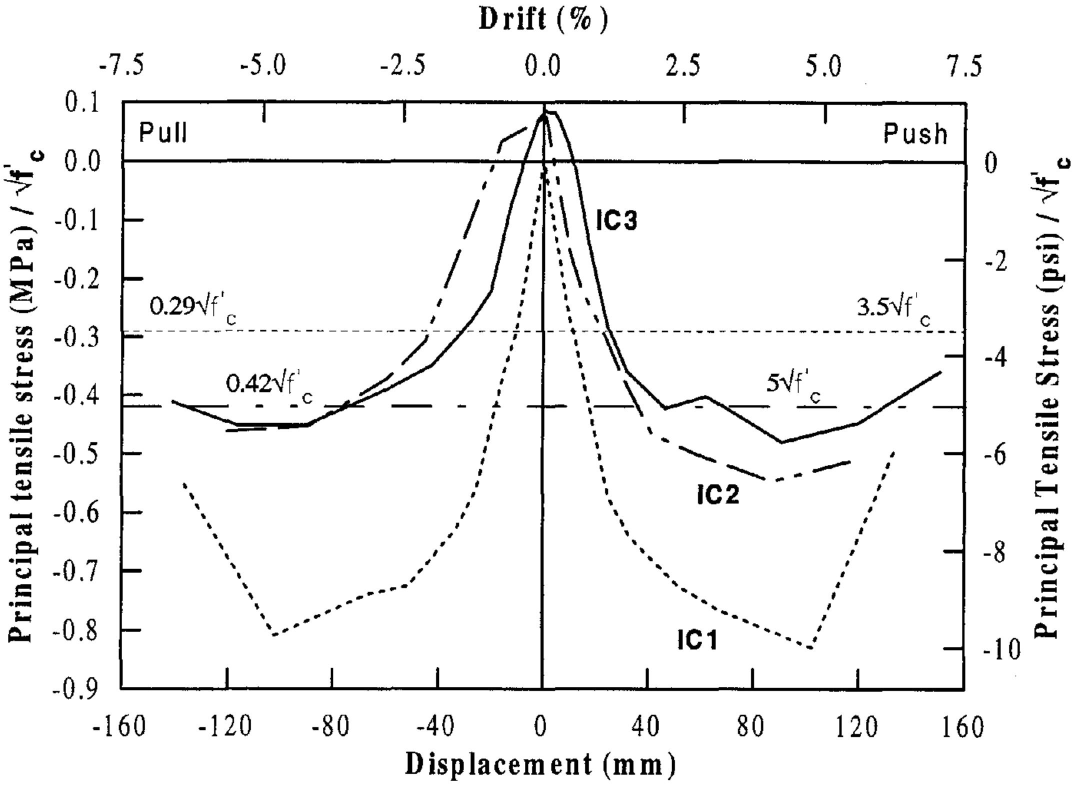

(a) using maximum joint shear stresses

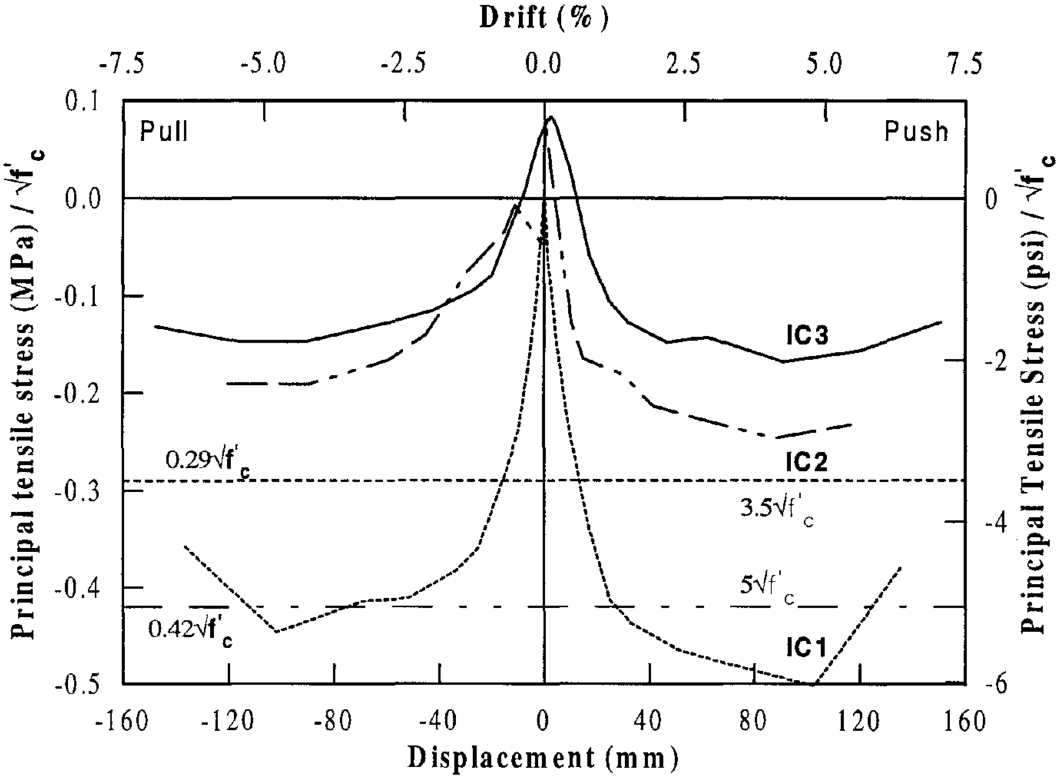

(b) using average joint shear stresses

Figure 7.4 Comparison of principal tensile stress envelopes as obtained for the redesigned joints using experimental data.

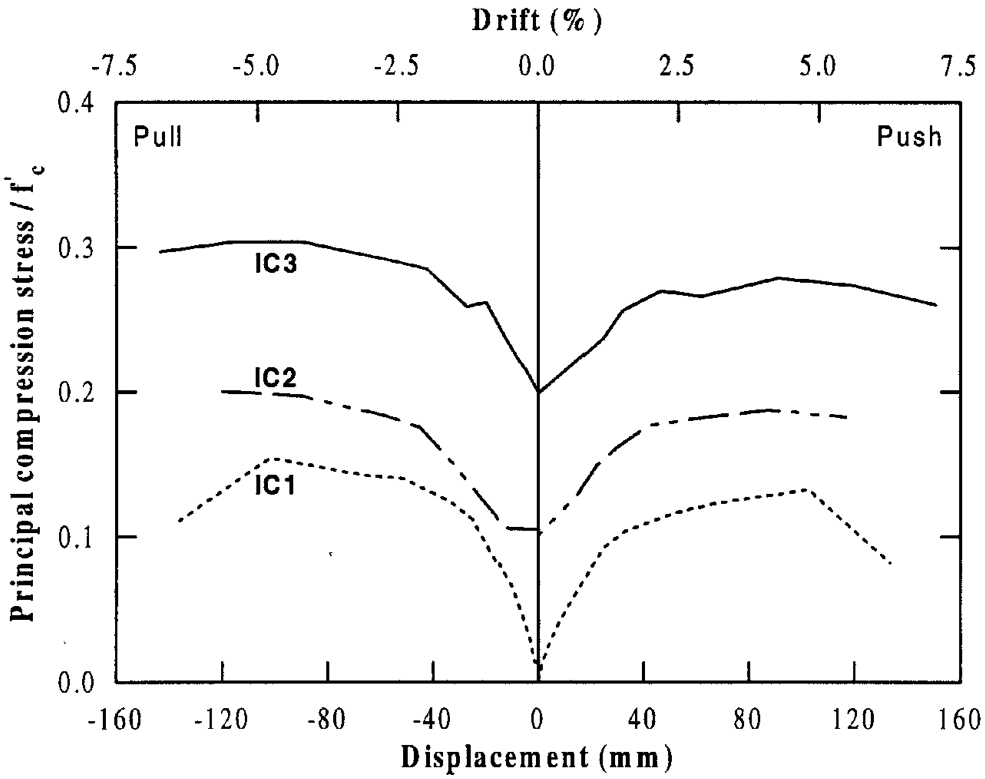

(a) using maximum joint shear stresses

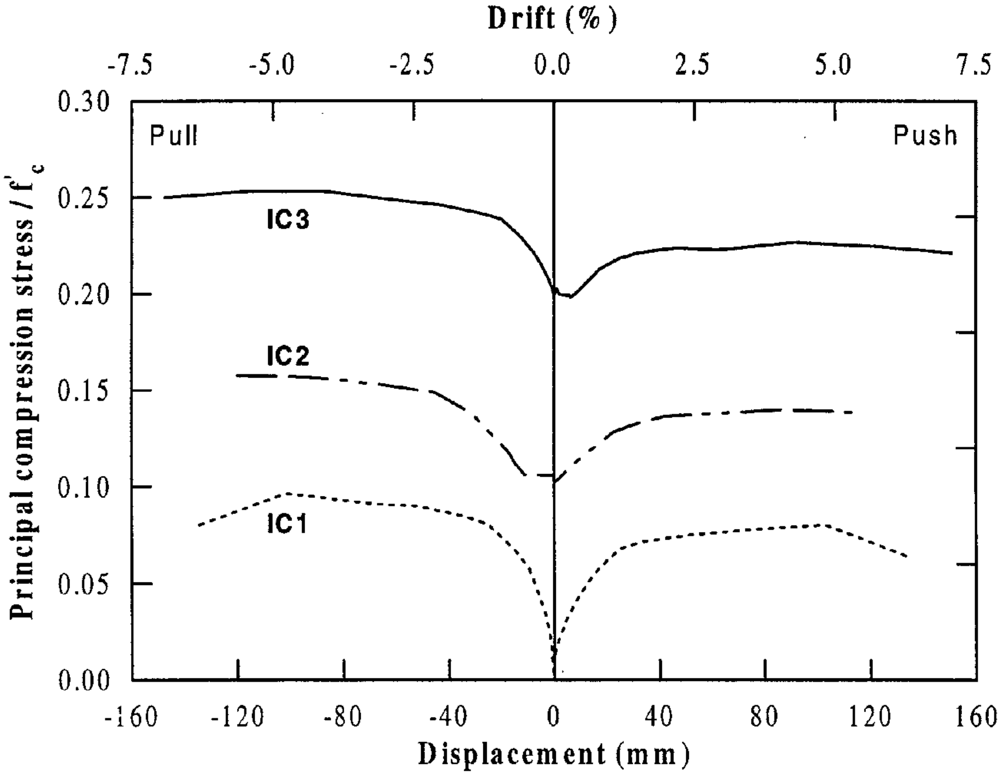

(b) using average joint shear stresses

Figure 7.5 Comparison of principal compression stress envelopes as obtained for the redesigned joints using experimental data.

neutral axis depth of the beam section adjacent to column tension side (i.e. by subjecting the beam section to the maximum positive moment) and a bond stress value of up to $\mathbf{2.5\sqrt{f_c'}}\left(\mathbf{30\sqrt{f_c'}}\text{ in psi units}\right)$ can be considered. Similarly, if the average joint principal tensile stress is estimated to be above the lower bounding value, nominal reinforcement in the joint region can be justified, provided the anchorage of the longitudinal column bars can be achieved by bond transfer within the joint diagonal strut.

The envelopes of principal stress presented in Figure 7.5 show that the cap beam prestressing significantly elevated the joint principal compression stress. In the test unit with a fully prestressed cap beam, the maximum principal compression stress reached the permissible stress which was established from design criteria of building joints [15]. However, there was no indication of concrete strut failure observed during the test. This is consistent with a recommendation [19] where it is suggested that it is adequate to limit the average joint principal compression stress to $\mathbf{0.3f'_c}$. In the reinforced concrete joint, in which the principal compression stress had its lowest value, well below the limiting stress, crushing of concrete occurred in the joint diagonal strut. A similar observation was also made in the tee joint of a recently tested reinforced concrete multi-column bent at UCSD [24].

In reinforced concrete bridge joints, significant amount of cracks develop in the joint region as seen for IC1. In order to mobilize the external joint reinforcement provided in the cap beam, high inelastic strains have to be developed in the joint reinforcement. This will, in effect, reduce the compressive strength of the joint core concrete. Further, the depth of the joint strut is shallow at the top corner, due to the absence of flexural compression stress resultant acting upon the joint from above, and increases towards the opposite bottom corner (Figure 4.3a). The compression force in the joint strut also increases with increasing strut depth [26]. Consequently, failure of the joint strut is likely to initiate in a localized region. Therefore, it may not be appropriate to justify the strut failure in a reinforced concrete joint based on the principal compression stress, which is obtained by applying an elastic theory to the overall dimensions of the joint. If the prestressing introduced in the joint is not sufficient to limit severe joint cracking and significant inelastic strains developing in the joint reinforcement, a similar problem may arise in prestressed joints as well. However, in general, it is expected that the amount of prestressing required in partially or fully prestressed joints is adequate enough to avoid severe joint cracking and development of significant inelastic strains in the joint reinforcement.

It is clear from the above discussion that an alternative approach is necessary to ensure that a brittle diagonal compression failure will not occur in concrete bridge joints subjected to inelastic response. This is further investigated in a companion report [26] on the analysis of bridge joints.

When severe cracking occurs and a strut failure develops in the joint, the horizontal displacement of the structure is significantly influenced by the joint shear rotation as seen for test unit IC1. This displacement component should be accounted for when assessing the force-displacement response of bridge structures. For this purpose, a relationship between joint shear strain and the maximum joint principal tensile stress was put forward by Priestley [17] for unreinforced concrete bridge joints. If the joint is designed with reinforcement, a higher joint shear strain is expected to develop, when compared to an unreinforced joint, before strength deteriorates and gradually leads to a compression strut failure. This can be seen in Figure 7.6 in which the maximum principal tensile stress developed in reinforced concrete joint IC1 is plotted as a function of joint shear strain. Also shown in this figure are the proposed joint shear strain and the principal tensile stress relation for unreinforced joints and an approximate envelope representative for the measured response of IC1. In Table 7.1, the data points corresponding to the two latter curves are presented. In establishing the envelope response of IC1, it was assumed that:

(a) initial stiffness before cracking is taken as twice that considered for unreinforced joints. Identical stiffness should be considered for both joints before cracking, but the suggested value correlates well with the experimental data.

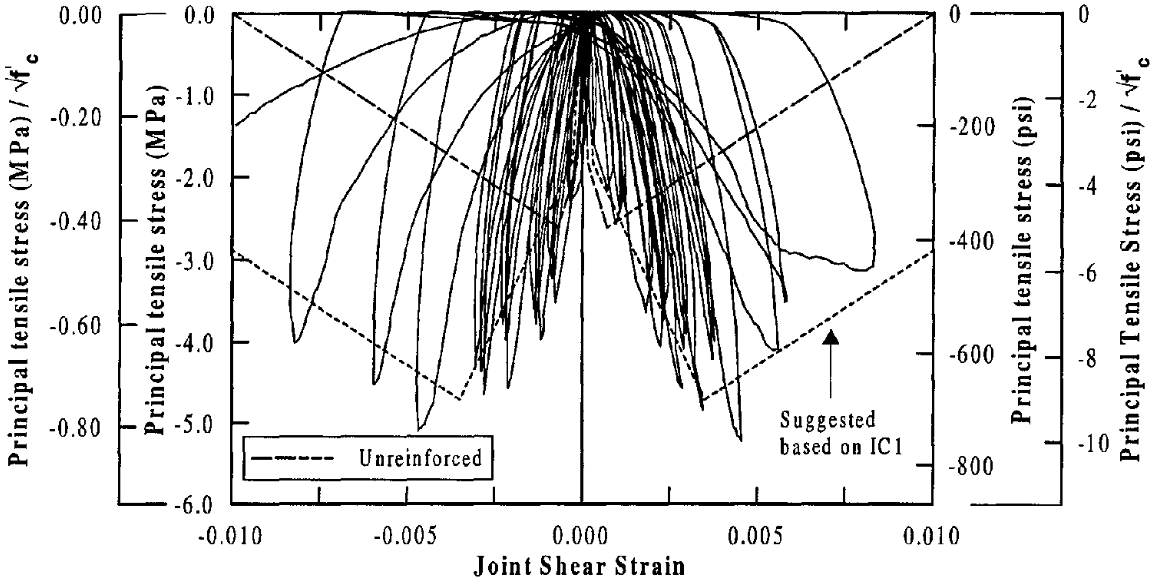

Figure 7.6 Joint shear strain as a function of maximum joint principal tensile stress for test unit IC1.

Table 7.1 Empirical relation for joint shear strain and maximum joint principal tensile stress.

For unreinforced joints [17]			Suggested based on IC1		
Shear Strain (Rotation in radians)	$\sqrt{f'_c}$		Shear Strain (Rotation in radians)	$\sqrt{f'_c}$	
	SI units	psi		SI units	psi
0	0	0	0	0	0
0.00015	0.29	3.5	0.0003	0.29	3.5
0.0007	0.42	5	0.0035	0.75	9
0.01	0	0	0.01	0.46	5.5

(b) the shear strain corresponds to the peak tensile stress was taken as five times that of the unreinforced joint. The peak value of the principal tensile stress was assumed to be $7.5\sqrt{f_c'}\left(9\sqrt{f_c'} \text{ in psi units}\right)$.

(c) the negative stiffness resulting from crushing of concrete in the joint core was assumed to be the same as that for the unreinforced joint. Consequently, it was found that the negative stiffness reached zero tensile stress at joint shear strain of 0.02 which is twice the value considered for unreinforced joints.

Although requiring verification against more test data, in the interim, the suggested relationship between principal tensile stress and joint shear strain is considered to be appropriate for the behavior of reinforced concrete bridge joints.

7.3 Design Recommendations

Based on the experimental investigation presented in this report, the following design recommendations are made for seismic design of cap beam/column concrete bridge tee joints.

7.3.1 Reinforced Concrete Joints

- Joint shear reinforcement shall be minimized by placing additional reinforcement in the bent cap adjacent to the joint.

- The required minimal reinforcement quantities in the joint region shall be obtained using the recommendations outlined in Section 4.1.3 or in reference [19].

- All longitudinal column reinforcement shall be extended as close to the top beam longitudinal reinforcement as possible.

- All the vertical stirrups in the joint region shall be provided as closed ties.

When a reinforced concrete joint is designed with the above recommendations, a satisfactory seismic response shall be expected for the joint within the maximum theoretical displacement capacity of the bent. At the *expected* ultimate displacement capacity of the system, some damage to the joint may occur as a result of significant inelastic strains developing in the joint reinforcement. However, in moderate to large earthquake excitations, the structure is not expected to reach its ultimate displacement capacity.

7.3.2 Prestressed Concrete Joints

- When the bent cap is designed with partially or fully prestressed details, a further reduction in the joint shear reinforcement shall be obtained in comparison to an equivalent reinforced concrete joint designed in accordance to Section 7.3.1.

- A prestressed joint shall be designed with nominal reinforcement within the joint and no additional reinforcement outside the joint in the cap beam if :
  - (a) the most extreme column tension bar can be anchored into the joint main diagonal strut by bond, or
  - (b) the average joint principal tensile stress is less than $\mathbf{0.29\sqrt{f'_c}}\left(\mathbf{3.5\sqrt{f'_c}}\text{ in psi units}\right)$.

- To ensure sufficient anchorage of the extreme longitudinal column tension bar, the depth of joint strut at the location of the reinforcement shall be approximated to the neutral axis depth of the beam section adjacent to column tension side and with a permissible bond stress value of up to $\mathbf{2.5\sqrt{f'_c}}\left(\mathbf{30\sqrt{f'_c}}\text{ in psi units}\right)$ as illustrated in Figure 7.7.

- All longitudinal column reinforcement shall be extended as close to the top beam longitudinal reinforcement as possible.

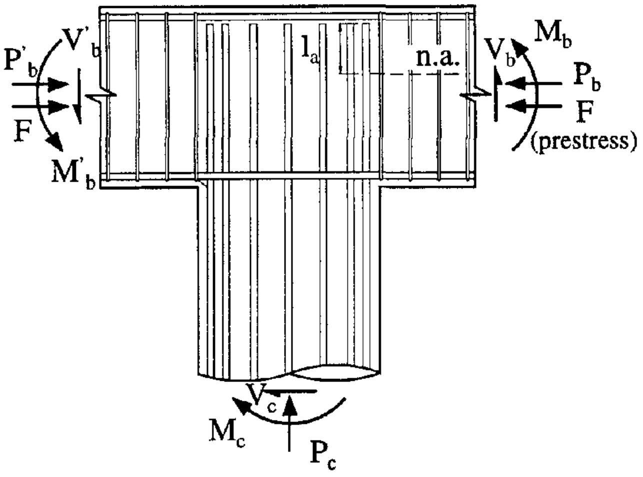

where

$$l_a * \pi d_b U_u \geq 1.4 f_y A_b$$

$$U_u \leq 2.5\sqrt{f'_c}\left(30\sqrt{f'_c} \text{ in psi units}\right)$$

note:
n.a. is found for the moment corresponding to column overstrength

Figure 7.7 Adequate anchorage of the column reinforcement into a prestressed tee joint.

- The nominal horizontal joint reinforcement shall be obtained using Eq. 4.6 while the nominal vertical reinforcement shall be taken as 8% of the total column longitudinal reinforcement (see Section 4.1.3).

- All the vertical stirrups in the joint region shall be provided as closed ties.

- If either of the criteria established for designing a prestressed joint with nominal reinforcement is not satisfied, an appropriate joint detail consisting of additional reinforcement in the cap beam shall be obtained using the procedures outlined in Sections 4.1.3 and 5.1.3.

- The average joint principal compression stress shall be limited to $\mathbf{0.3f'_c}$.

When a prestressed joint is designed with the above recommendations, nominal joint reinforcement details are generally expected. Because of the additional confinement provided to the joint by cap beam prestressing, a good dependable seismic performance shall be expected for the joint with almost no damage to the joint region.

REFERENCES

1. *AASHTO Standard Design Specifications for Highway Bridges*, American Association of State Highway and Transportation Officials, Washington, D. C., 1992.

2. Allahabadi, R. and Powell, G. H., *Drain-2DX User Guide*, Report No. UCB/EERC-88/06, Earthquake Engineering Research Center, University of California at Berkeley, California, March 1988.

3. American Concrete Institute, *Building code Requirements for Structural Concrete (ACI 318-95) and Commentary (ACI 318R-95),* Michigan, 1995.

4. Caltrans, *Bridge Design Specifications*, California Department of Transportation, State of California, Sacramento, California, 1993.

5. Eligehausen, R., Popov, E. P. and Bertero, V. V., *Local Bond Stress-Slip Relationships of Deformed Bars under Generalized Excitation*, Report No. UCB/EERC-83/23, Earthquake Engineering Research Center, University of California at Berkeley, California, October 1983.

6. Housner, G. W., *Competing Against Time*, Report to Governor George Deukmejian form the Governor's Board of Inquiry on the 1989 Loma Prieta Earthquake, California, May 1990.

7. Ingham, J. M., Priestley M. J. N. and Seible, F., *Seismic Performance of Bridge Knee Joints - Volume 1,* Structural Systems Research Report, Report No. SSRP 94/12, University of California at San Diego, California, June 1994.

8. Ingham, J. M., *Seismic Performance of Bridge Knee Joints*, Doctoral Dissertation, Division of Structural Engineering, University of California at San Diego, California, 1996.

9. King, D. J., M. J. N. Priestley and Park, R., *Computer Programs For Concrete Column Design*, Report 86-12, Department of Civil Engineering, University of Canterbury, Christchurch, New Zealand, 1986.

10. Kowalsky, M. J., Priestley M. J. N. and Seible, F., *Shear Behavior of Lightweight Concrete Columns under Seismic Conditions*, Structural Systems Research Report, Report No. SSRP 95/10, University of California at San Diego, California, 1995.

11. Lowes, L. N. and Moehle, J. P., *Seismic Behavior and Retrofit of Older Reinforced Concrete Bridge T-Joints*, Report No. UCB/EERC-95/09, Earthquake Engineering Research Center, University of California at Berkeley, California, September 1995.

12. MacRae, G. A., Priestley, M. J. N. and Seible, F., *Santa Monica Viaduct Retrofit-Large-scale Column-Cap Beam Joint Transverse Test - Preliminary Report*, Structural Systems Research Project, Report No. TR- 94/02, University of California at San Diego, California, 1994.

13. Mander, J.B., Priestley M. J. N., and Park, R., "Theoretical Stress-Strain Model For Confined Concrete", *Journal of the Structural Division, ASCE*, Vol. 114, No. 8, August 1988, pp. 1804-1826.

14. Park, R. and Paulay, T., *Reinforced Concrete Structures*, John Wiley & Sons, New York, 1975.

15. Paulay, T. and Priestly, M. J. N., *Seismic Design of Reinforced Concrete and Masonry Buildings*, John Wiley & Son, New York, 1992.

16. Priestley M. J. N., Ely, A., Scott, R. and Seible, F., *Seismic Safety Review of Santa Monica Viaduct Retrofit*, Report by the Seismic Safety Review Panel to Caltrans Office of Structures Design, Sacramento, California, January 1992.

17. Priestley M. J. N., *Assessment and Design of Joints for Single-Level Bridges with Circular Columns*, Structural Systems Research Report, Report No. SSRP 93/02, University of California at San Diego, California, February 1993.

18. Priestley M. J. N., Seible, F. and Benzoni, G., *Seismic Performance of Circular Columns with Low Longitudinal Steel Ratios*, Structural Systems Research Report, Report No. SSRP 94/08, University of California at San Diego, California, 1994.

19. Priestley, M. J. N., Seible, F. and Calvi, M., *Seismic Design and Retrofit of Bridges*, John Wiley & Sons, New York, 1996.

20. Roberts, J. E., "Research Based Seismic Design and Retrofit of California Bridges", *The First Annual Seismic Research Workshop*, California Department of Transportation, Division of Structures, Sacramento, California, 1991.

21. Seible F., and Igarashi, A., "Full Scale Testing of Masonry Structures under Simulated Seismic Loadings", *Experimental and Numerical Methods in Earthquake Engineering (J. Donea and P.M. Jones)*, 1991, pp.119-148.

22. Sritharan, S., *The Effects of Creep and Shrinkage on Concrete Structures*, Report No. 480, Department of Civil Engineering, University of Auckland, Auckland, New Zealand, 1990.

23. Sritharan, S., Priestley, M. J. N. and Seible, F., "Influence of Prestress on Column/Cap Beam Tee Joints", *The Fourth Caltrans Seismic Research Workshop*,

California Department of Transportation, Division of Structures, Sacramento, California, 1996.

24. Sritharan, S., Priestley M. J. N. and Seible, F., *Seismic Design and Performance of Concrete Multi-Column Bents for Bridges*, Structural Systems Research Report, Report No. SSRP 97/03, University of California at San Diego, California, June 1997.

25. Sritharan, S., Ingham, J. M., Priestley, M. J. N. and Seible, F., "Bond Slip of Column Reinforcement Anchored in Cap Beams", *The Gergely Symposium on Bond - ACI Spring Convention*, American Concrete Institute, Seattle, Washington, April 1997.

26. Sritharan, S., *Analysis of Concrete Bridge Joints Subjected to Seismic Excitation*, Doctoral Dissertation, Division of Structural Engineering, University of California at San Diego, California, (in preparation).

27. Standard Association of New Zealand, *Code of Practice for the Design of Concrete Structures*, NZS DZ 3101 Part 1 and Part2, Wellington, 1994.

28. Verma, R, Priestley M J N and Seible, F. "Assessment of Seismic Response and Steel Jacket Retrofit of Squat Circular Reinforced Concrete Bridge Columns". *University of California at San Diego.* Structural System Research Report, SSRP 92/05. California, 1993.

29. Zelinski, R., *Seismic Design Memo: Various Topics - Preliminary Guidelines*, Seismic Technology Section, California Department of Transportation, Sacramento, 1995.

APPENDIX A

ANALYSIS OF JOINT CRACKING

The horizontal actuator force required to induce joint shear cracking in the test unit was obtained assuming that joint should crack when the maximum, *not the average*, joint principal tensile stress reaches a value of $\mathbf{0.29\sqrt{f_c'}}\left(\mathbf{3.5\sqrt{f_c'}}\text{ in psi units}\right)$. The average principal tensile stress may be considered as a good representative value for the overall joint damage. However, cracking in the joint should correspond to the maximum principal tensile stress.

In establishing the joint cracking force, an iterative approach was employed using Eq. 4.1. For an assumed actuator force **F**, the average joint stress in the horizontal direction was obtained as follows:

$$\mathbf{f_h = \frac{P - 0.5F}{h_b b_j}} \tag{A1}$$

where **P** is the cap beam prestressing and **(P-0.5F)** represents the average joint axial force under the push direction of loading. When the test unit was subjected to a pull direction of loading, axial compression was induced in the joint, which was expected to delay the joint cracking. Therefore, the joint cracking force was obtained for the push direction of loading. The estimate of the average joint stress in the vertical direction due to gravity load was obtained as follows:

$$\mathbf{f_v = \frac{400}{2Db_j}} \tag{A2}$$

where **D** is the column diameter and it was assumed that $\mathbf{2Db_j}$ is the effective area, using a 45° dispersion [17]. Hence from Eq. 4.1, the joints shear stress $\mathbf{v_j}$ was determined. The maximum joint shear force was therefore:

$$\mathbf{V_{jv} = v_j * h_b d_j} \tag{A3}$$

From Figure A1, the maximum joint vertical joint shear force was also obtained from equilibrium conditions as follows:

$$\mathbf{V_{jv} = T_c - V_b} \tag{A4}$$

If the values of $\mathbf{V_{jv}}$ from Eqs. A3 and A4 were similar, then the assumed actuator force corresponded to the joint shear cracking force. Otherwise, a new value was considered for **F**, and the above steps were repeated.

1. Joint IC1

Joint cracking load was predicted prior to the test as follows:

Based on 28 days compressive strength, $\mathbf{f'_c = 38}$ **MPa** was expected on the day of testing.

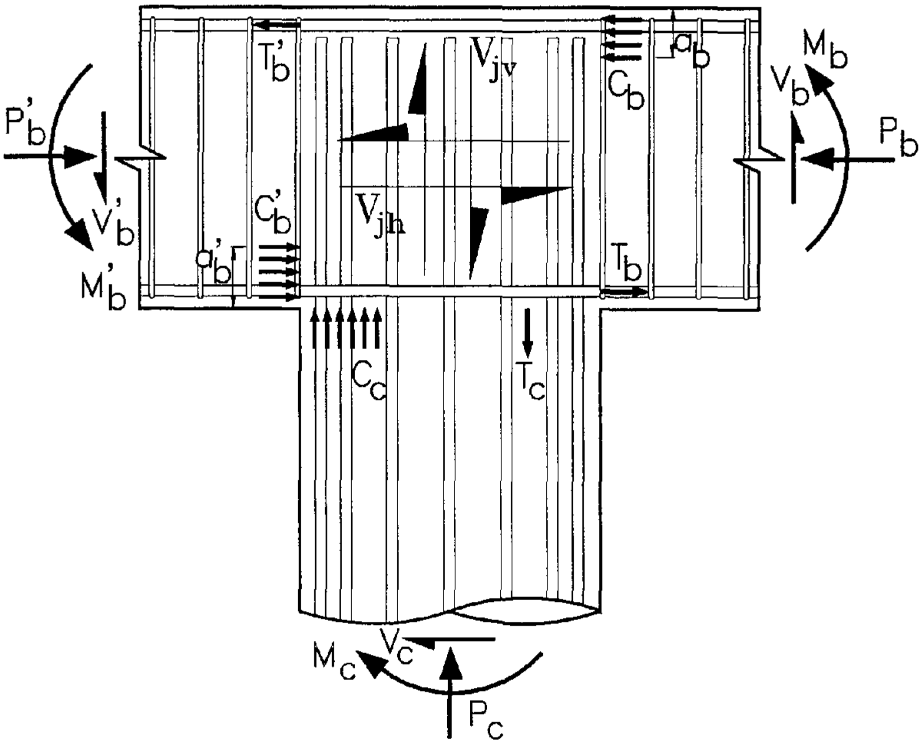

Figure A1 Forces acting on a bridge tee joint

Hence,

$$p_t = 0.29\sqrt{f_c'} = 1.79\,\text{MPa}$$

Assume **F = 220 kN**, Eq. A1 gives $f_h = \dfrac{0 - 0.5\text{x}220\text{x}10^3}{610\text{x}686} = -0.263\text{MPa}$

From A2, $f_v = \dfrac{400\text{x}10^3}{2\text{x}610\text{x}686} = 0.478\text{MPa}$

Hence, from Eq. 4.1, $v_j = 1.861\text{MPa}$, and

Eq. A3 gives, $V_{jv} = 1.861 * 610\text{x}686\text{x}10^{-3} = 779\text{kN}$

From equilibrium conditions, $V_{jv} = T_c - V_b = 783 + 5 = 788$ (close enough)

where **T**$_c$ was obtained analyzing the column section for the applied bending moment and axial force.

Therefore, it was concluded that the joint cracking was expected at a horizontal actuator force of 220 kN in the push direction of loading.

2. Joint IC2

The prediction of the joint cracking force was not calculated prior to the test. Using the measured compressive strength and **P = 1735 kN**, the horizontal joint cracking force **F = 356 kN** was obtained using the above procedure.

3. Joint IC3

The prediction of the joint cracking force for IC3 was also not calculated prior to the test. Using the measured compressive strength and **P = 2936 kN**, the horizontal joint cracking force **F = 400 kN** was obtained using the above procedure.

APPENDIX B

FORCE-DISPLACEMENT ENVELOPES

In the following tables, the numerical values of the predicted and experimentally measured displacement components of the redesigned test units are presented. The theoretical calculations were performed using the procedure outlined in Chapter 2, and the graphical representation of the data given in the tables are presented in the appropriate chapters.

Table B1: Theoretically calculated displacement components of test unit IC1 in mm ($\mu_m = 6.81$, $f = 0.241$ and $\mu_s = 5.68$)*.

Force	Column			Beam	Total
(kN)	Elastic	Plastic	Shear	flexibility	displacement
Push direction					
53	0.48	0.0	≈ 0	0.18	0.66
257	8.33	0.0	0.38	2.11	10.82
374	12.14	19.91	0.56	3.28	35.89
400	13.01	44.45	0.58	3.56	61.60
418	13.56	72.64	0.61	3.73	90.54
Pull direction					
-53	-0.48	0.0	≈ 0	-0.18	-0.66
-257	-8.33	0.0	-0.38	-1.88	-10.59
-374	-12.14	-19.91	-0.56	-2.85	-35.46
-400	-13.01	-44.45	-0.58	-3.07	-61.11
-418	-13.56	-72.64	-0.61	-3.20	-90.01

* μ_m = member ductility capacity from a fixed base analysis

f = system flexibility coefficient, and

μ_s = system ductility capacity (see Section 2.8 for details)

Table B2: Experimentally measured displacement components of test unit IC1 in mm.

Ductility μ_Δ	Column flexure	Beam flexibility	Joint shear	Total measured	Error (%)
Push direction					
1	10.45	3.15	2.05	16.96	-7.72
2	24.04	4.69	5.77	33.23	3.82
4	58.13	5.48	9.31	68.37	6.66
6	90.21	5.73	13.22	102.85	6.14
8	102.99	8.54	37.05	136.15	9.13
Pull direction					
-1	-11.79	-3.86	-0.93	-16.96	-2.24
-2	-26.38	-5.83	-2.61	-33.50	3.94
-4	-57.13	-7.88	-5.60	-68.61	2.92
-6	-80.97	-10.00	-9.12	-102.35	-2.21
-8	-94.30	-13.95	-44.13	-136.75	11.43

Table B3: Theoretically calculated displacement components of test unit IC2 in mm (μ_m = 6.81, f = 0.213 and μ_s = 5.79).

Force (kN)	Column			Beam flexibility	Total displacement
	Elastic	Plastic	Shear		
Push direction					
53	0.48	0.0	≈ 0	0.18	0.66
257	8.33	0.0	0.38	2.13	10.84
311	10.11	1.83	0.46	2.45	14.85
374	12.14	19.91	0.56	2.80	35.41
400	13.01	44.45	0.58	2.96	61.00
418	13.56	72.64	0.61	3.05	89.86
Pull direction					
-53	-0.48	0.0	≈ 0	-0.18	-0.66
-257	-8.33	0.0	-0.38	-1.99	-10.70
-311	-10.11	-1.83	-0.46	-2.29	-14.69
-374	-12.14	-19.91	-0.56	-2.62	-35.23
-400	-13.01	-44.45	-0.58	-2.77	-60.81
-418	-13.56	-72.64	-0.61	-2.87	-89.68

Table B4: Experimentally measured displacement components of test unit IC2 in mm.

Ductility μ_Δ	Column flexure	Beam flexibility	Joint shear[†]	Total measured	Error (%)
Push direction					
1	10.54	2.05	-	14.8	-14.9
2	23.84	3.86	-	29.73	-6.83
4	51.02	4.69	-	59.37	-6.17
6	78.21	5.63	-	89.41	-6.23
8	100.98	6.72	-	119.37	-9.78
Pull direction					
-1	-12.82	-0.08	-	-15.24	-15.35
-2	-25.79	-2.09	-	-30.16	-7.56
-4	-52.05	-1.75	-	-60.49	-11.06
-6	-76.53	-2.88	-	-90.58	-12.33
-8	-95.31	-5.91	-	-120.53	-16.02

[†] data was disturbed by the noise in the system (see Section 5.7.3)

Table B5: Theoretically calculated displacement components of test unit IC3 in mm ($\mu_m = 8.5$, f = 0.092 and $\mu_s = 7.87$).

Force (kN)	Column			Beam flexibility	Total displacement
	Elastic	Plastic	Shear		
Push direction					
53	0.48	0.0	≈ 0	0.15	0.63
262	8.64	0.0	0.38	0.72	9.74
351	11.61	8.81	0.51	0.97	21.90
400	13.20	36.22	0.58	1.57	51.57
445	14.68	97.38	0.66	1.93	114.65
Pull direction					
-53	-0.48	0.0	≈ 0	-0.15	-0.63
-262	-8.64	0.0	-0.38	-0.72	-9.74
-351	-11.61	-8.81	-0.51	-0.97	-21.90
-400	-13.20	-36.22	-0.58	-1.40	-51.40
-445	-14.68	-97.38	-0.66	-1.68	-114.40

Table B6: Experimentally measured displacement components of test unit IC3 in mm.

Ductility μ_Δ	Column flexure	Beam flexibility	Joint shear[†]	Total measured	Error (%)
Push direction					
1	12.92	1.92	-	17.27	-14.07
2	25.96	2.82	-	32.05	-10.20
4	56.84	3.22	-	62.13	-3.33
6	86.81	3.69	-	91.99	-1.62
8	114.57	4.76	-	122.32	-2.44
10	137.87	5.16	-	152.02	-5.91
Pull direction					
-1	-11.98	-3.20	-	-12.78	18.78
-2	-25.77	-3.69	-	-27.36	7.68
-4	-54.48	-4.12	-	-57.57	1.79
-6	-83.90	-4.55	-	-90.76	-2.55
-8	-105.15	-4.80	-	-117.38	-6.33
-10	-128.53	-5.16	-	-147.68	-9.47

[†] data was disturbed by the noise in the system (see Section 6.7.3 and Figure 6.25)

APPENDIX C

ANALYSIS OF HYSTERESIS LOOPS

Based on the measured force-displacement response of the test units, the area of the hysteresis loop and equivalent viscous damping coefficient were calculated for the first two loading cycles at different ductility levels. The results obtained for SM3 (as-built), IC1, IC2 and IC3 units are given in this appendix. In establishing equivalent viscous damping coefficient, ξ, the procedure outlined below was considered:

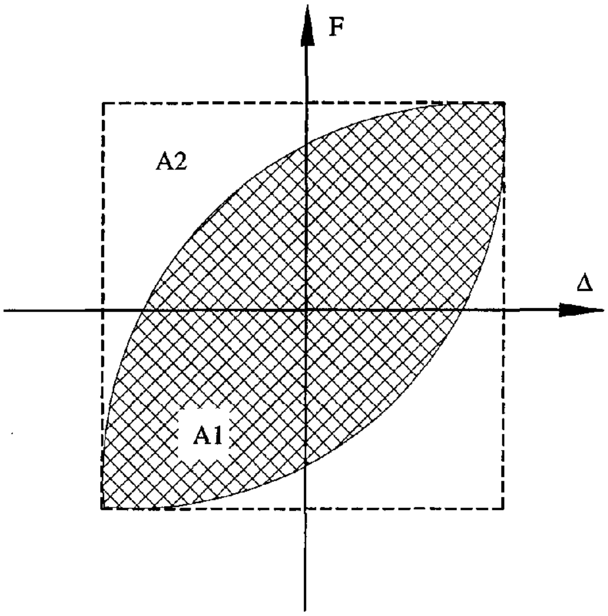

Figure C1 Hysteresis loop analysis.

In Figure C1, a force-displacement hysteresis loop is shown for one loading cycle. The area of this loop is A1. Considering the rectangular area A2, an equivalent viscous damping was obtained using the following equation:

$$\xi = \frac{2}{\pi} \frac{\mathbf{A1}}{\mathbf{A2}} \qquad \text{(C1)}$$

The values of A1 and ξ corresponding to the first two loading cycles are listed in the following tables:

Table C1: Hysteresis loop analysis of as-built unit SM3.

System Ductility	Cycle 1		Cycle 2	
μ_Δ	A1 (kNm)	ξ (%)	A1 (kNm)	ξ (%)
1	12.67	9.5	6.92	5.6
1.5	25.75	12.4	13.63	7.5
2	27.49	10.9	17.62	7.9
3	52.97	14.9	33.07	10.8
4.5	60.98	15.1	44.72	13.5
6	44.27	12.6	41.28	17.7

Table C2: Hysteresis loop analysis of redesigned unit IC1.

System Ductility	Cycle 1		Cycle 2	
μ_Δ	A1 (kNm)	ξ (%)	A1 (kNm)	ξ (%)
1	1.47	4.9	0.85	2.8
1.5	3.92	7.1	2.35	4.4
2	7.65	9.9	5.53	7.3
3	20.10	15.8	15.40	13.0
4	29.44	17.1	24.69	15.1
6	57.64	21.2	49.32	20.1
8	70.82	24.5	52.37	22.0

Table C3: Hysteresis loop analysis of redesigned unit IC2.

System Ductility	Cycle 1		Cycle 2	
μ_Δ	A1 (kNm)	ξ (%)	A1 (kNm)	ξ (%)
1	1.28	6.1	1.05	4.8
1.5	3.65	9.0	2.91	7.2
2	7.11	11.2	5.85	9.3
3	17.17	15.7	14.54	13.8
4	27.41	18.1	24.27	16.7
6	54.06	22.6	48.03	21.1
8	79.76	25.2	70.59	23.7

Table C4: Hysteresis loop analysis of redesigned unit IC3.

System Ductility	Cycle 1		Cycle 2	
μ_Δ	A1 (kNm)	ξ (%)	A1 (kNm)	ξ (%)
1	1.49	4.9	1.11	3.8
1.5	4.78	9.0	3.39	6.6
2	8.91	11.9	7.62	10.5
3	21.15	17.5	16.93	15.0
4	32.83	20.4	28.12	18.1
6	62.97	23.9	53.80	22.3
8	88.98	26.2	80.44	24.4
10	116.6	29.1	96.49	30.4

Reproduced by NTIS

National Technical Information Service
Springfield, VA 22161

This report was printed specifically for your order from nearly 3 million titles available in our collection.

For economy and efficiency, NTIS does not maintain stock of its vast collection of technical reports. Rather, most documents are printed for each order. Documents that are not in electronic format are reproduced from master archival copies and are the best possible reproductions available. If you have any questions concerning this document or any order you have placed with NTIS, please call our Customer Service Department at (703) 487-4660.

About NTIS

NTIS collects scientific, technical, engineering, and business related information — then organizes, maintains, and disseminates that information in a variety of formats — from microfiche to online services. The NTIS collection of nearly 3 million titles includes reports describing research conducted or sponsored by federal agencies and their contractors; statistical and business information; U.S. military publications; audiovisual products; computer software and electronic databases developed by federal agencies; training tools; and technical reports prepared by research organizations worldwide. Approximately 100,000 *new* titles are added and indexed into the NTIS collection annually.

For more information about NTIS products and services, call NTIS at (703) 487-4650 and request the free *NTIS Catalog of Products and Services*, PR-827LPG, or visit the NTIS Web site **http://www.ntis.gov.**

NTIS
Your indispensable resource for government-sponsored information—U.S. and worldwide

NTIS does not permit return of items for credit or refund. A replacement will be provided if an error is made in filling your order, if the item was received in damaged condition, or if the item is defective.

U.S. DEPARTMENT OF COMMERCE
Technology Administration
National Technical Information Service
Springfield, VA 22161 (703) 487-4650